

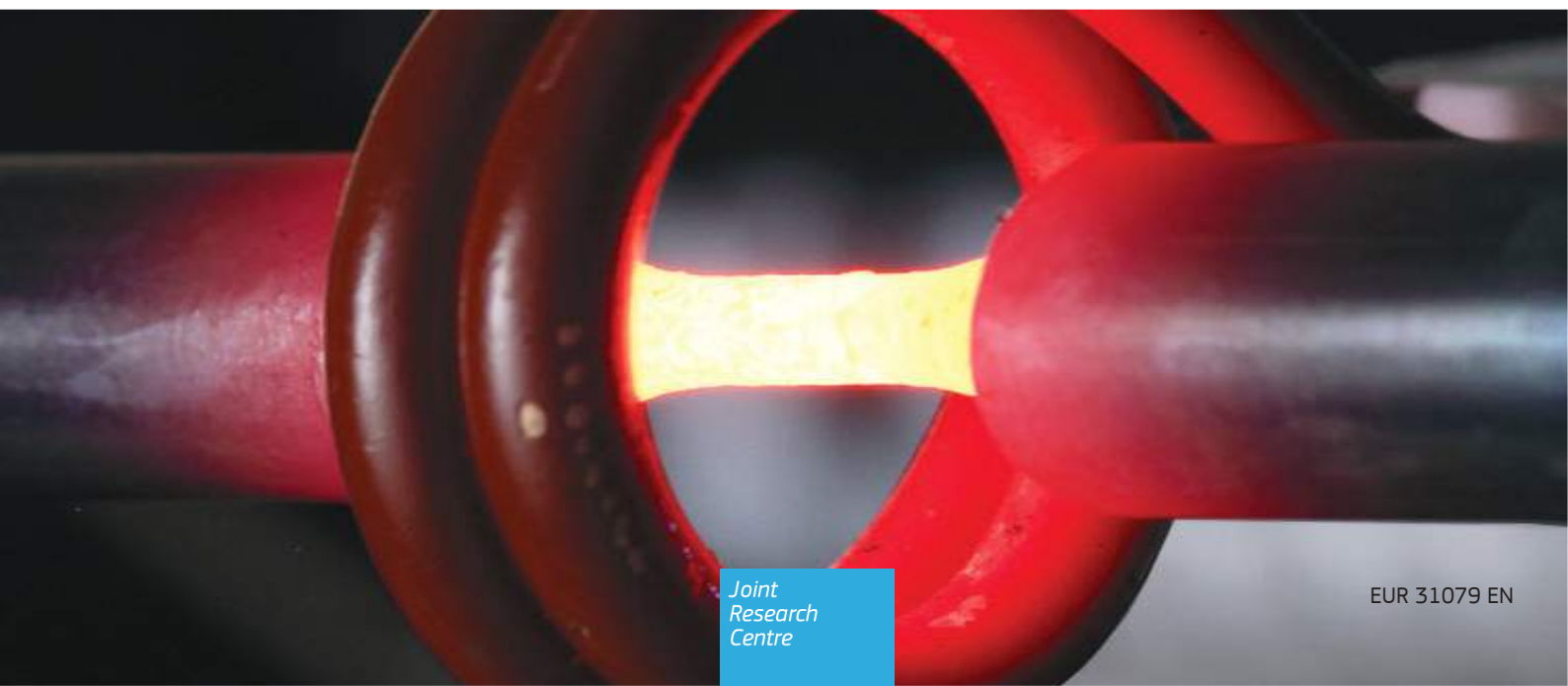


## JRC TECHNICAL REPORTS

# Review of the testing techniques and mechanical properties at high strain rate of nuclear reactor steels

*Results obtained in the period 1973-2003 at the JRC-Ispra in the frame of the containment of severe accidents program. Extensions to power fusion reactors.*

Albertini C., Cadoni E., Solomos G. and Tesio N.  
Peroni M. (editor)



This publication is a Technical report by the Joint Research Centre (JRC), the European Commission's science and knowledge service. It aims to provide evidence-based scientific support to the European policymaking process. The scientific output expressed does not imply a policy position of the European Commission. Neither the European Commission nor any person acting on behalf of the Commission is responsible for the use that might be made of this publication. For information on the methodology and quality underlying the data used in this publication for which the source is neither Eurostat nor other Commission services, users should contact the referenced source. The designations employed and the presentation of material on the maps do not imply the expression of any opinion whatsoever on the part of the European Union concerning the legal status of any country, territory, city or area or of its authorities, or concerning the delimitation of its frontiers or boundaries.

#### Contact Information

Name: Ezio Cadoni  
Address: University of Applied Science and Arts of Southern Switzerland  
Email: [ezio.cadoni@supsi.ch](mailto:ezio.cadoni@supsi.ch)  
Tel.: +41 58 6666377

#### EU Science Hub

<https://ec.europa.eu/jrc>

JRC128583

EUR 31079 EN

PDF ISBN 978-92-76-52773-2 ISSN 1831-9424 doi:10.2760/55004

Luxembourg: Publications Office of the European Union, 2022

© European Union, 2022



The reuse policy of the European Commission is implemented by the Commission Decision 2011/833/EU of 12 December 2011 on the reuse of Commission documents (OJ L 330, 14.12.2011, p. 39). Except otherwise noted, the reuse of this document is authorised under the Creative Commons Attribution 4.0 International (CC BY 4.0) licence (<https://creativecommons.org/licenses/by/4.0/>). This means that reuse is allowed provided appropriate credit is given and any changes are indicated. For any use or reproduction of photos or other material that is not owned by the EU, permission must be sought directly from the copyright holders.

All content © European Union, 2022

How to cite this report: Albertini C., Cadoni E., Solomos G. and Tesio N., Review of the testing techniques and mechanical properties at high strain rate of nuclear reactor steels, EUR 31079 EN, Publications Office of the European Union, Luxembourg, 2022, ISBN 978-92-79-52773-2, doi:10.2760/55004, JRC128583.

## Contents

Foreword .....	1
Acknowledgements .....	2
Abstract .....	3
1 Introduction .....	4
1.1 Historical evolution of the research .....	4
2 Dynamic mechanical properties of materials .....	6
2.1 Needs for the nuclear reactor safety studies .....	6
2.2 Dynamic response of materials and reactor safety .....	6
3 Overview of tested steels and testing conditions .....	8
3.1 Effects of high strain-rate and temperature .....	8
3.2 Effects of pre-damage at high strain-rate and high temperature .....	8
3.3 Size effects at high strain-rate .....	8
3.4 Effects of strain-rate histories typical of nuclear reactor malfunctions .....	9
4 Aims of the present report .....	10
5 Dynamic loading characteristics and related material testing devices .....	11
6 Detailed description of uniaxial dynamic testing devices .....	13
6.1 The Modified Hopkinson Bar for direct tension test .....	13
6.1.1 Progressing from the classical Hopkinson Bar to the JRC Universal Modified Hopkinson Bar (MHB) .....	13
6.1.2 The functioning of the Modified Hopkinson Bar in tension .....	14
6.2 The Universal Hydro Pneumatic Machine for testing at medium strain-rates .....	19
6.3 Application of the MHB and the HPM to dynamic testing of irradiated specimens of austenitic steels and alloys .....	23
6.4 Testing at high temperature with the MHB and the HPM .....	28
6.5 The JRC Large Modified Hopkinson Bar for fast dynamic testing of large specimens and structural components .....	29
6.5.1 Application of the Large MHB to high strain-rate testing of large steel specimens .....	30
7 Effects of strain-rate, environmental conditions and pre-damage on mechanical properties of nuclear reactor steels .....	32
7.1 Introduction .....	32
7.2 Effects of high strain-rate on as-received austenitic and ferritic steels at room temperature .....	32
7.3 Effects of high temperature and high strain-rate on as-received austenitic and ferritic steels .....	32
7.4 Effects of irradiation, high temperature and high strain-rate on austenitic stainless steels .....	46
7.5 Effects of the superposition of low cycle fatigue, irradiation, high temperature and high strain-rate on austenitic stainless steels AISI 304 and AISI 316H .....	46
7.6 Effects of creep damage, high temperature and high strain-rate on AISI 316H .....	51
7.7 Effects of welding, high temperature and high strain-rate on the austenitic stainless steel AISI 316H	51
7.8 Specimen size effects .....	55
7.9 Effects of strain-rate history on the stress-strain curves .....	55
8 New material database and assessment of nuclear reactor structures in case of severe accidents .....	70

8.1 Discussion.....	70
8.2 Improvements allowed by the new database to the safety assessment of aged reactor structures in case of severe accidents .....	71
9 Annex 1.....	73
9.1 List of materials.....	74
9.2 Chemical composition.....	75
9.3 Legend.....	77
9.4 Database.....	86
References.....	343
List of figures.....	349
List of tables.....	357

## **Foreword**

A prerequisite for a safety assessment of a nuclear installation under severe accident scenarios is the availability of reliable material data. In this direction, the motivation behind the work undertaken in this report has been the perceived need for retrieval and systematic collection of older JRC data concerning the mechanical characterisation of steels of nuclear fission reactors under dynamic loading conditions. The work itself was carried out in the framework of the two actions described below.

The Collaboration Agreement <sup>(1)</sup> signed by the Joint Research Centre (JRC) of the European Commission and the University of Applied Sciences and Arts of Southern Switzerland (SUPSI) had set as a general objective: "to contribute more effectively to understanding and resolving scientific issues in the field of assessing the mechanical vulnerability and/or robustness of structures to dynamic extreme loads as regards the behaviour of materials and structures to such conditions." In particular, one of the activities foreseen included: "To obtain the scientific data needed to perform such structural vulnerability studies. In this direction, existing results of older investigations, obtained at the JRC Materials Dynamic Testing Laboratory in the past Framework Programmes and in contract work, will be systematically collected in a database. Limited extent new testing may be envisaged".

At approximately the same period, within the activities of the EURATOM Seventh Framework Programme for Nuclear Research and Training -Fusion 2007, the launching of FEMaS (Fusion Energy Material Science - Coordination Action) was decided. The main aim of this coordination action was the enlargement of the European fusion material community to other European specialised materials R&D institutions, which might contribute to create at a faster time-scale and with higher quality the required knowledge over advanced characterisation methods of fusion materials using very small specimens; focus was especially put on the effects of high irradiation doses to the mechanical properties of the fusion materials. SUPSI's proposal, which was accepted in the FEMaS - Coordination Action<sup>(2)</sup> included:

- a. The consideration as advanced method for the characterisation of fusion materials of the Modified Hopkinson Bar (MHB) and of the Hydro-Pneumatic Machine (HPM) of the Joint Research Centre (JRC) technology because they had already been employed to characterise irradiated nuclear fission reactor steels using small specimens.
- b. A modern archive and a critical review and revision of the stress-strain curves of nuclear fission reactor steels irradiated from 2 to 30 dpa, tested in a large range of strain-rates, in the frame of successive Nuclear Fission Reactors Safety Programmes extended from 1973 to 2003, because a few of these steels (e.g. AISI316) are also candidates as fusion reactor materials.

Consequently, in order to achieve the objectives of the above two actions, a close collaboration was necessary and was made operative between the DynaMat Laboratory of SUPSI in Lugano (CH), represented by Prof. Dr. Ezio Cadoni, and the ELSA-HOPLAB of JRC-Ispra (EU), represented by Dr. George Solomos. For this purpose, JRC, as the owner of the dynamic testing technologies and of the dynamic material tests described at points a) and b), made the old test records and data (most of them in paper format) available to SUPSI for review and analyses. To render the above collaboration most efficient and productive it was also deemed necessary to resort to and engage in this activity Mr. Carlo Albertini, who was member of the Materials Dynamic Testing Laboratory from 1971 to 2000, initially as assistant to the laboratory Head Ing. Mario Montagnani, and subsequently as laboratory Head in the period 1990-2000. It was during these years that all the original testing technologies were developed and most of the data currently considered were produced, and in this sense he represents the scientific and historical memory of this report. The team was finally completed with the young engineer, Ing. Nicoletta Tesio, who patiently did most of the work of searching and retrieving the needed information from the old records and publications.

---

<sup>(1)</sup> Collaboration Agreement No 31237 between the European (Atomic Energy) Community and the University of Applied Sciences of Southern Switzerland, 12/02/2009.

<sup>(2)</sup> Project ID: 224752. Funded under: FP7-EURATOM-FUSION [https://cordis.europa.eu/project/rcn/89353\\_en.html](https://cordis.europa.eu/project/rcn/89353_en.html)

## Acknowledgements

The research was partially supported by the project FEMaS-Coordination Action, Project ID: 224752. Funded under: FP7-EURATOM-FUSION [https://cordis.europa.eu/project/rcn/89353\\_en.html](https://cordis.europa.eu/project/rcn/89353_en.html).

A special acknowledgement goes to Prof. Carlo Spinedi of the University of Applied Sciences and Arts of Southern Switzerland for his precious collaboration in recovering the data stored in older media and formats.

Finally, the authors wish to express their deep appreciation to Ing. Mario Montagnani, initiator of the Materials Dynamic Testing and Research at JRC Ispra, to whose memory they dedicate this work.

### **Authors**

**Carlo Albertini** is Former Head of the Materials Dynamic Testing Laboratory of the Joint Research Centre - European Commission

**Ezio Cadoni** is Professor at the University of Applied Sciences and Arts of Southern Switzerland. He has been Post-Doc grant holder and scientific auxiliary agent at Joint Research Centre - European Commission from March 1994 to September 1997.

**George Solomos** is Former Deputy Head of the Safety and Security of Buildings Unit, in charge of ELSA Large Hopkinson Bar Laboratory activities - Joint Research Centre - European Commission

**Nicoletta Tesio** is Researcher at the University of Applied Sciences and Arts of Southern Switzerland

### **Editor**

**Peroni Marco** is currently a scientific technical project manager of the Safety and Security of Buildings Unit - Joint Research Centre - European Commission

## **Abstract**

Safety is of paramount importance in nuclear energy production, and in particular where the industry is faced with the problem of extending the life of aged nuclear fission power plants. The re-assessment of the structural integrity of such aged nuclear reactors or other critical components under severe accident scenarios requires the measurement and/or the knowledge of the dynamic mechanical properties of their materials. A wealth of such data, produced over the last decades at the Joint Research Centre (JRC) of the European Commission, is provided in this report. They have been systematically collected from several dispersed sources and publications, and carefully controlled for their reliability. The materials investigated include mainly austenitic stainless steels (AISI 316, AISI 304, AISI 321, X6CrNiNb1810) and ferritic steels (ASME537, 20MnMoNi55, 6NiCrMo146, 22NiMoCr37). The data reported consist of stress-strain curves describing the uniaxial mechanical behaviour of the materials with respect to high strain-rate, high temperature, pre-damage by irradiation, fatigue, creep, thermal ageing, size effect and special strain-rate histories. Examples of testing conditions employed include strain rates reaching 1000/s, temperatures up to 900°C and irradiation levels of 30 dpa. The report also includes a description of the testing machines and techniques used, originally developed at the JRC, which are: the hydro-pneumatic machine, the modified Hopkinson bar, especially the very large Hopkinson bar, and the hot cell Hopkinson bar. As indicated, this review could also contribute in orientating research regarding the mechanical characterisation of irradiated steels for future fusion reactors. Finally, this publication timely coincides with the re-considerations about nuclear energy in the EU and its proposed inclusion by the Commission in the taxonomy of green energies.

# 1 Introduction

## 1.1 Historical evolution of the research

In 1957 the signing of the EURATOM Treaty led to the creation of a Joint Research Centre (JRC) directly depending on the European Commission, consisting, at that time, of four establishments, located at Ispra (Italy), Karlsruhe (Germany), Petten (The Netherlands), and Geel (Belgium). The mission of JRC was the development of a common research effort in the field of nuclear fission energy and reactor techniques including nuclear safety measures and the harmonisation of nuclear radiation measurements.

During the sixties the first joint project at JRC-Ispra was the construction of the Essor reactor, a prototype of organic liquid cooled reactor including the safety measures to contain the explosion effects due to accidental overpressures. Starting from the early seventies until the end of the twentieth century the research activity in the nuclear field of JRC-Ispra, was mainly concentrated on problems of nuclear reactor safety especially concerning the assessment of the steel or reinforced concrete containment structures for different types of nuclear reactors. These comprised Light Water Reactor (LWR), Pressurized Water Reactor (PWR) and Fast Breeder Reactor (FBR). Of concern was their resistance to the hypothetical accidental dynamic loadings like those due to gas explosions or liquid over-pressure arising in case of malfunctioning of some reactor components (e.g. cooling system, reactivity control bars etc.) or due to external accidents like impact of airplanes, terroristic attacks.

In particular at JRC-Ispra research activities were initiated regarding the steel reactor pressure vessel, containing the reactor core, and the steel containment shell surrounding the reactor pressure vessel and other reactor components. The assessment of the resistance of these structures against accidental dynamic loadings was conducted by means of calculations with Finite Element Codes, implementing the constitutive equations in dynamics of the steels of which the shell and the vessel were made. The calibration of these constitutive equations was supposed to be based on the stress-strain curve in tension of such steels measured at high strain-rates, ranging between one and a few hundred strain per second. Therefore to accomplish the above dynamic material testing programme of the high ductility steels new impact testing rigs had to be developed capable of generating the long duration pulses (durations ranging from tens of microseconds to a few milliseconds) of constant amplitude necessary to impose to the steel specimens the large displacements at constant speed and leading to fracture. Initially two were the basic set-ups developed:

- a hydro-pneumatic machine for strain-rate ranging from 1 to  $100 \text{ s}^{-1}$ , working in tension (Albertini and Montagnani, 1977);
- a Hopkinson bar for strain-rate ranging from 100 to  $1000 \text{ s}^{-1}$  modified for the generation of long duration pulses and for direct tension tests (Albertini and Montagnani, 1977, Montagnani et al., 1973, Albertini and Montagnani, 1974).

As will be thoroughly explained in Chapter 6, the main modification adopted in this new Hopkinson bar with respect to the classical scheme (Hopkinson, 1872, Hopkinson, 1914, Davis, 1948, Kolsky, 1949) concerned the generation of the loading pulse propagating in the input-output bar system. Due to the character of applied science of the research conducted at JRC, the new Hopkinson bar was patented in the years 1973-1974 (Montagnani et al., 1973). The first results obtained with the modified Hopkinson bar were published in the years 1974-1981 (Albertini and Montagnani, 1977, Albertini and Montagnani, 1974, Albertini and Montagnani, 1976, Albertini and Montagnani, 1983a, Albertini et al., 1979, Albertini et al., 1981), and concerned austenitic and ferritic virgin steels used for the down-scaled reactor containment shell models submitted to explosion experiments with the objective to validate the numerical computation codes (COVA code validation programme).

After this process of primary validation of the numerical codes the assessment of the resistance of the containment shells in the realistic working conditions had also to be performed by numerical computations which had implemented the dynamic constitutive equations of the austenitic and ferritic steels of the shell damaged by the environmental and loading conditions, characteristic of the nuclear reactor functioning. For this reason the modified Hopkinson bar and the hydro-pneumatic machine were installed in the hot cell laboratory of JRC-Ispra in order to measure the dynamic stress-strain curves at high temperatures (around  $550^\circ\text{C}$ ) of austenitic stainless steels previously submitted to welding, creep, low cycle fatigue and irradiation (2, 10 and 30 dpa) at elevated temperature. The results of this long term research were published in a series of ASTM special publications (Albertini et al., 1979, Albertini et al., 1981, Albertini et al., 1984a, Albertini et al., 1987a, Albertini et al., 1988) focusing on the mechanical properties of irradiated materials. Some dynamic material properties of the AISI 304L austenitic stainless steel irradiated and pre-fatigued are published here for the first time.

Due to the fact that most of the above research was performed using small specimens of 3mm diameter

and 5mm gauge length, in order to verify the specimen size effect on the dynamic material properties a new larger testing apparatus was conceived and constructed. Several tests similar to the above ones were afterwards performed by means of this new large modified Hopkinson bar. This apparatus allowed the tension testing at strain-rates (ranging between 20 and  $200\text{s}^{-1}$ ) of large specimens having a diameter of up to 30mm and gauge length of 50mm, whose results were compared with those of the 1/10 down-scaled small specimens of 3mm diameter and 5mm gauge length. This verification of the specimen size effect in dynamics was performed in the frame of the European projects RPVSA<sup>(3)</sup> and REVISA<sup>(4)</sup> and also in LISSAC<sup>(5)</sup> (Solomos et al., 2000, Solomos et al., 2004, Albertini et al., 2014, Solomos et al., 2003, Krieg et al., 2001, Solomos et al., 2002).

Finally, the effects due to special strain-rate histories on the stress-strain curves of the above steels have also been investigated. The aim was to simulate conditions of quasi-static increase of internal pressure followed by explosive dynamic loading and vice versa ((Albertini et al., 1995b, Eleiche et al., 1985, Albertini et al., 1989c)), and some results are presented in Chapter 7.

Clearly, in the assessment of containment shells against accidental dynamic loading the often generated stress multiaxiality should also be taken into account. This problem has raised the need of verifying in dynamics the yielding criteria and the material strength theories, which give rise to the equivalent stress flow curves. To this end biaxial versions of the modified Hopkinson bar and of the hydro-pneumatic machine, as well as of appropriate dynamic shear testing techniques were successfully developed. These results fall outside the scope of this report and are not included herein. Interested readers can find a wealth of such data and useful technical information in the relevant publications ((Albertini and Montagnani, 1979, Albertini and Montagnani, 1980, Albertini et al., 1989b, Solomos et al., 2000, Albertini, 1997), Albertini et al., 1990b, Albertini et al., 1991c, Albertini et al., 1991a)).

Reactor safety remains of paramount importance and economically strong countries depending on nuclear energy production are already faced with the problem of extending the life of aged nuclear reactors. It is clear that the re-assessment of such aged nuclear plants shall require the measurement of the dynamic mechanical properties of material taken directly from the aged reactor structures. The present report can provide precious help in such critical exercises as it describes in detail all the uniaxial applications of the hydro-pneumatic machine and of the modified Hopkinson bar, especially the large Hopkinson bar and the hot cell Hopkinson bar. More important, it also contains a large body of information on the dynamic mechanical properties in tension of as-received and pre-damaged nuclear steels, ordered in a data review manner, which might represent an important starting point in the re-assessment processes of aged nuclear plants. Finally the report could contribute to coping with characterisation problems of steels for future fusion reactors. The data review of the mechanical properties of irradiated steels can constitute a useful base for orientating the research regarding the effects of irradiation on fusion reactor steels.

<sup>(3)</sup> Project RPVSA: Reactor Pressure Vessel under Severe Accident Loading, FI4S-CT95-0002, Nuclear Fission Safety Programme, coordinated by FZKarlsruhe, 1996-1999.

<sup>(4)</sup> Project REVISA: Reactor Vessel Integrity in Severe Accidents, FI4S-CT96-0024 , Nuclear Fission Safety Programme, coordinated by CEA-Saclay, 1997-2000.

<sup>(5)</sup> Project LISSAC: Limit Strains for Severe Accident Conditions, FIKS-CT-1999-00012, Nuclear Fission Safety Programme, coordinated by FZKarlsruhe, 2000-2003.

## 2 Dynamic mechanical properties of materials

### 2.1 Needs for the nuclear reactor safety studies

Progress in the calculation of the dynamic loads following gas explosions allows the assessment of the resistance of steel containment shells provided that fracture criteria have been established for ductile steels, where considerable plasticity occurs before fracture. The method for evaluating the integrity of containment shells in case of explosion accidents consists of comparing the equivalent stress and the equivalent strain in the shell, determined by FEM calculations, with the stress and strain limits of the ductile fracture criteria. This analysis will be correct and reliable if both the dynamic loads acting on the shell are realistically known and the proper constitutive material model and ductile fracture criteria are effectively implemented in the code.

The constitutive material model and the ductile fracture criteria in dynamics are therefore indispensable and, as is evident, they can only be experimentally established via appropriate testing, representative of their actual loading conditions.

The tests should ideally be performed under the environmental conditions existing inside the reactor and after having submitted the specimen material to the working loads usually acting during the reactor functioning. Such environmental and loading conditions will be considered in the next two chapters.

### 2.2 Dynamic response of materials and reactor safety

The steel containment shells of nuclear reactors are designed to absorb the energy delivered by a hypothetical accident by means of the elasto-plastic deformation of the shell steel. Therefore the ideal stress/strain/strain-rate curves of the steel used for the containment shell should show not only high values of ultimate stress and fracture strain but also a stable dynamic plastic flow characterised by strain hardening, strain-rate hardening, high values of uniform strain, and no instabilities during plastic flow which might lead to early localisations compromising the response of the shell structure. Normally at room temperature the austenitic and ferritic steels used exhibit such a dynamic flow curve, close to the ideal one, as shown in Fig. 2.1 for the AISI 316H austenitic stainless steel (1.4541).

In reality nuclear reactor structures work under multiaxial loading, at high temperatures, and are submitted to thermo-mechanical loading cycles causing fatigue and creep damage, while further damage is due to irradiation, corrosion and stress corrosion. Therefore the capability of the containment shell to control a hypothetical accident is conferred to the elasto-plastic flow curves at high strain-rate of steels, which, despite being damaged by the above described processes, still possess dynamic stress-strain characteristics as much as possible resembling the ideal stress/strain/strain-rate curves described above. To check this fundamental point, within the context of the European Union Nuclear Fission Safety Programmes launched in the period 1973-2003, (chapter *Containment analysis of severe accidents in nuclear reactors*) an important amount of material impact tests were performed aimed at measuring the dynamic mechanical properties of nuclear reactor structural materials both in as-received and in pre-damaged conditions. Austenitic and ferritic steels were mainly studied, which are employed in Fast Breeder Reactors (FBR), Pressurized Water Reactors (PWR) and Light Water Reactors (LWR). Austenitic stainless steels are characterized by a good resistance to general corrosion at elevated temperature. This favours their widespread use in primary and auxiliary circuits of PWRs and in the containment structures of FBRs, where they work at temperatures ranging from 400°C to 550°C; also nuclear grade ferritic steels have been used for these nuclear reactor structures. Besides the harsh environment and the loads at normal operation, they may be subjected to many different types of dynamic loading in case of an accident.

The materials investigated were consequently the austenitic stainless steels (AISI 316, AISI 304, AISI 321, X6CrNiNb1810) and the ferritic steels (ASME537, 20MnMoNi55, 6NiCrMo146, 22NiMoCr37), most of which were tested in uniaxial tension and a few in biaxial tension at high strain rate, in a range of 6 orders of magnitude extended from  $10^{-3}$  to  $10^{+3} \text{ s}^{-1}$  and at temperatures from 20°C to 900°C. These testing conditions should reproduce the loading and environment conditions which are assumed to be found in a nuclear reactor in case of a severe accident. The steel specimens have also been tested in conditions of pre-damage equivalent to those of end-of-life of the reactor structures due to the foreseen long service period. Summarising, the large testing programme conducted at JRC has studied the influence on the tensile (shear) mechanical properties of nuclear austenitic and ferritic steels of the following parameters:

- High strain-rate
- High temperature
- Pre-damage by irradiation, fatigue, creep, thermal ageing
- Size effect

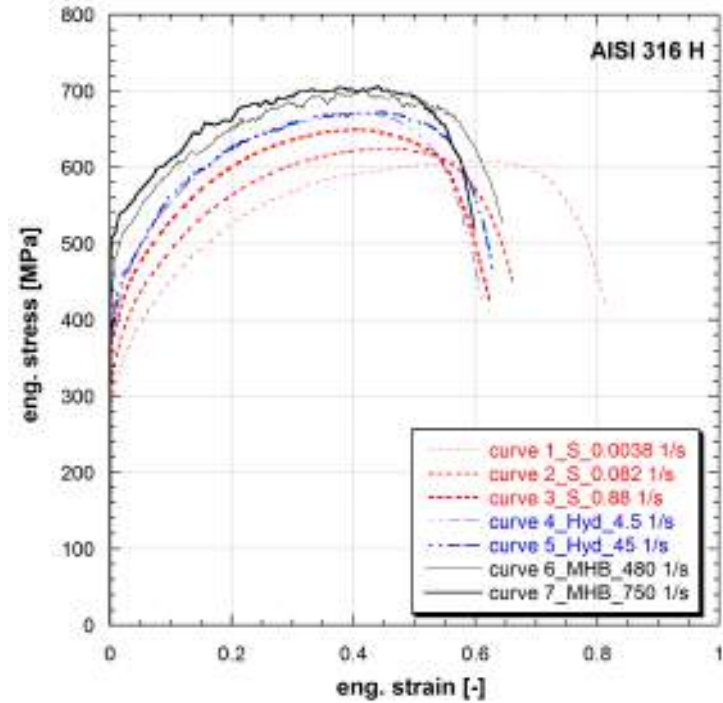


**Figure 2.1:** Stress vs. strain curves of AISI 316H stainless steel at different strain-rates and at room temperature. (S= Static, Hyd= Hydro-pneumatic machine, MHB= Modified Hopkinson Bar)

— Special strain-rate histories

As mentioned earlier, aspects concerning dynamic biaxial and shear tests are not included in this report. A detailed overview of the tested steels and of the realized testing and environmental conditions is reported in the next chapter.

### **3 Overview of tested steels and testing conditions**

#### **3.1 Effects of high strain-rate and temperature**

Among the materials thoroughly investigated were the austenitic stainless steels AISI 316, AISI 304 and AISI 321, which were tested in uniaxial tension in a strain-rate range of 6 orders of magnitude ranging from  $10^{-3}$  to  $10^{+3} \text{ s}^{-1}$  and at the temperatures of 20°C, 200°C, 300°C, 400°C, 500°C, 600°C, 700°C, 800°C and 900°C. These testing conditions attempted to reproduce the loading and environment conditions which are realistically assumed to be found in a nuclear reactor in case of a severe accident.

#### **3.2 Effects of pre-damage at high strain-rate and high temperature**

The steel specimens have also been tested in the same wide strain-rate range, at high temperatures (500°C) and in conditions of pre-damage equivalent to those of end-of-life of reactor structures due to the foreseen long service period. These steel specimens, before the dynamic testing, have been submitted to the following pre-damage conditions :

- Low cycle fatigue at different deformation levels (0.6 and 1%) and at different cycle ratios (0.2, 0.4, 0.6), temperature of 500°C and successive superposed irradiation to 2 dpa.
- Irradiation at increasing damage levels from 2 to 30 dpa.
- Creep loading at the temperature of 550°C at 0.4, 0.6, 0.8 of end-of-lifetime (1000 h).
- Different levels of temperature (R.T., 300°C, 400°C, 550°C, 600°C, 700°C).
- Thermal ageing at 550°C for 2000, 10000, 50000 hours.

The above described pre-damage conditions of the tested specimens might be considered as equivalent to those exerted on the real reactor structural materials by the thermo-mechanical cycles and by the radiation which exist inside a nuclear reactor during its service life. For performing such impact tests a special laboratory has been developed equipped with unique dynamic testing apparatuses capable of imposing large displacements at constant strain-rate in order to deform the very ductile austenitic stainless steel specimen up to fracture. A world-first achievement was to install such apparatuses in a hot cell in order to perform the impact tests on irradiated specimens. The material data obtained have been used to calibrate some visco-plastic constitutive equations (e.g. Perzyna, Bodner, Ludwig-Prandl) implemented in the FEM codes for the analysis of severe accident effects like explosion on reactor structures and containment shells (Albertini et al., 1983a, Eleiche et al., 1985, Micunovic et al., 2003, Micunovic et al., 2007, Albertini et al., 1991b). The total number of steel specimens tested has been about 1000. From each test the corresponding stress-strain curve has been constructed and the most important parameters were reported, always including yield stress, ultimate tensile strength, uniform strain and fracture strain.

#### **3.3 Size effects at high strain-rate**

Starting from the year 1994 in the frame of Shared Cost Actions (SCA) of the 4th and 5th Nuclear Fission Energy programme further mechanical tests have been performed at high strain-rates and at different temperatures on austenitic and ferritic steels used for the internal structures and the primary vessel. In fact the problem of the impact of a slug of molten corium and debris on the upper pressure vessel head as well as the dynamic pressure loading in the lower part of the vessel due to steam explosion were of concern in order to assess its integrity and overall performance. Strain-rate and temperature should be correctly included and size effects should be examined in order to assure the transferability of the small specimen results to the real structure. To this aim uniaxial tension tests have been performed on the materials used for the pressure vessel and its internal structures. These include: ferritic steel 20MnMoNi55 (vessel head), austenitic steel X6CrNiNb1819 (upper Internal Structure), ferritic steel 6NiCrMo146 (bolting) and ferritic steel 22NiMoCr37. Geometrically similar smooth cylindrical tension specimens of diameters 3 mm, 9mm and 30 mm have been tested at room and higher temperatures (400°C - 600°C) and at strain-rates ranging from quasi-static ( $10^{-3} \text{ s}^{-1}$ ) to dynamic  $200 \text{ s}^{-1}$  conditions. Notched cylindrical tension specimens of minimum diameter 2.4 mm, 7.2 mm and 24 mm have also been tested at the same conditions. In these SCAs about 300 dynamic tests have been performed and recorded in immediately usable current format. These data, collected in the period 1994-2003, are complementary to the data collected in the period 1973-1993, and it is intended to organise them in the same way and in the same database cited above. It has been in the frame of these SCA that the unique in the world Large Modified Hopkinson Bar, generating a 2.5 MN constant amplitude pulse with a 40 millisecond duration, has found a full exploitation.

### **3.4 Effects of strain-rate histories typical of nuclear reactor malfunctions**

The strain-rate histories which have been considered try to reproduce those which could load the containment structures in case of a hypothetical explosion type accident in a nuclear reactor.

Two typical such histories are the following:

1. deformation at high temperature and at quasi-static strain-rate, interrupted at a certain strain value and reloading at high temperature but at high strain-rate until fracture, thus simulating what happens to the containment shell material when the internal pressure of the containment or of the primary vessel increases slowly, followed by an explosive loading, both loads being due to some malfunctions of the nuclear reactor.
2. deformation at high temperature and at high strain-rate interrupted at a certain strain value and reloading at high temperature but at quasi-static strain-rate until fracture, thus simulating what happens to the material in case of an internal explosive loading followed by a quasi-static increase of the internal pressure.

The investigations on the effects of the above strain-rate histories have been performed on the steel AISI 316H and have been published in (Eleiche et al., 1985, Albertini et al., 1989b, Albertini et al., 1985b).

## **4 Aims of the present report**

The results of the tests listed in chapter 3section, because of the long time period of the testing activity (extending over 30 years), have been recorded using a very heterogeneous instrumentation and recording media, including, chronologically, analog magnetic tapes, analog diode oscilloscopes and more recently digital oscilloscopes and digital transient recorders. Due to the different formats, the large amount of the tests results could not be easily accessed today for a modern mathematical processing. There was also a real risk of losing these data because most of the researchers responsible for these older programmes have retired and the remaining ones in the laboratory either do not have the complete knowledge of the past data records or are entirely involved in different projects.

For these reasons, along with the commitments taken in the FEMaS-action, an urgency has been felt to retrieve and collect these widely dispersed data as in the meantime a large number of nuclear fission reactors in aged conditions are operated in Europe, and will soon require a safety assessment against severe accidents in order to verify if their reactor lifetime could be extended. The test results on pre-damaged materials described above would be crucial for this type of analysis. Thus the main objectives of the work conducted in the present project can be summarised as follows:

1. A critical review of the whole body of results regarding the dynamic material properties of nuclear steels employed for containment and internal structures of fission nuclear reactors which will permit to draw conclusions on the response of such steels in case of hypothetical accidents; such a critical review, based on the whole body of data, will be enhanced and richer than similar ones of the past.
2. The transformation of the old record formats of the impact test results into current formats which can be used in the modern computational processing; these updated dynamic material data will be organised in a modern Database, which is envisaged to be disseminated in Europe mainly towards Universities, Research Institutes and Industry involved in the safety assessment of nuclear power plants in case of severe accidents, or in the characterisation of irradiated proved and new steels for future fusion reactors.
3. The inclusion in the above body of fission reactor material data of the recently produced by SUPSI-DynaMat Lab data on dynamic material properties of steels for fusion reactors (Cadoni et al., 2011).
4. The presentation and detailed description of the analysis and methodology followed to transform the test records in the engineering stress/strain/strain-rate curves.
5. The presentation and detailed description of the original testing techniques used to generate the whole body of test data for fission reactors; as indicated, these techniques can be easily adapted and may find in the near future an important role in support of the characterisation of fusion reactor steels, where very small, highly irradiated specimens are used.

It is evident that a huge research effort has been made in Europe for producing these experimental data. The recovery, revision and modern storage of the whole body of experimental data through the above actions will contribute to saving this investment and will allow the use of the data for the re-assessment of the safety of aged nuclear reactors. As repeatedly stated, such a re-assessment is needed for the lifetime extension of several nuclear power plants, a problem which is of great socio-economic importance. The integration in a single, modern database of the dynamic mechanical properties of all these materials represents not only an indispensable tool for the analysis of aged nuclear reactor structures in Europe, but it also increases the competitive edge of the European nuclear industry worldwide.

## 5 Dynamic loading characteristics and related material testing devices

The aim of the successive research programmes in the period 1973–2003 concerning dynamic testing of reactor containment steels was that of delivering the dynamic mechanical properties of such steels, which was needed to design containment shells resistant to hypothetical internal and/or external explosions and plane crashes. In case of an explosion the propagation of pressure waves generates distinct impact loading conditions on the containment shell, ranging from extreme violent shocks to soft impact depending on the type of explosion and on the pressure amplitude attenuation with distance from the explosion centre. Trying to quantify it, it can be reasonably assumed that:

- Directly in contact with the explosion source there might be formation of **shock pressure waves** with a shock front having a sharp rise time of the order of  $1 \mu\text{s}$  or less, propagating in the material whose compressibility and bulk modulus do not remain constant and vary with the pressure level.
- Few meters from the source of the explosion the rise time of the loading pressure wave will be very short, ranging from  $10 \mu\text{s}$  to  $100 \mu\text{s}$ , giving rise to stress waves deforming the material at strain-rates from  $100 \text{ s}^{-1}$  to a few  $1000 \text{ s}^{-1}$ ; this deformation regime can be defined as **high strain-rate** and is characterised by stress wave propagation.
- At longer distances from the explosion source the pressure wave amplitude decreases and the rise time of the loading will be in the range  $200 \mu\text{s}$  to  $1000 \mu\text{s}$  imposing a deformation at strain-rates ranging from  $0.1 \text{ s}^{-1}$  to  $100 \text{ s}^{-1}$ , a range which can be considered as **medium strain-rate** where resonance phenomena are important.

A more detailed discussion establishing the above classification of strain-rate ranges and relating each of them to a corresponding most appropriate testing technique can be found in (Lindholm, 1971). Experiments reproducing on the material specimens the shock pressure waves leading to variation of the material compressibility and bulk modulus are mainly based on flyer plate impact and the records may be analysed through the Hugoniot relationships (Kolsky, 1949). Such testing techniques have not been considered in the above programmes because they reproduce extreme material state conditions not encountered in the containment shell assessment.

The testing techniques reproducing on the material specimens the stress waves deforming the material at high strain-rate ranging from  $100 \text{ s}^{-1}$  to a few  $1000 \text{ s}^{-1}$  are mainly based on the classical Hopkinson bar technique (Hopkinson, 1872, Hopkinson, 1914, Davis, 1948, Kolsky, 1949) and the test records are analysed by means of the uniaxial elastic stress wave propagation theory (Davis, 1948, Kolsky, 1949). The classical Hopkinson bar works in compression (originally) and generates short pulses through the launching of a projectile bar, and manages to deform only at small strains the ductile steels used for the containment shells. Therefore a modification of the classical Hopkinson bar technique was needed in order to perform direct tension tests at high strain-rate and generate the long duration pulses needed to deform ductile steels until fracture. Several testing machines (Lindholm, 1971) can be used for reproducing the medium strain-rates, ranging from  $0.1 \text{ s}^{-1}$  to  $100 \text{ s}^{-1}$ , but reliable, high-quality results have been obtained using an original Hydro-Pneumatic Machine (HPM) (Albertini and Montagnani, 1977) also introduced by the JRC in the year 1974. The MHB and the HPM will be described in detail in the following chapter.

Typical dynamic stress-strain curves in tension determined by means of these two apparatuses of the Joint Research Centre (JRC) technology for an ordinary construction steel are shown in Fig. 5.1. On each of the dynamic tensile stress-strain curves shown in Fig. 5.1 we can distinguish three distinct regions:

1. the yielding region, consisting of the elastic deformation and the yielding phase, a zone of varying extension often characterised by the upper yield stress peak followed by a drop to the lower yield stress, and terminating where the strain hardening phase begins,
2. the uniform plastic deformation region, characterised by the strain hardening phase, where the stress increases non-linearly with strain, extending up to the ultimate tensile strength (UTS),
3. the necking region, characterised by the localised deformation phase, where the load decreases non-linearly with strain, extending from the UTS point to the fracture point.

Normally (and for economic reasons) all three of the above regions of the dynamic stress-strain curves are measured by means of a single, uninterrupted dynamic tensile test (which brings the specimen to fracture), performed with the HPM at medium strain-rate and with the MHB at high strain-rate, respectively. As will be explained in the next chapter, in both the HPM and the MHB devices, conditions of specimen equilibrium are quickly created (despite the propagating stress waves) leading back the analysis of the dynamic test to that of

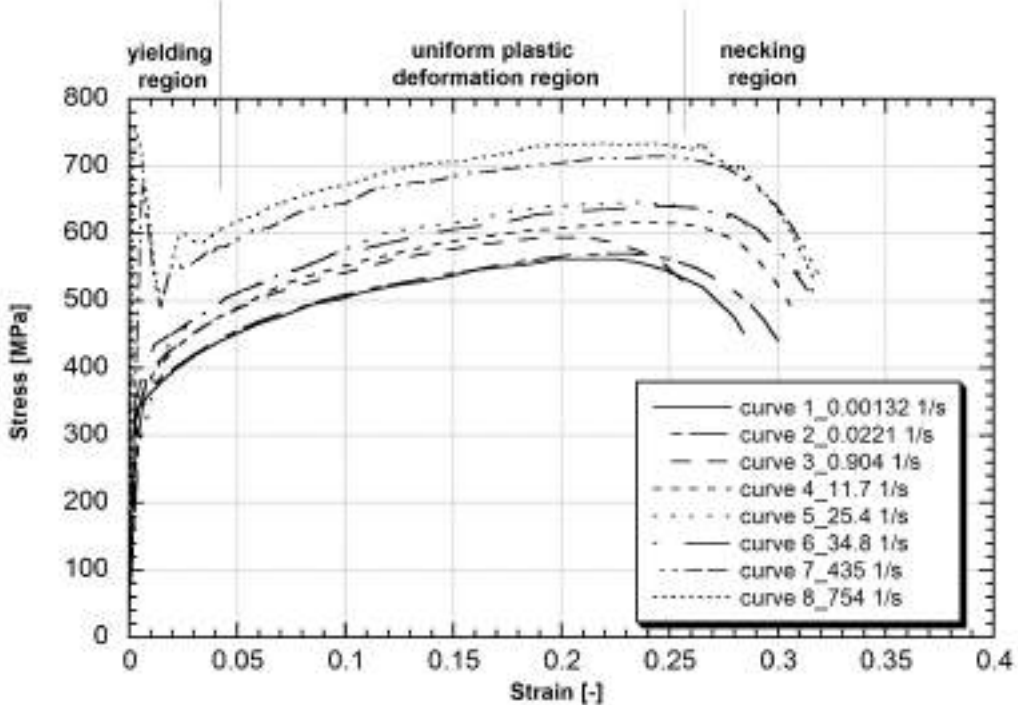


**Figure 5.1:** Stress vs. strain curves of FEE355 at room temperature for a wide range of strain-rates.

a quasi-static test. This is particularly true and assures good accuracy for the measurements of the non-linear deformation phases 2 and 3 because they are characterised by displacement and load changes of the same order of magnitude. However, it is not the case for the measurements of the region 1 (the elastic one up to the elastic limit or the upper yielding) of the curve mainly due to two reasons:

- the displacements to be measured during the linear phase 1 are up to two orders of magnitude smaller than those of the regions 2 and 3, consequently requiring special displacement measurement instrumentation, with much higher sensitivity and precision than that used for measuring the displacements of phase 2 and 3 of Fig. 5.1,
- the time to upper yield stress or to elastic limit, especially in high dynamics, is extremely short and may give problems of non-homogeneous stress distribution along the specimen gauge length, which must be taken into account when defining material properties.

## 6 Detailed description of uniaxial dynamic testing devices

### 6.1 The Modified Hopkinson Bar for direct tension test

#### 6.1.1 Progressing from the classical Hopkinson Bar to the JRC Universal Modified Hopkinson Bar (MHB)

The classical Hopkinson bar, after the pioneering work of J. Hopkinson father (Hopkinson, 1872) and B. Hopkinson son (Hopkinson, 1914), has been established in dynamic material testing, based mainly on the theoretical and experimental scientific work of R.M. Davis (Davis, 1948) and H. Kolsky (Kolsky, 1949). The classical Hopkinson bar (also known as SHPB - Split Hopkinson Pressure Bar or Kolsky bar) is an apparatus developed for compression tests at high strain-rate of small metal specimens, aiming at the determination of the stress-strain curves through the analysis of the experimental records with the elastic plane stress wave propagation theory in bars. The technique practically consists (Fig. 6.1) of applying a compression (or tension) stress pulse by striking a projectile normally to the transverse cross-section of a cylindrical bar, called the input or the incident bar, with the projectile striking giving rise to a stress wave propagating along the input bar, then acting on a specimen inserted between the input bar and another bar called the output or the transmitter bar. The specimen is deformed plastically until failure (depending on the strength and duration of the pulse) while the incident (input) and transmitter (output) bars remain in the elastic state.

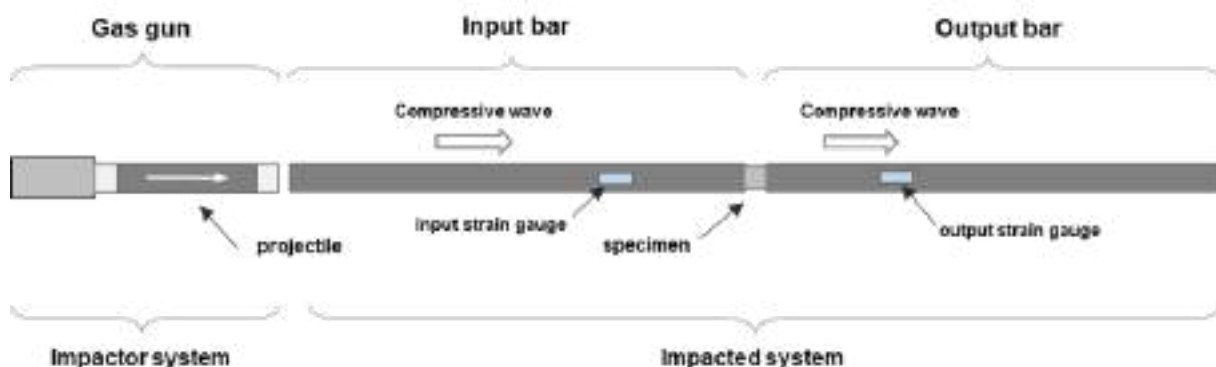


**Figure 6.1:** Classical Split Hopkinson Pressure Bar (SHPB)

The projectile is generally accelerated by a small gas gun apparatus (Fig. 6.1). When the projectile impacts the incident bar, a constant amplitude compressive pulse is generated in both the incident bar and the projectile. The length or duration of the compressive pulse generated in the input bar corresponds to the time taken by the elastic plane compression wave to travel from the impacting end of the projectile to the other end and back. The incident compression elastic plane stress wave propagates along the input bar, reaches the interface input bar-specimen (Fig.6.1) and dynamically loads the specimen. As a result of the interaction of the incident wave with the specimen which has a lower acoustic impedance, a reflected wave and a transmitted wave are generated at the interfaces input bar-specimen and specimen-output bar (Fig.6.1), respectively. Fulfilment of the following two basic assumptions is needed in order to be able to use the Hopkinson bar for an accurate measurement of the material mechanical properties at high strain-rate:

1. the bar diameter must be small in comparison with the pulse wave-length (Davis, 1948, Kolsky, 1949) so that the stresses and the velocities are propagated down the bars without any dispersion (the bars being elastically loaded);
2. the specimen length must be short so that the time taken by the wave to propagate through the specimen is short compared to the total time of the test. This condition allows many reflections to take place inside the specimen, necessary for reaching a homogeneous stress and strain distribution along the specimen gauge length, which also means equilibrium of the forces acting on the two ends of the specimen.

Having fulfilled the conditions 1. and 2. and being the two bars elastically loaded, the one-dimensional elastic plane stress wave propagation theory can be applied to the input bar-specimen-output bar system, as it is extensively shown in (Davis, 1948, Kolsky, 1949, Lindholm, 1971), leading to the calculation of stress, strain and strain-rate versus time in the specimen, by using the records of the incident, reflected and transmitted pulses. The discussion and demonstration of these basic relationships is presented in the next chapter. The limitations of this classical SHPB were soon realised, and the development of an improved apparatus was pursued (Modified Hopkinson Bar, MHB). This was particularly needed in order to make available a versatile equipment capable of working in tension, compression and shear at very high strain-rate but also capable of

generating the long duration pulses necessary to test at strain-rates around  $100\text{ s}^{-1}$  or less, imposing the large displacements required for fracturing the specimens of the ductile metals used in the nuclear structures. In fact, as an example of its necessity, we can consider the case of the dynamic test at strain-rate of  $100\text{ s}^{-1}$  of a steel specimen of 50 percent fracture strain, where the pulse duration needed for deforming such a specimen until fracture is of 5ms. Using the classical Hopkinson bar it would have required to launch a projectile of 12.5m length in order to obtain such a pulse duration. This is a really difficult task, in particular for what concerns the realisation of a plane impact of the projectile on the input bar, a prerequisite for the generation of an elastic stress plane wave pulse of rectangular form. In contrast, stretching and releasing a 12.5m long bar in the MHB (see its functioning below) would pose no problem. The MHB can also be considered as a universal testing device because it can easily be modified and applied for tension, compression and shear dynamic tests.

### 6.1.2 The functioning of the Modified Hopkinson Bar in tension

The development of the tension version of the modified Hopkinson bar (MHB) took place at the beginning of the seventies of the last century as described in the papers (Albertini and Montagnani, 1977, Montagnani et al., 1973, Albertini and Montagnani, 1974) and the patent listed in (Montagnani et al., 1973). The MHB functioning schematic is presented in Fig. 6.2.

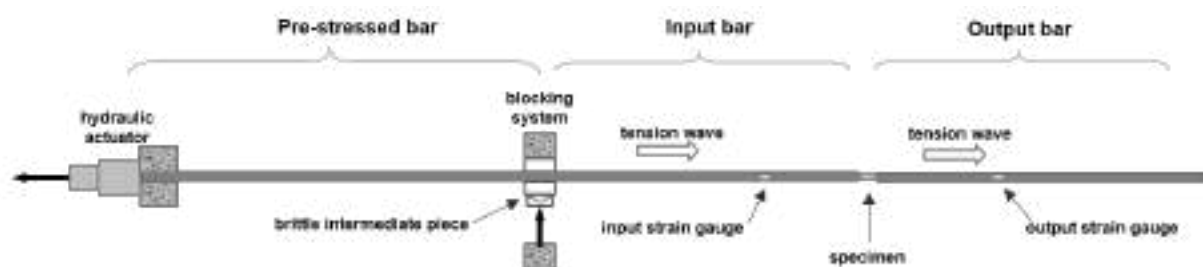


**Figure 6.2:** Modified Hopkinson Bar with pre-stressed bar loading device for tensile testing

The MHB consists of a pre-tensioned bar (substituting the projectile of the classical Hopkinson bar) which has as solid continuation the incident (input) bar, followed by the transmitter (output) bar and the specimen inserted between the two last bars. The MHB functioning is based on storing a certain amount of elastic mechanical energy in the pre-tensioned bar length by statically tensioning it up to a stress value lower than its elastic limit. To this aim the end section of the pre-tensioned bar contiguous to the incident bar is blocked utilizing a brittle intermediate piece and the other end is pulled by means of a hydraulic actuator. For conducting a test the specimen is first inserted between the incident and the transmitter bar, and once the proper elastic energy has been stored in the pre-tensioned bar, the brittle intermediate piece is ruptured giving rise to the simultaneous generation of two elastic plane waves:

- a plane elastic unloading wave starts from the bar section freed by the rupture of the brittle intermediate piece and propagates along the pre-tensioned bar unloading it (compression wave).
- a plane elastic tension wave starts from the same bar section and propagates along the incident bar loading it in tension, it reaches and loads the specimen until fracture, and it propagates and loads in tension the transmitter bar.

The duration of the generated tension pulse that loads the specimen corresponds to the travel time of the unloading wave from the unblocked bar section to the hydraulic actuator and back; its amplitude is half the static pre-stress value applied to the pre-tensioned bar by the hydraulic actuator. By using a rather long pre-tensioned bar it is possible to generate a tensile pulse of long duration allowing the deformation at constant high strain-rate until fracture of high ductility specimens. In that case the use of a transmitter bar of length correspondent to that of the pre-tensioned bar would be needed in order to deform the specimen under the clean and controlled loading history given by the incident tension pulse without the superposition of the wave reflections from the bar ends, which would render more complex the analysis of the records of the deformation of the specimen. This last test condition is also fundamental for the success of the dynamic testing of fragile specimens like those having been submitted to high irradiation doses.

The brittle intermediate piece, called also the *theta clamp*, because of its resemblance to the Greek alphabet letter  $\theta$ , shown in Fig. 6.3, has approximately the shape of a parallelogram whose sides (four metal rafters) are kept together by four supporting pieces placed at each vertex of the parallelogram:

- one of those supporting pieces is in contact with a hydraulic jack and the diagonally opposite piece is in contact with the end section of the pre-tensioned bar

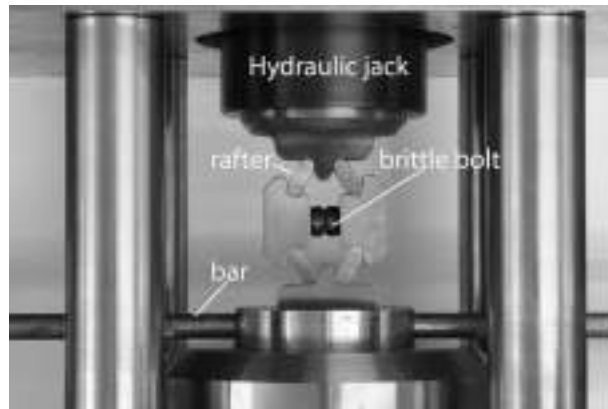


**Figure 6.3:** Blocking system called  $\theta$  theta clamp

- the two other supporting pieces, diagonally opposite, are held together by a notched brittle bolt.

Its functioning during the test is as follows. First, the hydraulic jack starts pushing on the vertex of the  $\theta$  parallelogram opposite to the vertex in contact with the bar, exerting a transverse force (loading simultaneously the sides of the parallelogram and the notched brittle bolt) on the end section of the pre-tensioned bar, thus blocking it by friction. Next, the other actuator at the end of the pre-tensioned bar starts statically pulling it to the desired level. After this phase of static pre-stressing for elastic energy storage has been completed, the transverse hydraulic jack increases the force passing through the parallelogram sides and the notched bolt until the notched bolt fractures in a brittle manner provoking the 'explosion' of the parallelogram. The controlled 'explosion' of the parallelogram is the key factor for assuring that:

- the end section of the pre-tensioned bar is very suddenly left free as needed for the generation of a tension pulse to have the very short rise time of about 30 microseconds.
- the end section of the pre-tensioned bar is left free in a clean manner without receiving undesired transverse bending pulses and therefore assuring that the tension wave propagating toward the specimen along the incident bar is an elastic plane wave without bending components.

Due to the importance of a faultless functioning of the  $\theta$  clamp for the scientific validity of the MHB tests and due to its originality, the  $\theta$  clamp has also been patented (Verheyden et al., ). In the MHB the bar diameter is small (e.g. 10mm) in comparison to the wavelength of the generated tension pulse, which can be of the order of some meters, therefore easily realising the conditions for the wave propagation without dispersion and absorption along the incident and transmitter bars. One (or more) electrical strain-gauge station is bonded on the incident bar at a certain distance from the specimen in order to record the deformation  $\epsilon_I$  of the bar provoked by the incident tension pulse during the propagation toward the specimen and the deformation  $\epsilon_R$  caused by the part of the incident tension pulse reflected at the interface incident bar-specimen (reflection which is correlated with the deformation of the specimen). The distance of the strain-gauge station from the specimen is usually chosen in a way that permits to distinguish clearly the record of the incident pulse from the record of the reflected pulse. A second strain-gauge station is bonded on the output bar at the same distance from the specimen as the strain-gauge station on the incident bar. This second strain-gauge station is used to record the deformation  $\epsilon_T$  caused on the bar by the part of the incident pulse which has been sustained by the specimen and has been therefore transmitted in the output bar. A record of an old dynamic tension test performed with the MHB is shown in Fig. 6.4, where it is possible to observe:

- the clean resolution of incident, reflected and transmitted pulses
- the sharp rise time of the incident pulse, of the order of 30 microseconds
- the almost constant amplitude of the incident pulse
- the almost constant amplitude of the reflected pulse
- the characteristic similarity of the record of the transmitted pulse with the stress-time record of a conventional tension test.

The record of Fig.6.4 is from one of the first tests with the MHB, done in the nineteen-seventies, and it has been registered using an electronic valve oscilloscope, type Tektronix. Also the successive analysis of the records, necessary for obtaining the dynamic stress-strain curves of the tested material (in this case an

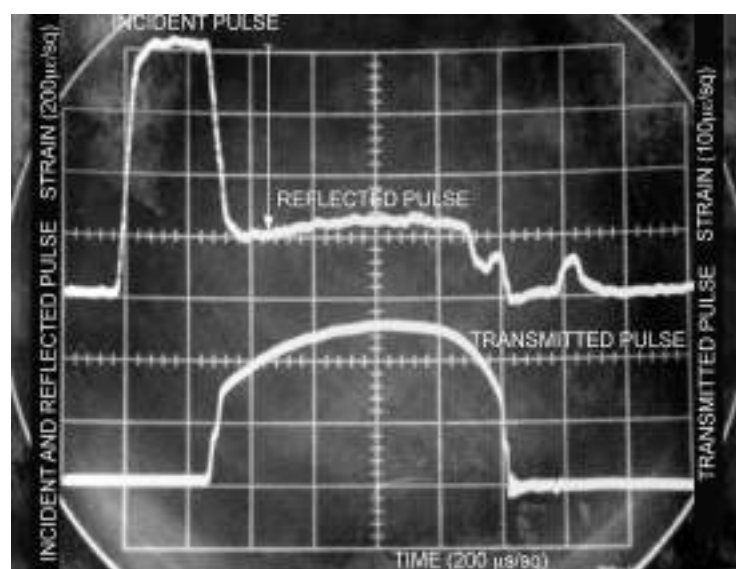


**Figure 6.4:** Record of a test with the MHB taken with a valve oscilloscope.

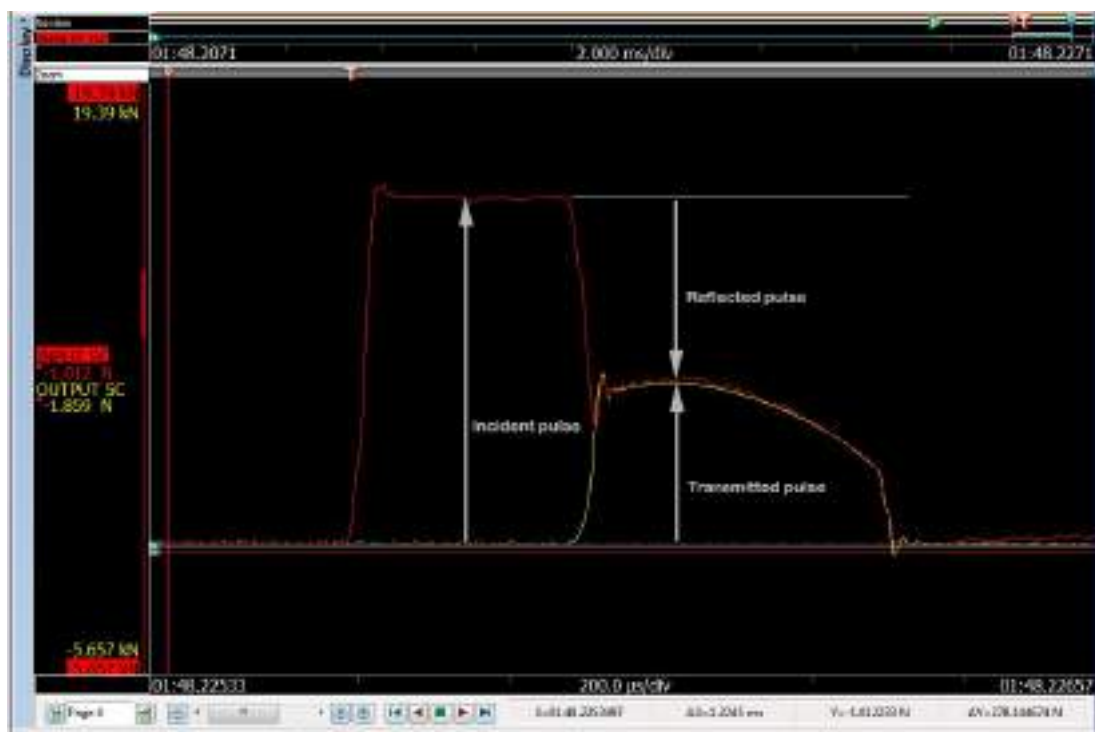


**Figure 6.5:** Record of a test with the MHB taken with modern transient recorder.

austenitic stainless steel), was performed using an analogic instrumentation. The record of a test with the MHB in Fig.6.5 has been taken recently using a digital transient recorder, where of course the successive analysis has been performed employing high precision digital instrumentation. Figures 6.4 and 6.5 provide a nice example showing how the records of the different instrumentation by which the dynamic stress-strain curves of the nuclear steels studied over 30 years have been measured and archived. This comparison shows the necessity of an update /modernisation and harmonization of the archiving in order to maintain usable the huge amount of dynamic stress-strain curves produced.

On the basis of the records of  $\epsilon_I, \epsilon_R, \epsilon_T$  of Figures 6.4 and 6.5, and considering the basic constitutive equation of the incident and transmitter elastic bar material and the one-dimensional wave propagation theory (Davis, 1948, Kolsky, 1949, Lindholm, 1971) it is possible to calculate the stress - strain - strain-rate curves of the specimen material according to the following procedure:

- constitutive equation (Hooke's law) of the elastic bar material

$$\sigma = E\epsilon \quad (1)$$

where  $\sigma$  is the longitudinal stress in the bar,  $E$  is the elastic modulus of the bar material,  $\epsilon$  is the corresponding longitudinal elastic deformation of the bar material

- the propagation velocity of one-dimensional elastic plane wave in the bar

$$C_0 = \sqrt{\frac{E}{\rho}} \quad (2)$$

where  $\rho$  is the bar material density

- the particle velocity in the elastic bar

$$v = C_0\epsilon = C_0 \frac{\sigma}{E} \quad (3)$$

- the forces acting at the incident and transmitter bar-specimen interfaces, respectively:

$$F_I(t) = A_{bar}E[\epsilon_I(t) + \epsilon_R(t)] \quad (4)$$

$$F_T(t) = A_{bar}E\epsilon_T(t) \quad (5)$$

where  $A_{bar}$  is the area of the bar cross-section and  $t$  is the time.

- the displacements of the incident and transmitter bar-specimen interfaces given, respectively, by:

$$d_I(t) = \int_0^t [v_I(t) - v_R(t)] dt = C_0 \int_0^t [\epsilon_I(t) - \epsilon_R(t)] dt \quad (6)$$

$$d_T(t) = \int_0^t [v_T(t)] dt = C_0 \int_0^t [\epsilon_T(t)] dt \quad (7)$$

Therefore the average values of engineering stress  $\sigma_{spec}$ , strain  $\epsilon_{spec}$  and strain-rate  $\dot{\epsilon}_{spec}$  in the specimen are:

$$\sigma_{spec}(t) = \frac{F_I(t) + F_T(t)}{2A_{spec}} = \frac{EA_{bar}}{2A_{spec}}[\epsilon_I(t) + \epsilon_R(t) + \epsilon_T(t)] \quad (8)$$

where  $A_{spec}$  is the cross-sectional area of the specimen at the gauge length,

$$\epsilon_{spec}(t) = \frac{d_I(t) - d_T(t)}{L_{spec}} = \frac{C_0}{L_{spec}} \int_0^t [\epsilon_I(t) - \epsilon_R(t) - \epsilon_T(t)] dt \quad (9)$$

where  $L_{spec}$  is the specimen gauge length

$$\dot{\epsilon}_{spec}(t) = \frac{C_0}{L_{spec}}[\epsilon_I(t) - \epsilon_R(t) - \epsilon_T(t)] \quad (10)$$

The specimen used for performing dynamic tension tests with the MHB for most of the austenitic and ferritic steels reported here, has a short gauge length, as shown in Fig.6.6. Therefore the time taken by the stress wave to pass through the specimen is very short (about two-three microseconds) in comparison with the duration of the test, and rapidly numerous reflections take place inside the specimen thus permitting a creation of equilibrium of forces at both ends of the specimen and a homogeneous stress distribution along the specimen gauge length. The specimen of Fig.6.6 is further characterized by:

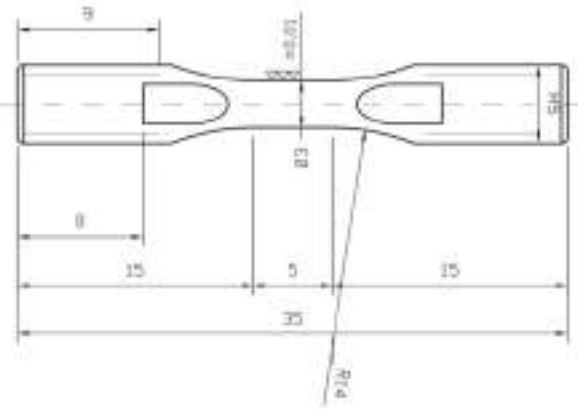


**Figure 6.6:** Specimen for a material tensile test with the MHB.

- threaded ends for the connections to the incident and transmitter bars; the threaded ends have demonstrated a good efficiency in transmitting the incident and transmitted elastic stress waves.
- large radius of fillets connecting the threaded ends to the central gauge length in order to avoid any stress concentrations.

The condition of force equilibrium of the specimen along its longitudinal axis is expressed by:

$$F_I(t) = F_T(t) \quad (11)$$

or

$$\epsilon_I(t) + \epsilon_R(t) = \epsilon_T(t) \quad (12)$$

which leads to the following simplified relationships for the engineering stress, strain and strain-rate in the specimen:

$$\sigma_{spec}(t) = E_{bar} \cdot \frac{A_{bar}}{A_{spec}} \epsilon_T(t) \quad (13)$$

$$\epsilon_{spec}(t) = -\frac{2 \cdot C_0}{L_{spec}} \int_0^t \epsilon_R(t) dt \quad (14)$$

$$\dot{\epsilon}_{spec}(t) = -\frac{2 \cdot C_0}{L_{spec}} \cdot \epsilon_R(t) \quad (15)$$

The simplified relationships 13, 14, 15 can be used for the determination of the stress, strain and strain-rate curves after verification of the condition 11 of force equilibrium of the specimen. An example of such a verification is shown in Fig. 6.5 and concerns a test done with the MHB on a Fig. 6.6 specimen.

As this verification of the force equilibrium of Fig. 6.5 is essential for the validity of the determined dynamic mechanical properties in tension, an extra effort has been made and the specimen equilibrium has thoroughly been checked for all nuclear steels which are the object of the updated archiving of this report.

Three examples of stress-strain curves at dynamic strain-rates determined by means of the relationships 13, 14, 15, starting from the records of the type shown in Figs. 6.4 and 6.5 of MHB tests, are included in Figures 6.7, 6.8, 6.9.

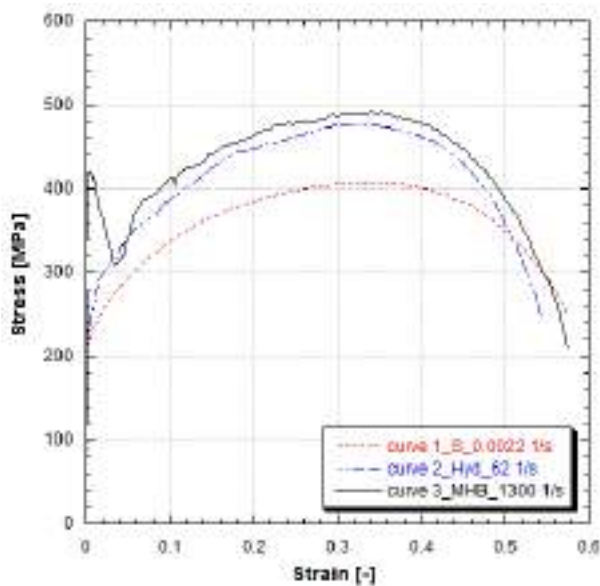


**Figure 6.7:** Engineering stress vs. strain curves of Ni201 steel in tension at room temperature.

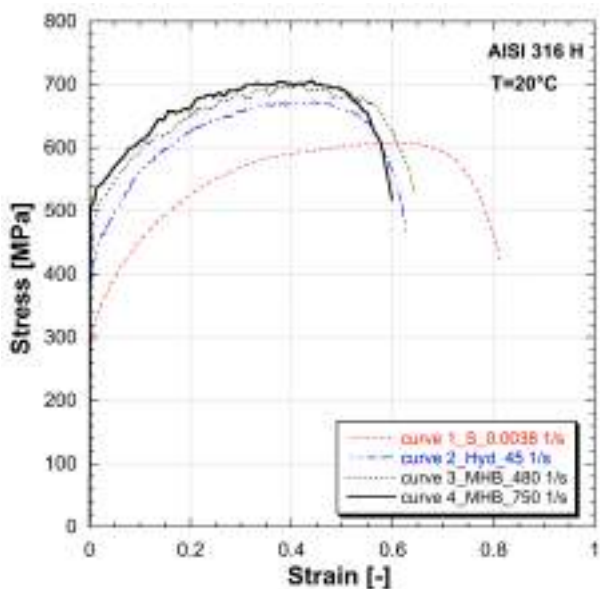


**Figure 6.8:** Engineering stress vs. strain curves of AISI 316H steel in tension at different strain-rates and at 20°C.

## 6.2 The Universal Hydro Pneumatic Machine for testing at medium strain-rates

The range of strain-rate extending from  $0.1$  to  $100 \text{ s}^{-1}$  can be defined as medium strain-rate regime, and is characterised by inertia and vibration phenomena caused by the multiple stress wave reflections which take place in the testing equipment when the test is started. Such phenomena, when not put under control, can provoke noisy oscillations in the measurement records which need to be filtered, with the effect of losing in accuracy and/or obscuring some other phenomena like the upper and lower yield peaks, strain ageing instabilities. The duration of the loading pulses for medium strain-rate tests is extended from milliseconds up to a few seconds. As an example one might consider the time needed to perform a test until fracture of a steel having a fracture strain of 50% :

- at the strain-rate of  $0.1 \text{ s}^{-1}$  the total test time is of 5 s.
- at the strain-rate of  $100 \text{ s}^{-1}$  the total test time is of 5 ms.

At the lowest strain-rate of the range ( $0.1 \text{ s}^{-1}$ , total test time 5 s) the load is already suddenly applied but not rapidly enough for the creation of critical stress wave propagation phenomena in the specimen and in the testing machine. In this case the most important phenomena, which must be controlled, relate to the inertia of the moving parts of the testing machine, whose masses must be kept as light as possible. At the highest strain-rate

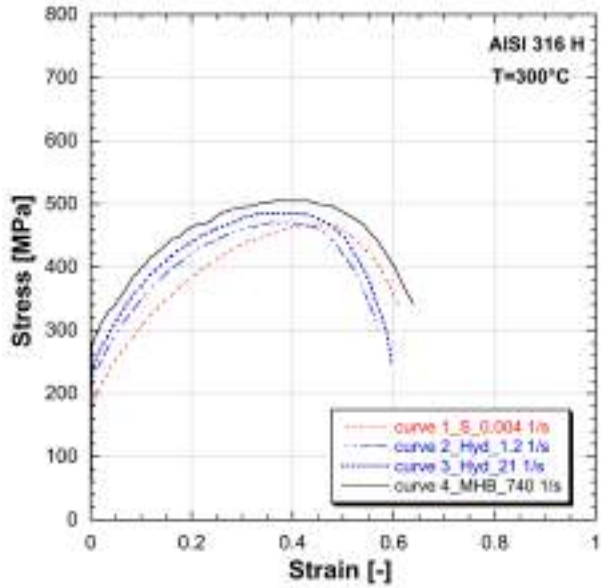


**Figure 6.9:** Engineering stress vs. strain curves of AISI 316H steel in tension at different strain-rates and at 300°C.

of the range ( $100 \text{ s}^{-1}$ , total test time 5 ms) the load application is already sufficiently rapid for giving rise to stress wave propagation phenomena especially in the testing machine. Of course, as claimed above, it can be argued that, the tests at strain-rate of  $100 \text{ s}^{-1}$  may in principle be performed with a Hopkinson Bar apparatus and the test can be analysed on the basis of the elastic plane stress wave propagation theory. Nevertheless, there are some obstacles of practical and physical nature impeding a direct employment of the Hopkinson bar, namely:

- the 5ms-duration of the loading pulse requires the launching of projectiles of 12.5 m length in the case of the classical Hopkinson bar (Davis, 1948,Kolsky, 1949,Lindholm, 1971), or the statical prestressing of a bar of the same length in case of the JRC Modified Hopkinson Bar (Albertini and Montagnani, 1977,Montagnani et al., 1973,Albertini and Montagnani, 1974)(obviously, the first solution is almost impossible to be easily realised).
- the limitation of physical nature often arises by the necessity to keep the amplitude of the generated loading pulse very near to the ultimate load of the specimen, with the consequence of entering in a non stable working regime for the Hopkinson bar, characterised by load oscillations and non-constant strain-rate.

Therefore it is useful to have the possibility of performing the tests at the strain-rate of  $100 \text{ s}^{-1}$  with dynamic testing apparatuses, not based on the stress wave propagation theory. As expected, the main difficulty with such apparatuses lies in the handling of the stress wave propagation and reflections which take place in the mechanical structures of the machine itself, which can give rise to oscillations and rebounds affecting the records of the test. Consequently, the length of the columns and of the dynamometric bars of these apparatuses should be kept as short as possible and also the inertia of the moving parts of the testing machine should be kept as light as possible. The Hydro-Pneumatic Machine, shortly HPM, developed at JRC Ispra already in the 1970s, is actually capable of covering the satisfactorily strain-rate range from 0.1 to  $100 \text{ s}^{-1}$ . Another characteristic of the HPM is that it can test specimens with the geometry of Fig. 6.6, rendering more reliable the direct comparison of the dynamic material mechanical properties determined at the different strain-rates using the HPM and the MHB.

Elaborating further, the testing machine at medium strain-rate should have not only short and light moving parts but also the length of the testing machine itself in the loading direction should be possibly kept short so that the time needed by the stress waves to travel through the different machine parts (columns, beams) is at least one order of magnitude smaller than the total test time. This means that at the strain-rate of  $100 \text{ s}^{-1}$  the maximum test machine length should be of about 0.5 m, resulting in a total travelling time of the stress wave through the machine length of about 100 microseconds, a time which is 50 times smaller than the above mentioned total testing time of 5 ms. The medium strain-rate hydro-pneumatic testing machine HPM developed at JRC fulfils the above requirements because the only moving part is a small weight piston whose length added to that of the dynamometric elastic bar is presently of 0.65 m, sufficiently close to the above mentioned value of 0.5 m. Therefore the inertia effects and the oscillations often affecting the records of commercially available medium strain-rate testing machines do not affect the records of the JRC-HPM.

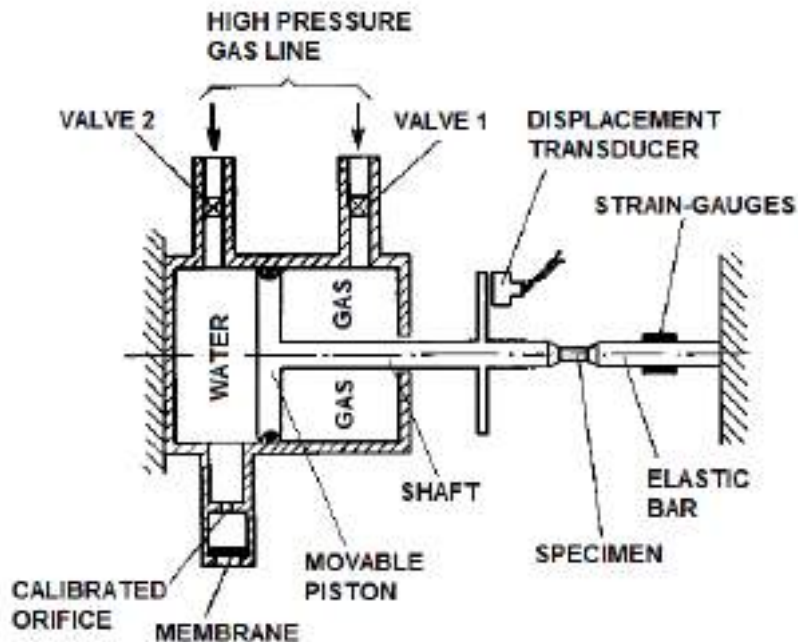


**Figure 6.10:** Schematic of Hydro-Pneumatic Machine for dynamic tensile tests at constant strain-rate ( $10^{-1}$  -  $100 \text{ s}^{-1}$ ).

The schematic of the HPM is shown in Fig. 6.10 where it can be seen that the machine consists of:

- a cylindrical tank divided in two chambers by a sealed piston; one chamber to be filled with gas at high pressure (e.g. 150 bars), the other chamber to be filled with water. The water chamber can discharge the water through a calibrated orifice when a membrane is ruptured or a rapid valve is opened in order to start the test.
- the piston shaft extends out of the gas chamber through a sealed opening, and its end is connected to the material specimen; on the shaft a target is attached, whose movement is measured by a displacement transducer.
- the elastic bar, one end of which is connected to the material specimen and the other end is rigidly fixed to the machine supporting structure; the elastic bar is instrumented with a strain-gauge station whose function is the measurement of the load resisted by the specimen during the test.

The functioning of the machine is as follows (see Fig. 6.10):

- water is filled in the upper tank-chamber and gas is filled in the lower tank-chamber; equal high pressure is established in the water and gas chambers so that the forces acting on the two piston faces are in equilibrium;
- the specimen is fixed to the piston shaft and to the elastic bar;
- by rupturing of the membrane that closes the water chamber (or by activating a rapid valve) the force exerted on the gas face of the piston prevails, accelerating the piston, which simultaneously loads the specimen and pushes water to flow out through the calibrated orifice; the force exerted by the gas pressure on the piston is then equilibrated by the resistance of the specimen plus the resistance of the water flow plus the friction forces, and as a result the piston attains a constant speed with the consequence of imposing a strain to the specimen with a constant strain-rate.

For the JRC HPM the lowest strain-rates are obtained inserting outflow orifices of about 0.5 mm while the highest strain-rates are obtained with orifices of 4 mm diameter. Practice has also shown that the movement of the piston at constant speed and therefore the constancy of the strain-rate during the test, depends mainly on the constancy of the force exerted by the gas on the piston. Good results in that sense have been obtained by effecting small gas volume changes during the test so that small is also the gas pressure decrease and the piston force decrease. This result has been obtained by maintaining small the stroke of the piston movement in order to limit to about 10 % the gas chamber volume increase during the test.

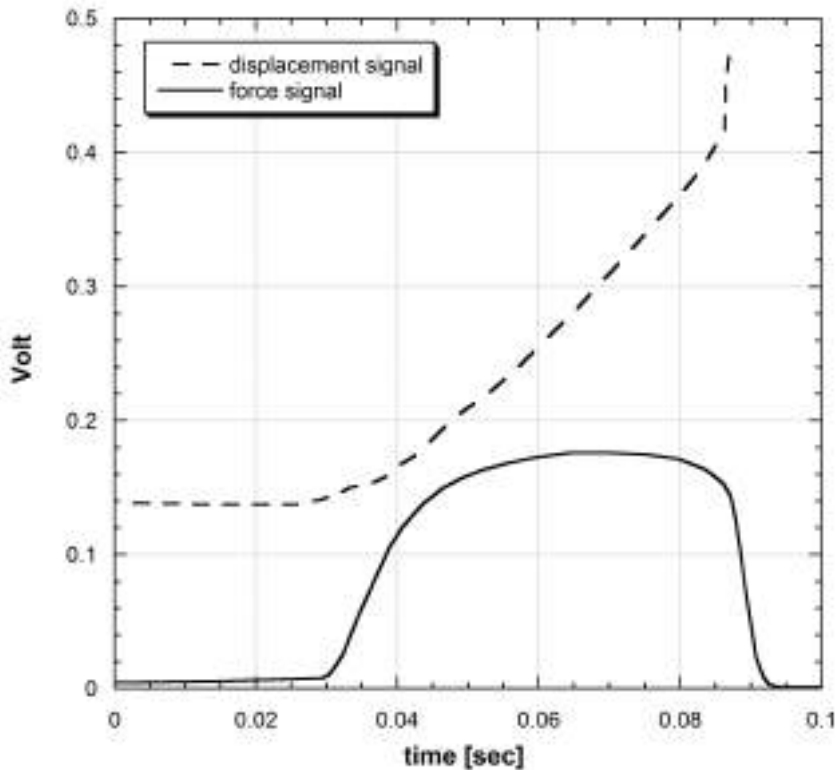


**Figure 6.11:** Record of a tension test with the Hydro-Pneumatic Machine, registered with a digital transient recorder.

The load  $P$  resisted by the specimen is measured by the dynamometric elastic stress bar and the specimen elongation  $\Delta L$  is measured by the displacement transducer sensing the displacement of the plate target fixed to the piston shaft. The engineering stress  $\sigma$ , engineering strain  $\epsilon$  and engineering strain-rate  $\dot{\epsilon}$  of the material specimen are given by the following relationships:

$$\sigma_{spec}(t) = \frac{P}{A_{spec}} \quad (16)$$

$$\epsilon_{spec}(t) = \frac{\Delta L}{L_0} \quad (17)$$

$$\dot{\epsilon}_{spec}(t) = \frac{\Delta \epsilon}{\Delta t} \quad (18)$$

where:

$A_{spec}$  = cross section area of the specimen gauge length;

$L_0$  = gauge length of the specimen;

$\Delta t$  = time needed for the plastic deformation  $\Delta \epsilon$ .

The records as functions of time of the load  $P$  and the elongation  $\Delta L$  of a medium strain-rate test performed in tension with the HPM are shown in Fig. 6.11 where we can observe that:

- no oscillations are visible on the records showing that no inertia and no wave reflection effects affect the test results;
- the record of the displacement  $\Delta L$  as a function of time is nearly linear during the plastic deformation, showing that plastic strain-rate is practically constant during the medium strain-rate test;
- there is characteristic similarity of the record of load versus time record with the stress versus time of a conventional quasi-static tension test of a metallic material.

### **6.3 Application of the MHB and the HPM to dynamic testing of irradiated specimens of austenitic steels and alloys**

As reported in previous chapters, a large program of dynamic tensile tests at room and high temperatures (up to 900°C), at strain-rates ranging between  $10^{-2}$  and  $10^3 \text{ s}^{-1}$ , has been performed at JRC-Ispra on small cylindrical specimens of 3mm diameter and 5 mm gauge length (see Fig.6.6) of AISI 316 and AISI 304 stainless steels, PE 16 Nimonic Alloy which have been previously irradiated at 2, 9 and 30 dpa. Part of the specimens of AISI 304 and AISI 316 has been submitted to low cycle fatigue at high temperature with the fatigue parameters quoted in chapter 3.2 before being irradiated at 2 dpa at high temperature. The experiments have been conducted in the frame of fast breeder reactor safety studies aimed to the containment of hypothetical reactor core explosive accidents.

Further to the above results showing the effects of irradiation, high temperature and high strain-rate on the stress-strain curves of the austenitic stainless steels, also the testing techniques used to obtain such results will be of interest for the characterization of the small irradiated specimens of the advanced steels for the fusion reactor. In fact downsized versions of the MHB and of the HPM can be proposed which could permit the mechanical characterization of advanced, highly irradiated fusion reactor steels by testing specimen of 1mm diameter or less.

Therefore, shown first is the experimental set-up employed for the implementation of the MHB and the HPM in the hot-cell laboratory of JRC-Ispra in order to test the irradiated specimens of 3mm diameter of Fig.6.6. This was the first time that a MHB (described in chapter 6.1.2) was installed with its whole length inside a large hot cell, where the testing operations were conducted using rather large telemanipulators, as shown in Figs.6.12, 6.13, 6.14 and 6.15:

- Figs. 6.12 and 6.13 show the MHB supporting structure installed inside the large hot cell; the total length of the MHB was about 10 m.
- Fig. 6.14 shows the external side of the large hot cell where the recording instrumentation of the MHB and the related telemanipulators were placed.
- Fig. 6.15 shows the input and output bars connected to the irradiated specimens inside the supporting structure placed in the large hot cell.

After a couple of years of experimenting with the large hot cell set-up of Figs.6.13 and 6.14, the MHB installation for the irradiated specimens was simplified by introducing a bespoke, home-made smaller hot cell, encompassing only the central part of the MHB with the irradiated specimen connected to the ends of the input and output bars. This home-made small hot cell was equipped with simpler telemanipulation devices, as those shown in the Figs.6.16, 6.17, 6.18 and 6.19:

- Fig. 6.16 shows the home-made small hot cell of about 1.2x1.8 m size, with the input and output bars entering the cell.
- Fig. 6.17 shows again the small hot cell with the prestressed bar and the input bar in perspective.
- Fig. 6.18 shows the recording instrumentation.
- Fig. 6.19 shows the interior of the small hot cell with the input and output bars connected to an irradiated specimen surrounded by a small oven during a high temperature dynamic test. The simple manipulation devices are also visible.

Fig. 6.20 also shows the hydro-pneumatic machine HPM (described before in chapter 6.2) installed in the hot cell for testing irradiated specimens at medium strain-rate.

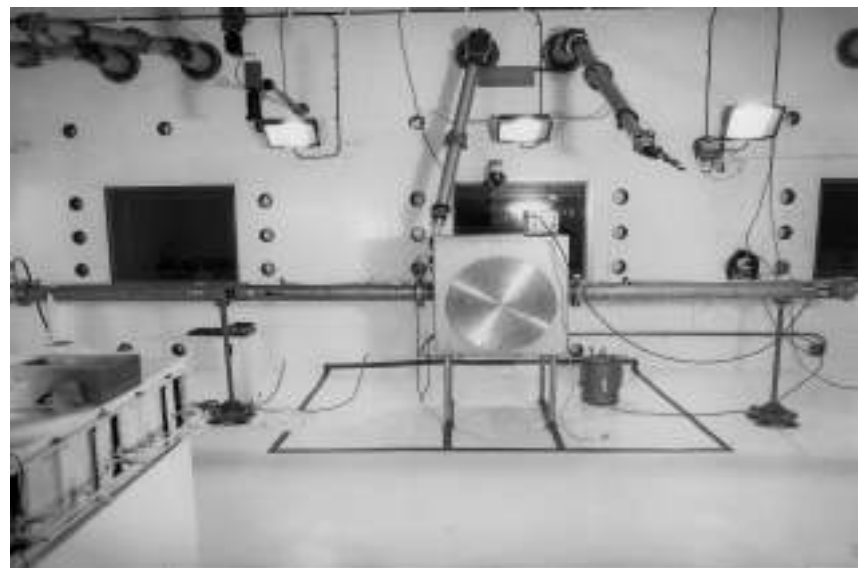


**Figure 6.12:** Modified Hopkinson Bar with telemanipulators inside a large hot cell.

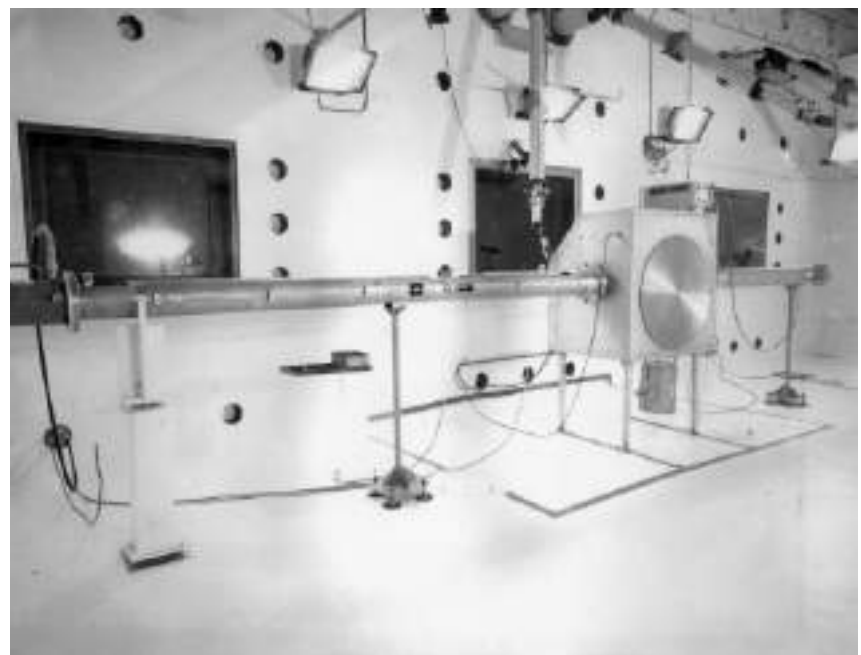


**Figure 6.13:** Modified Hopkinson Bar apparatus for dynamic tensile tests mounted in the hot cell.

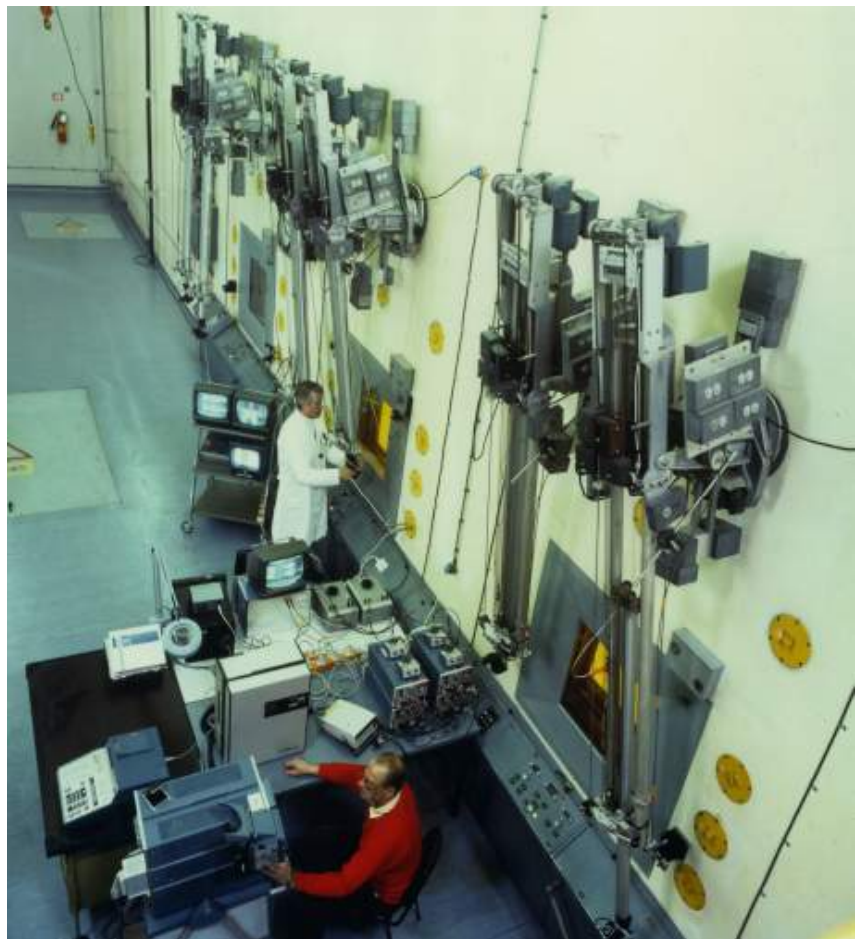


**Figure 6.14:** Telemanipulators and instrumentation serving the MHB in the large hot cell.



**Figure 6.15:** Irradiated specimen connected to input and output bars of the MHB in the large hot cell.

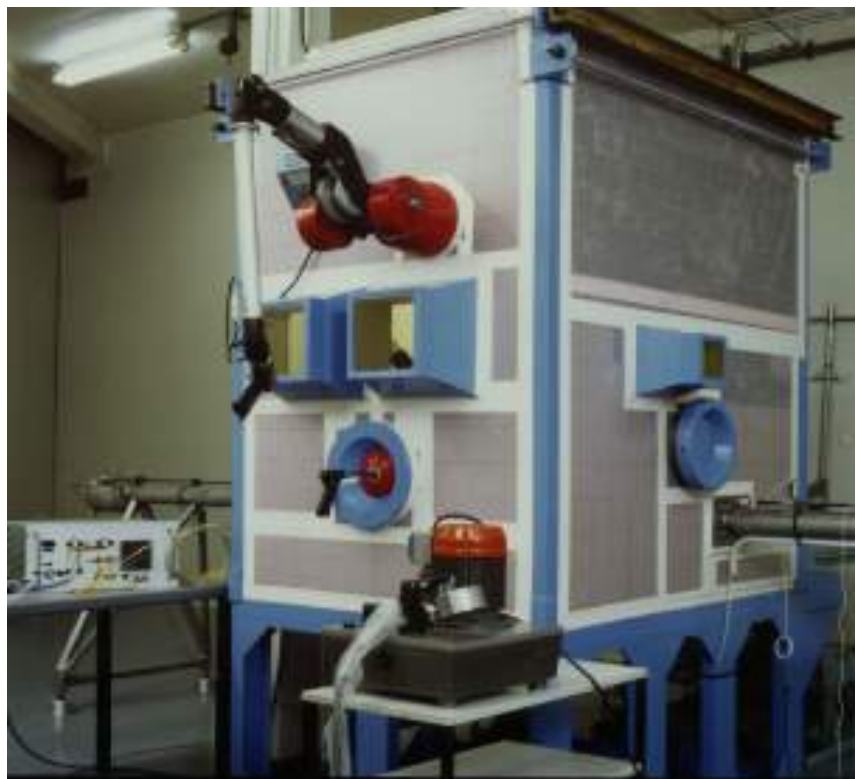


**Figure 6.16:** Small hot cell with the input bar (right) and output passing through the shield walls.



**Figure 6.17:** Small hot cell with view of the input and pre-tensioned bar of the MHB and of the operating small telemanipulator.

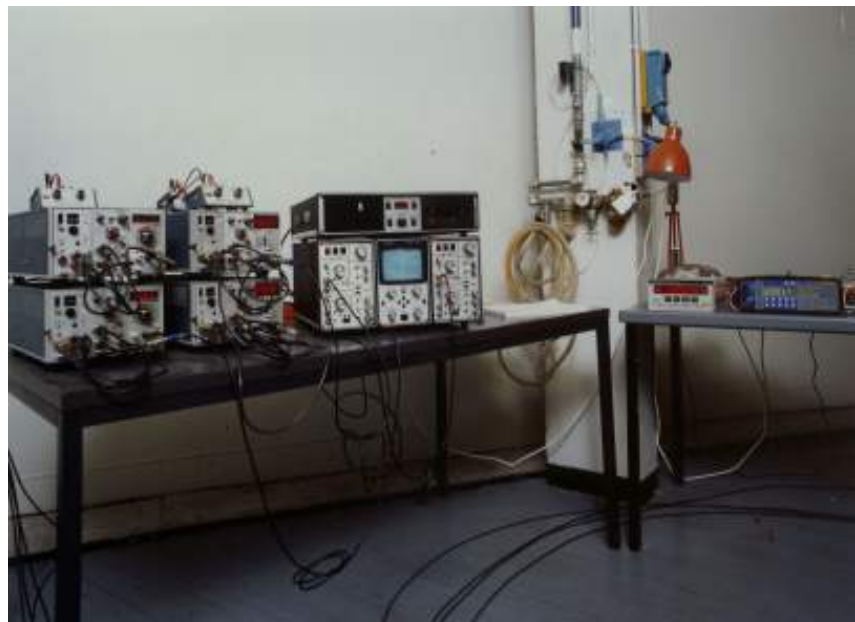


**Figure 6.18:** Recording instrumentation serving the MHB installed in the small hot cell.

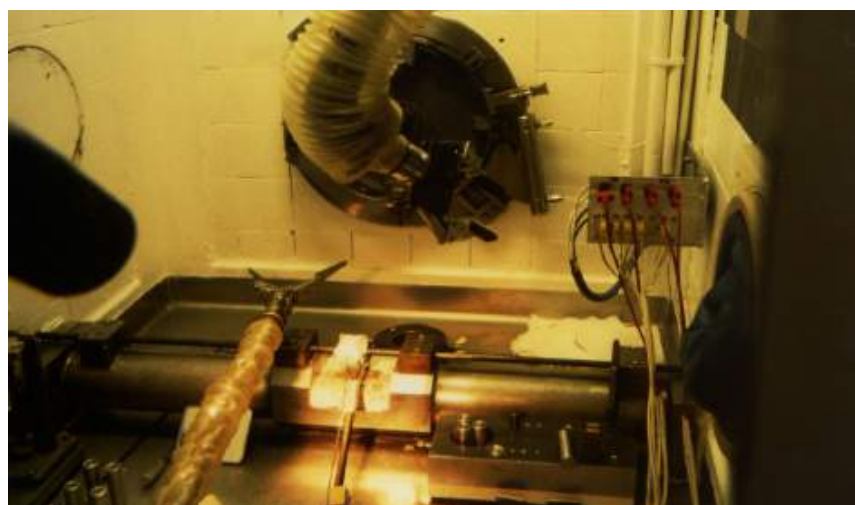


**Figure 6.19:** Interior of small hot cell: input, output bars and oven surrounding the specimen.

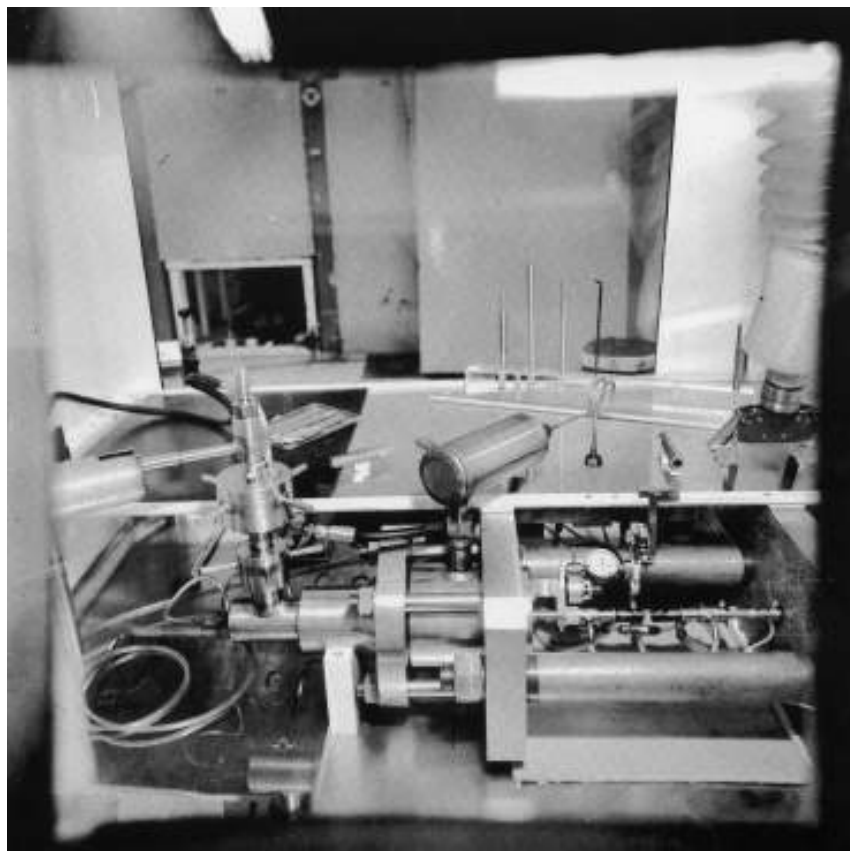


**Figure 6.20:** Hydro-Pneumatic machine for dynamic tensile test mounted in the large hot cell.

#### 6.4 Testing at high temperature with the MHB and the HPM

The high temperature tests with the MHB and the HPM are performed by heating first the specimen up to the desired temperature with an oven surrounding only the specimen, as sketched in Fig.6.21.

From Fig. 6.21 it can be seen that the internal cavity of the oven has a diameter slightly larger than that of the bars of MHB and HPM and a length slightly longer than the distance between the bar ends (with the specimen in place, screwed to the bar ends). The internal cavity dimensions of the oven are such that: i)the two bar ends close the cavity and help to ensure a homogeneous temperature distribution along the gauge length of the specimen; ii)the two bar ends are surrounded by the oven only over a very short length in order to reduce to

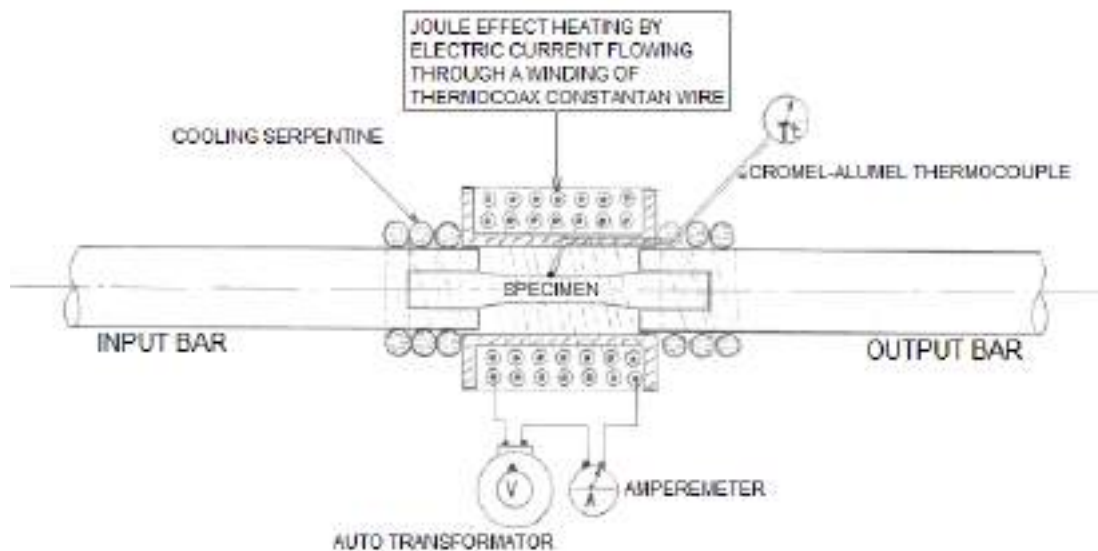


**Figure 6.21:** Specimen heating set-up for dynamic testing at high temperature with the MHB.

a minimum the heating of the bar extremes; in addition iii) the heating of the bars is maintained to a minimum also by the cooling action of cold water flowing through a serpentine placed around the bar ends, immediately adjacent to the oven, as shown in Fig. 6.21.

In the case of testing at high temperature with the MHB it is important to maintain the bar temperature as close as possible to the room temperature for two reasons:

- the temperature increase of the input and output bars changes the propagation speed of the elastic stress waves and as a consequence causes a wave dispersion which changes the amplitude of the incident, reflected and transmitted pulses. Nevertheless the problem is not always critical because, according to (Lindholm and Yeakley, 1968), bar temperature increase up to 150°C does not give rise to significant pulse amplitude changes and the issue can be neglected. If the changes of the wave speed due to bar temperature increases must be taken into account, recent studies propose a solution to this problem (Tong et al., 2001); a correction factor is also proposed in (Lindholm and Yeakley, 1968).
- the temperature increase of the bars may change the calibration of the strain-gauges because of the dependence of the electrical resistance of the strain-gauges on the temperature.

Clearly in the case of testing at high temperature with the HPM the heating of the elastic dynamometric bar should be avoided by means of the cooling serpentine (Fig. 6.21) only because of the potential change of the calibration of the strain-gauge station.

The oven used at JRC was home-made, consisting of a Constantan Thermocoax cable (a wire of Constantan alloy surrounded by an electrical insulation and inserted in a tubular shield) wrapped around a ceramic support (also a metal alloy for high temperatures can be used as support for testing temperatures up to 600°C) and fed by an electrical current at low voltage. In this manner test temperatures of up to 900°C were attained. A calibration procedure of the oven had to be performed in order to determine the correspondence of specimen temperature versus electrical current values. The fine test temperature control was realised by means of a thermocouple point welded to the gauge part of the specimen and by hand regulation of the electrical current just before starting the test. The reason of this final hand regulation of the temperature without interruption of the electric current was necessary in order to avoid the presence of extra-currents generated by the automated control of the temperature with interruption/restoration of electric circuits, and which could erroneously trigger the transient recorder.

## **6.5 The JRC Large Modified Hopkinson Bar for fast dynamic testing of large specimens and structural components**

At JRC-Ispra at the beginning of 1980s a large type of modified Hopkinson bar was designed and constructed in the frame of the Nuclear Reactor Safety Programme (containment of internal accidental explosions or impact of projectiles) in order to investigate:

- the effects of specimen size on the dynamic mechanical properties of the materials used for the steel containment shells;
- the dynamic mechanical response of specific points of the steel containment structures like welds, penetrations etc. which are difficult to be studied with small specimens;
- the dynamic mechanical properties of plane and reinforced concrete using real size aggregates and reinforcements.
- aspects of the process of numerical code validation by precision testing of structural components whose results should be compared with the numerical code predictions.

The apparatus was initially configured with two counteracting arms and its name was Large Dynamic Testing Facility, LDTF. Successively, in the 1990s its configuration was modified to one arm MHB, as shown in Fig. 6.24, which is similar to the small MHB of Fig. 6.2, and its name changed to HOPLAB (Hopkinson Large Bar). Its pretensioned, incident and transmitter bars are, respectively, 100m, 13m and 90m long, and it can deliver a loading pulse of 2.5MN amplitude and 40 ms duration with rise time of about 50  $\mu$ s. The HOPLAB was used also in the frame of Automotive Safety Programmes conducted in collaboration with the Automotive Industries in order to measure with precision the energy absorption of the structural components dedicated to mitigate the effect of crashes. The measurement of the dynamic response of the structural components of road safety barriers was also included in this programme. More recently, due to the problem of terrorism and attacks with explosives, the HOPLAB was also used in structural security related research.

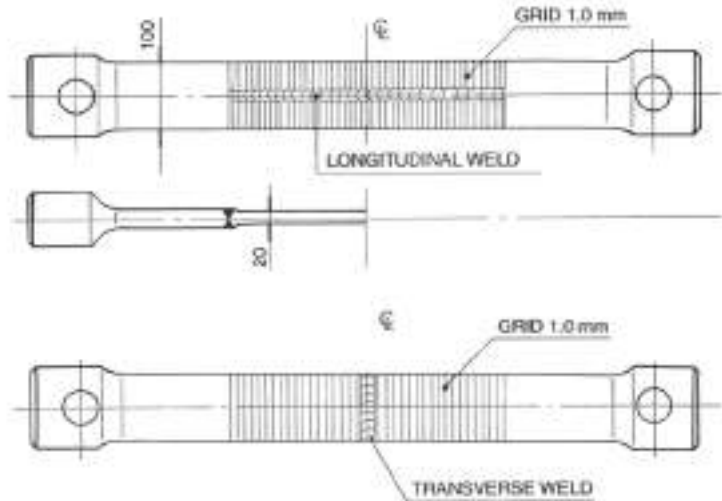


**Figure 6.22:** Large specimen for the study of the mechanical properties of real size welds at high strain-rate.

### 6.5.1 Application of the Large MHB to high strain-rate testing of large steel specimens

Several dynamic testing campaigns have been conducted on large steel specimens in the frame of Nuclear Reactor Safety programs. One of the first examples of a really large specimen, used to dynamically test real size welds, is represented in Fig. 6.22. The total length of the specimen is about 1m and the experiment has been carried out at the old LDTF.

Another significant testing campaign has aimed to verify the specimen size effects on the dynamic mechanical properties of structural steels widely used in nuclear reactor structures. For the austenitic steel X6CrNiNb1810 experiments have been performed with 3, 9 and 30mm-diameter cylindrical specimens, at room temperature and at 600°C. These specimens were geometrically similar, as shown in Fig. 6.23. The specimens of diameter 9 and 30 mm were tested with the Large MHB (HOPLAB) of Fig. 6.24 while the specimens of 3 mm diameter were tested with the small MHB of Fig. 6.2. Due to the fact that all experiments realise the same conditions of propagation of the elastic stress wave acting on the specimens, the records of the dynamic tests with large-medium-small specimens could be analysed applying the same theory of elastic plane stress wave propagation, resumed in the equations 13, 14, 15. The scale effect in the dynamic regime has thus been effectively investigated. The detailed results of the testing campaign are reported in (Solomos et al., 2004), where a major conclusion was that size effects at high strain-rate must be principally sought in parameters of local deformation and at regions of strong strain gradients. In Fig. 6.25 typical dynamic stress-strain curves of the three specimens are shown for room temperature. A similar investigation with 3, 9 and 30mm cylindrical specimens was undertaken for the nuclear ferritic steel 20MnMoNi55.



**Figure 6.23:** Specimens of 3, 9, 30mm diameter for the study of size effects at high strain-rate.



**Figure 6.24:** Schematic of Large MHB in the one-arm configuration for testing of large specimens.

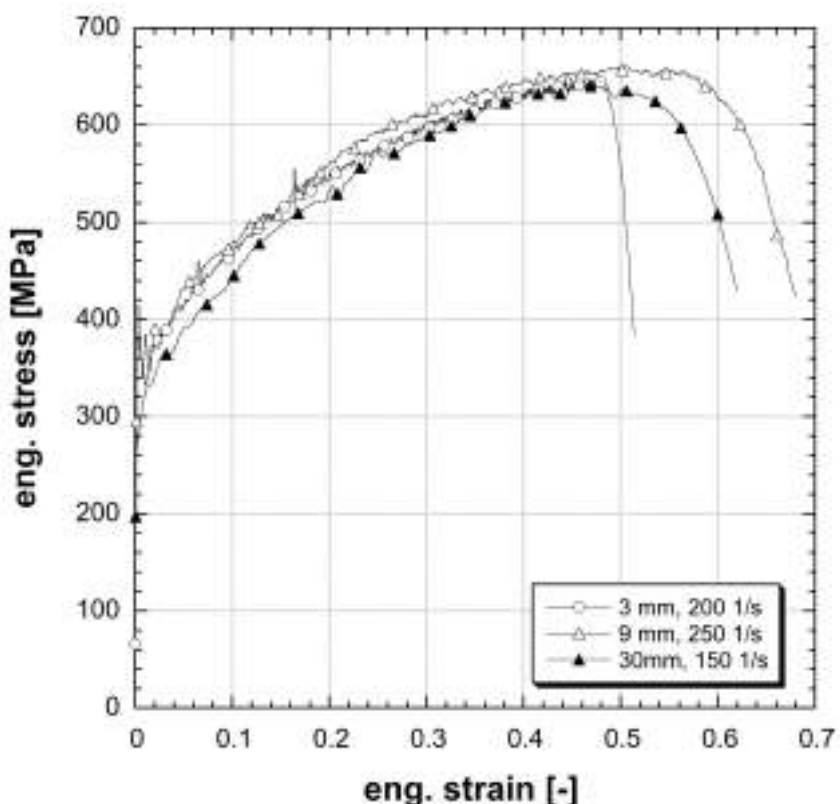


**Figure 6.25:** Stress-strain curves of 3, 9, 30mm diameter specimens of austenitic steel X6CrNiNb1810.

## **7 Effects of strain-rate, environmental conditions and pre-damage on mechanical properties of nuclear reactor steels**

### **7.1 Introduction**

As mentioned already, the data review comprises the whole body of the dynamic mechanical properties, in digitised format, concerning steels in as-received and pre-damaged conditions and used for containment shells and other mechanical structures of nuclear fission reactors. The new digitised format of the database should facilitate now the study and deepening of the analysis of the performance of the different steels against impact loading and energy absorption through controlled plastic deformation. In the following sections it is intended to show a few examples of the optimised analysis allowed by the new database. It is especially aimed at focusing attention to the main aspects of changes/degradation of the stress-strain curves of the tested steels due to high strain-rate, high temperature, irradiation, welding, creep, low cycle fatigue. Finally, on the basis of such analysis we briefly discuss qualitatively the possible effects that such changes/degradation of the dynamic stress-strain curves might have for the safety assessment of aged reactor structures against severe accidents provoking impact loading.

### **7.2 Effects of high strain-rate on as-received austenitic and ferritic steels at room temperature**

The effects of strain-rate increasing from  $10^{-2}$  to  $10^3 \text{ s}^{-1}$  on the stress-strain curves at room temperature of as-received austenitic stainless steels consist mainly of a marked increase of the stress at a given strain (strain-rate hardening) and of a reduction of uniform and fracture strain with increasing strain-rate. Such phenomena are illustrated in Figs. 7.1, 7.2, 7.3, 7.4, 7.5, respectively, for the austenitic stainless steels AISI 304L, AISI 321, AISI 316L, AISI 316H, X6CrNiNb1810. These figures show also strain hardening for the stress-strain curves of these steels at each strain-rate.

The effects of strain-rate increase in the same range as above on the stress-strain curves of ferritic steels ASME 537 and 20MnMoNi55 consist also of a marked strain-rate hardening but with practically no reduction of ductility, as illustrated, respectively, in Fig. 7.6 and Fig. 7.8. The stress-strain curves of each strain-rate show strain hardening, too. On the same figures one observes that the stress-strain curves at the highest strain-rate of the above two ferritic steels show also a marked initial yield instability characterised by an upper and lower yield stress at the passage from elastic to plastic deformation, whose effects will be discussed later.

### **7.3 Effects of high temperature and high strain-rate on as-received austenitic and ferritic steels**

The dynamic stress-strain curves of the same austenitic stainless steels mentioned above in the preceding Section have been measured at higher temperatures ranging from  $100^\circ\text{C}$  to  $950^\circ\text{C}$  also in the strain-rate range from  $10^{-2}$  to  $10^3 \text{ s}^{-1}$ ; the curves are shown in Figs. 7.9, 7.10, 7.11, 7.12, 7.13, 7.14, 7.15, 7.16, 7.17, 7.18, 7.19, 7.20, 7.21, 7.22, 7.23, 7.24, 7.25, 7.26 and 7.5.

At temperatures ranging from  $100^\circ\text{C}$  to  $400^\circ\text{C}$  (up to  $550^\circ\text{C}$  for the steel AISI 316H, Fig. 7.16) from the observation of the Figs 7.9 to 7.16 one can state that the dynamic stress-strain curves of the austenitic stainless steels show moderate strain-rate hardening and the curves at each strain-rate exhibit strain hardening.

At temperatures ranging from  $500^\circ\text{C}$  to  $650^\circ\text{C}$  from the Fig. 7.16 to 7.20 one can observe that the dynamic stress-strain curves of austenitic stainless steels show moderate strain-rate softening (where the stress at a given strain decreases with increasing strain-rate) and reduction of uniform strain. Such phenomena are graphically quantified in Fig. 7.24, Fig. 7.25, Fig. 7.26, Fig. 7.27, respectively, for the steels AISI 316L, 316H and X6CrNiNb1810.

The quasi-static flow curves of AISI 316L (Fig. 7.17) and 316H (Fig. 7.19), respectively, at the temperatures of  $550$  and  $650^\circ\text{C}$  show oscillations typical of dynamic strain ageing, while the dynamic flow curves of Figs. 7.17, 7.18, 7.19 show oscillations typical of early localisations.

At the testing temperatures from  $750^\circ\text{C}$  to  $950^\circ\text{C}$  a marked strain-rate hardening is shown by the dynamic stress-strain curves of the austenitic stainless steels AISI 316L and AISI 321, as illustrated in Figs. 7.21, 7.22, and 7.23.

The dynamic flow curves of the ferritic steels ASME 537 and 20MnMoNi55 show also the phenomenon of strain-rate softening (Figs. 7.7, 7.8), respectively, at the temperatures of  $300^\circ\text{C}$  and  $400^\circ\text{C}$ .

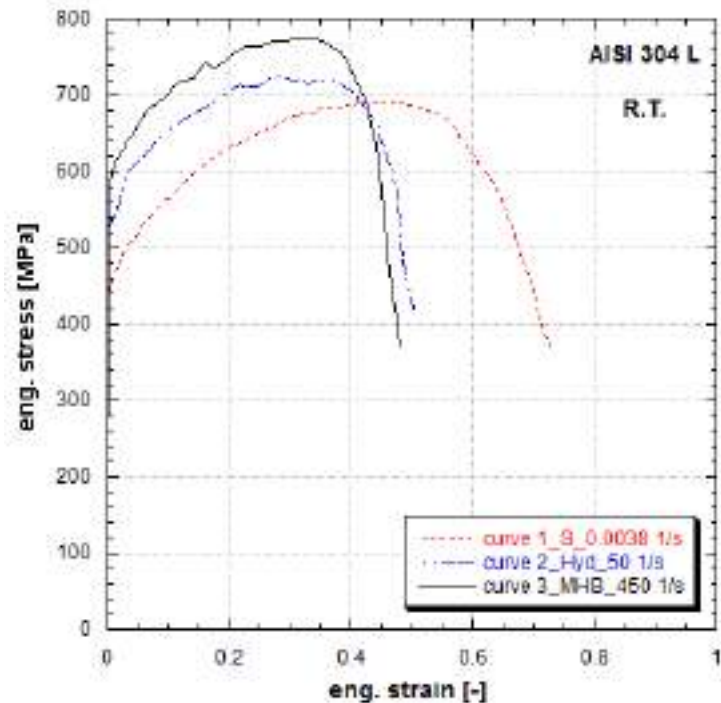


**Figure 7.1:** Engineering stress vs. strain curves of AISI 304L steel as-received from quasi-static to high strain-rate, at ambient temperature (Albertini and Montagnani, 1980) (Ref.Mat.1).

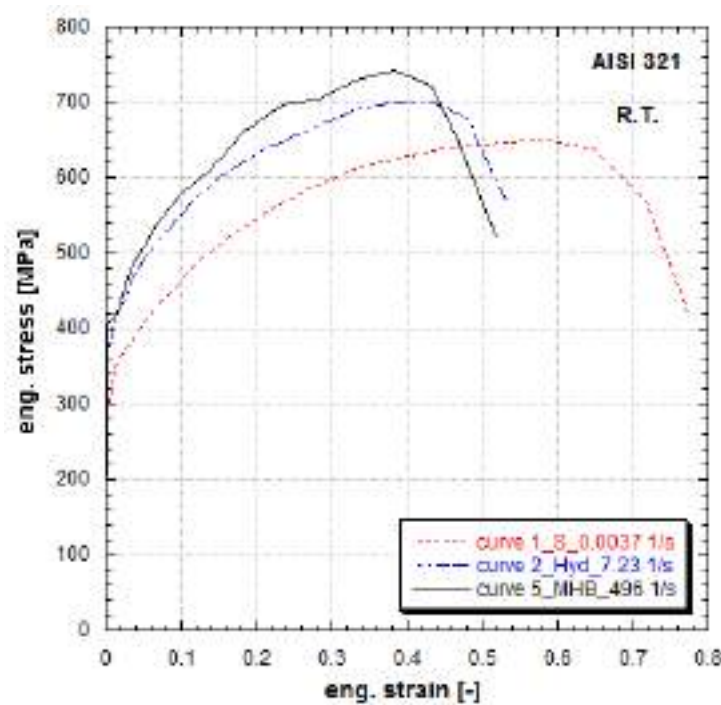


**Figure 7.2:** Engineering stress vs. strain curves of AISI 321 stainless steel (Albertini and Montagnani, 1980),(Albertini and Montagnani, 1983a) from quasi-static to high strain-rate, at ambient temperature (Ref.Mat.2).

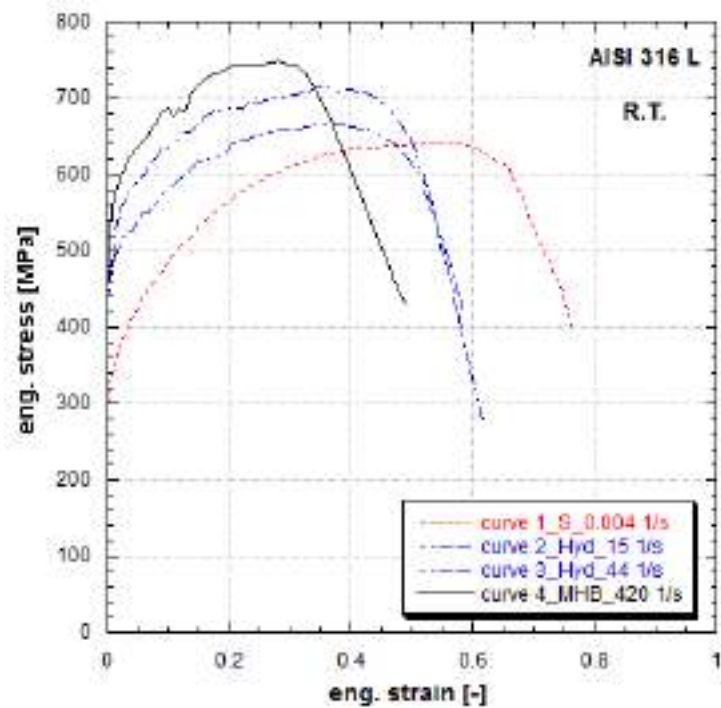


**Figure 7.3:** Engineering stress vs. strain curves of AISI 316L stainless steel from quasi-static to high strain-rate at ambient temperature (Albertini and Montagnani, 1978), (Albertini et al., 1978), (Albertini et al., 1979), (Albertini and Montagnani, 1980), (Albertini et al., 1980), (Albertini and Montagnani, 1981a), (Albertini et al., 1982), (Albertini and Montagnani, 1983b) (Ref.Mat.3).

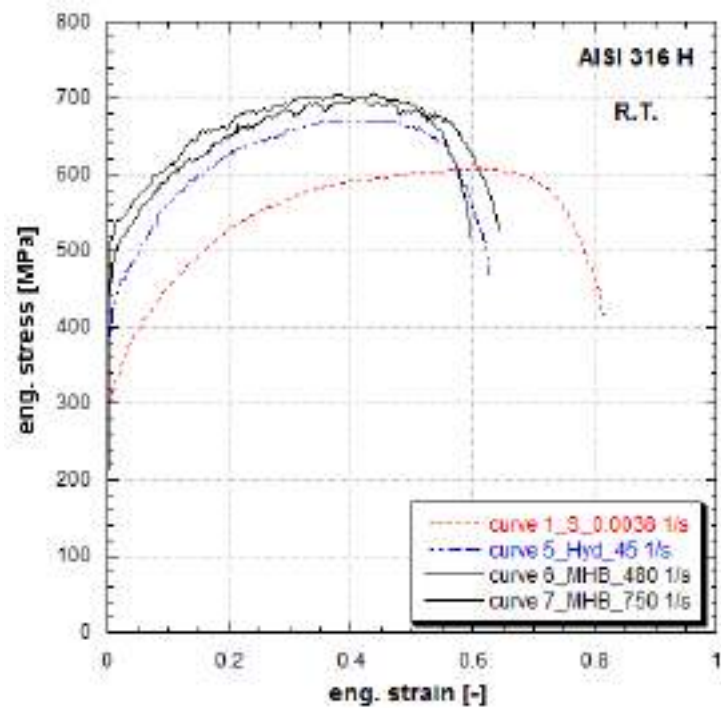


**Figure 7.4:** Engineering stress vs. strain curves of AISI 316H as-received stainless steel from quasi-static to high strain-rate at ambient temperature (Albertini et al., 1983b), (Albertini et al., 1983a), (Albertini et al., 1984b).

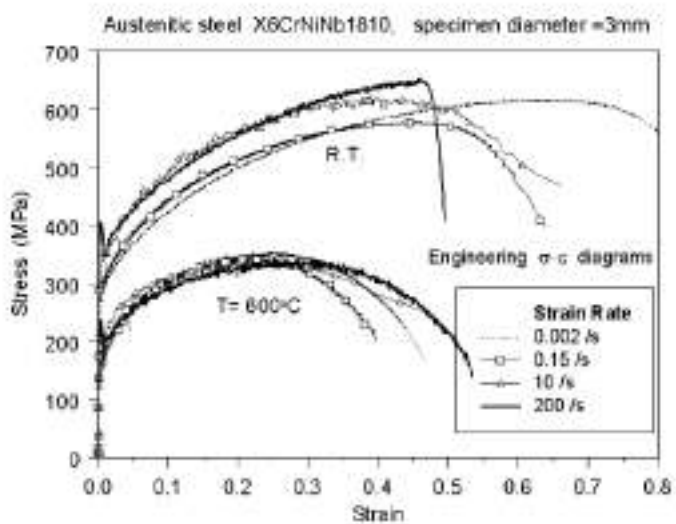


**Figure 7.5:** Engineering stress vs. strain curves of X6CrNiNb1810 steel for several strain-rates and two temperatures (Solomos et al., 2004, Solomos et al., 2003).

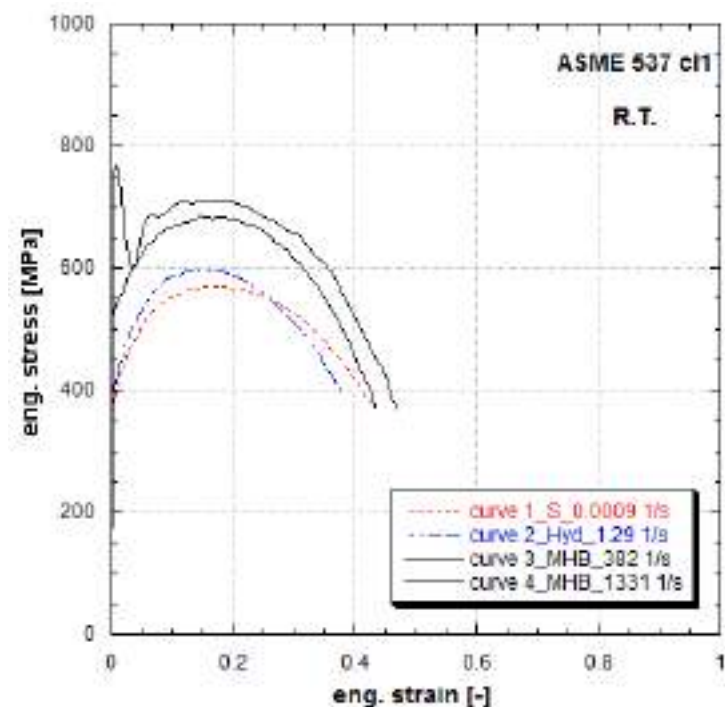


**Figure 7.6:** Engineering stress vs. strain curves of ASME 537 cl1 steel from quasi-static to high strain-rate at ambient temperature (Albertini, 1997).

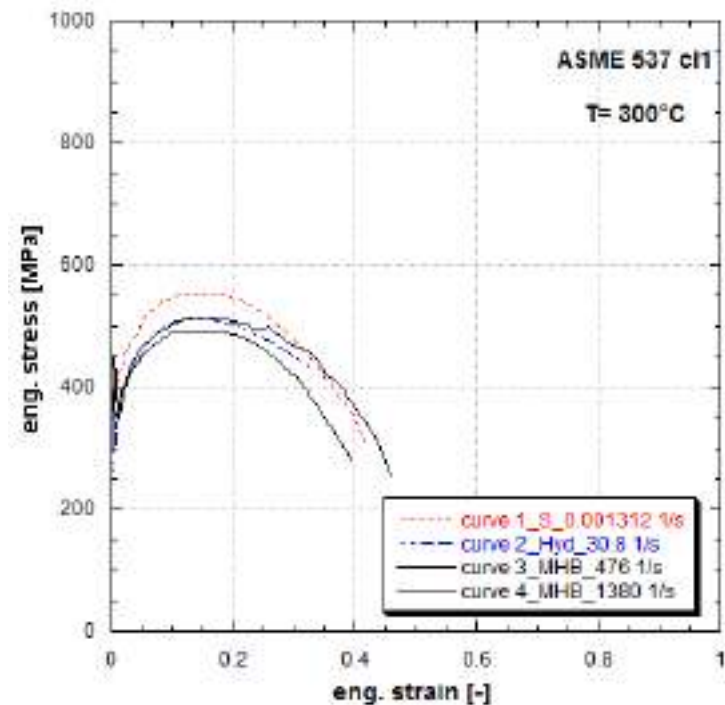


**Figure 7.7:** Engineering stress vs. strain curves of ASME 537 cl1 at 300°C at several strain-rates (Albertini, 1997).

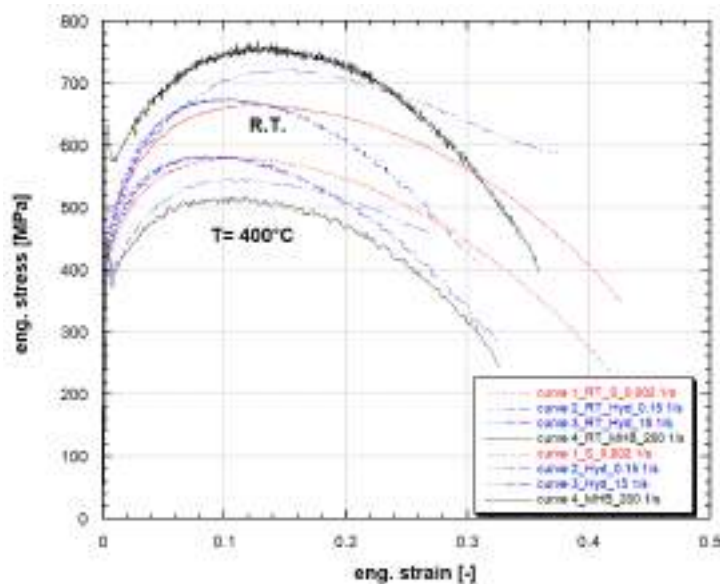


**Figure 7.8:** Engineering stress vs. strain curves of 20MnMoNi55 at different strain-rates at R.T. and 400°C (Solomos et al., 2004, Solomos et al., 2003).

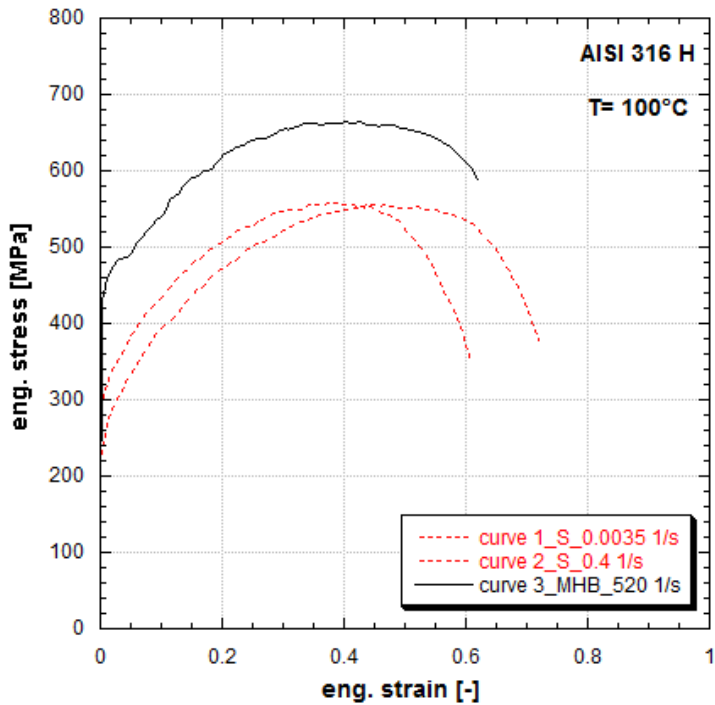


**Figure 7.9:** Engineering stress vs. strain curves of AISI 316H (Ref.Mat) at different strain-rates and 100°C (Birch et al., 1988, Albertini et al., 1985b).

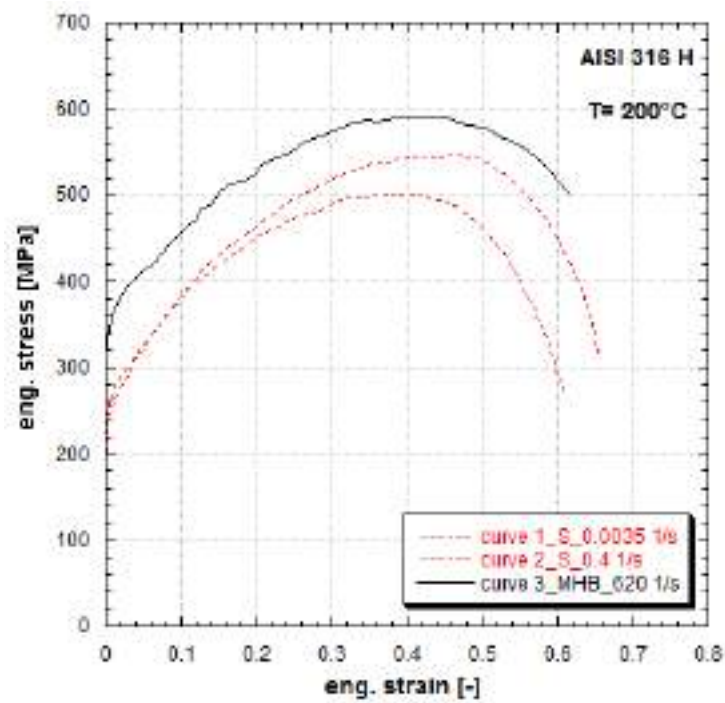


**Figure 7.10:** Engineering stress vs. strain curves of AISI 316H stainless steel at different strain-rates and 200°C (Birch et al., 1988, Albertini et al., 1985b).

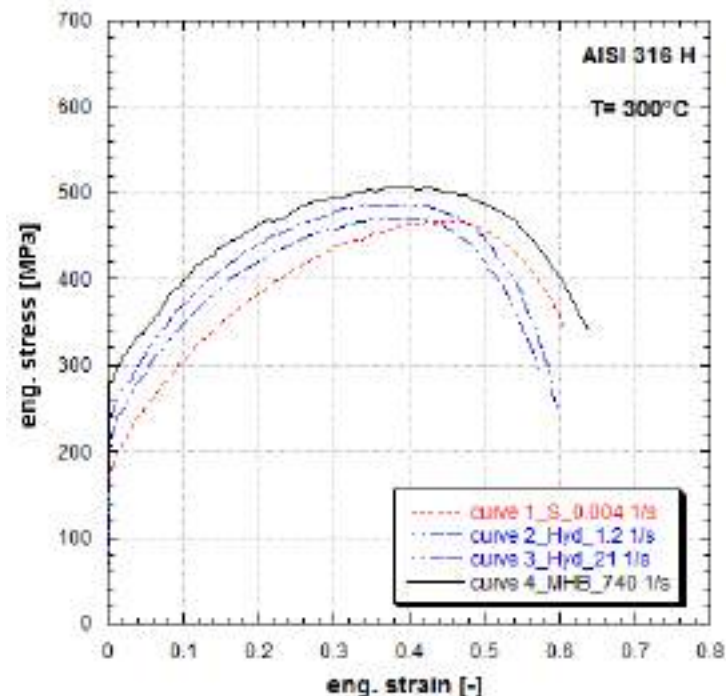


**Figure 7.11:** Engineering stress vs. strain curves of AISI 316H stainless steel at different strain-rates and 300°C (Birch et al., 1988, Albertini et al., 1985b).

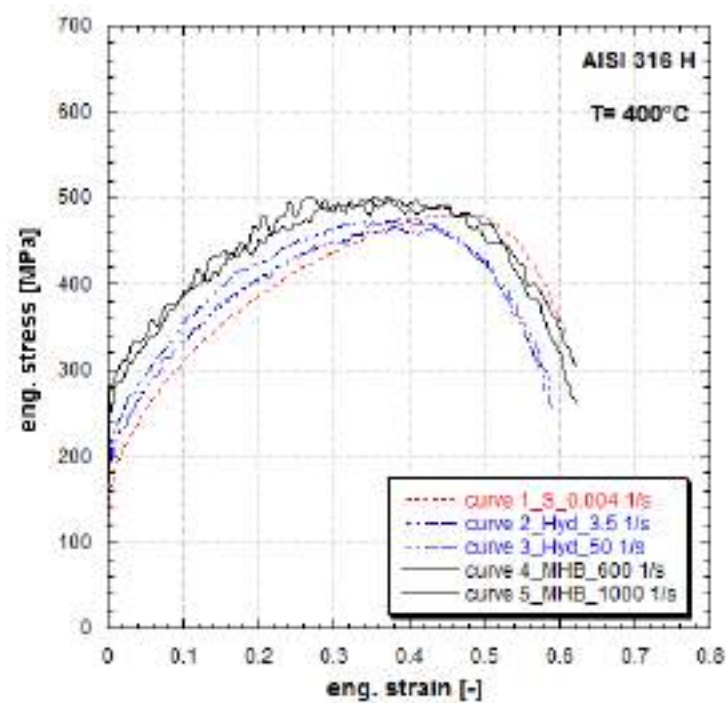


**Figure 7.12:** Engineering stress vs. strain curves of AISI 316H stainless steel at different strain-rates and 400°C (Birch et al., 1988, Albertini et al., 1985b).

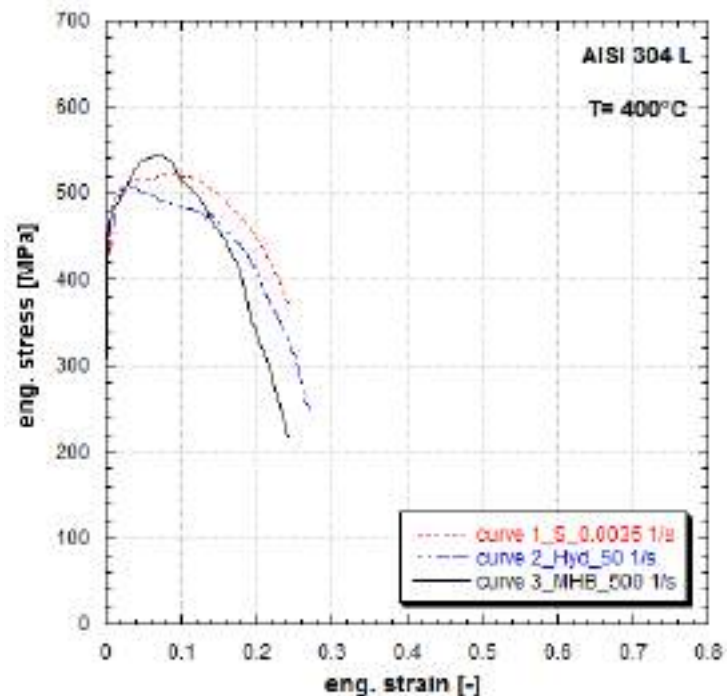


**Figure 7.13:** Engineering stress vs. strain curves of AISI 304L (Ref.Mat.1) stainless steel at 400°C (Albertini and Montagnani, 1980) at quasi-static and high strain-rate.

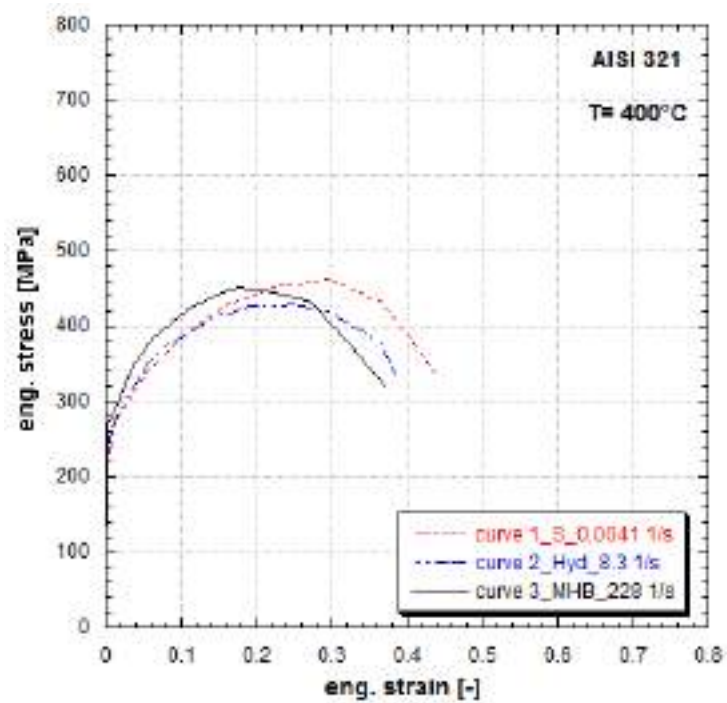


**Figure 7.14:** Engineering stress vs. strain curves of AISI 321(Ref.Mat.2) stainless steel at 400°C (Albertini and Montagnani, 1980) at quasi-static and high strain-rate.

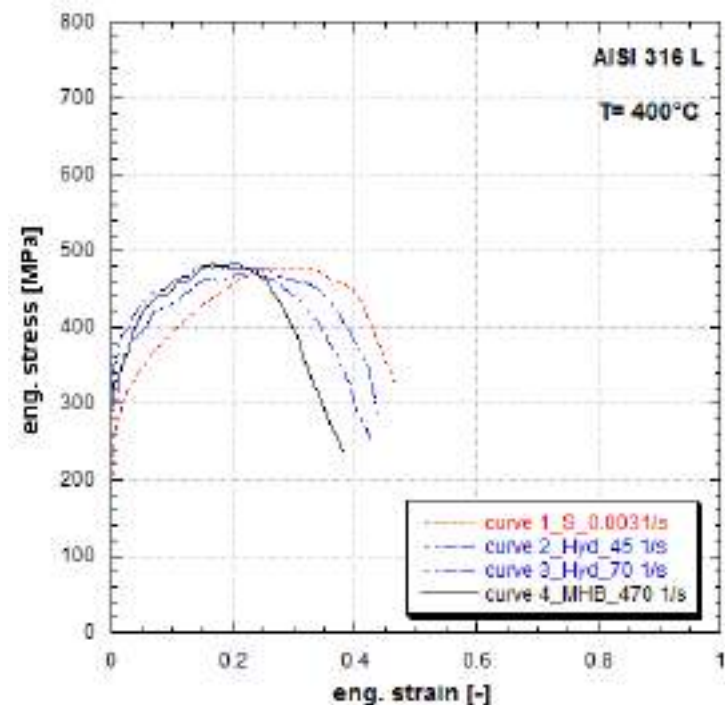


**Figure 7.15:** Engineering stress vs. strain curves of AISI 316L (Ref.Mat.3) stainless steel at different strain-rates and 400°C (Albertini et al., 1983a,Eleiche et al., 1985).

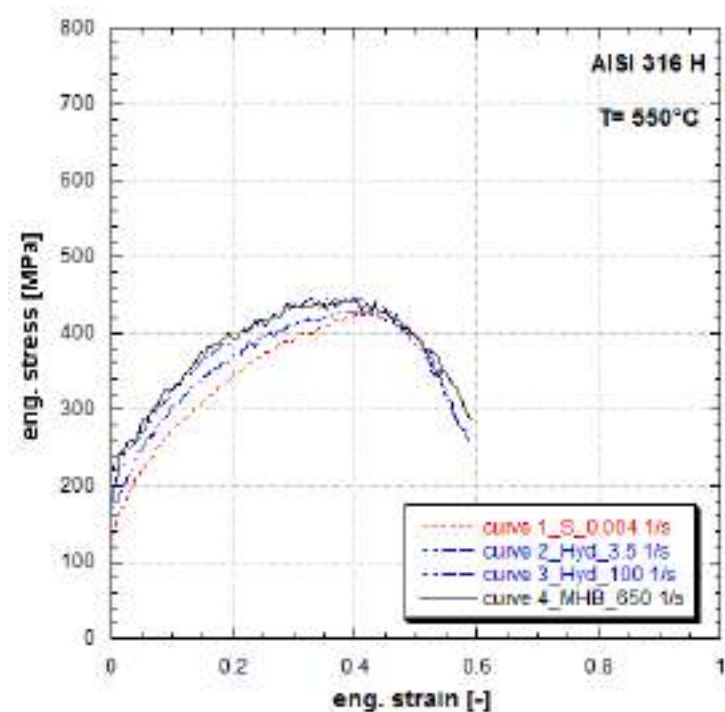


**Figure 7.16:** Engineering stress vs. strain curves of AISI 316H stainless steel at different strain-rates and 550°C (Albertini et al., 1983a,Albertini and Montagnani, 1983b,Albertini and Labibes, a,Birch et al., 1988,Albertini et al., 1985b).

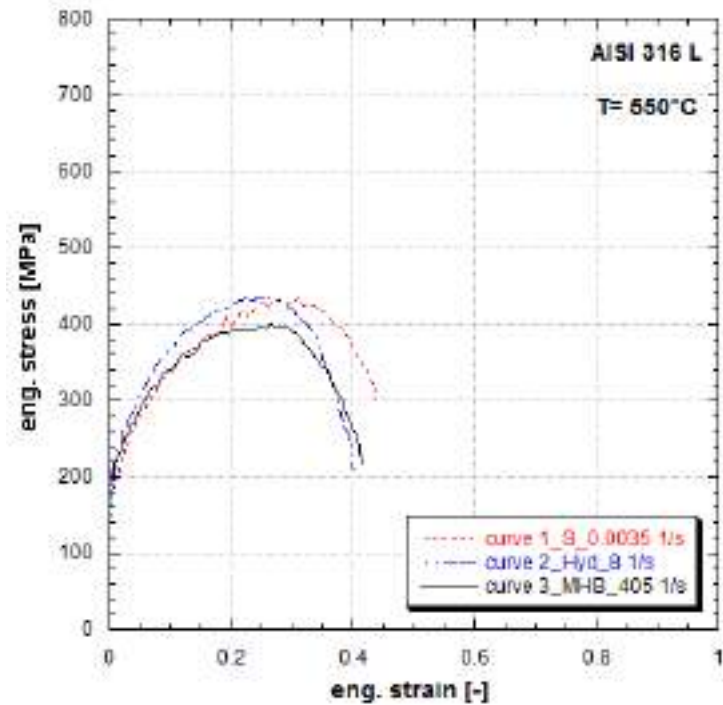


**Figure 7.17:** Engineering stress vs. strain curves of AISI 316L stainless steel at different strain-rates and 550°C (Albertini and Montagnani, 1978, Albertini and Montagnani, 1979, Albertini and Montagnani, 1980).

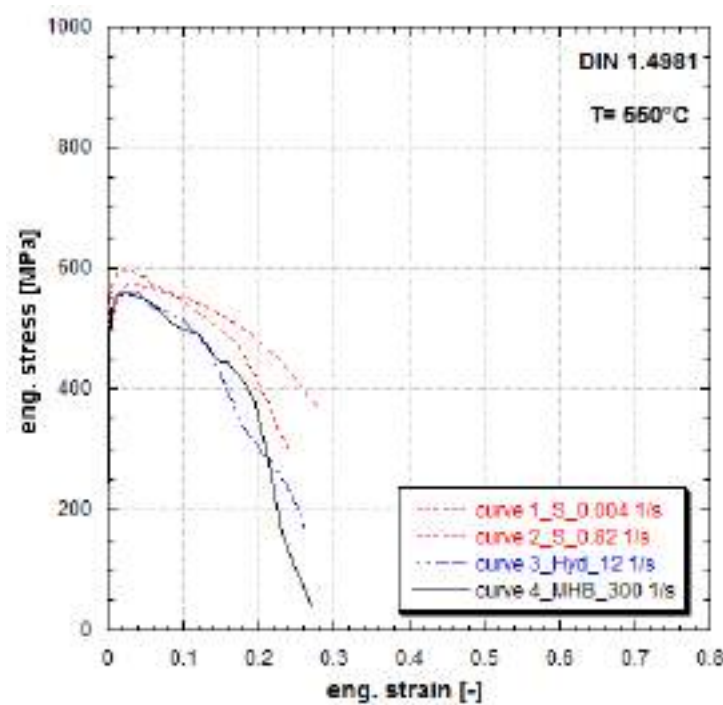


**Figure 7.18:** Engineering stress vs. strain curves of DIN 1.4981 stainless steel at different strain-rates and 550°C (Albertini et al., 1987b).

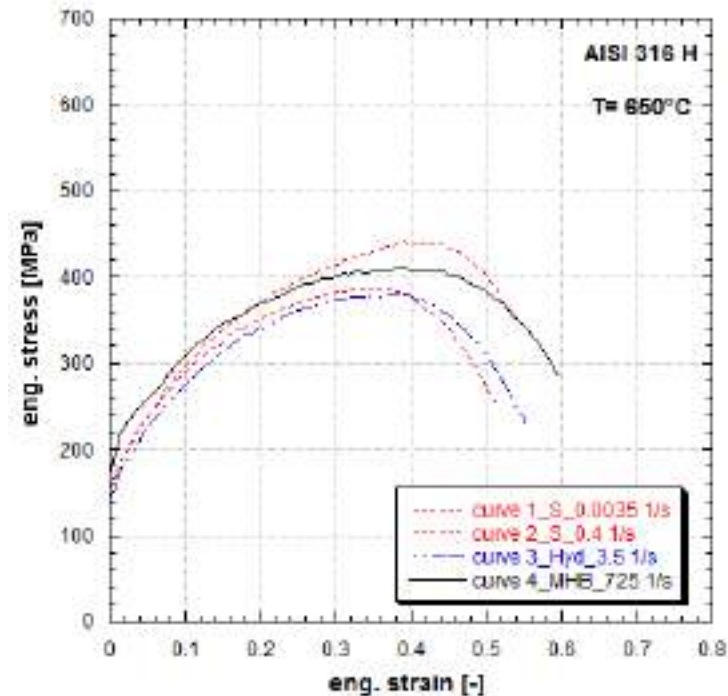


**Figure 7.19:** Engineering stress vs. strain curves of AISI 316H stainless steel at different strain-rates and 650°C (Birch et al., 1988; Albertini et al., 1985b).

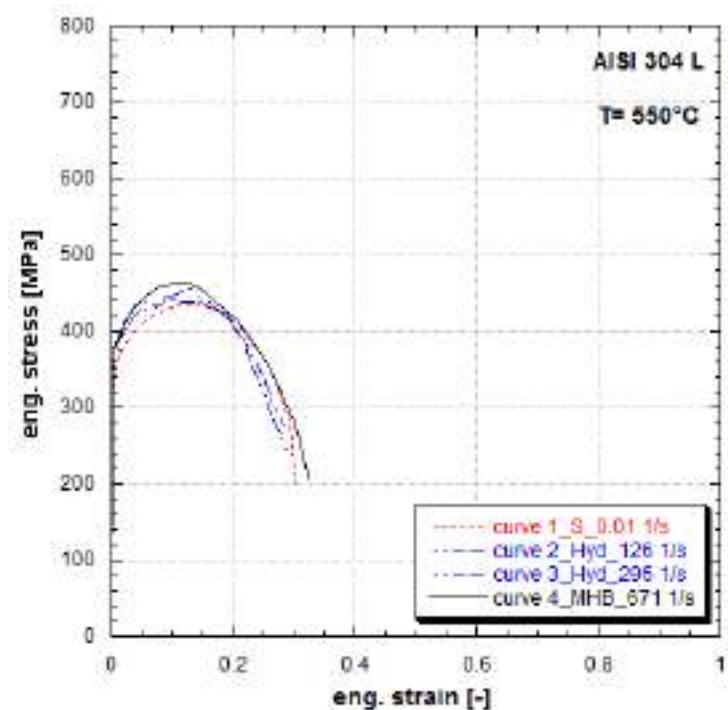


**Figure 7.20:** Engineering stress vs. strain curves of AISI 304L as-received stainless steel at different strain-rates and 550°C (Albertini and Montagnani, 1976).

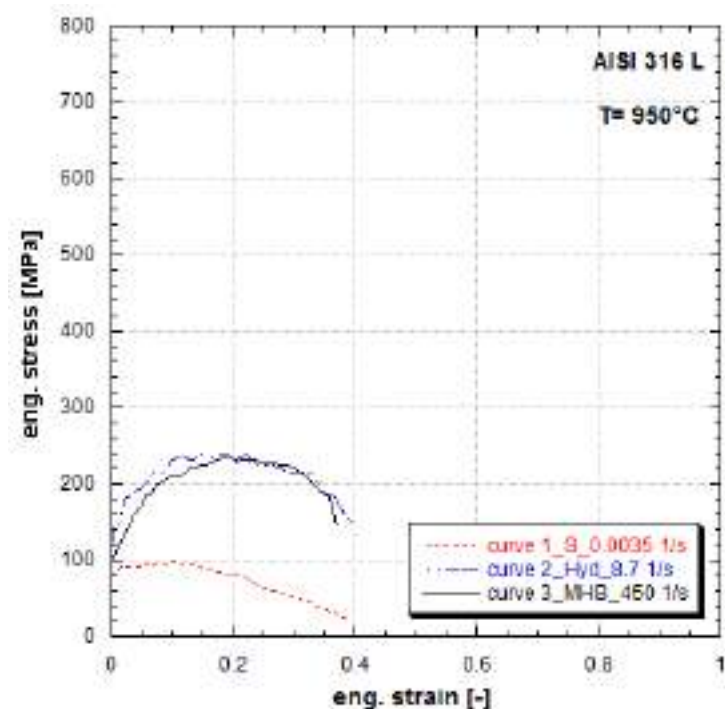


**Figure 7.21:** Engineering stress vs. strain curves of AISI 316L as-received stainless steel at different strain-rates and 950°C (Albertini et al., 1991b).

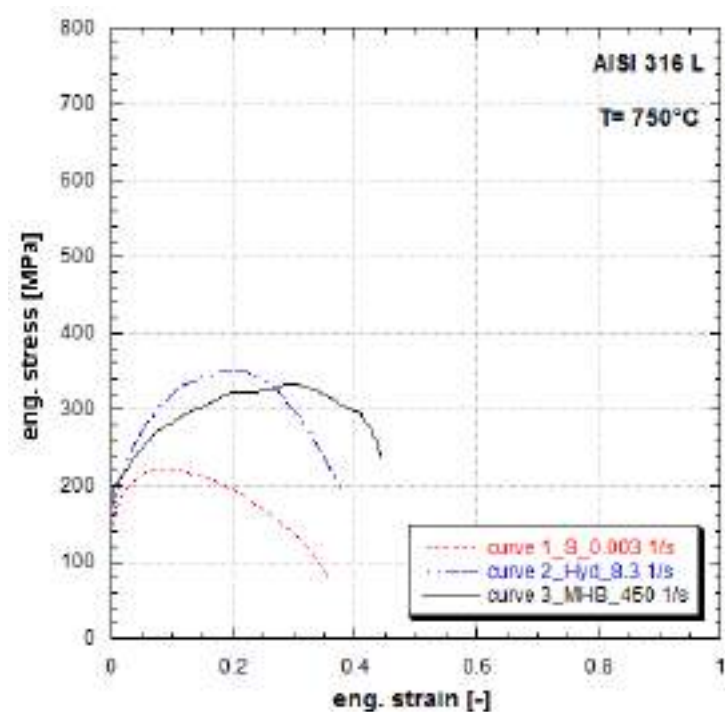


**Figure 7.22:** Engineering stress vs. strain curves of AISI 316L as-received stainless steel at different strain-rates and 750°C (Albertini and Montagnani, 1980).

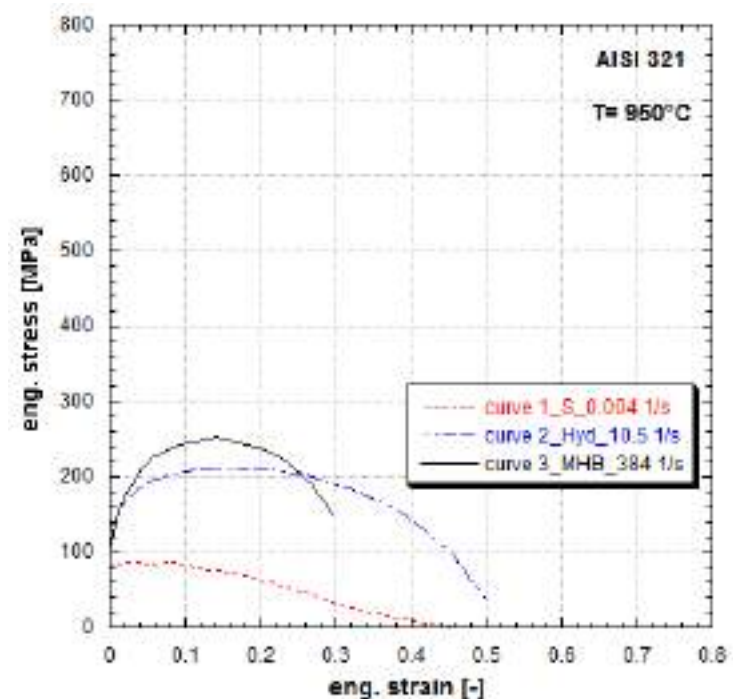


**Figure 7.23:** Engineering stress vs. strain curves of AISI 321 as-received stainless steel at different strain-rates and 950°C (Albertini and Montagnani, 1980).

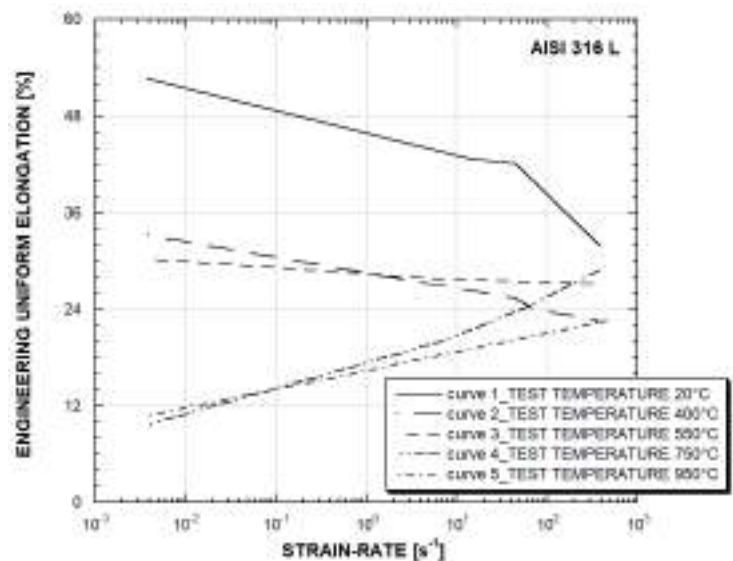


**Figure 7.24:** Effect of strain-rate on the engineering uniform elongation of AISI 316L at different temperatures.

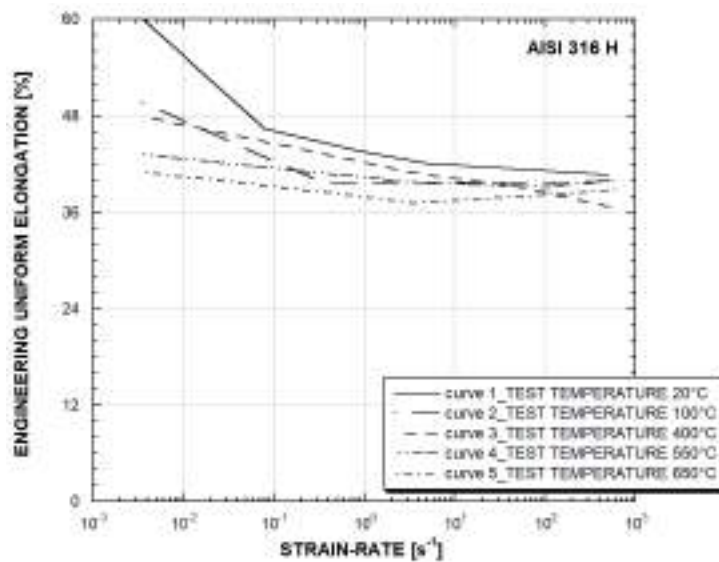


**Figure 7.25:** Effect of strain-rate on the engineering uniform elongation of AISI 316H at different temperatures.

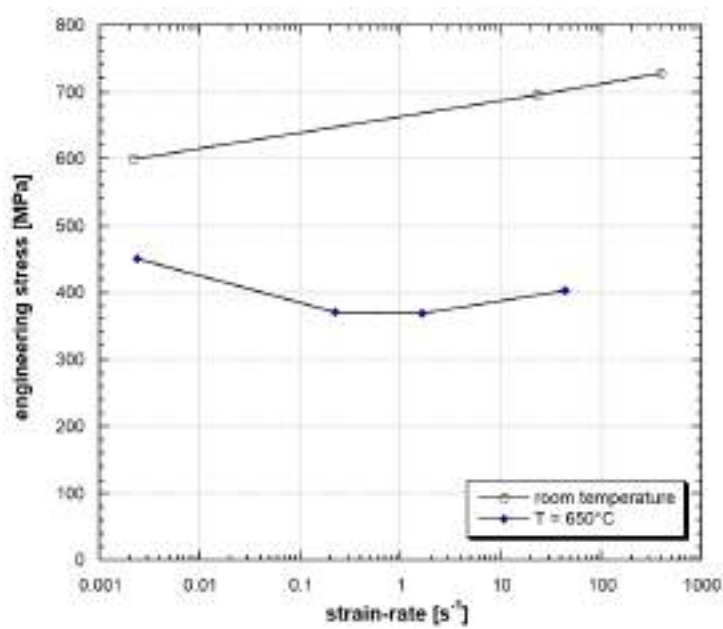


**Figure 7.26:** Effect of strain-rate on the ultimate tensile strength at room temperature and 650°C of AISI 316H as-received stainless steel.

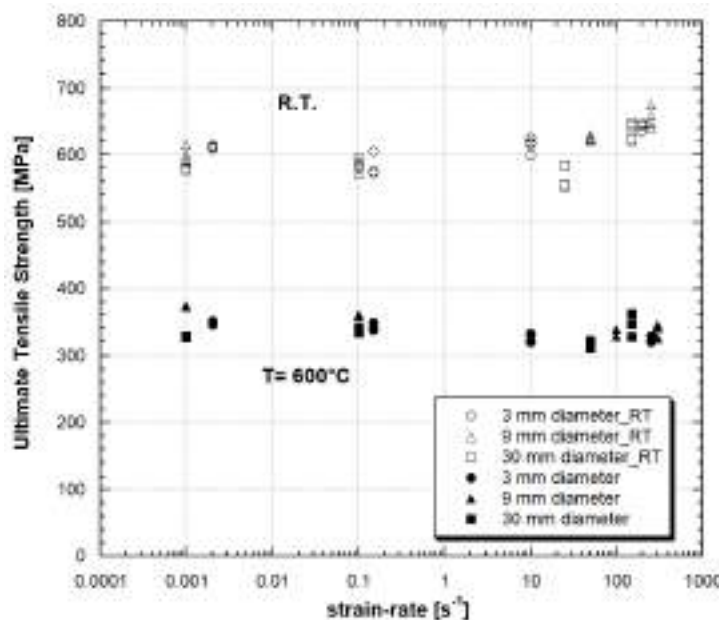


**Figure 7.27:** Effect of strain-rate on the ultimate tensile strength at room temperature and 600°C of X6CrNiNb1810 as-received stainless steel.

#### 7.4 Effects of irradiation, high temperature and high strain-rate on austenitic stainless steels

The dynamic stress-strain curves at room and higher temperature (400, 500, 550°C) of the austenitic stainless steels AISI 316L, 316H, 304L and of the Nimonic Alloy Pe16 after irradiation in the HFR reactor at the doses of 2 dpa<sup>(6)</sup>, 9.2 dpa, 30 dpa have been measured. A few examples from the extensive programme are reported here (Albertini et al., 1979, Albertini et al., 1981, Albertini et al., 1984a, Albertini et al., 1987a, Albertini et al., 1988), shown in Fig. 7.28 for AISI 304L, in Fig. 7.29, 7.30, 7.31, 7.32, regarding AISI 316L and Fig. 7.33, 7.34, 7.35 for PE16.

From Fig. 7.29 to Fig. 7.32 we observe that the effects of irradiation of AISI 316L (comparison of the flow curves at the same strain-rate) consist mainly of a strong increase of the flow stress at a given strain (damage hardening) and of a reduction of uniform and fracture strain. The dynamic flow curves at 550°C of the AISI 316L irradiated to 9.2 dpa show a marked strain-rate softening and reduction of uniform and fracture strain (Fig. 7.29 to Fig. 7.32). The same phenomena of strain-rate softening and reduction of uniform and fracture strain characterise the dynamic flow curves of the nimonic alloy PE16 irradiated at 9.2 dpa and tested at 500°C, as shown in Fig. 7.33. The damage hardening due to irradiation can be seen by comparing Figs. 7.34 and 7.33 regarding thermally aged and irradiated PE16, while the damage hardening and strain-rate softening due to thermal ageing in sodium at 500°C is observed from the comparison of Figs. 7.34 and 7.35. Finally, the effects of high irradiation (30 dpa) are depicted in Fig. 7.28, where the as-received (a) and irradiated specimens are shown (Albertini et al., 2014).

#### 7.5 Effects of the superposition of low cycle fatigue, irradiation, high temperature and high strain-rate on austenitic stainless steels AISI 304 and AISI 316H

This research programme was a collaboration between the Japanese institute PNC and the JRC. Specimens of SUS 304 (steel corresponding to AISI 304) and AISI 316H have been submitted to low cycle fatigue at 550°C by the Japanese PNC with the following cycle parameters:

- $n/N_f = 0.2, 0.4, 0.6$ .
- strain range = 0.6%, 1%.

where  $n$  is the actual number of cycles,  $N_f$  the number of cycles to fracture.

<sup>(6)</sup> Radiation in nuclear reactors, mainly consisting of neutrons, ions, electrons and gamma rays, can alter structural materials. Grossly explained, such radiation has the capability to displace an atom from its lattice site, thus leaving a vacancy behind and generating an interstitial atom in a location between lattice sites, where the displaced atom eventually stops. This type of material damage is represented by the "dpa = displacements per atom". Its effects may include increased material hardness, reduction in ductility, increased brittleness and susceptibility to environmentally induced cracking (from Wikipedia).

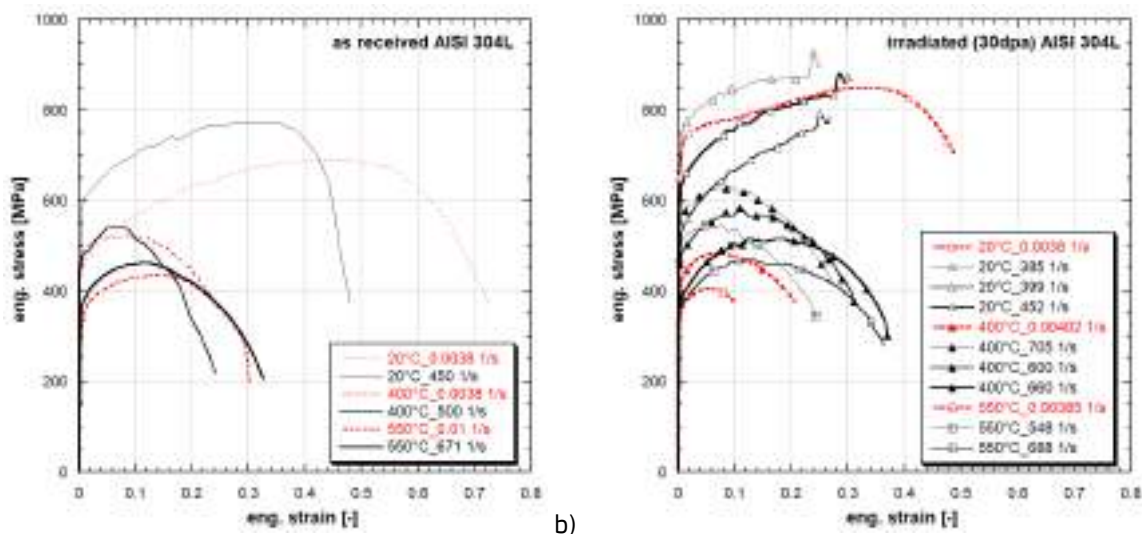


**Figure 7.28:** Stress vs. strain curve of AISI 304L at different strain-rates and temperatures: a) As-received; b) Irradiated at 30 dpa.

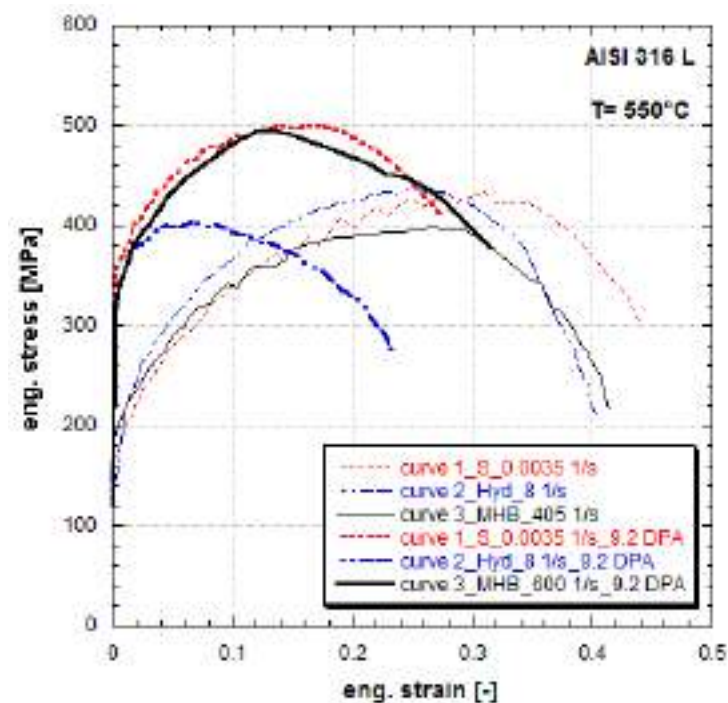


**Figure 7.29:** Engineering stress vs. strain curves of AISI 316L as-received and irradiated to 9.2 dpa at 550°C and different strain-rates (Albertini et al., 1984a).

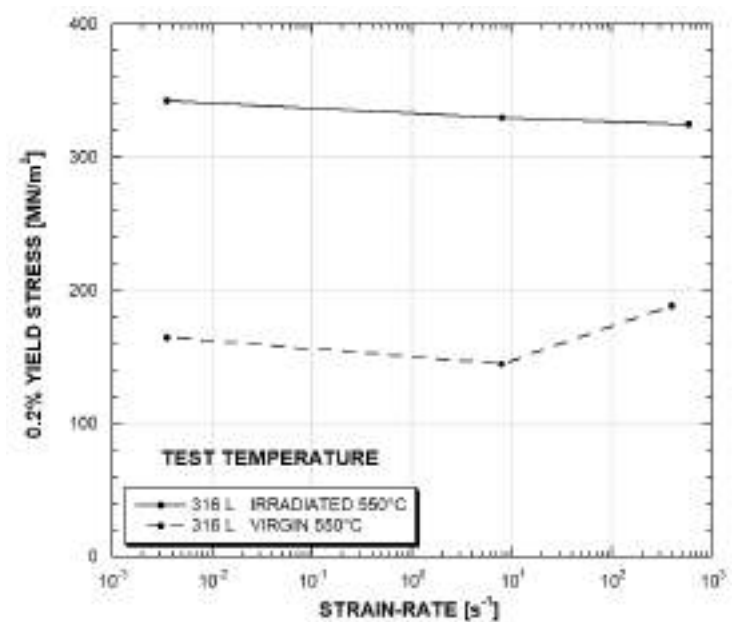


**Figure 7.30:** Effect of strain-rate on the 0.2% yield stress of AISI 316L stainless steel irradiated to 9.2 dpa in sodium at 550°C (Albertini et al., 1984a).

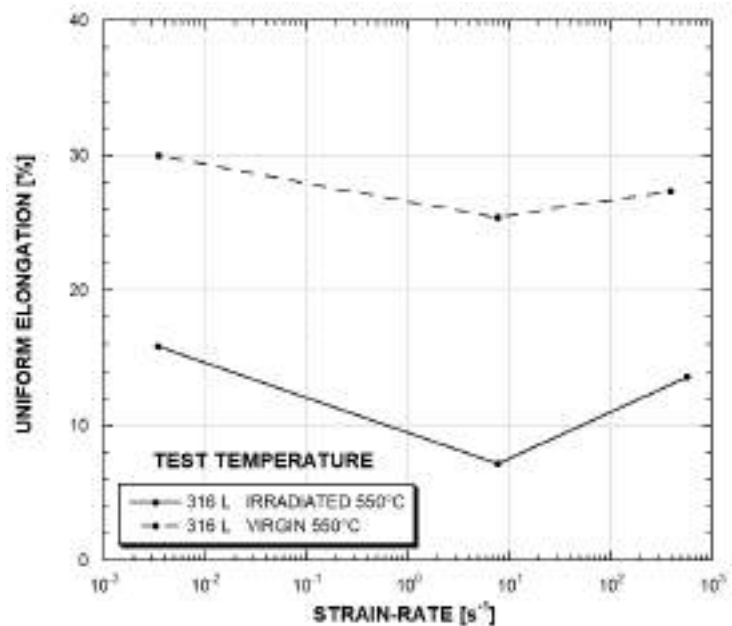


**Figure 7.31:** Effect of strain-rate on the uniform elongation of AISI 316L stainless steel irradiated to 9.2 dpa in sodium at 550°C (Albertini et al., 1984a).

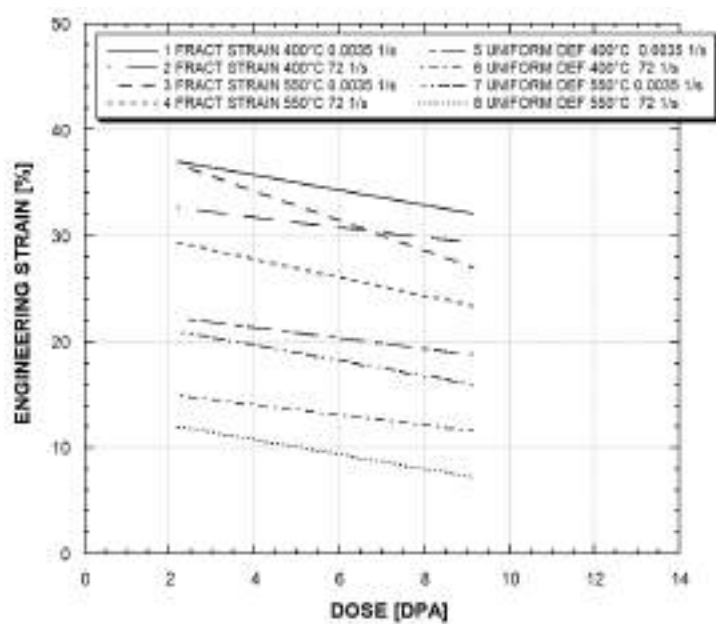


**Figure 7.32:** Effect of dose on fracture strain an uniform deformation of AISI 316L stainless steel irradiated at 400°C (2.2 dpa) and at 500°C (9.2 dpa) (Albertini et al., 1984a).

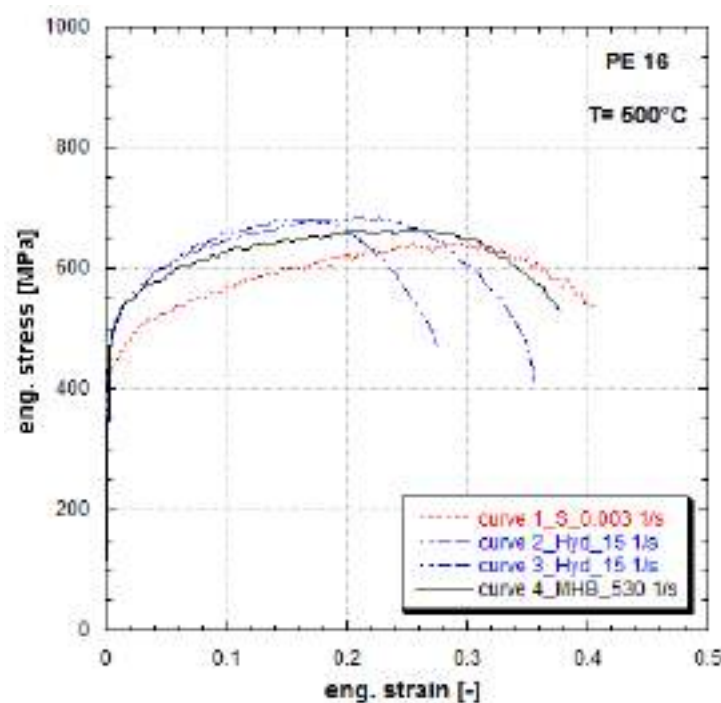


**Figure 7.33:** Engineering stress vs. strain curves for PE16 nimonic alloy irradiated to 9.2 dpa tested at different strain-rates and 500°C (Albertini et al., 1987a).

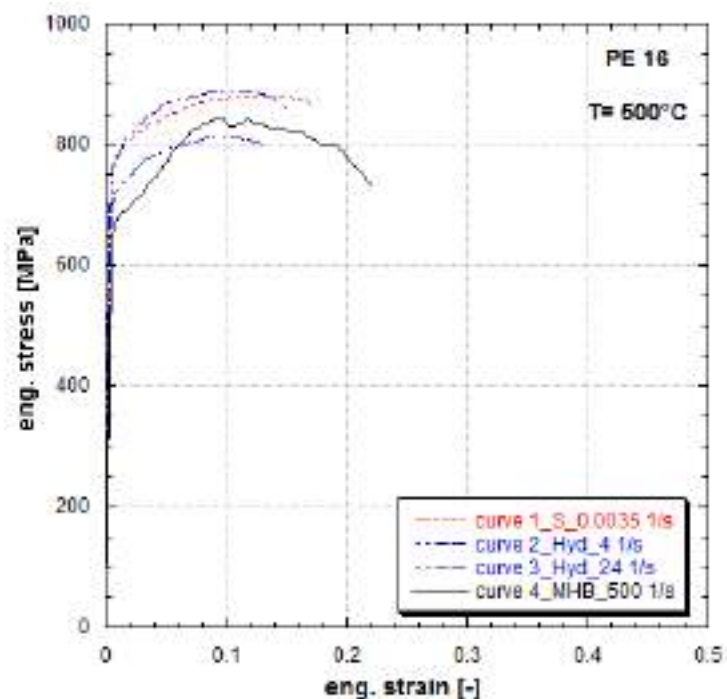


**Figure 7.34:** Engineering stress vs. strain curves for PE16 nimonic alloy thermally aged for 9864 hours in sodium tested at different strain-rates and 500°C (Albertini et al., 1987a).

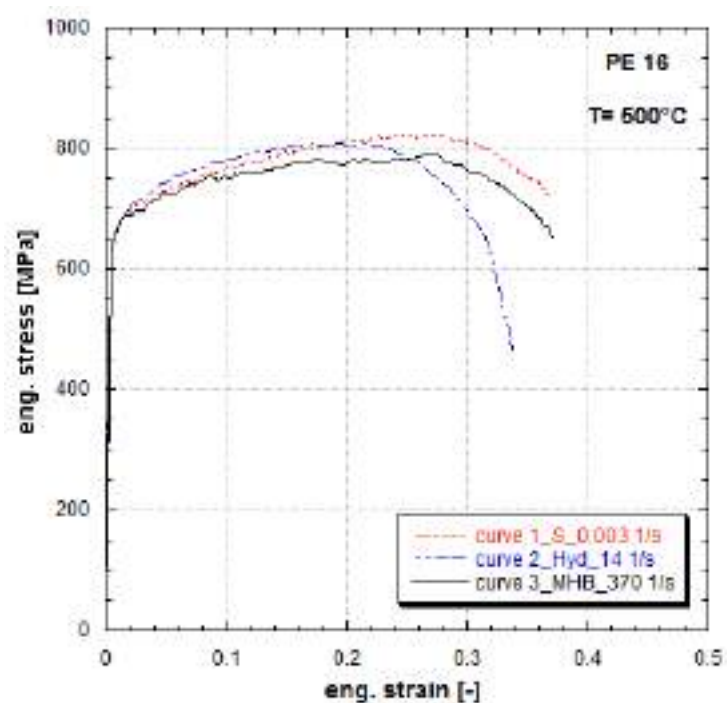


**Figure 7.35:** Engineering stress vs. strain curves for PE16 nimonic alloy as-received tested at different strain-rates and 500°C (Albertini et al., 1987a).

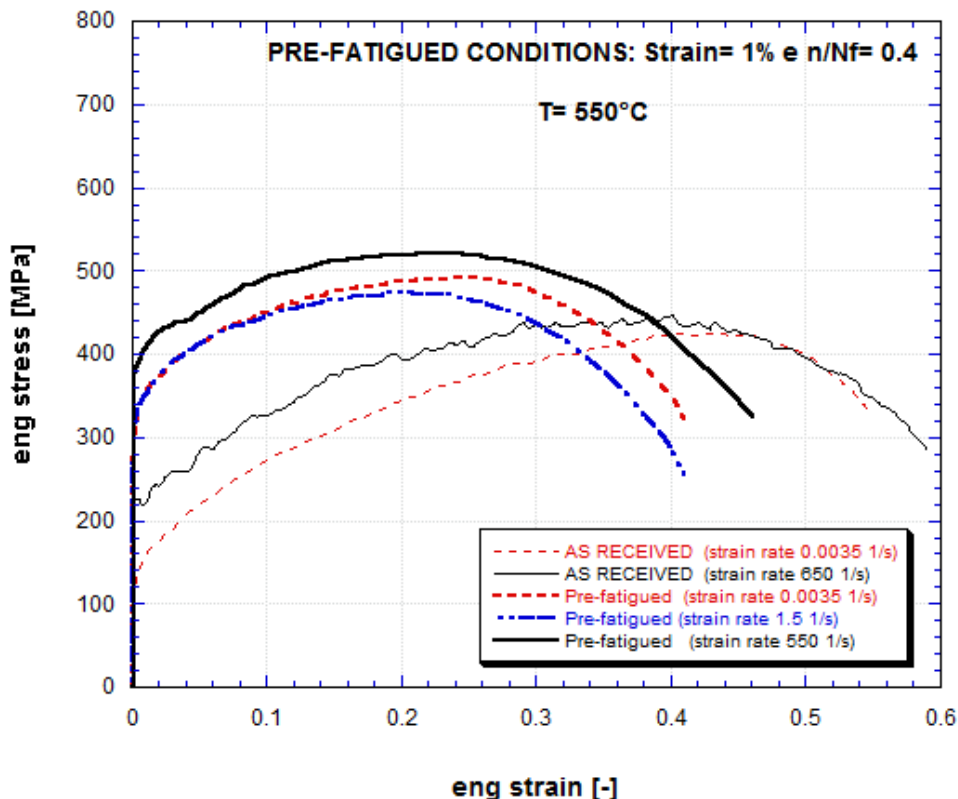


**Figure 7.36:** Enginnering stress vs. strain curves for AISI 316H as-received and prefatigued tested at different strain-rates and 550°C.

The pre-fatigued specimens were then irradiated by JRC at 2 dpa in the HFR reactor in Petten (The Netherlands) at the temperature of 550°C. The only pre-fatigued specimens and the pre-fatigued+irradiated specimens were then submitted to high strain-rate tension tests at high temperature (550°C). The detailed results of this large programme have been reported in (Albertini et al., 1988) for AISI 316H and in the present database from which some representative results are reported:

- The dynamic stress-strain curves of the only pre-fatigued AISI 316H (Fig. 7.36) show damage hardening , strain-rate hardening and reduction of ductility.
- The dynamic stress-strain curves of AISI 316H specimen previously submitted to superposition of low cycle fatigue and irradiation show (Figs. 7.37, 7.38, 7.39, 7.40) damage hardening, strain-rate softening and reduction of the uniform strain to about one third of that of the as-received material.

## 7.6 Effects of creep damage, high temperature and high strain-rate on AISI 316H

Specimens of AISI 316H have been submitted to creep tests in the following conditions:

- 300 MPa
- 550°C
- 400, 800, 1200 Hours (respectively 0.2, 0.4, 0.6 of the life time of 2000 hours).

Then these specimens have been tested at high strain-rate and at high temperature. The results are reported in (Albertini et al., 1989c, Albertini et al., 1990a, Albertini and Montagnani, 1990). Few representative results are reported in Figs. 7.41, 7.42, 7.43. From these figures we can observe that the dynamic stress-strain curves of the creep damaged specimens show damage hardening, strain-rate hardening, a marked reduction of uniform and fracture strain and marked instabilities along the flow curves.

## 7.7 Effects of welding, high temperature and high strain-rate on the austenitic stainless steel AISI 316H

The results of this investigation regarding the comparison of the dynamic stress-strain curves at high temperatures of AISI 316L, AISI 316H, AISI 304L in as-received conditions, in welded conditions and heat affected zone conditions are reported in (Albertini and Montagnani, 1978) from which the Figs. 7.44, 7.45, 7.46, 7.47, 7.48 7.49 regarding AISI 316H have been taken. From such figures it can be observed that the steel AISI 316H base

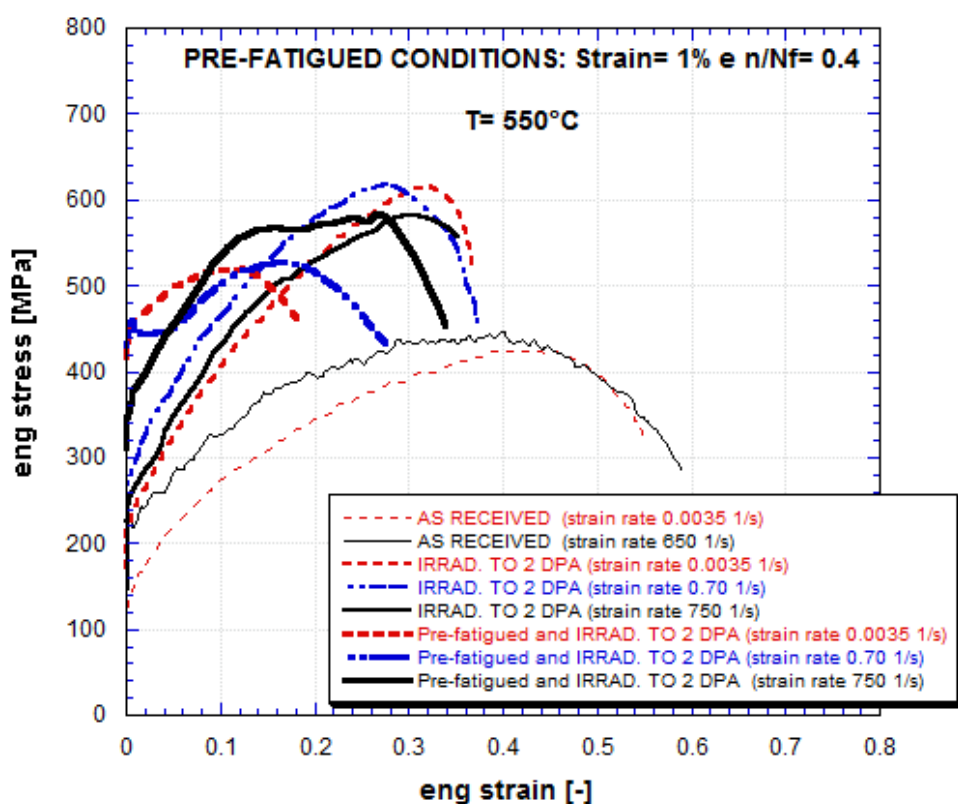


**Figure 7.37:** Engineering stress vs. strain curves for AISI 316H as-received, prefatigued and irradiated to 2.2 dpa tested at different strain-rates and 550°C.

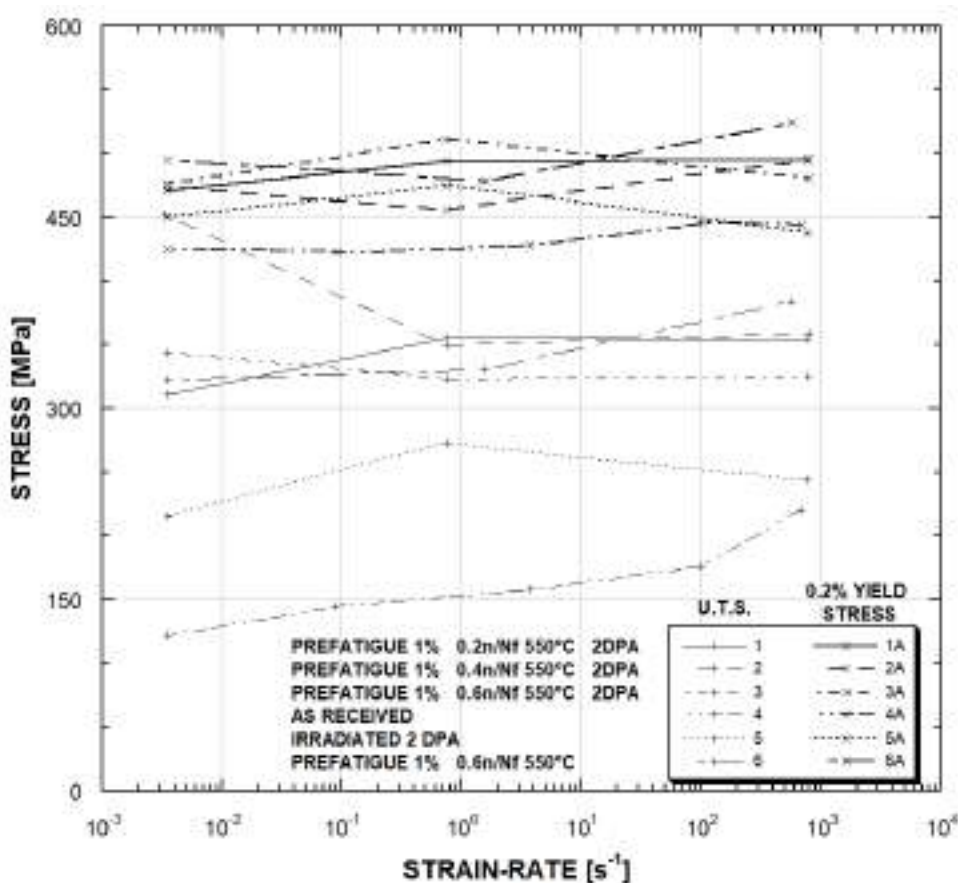


**Figure 7.38:** Engineering ultimate tensile strength vs. strain-rate, engineering 0.2% yield stress vs. strain-rate; AISI 316H stainless steel prefatigued with cycle strain range 1% and irradiated to 2.2 dpa (550°C).

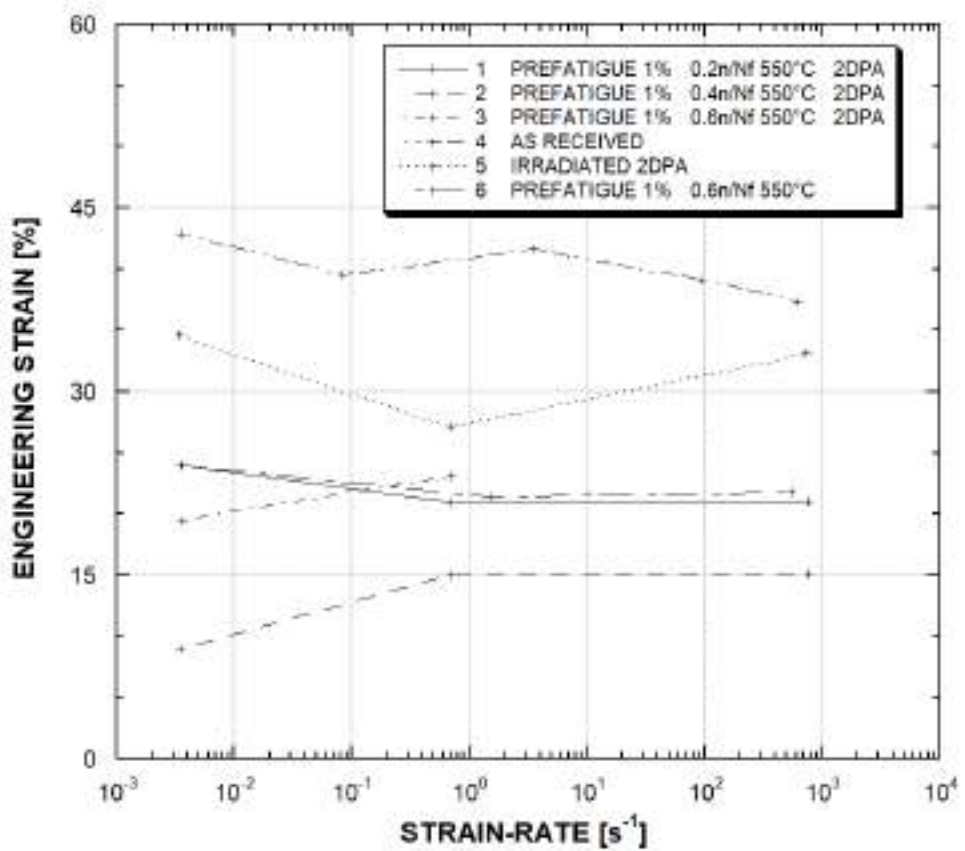


**Figure 7.39:** Uniform strain vs. strain-rate, AISI 316H stainless steel prefatigued with cycle strain range 1% and irradiated to 2.2 dpa (550°C).

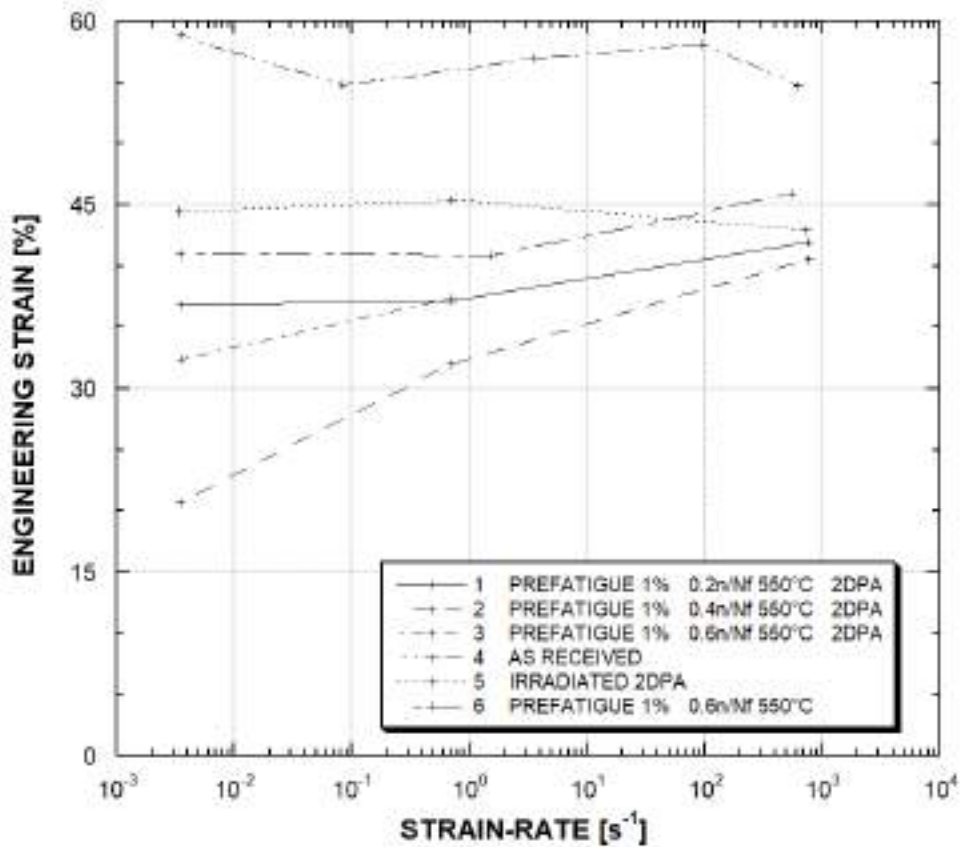


**Figure 7.40:** Fracture strain vs. strain-rate, AISI 316H stainless steel prefatigued with cycle strain range 1% and irradiated to 2.2 dpa (550°C).

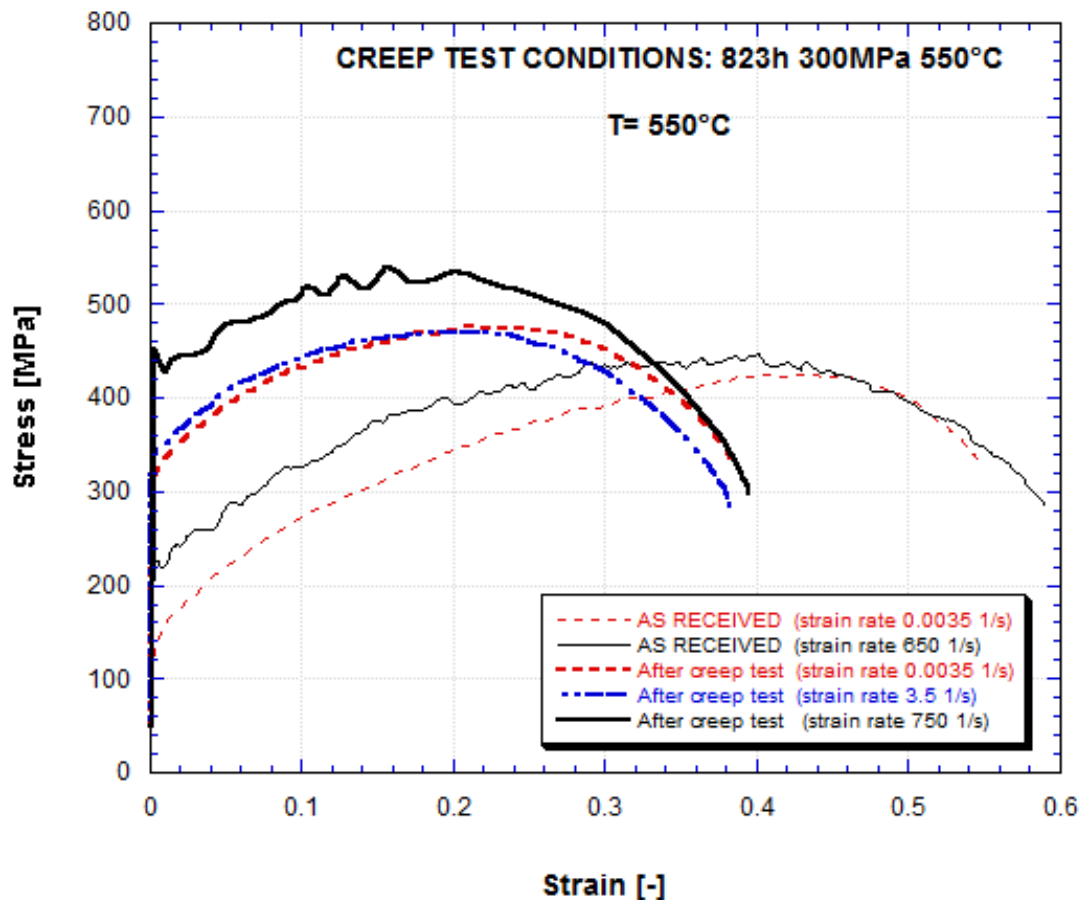


**Figure 7.41:** Engineering stress vs. strain curves for AISI 316H as-received and after creep test (550°C).

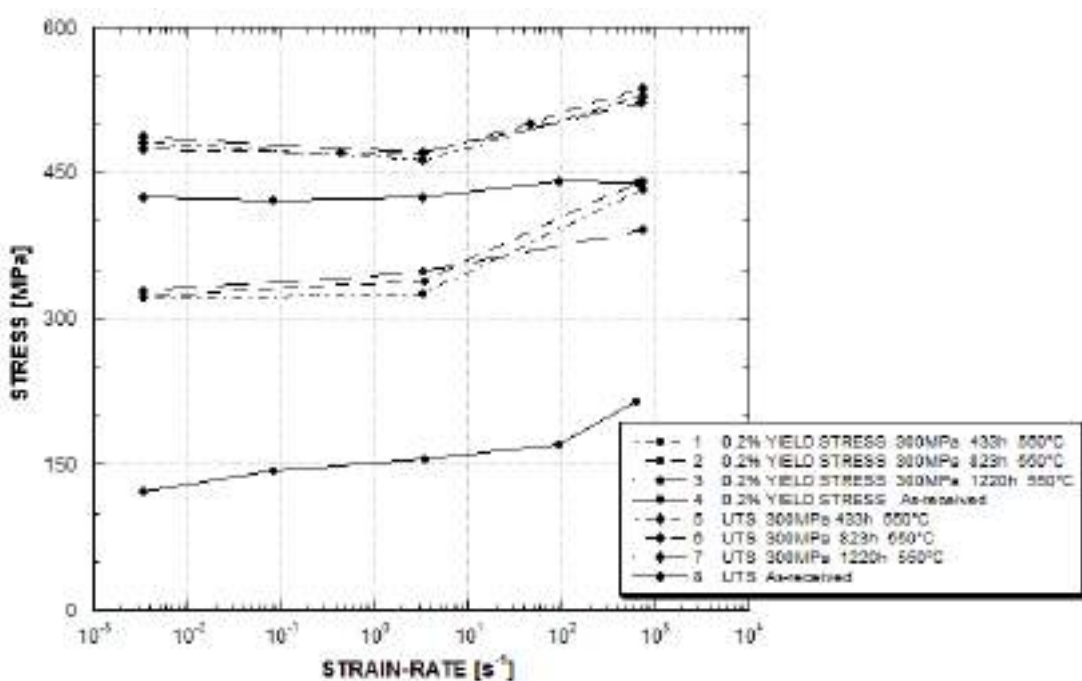


**Figure 7.42:** Engineering 0.2% yield stress and ultimate tensile strength of as-received and after creep test vs. strain-rate of AISI 316H stainless steel (550°C).

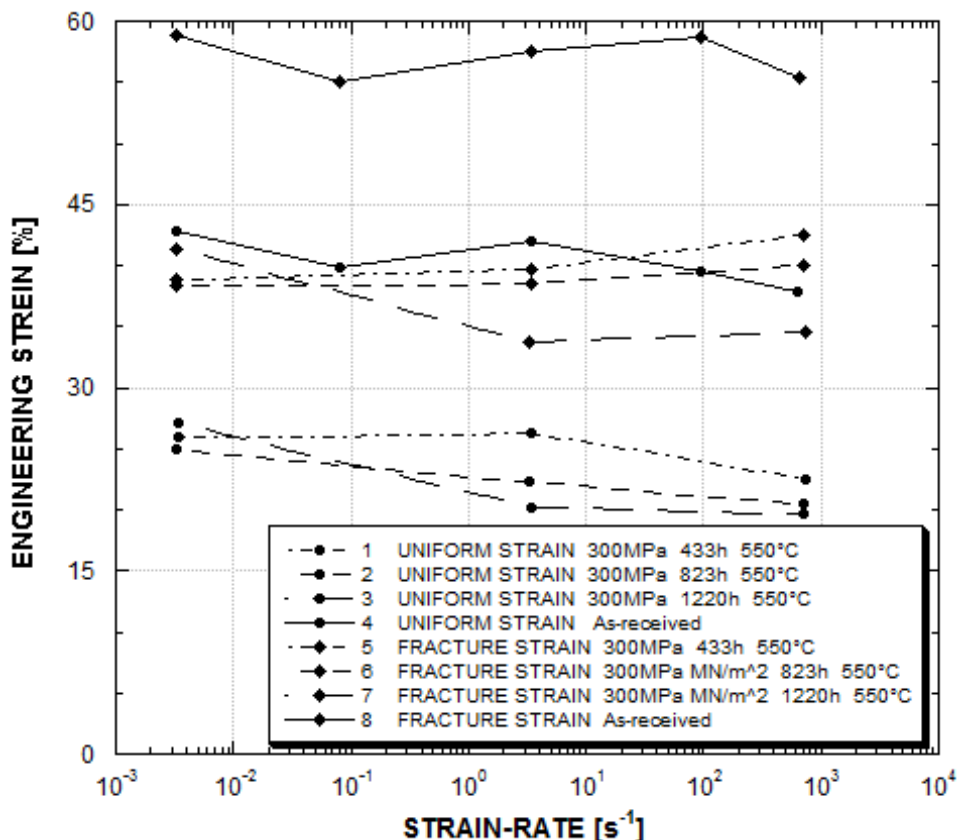


**Figure 7.43:** Engineering uniform strain and fracture strain of as-received and after creep test vs. strain-rate of AISI 316H stainless steel (550°C).

material, weld material and heat affected zone material, tested at 400°C, showed:

- very similar in strength and ductility quasi-static flow curves.
- a strain hardening and a strain-rate hardening behaviour for the dynamic flow curves of AISI 316H base material together with a marked reduction of uniform and fracture strain.
- a strain-rate softening and instabilities oscillations for the dynamic flow curves of AISI 316H weld and weld+heat affected zone materials.

## 7.8 Specimen size effects

The main conclusions of the large study, described in paragraph 6.5.1, of the specimen size effects on the quasi-static and dynamic stress-strain curves of austenitic and ferritic steels, including AISI 316, were the followings:

- the quasi-static and dynamic stress-strain curves of the studied austenitic and ferritic steels do not depend on the specimen size (cylindrical specimens of 3, 9 and 30mm diameter) when considering the uniform deformation phase preceding the necking of the flow curves, which means that the flow curves of the three specimen size are in good coincidence up to the point identifying the ultimate tensile strength and the uniform strain; size effect evidence on the flow curves arises during the necking phase.

## 7.9 Effects of strain-rate history on the stress-strain curves

The investigations on the effects of the strain rate history, reported below, have been published in (Eleiche et al., 1985, Albertini et al., 1989b, Albertini et al., 1985b) and only the most significant points of the testing methods and results will be reported here in some extent. The phenomena observed are characteristic of the dynamic stress-strain curves of the austenitic stainless steel, therefore important to be included in the related constitutive equations implemented in the numerical simulations aimed to explain what might be the response

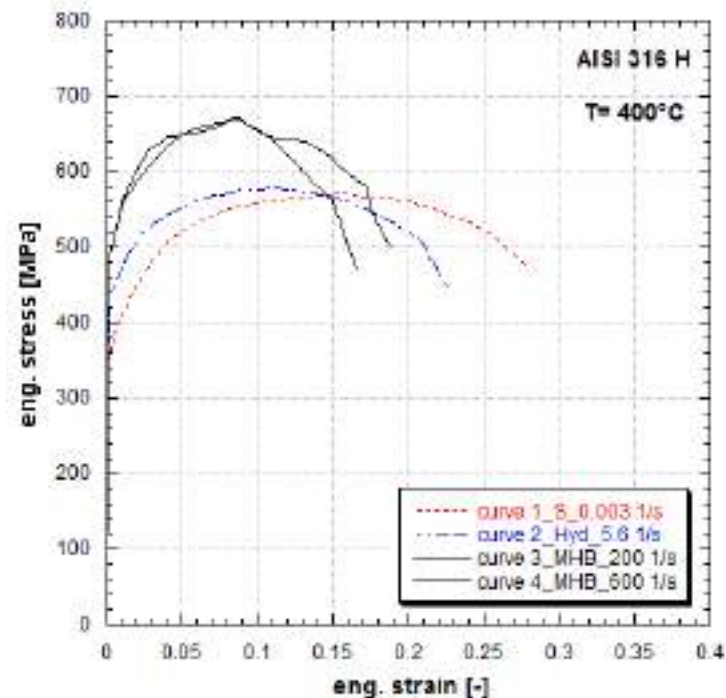


**Figure 7.44:** Engineering stress vs. strain curves for AISI 316H stainless steel base material (collaboration EURATOM-U.K.A.E.A.) tested at 400°C (Albertini and Montagnani, 1978).

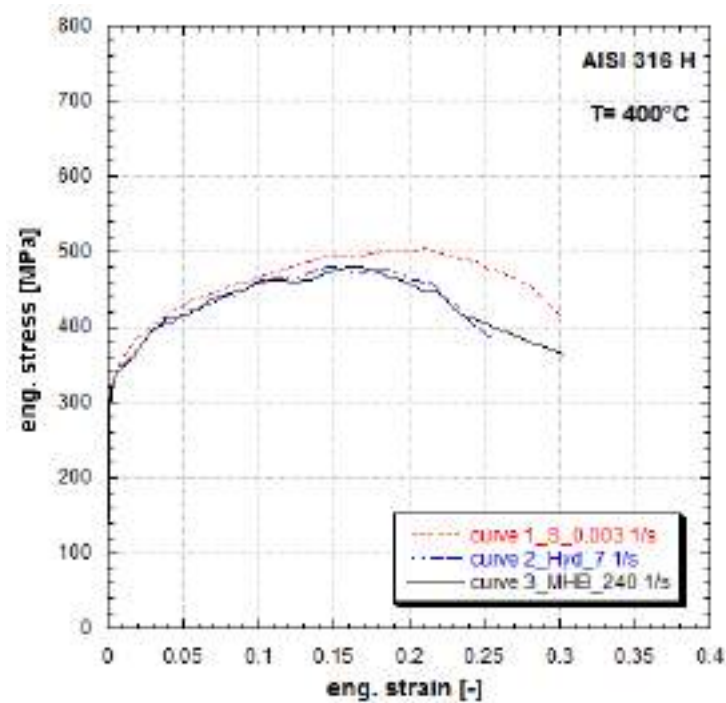


**Figure 7.45:** Engineering stress vs. strain curves for AISI 316H stainless steel weld+heat affected zone material tested at different strain-rates and 400°C (collaboration EURATOM-U.K.A.E.A.) (Albertini and Montagnani, 1978).

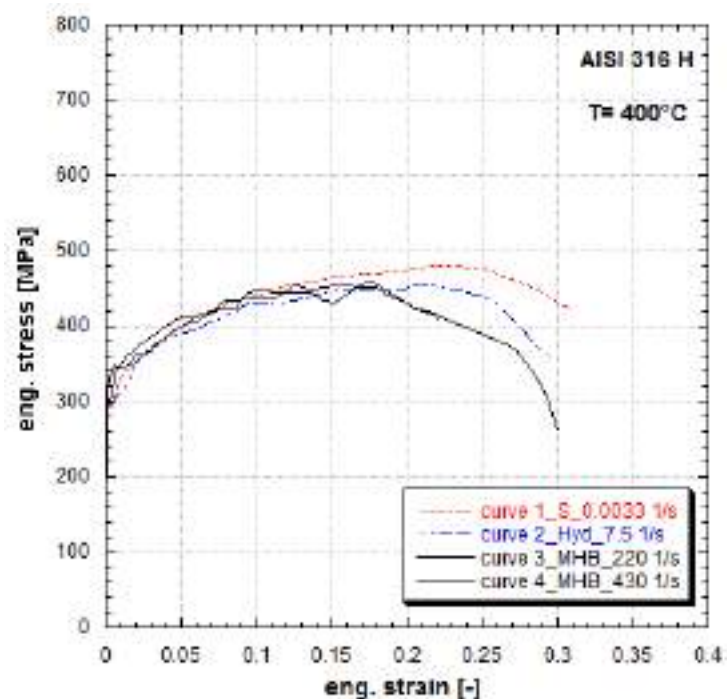


**Figure 7.46:** Engineering stress vs. strain curves for AISI 316H stainless steel weld material tested at different strain-rates and 400°C (collaboration EURATOM-U.K.A.E.A.) (Albertini and Montagnani, 1978).

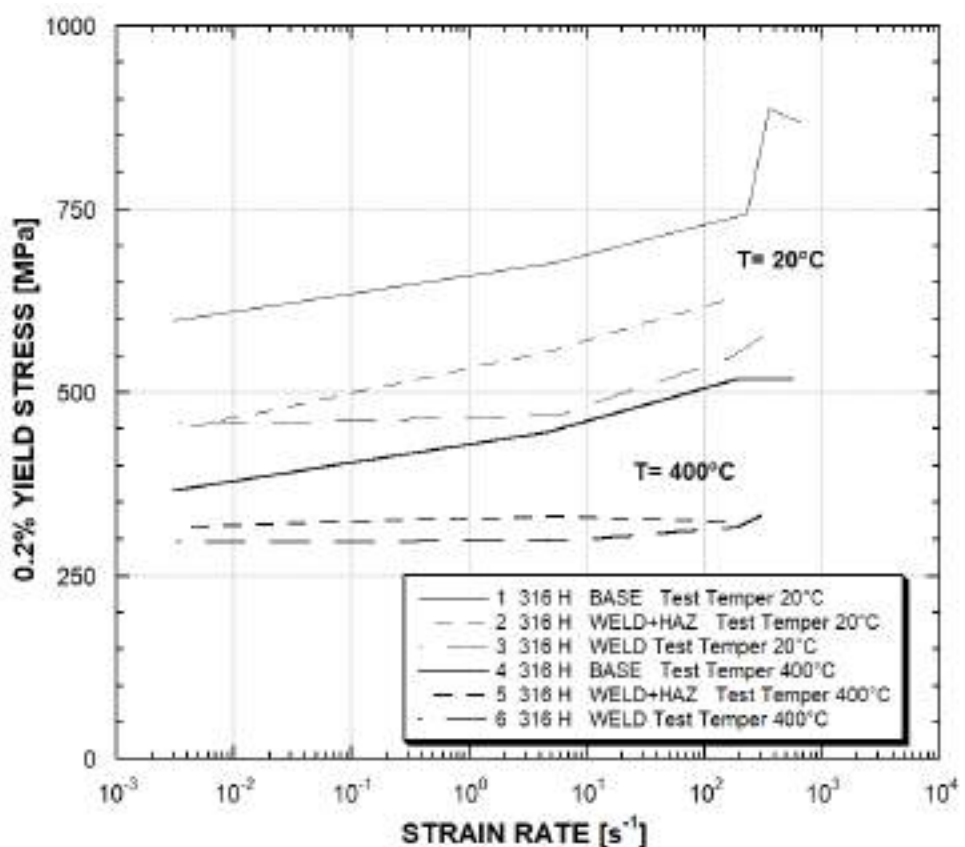


**Figure 7.47:** Effect of strain-rate on 0.2% yield stress of AISI 316H stainless steel base, weld, weld+heat affected zone materials tested at room temperature and 400°C (collaboration EURATOM-U.K.A.E.A.) (Albertini and Montagnani, 1978).

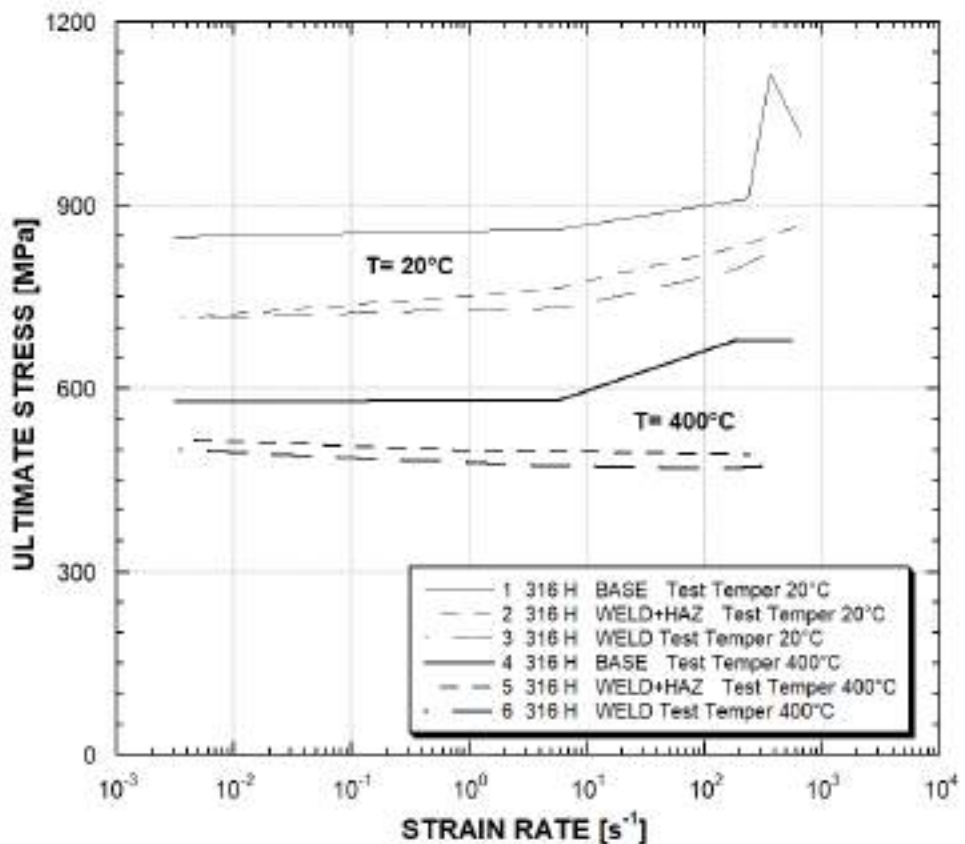


**Figure 7.48:** Effect of strain-rate on the ultimate tensile strength of AISI 316H stainless steel base, weld, weld+heat affected zone materials tested at room temperature and 400°C (collaboration EURATOM-U.K.A.E.A.) (Albertini and Montagnani, 1978).

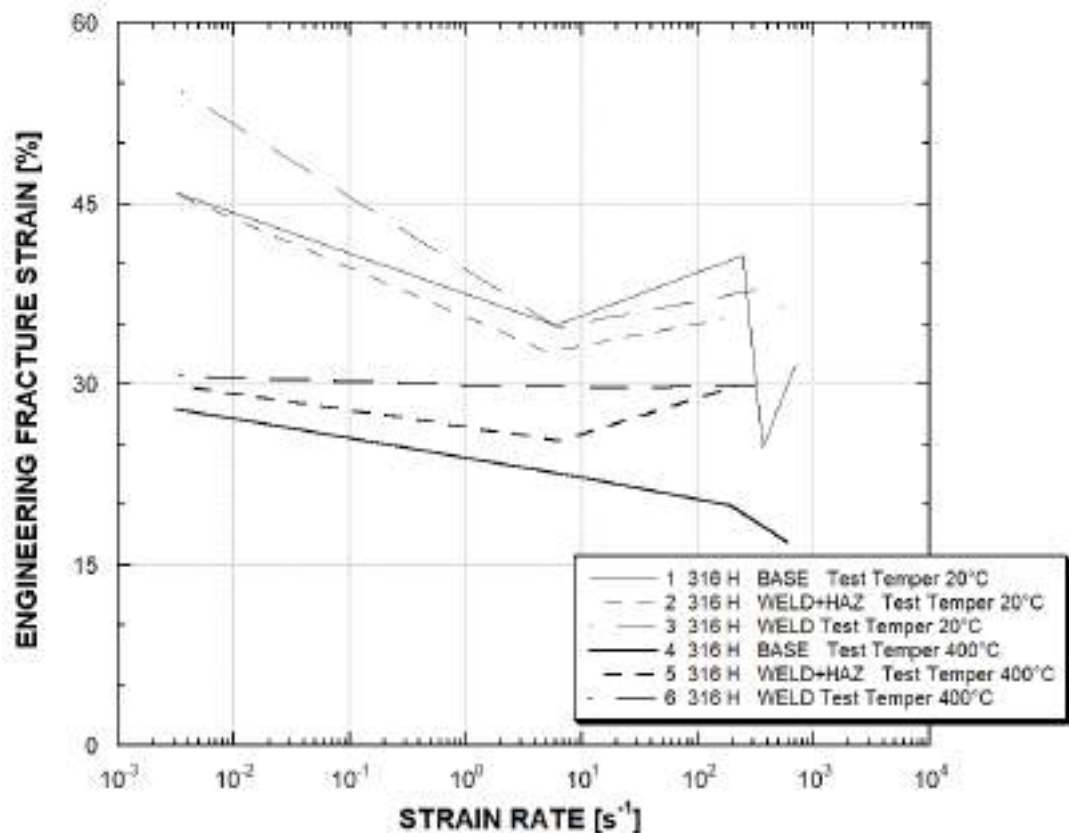


**Figure 7.49:** Effect of strain-rate on engineering fracture strain of AISI 316H stainless steel base, weld, weld+heat affected zone materials tested at room temperature and 400°C (collaboration EURATOM-U.K.A.E.A.) (Albertini and Montagnani, 1978).

of the containment structures under the loading histories illustrated below.

Attention is drawn to the fact that, adhering to the original presentation in the above publications, all stress-strain curves of this Section are denominated as "true". They have resulted by simply converting the engineering curves into true ones using the standard formulae. However this is correct up to the ultimate tensile strength, where necking sets in, and therefore the descending, last part of the curves should be discarded.

The strain-rate histories which have been considered try to represent those which could load the containment structures in case of a hypothetical explosive type accident in a nuclear reactor.

Two such typical histories are the following:

1. Deformation at high temperature and at quasi-static strain-rate interrupted at a certain strain value and reloading at high temperature and at high strain-rate until fracture. This would simulate what happens to the containment shell material when the internal pressure of the containment or of the primary vessel increases slowly, followed by an explosive loading, both loads being due to some malfunctions of the nuclear reactor. The strain-rate history has a jump from quasi-static to high strain-rate.
2. Deformation at high temperature and at high strain rate interrupted at a certain strain value and reloading at high temperature and at quasi-static strain rate until fracture. This would simulate what happens to the material in case of an internal explosive loading followed by a quasi-static increase of the internal pressure. The strain rate history has a jump from high to quasi-static strain rate.

The experiments to study the effects of strain-rate histories have been performed on the AISI 316H stainless steel using the specimens shown in Fig. 6.6. The tests to realize the above strain-rate history 1 have been performed by deforming the specimens, at quasi-static strain-rate, using a commercial tensile testing machine, interrupting the test at the desired value of strain and successively reloading the specimen at high strain-rate until fracture using the MHB.

The tests to realize the above strain-rate history 2 have been performed by deforming the specimen at high strain-rate, using the MHB described in chapter 6 section with the addition of supplementary bars, interrupting the test at the desired value of strain, and successively reloading the specimen to fracture at quasi-static strain-rate using a commercial tensile testing machine.

The MHB used for the interrupted dynamic tests was re-configured as follows:

- the length of the pre-tensioned bar was changed and fixed to the value needed to generate a tension incident pulse of the duration necessary to attain the desired strain value of the specimen;
- the transmitter bar was prolonged by an equal bar (of the same length and diameter) through a joint allowing the passage of a tension pulse but impeding the return into the transmitter bar of compression pulses (see Fig. 7.50 flip-flop connection); in this way the specimen is loaded only by the incident tension pulse avoiding the load effects of the undesired compression pulses reflected by the transmitter bar end;
- for the same reason as above the end of the pre-tensioned bar is in contact with a ballistic pendulum (Fig. 7.50) catching the compression wave travelling along the pre-tensioned bar, thus avoiding the return of the reflection of such wave to the specimen.

The addition of the above two supplementary bars permits to deform the specimen under the action of a tension pulse well-known in duration and amplitude. The record of Fig. 7.51 shows that no reflected pulses from the bar ends arrive to the specimen.

The presence of dynamic softening and strain ageing effects has first been investigated with tests conducted exclusively under static or dynamic strain-rate (no strain-rate jumping). In Figs. 7.52 and 7.53 the stress-strain curves of AISI 316H are shown, obtained by monotonic loading and repeated loading both at quasi-static and high strain-rate, respectively, at ambient temperature and at 550°C. The effects of thermal softening due to adiabatic deformation conditions can be observed in Fig. 7.52 by comparing the monotonic dynamic curve B with the interrupted dynamic curves, where, for a given total strain, the monotonic flow curve is generally lower than the interrupted flow curve. This effect decreases with increasing temperature as shown in Fig. 7.53 for the curves at 550°C.

The results obtained at ambient and high temperatures ranging from 100 to 650°C follow next for the above described strain-rate histories:

1. pre-straining at quasi-static strain-rate, unloading, then continue re-straining at high strain-rate up to fracture;
2. pre-straining at high strain-rate, unloading, then continue re-straining at quasi-static strain-rate to fracture.

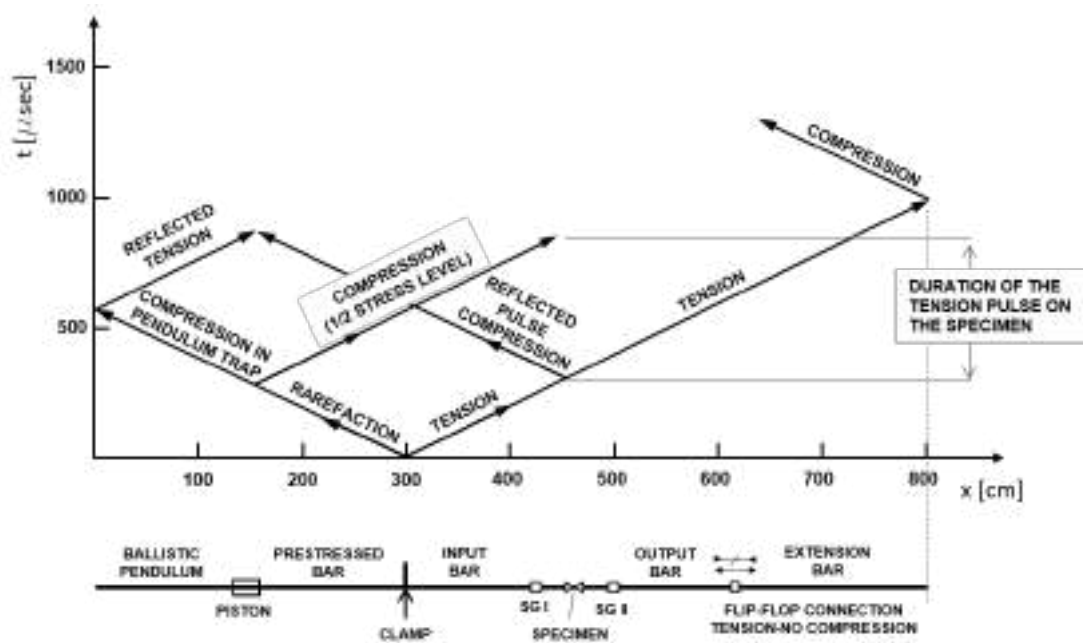


**Figure 7.50:** Wave transmission and reflection diagram along the Hopkinson bar, reconfigured with the addition of an extension bar and a ballistic pendulum.

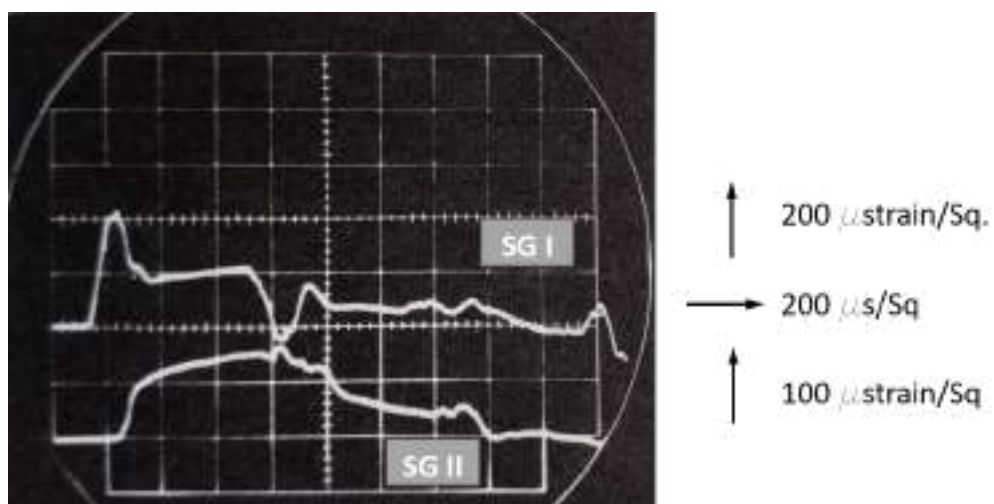


**Figure 7.51:** Oscilloscope traces of the records of test performed with the Hopkinson bar, re-configured with the addition of a bar as a ballistic pendulum upstream (on the pre-tensioned bar) and of an extension bar downstream (on the transmitter bar) (Albertini et al., 1985b).

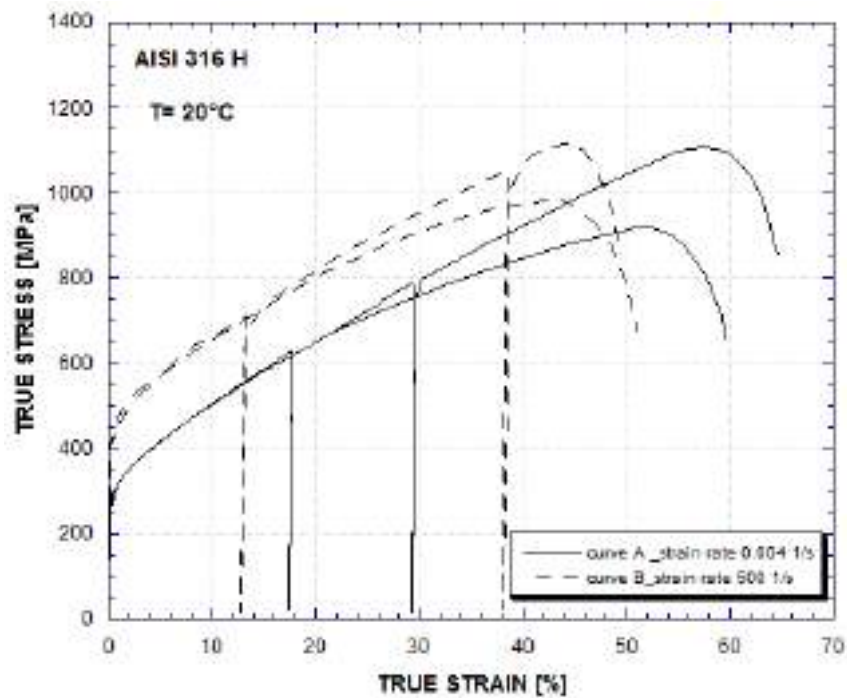


**Figure 7.52:** True stress vs. true strain curves of AISI 316H for interrupted and monotonic quasi-static ( $0.004\text{ s}^{-1}$ ) and dynamic ( $500\text{s}^{-1}$ ) loading at  $20^\circ\text{C}$  (Albertini et al., 1985b).

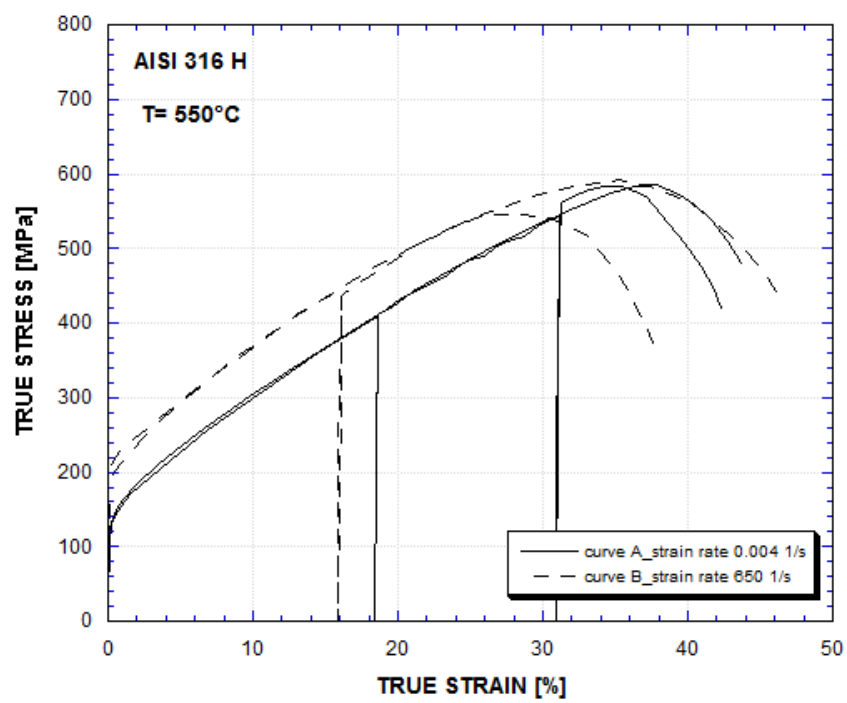


**Figure 7.53:** True stress vs. true strain curves of AISI 316H for interrupted and monotonic quasi-static ( $0.004\text{ s}^{-1}$ ) and dynamic ( $500\text{s}^{-1}$ ) loading at  $550^\circ\text{C}$  (Albertini et al., 1985b).

These strain-rate jump results are presented in Figs. 7.54 to 7.65. The dynamic flow curves of the interrupted strain-rate jump tests from quasi-static to dynamic have been corrected to isothermal dynamic flow curves following the procedure described in (Albertini et al., 1989b). On each of the diagrams shown in Fig. 7.54 to 7.65, the curves A and B represent the stress-strain relationships obtained by monotonic tensile tests to fracture at quasi-static and high strain-rate, respectively. The other curves on these diagrams represent the stress-strain relationships obtained by interrupting the dynamic (or the quasi-static) tensile tests at different strain levels, and then continuing them with a quasi-static (or dynamic) strain rate. Each monotonic curve in these figures is the average of results from 3 to 4 tests, while the other curves are the result of a single test for each value of prestrain. The monotonic flow curves A and B from ambient temperature to 550°C show an increase of the flow stress at a given strain with increasing strain-rate, while at 650°C at large strains strain-rate softening appears, probably due to the dynamic strain ageing revealed by the serrations on the quasi-static monotonic flow curve.

The results of quasi-static to dynamic strain-rate jump (Figs. 7.54 to 7.58) show that, at all testing temperatures, two types of behaviour can be distinguished:

- For pre-strains less than 0.10, the dynamic reloading curve is characterised by a well-defined yield point whose level is higher than the maximum reached in quasi-static pre-straining, but which is very close to the flow stress level reached at the same strain-rate in a test conducted exclusively at the dynamic rate.
- For pre-strains larger than 0.10, the yield stress levels reached on dynamic reloading are even higher than the corresponding levels at the same strains on dynamic monotonic curves B. At the high strains and at elevated temperatures, the situation becomes much more complicated due to the occurrence of Dynamic Strain Ageing with accompanying changes in dislocation cell structures and sub-grain formations, as suggested in (Michel et al., 1973).

The general trend of the dynamic to quasi-static strain-rate jump behaviour is complex and presumably governed, as in many other metals (Baird, 1971), by strain ageing phenomena, which depend on dynamic pre-strain and on temperature. The dependence on dynamic pre-strain is shown at the ambient temperature (Fig. 7.59) where an increasing static strain ageing (ageing after straining) may be observed with increasing dynamic pre-strain. The same dependence is also observed at 300, 400, and 550°C (Figs. 7.62, 7.63, 7.64). Furthermore, the quasi-static reloading curves at 400, 550 and 650°C (Figs. 7.63, 7.64, 7.65) also show phenomena of dynamic strain ageing (ageing during straining) manifested by serrations along the flow curves. At 200 and 650°C (Figs. 7.61 and 7.65), overageing is also exhibited where the quasi-static reloading curves lie below the monotonic ones. It is interesting to note that the same strain ageing phenomena were also observed on the dynamic reloading curves obtained at 300, 400, 550 and 650°C after quasi-static prestraining (Figs. 7.55, 7.56, 7.57, and 7.58).

The complicated physical and micro-structural aspects of strain ageing have been discussed in detail by other investigators (Michel et al., 1973, Baird, 1971). The present experimental results put in evidence that the static strain ageing effects are present in the quasi-static and in the dynamic reloading flow curves obtained after pre-straining at a different strain-rate, but are practically absent in the reloading flow curves obtained after pre-straining at the same strain-rate (Figs. 7.52 and 7.53). This fact would reflect the difference in the governing deformation modes and the microstructures developed during high and low strain-rate pre-straining. It is the passage from one deformation mode to the other which provokes the static and dynamic strain ageing instabilities. Preliminary scanning electron microscopy observations of the specimen fracture surfaces seem to confirm this interpretation. When analysed, at all temperatures the fracture surfaces which were full of holes and dimples indicative of ductile fracture, revealed:

- A more uniform distribution of hole diameters in specimens subjected to monotonic loading than in those subjected to interrupted strain-rate jump loading
- A larger average value of the distribution of the holes in specimens subjected to monotonic loading than in those submitted to interrupted strain-rate jump loading
- In specimen broken at quasi-static strain-rate, higher values of dynamic pre-strain causes a decrease of the average value of the distribution of the hole diameters.

From the phenomenological point of view, strain and strain-rate histories have an important effect on the stress-strain relationships, which becomes greater at large pre-strains and higher temperatures. In particular, the results presented here permit to affirm that at large values of total strain and at high temperatures strain ageing phenomena must be accurately modelled and incorporated in the constitutive equations used for numerical simulation of nuclear reactor accidents. This can be achieved with the help of microstructural observations on a fine scale during and /or after testing, since current physical interpretations of such phenomena call for interactions between dislocations and interstitials of various nature and with precipitating particles (Michel et al.,

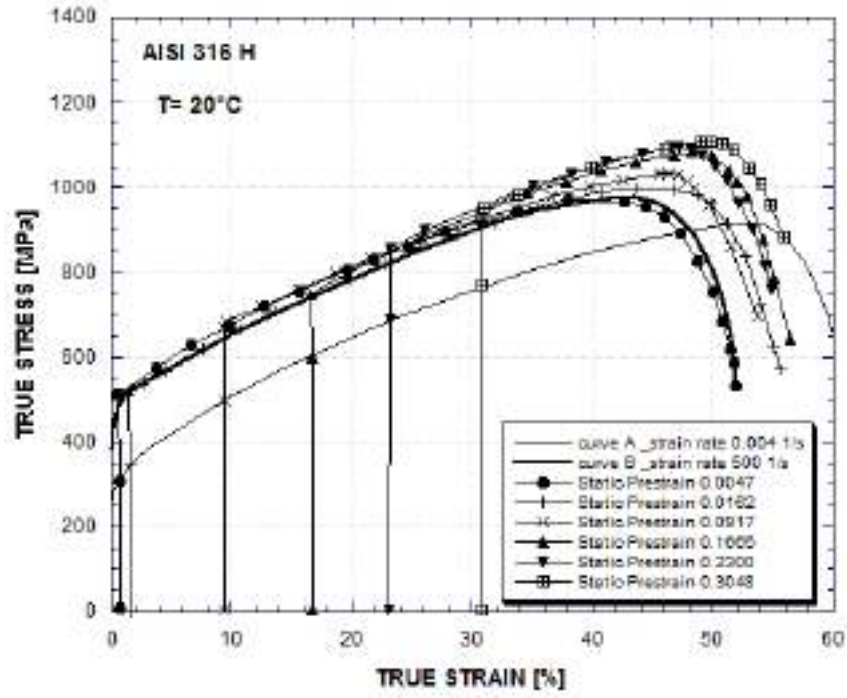


**Figure 7.54:** Monotonic and interrupted quasi-static to dynamic jump true stress vs. true strain curves at 20°C (Albertini et al., 1985b).

1973, Baird, 1971).

From the foregoing, it appears that the dynamic tensile loading and its history introduces in the deformation process of steels, in addition to the instabilities at yield and necking, new ones induced by strain ageing and thermal-softening, and characterised by strain localisation which can rapidly lead to fracture. Such tendency to early localisation can be observed on the Figs. 7.54 to 7.65 where uniform deformation and fracture strains of the flow curves from strain-rate jump tests have values lower than those from the monotonic flow curves. These phenomena, which are usually exhibited by material specimens tested in the laboratory, could also appear in structures due to uncontrolled stress wave propagation caused by accidents. Thus, dynamic deformation appears like a very unstable process necessitating thorough understanding and careful control in order to avoid premature fracture. In fact, the nil strain-rate sensitivity shown by the flow curves at the highest temperatures is due to the adiabatic thermal softening at the dynamic strain-rate and to the dynamic strain ageing at the quasi-static one, both phenomena leading to strain concentrations and fracture.

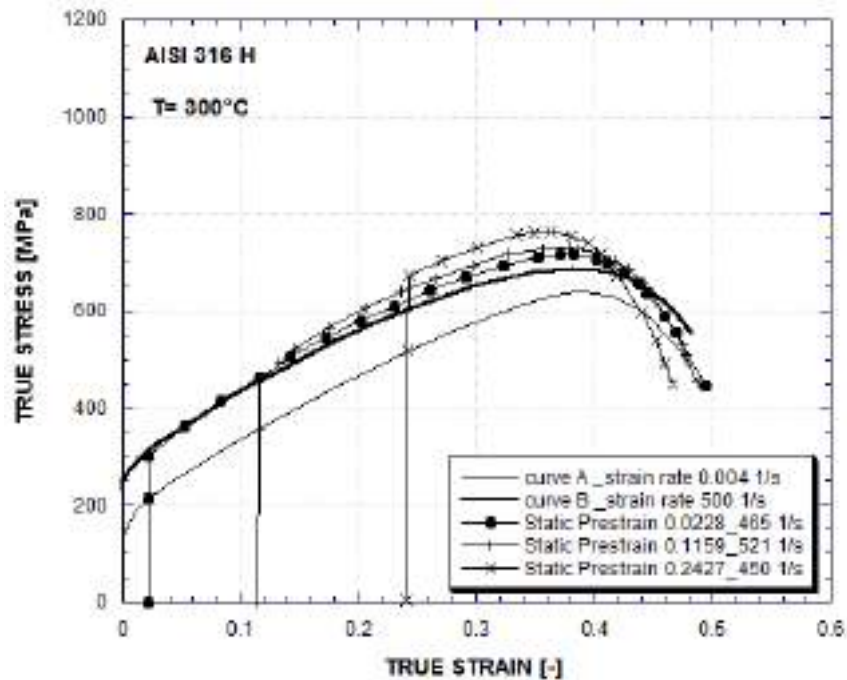


**Figure 7.55:** Monotonic and interrupted quasi-static to dynamic jump true stress vs. true strain curves at 300°C (Albertini et al., 1985b).

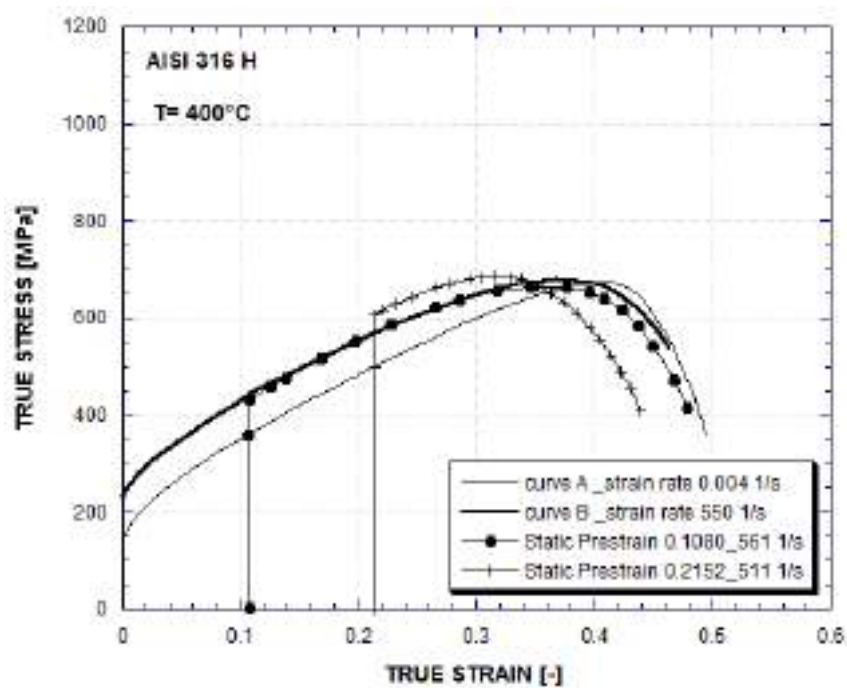


**Figure 7.56:** Monotonic and interrupted quasi-static to dynamic jump true stress vs. true strain curves at 400°C (Albertini et al., 1985b).

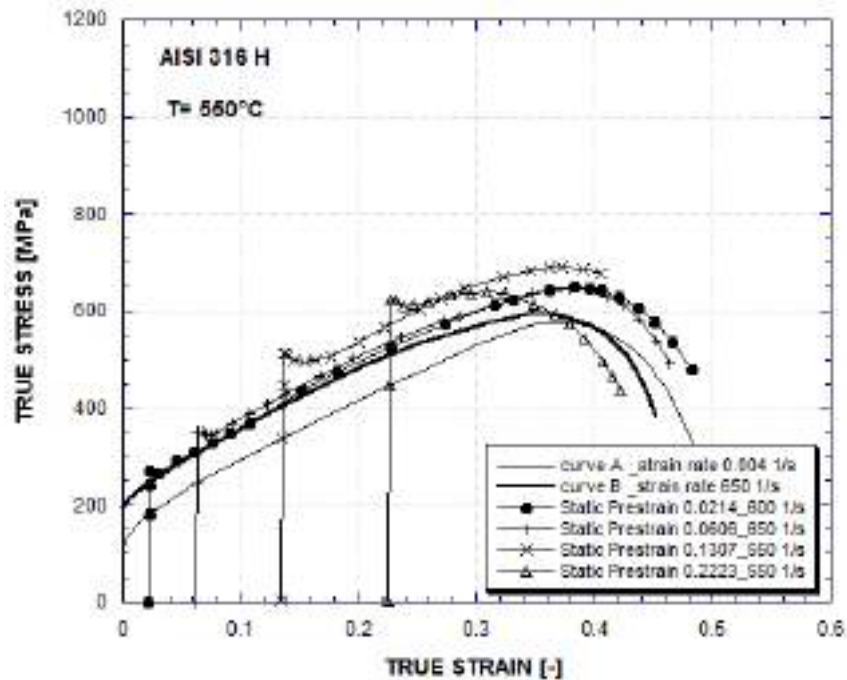


**Figure 7.57:** Monotonic and interrupted quasi-static to dynamic jump true stress vs. true strain curves at 550°C (Albertini et al., 1985b).

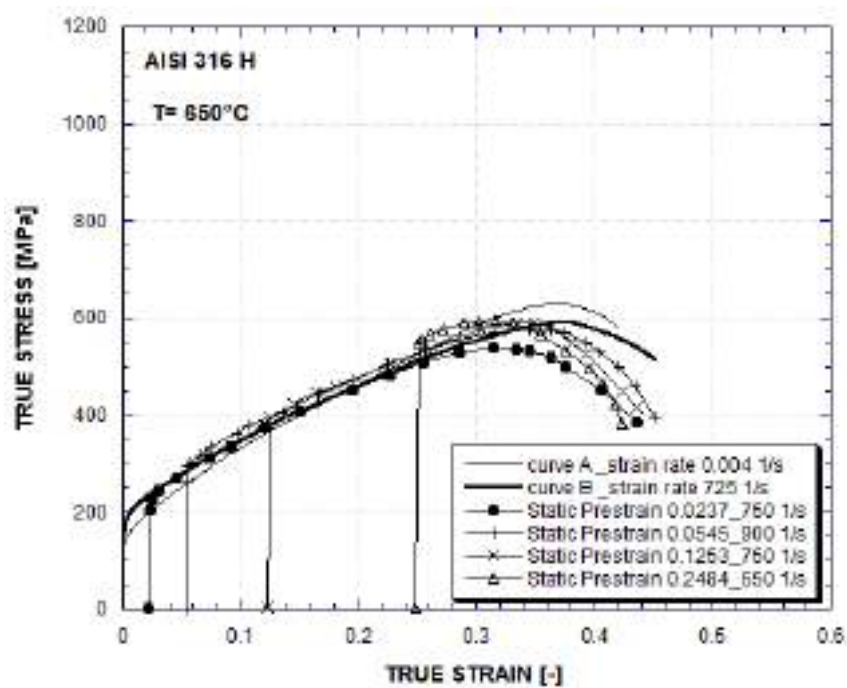


**Figure 7.58:** Monotonic and interrupted quasi-static to dynamic jump true stress vs. true strain curves at 650°C (Albertini et al., 1985b).

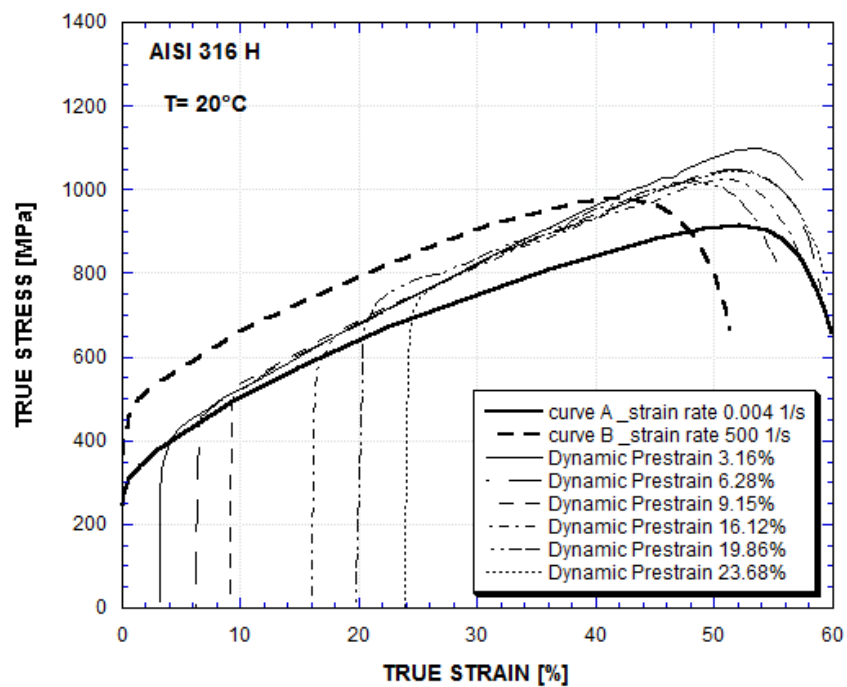


**Figure 7.59:** Monotonic and interrupted dynamic to quasi-static jump true stress vs. true strain curves at 20°C (Albertini et al., 1985b).

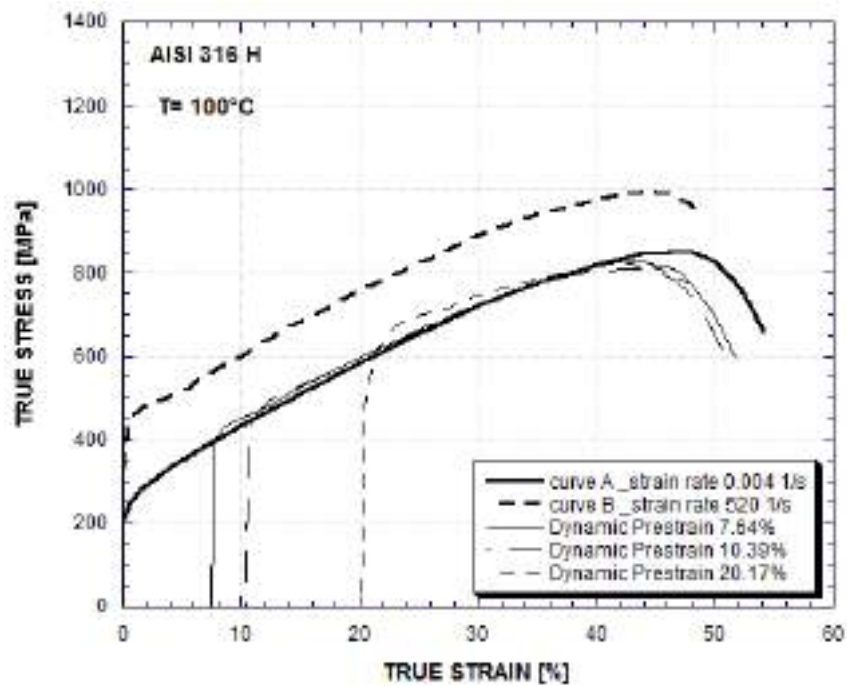


**Figure 7.60:** Monotonic and interrupted dynamic to quasi-static jump true stress vs. true strain curves at 100°C (Albertini et al., 1985b).

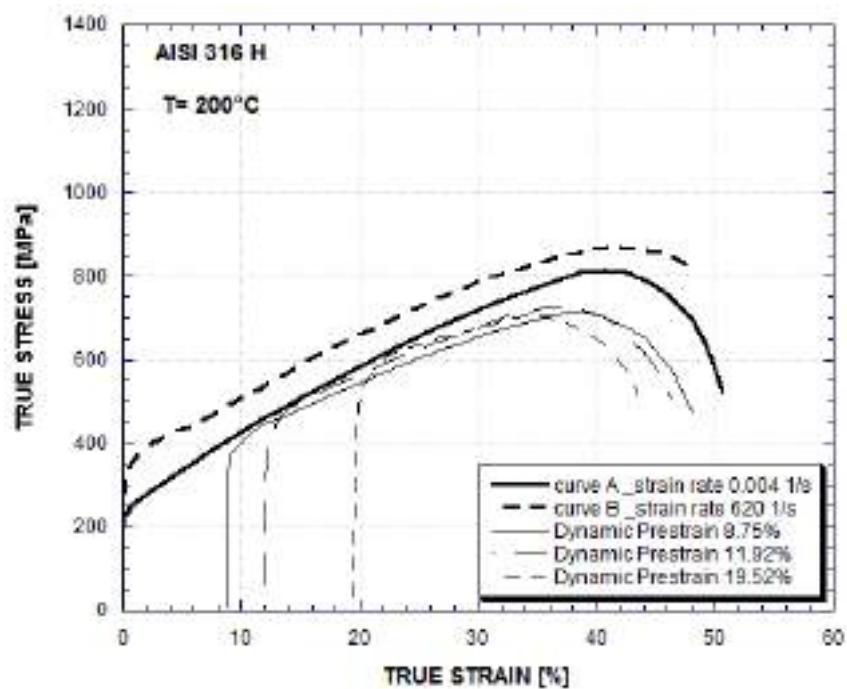


**Figure 7.61:** Monotonic and interrupted dynamic to quasi-static jump true stress vs. true strain curves at 200°C (Albertini et al., 1985b).

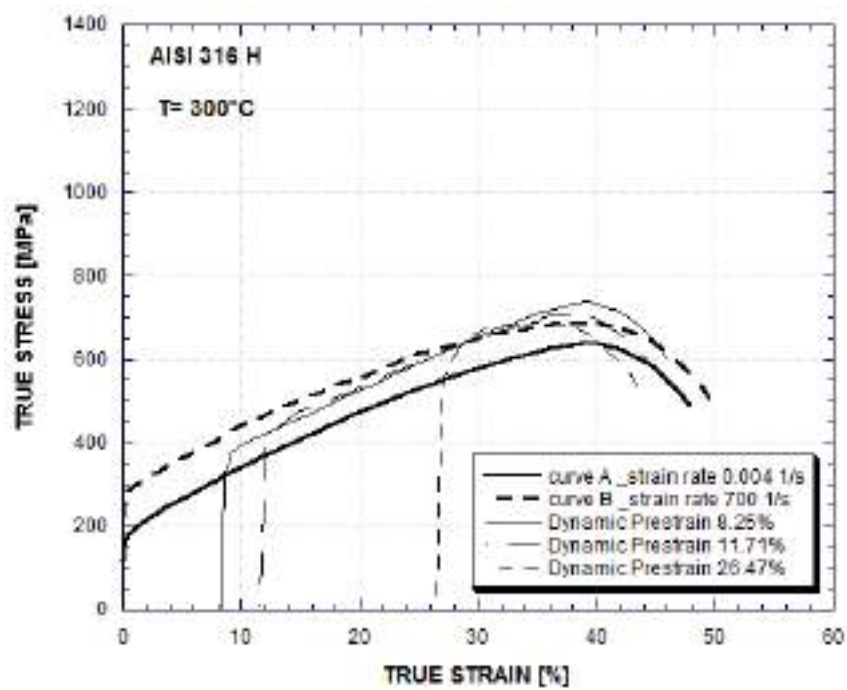


**Figure 7.62:** Monotonic and interrupted dynamic to quasi-static jump true stress vs. true strain curves at 300°C (Albertini et al., 1985b).

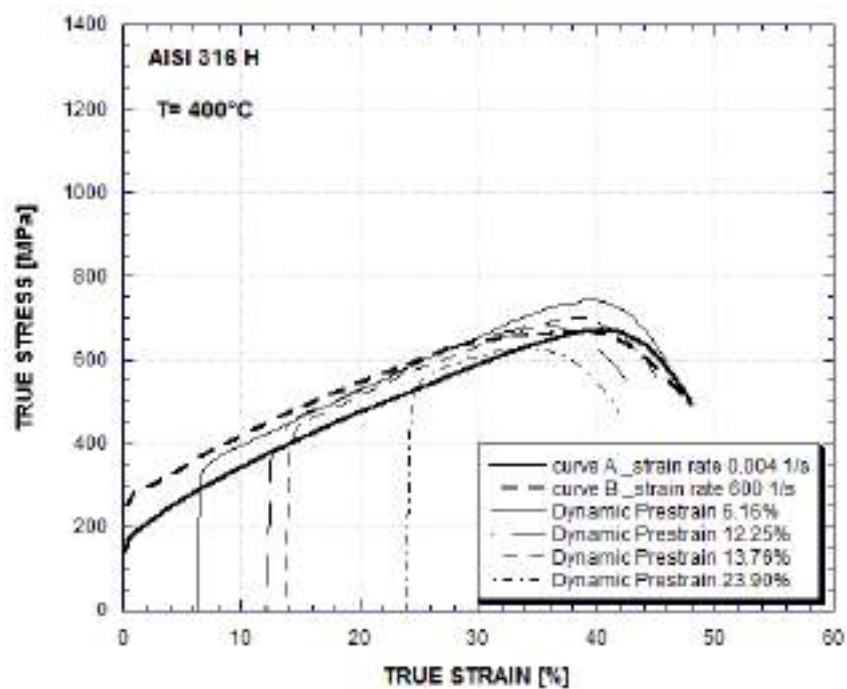


**Figure 7.63:** Monotonic and interrupted dynamic to quasi-static jump true stress vs. true strain curves at 400°C (Albertini et al., 1985b).

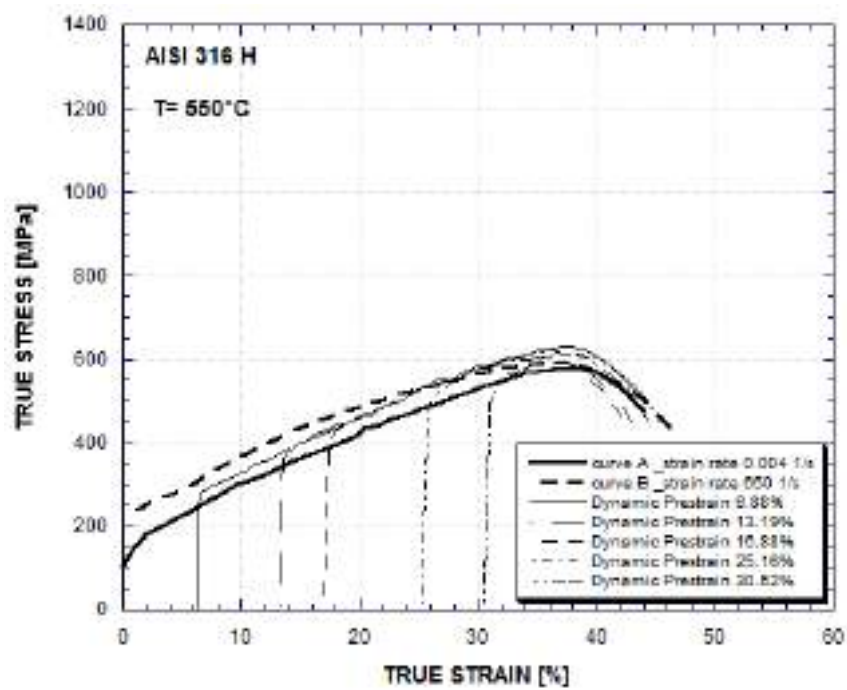


**Figure 7.64:** Monotonic and interrupted dynamic to quasi-static jump true stress vs. true strain curves at 550°C (Albertini et al., 1985b).

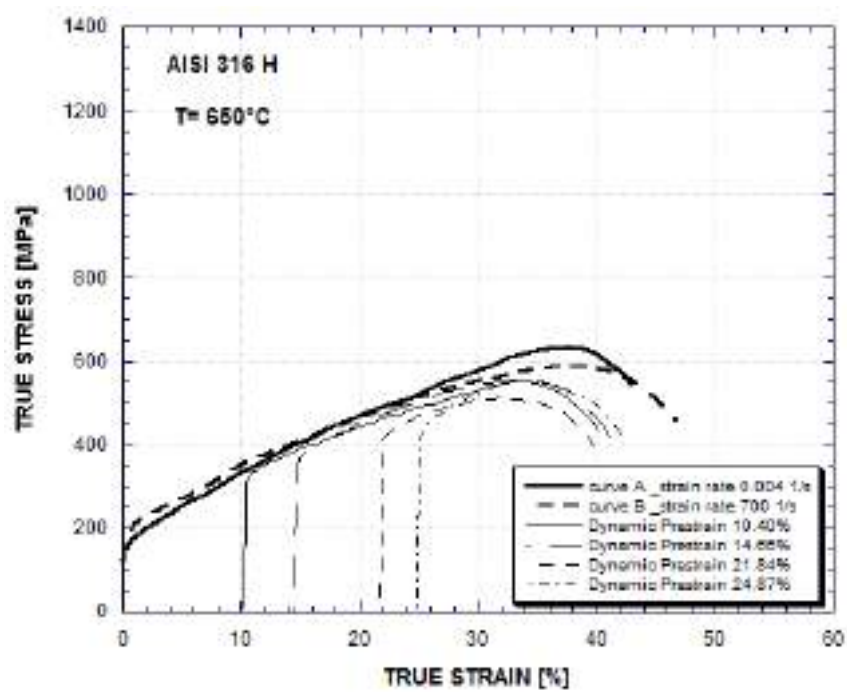


**Figure 7.65:** Monotonic and interrupted dynamic to quasi-static jump true stress vs. true strain curves at 650°C (Albertini et al., 1985b).

## **8 New material database and assessment of nuclear reactor structures in case of severe accidents**

### **8.1 Discussion**

The stress-strain curves in uniaxial tension of five austenitic stainless steels (AISI 316L, AISI 316H, AISI 304L, AISI 321, X6CrNiNb1810), two ferritic steels (ASME 537, 20MnMoNi55), the Nimonic alloy PE16, all materials used for the construction of nuclear fission reactor structures, have been reviewed. The materials have been tested in the as-received and pre-damaged conditions, at room temperature, at the high service temperatures of reactor structures, at the high strain-rates up to  $10^3 \text{ s}^{-1}$  and strain-rate histories imposed by impact loading in case of severe accidents. As will be seen in Annex 1, the database is richer and includes substantially more materials, not necessarily exhaustively tested.

For all the studied austenitic stainless steels in as-received conditions a common behaviour at high strain-rate and at room temperature has been found where the dynamic stress-strain curves show strain hardening, strain-rate hardening and a reduction of uniform and fracture strains. Despite the reduction of ductility the deformation energy (and therefore the capability of absorbing the energy delivered by the accident) of such steels remains nearly constant at each strain-rate because of the compensation of ductility loss through the strain-rate hardening.

The dynamic stress-strain curves of the studied ferritic steels in as-received conditions show strain hardening, strain-rate hardening and no reduction of uniform and fracture strains, which implies a slight increase of the deformation energy with increasing strain-rate. Therefore in case of severe accidents at room temperature with deformation of the reactor structures at high strain-rate the studied as-received austenitic and ferritic steels maintain the same capability of absorbing the accident energy both at low and high strain-rate, with a slightly better performance in that sense of the ferritic steels. Furthermore the strain hardening and the strain-rate hardening of these materials is a good premise for a stable response of the structures to severe accident dynamic conditions because the impulsive load imposes increasing particle speed to the structure with the consequence of increasing also the resistance of the material and then of the structure.

All the studied austenitic and ferritic steels in the as-received conditions the stress-strain curves in the temperature range from 300 to  $650^\circ\text{C}$  show a phenomenon of strain-rate softening, which means a reduction of the stress at a given strain at the strain-rates higher than the quasi-static strain-rate. For the austenitic stainless steels in the above temperature range the strain-rate softening is also accompanied by a reduction of uniform and fracture strain and by the appearance of instabilities along the flow curves. This behaviour can be attributed to:

- the increase of temperature of the specimen due to the adiabatic deformation conditions created by the dynamic loading, which softens the dynamic flow curve and fosters early localisations giving rise to instabilities of the flow curve; such instabilities are enhanced by quasi-static pre-strain of the steel provoking strain ageing phenomena.
- the presence at low strain-rate (and not at high strain-rate) of dynamic strain ageing phenomena which harden the quasi-static flow curve.

As discussed in Chapter 7 section, it is important to ascertain the causes of strain-rate softening and of the instabilities of the dynamic flow curves in view of both the choice of the material giving the best dynamic response and of the constitutive models better describing the experimentally observed material behaviour. It is also important to underline the excellent performance of the Modified Hopkinson Bar in revealing and measuring with high reliability all physical phenomena intervening during plastic flow in dynamics, like upper and lower initial yield, strain ageing instabilities, necking.

The stress-strain curves at high strain-rate and at high temperature of austenitic stainless steels show often initial yield oscillations, e.g. as a consequence of the complex strain-rate histories, which could occur in case of severe accidents (see Fig. 7.57). Initial yield oscillations at high strain-rate for AISI 304L steel are reported in (Dodd et al., 1973). There are also shown, in Figs. 7.8 and 7.6 7.7, respectively for the ferritic steels 20MnMoNi55 and ASME 537. The physical nature of these oscillations is attributed to impeded dislocation movement giving rise to an early localisation as Lueders bands, before gross plastic deformation begins (Campbell, 1973). Normally, such initial yield oscillations of the stress-strain curves of steels are neglected in the material models implemented in the numerical simulation FEM tools. However it has been experimentally ascertained that these initial yield oscillations of the dynamic stress-strain curve have a direct effect on the dynamic load-displacement curve of structures (such as crash absorbers). Therefore an effort should be done for the further investigation

and implementation of material models including such phenomena in the codes for the numerical simulations of severe accidents.

Experimental evidence has also shown that at elevated temperatures ranging from 300 to 650°C all the above mentioned as-received austenitic and ferritic steels, including the welded and heat-affected zone material, exhibit at high strain-rate a reduced capability of absorbing by deformation the accident energy with respect to the quasi-static strain-rate. This behaviour raises some questions whether a stable response of the structure to the severe accident impact loading can be achieved at such temperatures.

The dynamic stress-strain curves of the austenitic steels AISI 316L, AISI 304 and of the Nimonic alloy PE16 irradiated up to 9.2 dpa and tested in the high temperature ranging from 400 to 550°C show also the phenomenon of strain-rate softening and marked reduction of uniform and fracture strains. Remarkable is the case of AISI 316L at the medium strain-rate of  $8\text{ s}^{-1}$  (Fig. 7.29), where the deformation energy of the irradiated material is reduced to about one half that of the as-received material.

Strain-rate softening and reduction of uniform and fracture strains are also characteristics of the response shown by the dynamic stress-strain curves of the austenitic stainless steel AISI 316H tested at 550°C after having been submitted to irradiation at 2dpa and to low cycle fatigue. These phenomena reduce the deformation energy of the pre-damaged material to about one half that of the as-received material. It should be here remarked that it is the superposition of the irradiation to the low cycle fatigue damage which gives rise to the reduction of the deformation energy of the pre-damaged material. In fact, as shown in Fig. 7.63, the dynamic flow curves of AISI 316H pre-damaged only by low cycle fatigue show damage hardening, strain hardening and strain-rate hardening and do not practically show reduction of deformation energy. From the above considerations it follows that the main responsible for the degradation phenomena in the dynamic stress-strain curves is, as expected, the combined action of high strain-rate, high temperatures (between 300 and 650°C), irradiation and thermo-mechanical service loading including low cycle fatigue and creep.

Due to the serious consequences that a failure of nuclear reactor structures might have, the problem of reactor safety requires a reliable structural assessment based on advanced computations implementing material models calibrated on accurate physical data obtained by testing under impact loading the materials, progressively damaged up to the end-of-life conditions.

Due to the multifactorial nature of the mechanical degradation process, ideally the tested material should originate from an aged reactor structure itself or submitted to a thermo-mechanical and irradiation process as similar as possible to that at a real reactor.

The JRC testing technology at high strain-rate and at high temperature with the use of the hydro-pneumatic machine and of the modified Hopkinson bar installed in a hot cell has permitted to obtain the results on irradiated+thermo-mechanically aged material now archived and updated in the new database. This technology has been widely recognised and appreciated by the scientific nuclear Community, and might even be implemented in a dynamic testing campaign on specimens worked out from aged reactor structures.

Several material constitutive models may be used to represent the response at high strain-rate of the materials reported in this report, such as the generalised constitutive equations proposed by Perzyna (Albertini et al., 1983a, Perzyna, 1980) and by Zener-Hollomon (Zener and Hollomon, 1944, Micunovic et al., 2003), which have been calibrated using the uniform strain branch of the experimental true stress-strain-strain-rate curves. These constitutive equations would be able to describe with good approximation the strain-rate hardening phenomena and might be readily implemented in the FEM codes because of their mathematical simplicity. Nevertheless they could not describe the strain-rate softening phenomena, mainly due to the combined effects of high temperature-irradiation-low cycle fatigue. The possibility to include these latter phenomena is essential for the analysis of structural behaviour in the case of severe accidents. Progress in this field might be achieved by employing the Zerilli-Armstrong constitutive equation (Zerilli and Armstrong, 1987), based on dislocation mechanics, which allows specialised expressions for face-centred-cubic and body-centred-cubic metals, including grain size and thermal softening effects.

## **8.2 Improvements allowed by the new database to the safety assessment of aged reactor structures in case of severe accidents**

A qualitative review has been made of the published results on nuclear steels dynamic testing obtained in the frame of the Safety Programme of Pressurised Water Reactors, Fast Breeder Reactors and Light Water Reactors, conducted at JRC over the last decades. The review regarded the tensile stress-strain curves measured at high strain-rate and at high temperature of some austenitic stainless steels (AISI 316L, AISI 316H, AISI 304, AISI 321, X6CrNiNb1810) pre-damaged by irradiation, creep, low cycle fatigue, welding, biaxial loading, and of two ferritic steels (ASME 537, 20MnMoNi55). As explained in the previous Section, under such conditions several complex

phenomena take place and the response of these materials may be quite complicated. It needs, however, to be effectively described through appropriate constitutive equations and successively implemented in FEM codes, if reliable assessments of the reactor safety under severe accidents are to be obtained.

The digital database of the dynamic stress-strain curves of the austenitic and ferritic steels, developed in this project, should allow a systematic investigation and should be a useful tool in order to give a reliable answer to the questions of the response of aged reactor structures to severe impact loading. In fact the new database allows a precise parameterisation of the observed phenomena, like strain and strain-rate hardening, strain-rate softening, instabilities due to strain ageing and dynamic strain ageing, reduction of ductility, on the basis of the whole body of the dynamic stress-strain curves, using the powerful tools of the digital technology. The parameters giving the measure of the observed phenomena should be easily and repetitively used for the optimal calibration of material models to be implemented in the numerical simulations of the aged reactor structures response to severe impact loading. To improve and render more realistic the numerical simulations further investigations of the dynamic stress-strain curves of aged materials directly taken from operational reactors could be contemplated and performed by means of the JRC HPM and MHB machines installed in a hot cell. As previously discussed, the same technology can be readily transferred to the testing of the small irradiated specimens of fusion reactors steels.

## **9 Annex 1**

## **9.1 List of materials**

- AISI 304
- AISI 304 (Ref.Mat.4)
- SUS 304
- Ni201
- AISI 304L
- AISI 304L (Ref.Mat.1)
- AISI 304H
- AISI 316
- AISI 316L
- AISI 316L (Ref.Mat.3)
- AISI 316H (Ref.Mat.UKAEA)
- AISI 316H (Ref.Mat.)
- SS400
- SL9N590
- ASME 537cl1 (Ref.Mat.6)
- PE16 (Ref.Mat.5)
- AISI 321 (Ref.Mat.2)
- DIN 1.4306, 1.4981, ST35
- AISI 347
- Steel X52, X60
- Fe360, Fe430
- EN 2 STEEL
- Aluminium 6061
- Mild steel 4mm, 6mm
- Carbon steel
- AUSTENITIC X6CrNiNb1810
- FERRITIC 20MnMoNi55
- FERRITIC 22NiMoCr37
- FERRITIC 26NiCrMo146
- Eurofer97

The  $\sigma - \epsilon - \dot{\epsilon}$  curves marked with equal "Ref.Mat...." are obtained from specimens originating from the same plate, sheet or bar.

## 9.2 Chemical composition

— AISI 304 L (Ref.Mat.1)

	Wt%		Wt%		Wt%
C	0.020	Si	< 0.1	Mn	1.880
P	< 0.05	S	0.004	Cr	18.90
Mo	0.27	Ni	9.2	Nb	< 0.01

— AISI 316 L (Ref.Mat.3)

	Wt%		Wt%		Wt%
C	0.030	Si	0.40	Mn	1.82
P	< 0.05	S	0.007	Cr	16.00
Mo	2.74	Ni	13.3	Nb	< 0.01

— AISI 316 H (Ref.Mat.UKAEA)

	Wt%		Wt%		Wt%
C	0.040	Si	0.31	Mn	1.31
P	0.023	S	0.020	Cr	17.47
Mo	2.63	Ni	11.64	-	-

— AISI 316 H (Ref.Mat.)

	Wt%		Wt%		Wt%
C	0.053	Si	0.35	Mn	1.65
P	0.020	S	0.008	Cr	16.90
Mo	2.45	Ni	12.40	Nb	0.006
Ti	0.006	B	0.001	Co	0.023
Cu	0.080	N	0.082	W	0.023
V	0.087	Zr	0.001	Ta	0.002
Se	0.002	Sn	0.005	-	-

— PE16 (Ref.Mat.5)

	Wt%		Wt%		Wt%
C	0.050	Si	0.21	Mn	0.050
S	0.003	Cr	16.75	Mo	3.73
Ni	43.70	Ti	1.230	B	0.002
Co	0.090	Cu	0.060	Al	1.30
Fe	balance	-	-	-	-

— AISI 321 (Ref.Mat.2)

	Wt%		Wt%		Wt%
C	0.070	Si	0.25	Mn	1.840
P	0.032	S	0.010	Cr	16.70
Ni	10.25	Ti	0.38	-	-

— DIN 1.4306

	Wt%		Wt%		Wt%
C	0.024	Si	0.36	Mn	1.160
P	0.020	S	0.012	Cr	18.40
Ni	10.20	-	-	-	-

— DIN 1.4981

	Wt%		Wt%		Wt%
C	0.100	Si	0.45	Mn	1.250
Cr	16.50	Mo	1.800	Ni	16.50
Nb	<1.0	-	-	-	-

— AUSTENITIC X6CrNiNb1810

	Wt%		Wt%		Wt%
C	0.025	Si	0.32	Mn	1.70
P	0.028	S	0.002	Cr	18.00
Co	0.08	Ni	10.36	Nb	0.43

— FERRITIC 20MnMoNi55

	Wt%		Wt%		Wt%
C	0.20	Si	0.28	Mn	1.30
P	0.009	S	0.002	Cr	0.11
Mo	0.47	Ni	0.65	V	0.005
Al	0.028	N	0.005	Cu	0.03
Co	0.01	Sn	0.006	As	0.008
Ta	0.005	-	-	-	-

— FERRITIC 22NiMoCr37

	Wt%		Wt%		Wt%
C	0.22	Si	0.19	Mn	0.89
P	0.007	S	0.007	Cr	0.40
Mo	0.55	Ni	0.87	Co	0.011
Al	0.019	Nb	0.43	Cu	0.04
Sb	0.001	Sn	0.008	As	0.009
Ta	<0.005	V	<0.01	-	-

— FERRITIC 26NiCrMo146

	Wt%		Wt%		Wt%
C	0.25-0.30	Si	0.15-0.30	Mn	0.30-0.50
P	<0.020	S	<0.010	Cr	1.20-1.50
Mo	0.35-0.50	Ni	3.40-3.80	V	<0.12
Al	0.020-0.050	-	-	-	-

— Eurofer97

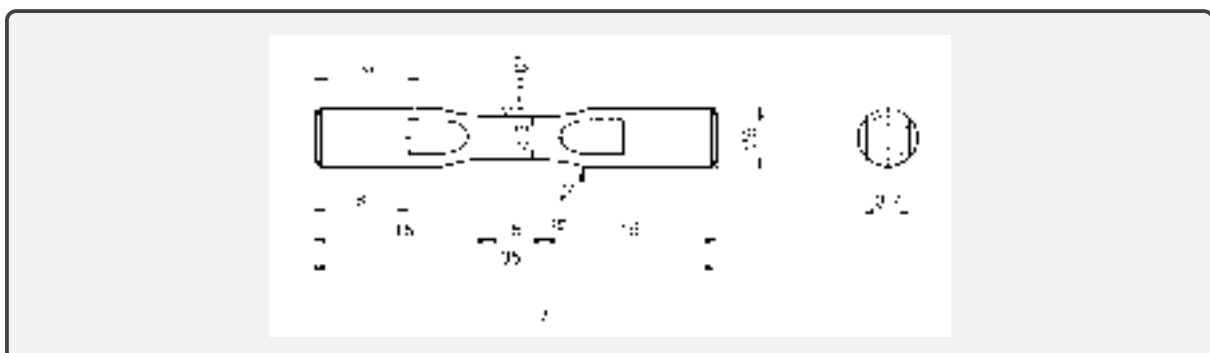
	Wt%		Wt%		Wt%
C	0.12	Si	0.06	Mn	0.47
P	<0.005	S	0.04	Cr	8.9
Mo	<0.005	Ni	0.02	V	0.2
Ta	0.15	-	-	-	-

### 9.3 Legend



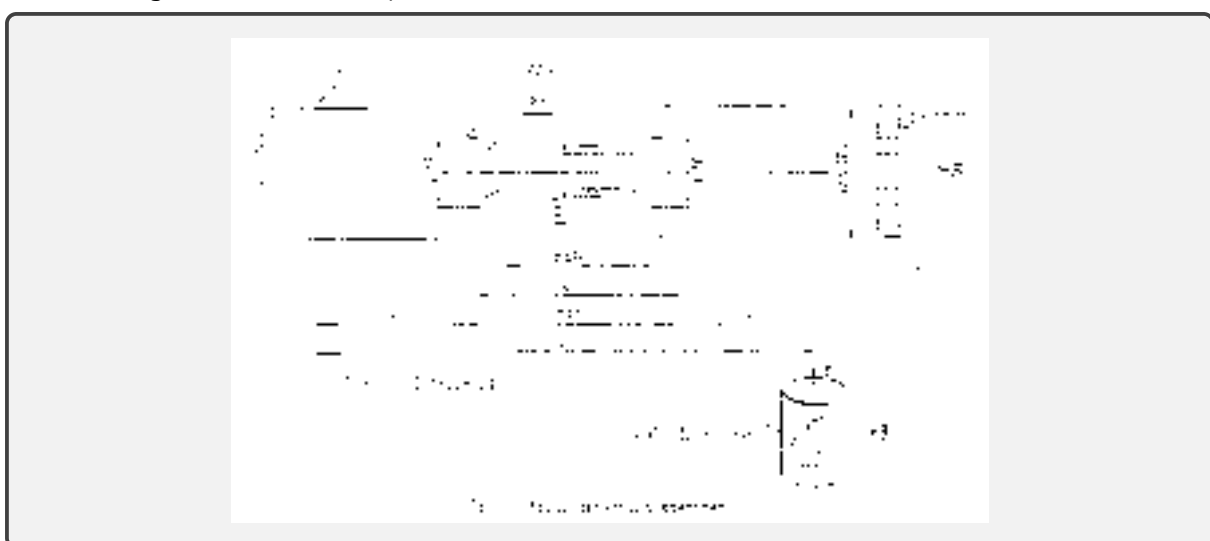
### Round specimen

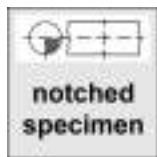
### Specimen geometry:



## Plate specimen

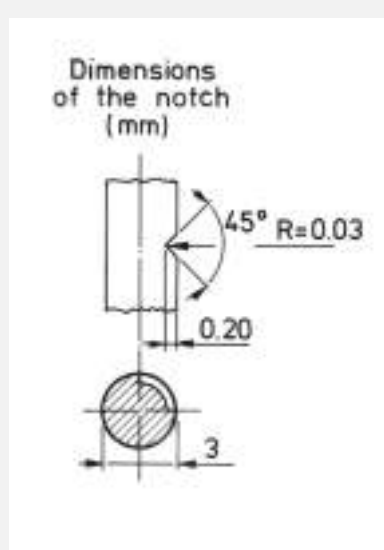
Different geometries. For example:

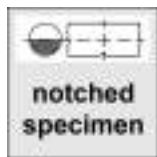




Notched specimen

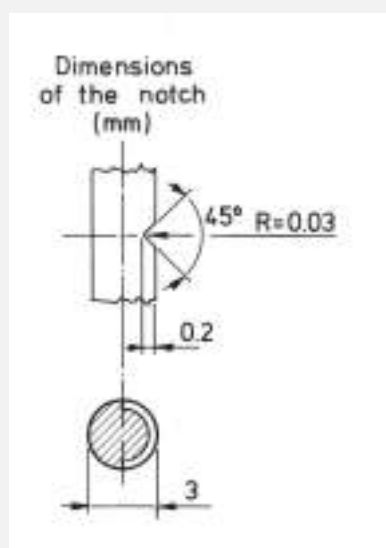
Specimen geometry:

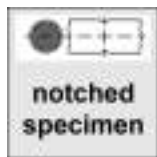




Notched specimen

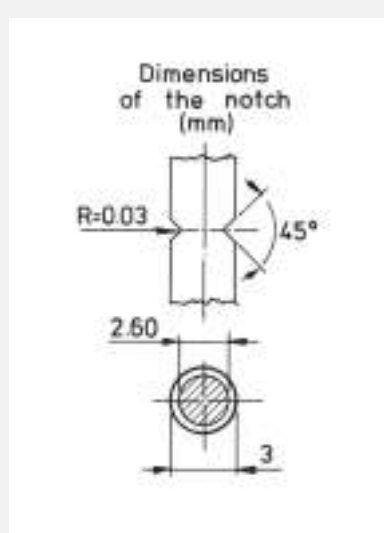
Specimen geometry:





Notched specimen

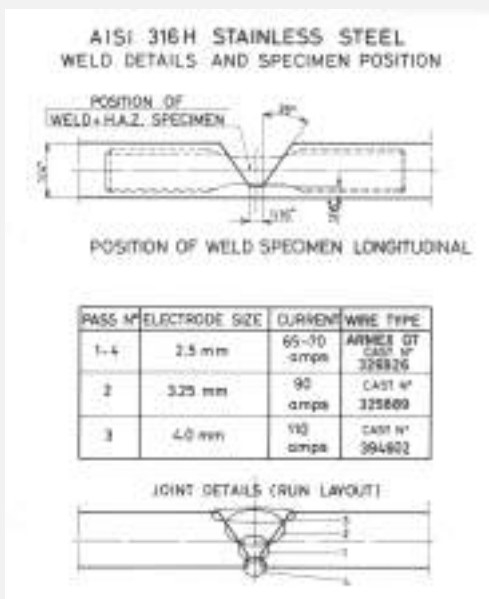
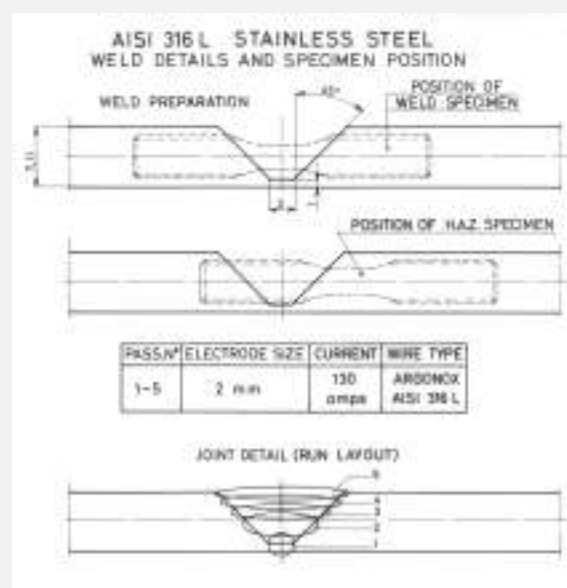
Specimen geometry:

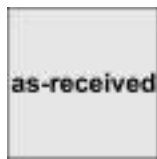




Weld and Weld+Heat Affected Zone specimens

Weld details and specimen position:





As received material



Virgin material



Cold worked material



Test temperature

All test temperatures:

-100°C	20°C	100°C	200°C	300°C	350°C	400°C
500°C	550°C	600°C	650°C	750°C	850°C	950°C



Irradiated material

Specimens irradiated in sodium at different temperature in HFR Reactor



Thermally aged material

Specimens thermally aged in sodium at different temperature and time





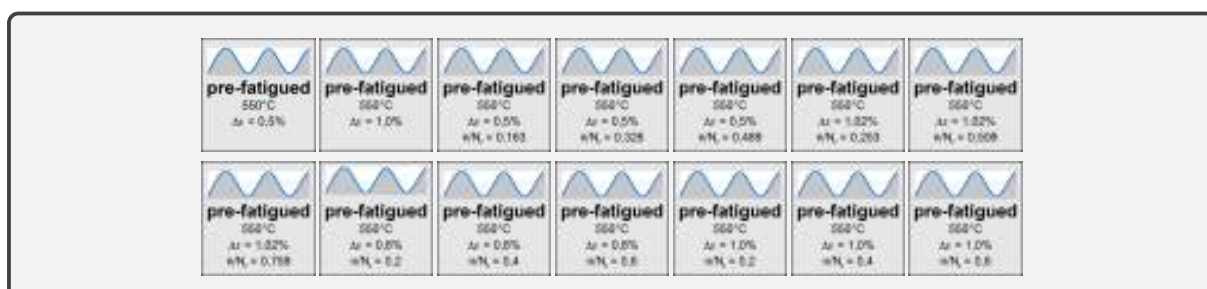
Creep material

Creep condition:



Pre-fatigued material

All pre-fatigued condition:



**carbon steel**  
6 mm  
thickness

Specimen coming from a sheet 6mm thick

**from**  
**aluminium**  
**sheet 2 mm**  
**thickness**

**from**  
**aluminium**  
**sheet 3 mm**  
**thickness**

Specimen coming from aluminium sheets 2, 3mm thick

**inner tank**  
1,6 mm

**inner tank**  
2,0 mm

Specimen coming from sheets 1.6, 2mm thick, used for the construction of the inner tank

**mild steel**  
wall of  
1/12 vessels  
4 mm  
thickness

**mild steel**  
**shield tank**  
**of 1/12 vessels**  
6 mm  
thickness

Specimen coming from sheets 4, 6mm thick of vessel models down scaled 1/12.

## **9.4 Database**

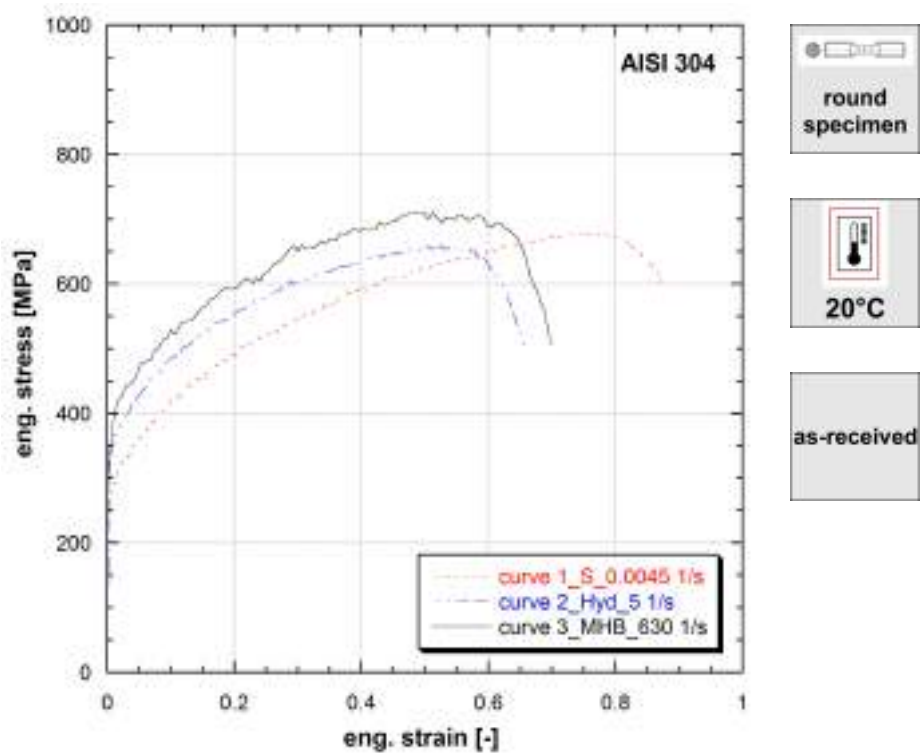


**Figure 9.1:** Stress vs strain curves of AISI 304 (Ref.Mat.4)

**Note 9.1** Ref.Mat.4

Strain rate [1/s]	Yield stress [MPa]	Ultimate tensile strength [MPa]	Uniform strain [-]	Fracture stress [MPa]	Fracture strain [-]
0.0045	263	678	0.742	595	0.880
5	337	659	0.525	494	0.660
630	340	710	0.499	504	0.699

**Table 1:** Mechanical properties of AISI 304 (Ref.Mat.4)

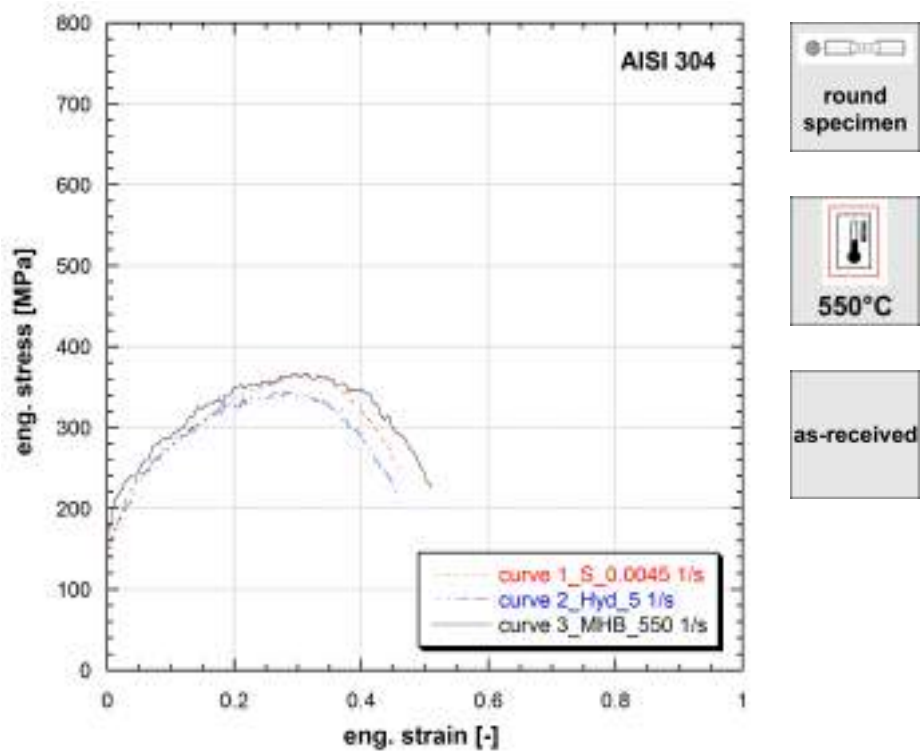


**Figure 9.2:** Stress vs strain curves of AISI 304 (Ref.Mat.4)

**Note 9.2** Ref.Mat.4

Strain rate [1/s]	Yield stress [MPa]	Ultimate tensile strength [MPa]	Uniform strain [-]	Fracture stress [MPa]	Fracture strain [-]
0.0045	145	367	0.315	249	0.461
5	143	345	0.279	201	0.460
550	176	368	0.313	226	0.510

**Table 2:** Mechanical properties of AISI 304 (Ref.Mat.4)

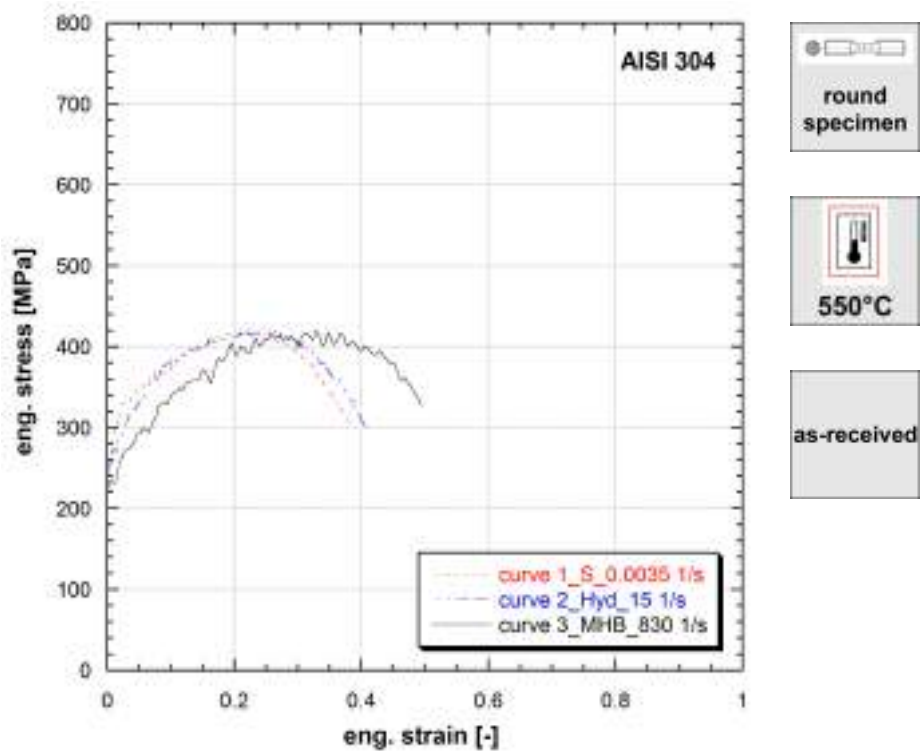


**Figure 9.3:** Stress vs strain curves of AISI 304 (Ref.Mat.4)

**Note 9.3** Ref.Mat.4

Strain rate [1/s]	Yield stress [MPa]	Ultimate tensile strength [MPa]	Uniform strain [-]	Fracture stress [MPa]	Fracture strain [-]
0.0035	256	415	0.238	302	0.382
15	249	421	0.260	292	0.411
830	233	420	0.329	327	0.494

**Table 3:** Mechanical properties of AISI 304 (Ref.Mat.4)

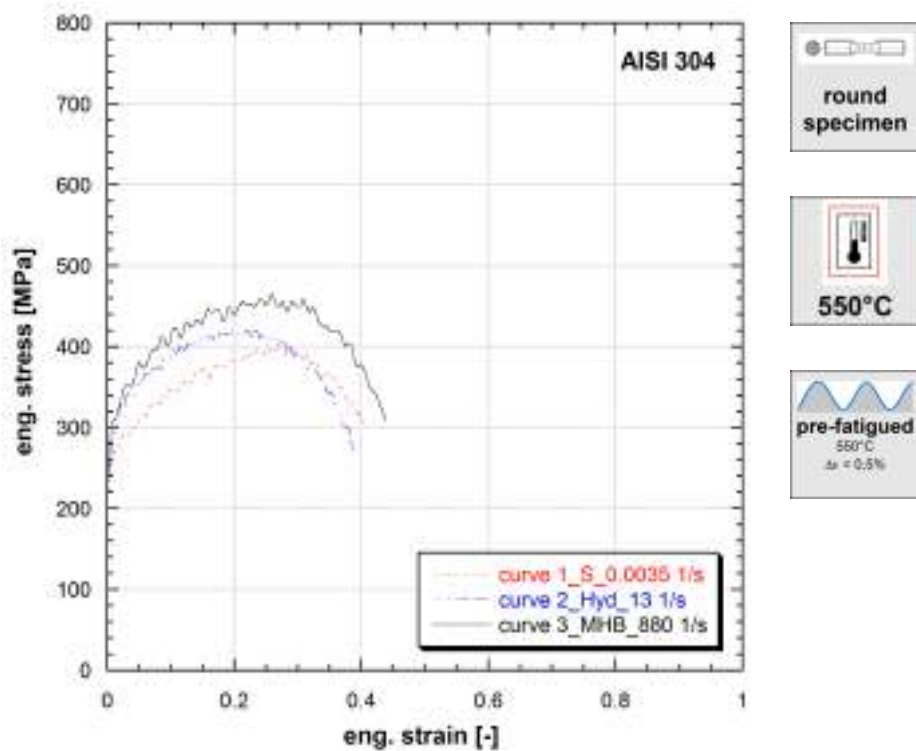


**Figure 9.4:** Stress vs strain curves of AISI 304 (Ref.Mat.4)

**Note 9.4** Ref.Mat.4

Strain rate [1/s]	Yield stress [MPa]	Ultimate tensile strength [MPa]	Uniform strain [-]	Fracture stress [MPa]	Fracture strain [-]
0.0035	219	397	0.253	305	0.403
15	250	421	0.197	270	0.386
880	265	465	0.258	308	0.439

**Table 4:** Mechanical properties of AISI 304 (Ref.Mat.4)

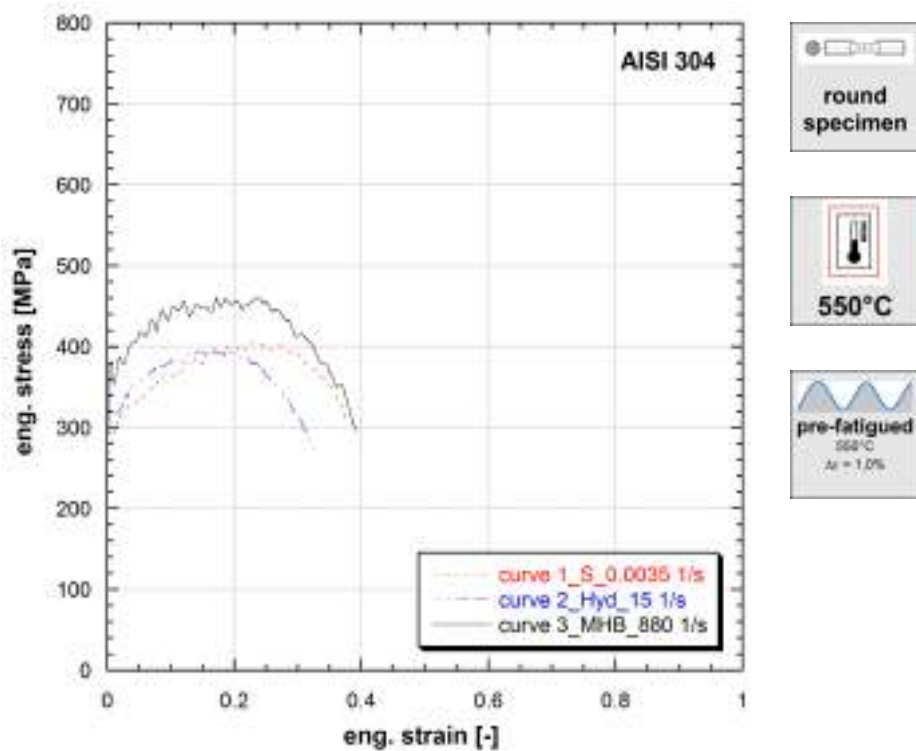


**Figure 9.5:** Stress vs strain curves of AISI 304 (Ref.Mat.4)

**Note 9.5** Ref.Mat.4

Strain rate [1/s]	Yield stress [MPa]	Ultimate tensile strength [MPa]	Uniform strain [-]	Fracture stress [MPa]	Fracture strain [-]
0.0035	267	406	0.230	299	0.391
15	299	394	0.143	263	0.331
880	363	461	0.171	295	0.393

**Table 5:** Mechanical properties of AISI 304 (Ref.Mat.4)

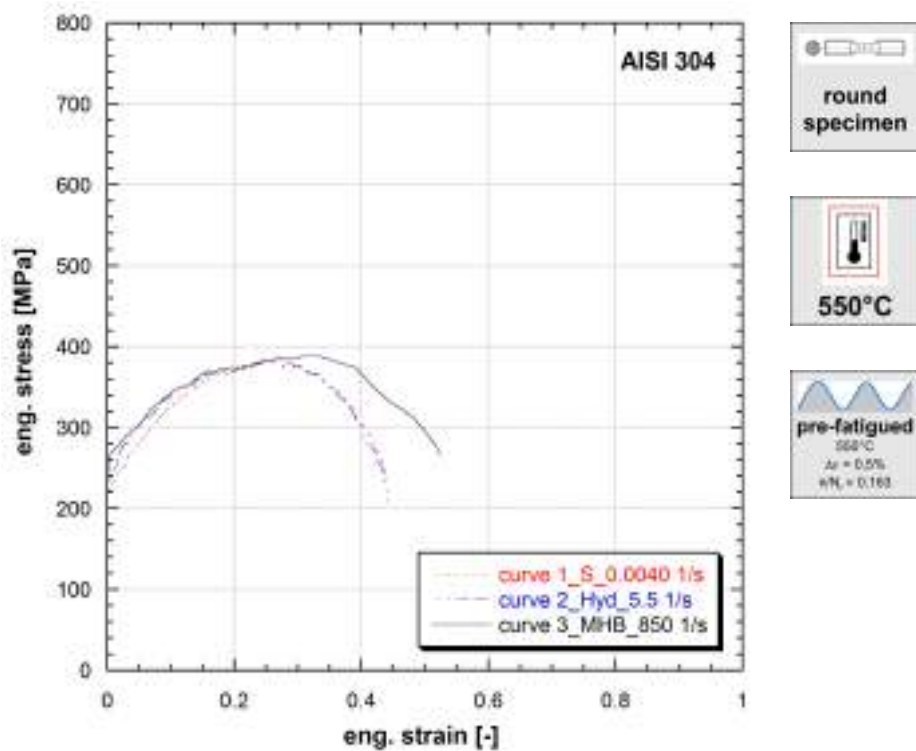


**Figure 9.6:** Stress vs strain curves of AISI 304 (Ref.Mat.4)

**Note 9.6** Ref.Mat.4

Strain rate [1/s]	Yield stress [MPa]	Ultimate tensile strength [MPa]	Uniform strain [-]	Fracture stress [MPa]	Fracture strain [-]
0.004	217	388	0.270	231	0.440
5.5	229	382	0.244	206	0.442
850	264	388	0.307	266	0.524

**Table 6:** Mechanical properties of AISI 304 (Ref.Mat.4)

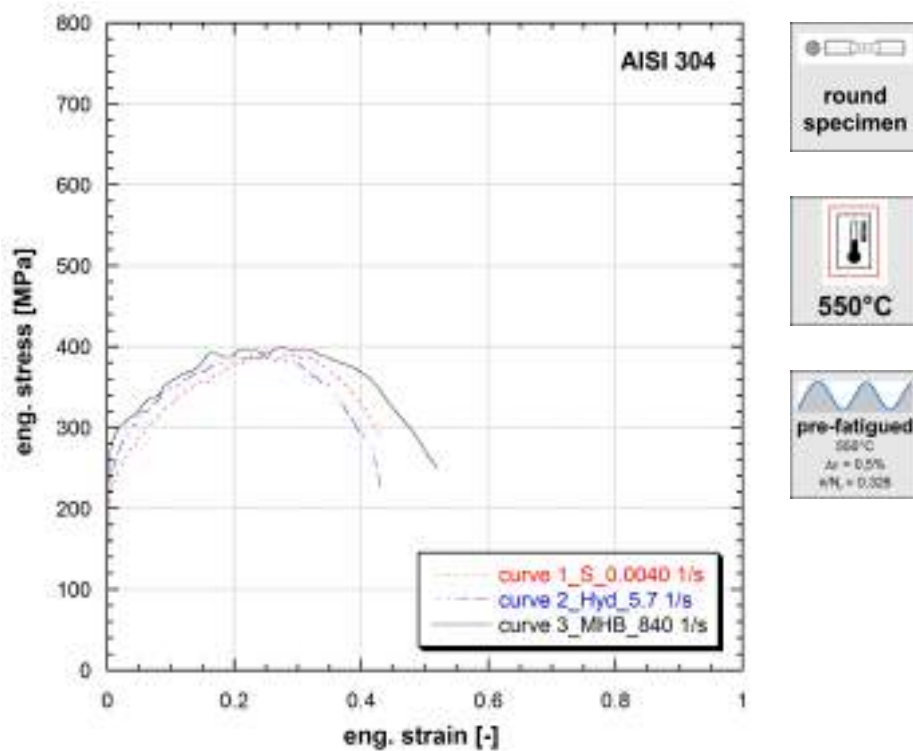


**Figure 9.7:** Stress vs strain curves of AISI 304 (Ref.Mat.4)

**Note 9.7** Ref.Mat.4

Strain rate [1/s]	Yield stress [MPa]	Ultimate tensile strength [MPa]	Uniform strain [-]	Fracture stress [MPa]	Fracture strain [-]
0.004	203	391	0.275	287	0.431
5.7	221	389	0.227	219	0.432
840	263	398	0.270	250	0.520

**Table 7:** Mechanical properties of AISI 304 (Ref.Mat.4)

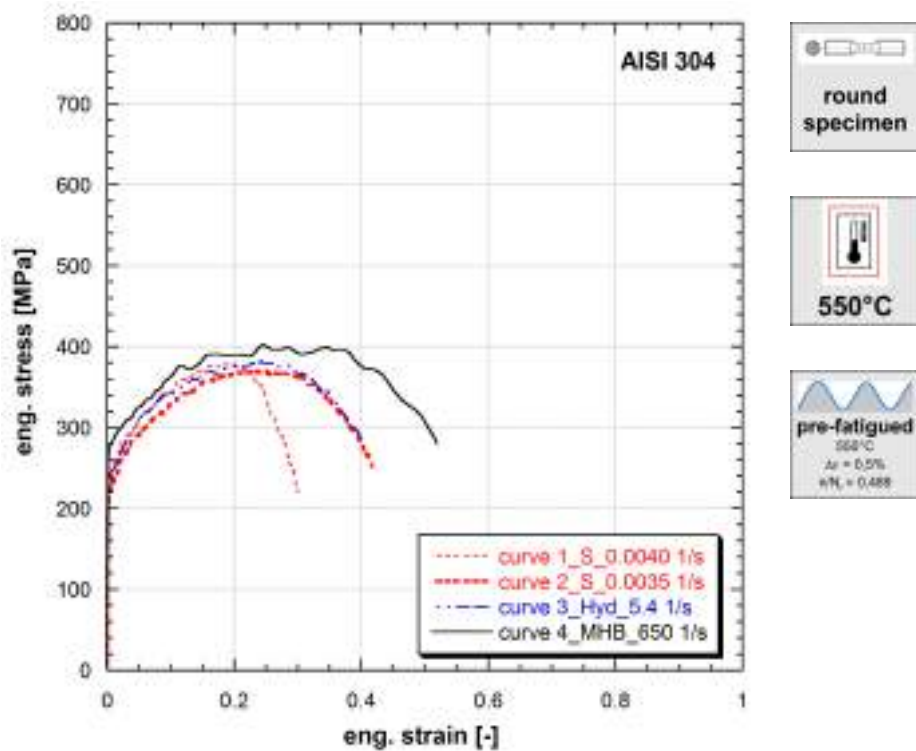


**Figure 9.8:** Stress vs strain curves of AISI 304 (Ref.Mat.4)

**Note 9.8** Ref.Mat.4

Strain rate [1/s]	Yield stress [MPa]	Ultimate tensile strength [MPa]	Uniform strain [-]	Fracture stress [MPa]	Fracture strain [-]
0.004	242	380	0.180	220	0.300
0.0035	214	372	0.246	253	0.416
5.4	226	382	0.243	280	0.406
650	277	402	0.245	280	0.520

**Table 8:** Mechanical properties of AISI 304 (Ref.Mat.4)

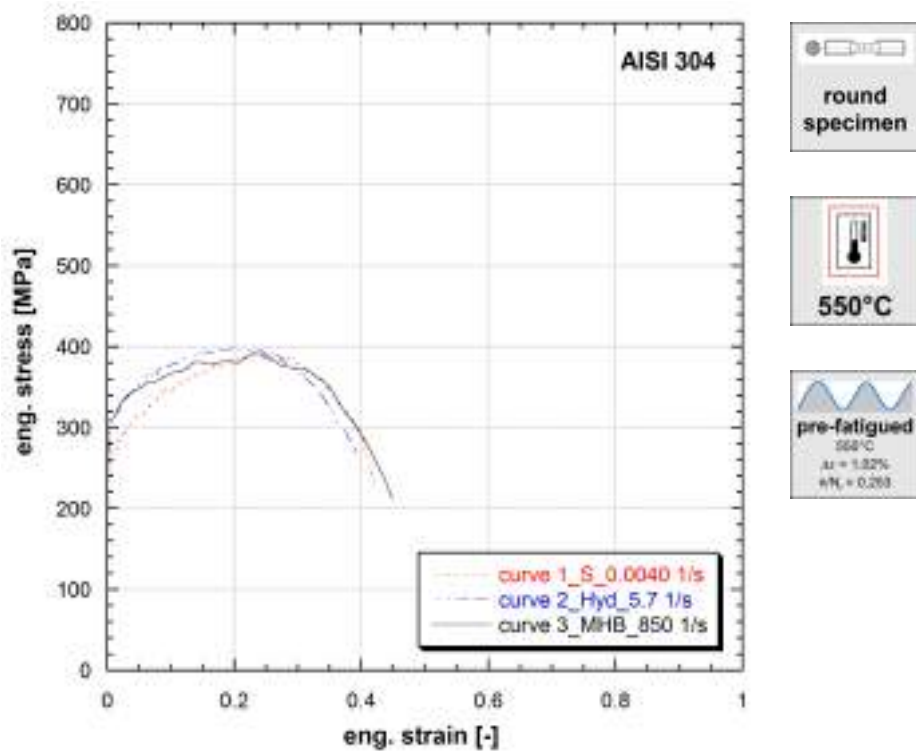


**Figure 9.9:** Stress vs strain curves of AISI 304 (Ref.Mat.4)

**Note 9.9** Ref.Mat.4

Strain rate [1/s]	Yield stress [MPa]	Ultimate tensile strength [MPa]	Uniform strain [-]	Fracture stress [MPa]	Fracture strain [-]
0.004	256	390	0.231	222	0.425
5.7	294	399	0.198	269	0.393
850	310	393	0.234	211	0.450

**Table 9:** Mechanical properties of AISI 304 (Ref.Mat.4)

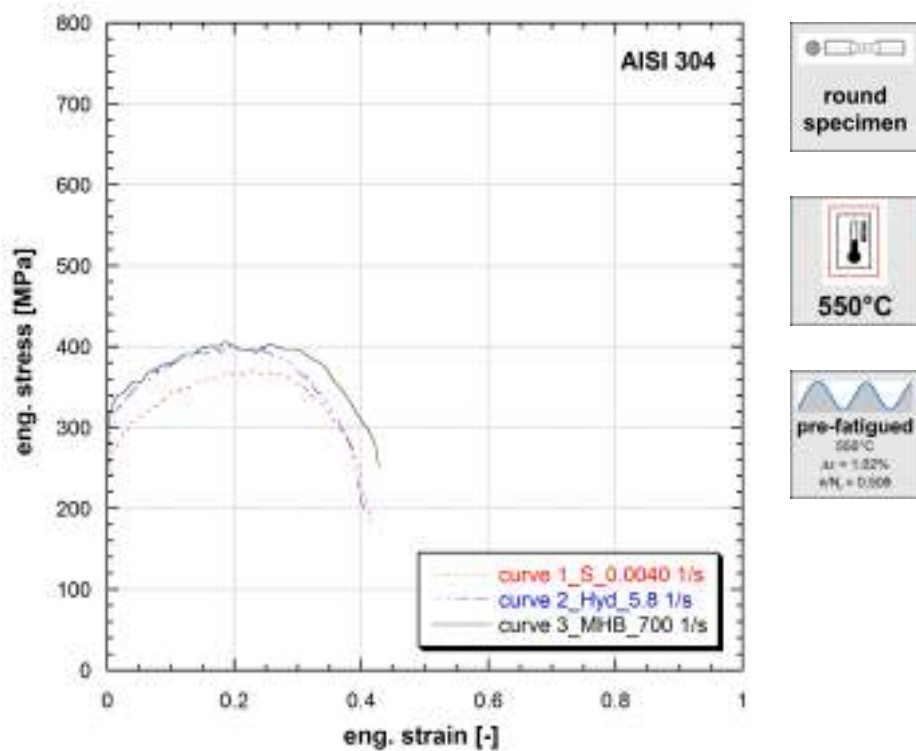


**Figure 9.10:** Stress vs strain curves of AISI 304 (Ref.Mat.4)

**Note 9.10** Ref.Mat.4

Strain rate [1/s]	Yield stress [MPa]	Ultimate tensile strength [MPa]	Uniform strain [-]	Fracture stress [MPa]	Fracture strain [-]
0.004	257	369	0.251	177	0.415
5.8	292	402	0.194	193	0.407
700	312	405	0.189	252	0.428

**Table 10:** Mechanical properties of AISI 304 (Ref.Mat.4)

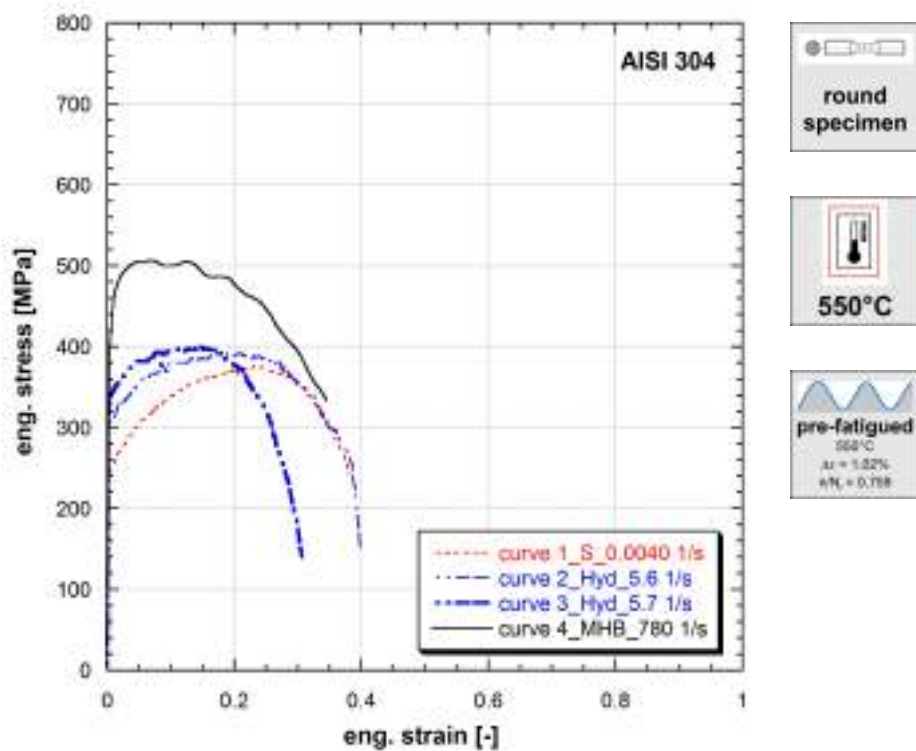


**Figure 9.11:** Stress vs strain curves of AISI 304 (Ref.Mat.4)

**Note 9.11** Ref.Mat.4

Strain rate [1/s]	Yield stress [MPa]	Ultimate tensile strength [MPa]	Uniform strain [-]	Fracture stress [MPa]	Fracture strain [-]
0.004	245	377	0.232	242	0.380
5.6	307	394	0.178	152	0.398
5.7	335	400	0.148	140	0.307
780	410	506	0.068	333	0.345

**Table 11:** Mechanical properties of AISI 304 (Ref.Mat.4)

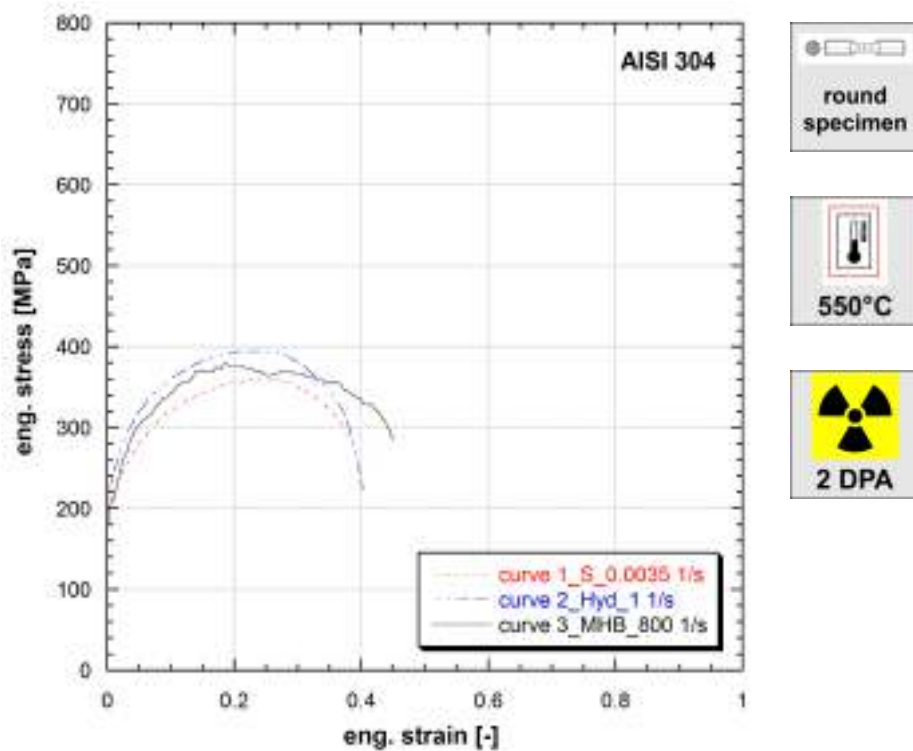


**Figure 9.12:** Stress vs strain curves of AISI 304 (Ref.Mat.4)

**Note 9.12** Ref.Mat.4

*Irradiated in sodium at 550°C in HFR reactor.*

Strain rate [1/s]	Yield stress [MPa]	Ultimate tensile strength [MPa]	Uniform strain [-]	Fracture stress [MPa]	Fracture strain [-]
0.0035	197	360	0.263	262	0.395
1	211	395	0.212	223	0.403
800	201	379	0.187	286	0.453

**Table 12:** Mechanical properties of AISI 304 (Ref.Mat.4)

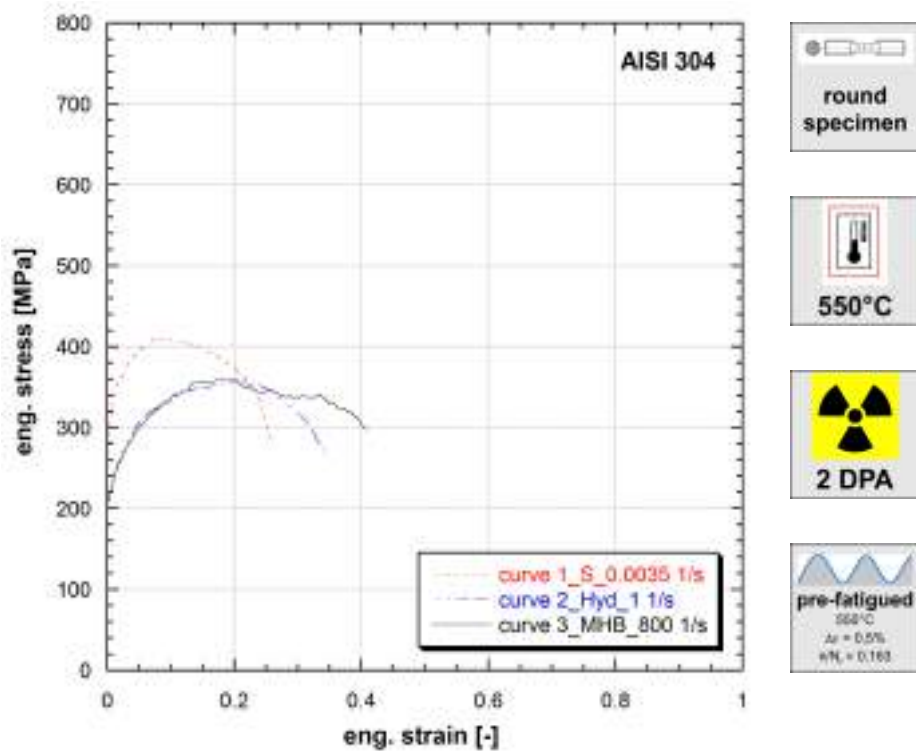


**Figure 9.13:** Stress vs strain curves of AISI 304 (Ref.Mat.4)

**Note 9.13** Ref.Mat.4

*Irradiated in sodium at 550°C in HFR reactor.*

Strain rate [1/s]	Yield stress [MPa]	Ultimate tensile strength [MPa]	Uniform strain [-]	Fracture stress [MPa]	Fracture strain [-]
0.0035	300	410	0.090	281	0.260
1	204	357	0.200	267	0.345
800	215	360	0.184	298	0.409

**Table 13:** Mechanical properties of AISI 304 (Ref.Mat.4)

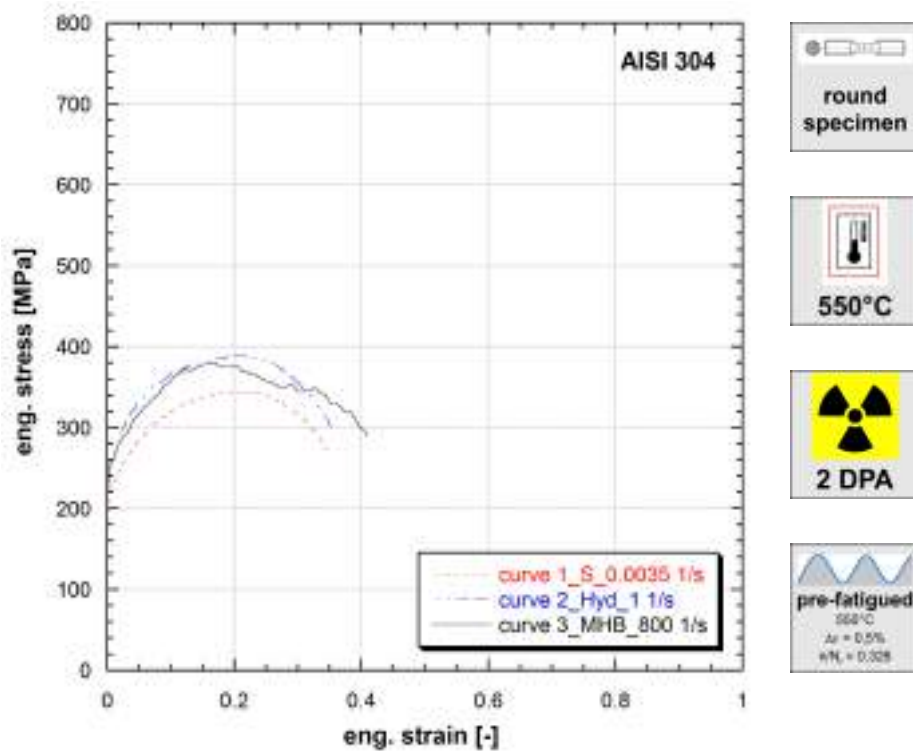


**Figure 9.14:** Stress vs strain curves of AISI 304 (Ref.Mat.4)

**Note 9.14** Ref.Mat.4

*Irradiated in sodium at 550°C in HFR reactor.*

Strain rate [1/s]	Yield stress [MPa]	Ultimate tensile strength [MPa]	Uniform strain [-]	Fracture stress [MPa]	Fracture strain [-]
0.0035	200	344	0.209	270	0.345
1	243	389	0.203	301	0.352
800	246	381	0.167	289	0.409

**Table 14:** Mechanical properties of AISI 304 (Ref.Mat.4)

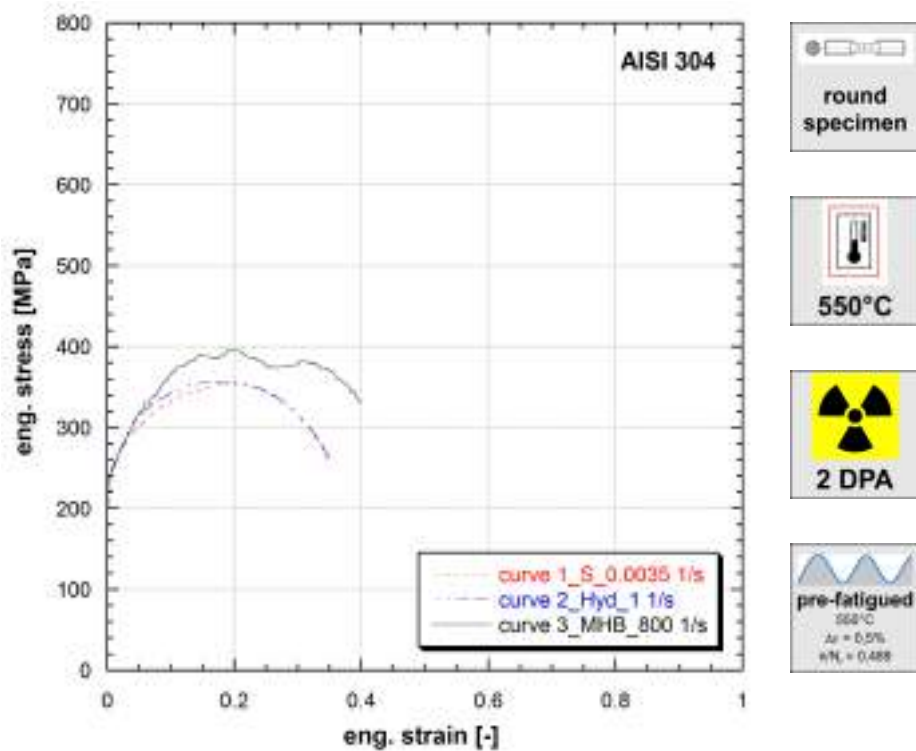


**Figure 9.15:** Stress vs strain curves of AISI 304 (Ref.Mat.4)

**Note 9.15** Ref.Mat.4

*Irradiated in sodium at 550°C in HFR reactor.*

Strain rate [1/s]	Yield stress [MPa]	Ultimate tensile strength [MPa]	Uniform strain [-]	Fracture stress [MPa]	Fracture strain [-]
0.0035	236	353	0.208	261	0.345
1	218	357	0.195	256	0.355
800	238	397	0.193	330	0.400

**Table 15:** Mechanical properties of AISI 304 (Ref.Mat.4)

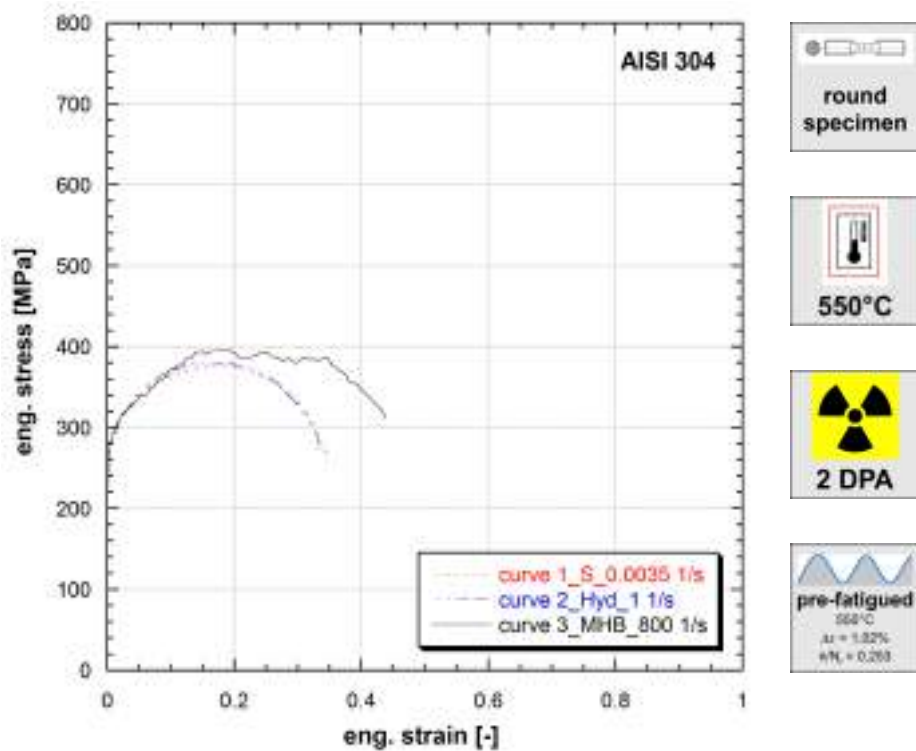


**Figure 9.16:** Stress vs strain curves of AISI 304 (Ref.Mat.4)

**Note 9.16** Ref.Mat.4

*Irradiated in sodium at 550°C in HFR reactor.*

Strain rate [1/s]	Yield stress [MPa]	Ultimate tensile strength [MPa]	Uniform strain [-]	Fracture stress [MPa]	Fracture strain [-]
0.0035	271	376	0.189	262	0.349
1	263	380	0.155	272	0.334
800	272	396	0.185	312	0.439

**Table 16:** Mechanical properties of AISI 304 (Ref.Mat.4)

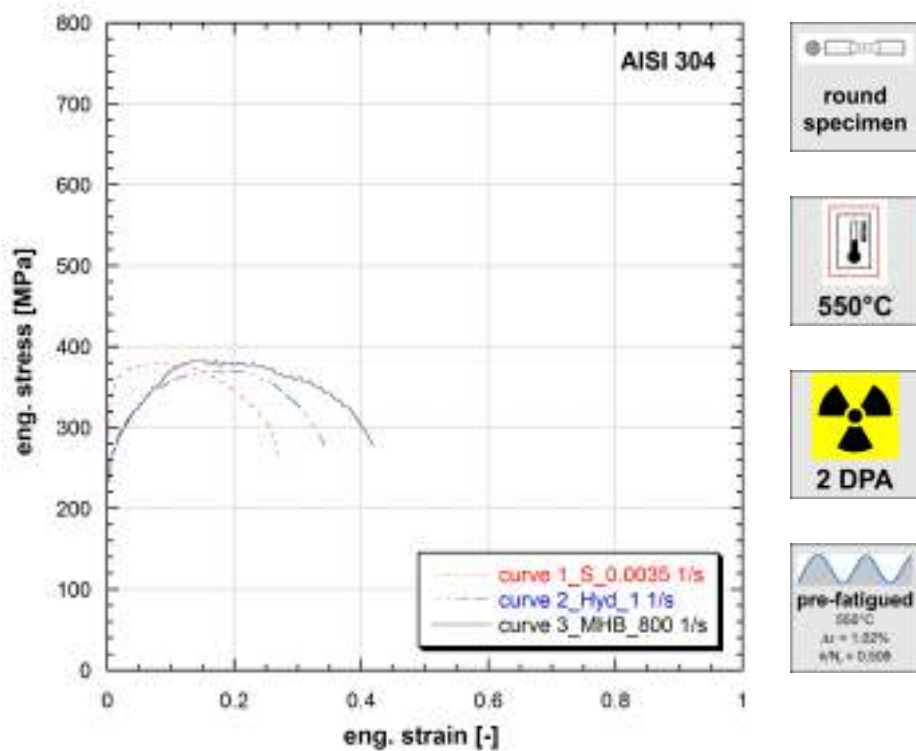


**Figure 9.17:** Stress vs strain curves of AISI 304 (Ref.Mat.4)

**Note 9.17** Ref.Mat.4

*Irradiated in sodium at 550°C in HFR reactor.*

Strain rate [1/s]	Yield stress [MPa]	Ultimate tensile strength [MPa]	Uniform strain [-]	Fracture stress [MPa]	Fracture strain [-]
0.0035	310	379	0.081	266	0.269
1	238	370	0.188	277	0.341
800	257	383	0.171	278	0.420

**Table 17:** Mechanical properties of AISI 304 (Ref.Mat.4)

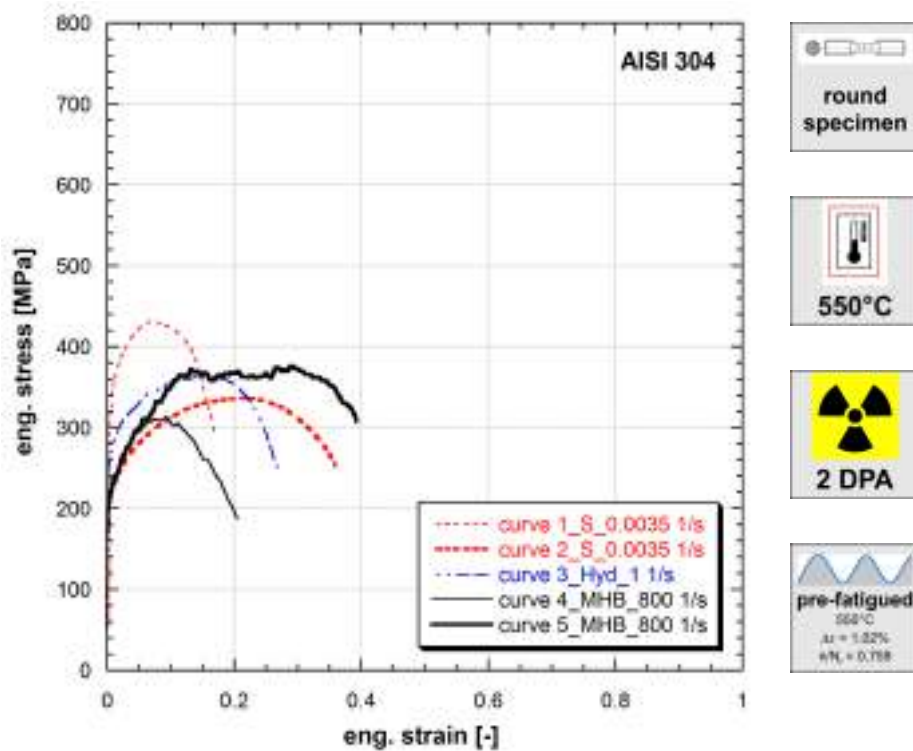


**Figure 9.18:** Stress vs strain curves of AISI 304 (Ref.Mat.4)

**Note 9.18** Ref.Mat.4

*Irradiated in sodium at 550°C in HFR reactor.*

Strain rate [1/s]	Yield stress [MPa]	Ultimate tensile strength [MPa]	Uniform strain [-]	Fracture stress [MPa]	Fracture strain [-]
0.0035	308	431	0.070	296	0.167
0.0035	206	336	0.215	253	0.359
1	260	363	0.148	245	0.270
800	221	313	0.092	187	0.205
800	213	376	0.291	307	0.392

**Table 18:** Mechanical properties of AISI 304 (Ref.Mat.4)

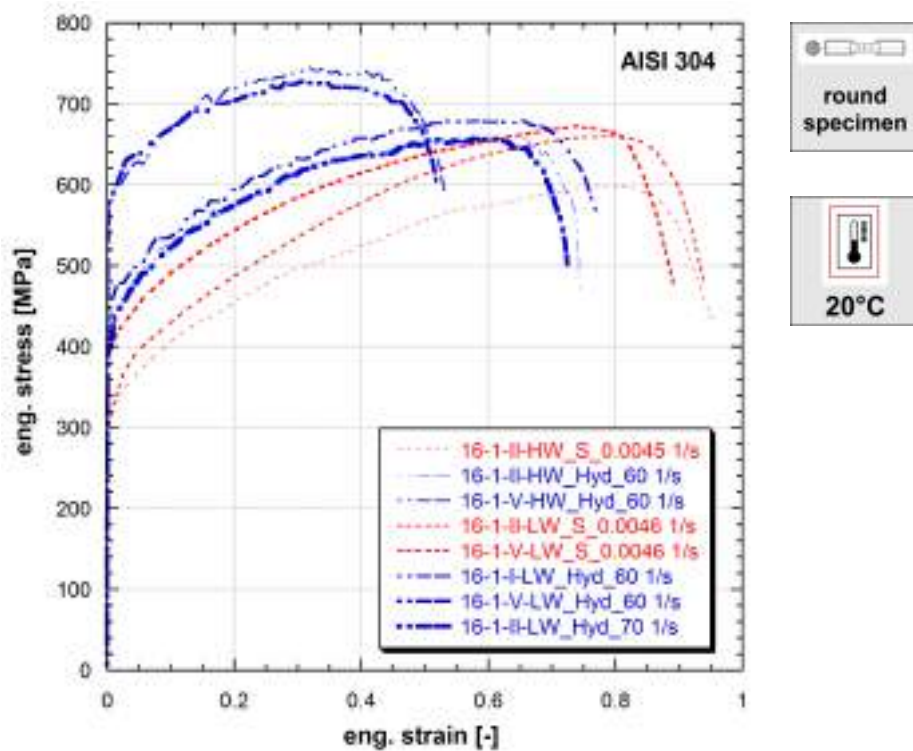


**Figure 9.19:** Stress vs strain curves of AISI 304

**Note 9.19** Specimens taken from different position of a down scaled reactor tank model of COVA program.

Strain rate [1/s]	Yield stress [MPa]	Ultimate tensile strength [MPa]	Uniform strain [-]	Fracture stress [MPa]	Fracture strain [-]
0.0045	301	598	0.810	430	0.953
60	401	661	0.575	462	0.744
60	574	745	0.320	588	0.531
0.0046	303	661	0.798	480	0.939
0.0046	393	672	0.738	478	0.890
60	447	679	0.651	564	0.771
60	581	728	0.306	598	0.520
70	395	658	0.605	501	0.725

**Table 19:** Mechanical properties of AISI 304

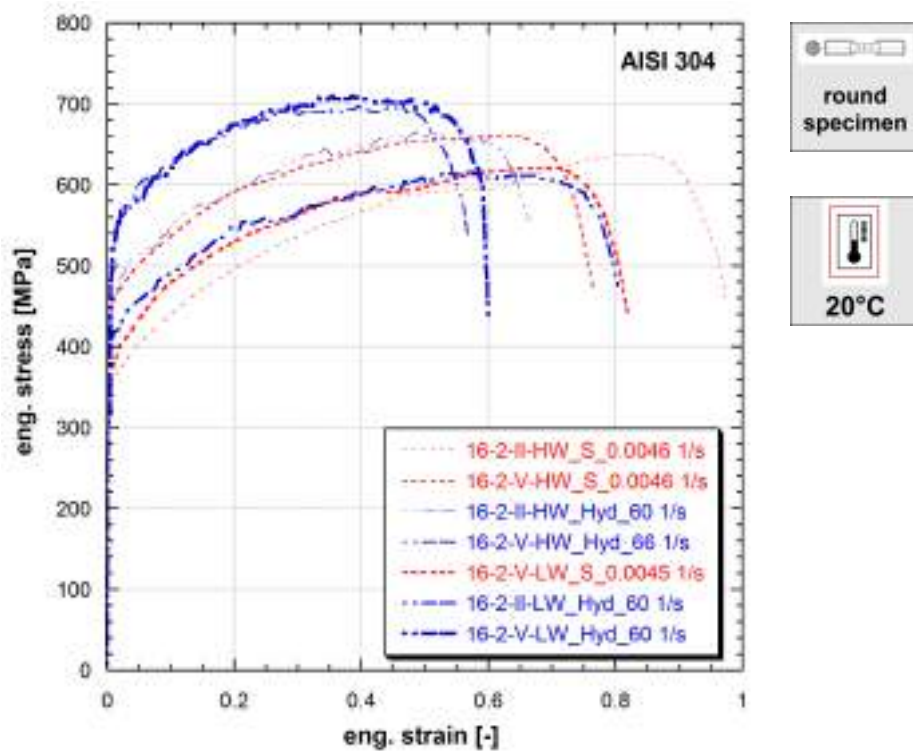


**Figure 9.20:** Stress vs strain curves of AISI 304

**Note 9.20** Specimens taken from different position of a down scaled reactor tank model of the COVA program.

Strain rate [1/s]	Yield stress [MPa]	Ultimate tensile strength [MPa]	Uniform strain [-]	Fracture stress [MPa]	Fracture strain [-]
0.0046	329	638	0.859	458	0.974
0.0046	438	661	0.652	467	0.767
60	411	666	0.486	556	0.664
66	462	702	0.462	539	0.567
0.0045	353	621	0.711	438	0.820
60	380	616	0.569	474	0.804
60	307	710	0.354	439	0.600

**Table 20:** Mechanical properties of AISI 304

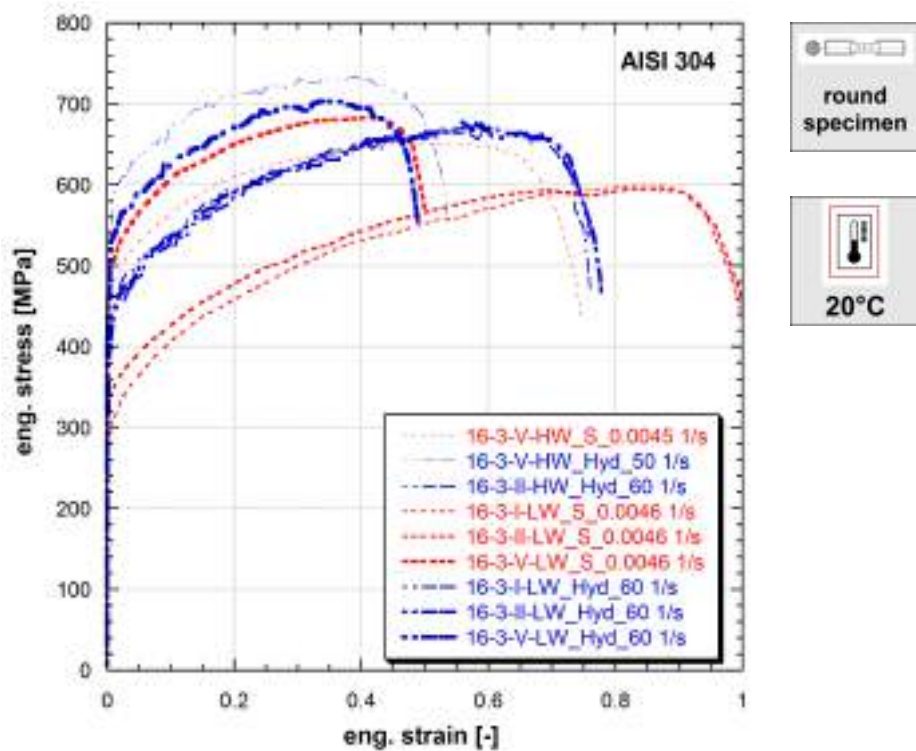


**Figure 9.21:** Stress vs strain curves of AISI 304

Strain rate [1/s]	Yield stress [MPa]	Ultimate tensile strength [MPa]	Uniform strain [-]	Fracture stress [MPa]	Fracture strain [-]
0.0045	449	651	0.511	439	0.746
50	520	735	0.389	555	0.536
60	456	667	0.534	472	0.760
0.0046	287	599	0.827	409	1.008
0.0046	329	595	0.827	408	1.010
0.0046	484	683	0.408	571	0.499
60	380	676	0.589	536	0.758
60	398	677	0.559	468	0.777
60	460	703	0.336	551	0.489

**Table 21:** Mechanical properties of AISI 304

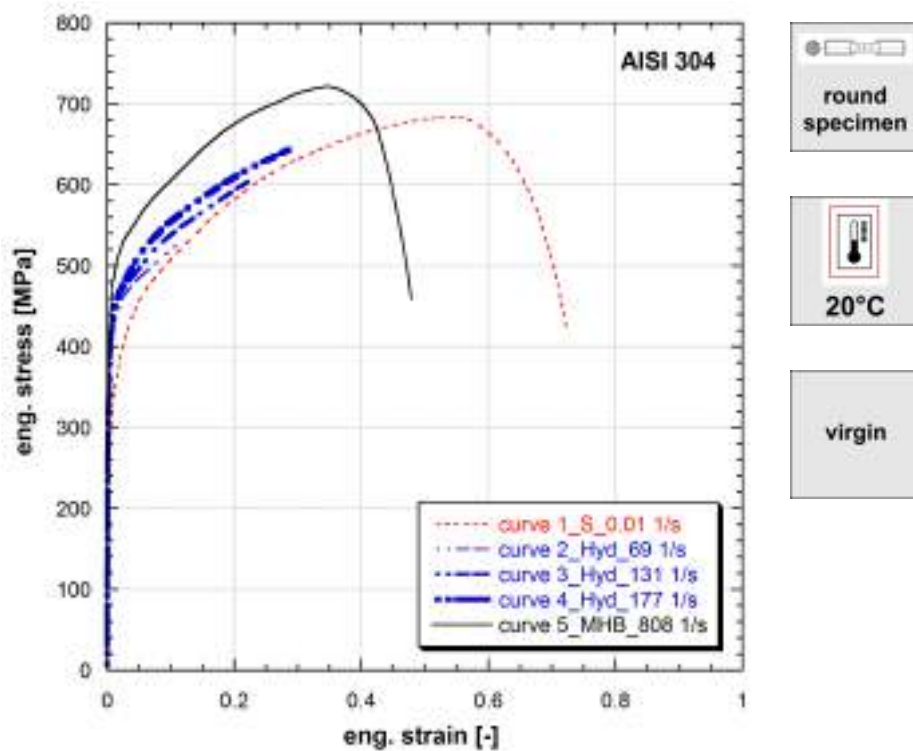


**Figure 9.22:** Stress vs strain curves of AISI 304

Strain rate [1/s]	Yield stress [MPa]	Ultimate tensile strength [MPa]	Uniform strain [-]	Fracture stress [MPa]	Fracture strain [-]
0.01	243	684	0.539	424	0.722
69	321	-	-	-	-
131	342	-	-	-	-
177	381	-	-	-	-
808	430	722	0.346	459	0.478

**Table 22:** Mechanical properties of AISI 304

Published in (Albertini and Montagnani, 1974), (Albertini and Montagnani, 1976).

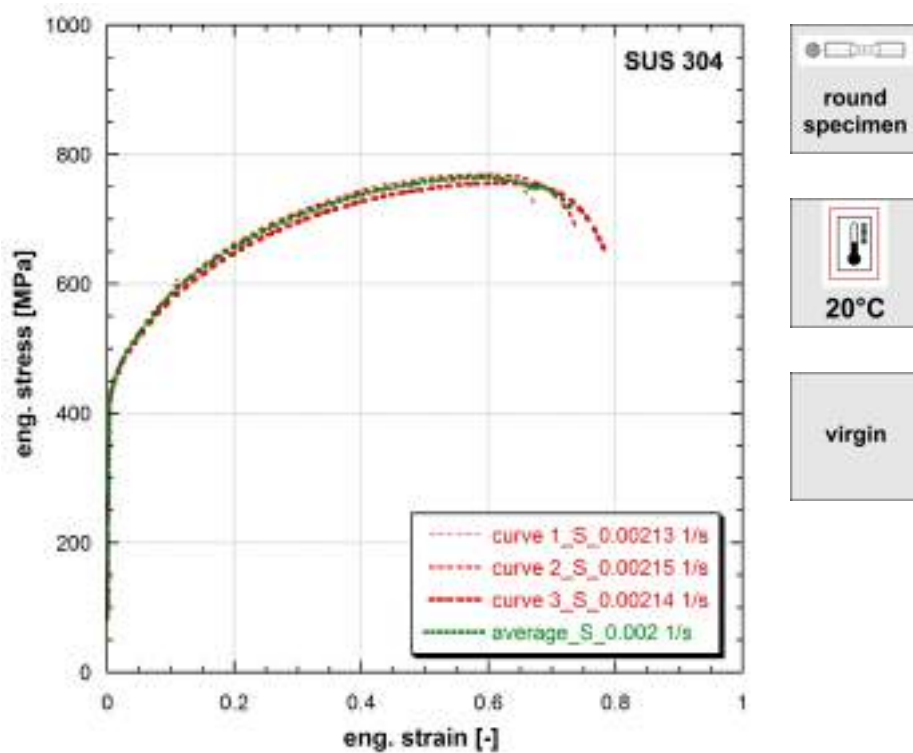


**Figure 9.23:** Stress vs strain curves of SUS 304

Strain rate [1/s]	Yield stress [MPa]	Ultimate tensile strength [MPa]	Uniform strain [-]	Fracture stress [MPa]	Fracture strain [-]
0.00213	425	769	0.563	719	0.676
0.00215	444	769	0.605	678	0.743
0.00214	438	756	0.619	649	0.785
0.002	425	764	0.579	710	0.735

**Table 23:** Mechanical properties of SUS 304

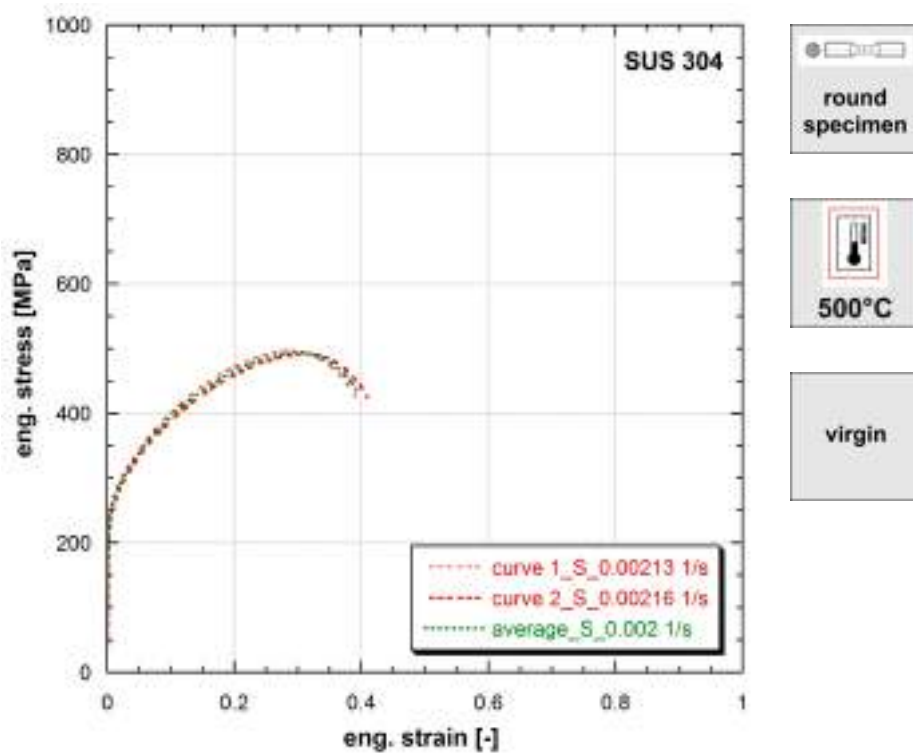


**Figure 9.24:** Stress vs strain curves of SUS 304

Strain rate [1/s]	Yield stress [MPa]	Ultimate tensile strength [MPa]	Uniform strain [-]	Fracture stress [MPa]	Fracture strain [-]
0.00213	258	497	0.288	419	0.395
0.00216	236	493	0.315	425	0.409
0.002	242	494	0.295	436	0.393

**Table 24:** Mechanical properties of SUS 304

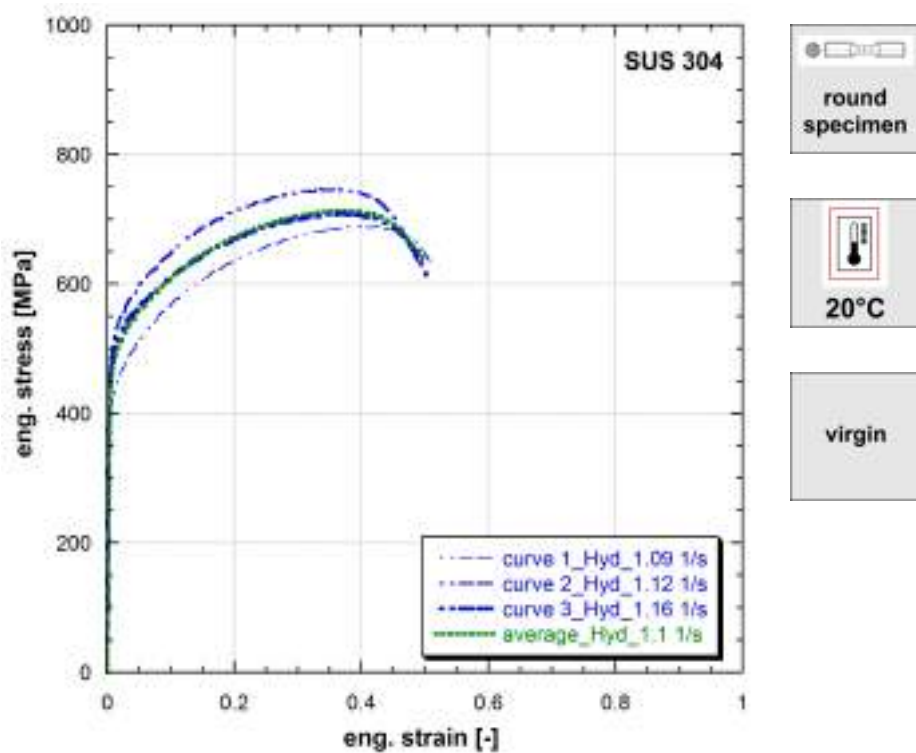


**Figure 9.25:** Stress vs strain curves of SUS 304

Strain rate [1/s]	Yield stress [MPa]	Ultimate tensile strength [MPa]	Uniform strain [-]	Fracture stress [MPa]	Fracture strain [-]
1.09	410	690	0.349	627	0.513
1.12	496	747	0.358	636	0.488
1.16	482	709	0.370	606	0.506
1.1	457	714	0.370	629	0.502

**Table 25:** Mechanical properties of SUS 304

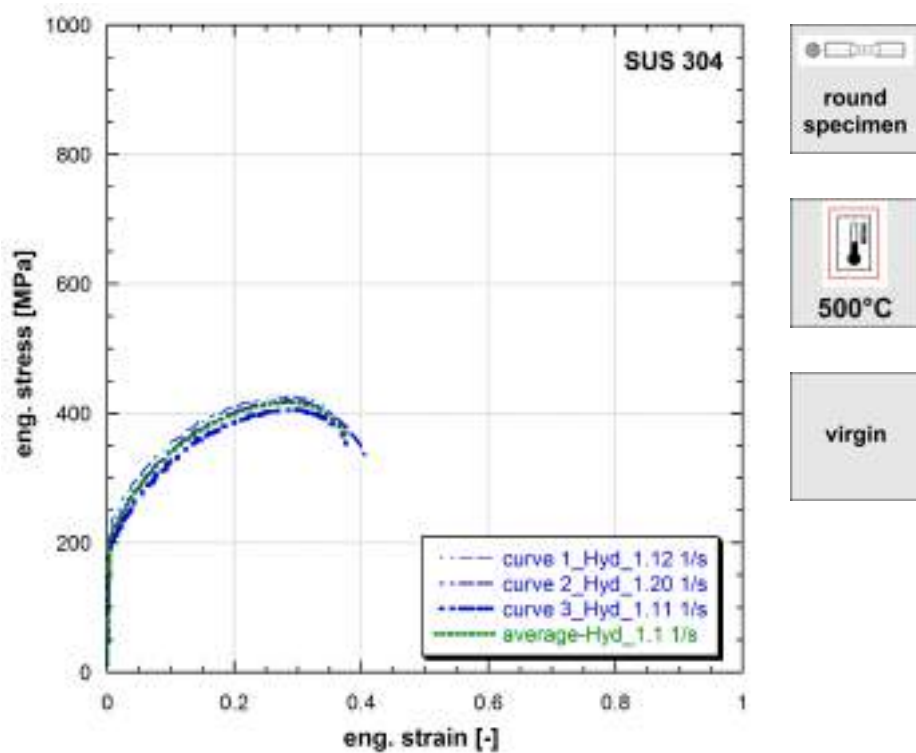


**Figure 9.26:** Stress vs strain curves of SUS 304

Strain rate [1/s]	Yield stress [MPa]	Ultimate tensile strength [MPa]	Uniform strain [-]	Fracture stress [MPa]	Fracture strain [-]
1.12	232	427	0.292	397	0.355
1.2	203	422	0.280	325	0.413
1.11	193	406	0.276	351	0.377
1.1	206	417	0.284	368	0.375

**Table 26:** Mechanical properties of SUS 304

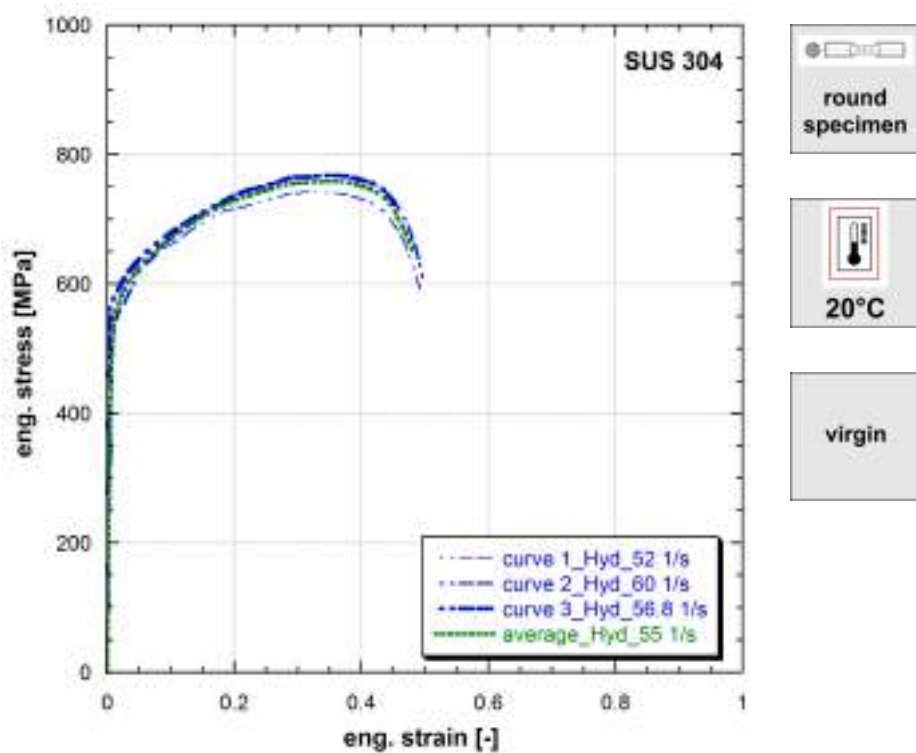


**Figure 9.27:** Stress vs strain curves of SUS 304

Strain rate [1/s]	Yield stress [MPa]	Ultimate tensile strength [MPa]	Uniform strain [-]	Fracture stress [MPa]	Fracture strain [-]
52	544	742	0.314	590	0.493
60	507	768	0.365	611	0.496
57	580	767	0.361	722	0.455
55	542	758	0.357	648	0.481

**Table 27:** Mechanical properties of SUS 304

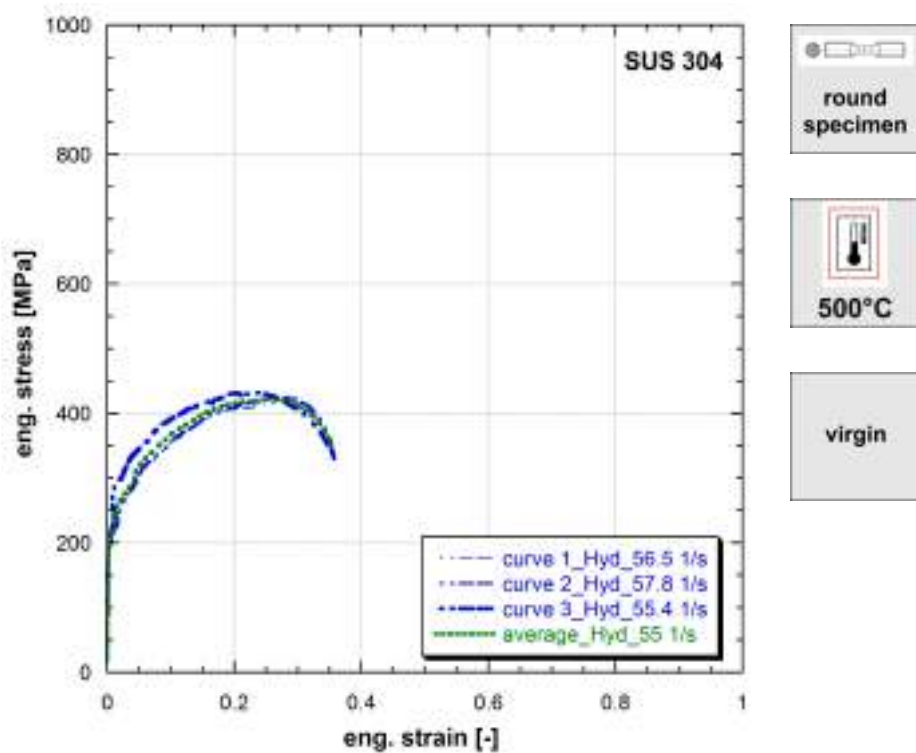


**Figure 9.28:** Stress vs strain curves of SUS 304

Strain rate [1/s]	Yield stress [MPa]	Ultimate tensile strength [MPa]	Uniform strain [-]	Fracture stress [MPa]	Fracture strain [-]
56.5	193	419	0.271	354	0.354
57.8	199	425	0.275	354	0.352
55.4	210	432	0.242	331	0.357
55	201	422	0.260	351	0.353

**Table 28:** Mechanical properties of SUS 304

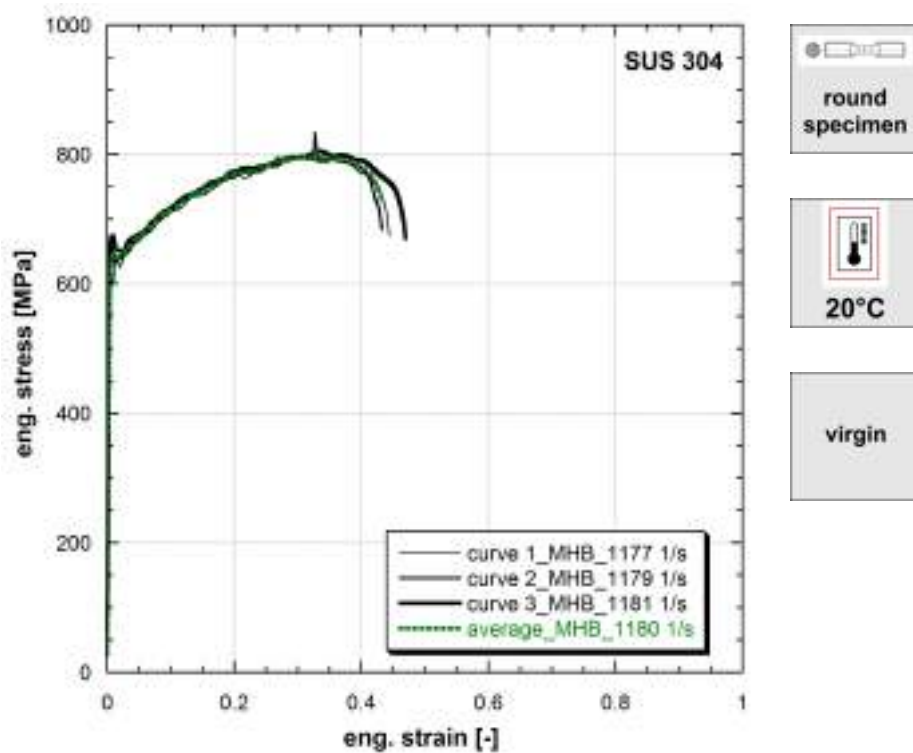


**Figure 9.29:** Stress vs strain curves of SUS 304

Strain rate [1/s]	Yield stress [MPa]	Ultimate tensile strength [MPa]	Uniform strain [-]	Fracture stress [MPa]	Fracture strain [-]
1177	625	797	0.276	675	0.444
1179	653	833	0.327	685	0.432
1181	672	805	0.337	671	0.470
1180	633	808	0.327	732	0.431

**Table 29:** Mechanical properties of SUS 304

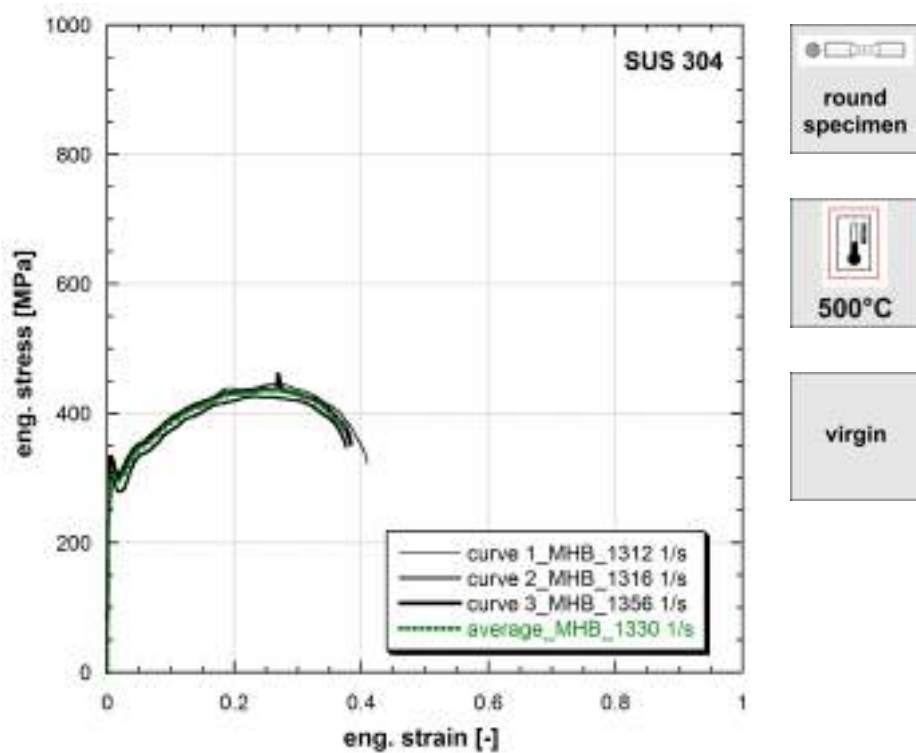


**Figure 9.30:** Stress vs strain curves of SUS 304

Strain rate [1/s]	Yield stress [MPa]	Ultimate tensile strength [MPa]	Uniform strain [-]	Fracture stress [MPa]	Fracture strain [-]
1312	246	446	0.266	322	0.410
1316	308	427	0.231	348	0.376
1356	335	460	0.269	353	0.383
1330	297	441	0.270	372	0.376

**Table 30:** Mechanical properties of SUS 304

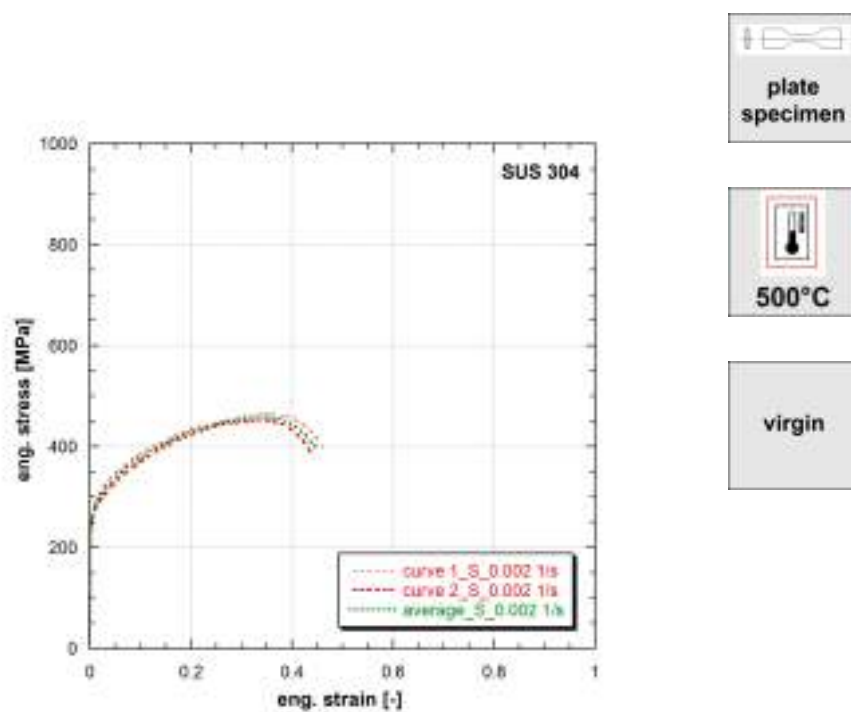


**Figure 9.31:** Stress vs strain curves of SUS 304

Strain rate [1/s]	Yield stress [MPa]	Ultimate tensile strength [MPa]	Uniform strain [-]	Fracture stress [MPa]	Fracture strain [-]
0.002	263	465	0.352	399	0.460
0.002	255	452	0.343	383	0.440
0.002	259	458	0.340	396	0.450

**Table 31:** Mechanical properties of SUS 304

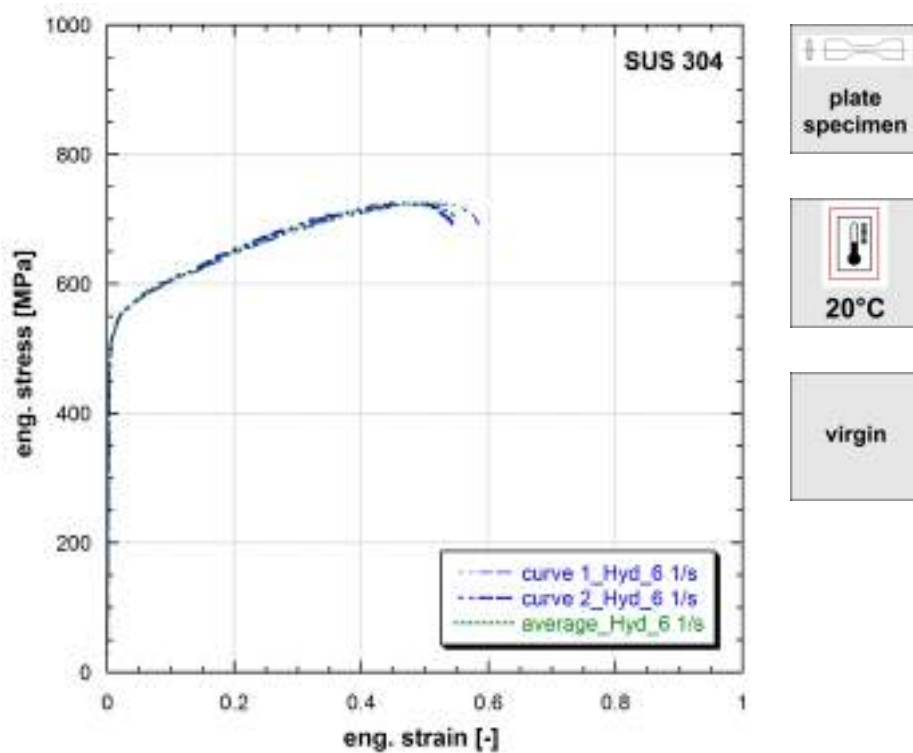


**Figure 9.32:** Stress vs strain curves of SUS 304

Strain rate [1/s]	Yield stress [MPa]	Ultimate tensile strength [MPa]	Uniform strain [-]	Fracture stress [MPa]	Fracture strain [-]
6	503	725	0.515	692	0.585
6	490	725	0.464	689	0.546
6	502	724	0.483	706	0.546

**Table 32:** Mechanical properties of SUS 304

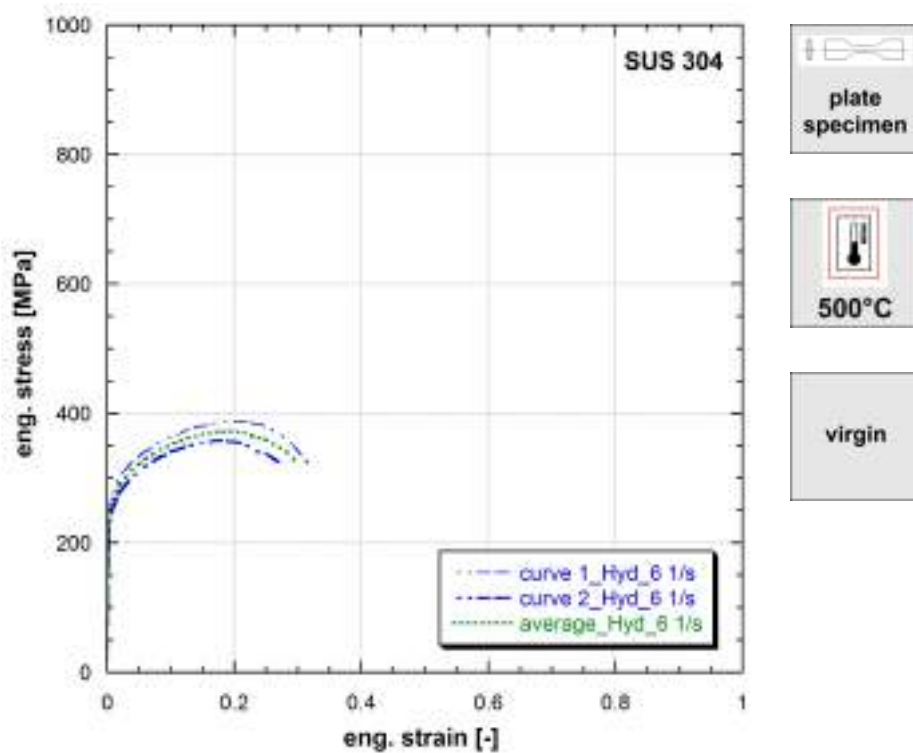


**Figure 9.33:** Stress vs strain curves of SUS 304

Strain rate [1/s]	Yield stress [MPa]	Ultimate tensile strength [MPa]	Uniform strain [-]	Fracture stress [MPa]	Fracture strain [-]
6	257	388	0.195	323	0.316
6	230	358	0.175	322	0.277
6	241	372	0.192	326	0.297

**Table 33:** Mechanical properties of SUS 304

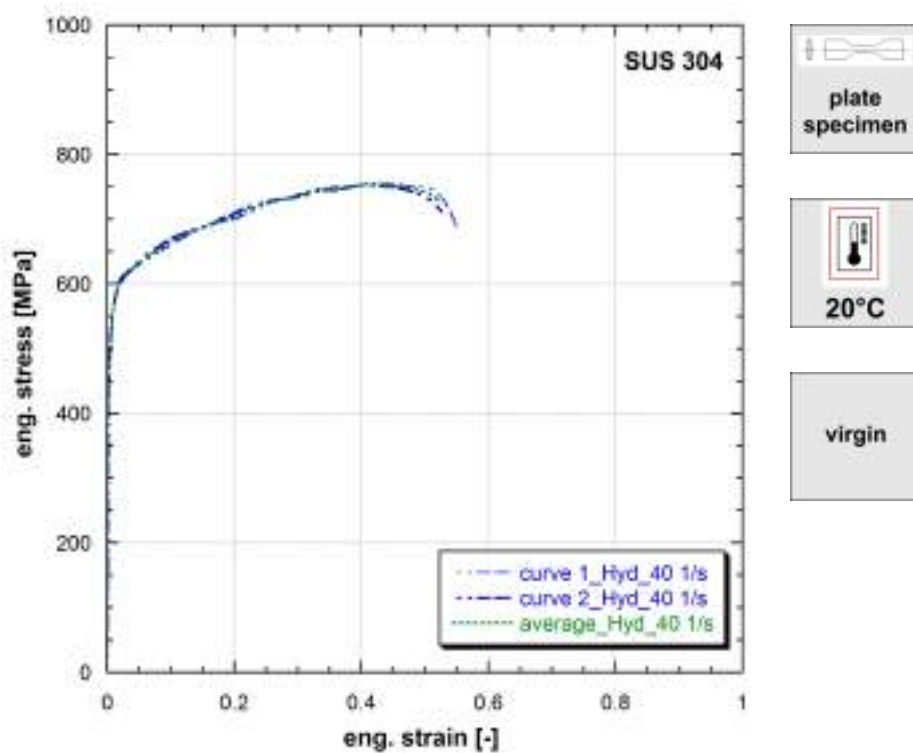


**Figure 9.34:** Stress vs strain curves of SUS 304

Strain rate [1/s]	Yield stress [MPa]	Ultimate tensile strength [MPa]	Uniform strain [-]	Fracture stress [MPa]	Fracture strain [-]
40	437	755	0.426	683	0.552
40	507	752	0.409	712	0.526
40	433	754	0.420	727	0.524

**Table 34:** Mechanical properties of SUS 304

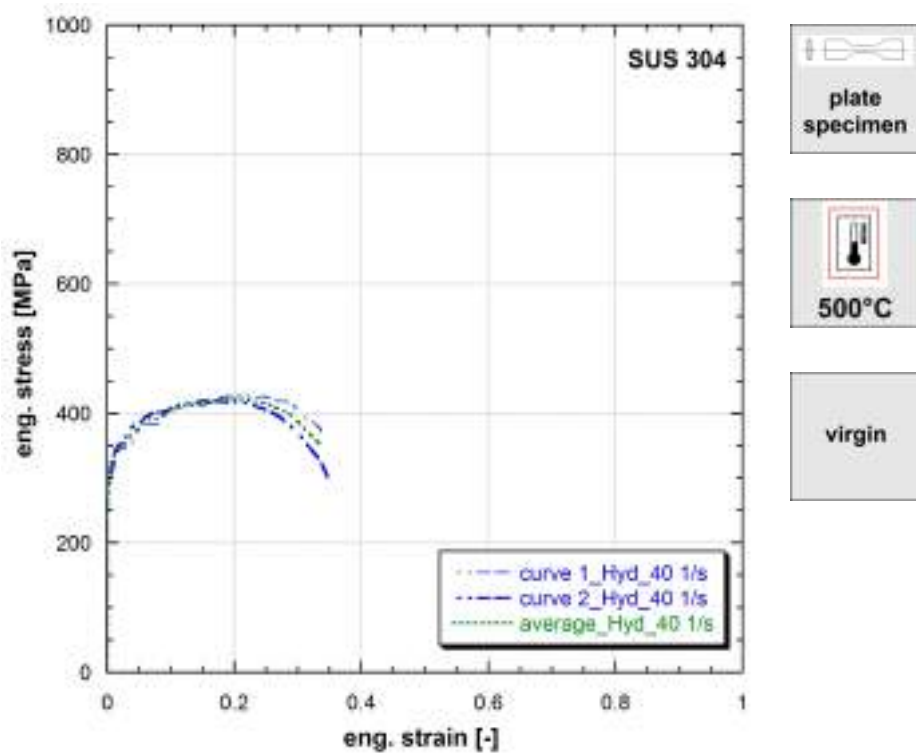


**Figure 9.35:** Stress vs strain curves of SUS 304

Strain rate [1/s]	Yield stress [MPa]	Ultimate tensile strength [MPa]	Uniform strain [-]	Fracture stress [MPa]	Fracture strain [-]
40	302	428	0.213	372	0.337
40	289	420	0.155	301	0.347
40	292	423	0.210	351	0.335

**Table 35:** Mechanical properties of SUS 304

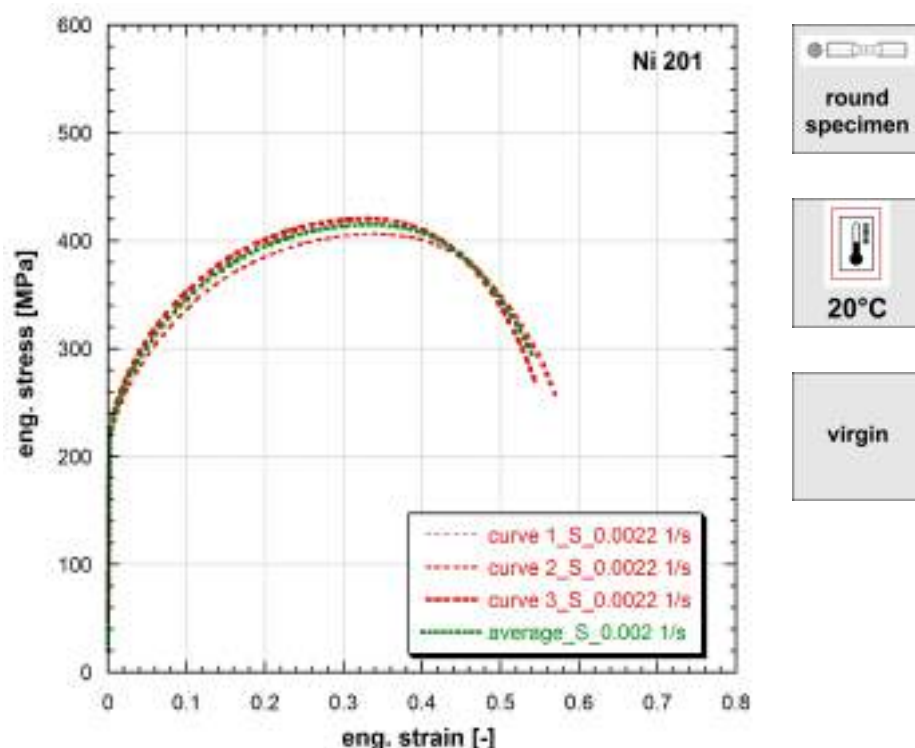


**Figure 9.36:** Stress vs strain curves of Ni 201

Strain rate [1/s]	Yield stress [MPa]	Ultimate tensile strength [MPa]	Uniform strain [-]	Fracture stress [MPa]	Fracture strain [-]
0.0022	227	419	0.340	257	0.568
0.0022	225	406	0.342	252	0.573
0.0022	233	421	0.323	271	0.544
0.002	228	415	0.337	290	0.543

**Table 36:** Mechanical properties of Ni 201

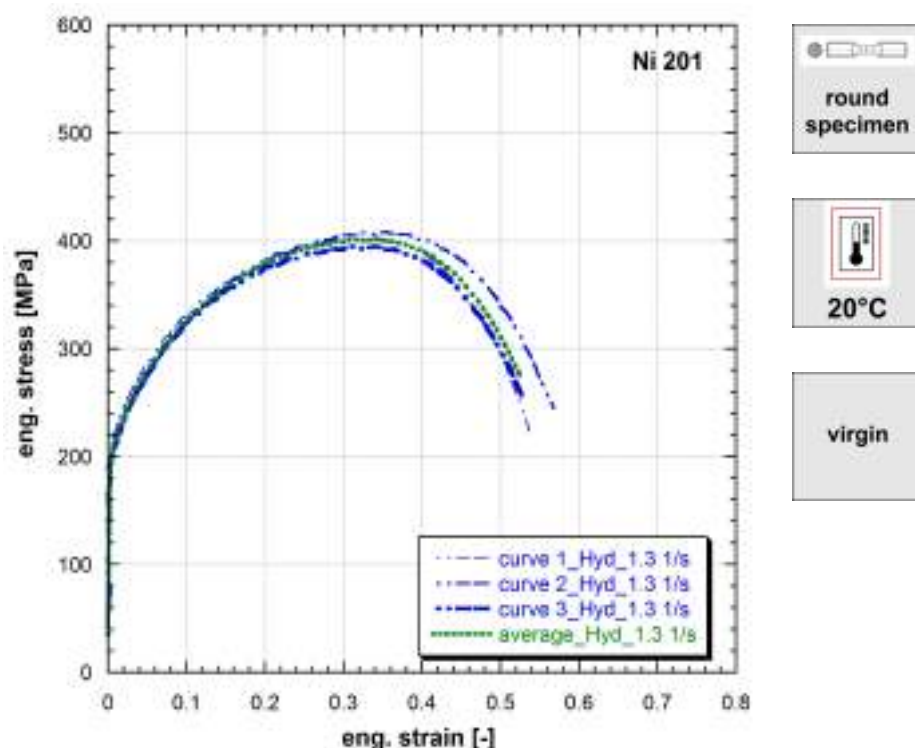


**Figure 9.37:** Stress vs strain curves of Ni 201

Strain rate [1/s]	Yield stress [MPa]	Ultimate tensile strength [MPa]	Uniform strain [-]	Fracture stress [MPa]	Fracture strain [-]
1.3	207	403	0.311	218	0.538
1.3	197	408	0.353	245	0.568
1.3	206	395	0.339	253	0.529
1.3	203	401	0.342	272	0.527

**Table 37:** Mechanical properties of Ni 201

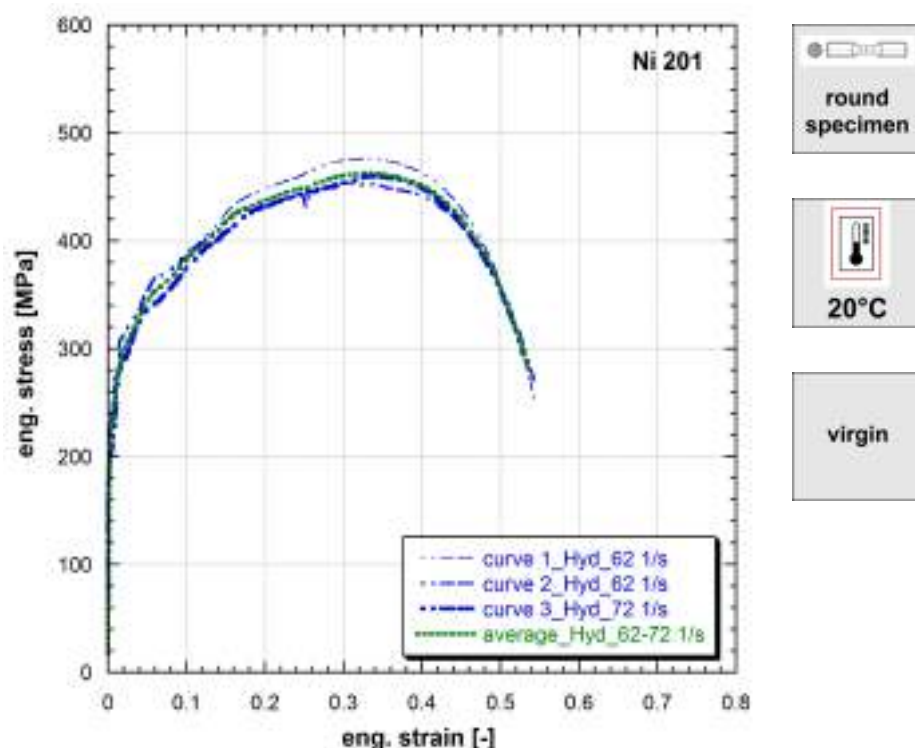


**Figure 9.38:** Stress vs strain curves of Ni 201

Strain rate [1/s]	Yield stress [MPa]	Ultimate tensile strength [MPa]	Uniform strain [-]	Fracture stress [MPa]	Fracture strain [-]
62	242	477	0.336	251	0.544
62	239	454	0.315	271	0.542
72	207	460	0.345	295	0.529
62-72	227	463	0.335	275	0.538

**Table 38:** Mechanical properties of Ni 201

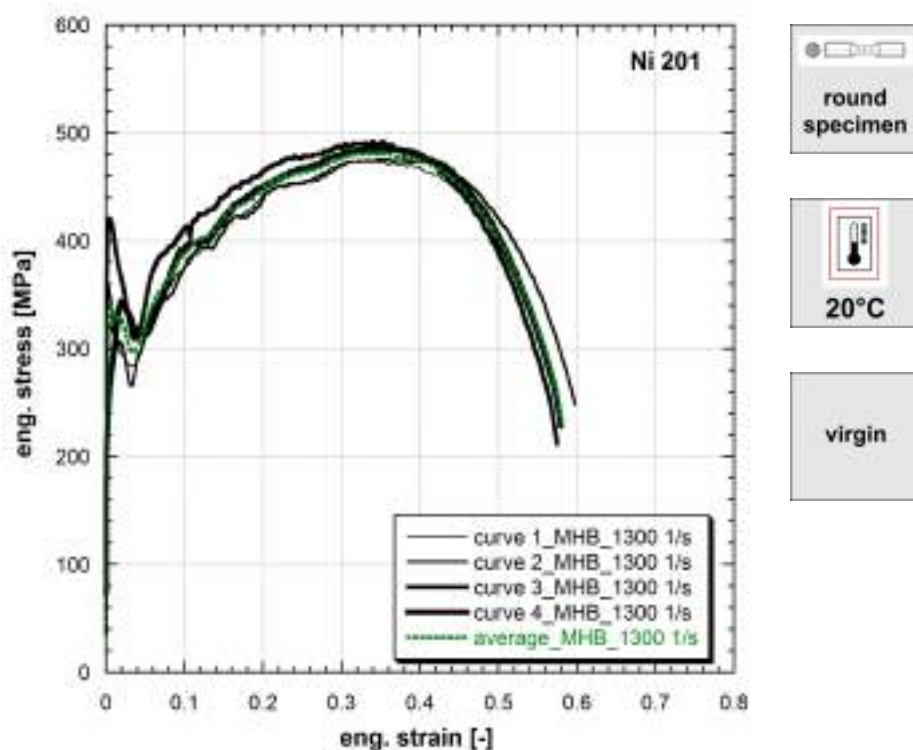


**Figure 9.39:** Stress vs strain curves of Ni 201

Strain rate [1/s]	Yield stress [MPa]	Ultimate tensile strength [MPa]	Uniform strain [-]	Fracture stress [MPa]	Fracture strain [-]
1300	320	475	0.332	255	0.574
1300	348	476	0.354	248	0.597
1300	418	492	0.340	212	0.575
1300	263	486	0.336	229	0.580
1300	338	482	0.353	230	0.582

**Table 39:** Mechanical properties of Ni 201

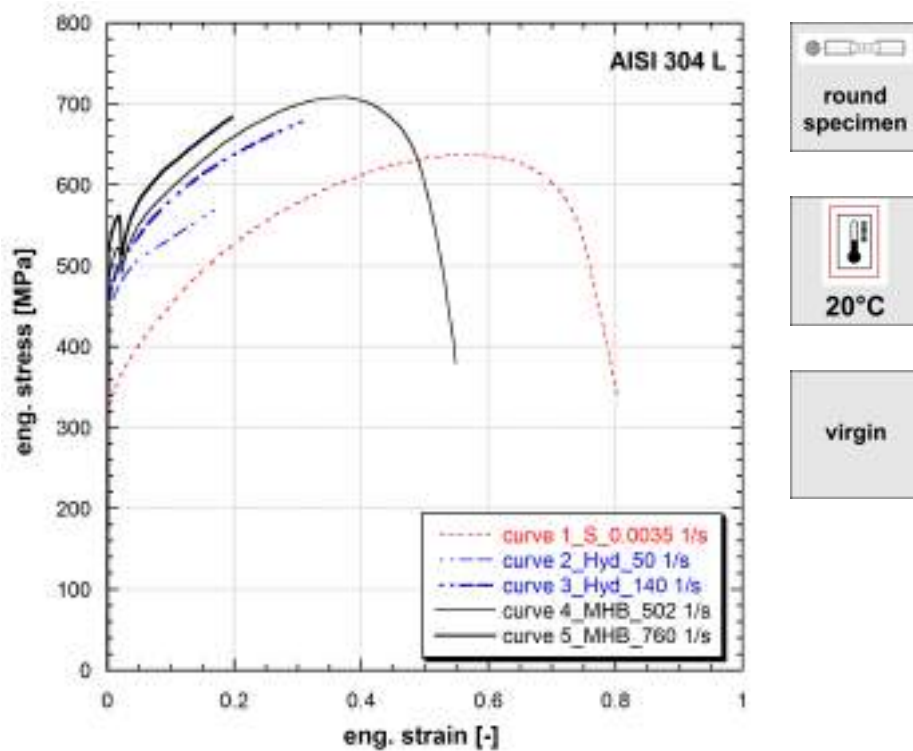


**Figure 9.40:** Stress vs strain curves of AISI 304 L

Strain rate [1/s]	Yield stress [MPa]	Ultimate tensile strength [MPa]	Uniform strain [-]	Fracture stress [MPa]	Fracture strain [-]
0.0035	324	638	0.549	337	0.804
50	433	-	-	-	-
140	462	-	-	-	-
502	487	708	0.376	379	0.549
760	527	-	-	-	-

**Table 40:** Mechanical properties of AISI 304L

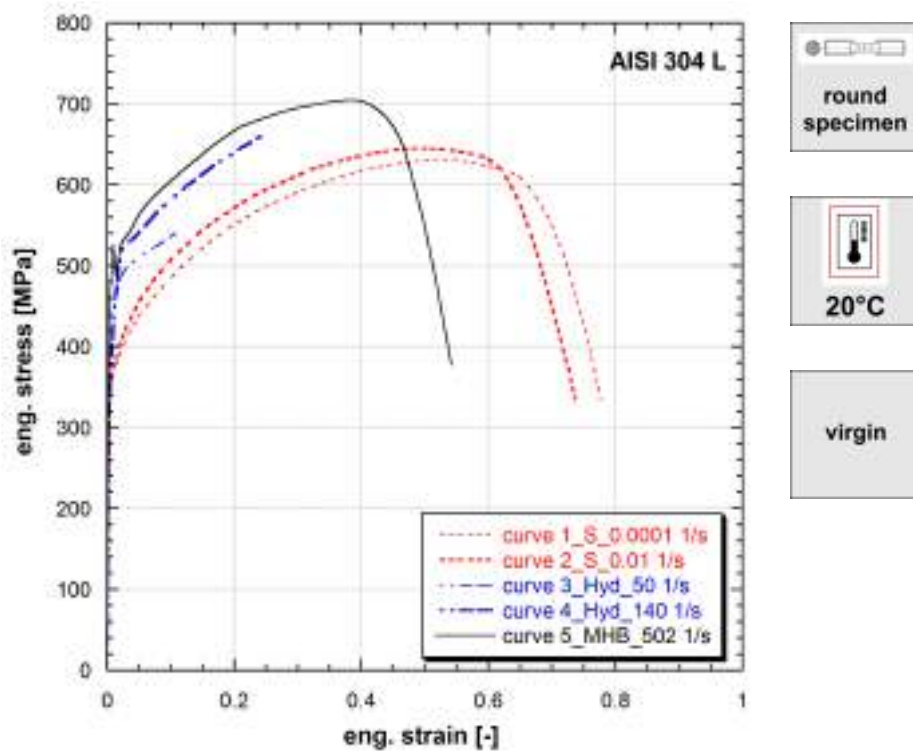


**Figure 9.41:** Stress vs strain curves of AISI 304 L

Strain rate [1/s]	Yield stress [MPa]	Ultimate tensile strength [MPa]	Uniform strain [-]	Fracture stress [MPa]	Fracture strain [-]
0.0001		630	0.521	335	0.777
0.01	333	645	0.510	336	0.737
50	342	-	-	-	-
140	362	-	-	-	-
502	482	705	0.375	377	0.542

**Table 41:** Mechanical properties of AISI 304L

Published in (Albertini and Montagnani, 1974), (Albertini and Montagnani, 1976).

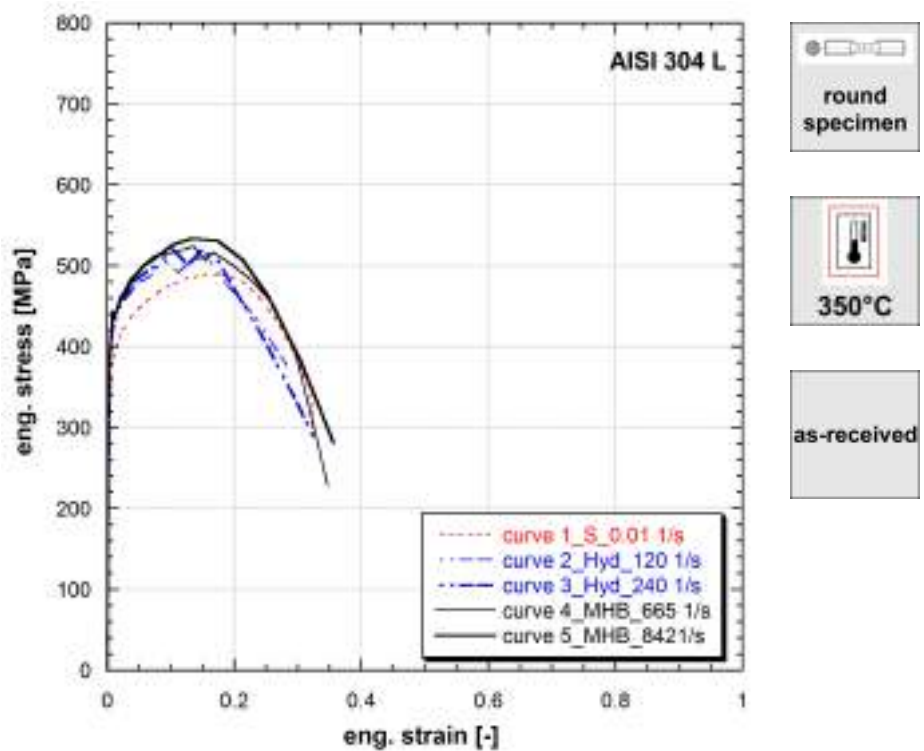


**Figure 9.42:** Stress vs strain curves of AISI 304 L

Strain rate [1/s]	Yield stress [MPa]	Ultimate tensile strength [MPa]	Uniform strain [-]	Fracture stress [MPa]	Fracture strain [-]
0.01	332	489	0.170	288	0.324
120	372	511	0.158	377	0.284
240	387	520	0.103	288	0.325
665	393	524	0.136	228	0.347
842	398	534	0.133	281	0.356

**Table 42:** Mechanical properties of AISI 304L

Published in (Albertini and Montagnani, 1976).

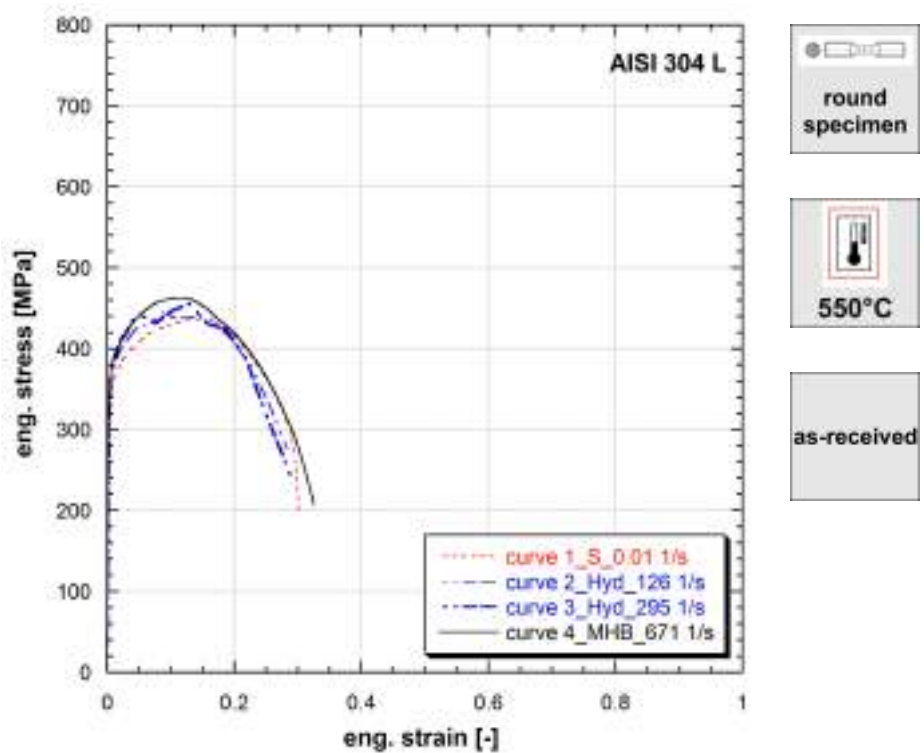


**Figure 9.43:** Stress vs strain curves of AISI 304 L

Strain rate [1/s]	Yield stress [MPa]	Ultimate tensile strength [MPa]	Uniform strain [-]	Fracture stress [MPa]	Fracture strain [-]
0.01	312	435	0.149	201	0.301
126	342	444	0.088	276	0.284
295	347	455	0.130	237	0.292
671	362	463	0.108	208	0.326

**Table 43:** Mechanical properties of AISI 304L

Published in (Albertini and Montagnani, 1976).

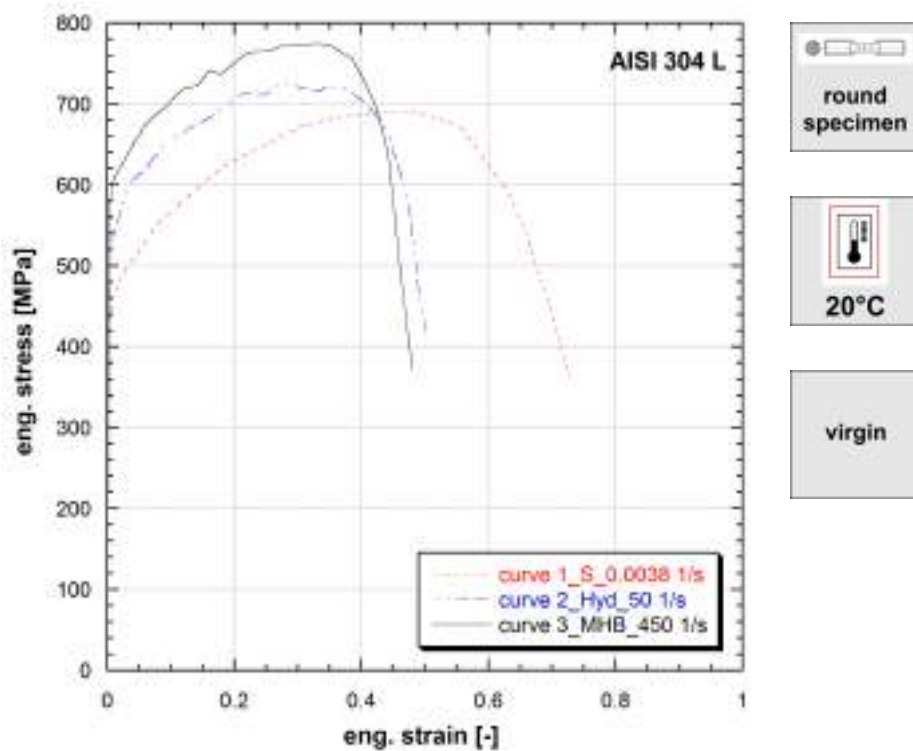


**Figure 9.44:** Stress vs strain curves of AISI 304 L (Ref.Mat.1)

**Note 9.44** Ref.Mat.1

Strain rate [1/s]	Yield stress [MPa]	Ultimate tensile strength [MPa]	Uniform strain [-]	Fracture stress [MPa]	Fracture strain [-]
0.0038	436	690	0.442	364	0.729
50	524	725	0.278	417	0.503
450	582	774	0.333	372	0.480

**Table 44:** Mechanical properties of AISI 304L (Ref.Mat.1)

Published in (Albertini and Montagnani, 1980), (Albertini et al., 1980).

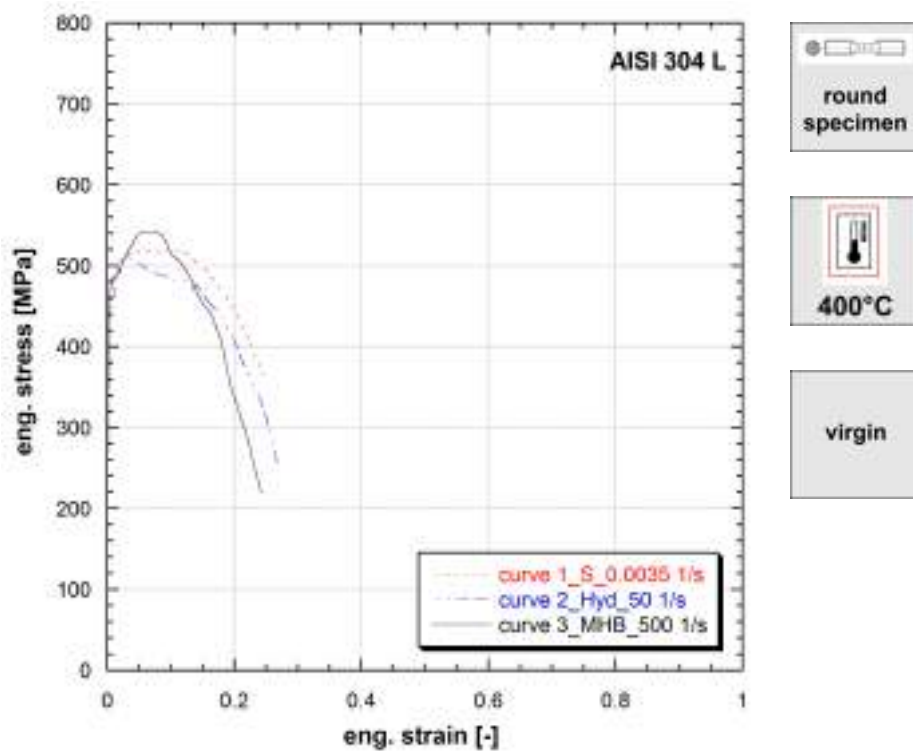


**Figure 9.45:** Stress vs strain curves of AISI 304 L (Ref.Mat.1)

**Note 9.45** Ref.Mat.1

Strain rate [1/s]	Yield stress [MPa]	Ultimate tensile strength [MPa]	Uniform strain [-]	Fracture stress [MPa]	Fracture strain [-]
0.0035	450	520	0.089	366	0.245
50	437	511	0.033	252	0.269
500	462	543	0.074	219	0.243

**Table 45:** Mechanical properties of AISI 304L (Ref.Mat.1)

Published in (Albertini and Montagnani, 1980), (Albertini et al., 1980).

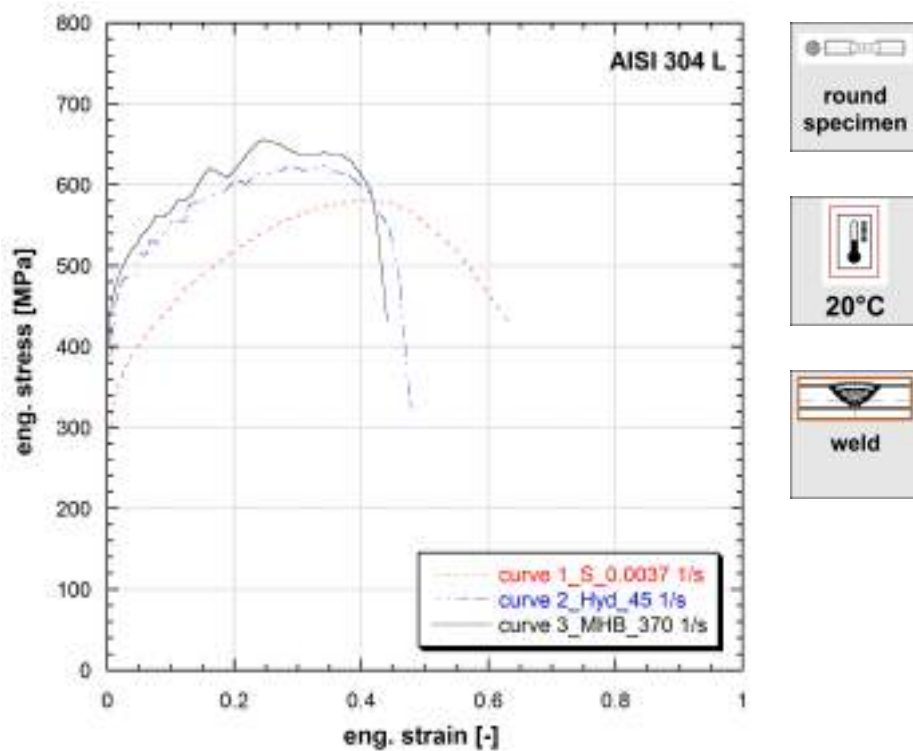


**Figure 9.46:** Stress vs strain curves of AISI 304 L (Ref.Mat.1)

**Note 9.46** Ref.Mat.1

Argon arc welding.

Strain rate [1/s]	Yield stress [MPa]	Ultimate tensile strength [MPa]	Uniform strain [-]	Fracture stress [MPa]	Fracture strain [-]
0.0037	287	581	0.416	427	0.634
45	384	625	0.333	323	0.478
370	427	656	0.245	432	0.441

**Table 46:** Mechanical properties of AISI 304L (Ref.Mat.1)

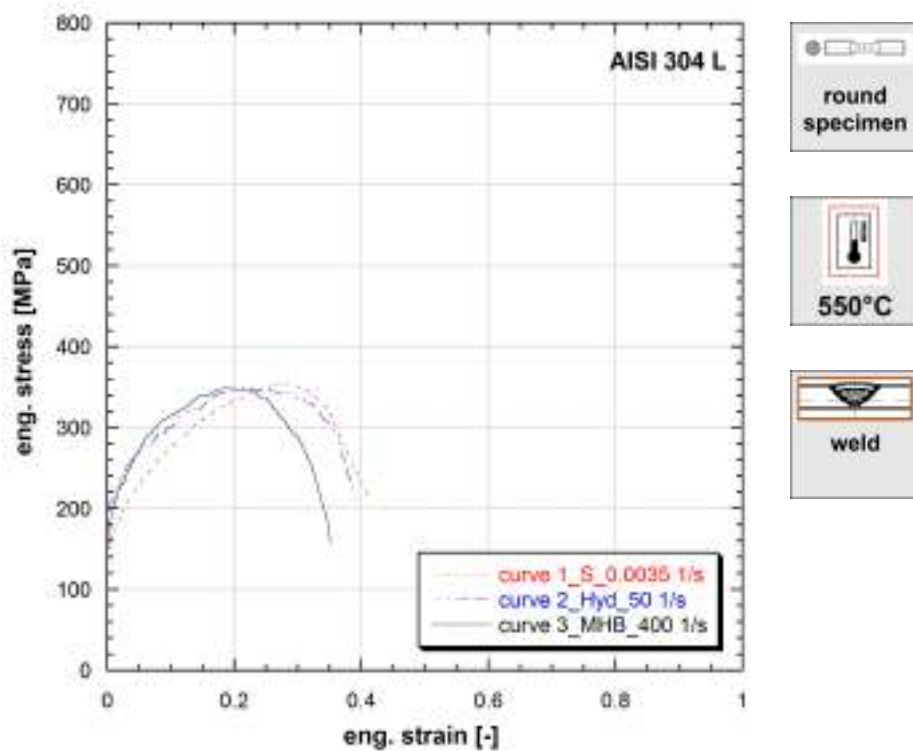


**Figure 9.47:** Stress vs strain curves of AISI 304 L (Ref.Mat.1)

**Note 9.47** Ref.Mat.1

Argon arc welding.

Strain rate [1/s]	Yield stress [MPa]	Ultimate tensile strength [MPa]	Uniform strain [-]	Fracture stress [MPa]	Fracture strain [-]
0.0035	142	355	0.277	213	0.412
50	198	349	0.205	206	0.392
400	171	348	0.184	158	0.351

**Table 47:** Mechanical properties of AISI 304L (Ref.Mat.1)

Published in (Albertini and Montagnani, 1980).

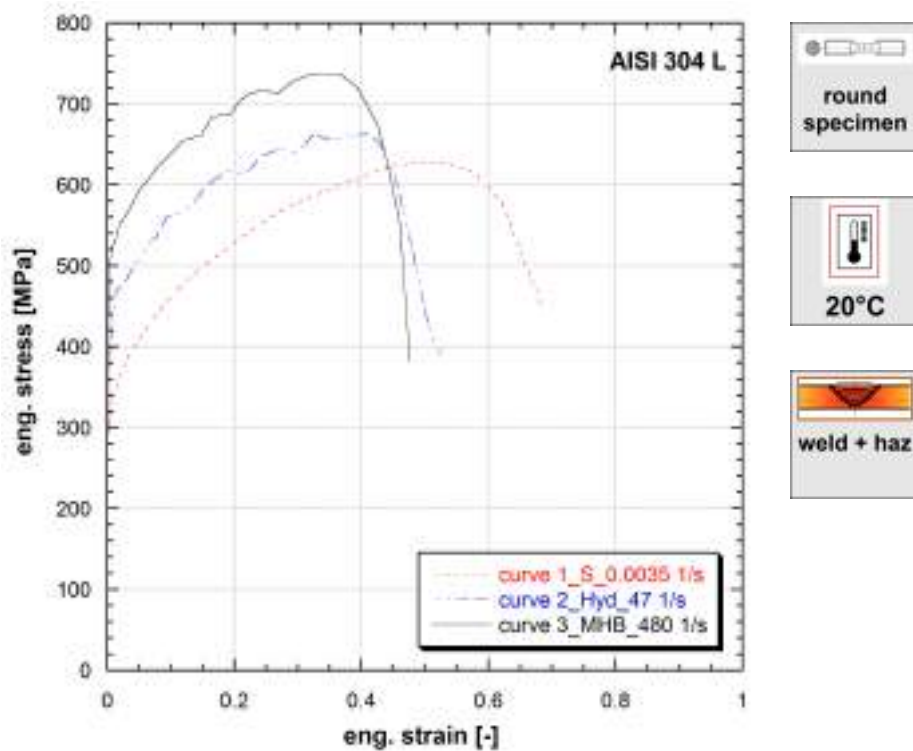


**Figure 9.48:** Stress vs strain curves of AISI 304 L (Ref.Mat.1)

**Note 9.48** Ref.Mat.1

*Argon arc welding.*

Strain rate [1/s]	Yield stress [MPa]	Ultimate tensile strength [MPa]	Uniform strain [-]	Fracture stress [MPa]	Fracture strain [-]
0.0035	298	628	0.500	453	0.683
47	371	665	0.327	391	0.525
480	502	738	0.366	382	0.477

**Table 48:** Mechanical properties of AISI 304L (Ref.Mat.1)

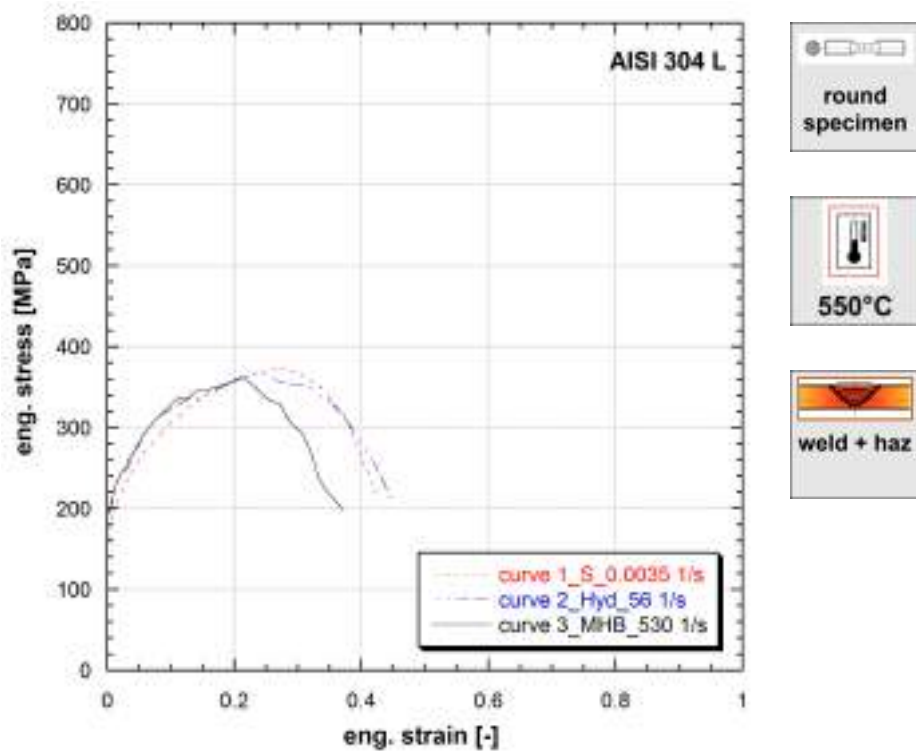


**Figure 9.49:** Stress vs strain curves of AISI 304 L (Ref.Mat.1)

**Note 9.49** Ref.Mat.1

Argon arc welding.

Strain rate [1/s]	Yield stress [MPa]	Ultimate tensile strength [MPa]	Uniform strain [-]	Fracture stress [MPa]	Fracture strain [-]
0.0035	166	373	0.270	211	0.428
56	197	366	0.227	203	0.451
530	197	358	0.221	198	0.372

**Table 49:** Mechanical properties of AISI 304L (Ref.Mat.1)

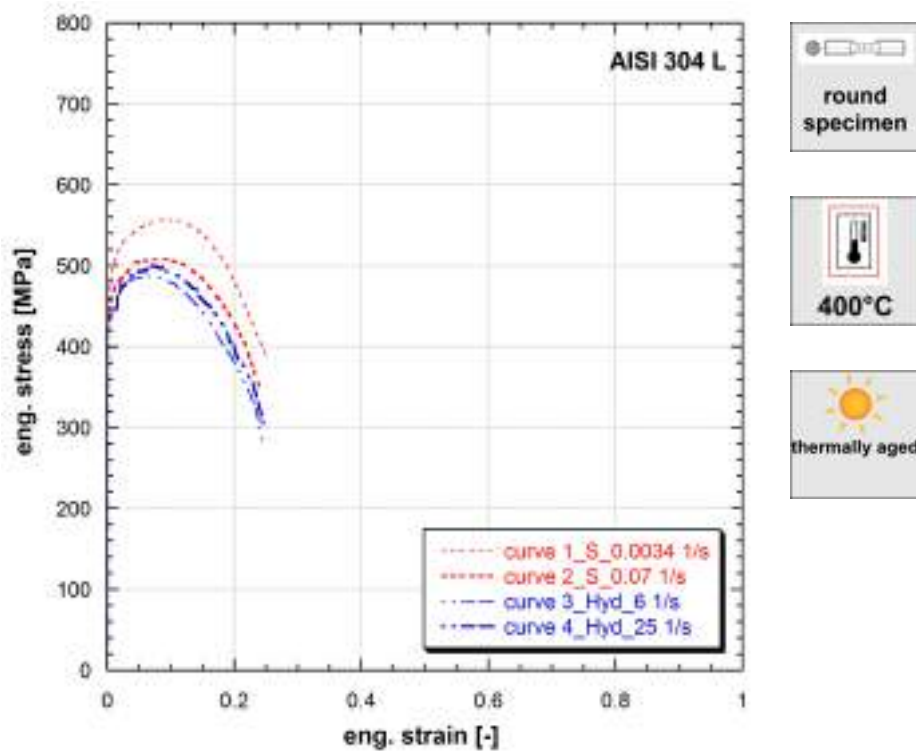


**Figure 9.50:** Stress vs strain curves of AISI 304 L (Ref.Mat.1)

**Note 9.50** Ref.Mat.1

*Thermally aged in sodium for 3264 hours at 550°C.*

Strain rate [1/s]	Yield stress [MPa]	Ultimate tensile strength [MPa]	Uniform strain [-]	Fracture stress [MPa]	Fracture strain [-]
0.0034	460	557	0.086	390	0.249
0.07	443	508	0.097	350	0.239
6	427	487	0.064	283	0.246
25	433	501	0.072	296	0.249

**Table 50:** Mechanical properties of AISI 304L (Ref.Mat.1)

*Published in (Albertini et al., 1981).*

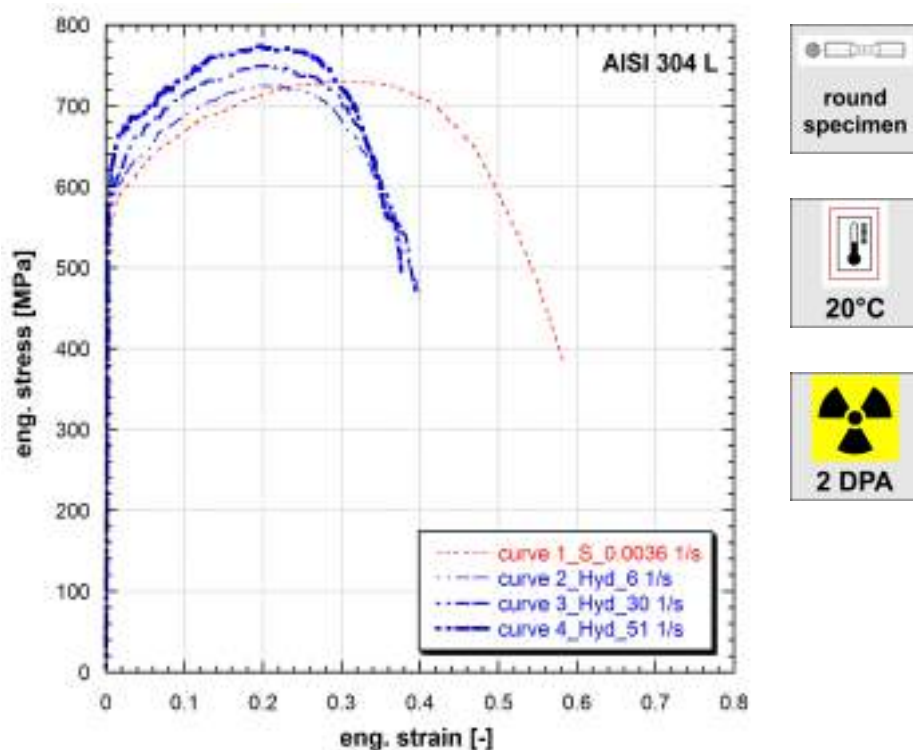


**Figure 9.51:** Stress vs strain curves of AISI 304 L (Ref.Mat.1)

**Note 9.51** Ref.Mat.1

*Irradiated in sodium at 550°C in HFR reactor, for 3000 hours.*

Strain rate [1/s]	Yield stress [MPa]	Ultimate tensile strength [MPa]	Uniform strain [-]	Fracture stress [MPa]	Fracture strain [-]
0.0036	542	729	0.288	384	0.583
6	569	726	0.195	463	0.402
30	580	749	0.201	473	0.393
51	598	774	0.197	496	0.376

**Table 51:** Mechanical properties of AISI 304L (Ref.Mat.1)

*Published in (Albertini et al., 1981).*

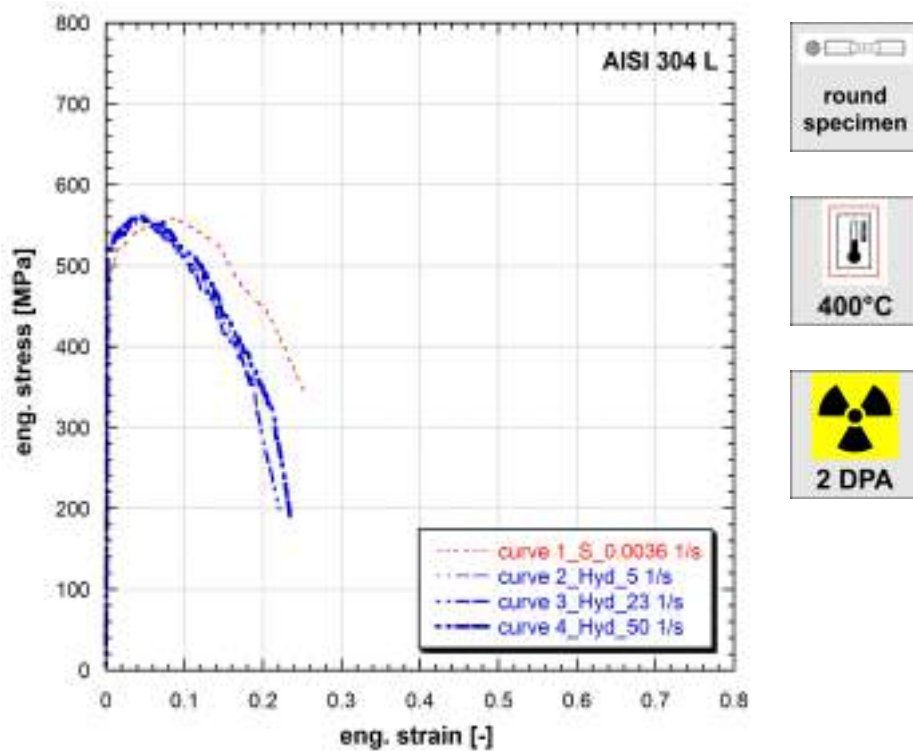


**Figure 9.52:** Stress vs strain curves of AISI 304 L (Ref.Mat.1)

**Note 9.52** Ref.Mat.1

*Irradiated in sodium at 550°C in HFR reactor, for 3000 hours.*

Strain rate [1/s]	Yield stress [MPa]	Ultimate tensile strength [MPa]	Uniform strain [-]	Fracture stress [MPa]	Fracture strain [-]
0.0036	477	557	0.091	346	0.252
5	513	558	0.047	348	0.187
23	510	557	0.036	196	0.222
50	520	562	0.047	191	0.234

**Table 52:** Mechanical properties of AISI 304L (Ref.Mat.1)

*Published in (Albertini et al., 1981), (Albertini and Montagnani, 1980), (Albertini et al., 1980).*

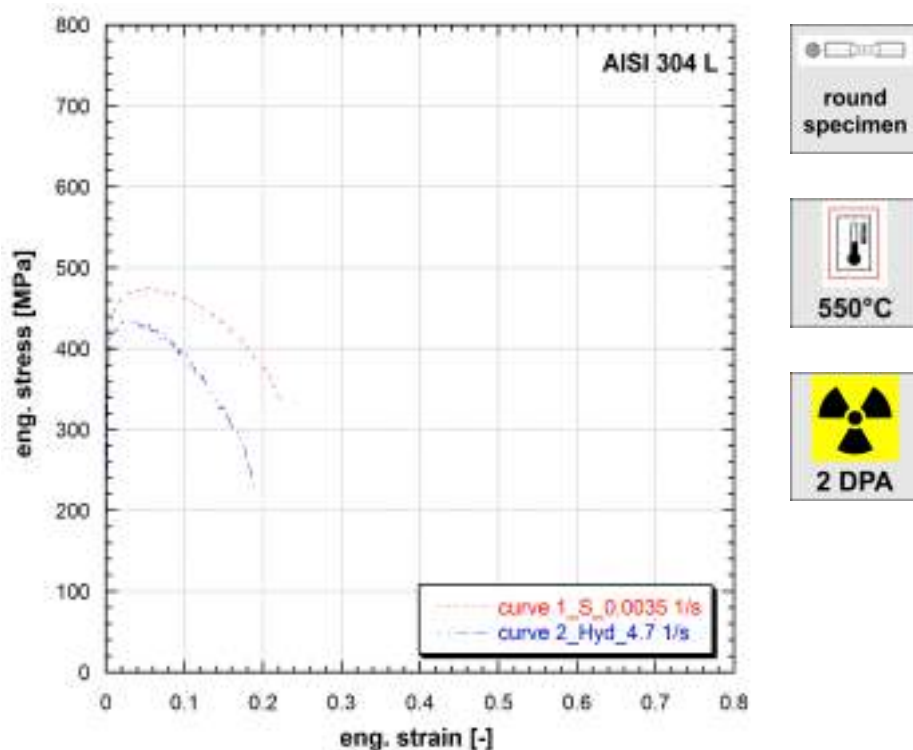


**Figure 9.53:** Stress vs strain curves of AISI 304 L (Ref.Mat.1)

**Note 9.53** Ref.Mat.1

Irradiated in sodium at 550°C in HFR reactor, for 3000 hours.

Strain rate [1/s]	Yield stress [MPa]	Ultimate tensile strength [MPa]	Uniform strain [-]	Fracture stress [MPa]	Fracture strain [-]
0.0035	410	475	0.055	335	0.224
4.7	413	434	0.022	230	0.187

**Table 53:** Mechanical properties of AISI 304L (Ref.Mat.1)

Published in (Albertini et al., 1981).

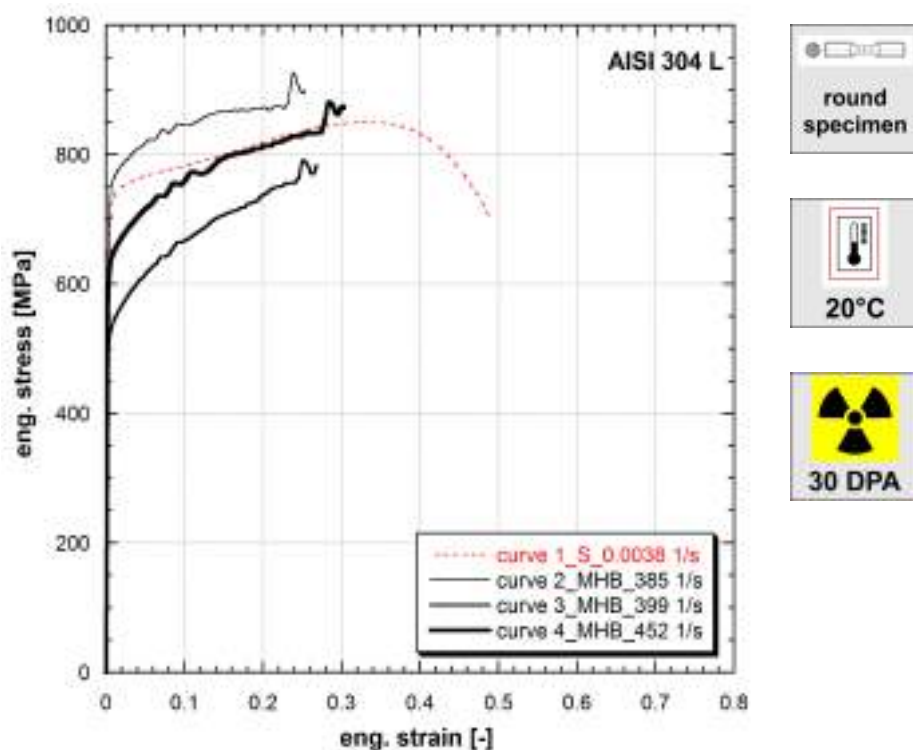


**Figure 9.54:** Stress vs strain curves of AISI 304 L (Ref.Mat.1)

**Note 9.54** Ref.Mat.1

*Irradiated in sodium at 550°C in HFR reactor, for 30000 hours.*

Strain rate [1/s]	Yield stress [MPa]	Ultimate tensile strength [MPa]	Uniform strain [-]	Fracture stress [MPa]	Fracture strain [-]
0.0038	686	849	0.346	703	0.489
385	720	926	0.239	898	0.254
399	512	791	0.250	784	0.268
452	622	881	0.285	872	0.304

**Table 54:** Mechanical properties of AISI 304L (Ref.Mat.1)

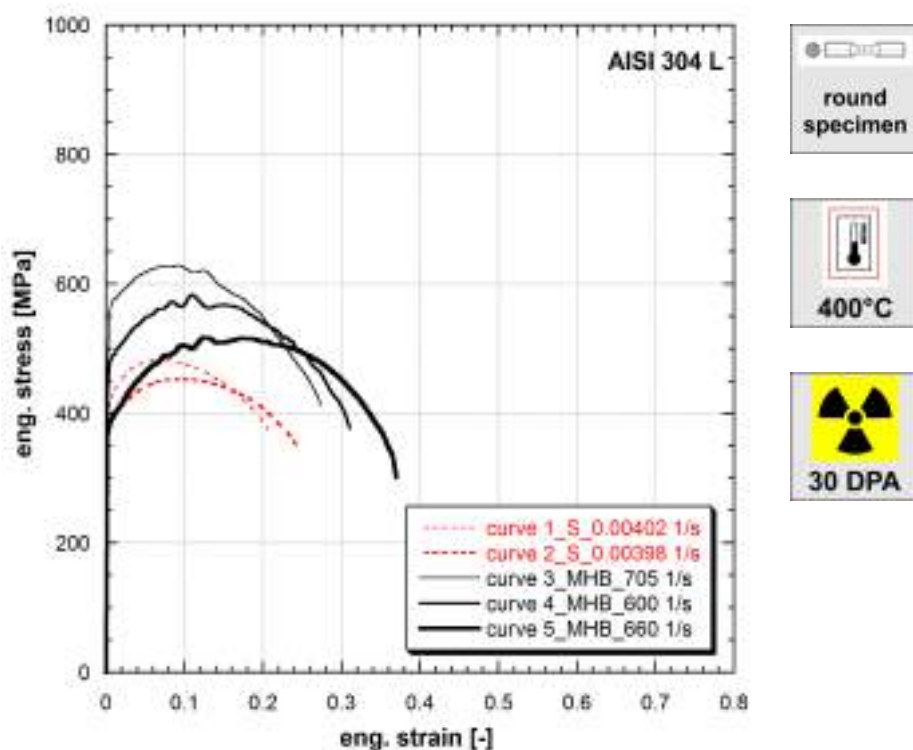


**Figure 9.55:** Stress vs strain curves of AISI 304 L (Ref.Mat.1)

**Note 9.55** Ref.Mat.1

*Irradiated in sodium at 550°C in HFR reactor, for 30000 hours.*

Strain rate [1/s]	Yield stress [MPa]	Ultimate tensile strength [MPa]	Uniform strain [-]	Fracture stress [MPa]	Fracture strain [-]
0.00402	408	483	0.077	376	0.207
0.00398	378	453	0.100	352	0.242
705	554	628	0.091	412	0.273
600	470	583	0.109	377	0.311
660	379	517	0.124	301	0.370

**Table 55:** Mechanical properties of AISI 304L (Ref.Mat.1)

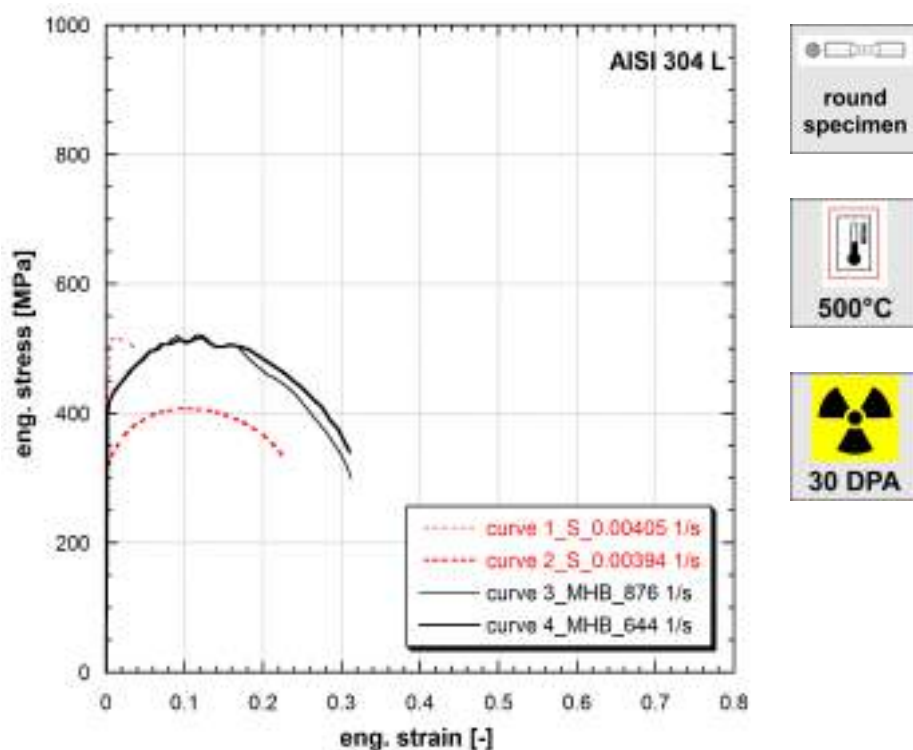


**Figure 9.56:** Stress vs strain curves of AISI 304 L (Ref.Mat.1)

**Note 9.56** Ref.Mat.1

*Irradiated in sodium at 550°C in HFR reactor, for 30000 hours.*

Strain rate [1/s]	Yield stress [MPa]	Ultimate tensile strength [MPa]	Uniform strain [-]	Fracture stress [MPa]	Fracture strain [-]
0.00405	481	516	0.014	497	0.039
0.00394	319	407	0.092	336	0.224
876	417	521	0.116	300	0.312
644	419	517	0.119	340	0.311

**Table 56:** Mechanical properties of AISI 304L (Ref.Mat.1)

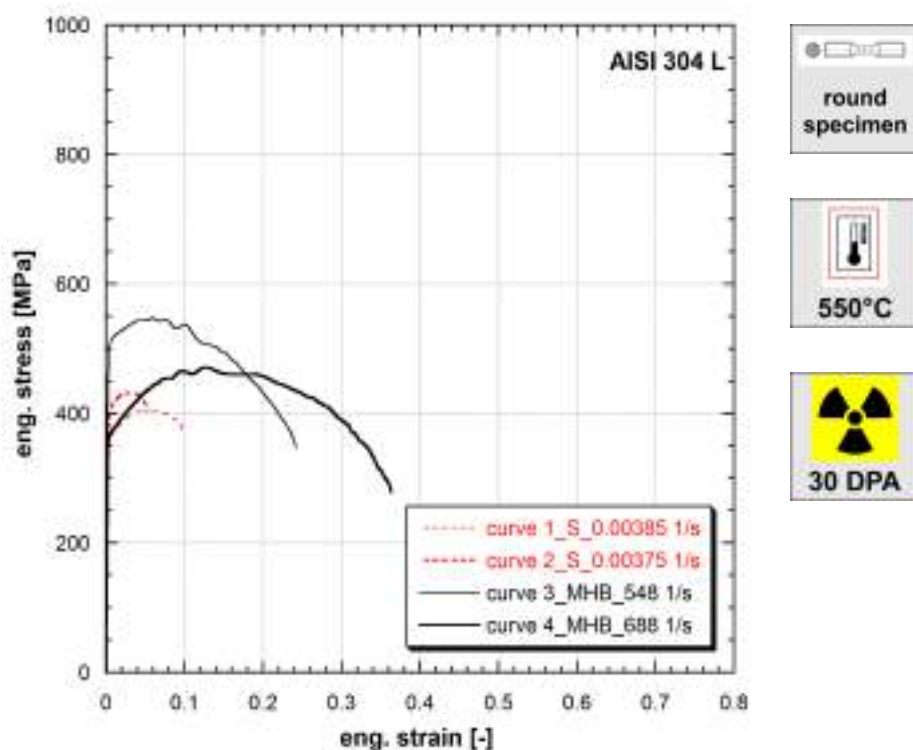


**Figure 9.57:** Stress vs strain curves of AISI 304 L (Ref.Mat.1)

**Note 9.57** Ref.Mat.1

*Irradiated in sodium at 550°C in HFR reactor, for 30000 hours.*

Strain rate [1/s]	Yield stress [MPa]	Ultimate tensile strength [MPa]	Uniform strain [-]	Fracture stress [MPa]	Fracture strain [-]
0.00385	331	405	0.054	374	0.099
0.00375	389	432	0.028	412	0.051
548	505	548	0.059	346	0.242
688	360	471	0.129	278	0.363

**Table 57:** Mechanical properties of AISI 304L (Ref.Mat.1)

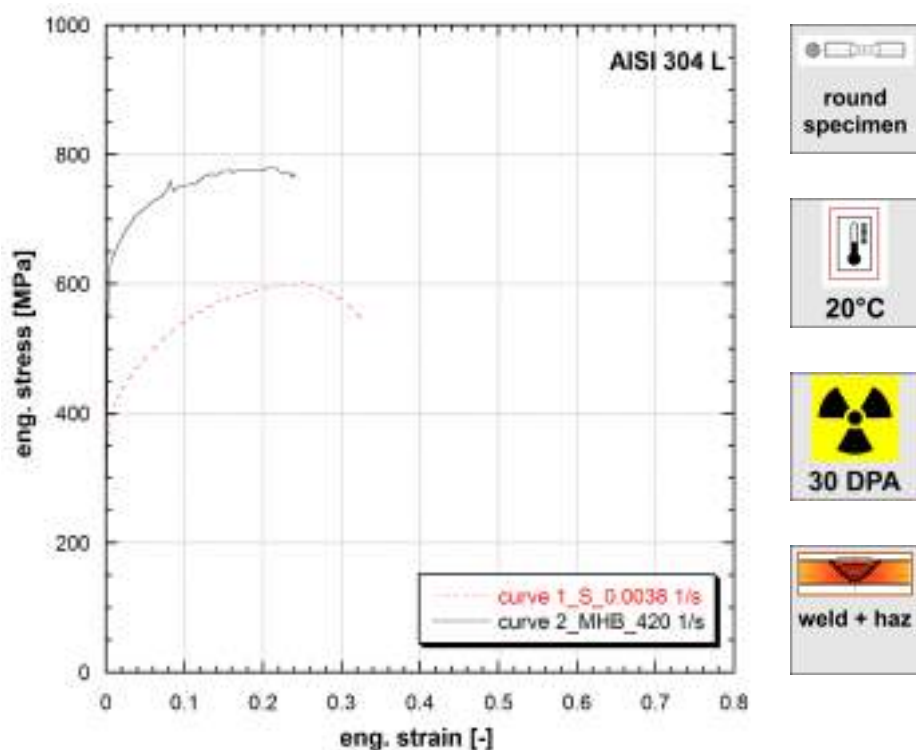


**Figure 9.58:** Stress vs strain curves of AISI 304 L (Ref.Mat.1)

**Note 9.58** Ref.Mat.1

*Irradiated in sodium at 550°C in HFR reactor, for 30000 hours.*

*Argon arc welding.*

Strain rate [1/s]	Yield stress [MPa]	Ultimate tensile strength [MPa]	Uniform strain [-]	Fracture stress [MPa]	Fracture strain [-]
0.0038	375	600	0.251	541	0.327
420	613	778	0.203	764	0.242

**Table 58:** Mechanical properties of AISI 304L (Ref.Mat.1)

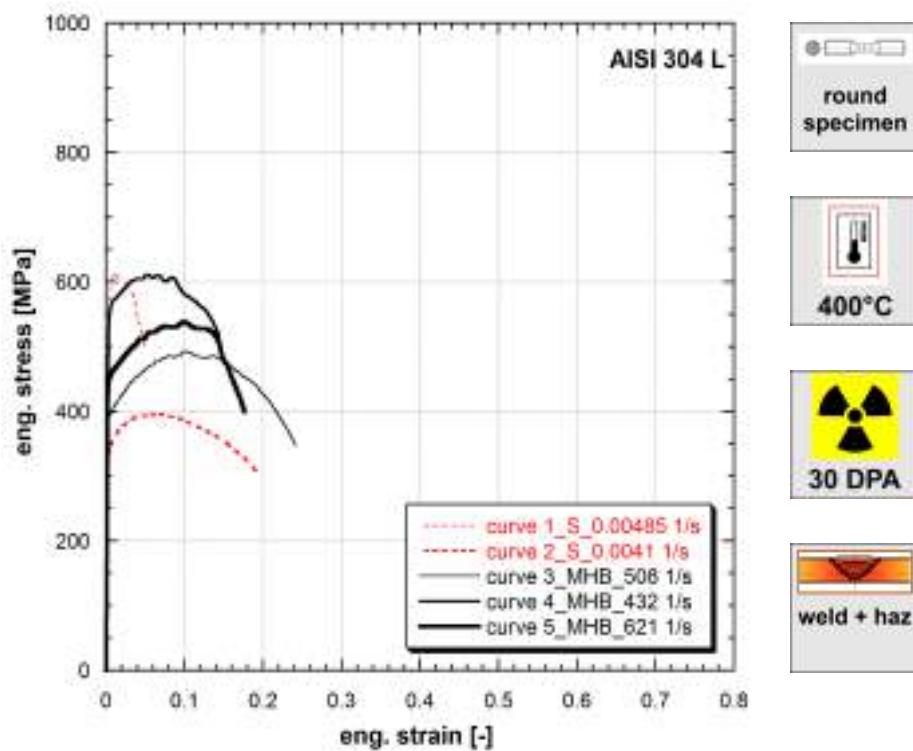


**Figure 9.59:** Stress vs strain curves of AISI 304 L (Ref.Mat.1)

**Note 9.59** Ref.Mat.1

*Irradiated in sodium at 550°C in HFR reactor, for 30000 hours.*

*Argon arc welding.*

Strain rate [1/s]	Yield stress [MPa]	Ultimate tensile strength [MPa]	Uniform strain [-]	Fracture stress [MPa]	Fracture strain [-]
0.00485	583	612	0.009	499	0.049
0.0041	331	396	0.068	301	0.195
508	390	493	0.098	347	0.242
432	557	611	0.055	517	0.144
621	453	538	0.098	400	0.177

**Table 59:** Mechanical properties of AISI 304L (Ref.Mat.1)

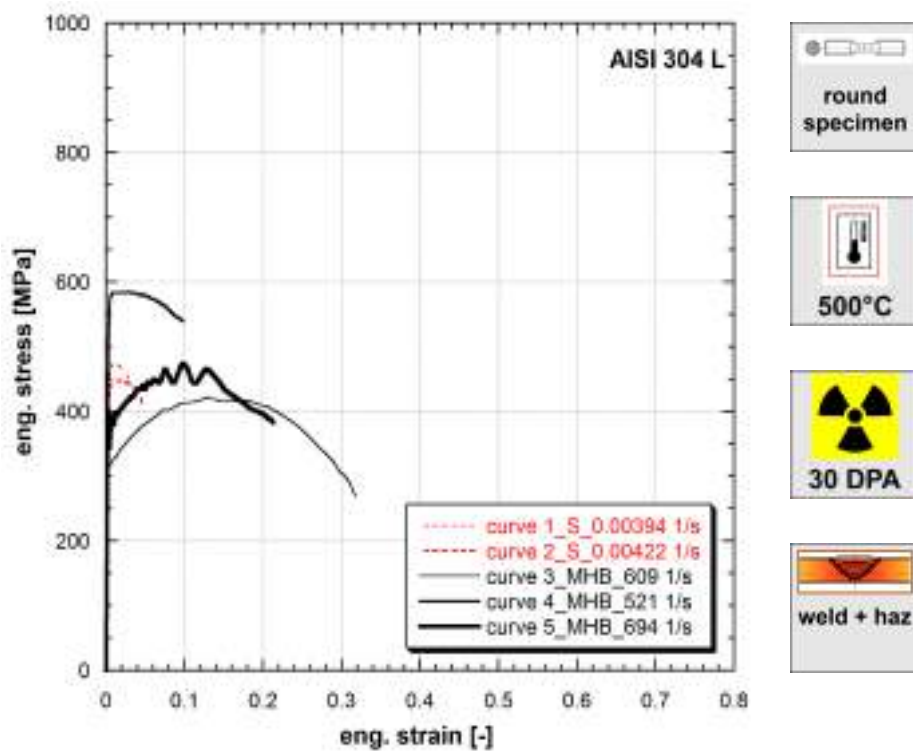


**Figure 9.60:** Stress vs strain curves of AISI 304 L (Ref.Mat.1)

**Note 9.60** Ref.Mat.1

*Irradiated in sodium at 550°C in HFR reactor, for 30000 hours.*

*Argon arc welding.*

Strain rate [1/s]	Yield stress [MPa]	Ultimate tensile strength [MPa]	Uniform strain [-]	Fracture stress [MPa]	Fracture strain [-]
0.00394	444	473	0.009	443	0.031
0.00422	431	448	0.015	412	0.046
609	317	422	0.130	269	0.318
521	573	585	0.029	539	0.098
694	370	474	0.097	382	0.213

**Table 60:** Mechanical properties of AISI 304L (Ref.Mat.1)

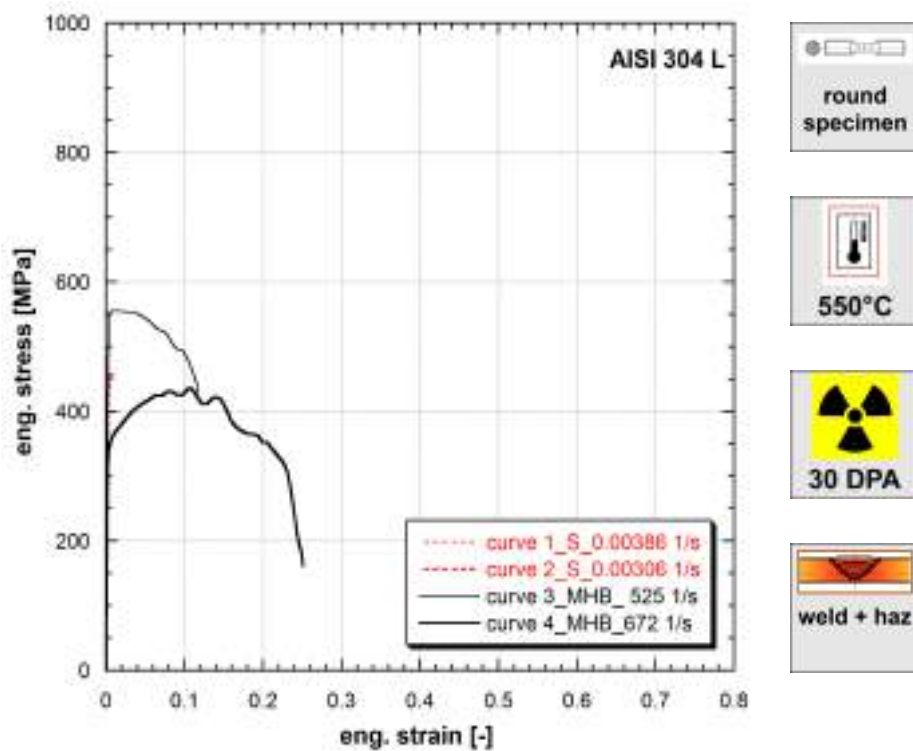


**Figure 9.61:** Stress vs strain curves of AISI 304 L (Ref.Mat.1)

**Note 9.61** Ref.Mat.1

*Irradiated in sodium at 550°C in HFR reactor, for 30000 hours.*

*Argon arc welding.*

Strain rate [1/s]	Yield stress [MPa]	Ultimate tensile strength [MPa]	Uniform strain [-]	Fracture stress [MPa]	Fracture strain [-]
0.00386	450	460	0.006		
0.00306	450	456	0.012		
525	543	555	0.016	429	0.117
672	343	436	0.108	161	0.251

**Table 61:** Mechanical properties of AISI 304L (Ref.Mat.1)

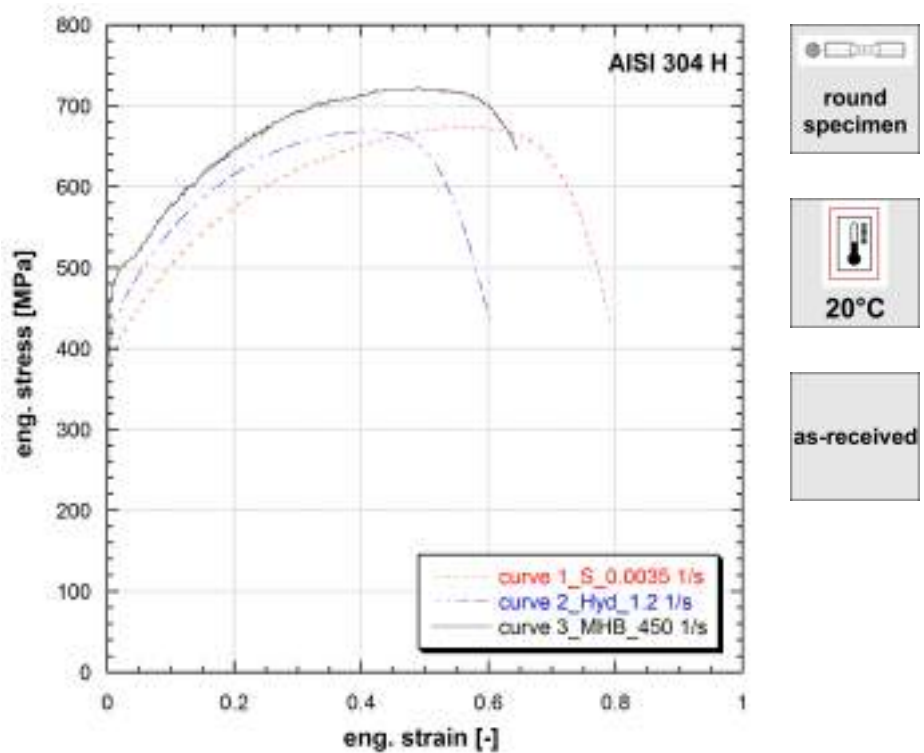


**Figure 9.62:** Stress vs strain curves of AISI 304 H

**Note 9.62** Stainless Steel EN 1.4948. Austenitic, creep resistant.

Strain rate [1/s]	Yield stress [MPa]	Ultimate tensile strength [MPa]	Uniform strain [-]	Fracture stress [MPa]	Fracture strain [-]
0.0035	377	673	0.559	434	0.790
1.2	404	668	0.420	426	0.605
450	459	723	0.489	645	0.644

**Table 62:** Mechanical properties of AISI 304 H

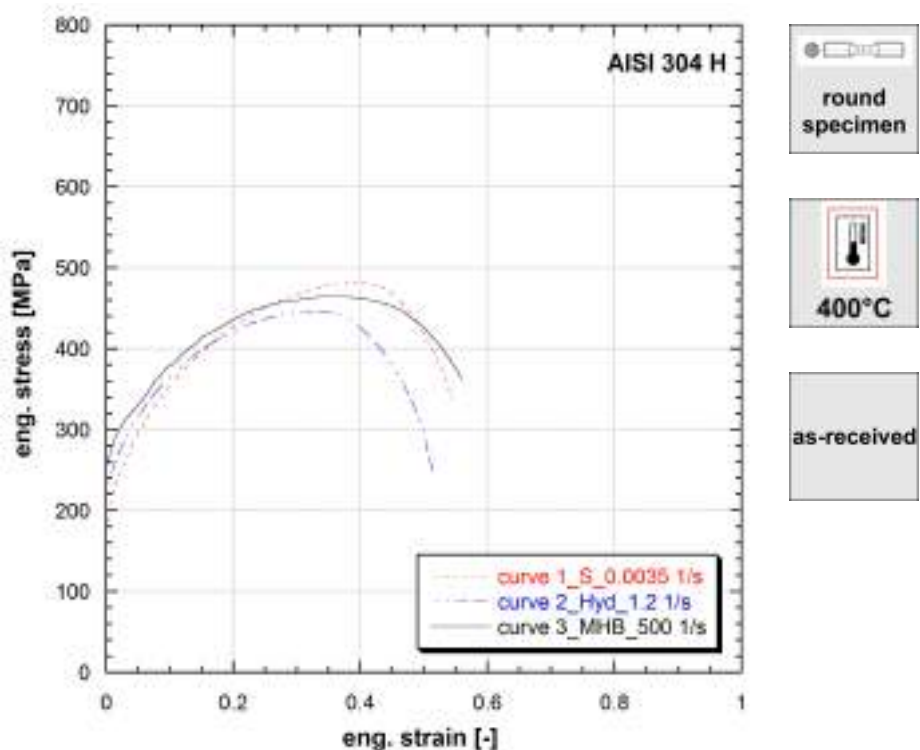


**Figure 9.63:** Stress vs strain curves of AISI 304 H

**Note 9.63** Stainless Steel EN 1.4948. Austenitic, creep resistant.

Strain rate [1/s]	Yield stress [MPa]	Ultimate tensile strength [MPa]	Uniform strain [-]	Fracture stress [MPa]	Fracture strain [-]
0.0035	188	482	0.403	338	0.545
1.2	228	446	0.315	242	0.515
500	262	464	0.360	362	0.560

**Table 63:** Mechanical properties of AISI 304 H

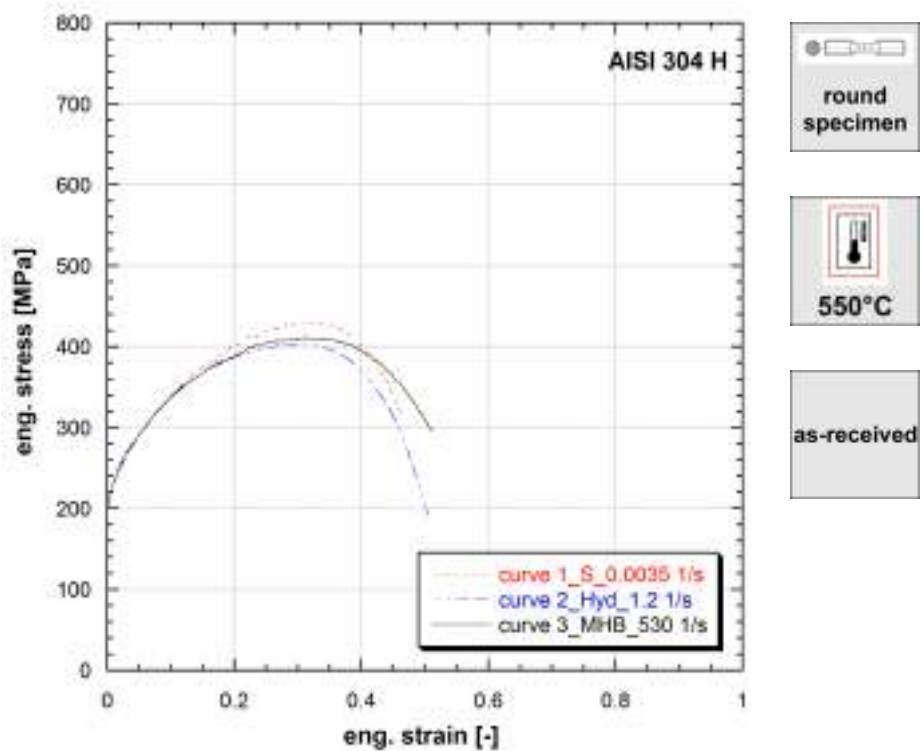


**Figure 9.64:** Stress vs strain curves of AISI 304 H

**Note 9.64** Stainless Steel EN 1.4948. Austenitic, creep resistant.

Strain rate [1/s]	Yield stress [MPa]	Ultimate tensile strength [MPa]	Uniform strain [-]	Fracture stress [MPa]	Fracture strain
0.0035	215	430	0.328	315	0.464
1.2	215	403	0.310	192	0.505
530	212	412	0.312	295	0.512

**Table 64:** Mechanical properties of AISI 304 H

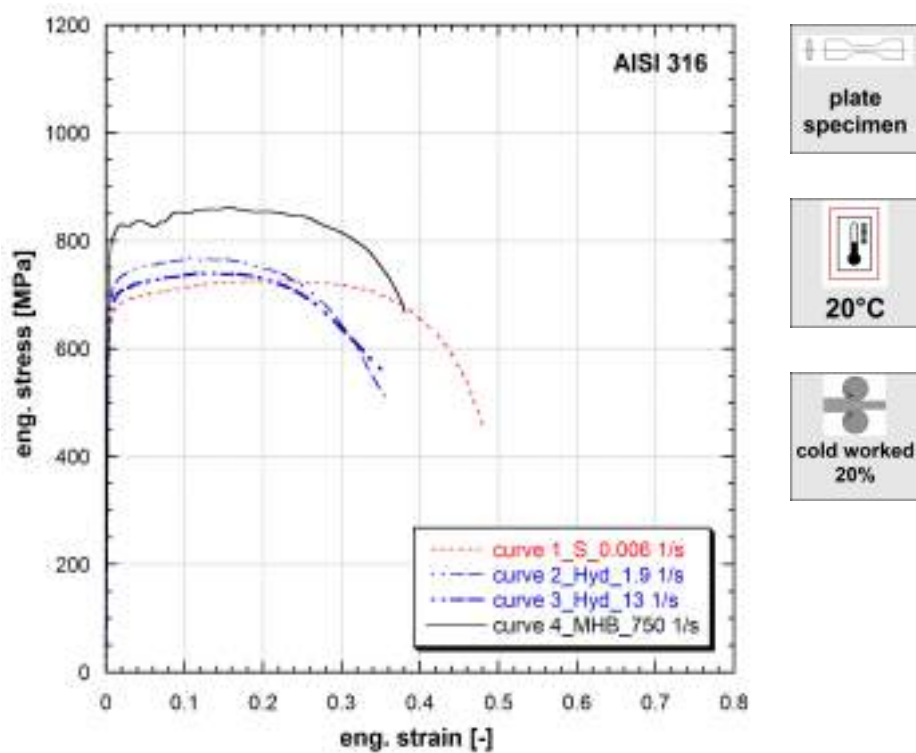


**Figure 9.65:** Stress vs strain curves of AISI 316

Strain rate [1/s]	Yield stress [MPa]	Ultimate tensile strength [MPa]	Uniform strain [-]	Fracture stress [MPa]	Fracture strain [-]
0.006	642	725	0.235	456	0.481
1.9	678	766	0.115	497	0.361
13	667	740	0.132	560	0.352
750	783	861	0.158	667	0.381

**Table 65:** Mechanical properties of AISI 316

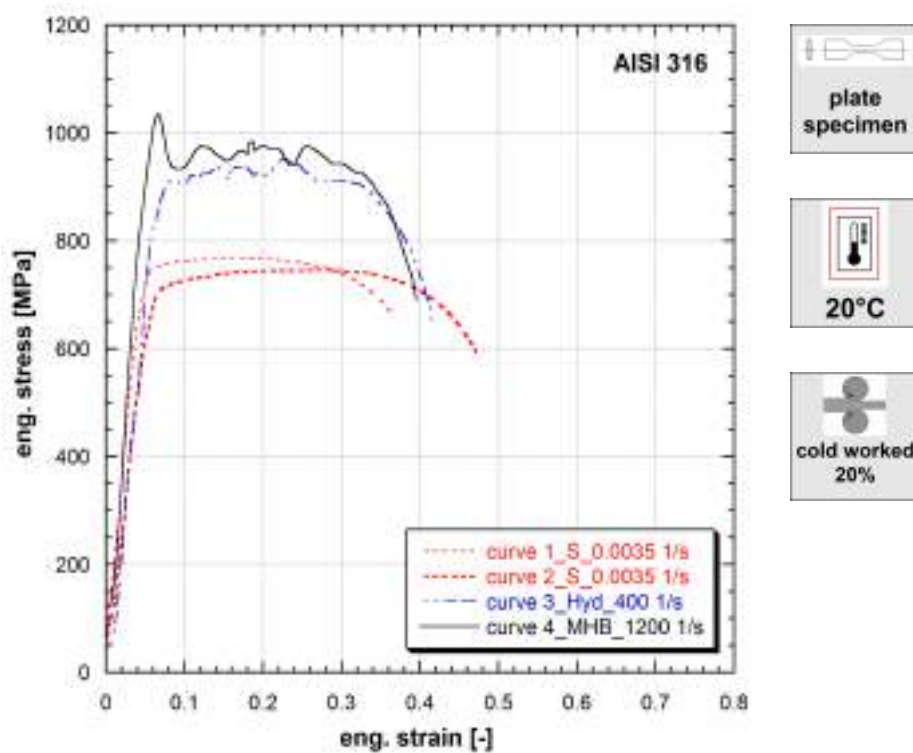


**Figure 9.66:** Stress vs strain curves of AISI 316

Strain rate [1/s]	Yield stress [MPa]	Ultimate tensile strength [MPa]	Uniform strain [-]	Fracture stress [MPa]	Fracture strain [-]
0.0035	-	766	0.192	658	0.367
0.0035	-	746	0.288	594	0.471
400	-	952	0.225	649	0.415
1200	-	1034	0.067	689	0.395

**Table 66:** Mechanical properties of AISI 316

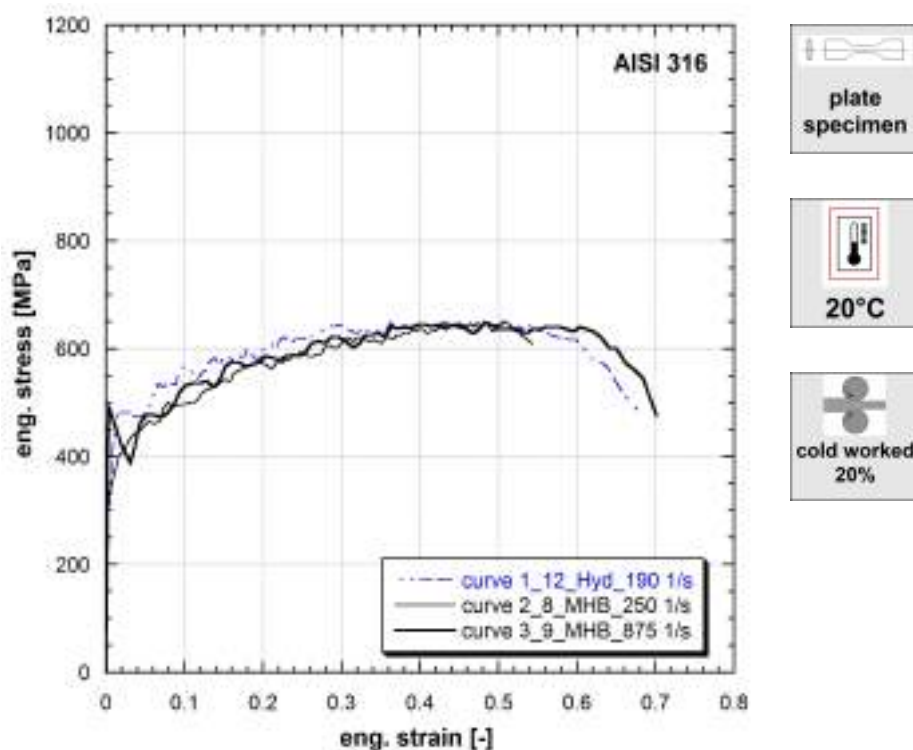


**Figure 9.67:** Stress vs strain curves of AISI 316

**Note 9.67** Specimens longitudinally cut from a hexagonal can of a F.B.R (Fast Breeder Reactor) by electrical discharge machining.

Strain rate [1/s]	Yield stress [MPa]	Ultimate tensile strength [MPa]	Uniform strain [-]	Fracture stress [MPa]	Fracture strain [-]
875	490	649	0.483	476	0.702
250	326	651	0.506	609	0.543
190	309	649	0.436	487	0.677

**Table 67:** Mechanical properties of AISI 316

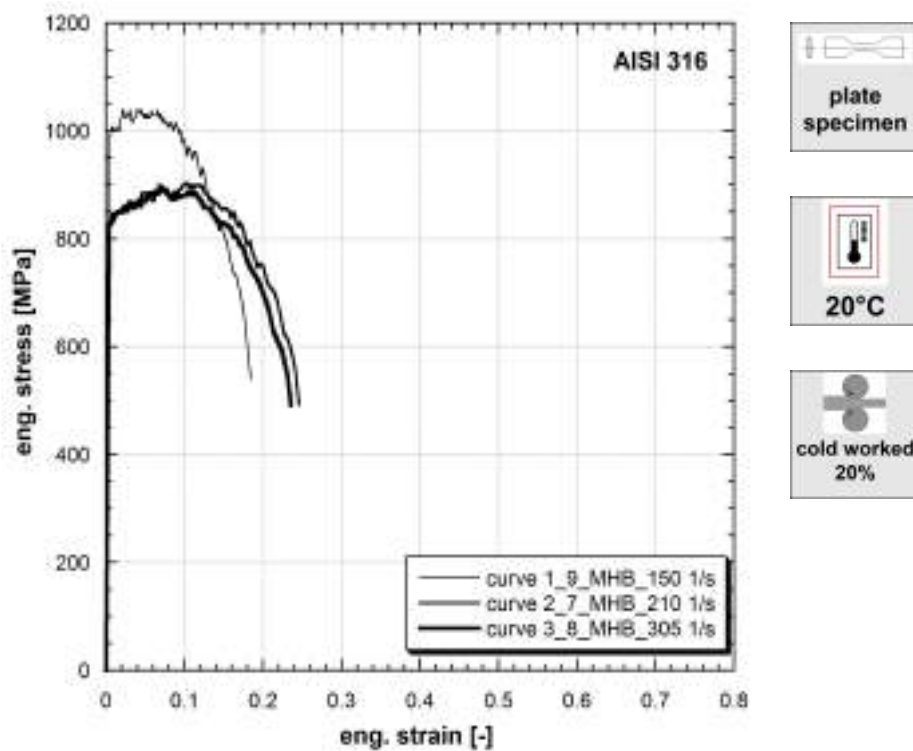


**Figure 9.68:** Stress vs strain curves of AISI 316

**Note 9.68** Specimens longitudinally cut from a hexagonal can of a F.B.R (Fast Breeder Reactor) by electrical discharge machining.

9: corner of the hexcan.

7: mid-length of the face.

8: quarter-length of the face.

Strain rate [1/s]	Yield stress [MPa]	Ultimate tensile strength [MPa]	Uniform strain [-]	Fracture stress [MPa]	Fracture strain [-]
210	836	904	0.103	492	0.246
305	827	892	0.069	491	0.236
150	1000	1038	0.046	539	0.185

**Table 68:** Mechanical properties of AISI 316

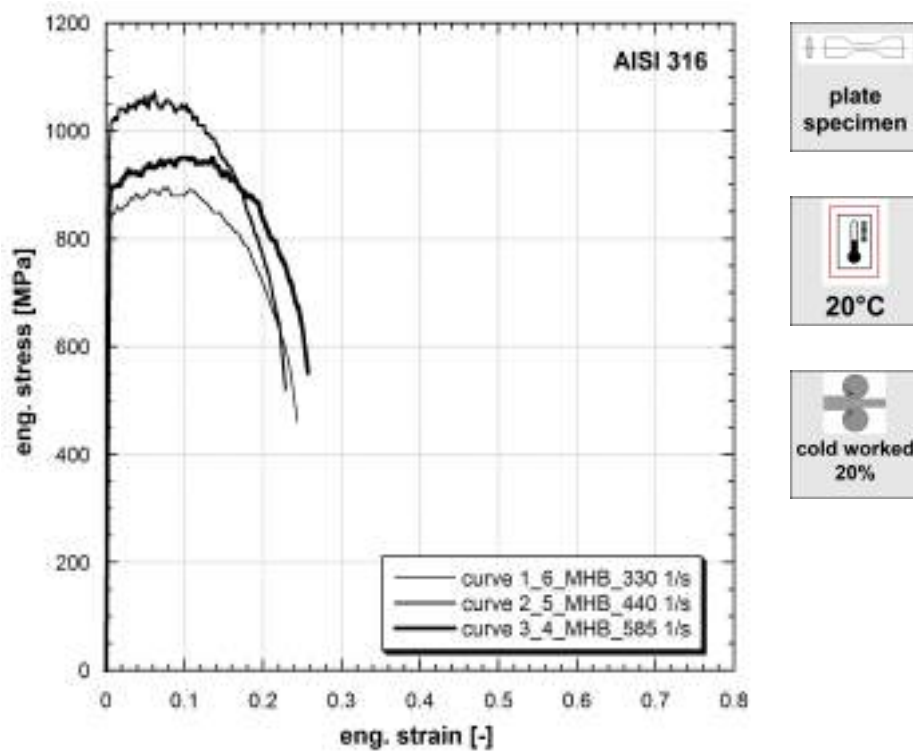


**Figure 9.69:** Stress vs strain curves of AISI 316

**Note 9.69** Specimens longitudinally cut from a hexagonal can of a F.B.R (Fast Breeder Reactor) by electrical discharge machining.

5: corner of the hexcan.

4-6: quarter-length of the face.

Strain rate [1/s]	Yield stress [MPa]	Ultimate tensile strength [MPa]	Uniform strain [-]	Fracture stress [MPa]	Fracture strain [-]
330	834	895	0.080	461	0.244
440	1017	1072	0.062	520	0.228
585	893	950	0.103	552	0.257

**Table 69:** Mechanical properties of AISI 316

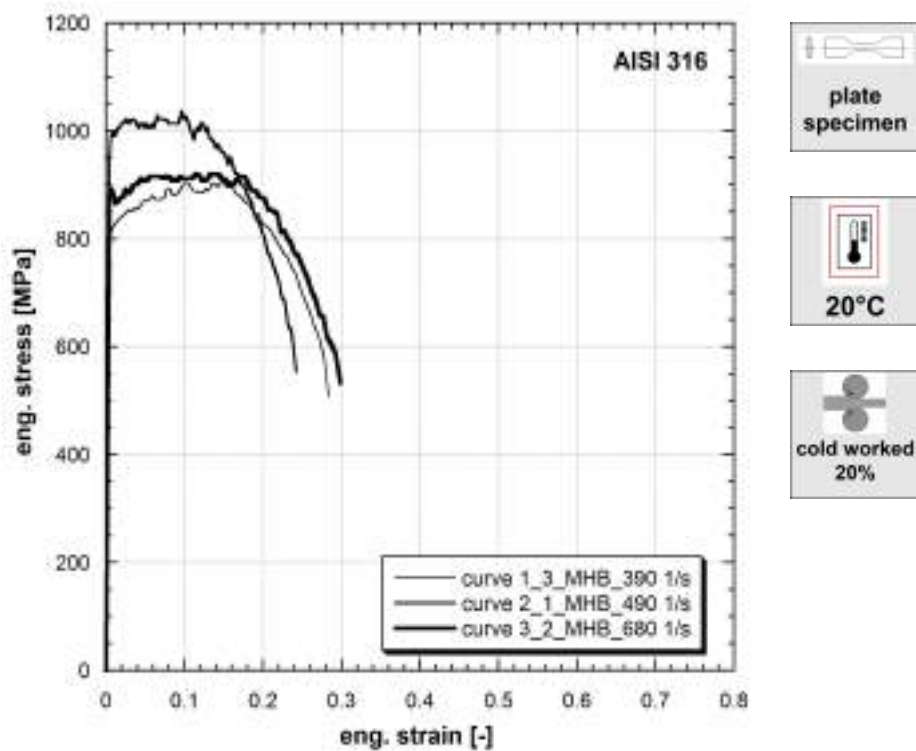


**Figure 9.70:** Stress vs strain curves of AISI 316

**Note 9.70** Specimens longitudinally cut from a hexagonal can of a F.B.R (Fast Breeder Reactor) by electrical discharge machining.

- 1: corner of the hexcan.
- 3: mid-length of the face.
- 2: quarter-length of the face.

Strain rate [1/s]	Yield stress [MPa]	Ultimate tensile strength [MPa]	Uniform strain [-]	Fracture stress [MPa]	Fracture strain [-]
390	811	907	0.150	508	0.284
490	994	1037	0.096	553	0.242
680	889	920	0.133	532	0.299

**Table 70:** Mechanical properties of AISI 316

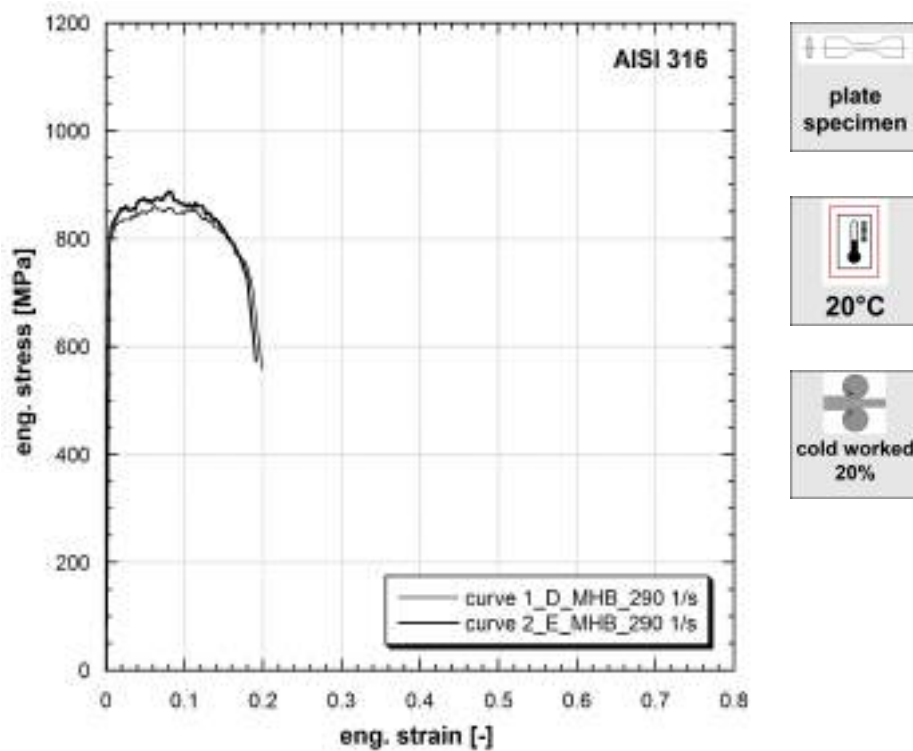


**Figure 9.71:** Stress vs strain curves of AISI 316

**Note 9.71** Specimens transversally cut from a hexagonal can of a F.B.R (Fast Breeder Reactor) by electrical discharge machining.

Strain rate [1/s]	Yield stress [MPa]	Ultimate tensile strength [MPa]	Uniform strain [-]	Fracture stress [MPa]	Fracture strain [-]
290	803	861	0.062	558	0.199
290	817	888	0.081	572	0.191

**Table 71:** Mechanical properties of AISI 316

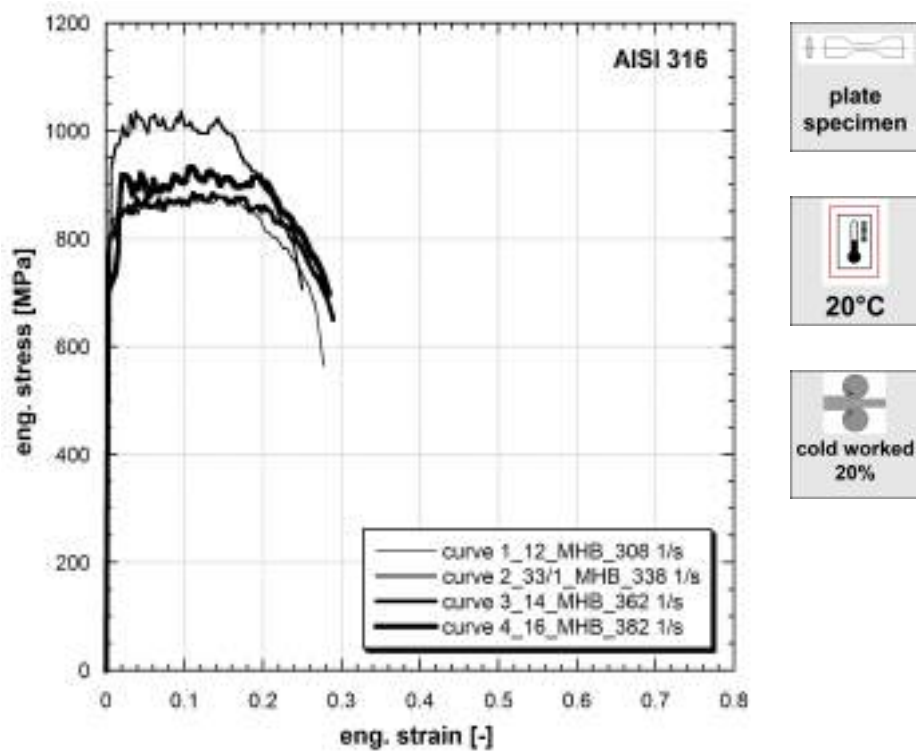


**Figure 9.72:** Stress vs strain curves of AISI 316

**Note 9.72** Preliminary tests on specimens from hexagonal can of a F.B.R (Fast Breeder Reactor).

Strain rate [1/s]	Yield stress [MPa]	Ultimate tensile strength [MPa]	Uniform strain [-]	Fracture stress [MPa]	Fracture strain [-]
308	815	881	0.145	564	0.278
338	869	1037	0.095	707	0.250
362	807	885	0.111	649	0.290
382	714	933	0.109	697	0.284

**Table 72:** Mechanical properties of AISI 316

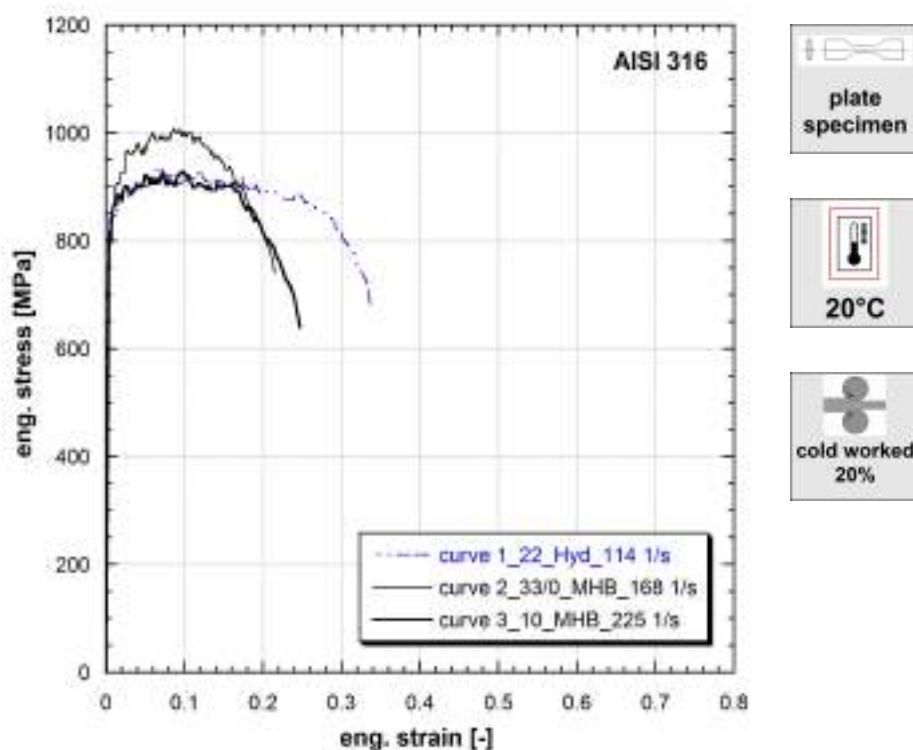


**Figure 9.73:** Stress vs strain curves of AISI 316

**Note 9.73** Preliminary tests on specimens from hexagonal can of a F.B.R (Fast Breeder Reactor).

Strain rate [1/s]	Yield stress [MPa]	Ultimate tensile strength [MPa]	Uniform strain [-]	Fracture stress [MPa]	Fracture strain [-]
114	843	937	0.065	677	0.337
168	827	1008	0.087	740	0.215
225	797	929	0.098	639	0.247

**Table 73:** Mechanical properties of AISI 316

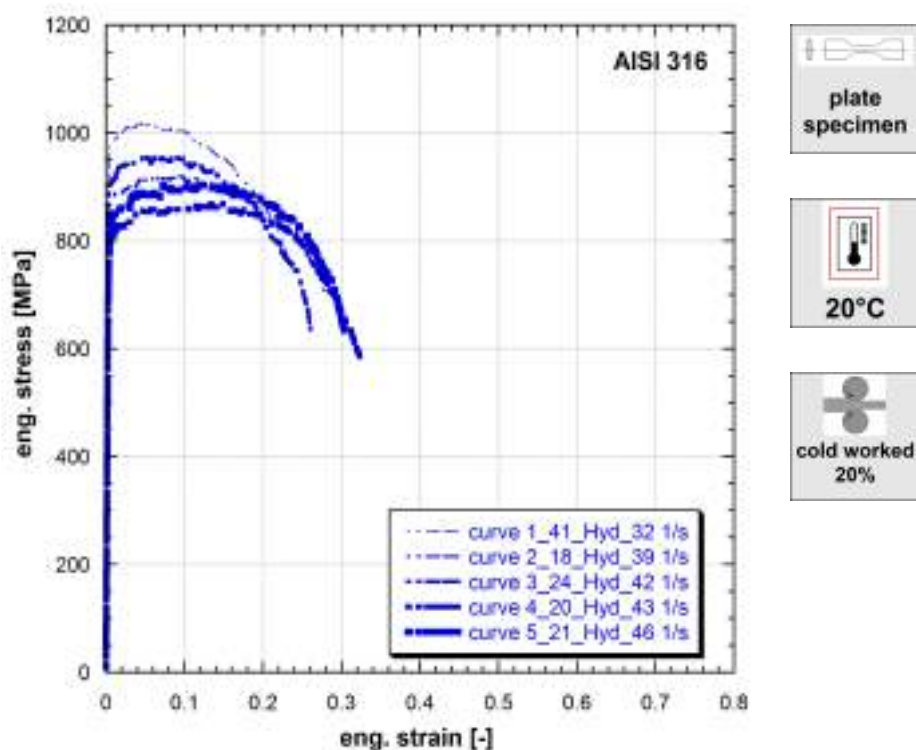


**Figure 9.74:** Stress vs strain curves of AISI 316

**Note 9.74** Preliminary tests on specimens from hexagonal can of a F.B.R (Fast Breeder Reactor).

Strain rate [1/s]	Yield stress [MPa]	Ultimate tensile strength [MPa]	Uniform strain [-]	Fracture stress [MPa]	Fracture strain [-]
32	983	1017	0.053	741	0.241
39	870	920	0.066	701	0.281
42	907	959	0.087	629	0.261
43	807	870	0.150	586	0.324
46	803	906	0.118	634	0.304

**Table 74:** Mechanical properties of AISI 316

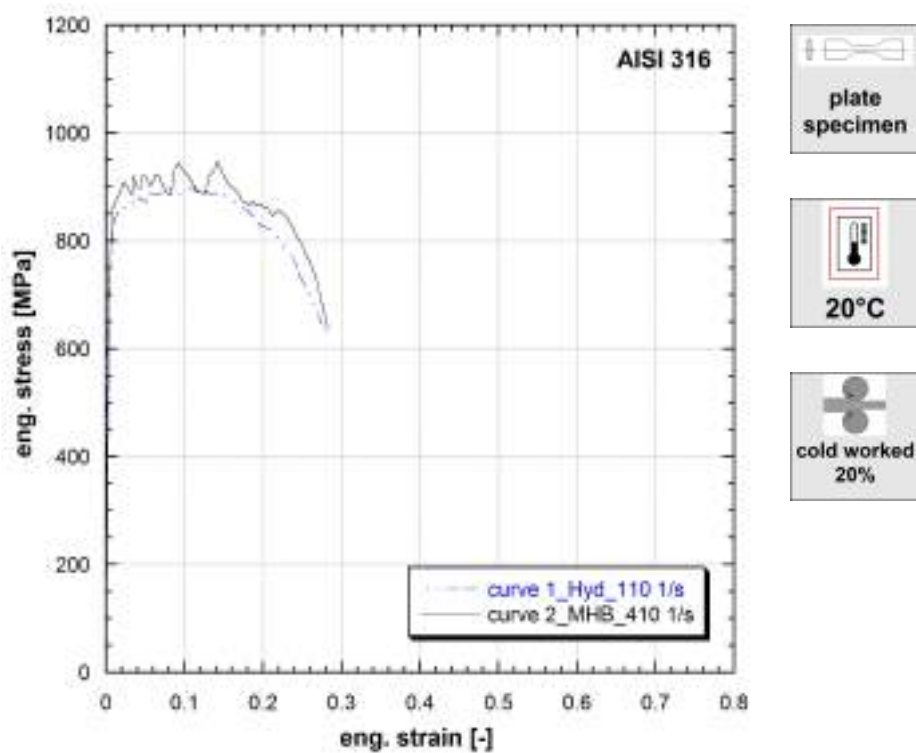


**Figure 9.75:** Stress vs strain curves of AISI 316

Strain rate	Yield stress [MPa]	Ultimate tensile strength [MPa]	Uniform strain [-]	Fracture stress [MPa]	Fracture strain [-]
[1/s]					
110	742	899	0.111	631	0.280
410	778	947	0.142	637	0.283

**Table 75:** Mechanical properties of AISI 316

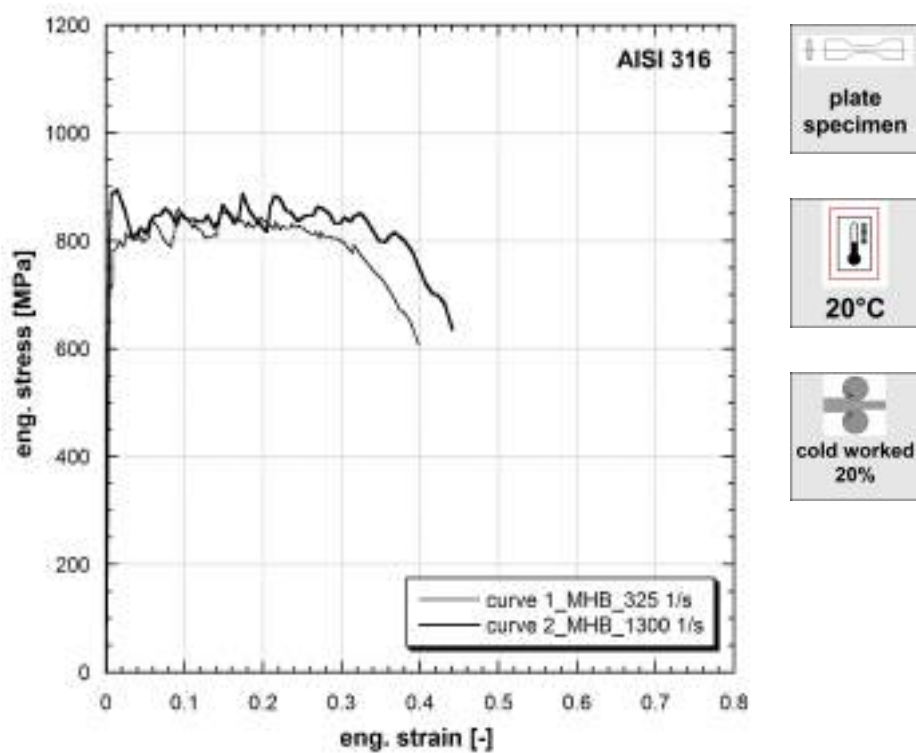


**Figure 9.76:** Stress vs strain curves of AISI 316

Strain rate [1/s]	Yield stress [MPa]	Ultimate tensile strength [MPa]	Uniform strain [-]	Fracture stress [MPa]	Fracture strain [-]
325	707	859	0.093	608	0.399
1300	867	895	0.014	636	0.441

**Table 76:** Mechanical properties of AISI 316

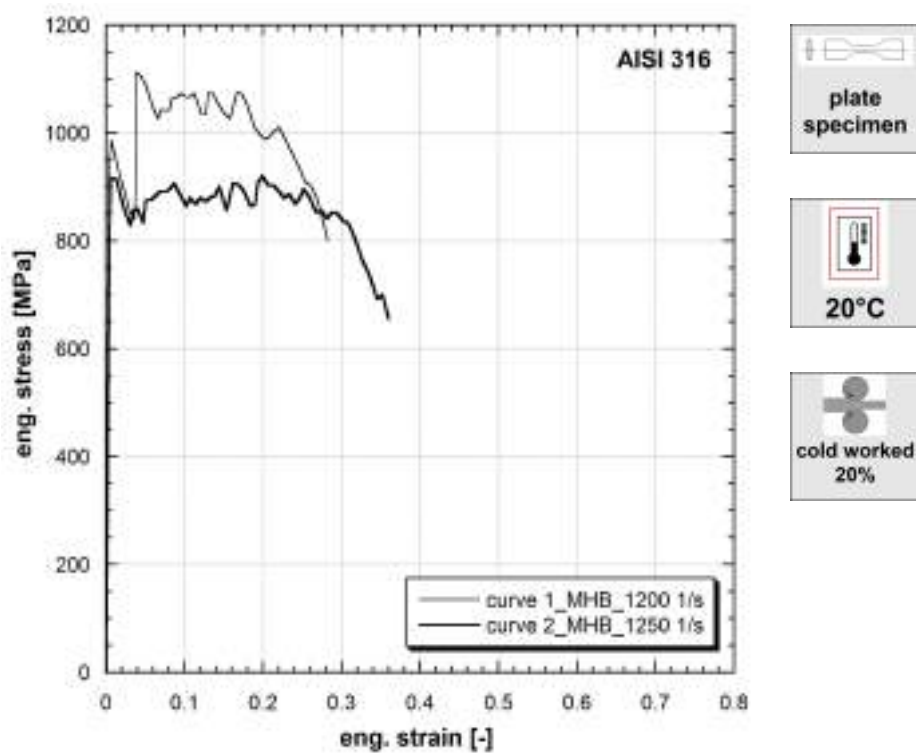


**Figure 9.77:** Stress vs strain curves of AISI 316

Strain rate [1/s]	Yield stress [MPa]	Ultimate tensile strength [MPa]	Uniform strain [-]	Fracture stress [MPa]	Fracture strain [-]
1200	978	1112	0.039	800	0.283
1250	916	920	0.199	655	0.360

**Table 77:** Mechanical properties of AISI 316

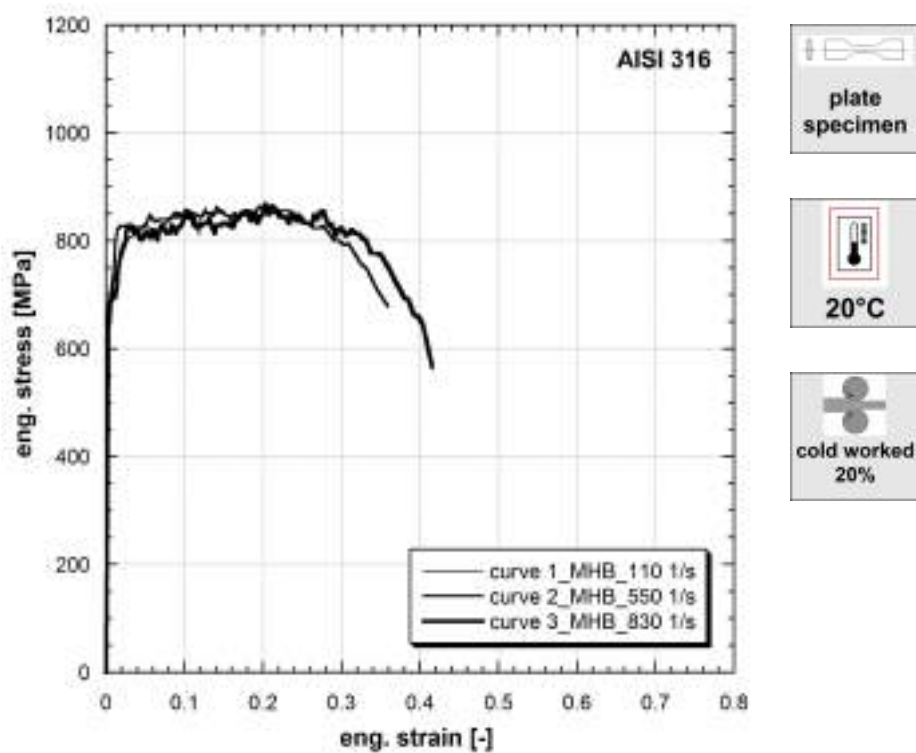


**Figure 9.78:** Stress vs strain curves of AISI 316

Strain rate [1/s]	Yield stress [MPa]	Ultimate tensile strength [MPa]	Uniform strain [-]	Fracture stress [MPa]	Fracture strain [-]
110	642	860	0.127	841	0.219
550	697	864	0.195	679	0.359
830	685	868	0.202	565	0.416

**Table 78:** Mechanical properties of AISI 316

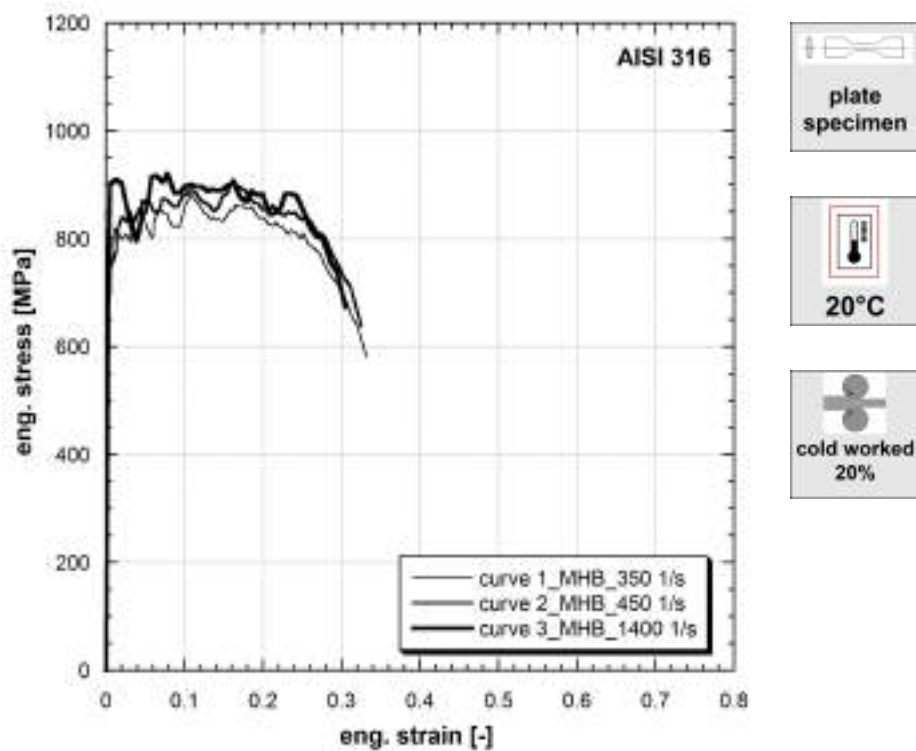


**Figure 9.79:** Stress vs strain curves of AISI 316

Strain rate [1/s]	Yield stress [MPa]	Ultimate tensile strength [MPa]	Uniform strain [-]	Fracture stress [MPa]	Fracture strain [-]
350	753	884	0.108	580	0.332
450	737	910	0.162	638	0.326
1400	901	921	0.079	673	0.305

**Table 79:** Mechanical properties of AISI 316

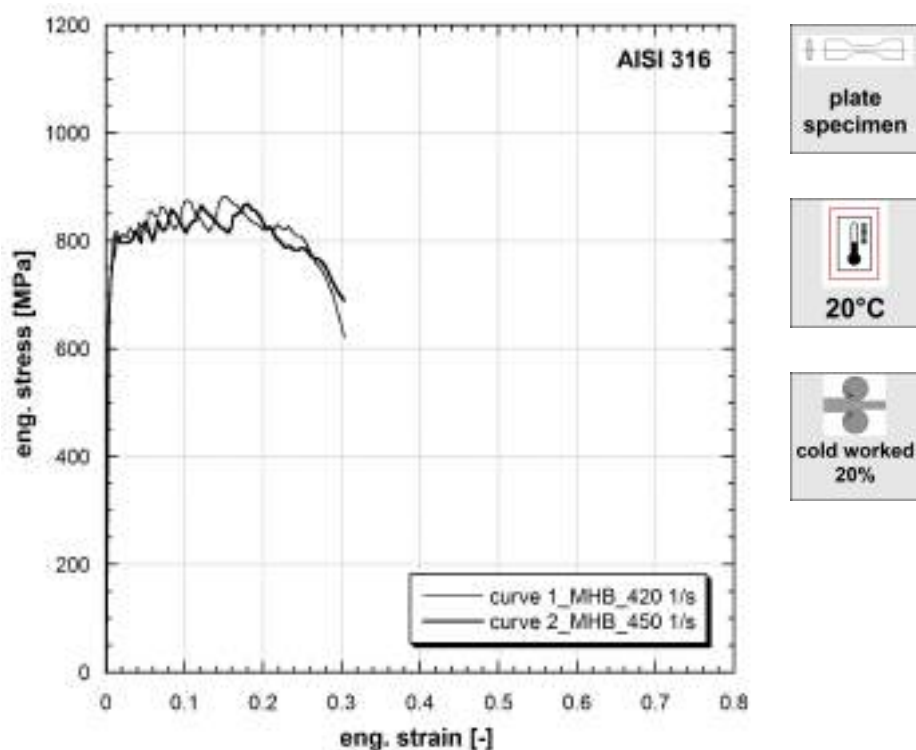


**Figure 9.80:** Stress vs strain curves of AISI 316

Strain rate [1/s]	Yield stress [MPa]	Ultimate tensile strength [MPa]	Uniform strain [-]	Fracture stress [MPa]	Fracture strain [-]
420	697	882	0.151	620	0.304
450	703	869	0.180	689	0.304

**Table 80:** Mechanical properties of AISI 316

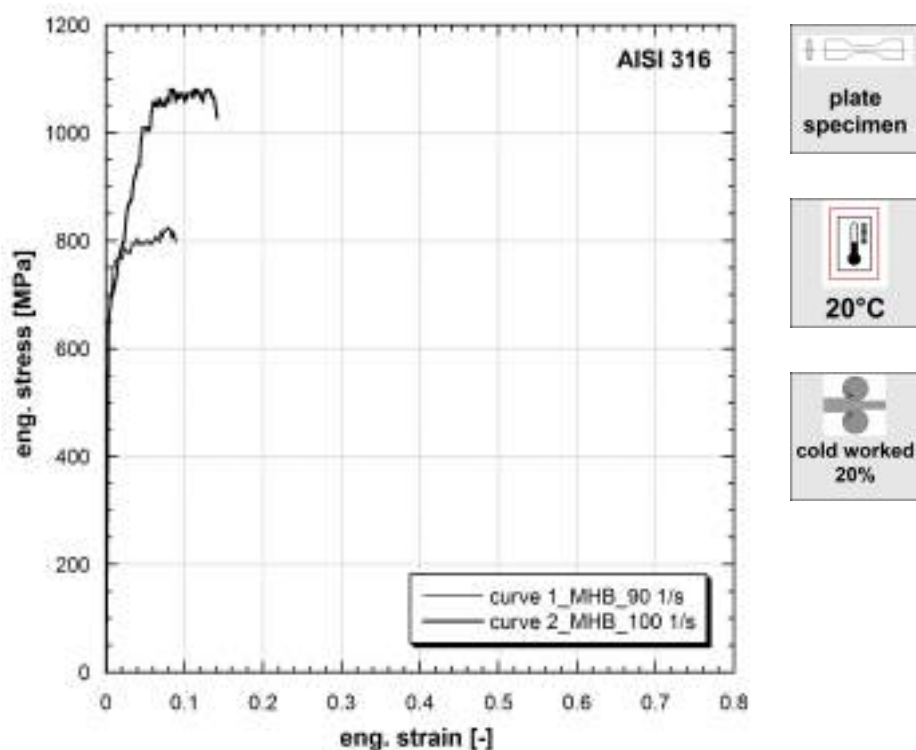


**Figure 9.81:** Stress vs strain curves of interrupted tests of AISI 316

Strain rate [1/s]	Yield stress [MPa]	Ultimate tensile strength [MPa]	Uniform strain [-]	Fracture stress [MPa]	Fracture strain [-]
90	697	-	-	-	-
100	673	-	-	-	-

**Table 81:** Mechanical properties of AISI 316

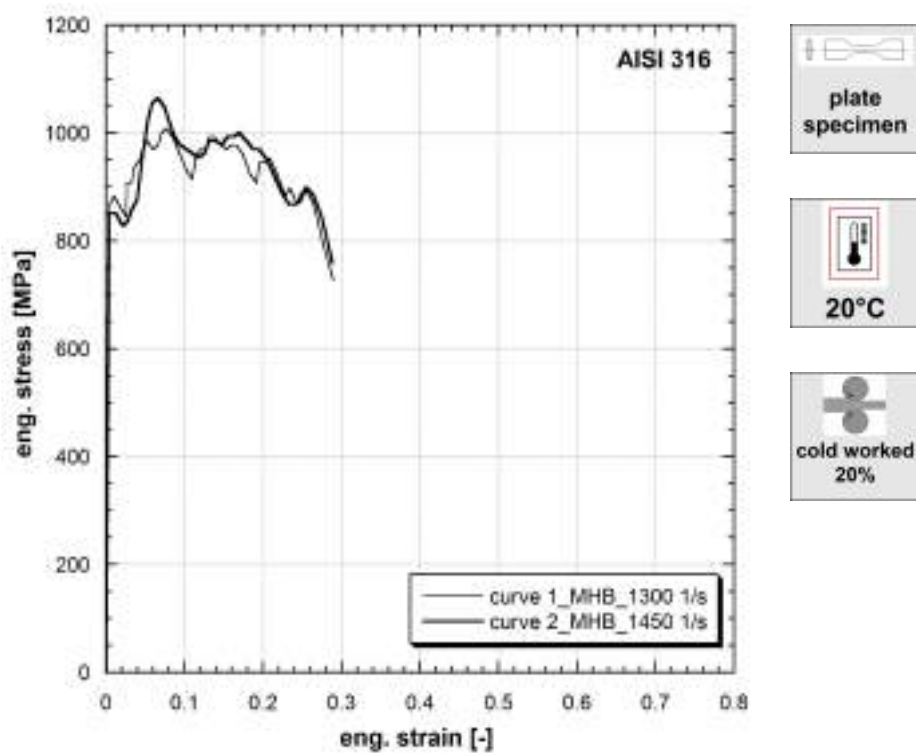


**Figure 9.82:** Stress vs strain curves of AISI 316

Strain rate [1/s]	Yield stress [MPa]	Ultimate tensile strength [MPa]	Uniform strain [-]	Fracture stress [MPa]	Fracture strain [-]
1300	873	1008	0.077	726	0.290
1450	846	1065	0.066	758	0.288

**Table 82:** Mechanical properties of AISI 316

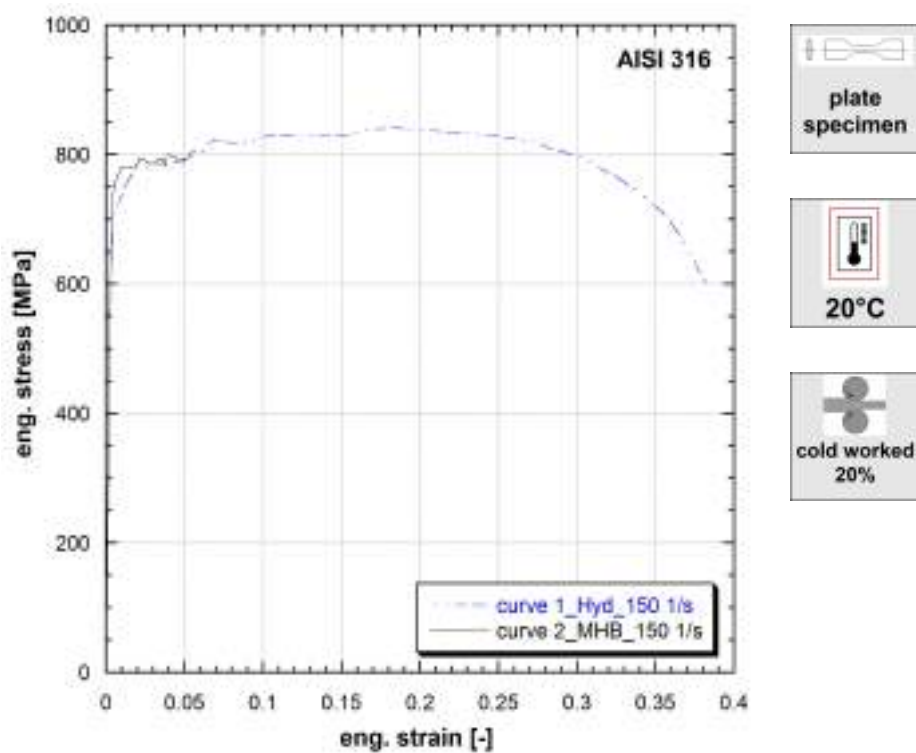


**Figure 9.83:** Stress vs strain curves of AISI 316

**Note 9.83** Comparison between tests performed by HPM and MHB at the same strain-rate.

Strain rate [1/s]	Yield stress [MPa]	Ultimate tensile strength [MPa]	Uniform strain [-]	Fracture stress [MPa]	Fracture strain [-]
150	712	841	0.183	602	0.383
150	758	-	-	-	-

**Table 83:** Mechanical properties of AISI 316

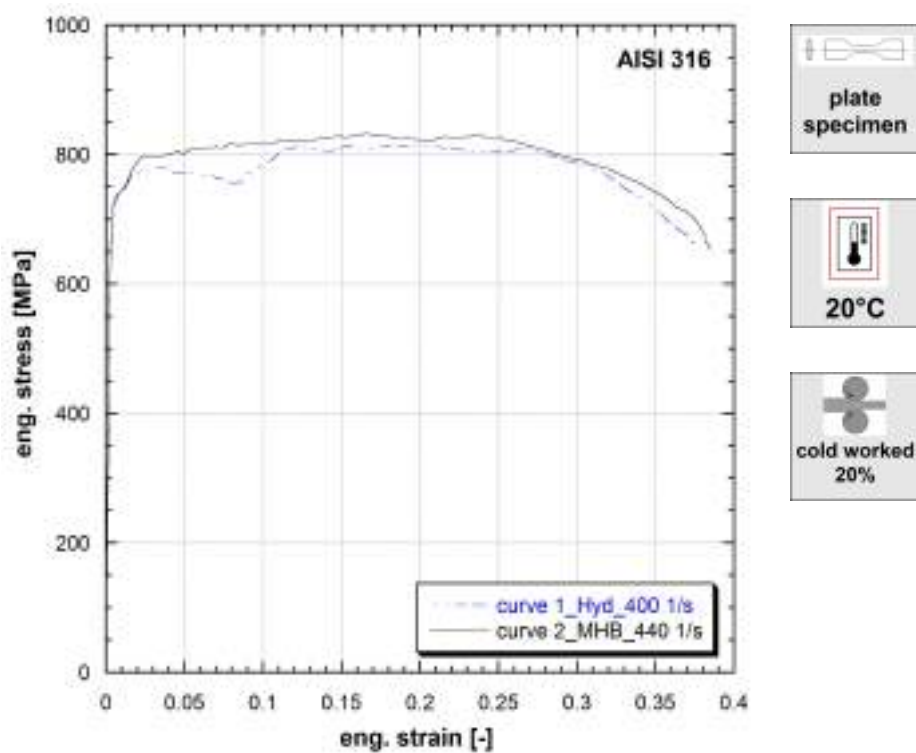


**Figure 9.84:** Stress vs strain curves of AISI 316

**Note 9.84** Comparison between tests performed by HPM and MHB at the same strain-rate.

Strain rate [1/s]	Yield stress [MPa]	Ultimate tensile strength [MPa]	Uniform strain [-]	Fracture stress [MPa]	Fracture strain [-]
400	714	813	0.154	651	0.378
440	730	832	0.165	652	0.385

**Table 84:** Mechanical properties of AISI 316

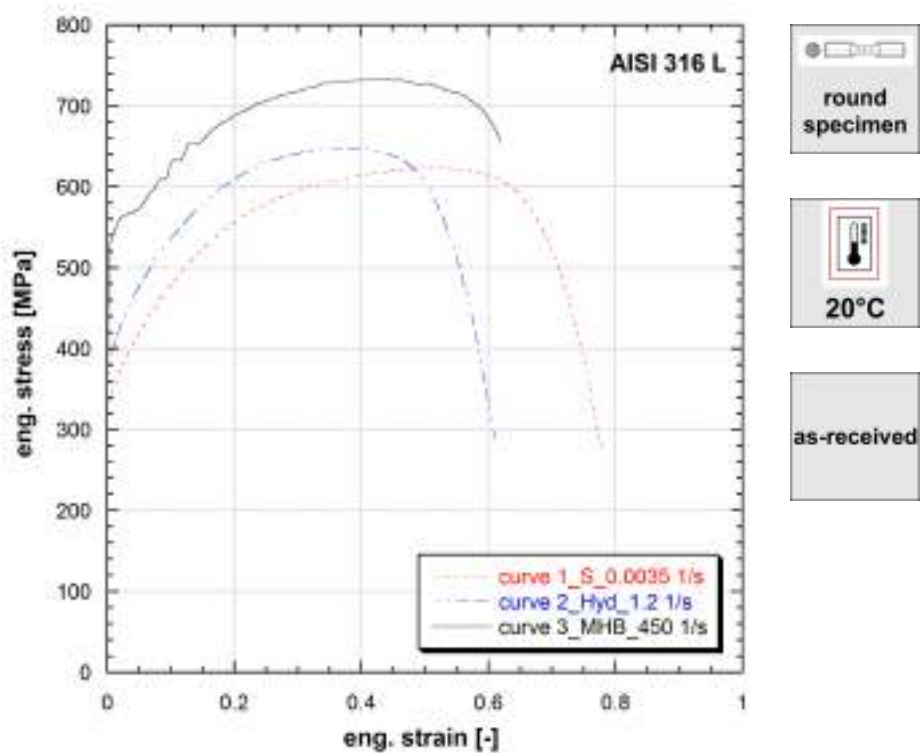


**Figure 9.85:** Stress vs strain curves of AISI 316 L

Strain rate [1/s]	Yield stress [MPa]	Ultimate tensile strength [MPa]	Uniform strain [-]	Fracture stress [MPa]	Fracture strain [-]
0.0035	327	623	0.501	270	0.779
1.2	366	648	0.362	289	0.609
450	519	732	0.423	656	0.619

**Table 85:** Mechanical properties of AISI 316 L

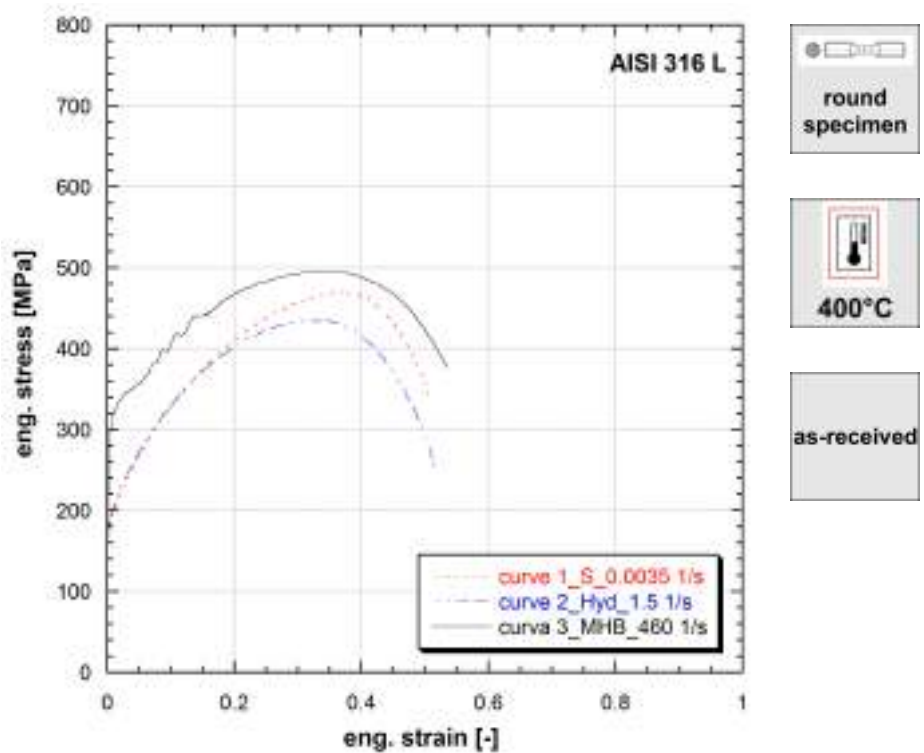


**Figure 9.86:** Stress vs strain curves of AISI 316 L

Strain rate [1/s]	Yield stress [MPa]	Ultimate tensile strength [MPa]	Uniform strain [-]	Fracture stress [MPa]	Fracture strain [-]
0.0035	174	470	0.366	342	0.505
1.5	182	435	0.335	255	0.515
460	299	495	0.363	376	0.535

**Table 86:** Mechanical properties of AISI 316 L

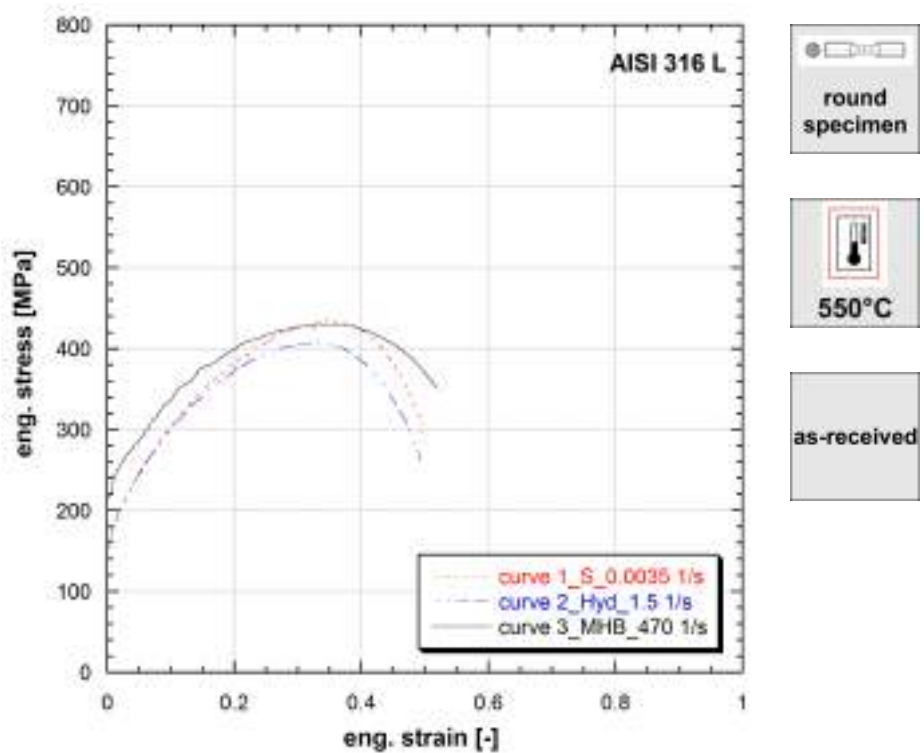


**Figure 9.87:** Stress vs strain curves of AISI 316 L

Strain rate [1/s]	Yield stress [MPa]	Ultimate tensile strength [MPa]	Uniform strain [-]	Fracture stress [MPa]	Fracture strain [-]
0.0035	163	436	0.348	296	0.495
1.5	159	408	0.328	262	0.493
470	218	431	0.332	350	0.520

**Table 87:** Mechanical properties of AISI 316 L

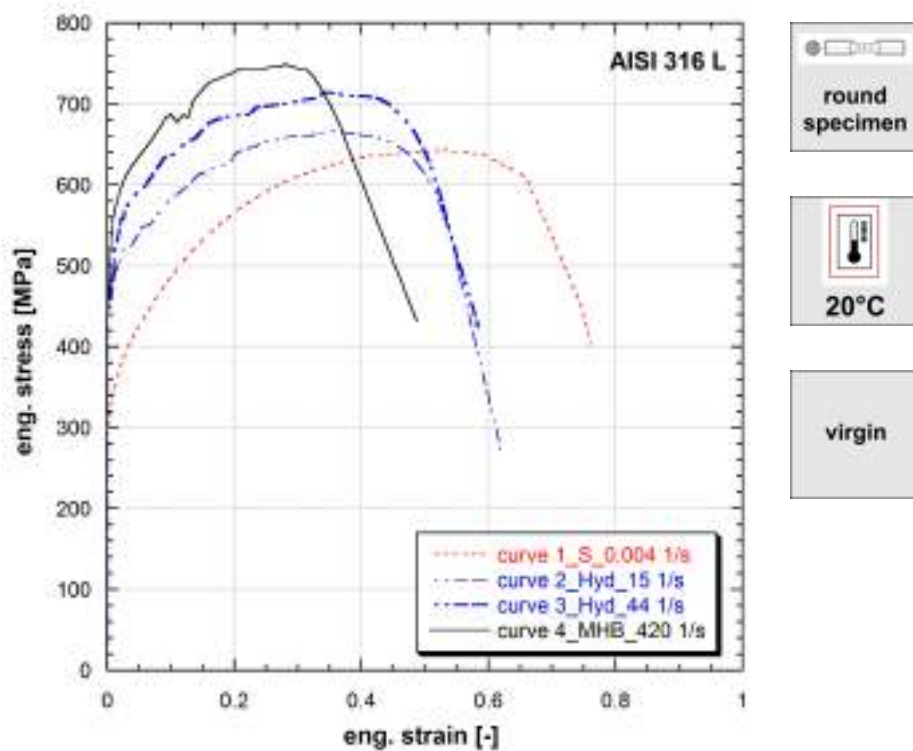


**Figure 9.88:** Stress vs strain curves of AISI 316 L (Ref.Mat.3)

**Note 9.88** Ref.Mat.3

Strain rate [1/s]	Yield stress [MPa]	Ultimate tensile strength [MPa]	Uniform strain [-]	Fracture stress [MPa]	Fracture strain [-]
0.004	309	642	0.533	402	0.761
15	442	667	0.361	273	0.619
44	453	714	0.339	424	0.584
420	473	749	0.279	431	0.488

**Table 88:** Mechanical properties of AISI 316 L (Ref.Mat.3)

Published in (Albertini and Montagnani, 1979), (Albertini and Montagnani, 1980), (Albertini and Montagnani, 1978), (Albertini and Montagnani, 1983b), (Albertini and Genet, 1979), (Albertini et al., 1980), (Albertini and Montagnani, 1981a), (Albertini et al., 1982).

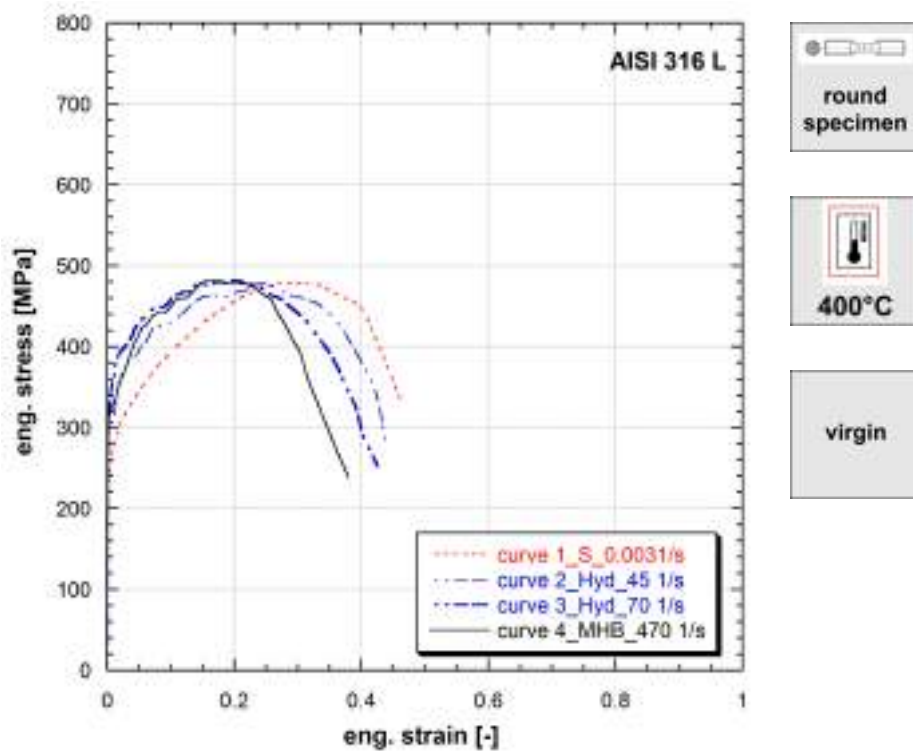


**Figure 9.89:** Stress vs strain curves of AISI 316 L (Ref.Mat.3)

**Note 9.89** Ref.Mat.3

Strain rate [1/s]	Yield stress [MPa]	Ultimate tensile strength [MPa]	Uniform strain [-]	Fracture stress [MPa]	Fracture strain [-]
0.003	239	479	0.314	330	0.464
45	294	478	0.250	279	0.438
70	326	482	0.201	253	0.426
470	311	481	0.167	238	0.379

**Table 89:** Mechanical properties of AISI 316 L (Ref.Mat.3)

Published in (Albertini and Genet, 1979).

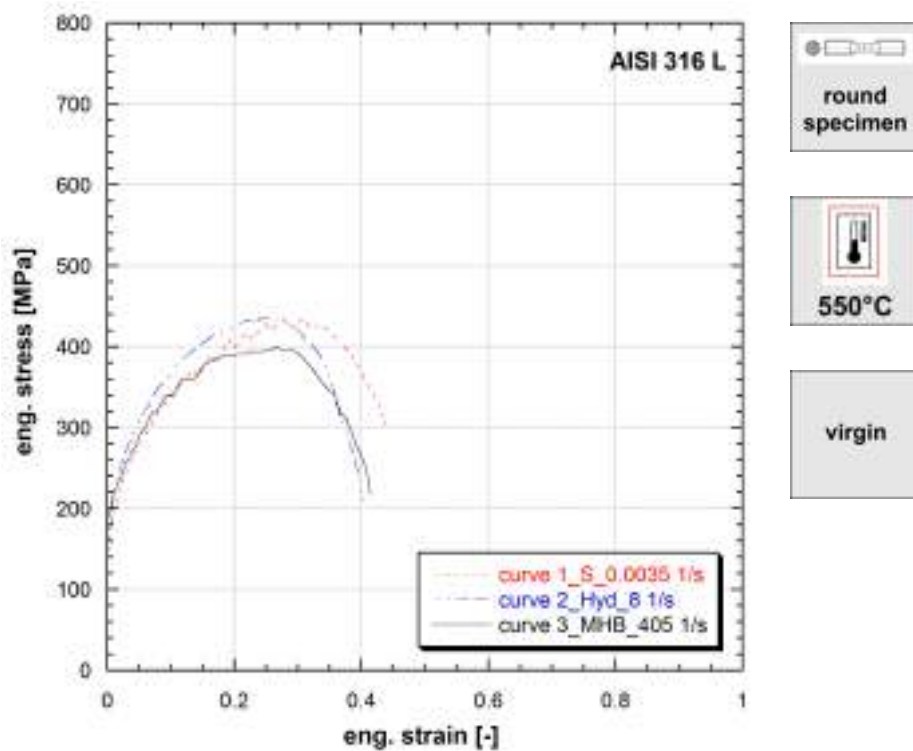


**Figure 9.90:** Stress vs strain curves of AISI 316 L (Ref.Mat.3)

**Note 9.90** Ref.Mat.3

Strain rate [1/s]	Yield stress [MPa]	Ultimate tensile strength [MPa]	Uniform strain [-]	Fracture stress [MPa]	Fracture strain [-]
0.0035	167	434	0.310	303	0.439
8	150	436	0.248	210	0.402
405	190	400	0.266	217	0.414

**Table 90:** Mechanical properties of AISI 316 L (Ref.Mat.3)

Published in (Albertini and Montagnani, 1980), (Albertini and Montagnani, 1978), (Albertini and Genet, 1979), (Albertini et al., 1980), (Albertini and Montagnani, 1981b).

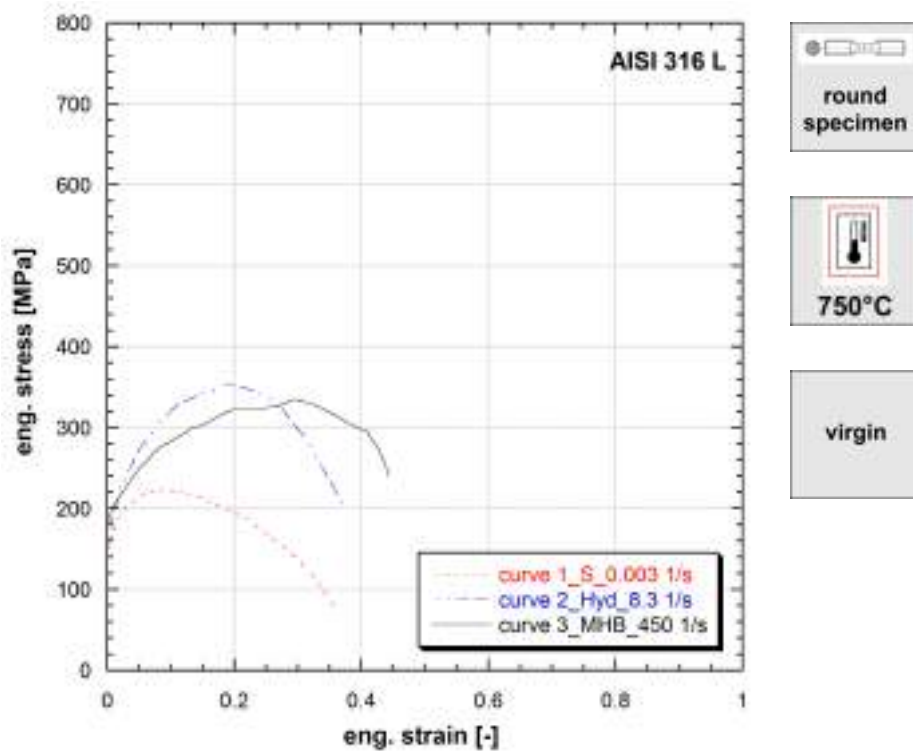


**Figure 9.91:** Stress vs strain curves of AISI 316 L (Ref.Mat.3)

**Note 9.91** Ref.Mat.3

Strain rate [1/s]	Yield stress [MPa]	Ultimate tensile strength [MPa]	Uniform strain [-]	Fracture stress [MPa]	Fracture strain [-]
0.003	149	222	0.091	75	0.360
8.3	161	352	0.196	198	0.377
450	188	334	0.292	239	0.443

**Table 91:** Mechanical properties of AISI 316 L (Ref.Mat.3)

Published in (Albertini and Montagnani, 1980).

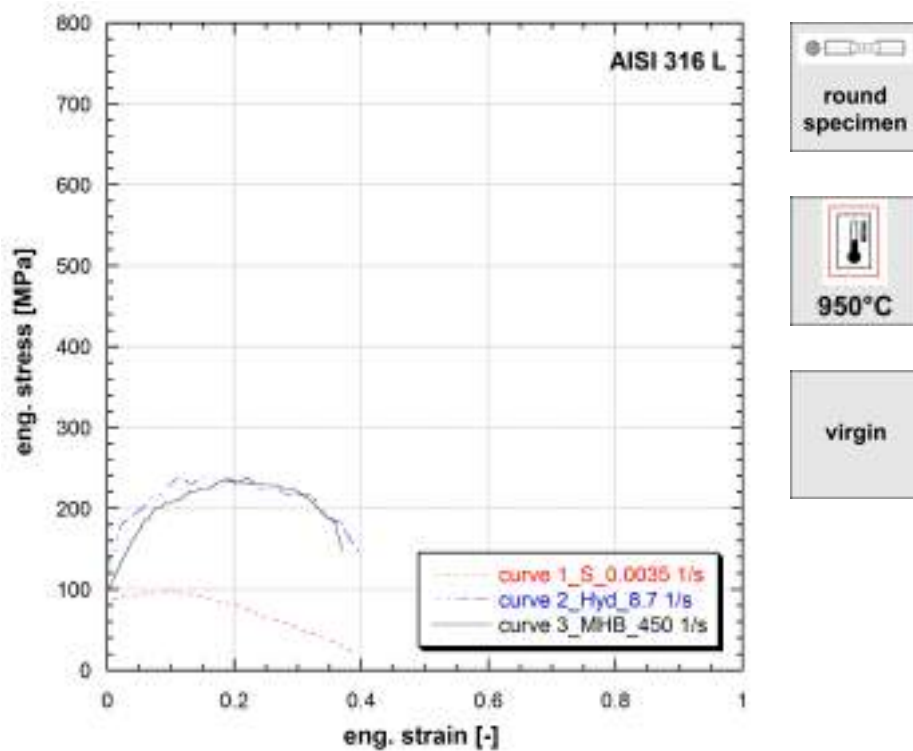


**Figure 9.92:** Stress vs strain curves of AISI 316 L (Ref.Mat.3)

**Note 9.92** Ref.Mat.3

Strain rate [1/s]	Yield stress [MPa]	Ultimate tensile strength [MPa]	Uniform strain [-]	Fracture stress [MPa]	Fracture strain [-]
0.0035	83	97	0.106	19	0.393
8.7	140	238	0.183	142	0.400
450	105	238	0.221	148	0.370

**Table 92:** Mechanical properties of AISI 316 L (Ref.Mat.3)

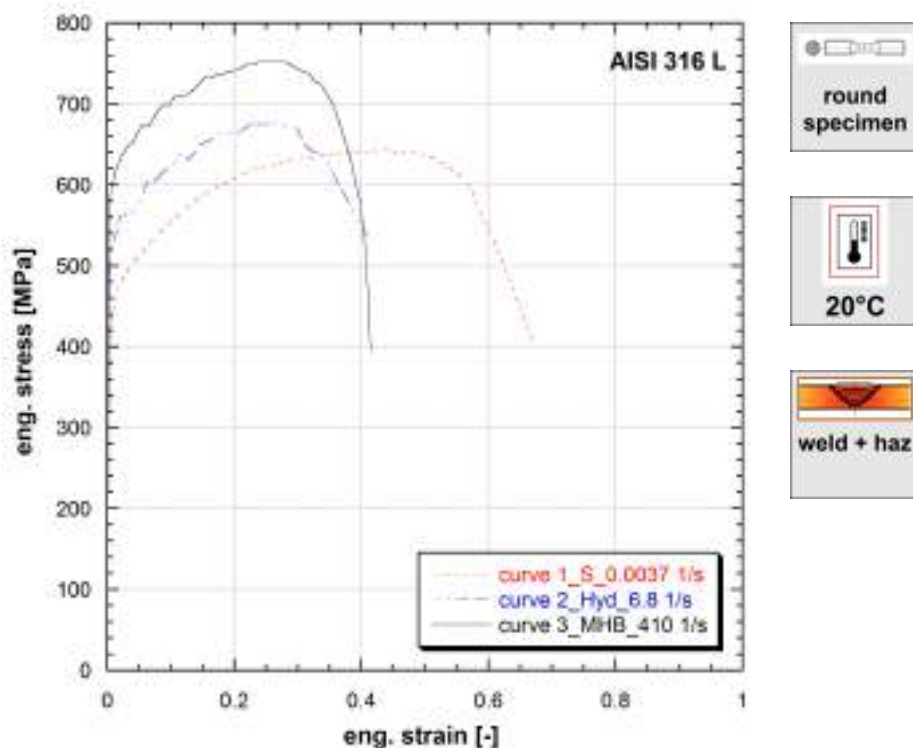


**Figure 9.93:** Stress vs strain curves of AISI 316 L (Ref.Mat.3)

**Note 9.93** Ref.Mat.3

Argon arc welding.

Strain rate [1/s]	Yield stress [MPa]	Ultimate tensile strength [MPa]	Uniform strain [-]	Fracture stress [MPa]	Fracture strain [-]
0.0037	416	643	0.444	405	0.671
6.8	491	676	0.269	537	0.411
410	584	752	0.280	395	0.415

**Table 93:** Mechanical properties of AISI 316 L (Ref.Mat.3)

Published in (Albertini and Montagnani, 1978).

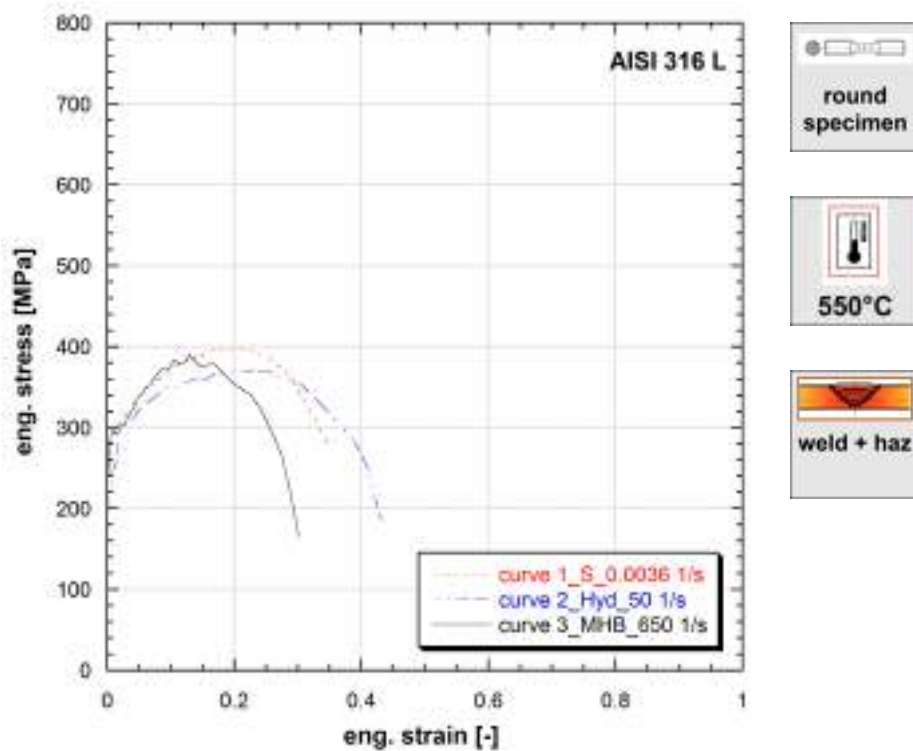


**Figure 9.94:** Stress vs strain curves of AISI 316 L (Ref.Mat.3)

**Note 9.94** Ref.Mat.3

Argon arc welding.

Strain rate [1/s]	Yield stress [MPa]	Ultimate tensile strength [MPa]	Uniform strain [-]	Fracture stress [MPa]	Fracture strain [-]
0.0036	256	398	0.183	274	0.351
50	220	372	0.234	185	0.432
650	266	390	0.129	164	0.302

**Table 94:** Mechanical properties of AISI 316 L (Ref.Mat.3)

Published in (Albertini and Montagnani, 1978).

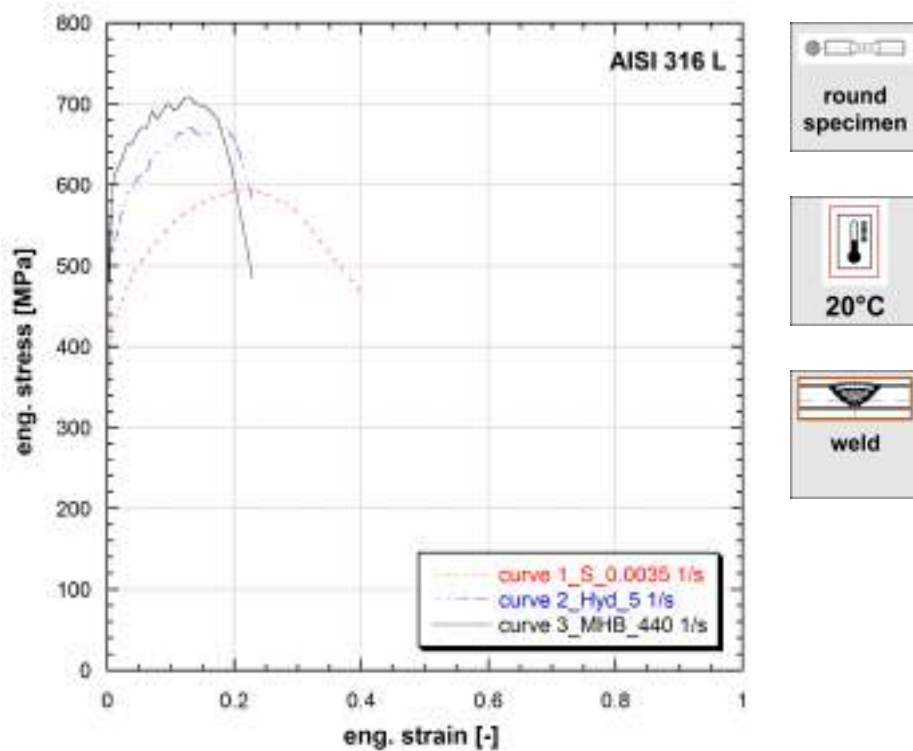


**Figure 9.95:** Stress vs strain curves of AISI 316 L (Ref.Mat.3)

**Note 9.95** Ref.Mat.3

*Argon arc welding.*

Strain rate [1/s]	Yield stress [MPa]	Ultimate tensile strength [MPa]	Uniform strain [-]	Fracture stress [MPa]	Fracture strain [-]
0.0035	402	596	0.223	461	0.404
5	504	671	0.168	581	0.229
440	518	709	0.130	483	0.229

**Table 95:** Mechanical properties of AISI 316 L (Ref.Mat.3)

Published in (Albertini and Montagnani, 1980), (Albertini and Montagnani, 1978).

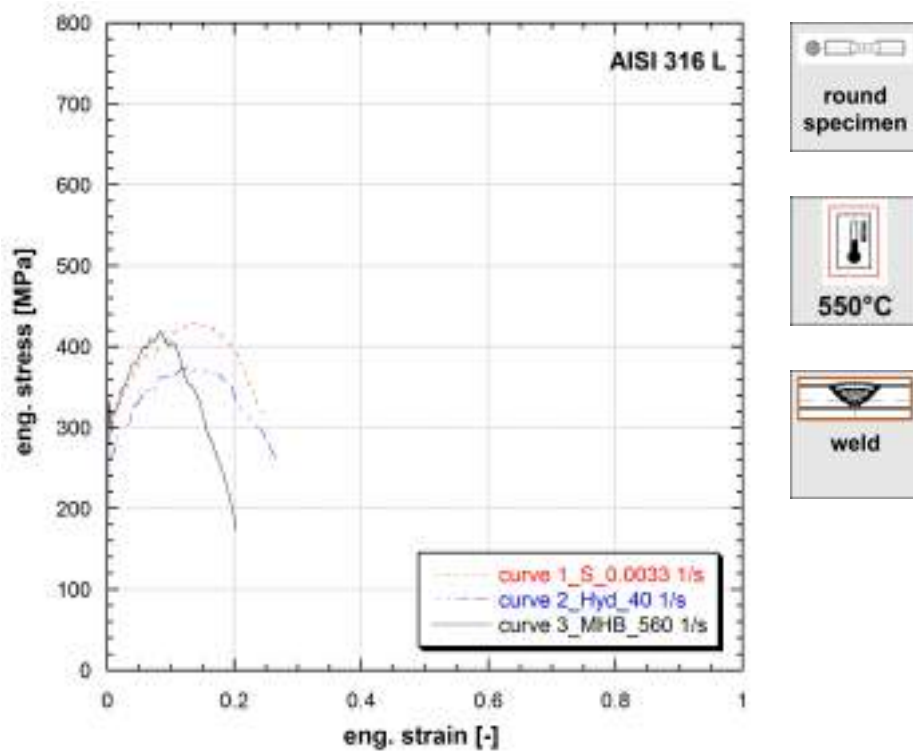


**Figure 9.96:** Stress vs strain curves of AISI 316 L (Ref.Mat.3)

**Note 9.96** Ref.Mat.3

*Argon arc welding.*

Strain rate [1/s]	Yield stress [MPa]	Ultimate tensile strength [MPa]	Uniform strain [-]	Fracture stress [MPa]	Fracture strain [-]
0.0033	283	429	0.131	317	0.243
40	264	375	0.144	259	0.267
560	318	419	0.084	173	0.203

**Table 96:** Mechanical properties of AISI 316 L (Ref.Mat.3)

Published in (Albertini and Montagnani, 1980), (Albertini and Montagnani, 1978), (Albertini et al., 1980).

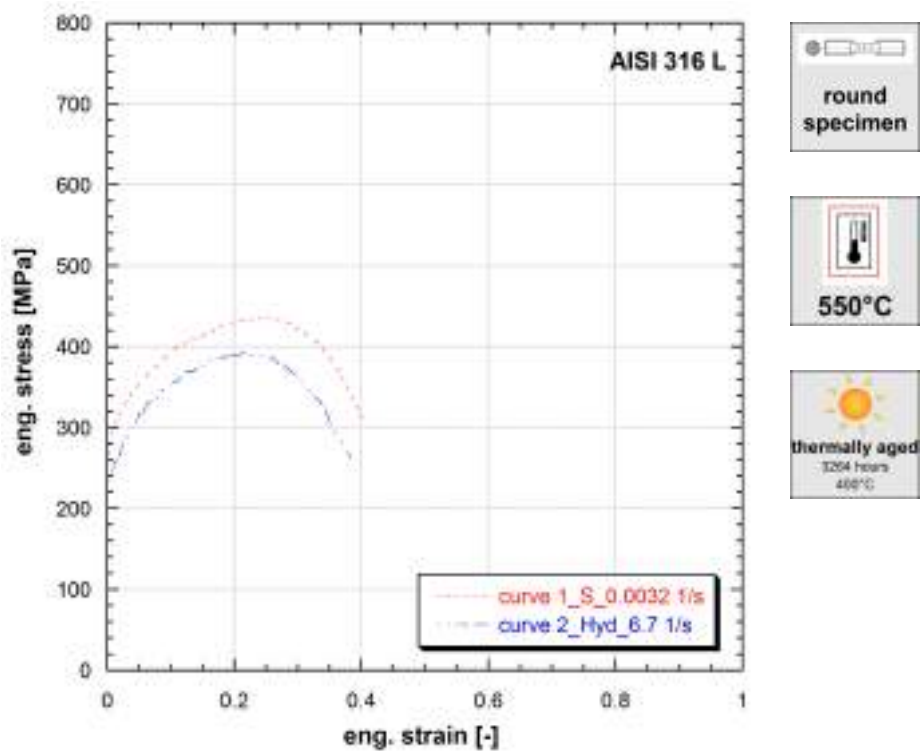


**Figure 9.97:** Stress vs strain curves of AISI 316 L (Ref.Mat.3)

**Note 9.97** Ref.Mat.3

Strain rate [1/s]	Yield stress [MPa]	Ultimate tensile strength [MPa]	Uniform strain [-]	Fracture stress [MPa]	Fracture strain [-]
0.0032	268	434	0.257	307	0.405
6.7	229	392	0.213	262	0.384

**Table 97:** Mechanical properties of AISI 316 L (Ref.Mat.3)

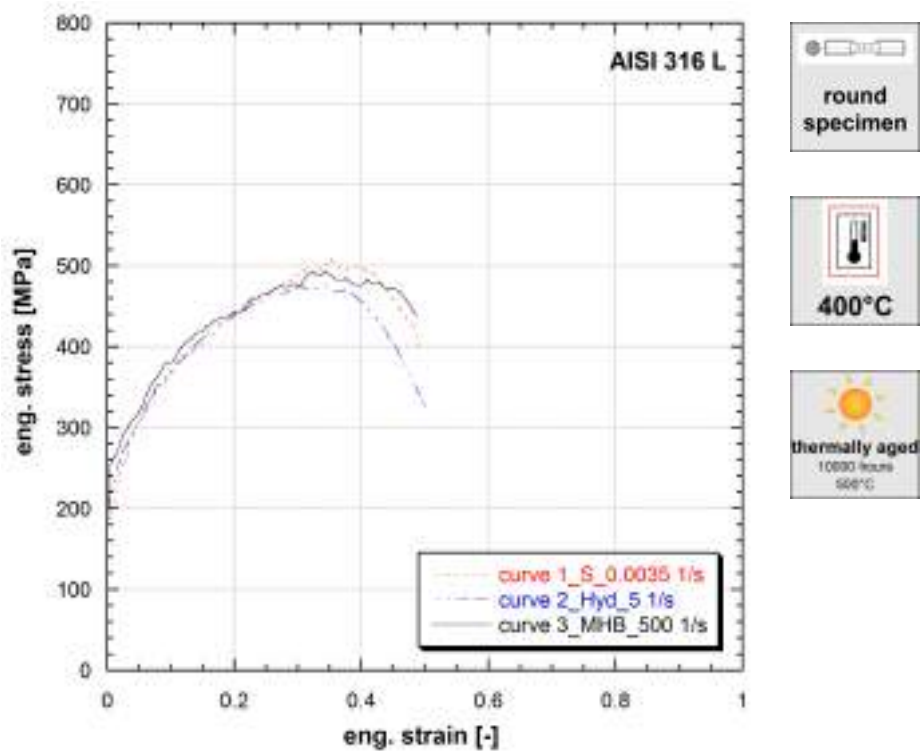


**Figure 9.98:** Stress vs strain curves of AISI 316 L (Ref.Mat.3)

**Note 9.98** Ref.Mat.3

Strain rate [1/s]	Yield stress [MPa]	Ultimate tensile strength [MPa]	Uniform strain [-]	Fracture stress [MPa]	Fracture strain [-]
0.0035	189	507	0.352	399	0.490
5	208	475	0.348	326	0.499
500	246	493	0.343	438	0.487

**Table 98:** Mechanical properties of AISI 316 L (Ref.Mat.3)

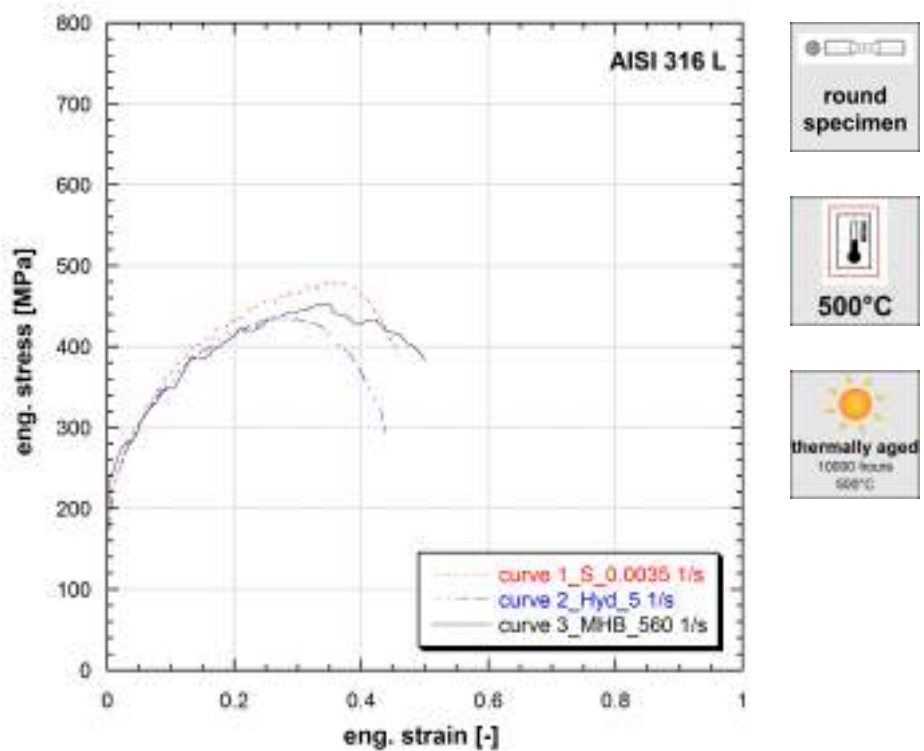


**Figure 9.99:** Stress vs strain curves of AISI 316 L (Ref.Mat.3)

**Note 9.99** Ref.Mat.3

Strain rate [1/s]	Yield stress [MPa]	Ultimate tensile strength [MPa]	Uniform strain [-]	Fracture stress [MPa]	Fracture strain [-]
0.0035	185	479	0.369	390	0.460
5	172	434	0.283	293	0.438
560	229	453	0.348	383	0.499

**Table 99:** Mechanical properties of AISI 316 L (Ref.Mat.3)

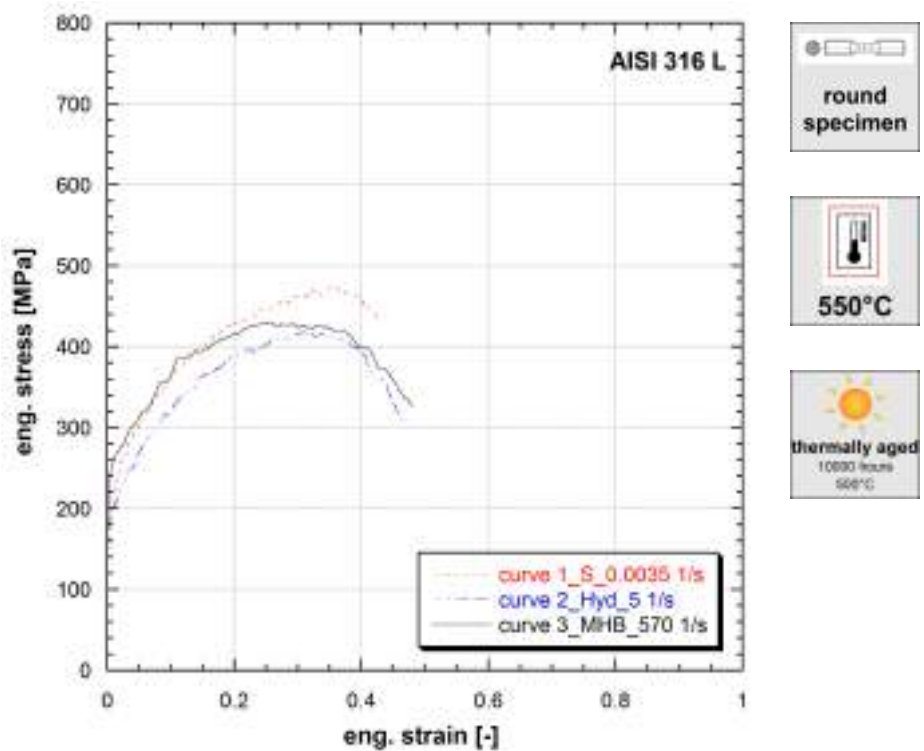


**Figure 9.100:** Stress vs strain curves of AISI 316 L (Ref.Mat.3)

**Note 9.100** Ref.Mat.3

Strain rate [1/s]	Yield stress [MPa]	Ultimate tensile strength [MPa]	Uniform strain [-]	Fracture stress [MPa]	Fracture strain [-]
0.0035	180	474	0.352	432	0.431
5	177	418	0.308	299	0.471
570	235	430	0.256	326	0.481

**Table 100:** Mechanical properties of AISI 316 L (Ref.Mat.3)

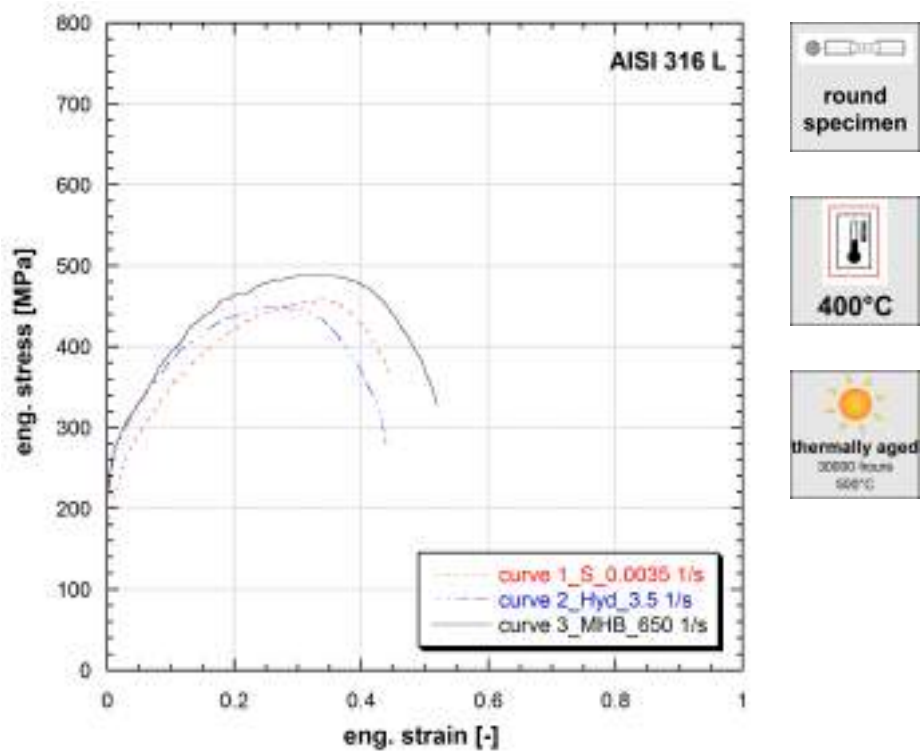


**Figure 9.101:** Stress vs strain curves of AISI 316 L (Ref.Mat.3)

**Note 9.101** Ref.Mat.3

Strain rate [1/s]	Yield stress [MPa]	Ultimate tensile strength [MPa]	Uniform strain [-]	Fracture stress [MPa]	Fracture strain [-]
0.0035	186	457	0.336	360	0.448
3.5	225	450	0.254	280	0.439
650	240	490	0.324	327	0.519

**Table 101:** Mechanical properties of AISI 316 L (Ref.Mat.3)

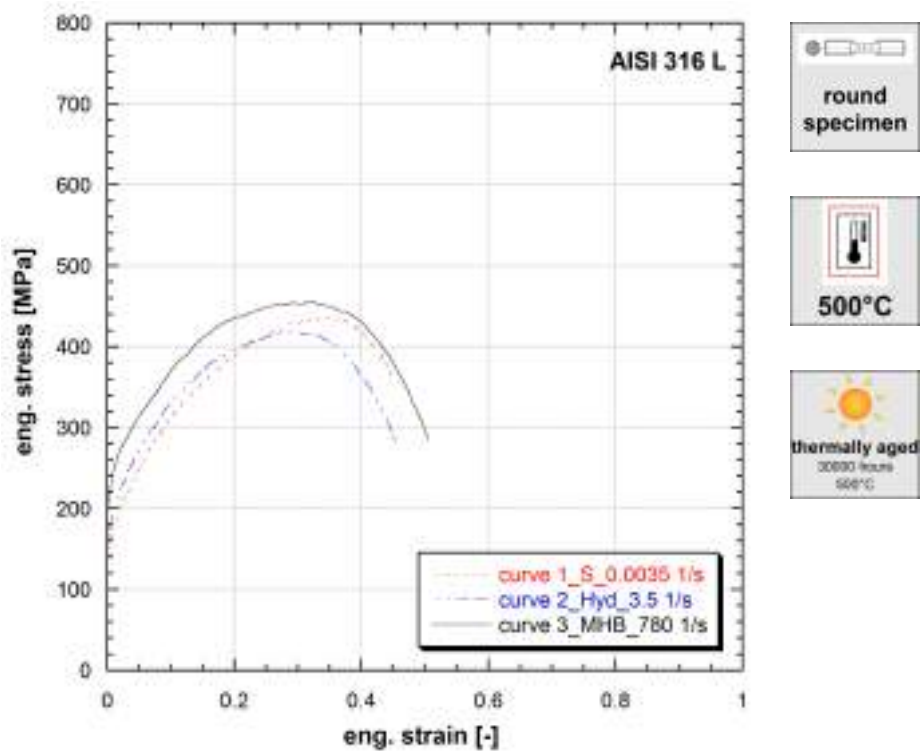


**Figure 9.102:** Stress vs strain curves of AISI 316 L (Ref.Mat.3)

**Note 9.102** Ref.Mat.3

Strain rate [1/s]	Yield stress [MPa]	Ultimate tensile strength [MPa]	Uniform strain [-]	Fracture stress [MPa]	Fracture strain [-]
0.0035	139	434	0.358	355	0.453
3.5	168	418	0.299	283	0.454
780	211	455	0.317	285	0.505

**Table 102:** Mechanical properties of AISI 316 L (Ref.Mat.3)

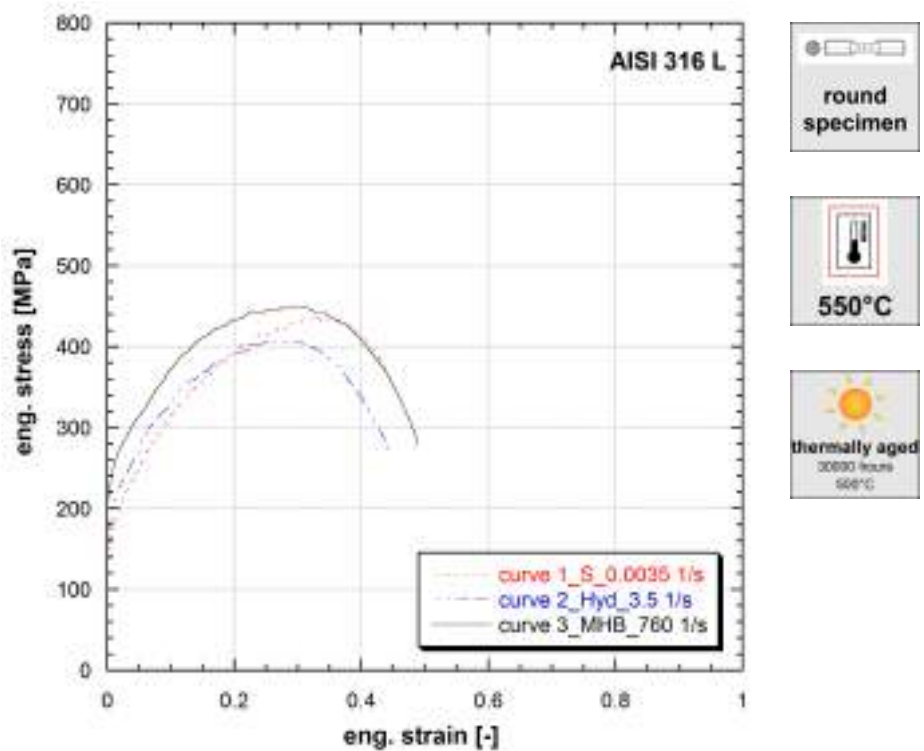


**Figure 9.103:** Stress vs strain curves of AISI 316 L (Ref.Mat.3)

**Note 9.103** Ref.Mat.3

Strain rate [1/s]	Yield stress [MPa]	Ultimate tensile strength [MPa]	Uniform strain [-]	Fracture stress [MPa]	Fracture strain [-]
0.0035	138	438	0.328	346	0.454
3.5	171	407	0.280	273	0.441
760	219	449	0.288	278	0.489

**Table 103:** Mechanical properties of AISI 316 L (Ref.Mat.3)

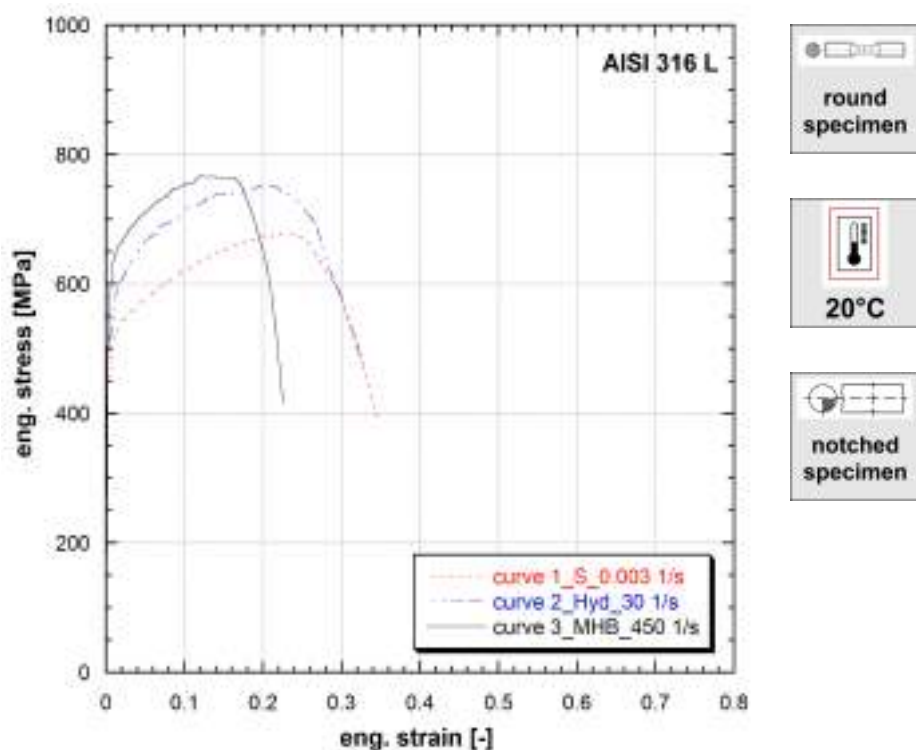


**Figure 9.104:** Stress vs strain curves of AISI 316 L (Ref.Mat.3)

**Note 9.104** Ref.Mat.3

Strain rate [1/s]	Yield stress [MPa]	Ultimate tensile strength [MPa]	Uniform strain [-]	Fracture stress [MPa]	Fracture strain [-]
0.003	462	678	0.229	388	0.348
30	516	752	0.195	473	0.328
450	576	766	0.119	417	0.226

**Table 104:** Mechanical properties of AISI 316 L (Ref.Mat.3)

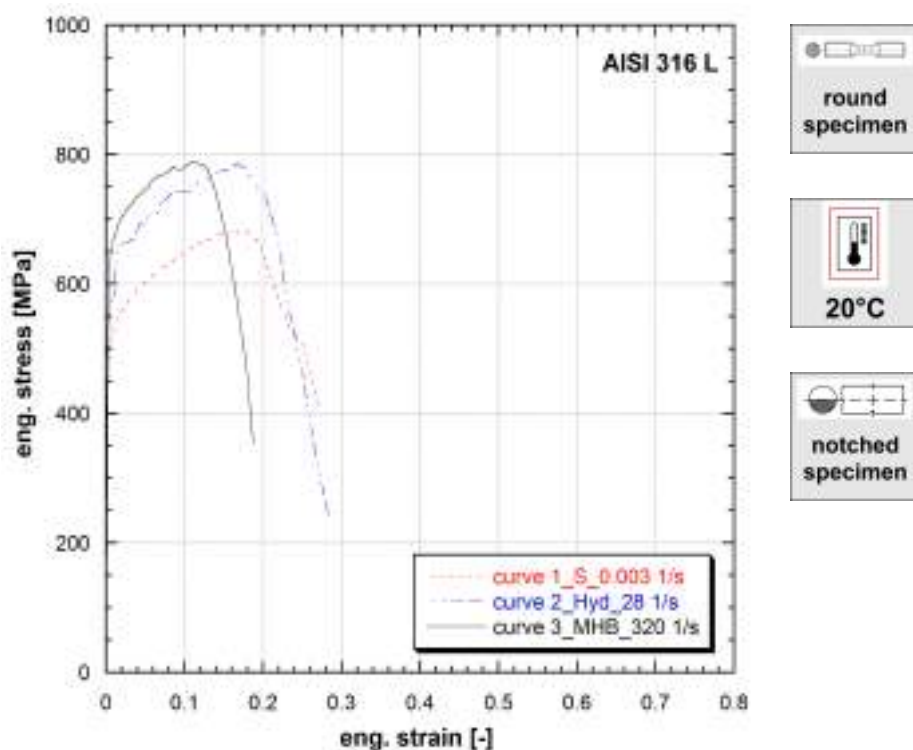


**Figure 9.105:** Stress vs strain curves of AISI 316 L (Ref.Mat.3)

**Note 9.105** Ref.Mat.3

Strain rate [1/s]	Yield stress [MPa]	Ultimate tensile strength [MPa]	Uniform strain [-]	Fracture stress [MPa]	Fracture strain [-]
0.003	499	681	0.179	404	0.274
28	571	786	0.167	245	0.283
320	636	789	0.110	353	0.187

**Table 105:** Mechanical properties of AISI 316 L (Ref.Mat.3)

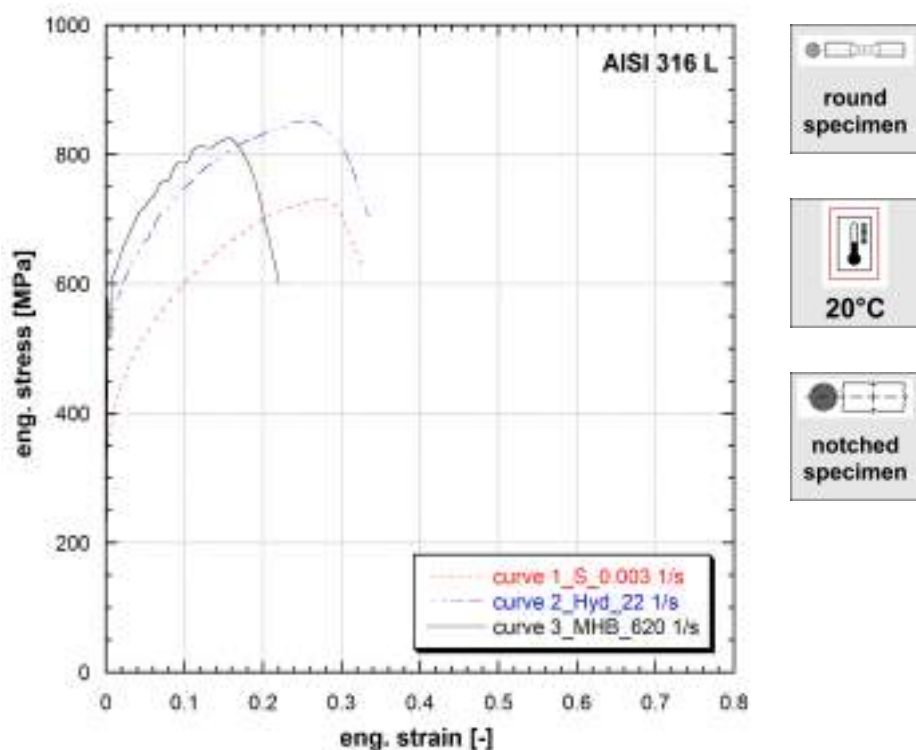


**Figure 9.106:** Stress vs strain curves of AISI 316 L (Ref.Mat.3)

**Note 9.106** Ref.Mat.3

Strain rate [1/s]	Yield stress [MPa]	Ultimate tensile strength [MPa]	Uniform strain [-]	Fracture stress [MPa]	Fracture strain [-]
0.003	361	731	0.280	623	0.328
22	519	851	0.239	703	0.334
620	544	825	0.159	599	0.221

**Table 106:** Mechanical properties of AISI 316 L (Ref.Mat.3)

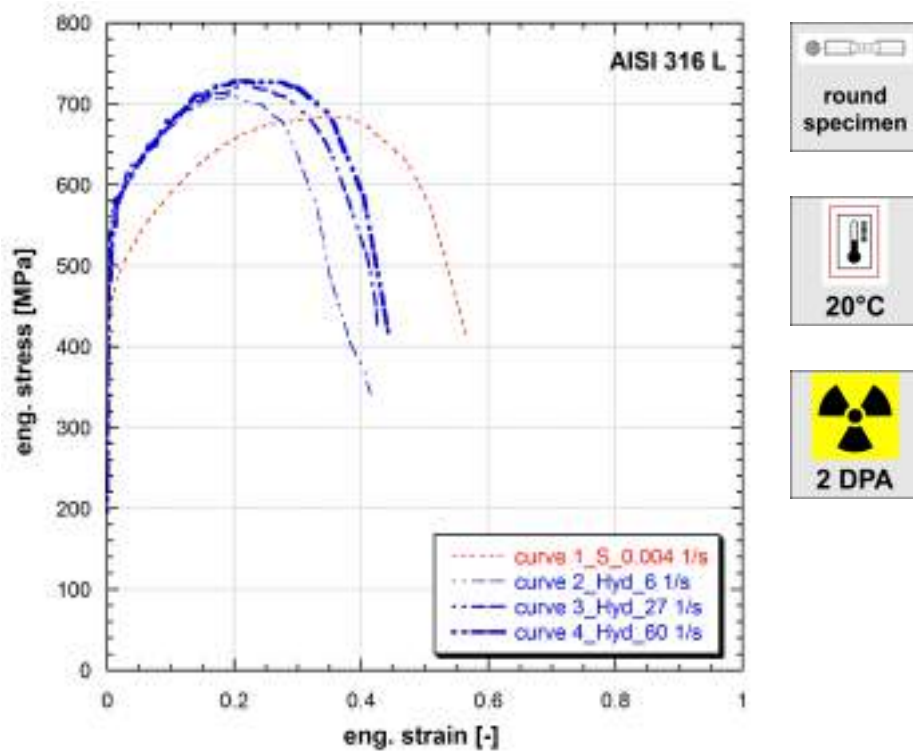


**Figure 9.107:** Stress vs strain curves of AISI 316 L (Ref.Mat.3)

**Note 9.107** Ref.Mat.3

*Irradiated in sodium at 400°C in HFR reactor, for 3000 hours.*

Strain rate [1/s]	Yield stress [MPa]	Ultimate tensile strength [MPa]	Uniform strain [-]	Fracture stress [MPa]	Fracture strain [-]
0.004	436	684	0.362	411	0.567
6	544	710	0.194	341	0.415
27	536	726	0.210	419	0.425
60	491	729	0.246	414	0.443

**Table 107:** Mechanical properties of AISI 316 L (Ref.Mat.3)

*Published in (Albertini et al., 1979), (Albertini and Montagnani, 1980), (Albertini and Genet, 1979).*

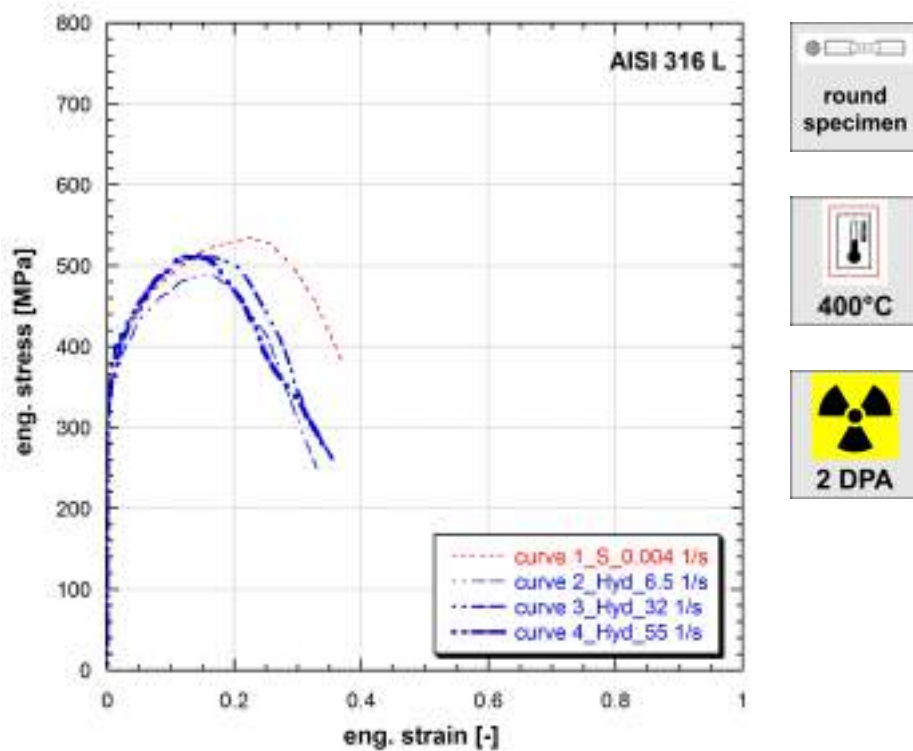


**Figure 9.108:** Stress vs strain curves of AISI 316 L (Ref.Mat.3)

**Note 9.108** Ref.Mat.3

*Irradiated in sodium at 400°C in HFR reactor, for 3000 hours.*

Strain rate [1/s]	Yield stress [MPa]	Ultimate tensile strength [MPa]	Uniform strain [-]	Fracture stress [MPa]	Fracture strain [-]
0.004	310	534	0.224	380	0.370
6.5	322	490	0.148	250	0.330
32	360	514	0.144	257	0.358
55	335	511	0.125	280	0.339

**Table 108:** Mechanical properties of AISI 316 L (Ref.Mat.3)

*Published in (Albertini et al., 1979), (Albertini and Genet, 1979).*

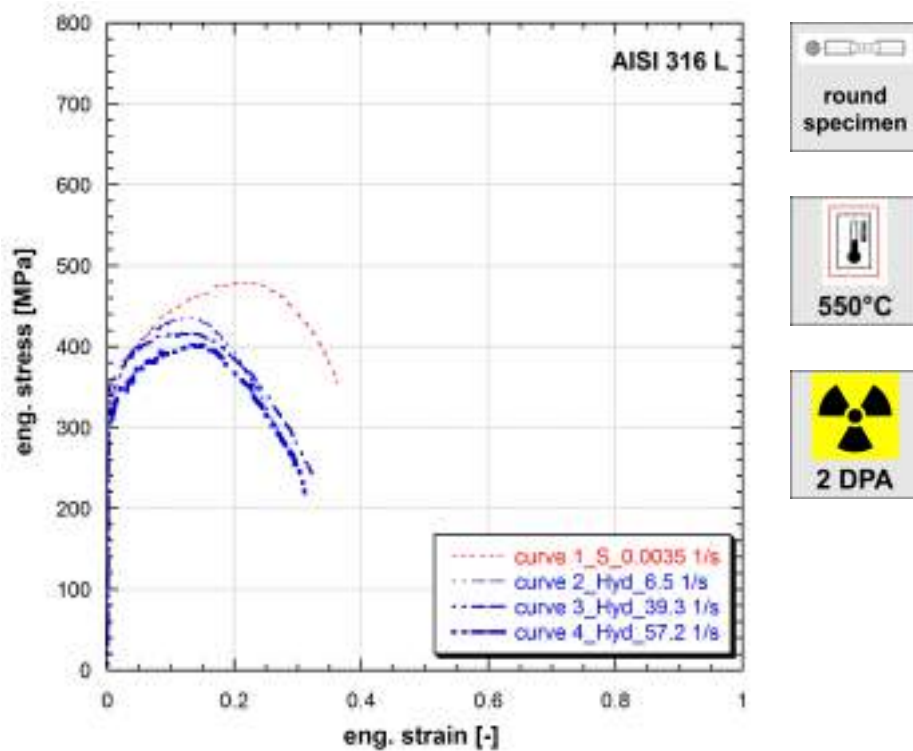


**Figure 9.109:** Stress vs strain curves of AISI 316 L (Ref.Mat.3)

**Note 9.109** Ref.Mat.3

*Irradiated in sodium at 400°C in HFR reactor, for 3000 hours.*

Strain rate [1/s]	Yield stress [MPa]	Ultimate tensile strength [MPa]	Uniform strain [-]	Fracture stress [MPa]	Fracture strain [-]
0.0035	311	478	0.204	355	0.363
6.5	332	436	0.124	252	0.292
39.3	347	416	0.132	237	0.324
57.2	297	402	0.132	217	0.312

**Table 109:** Mechanical properties of AISI 316 L (Ref.Mat.3)

*Published in (Albertini and Montagnani, 1980), (Albertini and Montagnani, 1983b), (Albertini and Genet, 1979), (Albertini et al., 1980), (Albertini and Montagnani, 1981a).*

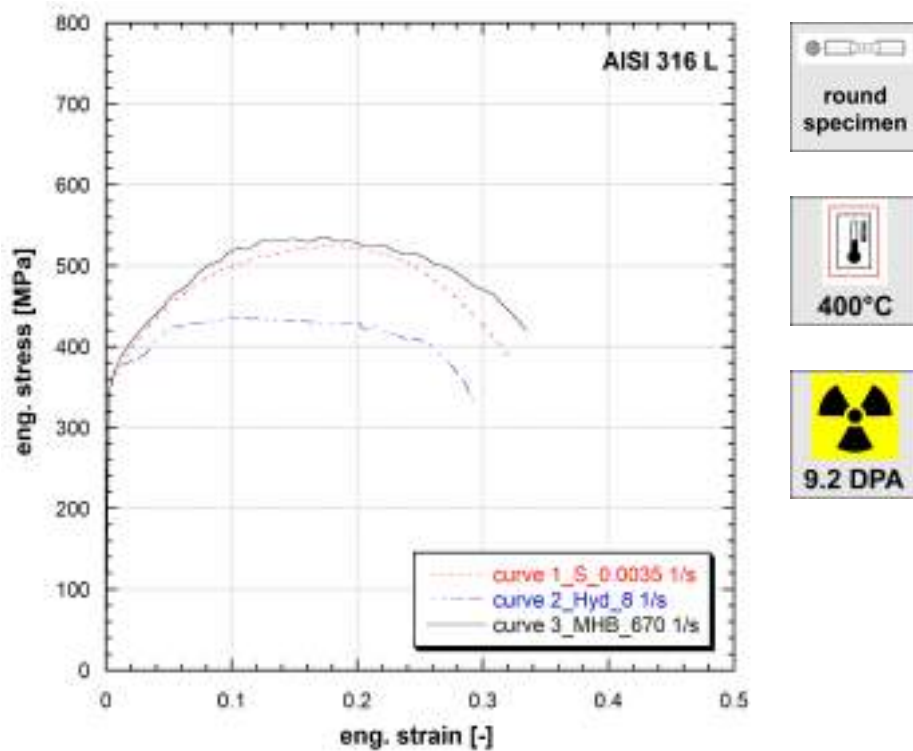


**Figure 9.110:** Stress vs strain curves of AISI 316 L (Ref.Mat.3)

**Note 9.110** Ref.Mat.3 *Irradiated in sodium at 500°C in HFR reactor, for 10000 hours.*

Strain rate [1/s]	Yield stress [MPa]	Ultimate tensile strength [MPa]	Uniform strain [-]	Fracture stress [MPa]	Fracture strain [-]
0.0035	345	524	0.175	389	0.320
8	357	437	0.101	334	0.292
670	348	536	0.171	420	0.335

**Table 110:** Mechanical properties of AISI 316 L (Ref.Mat.3)

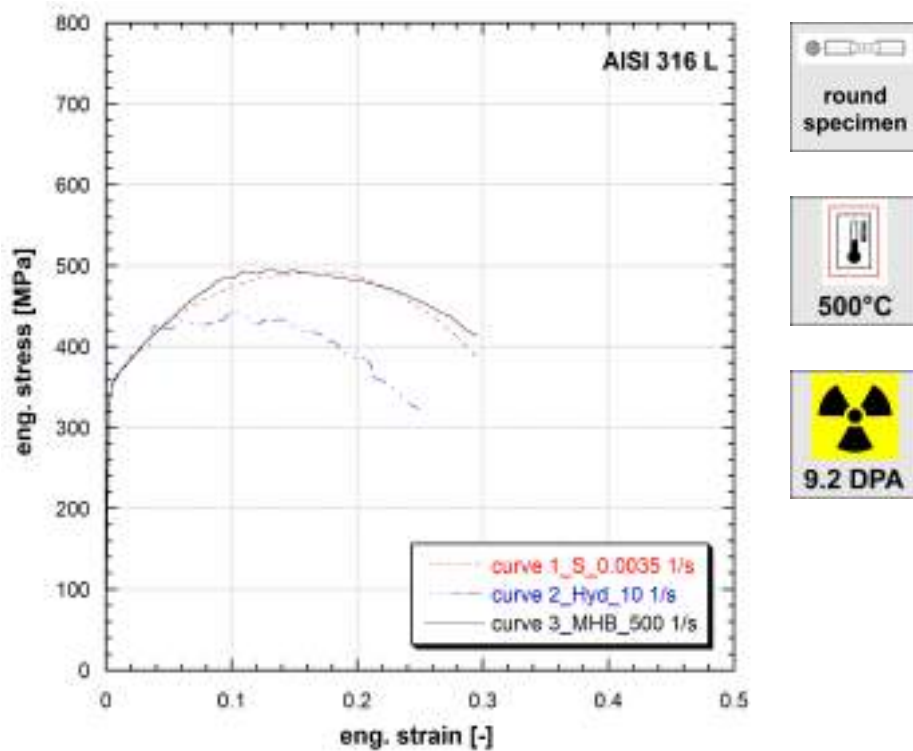


**Figure 9.111:** Stress vs strain curves of AISI 316 L (Ref.Mat.3)

**Note 9.111** Ref.Mat.3 *Irradiated in sodium at 500°C in HFR reactor, for 10000 hours.*

Strain rate [1/s]	Yield stress [MPa]	Ultimate tensile strength [MPa]	Uniform strain [-]	Fracture stress [MPa]	Fracture strain [-]
0.0035	346	492	0.17	289	0.295
10	349	442	0.100	320	0.252
500	335	495	0.134	414	0.296

**Table 111:** Mechanical properties of AISI 316 L (Ref.Mat.3)

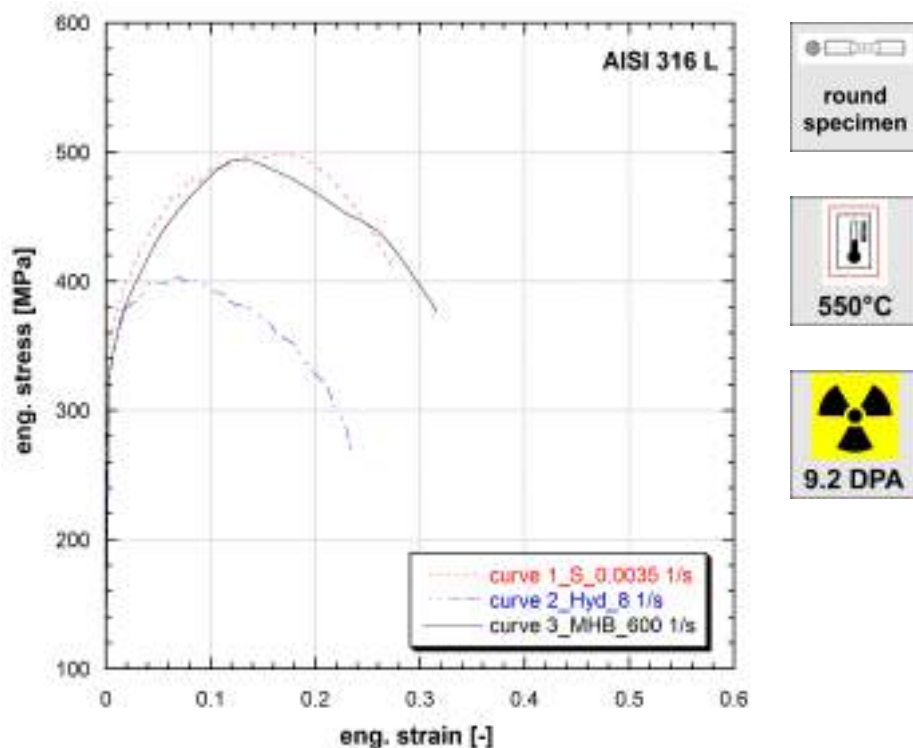


**Figure 9.112:** Stress vs strain curves of AISI 316 L (Ref.Mat.3)

**Note 9.112** Ref.Mat.3 *Irradiated in sodium at 500°C in HFR reactor, for 10000 hours.*

Strain rate [1/s]	Yield stress [MPa]	Ultimate tensile strength [MPa]	Uniform strain [-]	Fracture stress [MPa]	Fracture strain [-]
0.0035	358	498	0.138	410	0.273
8	331	402	0.067	270	0.234
600	335	494	0.132	376	0.316

**Table 112:** Mechanical properties of AISI 316 L (Ref.Mat.3)

*Published in (Albertini et al., 1984a).*

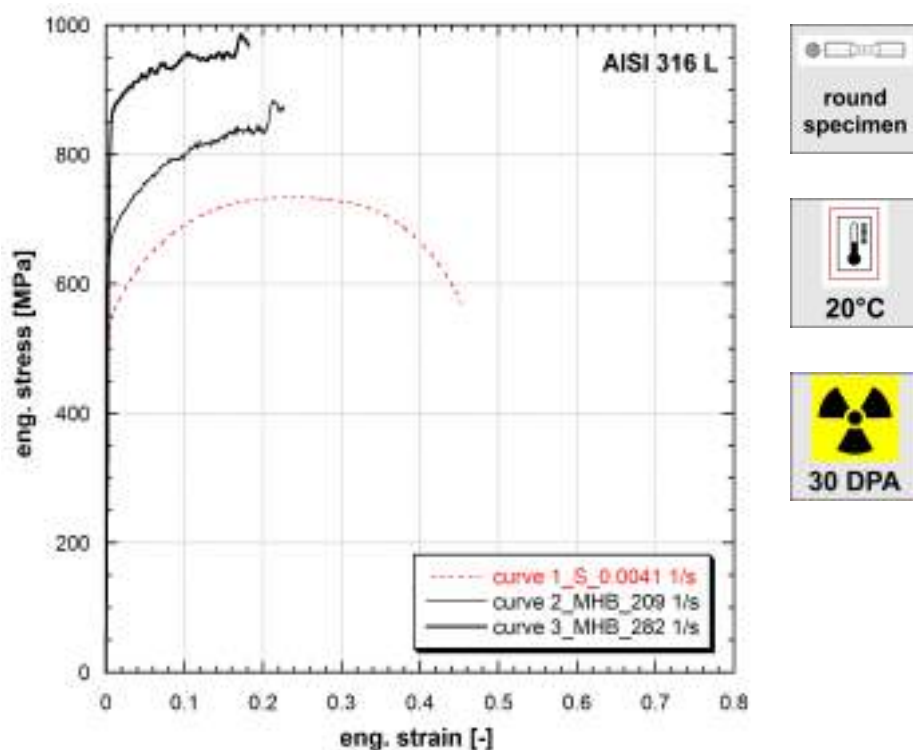


**Figure 9.113:** Stress vs strain curves of AISI 316 L (Ref.Mat.3)

**Note 9.113** Ref.Mat.3

Irradiated in sodium at 500°C in HFR reactor, for 30000 hours.

Strain rate [1/s]	Yield stress [MPa]	Ultimate tensile strength [MPa]	Uniform strain [-]	Fracture stress [MPa]	Fracture strain [-]
0.0041	522	734	0.235	570	0.453
209	658	-	-	-	-
282	839	-	-	-	-

**Table 113:** Mechanical properties of AISI 316 L (Ref.Mat.3)

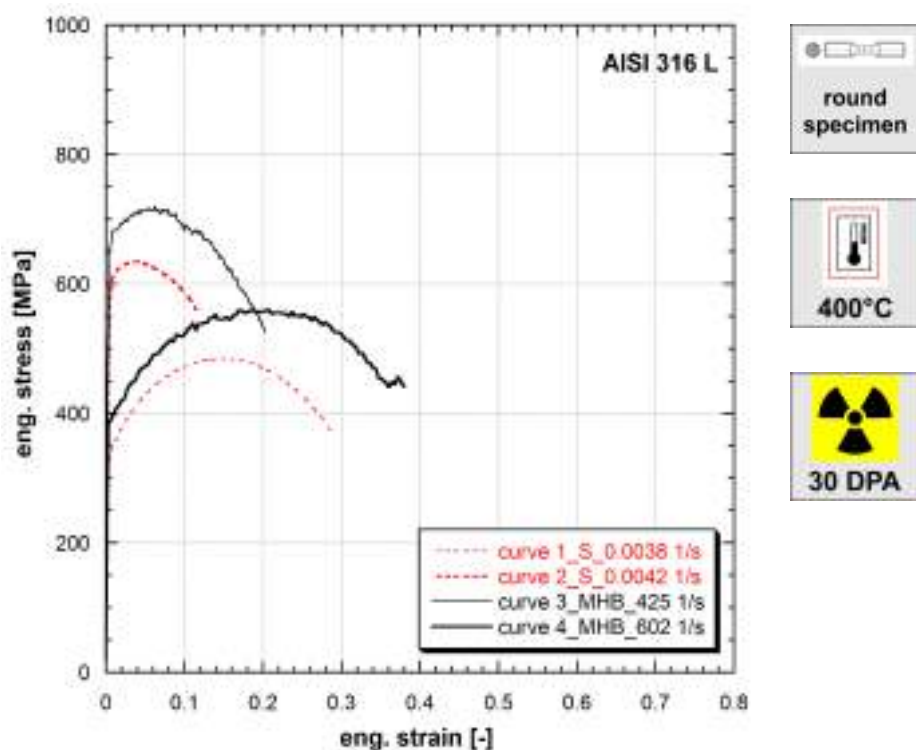


**Figure 9.114:** Stress vs strain curves of AISI 316 L (Ref.Mat.3)

**Note 9.114** Ref.Mat.3

*Irradiated in sodium at 500°C in HFR reactor, for 30000 hours.*

Strain rate [1/s]	Yield stress [MPa]	Ultimate tensile strength [MPa]	Uniform strain [-]	Fracture stress [MPa]	Fracture strain [-]
0.0038	324	484	0.152	369	0.288
0.0042	576	635	0.037	556	0.117
425	660	719	0.063	525	0.202
602	385	560	0.186	441	0.361

**Table 114:** Mechanical properties of AISI 316 L (Ref.Mat.3)

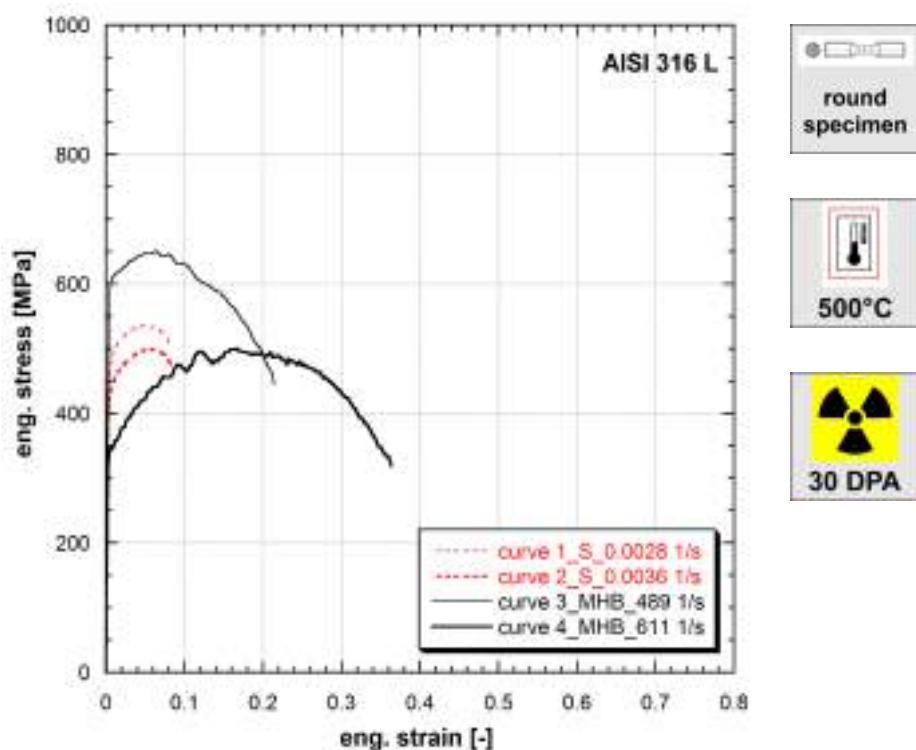


**Figure 9.115:** Stress vs strain curves of AISI 316 L (Ref.Mat.3)

**Note 9.115** Ref.Mat.3

*Irradiated in sodium at 500°C in HFR reactor, for 30000 hours.*

Strain rate [1/s]	Yield stress [MPa]	Ultimate tensile strength [MPa]	Uniform strain [-]	Fracture stress [MPa]	Fracture strain [-]
0.0028	465	535	0.053	503	0.083
0.0036	424	499	0.061	469	0.084
489	597	650	0.063	445	0.215
611	338	500	0.167	318	0.363

**Table 115:** Mechanical properties of AISI 316 L (Ref.Mat.3)

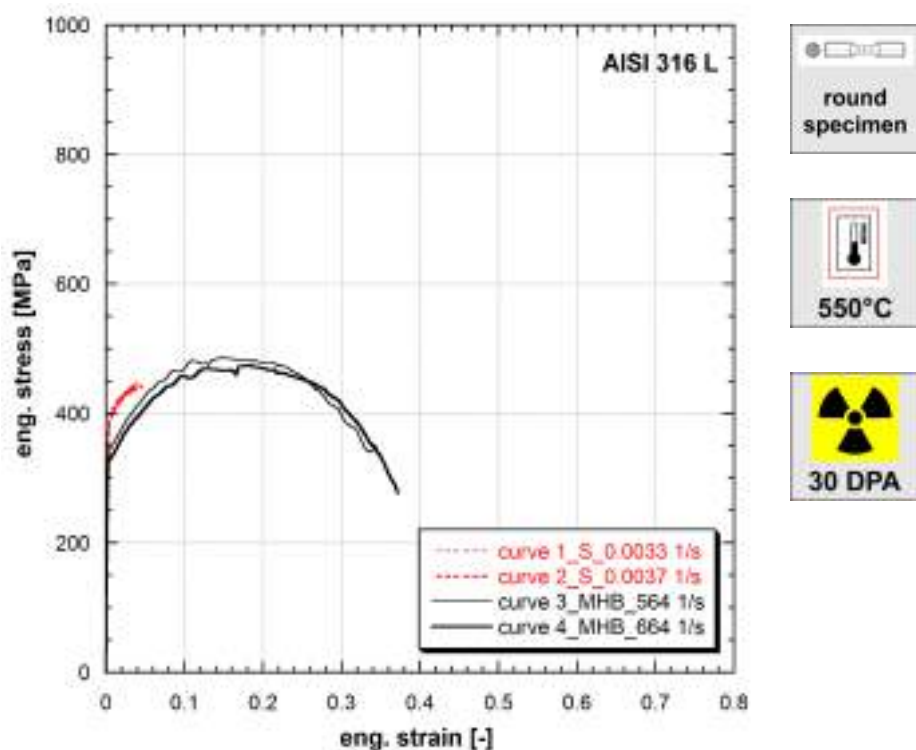


**Figure 9.116:** Stress vs strain curves of AISI 316 L (Ref.Mat.3)

**Note 9.116** Ref.Mat.3

*Irradiated in sodium at 500°C in HFR reactor, for 30000 hours.*

Strain rate [1/s]	Yield stress [MPa]	Ultimate tensile strength [MPa]	Uniform strain [-]	Fracture stress [MPa]	Fracture strain [-]
0.0033	383	447	0.039	447	0.039
0.0037	383	439	0.037	439	0.037
564	345	487	0.150	340	0.337
664	327	474	0.184	277	0.372

**Table 116:** Mechanical properties of AISI 316 L (Ref.Mat.3)

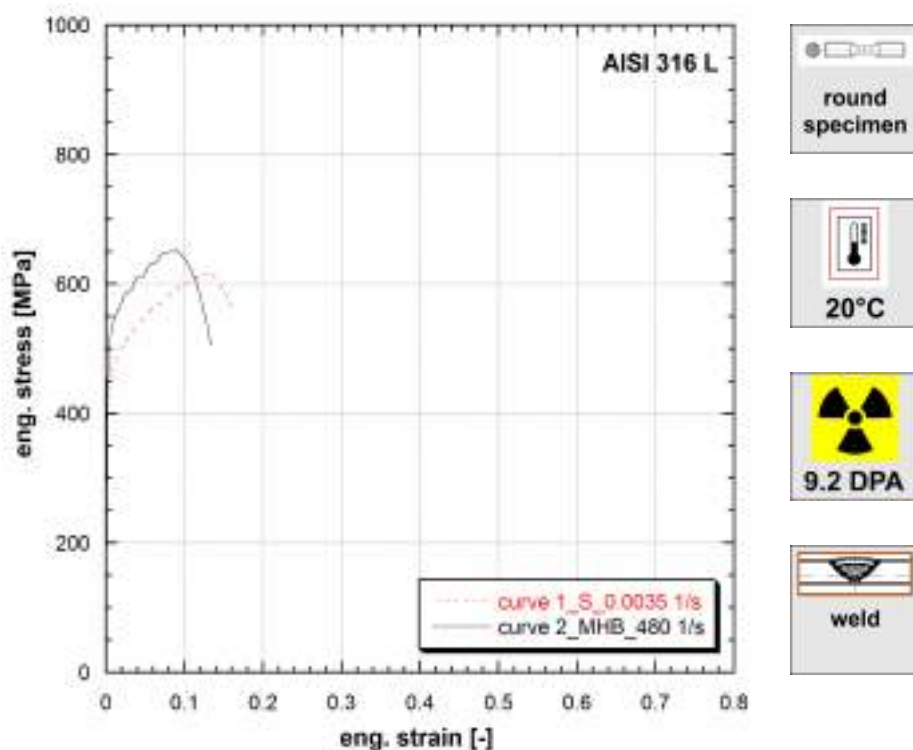


**Figure 9.117:** Stress vs strain curves of AISI 316 L (Ref.Mat.3)

**Note 9.117** Ref.Mat.3

*Irradiated in sodium at 500°C in HFR reactor, for 10000 hours.*

*Argon arc welding.*

Strain rate [1/s]	Yield stress [MPa]	Ultimate tensile strength [MPa]	Uniform strain [-]	Fracture stress [MPa]	Fracture strain [-]
0.0035	434	614	0.129	565	0.160
480	500	651	0.088	505	0.134

**Table 117:** Mechanical properties of AISI 316 L (Ref.Mat.3)

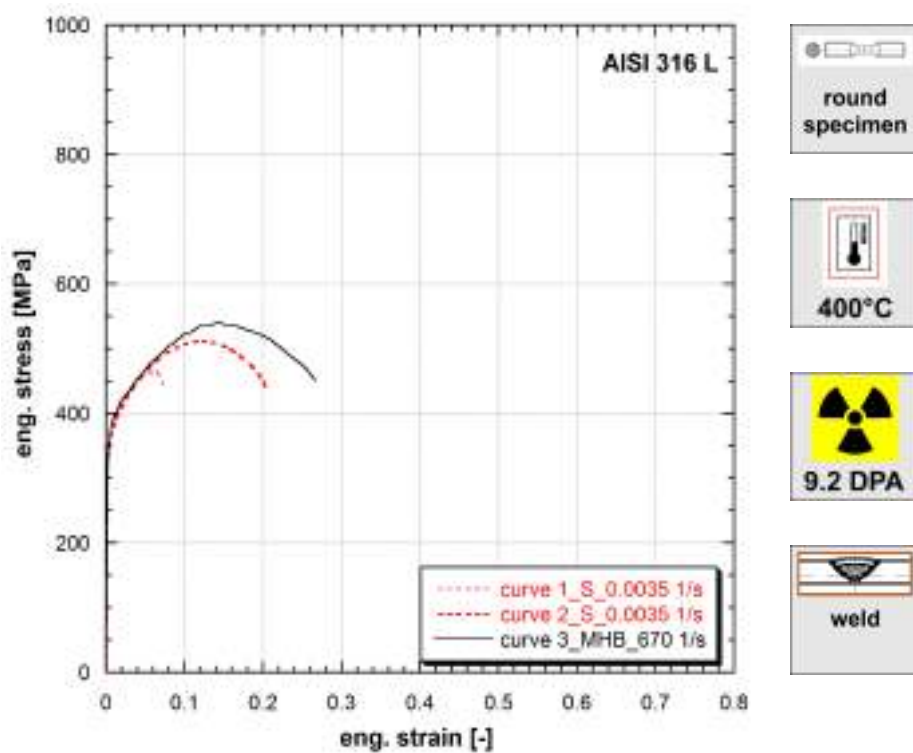


**Figure 9.118:** Stress vs strain curves of AISI 316 L (Ref.Mat.3)

**Note 9.118** Ref.Mat.3

*Irradiated in sodium at 500°C in HFR reactor, for 10000 hours.*

*Argon arc welding.*

Strain rate [1/s]	Yield stress [MPa]	Ultimate tensile strength [MPa]	Uniform strain [-]	Fracture stress [MPa]	Fracture strain [-]
0.0035	356	465	0.062	445	0.073
0.0035	344	512	0.122	433	0.205
670	358	540	0.143	451	0.267

**Table 118:** Mechanical properties of AISI 316 L (Ref.Mat.3)

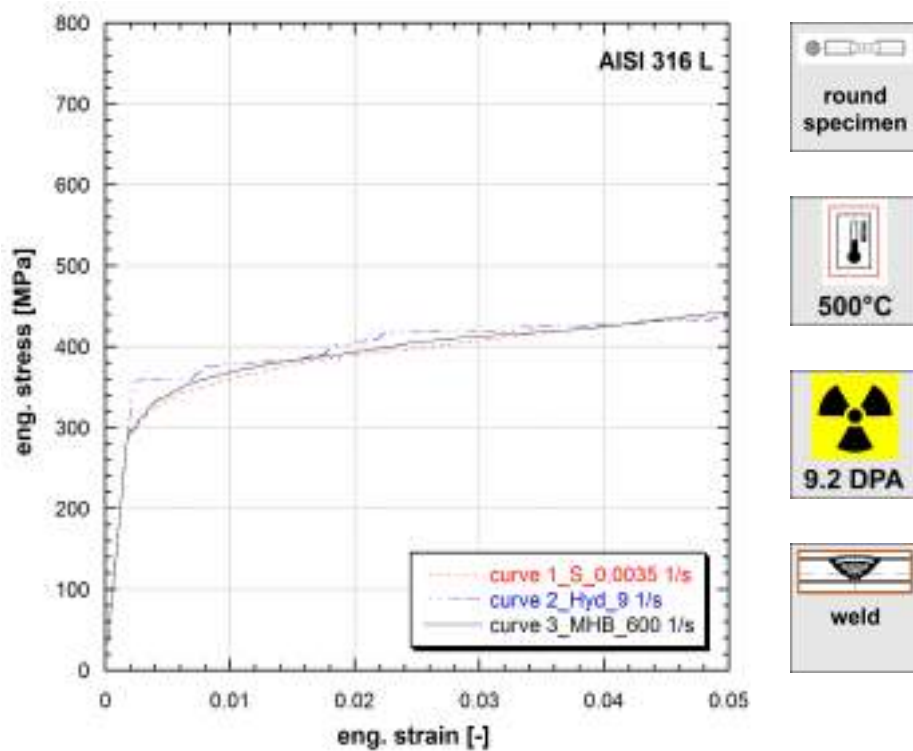


**Figure 9.119:** Stress vs strain curves of AISI 316 L (Ref.Mat.3)

**Note 9.119** Ref.Mat.3

*Irradiated in sodium at 500°C in HFR reactor, for 10000 hours.*

*Argon arc welding.*

Strain rate [1/s]	Yield stress [MPa]	Ultimate tensile strength [MPa]	Uniform strain [-]	Fracture stress [MPa]	Fracture strain [-]
0.0035	325	-	-	-	-
9	358	-	-	-	-
600	332	-	-	-	-

**Table 119:** Mechanical properties of AISI 316 L (Ref.Mat.3)

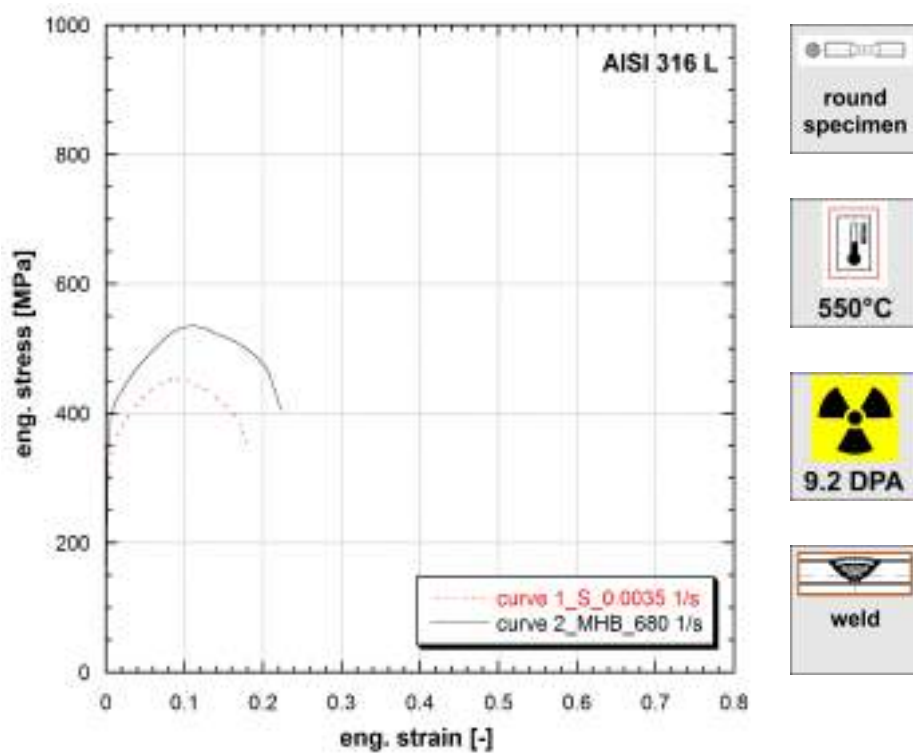


**Figure 9.120:** Stress vs strain curves of AISI 316 L (Ref.Mat.3)

**Note 9.120** Ref.Mat.3

*Irradiated in sodium at 500°C in HFR reactor, for 10000 hours.*

*Argon arc welding.*

Strain rate [1/s]	Yield stress [MPa]	Ultimate tensile strength [MPa]	Uniform strain [-]	Fracture stress [MPa]	Fracture strain [-]
0.0035	308	456	0.086	341	0.183
680	376	536	0.111	405	0.223

**Table 120:** Mechanical properties of AISI 316 L (Ref.Mat.3)

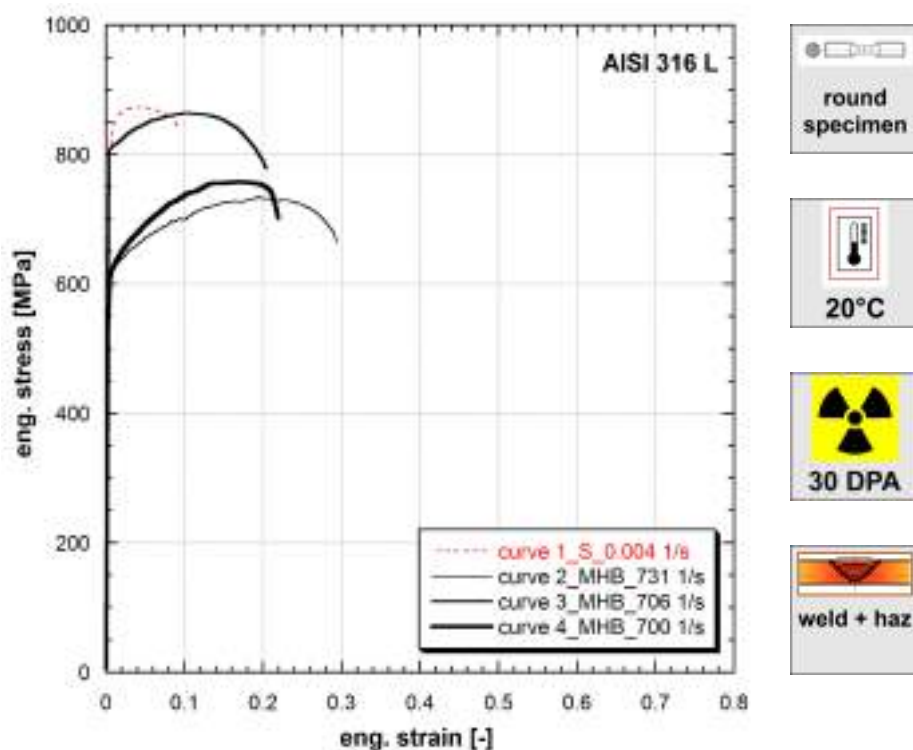


**Figure 9.121:** Stress vs strain curves of AISI 316 L (Ref.Mat.3)

**Note 9.121** Ref.Mat.3

*Irradiated in sodium at 500°C in HFR reactor, for 30000 hours.*

*Argon arc welding.*

Strain rate [1/s]	Yield stress [MPa]	Ultimate tensile strength [MPa]	Uniform strain [-]	Fracture stress [MPa]	Fracture strain [-]
0.004	803	872	0.042	838	0.093
700	593	758	0.169	702	0.219
706	813	864	0.099	779	0.204
731	613	734	0.194	664	0.294

**Table 121:** Mechanical properties of AISI 316 L (Ref.Mat.3)

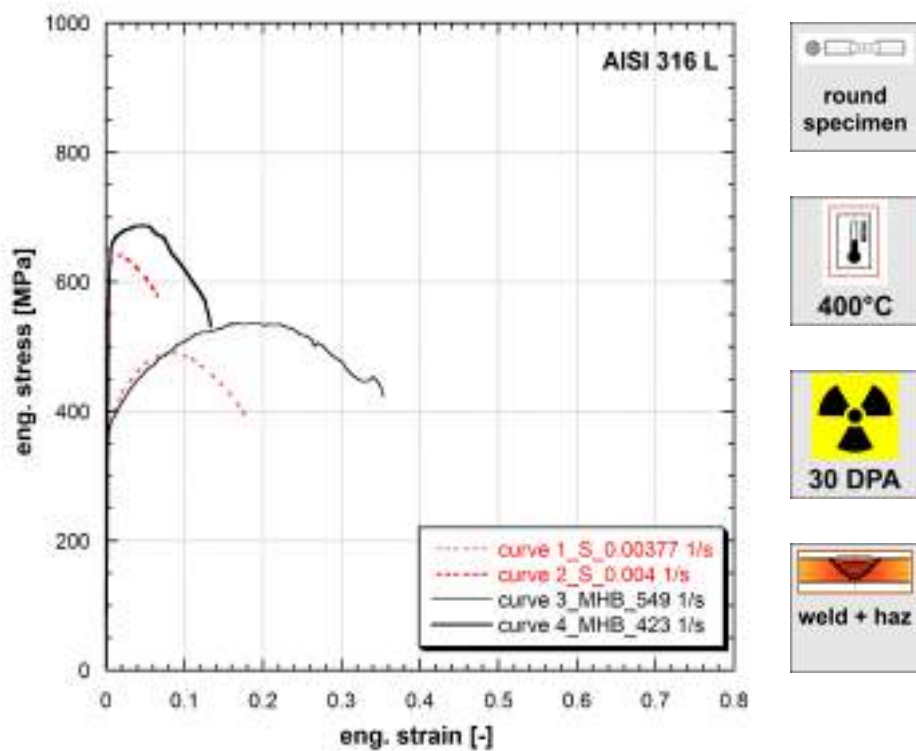


**Figure 9.122:** Stress vs strain curves of AISI 316 L (Ref.Mat.3)

**Note 9.122** Ref.Mat.3

*Irradiated in sodium at 500°C in HFR reactor, for 30000 hours.*

*Argon arc welding.*

Strain rate [1/s]	Yield stress [MPa]	Ultimate tensile strength [MPa]	Uniform strain [-]	Fracture stress [MPa]	Fracture strain [-]
0.00377	361	490	0.081	391	0.178
0.004	622	642	0.014	578	0.065
423	642	688	0.046	532	0.133
549	372	536	0.159	422	0.354

**Table 122:** Mechanical properties of AISI 316 L (Ref.Mat.3)

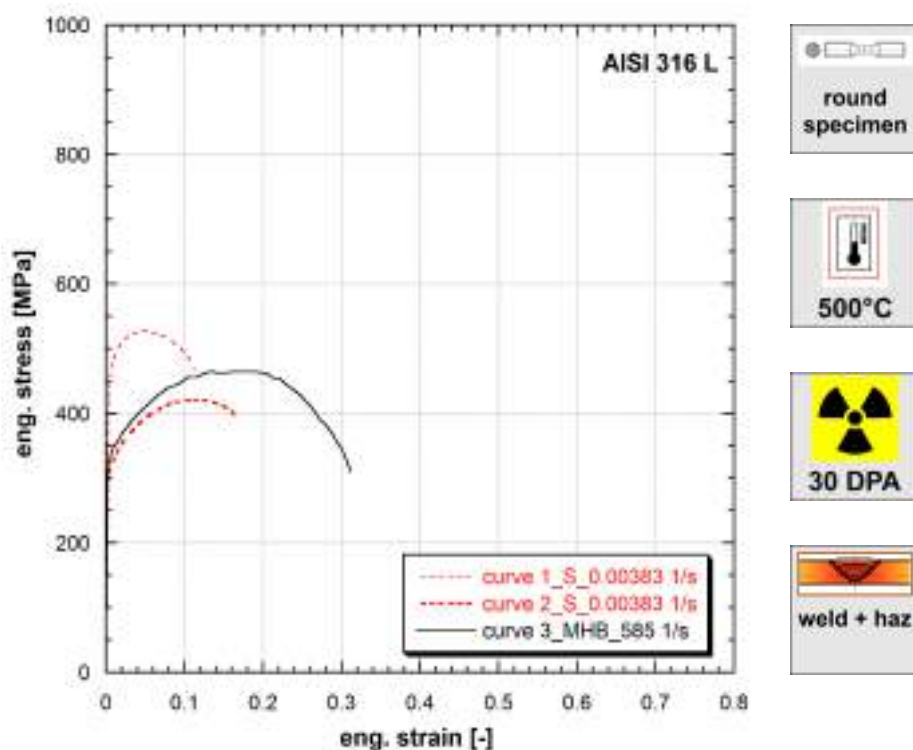


**Figure 9.123:** Stress vs strain curves of AISI 316 L (Ref.Mat.3)

**Note 9.123** Ref.Mat.3

*Irradiated in sodium at 500°C in HFR reactor, for 30000 hours.*

*Argon arc welding.*

Strain rate [1/s]	Yield stress [MPa]	Ultimate tensile strength [MPa]	Uniform strain [-]	Fracture stress [MPa]	Fracture strain [-]
0.00383	304	421	0.112	395	0.164
0.00383	449	527	0.049	467	0.112
585	327	465	0.136	309	0.312

**Table 123:** Mechanical properties of AISI 316 L (Ref.Mat.3)

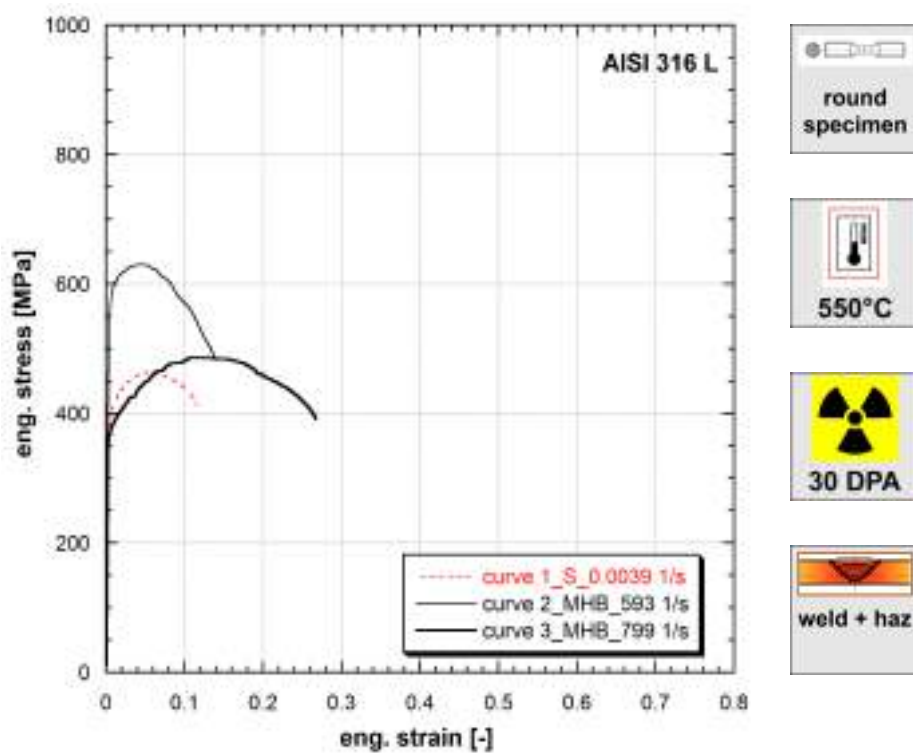


**Figure 9.124:** Stress vs strain curves of AISI 316 L (Ref.Mat.3)

**Note 9.124** Ref.Mat.3

*Irradiated in sodium at 500°C in HFR reactor, for 30000 hours.*

*Argon arc welding.*

Strain rate [1/s]	Yield stress [MPa]	Ultimate tensile strength [MPa]	Uniform strain [-]	Fracture stress [MPa]	Fracture strain [-]
0.0039	373	463	0.052	413	0.115
593	549	630	0.047	482	0.139
799	364	486	0.107	391	0.267

**Table 124:** Mechanical properties of AISI 316 L (Ref.Mat.3)

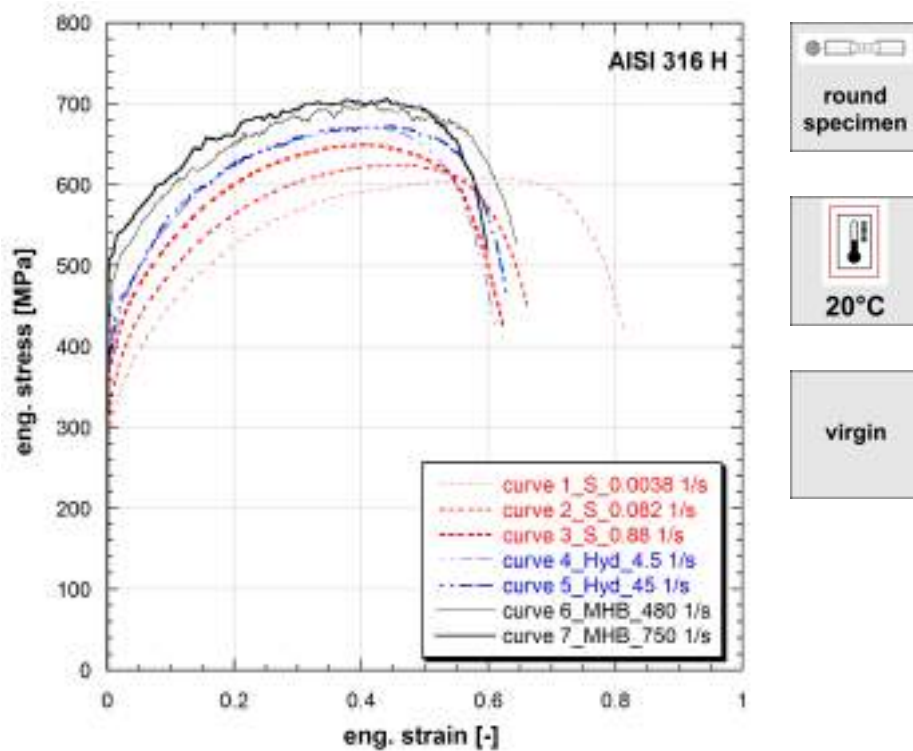


**Figure 9.125:** Stress vs strain curves of AISI 316 H (Ref.Mat.)

**Note 9.125** Ref.Mat.

Strain rate [1/s]	Yield stress [MPa]	Ultimate tensile strength [MPa]	Uniform strain [-]	Fracture stress [MPa]	Fracture strain [-]
0.0038	287	608	0.637	416	0.814
0.082	320	624	0.459	452	0.659
0.88	375	650	0.406	427	0.622
4.5	389	670	0.425	427	0.611
45	389	673	0.448	468	0.628
480	442	701	0.414	527	0.645
750	509	707	0.439	518	0.598

**Table 125:** Mechanical properties of AISI 316 H (Ref.Mat.)

Published in (Albertini et al., 1983a), (Albertini et al., 1984b), (Albertini and Montagnani, 1983b), (Albertini et al., 1983b).

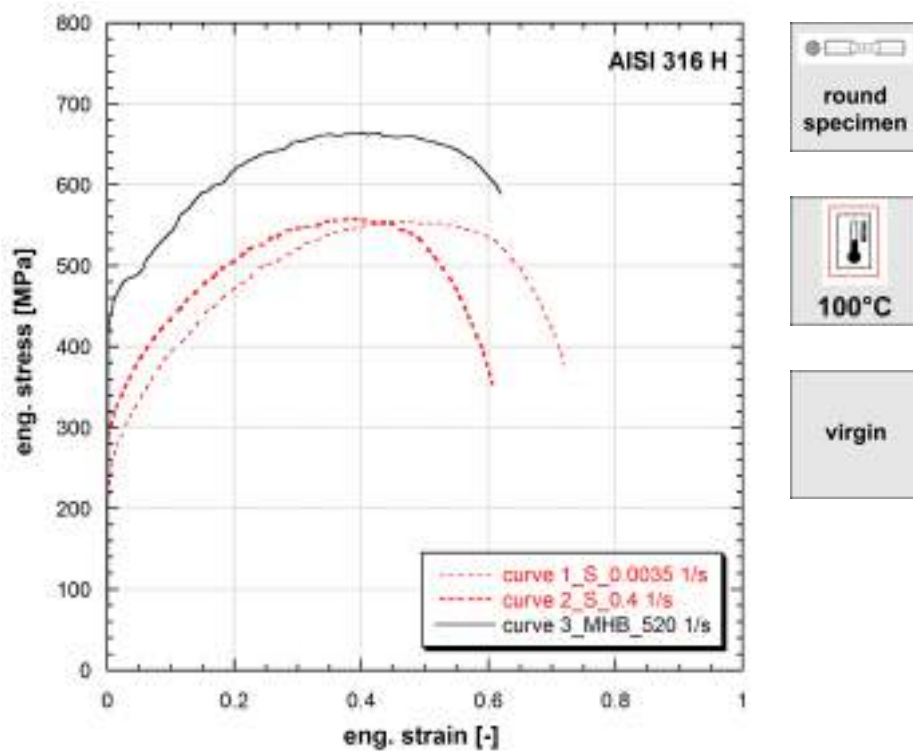


**Figure 9.126:** Stress vs strain curves of AISI 316 H (Ref.Mat.)

**Note 9.126** Ref.Mat.

Strain rate [1/s]	Yield stress [MPa]	Ultimate tensile strength [MPa]	Uniform strain [-]	Fracture stress [MPa]	Fracture strain [-]
0.0035	218	555	0.441	377	0.719
0.4	291	558	0.388	353	0.607
520	430	664	0.402	589	0.620

**Table 126:** Mechanical properties of AISI 316 H (Ref.Mat.)

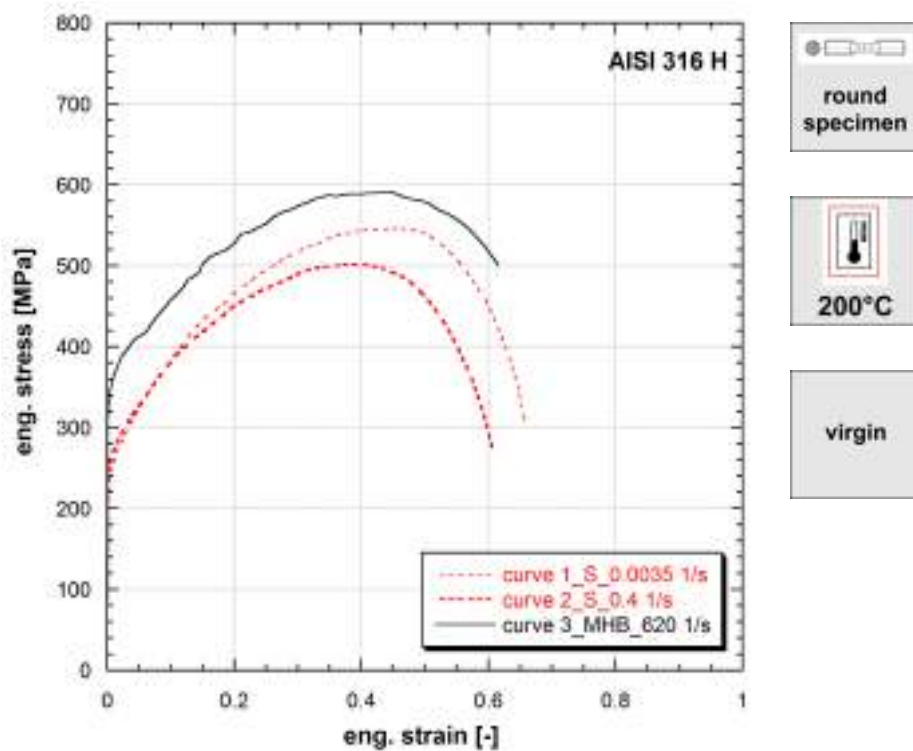


**Figure 9.127:** Stress vs strain curves of AISI 316 H (Ref.Mat.)

**Note 9.127** Ref.Mat.

Strain rate [1/s]	Yield stress [MPa]	Ultimate tensile strength [MPa]	Uniform strain [-]	Fracture stress [MPa]	Fracture strain [-]
0.0035	233	546	0.459	310	0.657
0.4	250	502	0.399	269	0.608
620	333	591	0.447	501	0.615

**Table 127:** Mechanical properties of AISI 316 H (Ref.Mat.)

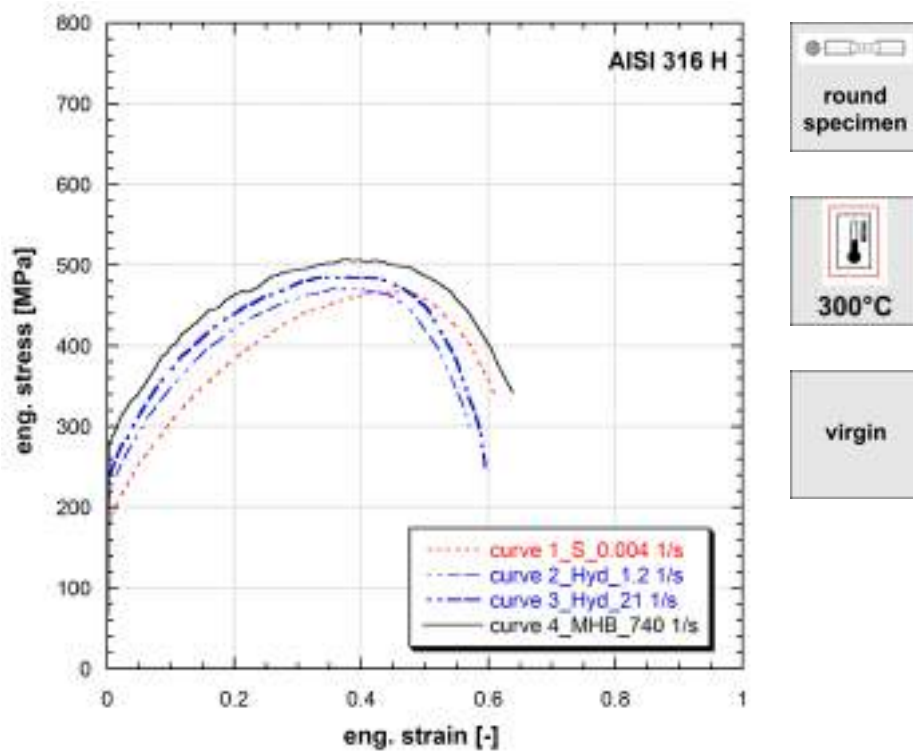


**Figure 9.128:** Stress vs strain curves of AISI 316 H (Ref.Mat.)

**Note 9.128** Ref.Mat.

Strain rate [1/s]	Yield stress [MPa]	Ultimate tensile strength [MPa]	Uniform strain [-]	Fracture stress [MPa]	Fracture strain [-]
0.004	173	467	0.464	339	0.610
1.2	207	470	0.396	293	0.572
21	235	485	0.342	250	0.595
740	277	507	0.377	342	0.639

**Table 128:** Mechanical properties of AISI 316 H (Ref.Mat.)

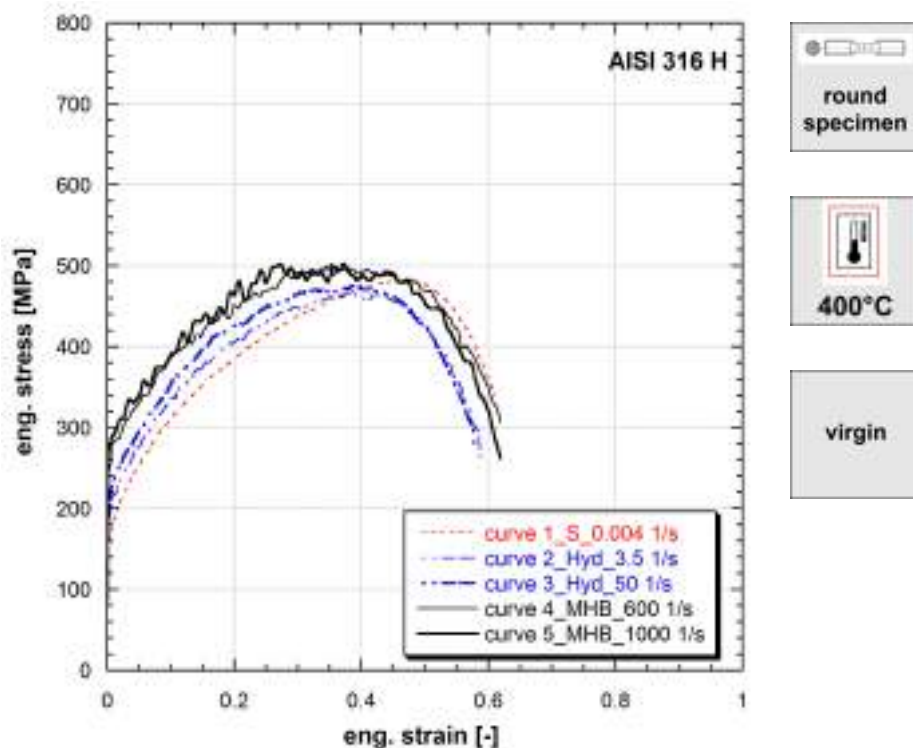


**Figure 9.129:** Stress vs strain curves of AISI 316 H (Ref.Mat.)

**Note 9.129** Ref.Mat.

Strain rate [1/s]	Yield stress [MPa]	Ultimate tensile strength [MPa]	Uniform strain [-]	Fracture stress [MPa]	Fracture strain [-]
0.004	162	480	0.485	340	0.609
3.5	187	466	0.433	251	0.589
50	192	476	0.391	276	0.579
600	248	502	0.353	306	0.619
1000	277	502	0.372	262	0.619

**Table 129:** Mechanical properties of AISI 316 H (Ref.Mat.)

Published in (Albertini and Montagnani, 1983b), (Albertini et al., 1983b).

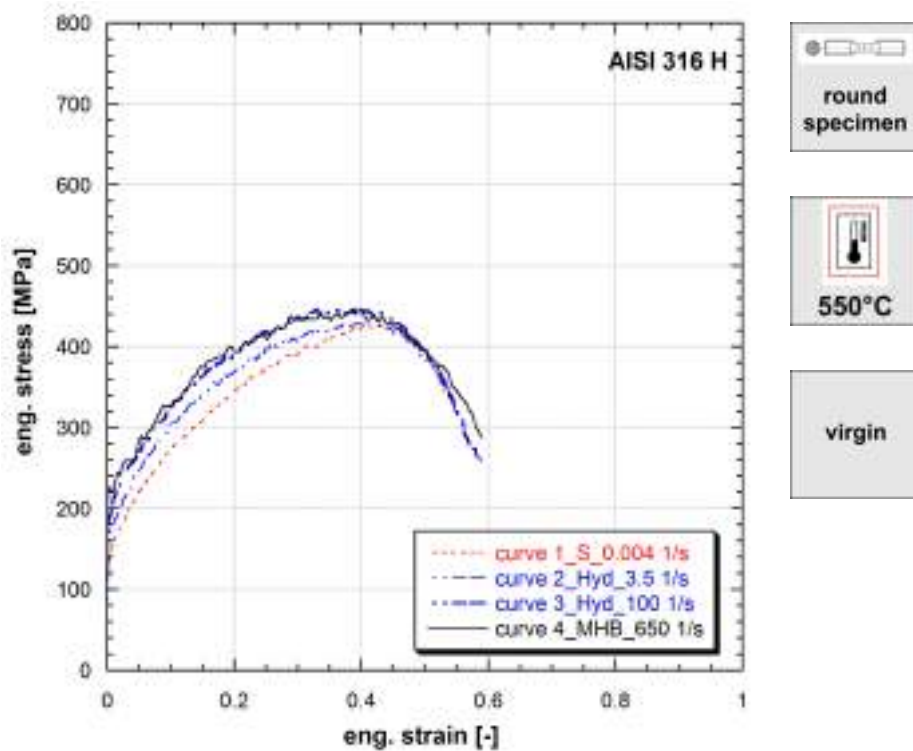


**Figure 9.130:** Stress vs strain curves of AISI 316 H (Ref.Mat.)

**Note 9.130** Ref.Mat.

Strain rate [1/s]	Yield stress [MPa]	Ultimate tensile strength [MPa]	Uniform strain [-]	Fracture stress [MPa]	Fracture strain [-]
0.004	133	425	0.440	327	0.549
3.5	160	430	0.409	258	0.588
100	188	446	0.388	266	0.580
650	226	446	0.399	287	0.589

**Table 130:** Mechanical properties of AISI 316 H (Ref.Mat.)

Published in (Albertini et al., 1983a), (Albertini et al., 1983b).

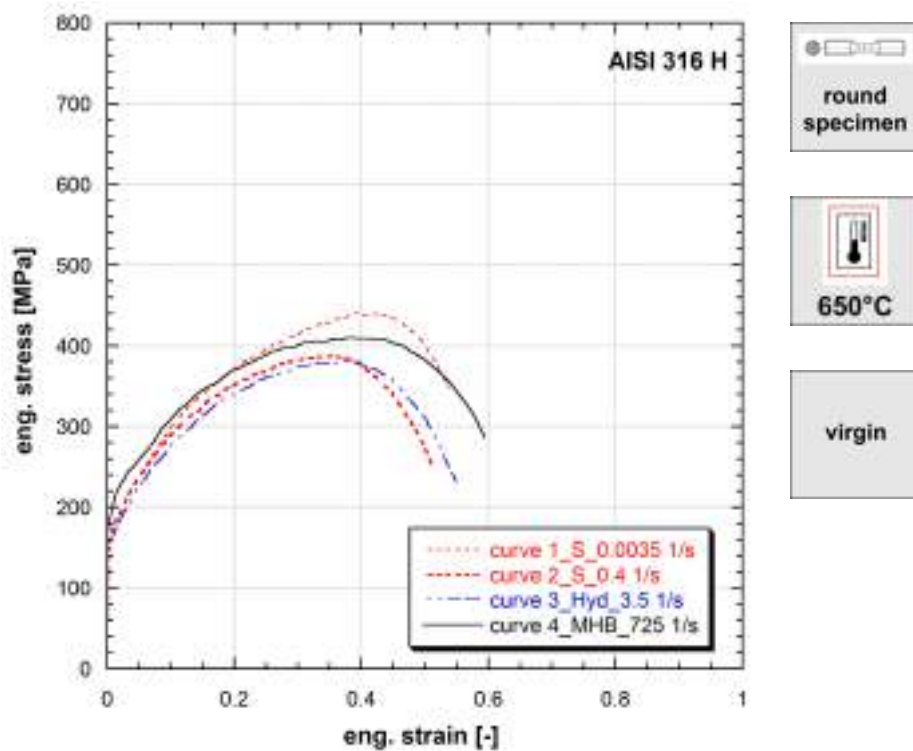


**Figure 9.131:** Stress vs strain curves of AISI 316 H (Ref.Mat.)

**Note 9.131** Ref.Mat.

Strain rate [1/s]	Yield stress [MPa]	Ultimate tensile strength [MPa]	Uniform strain [-]	Fracture stress [MPa]	Fracture strain [-]
0.0035	155	441	0.391	348	0.538
0.4	158	387	0.355	254	0.510
3.5	139	380	0.374	231	0.550
725	177	410	0.381	285	0.595

**Table 131:** Mechanical properties of AISI 316 H (Ref.Mat.)

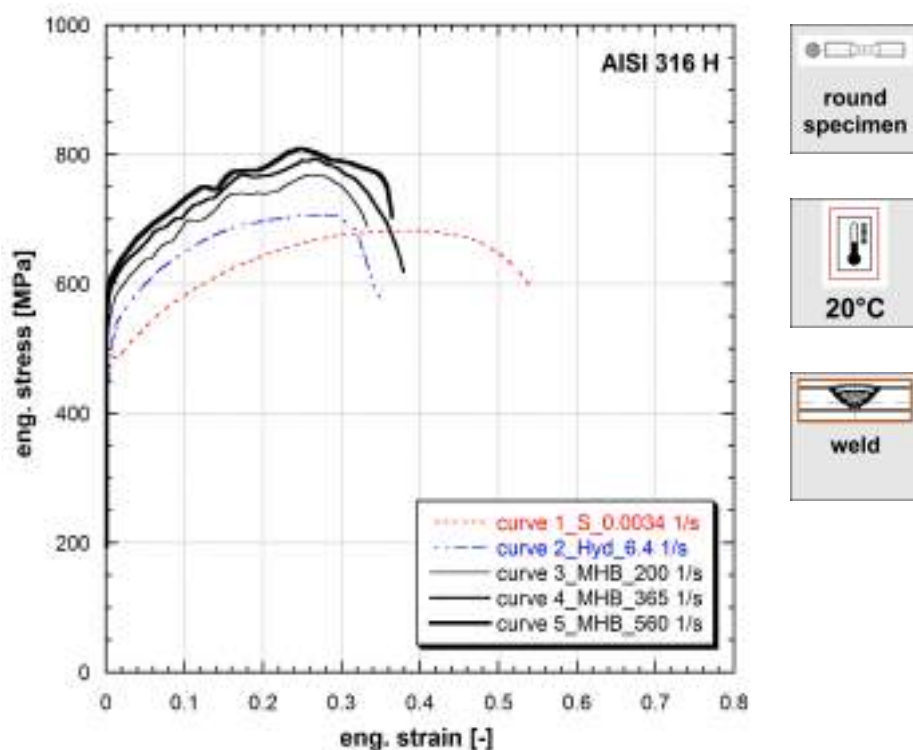


**Figure 9.132:** Stress vs strain curves of AISI 316 H (Ref.Mat.UKAEA)

**Note 9.132** Ref.Mat.UKAEA Argon arc welding.

Strain rate [1/s]	Yield stress [MPa]	Ultimate tensile strength [MPa]	Uniform strain [-]	Fracture stress [MPa]	Fracture strain [-]
0.0034	458	682	0.393	594	0.543
6.4	483	706	0.273	580	0.348
200	528	768	0.265	689	0.333
365	581	794	0.264	618	0.379
560	586	809	0.246	704	0.364

**Table 132:** Mechanical properties of AISI 316 H (Ref.Mat.UKAEA)

Published in (Albertini and Montagnani, 1978).

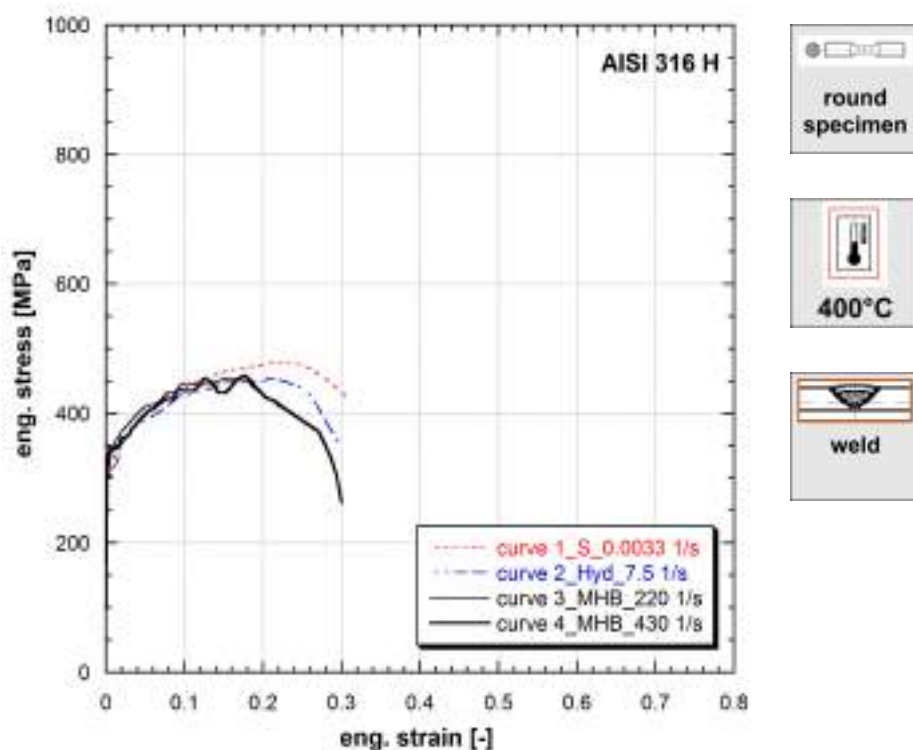


**Figure 9.133:** Stress vs strain curves of AISI 316 H (Ref.Mat.UKAEA)

**Note 9.133** Ref.Mat.UKAEA Argon arc welding.

Strain rate [1/s]	Yield stress [MPa]	Ultimate tensile strength [MPa]	Uniform strain [-]	Fracture stress [MPa]	Fracture strain [-]
0.0033	300	479	0.228	423	0.308
7.5	293	455	0.207	354	0.298
220	317	453	0.153	410	0.221
430	343	459	0.177	262	0.300

**Table 133:** Mechanical properties of AISI 316 H (Ref.Mat.UKAEA)

Published in (Albertini and Montagnani, 1978).

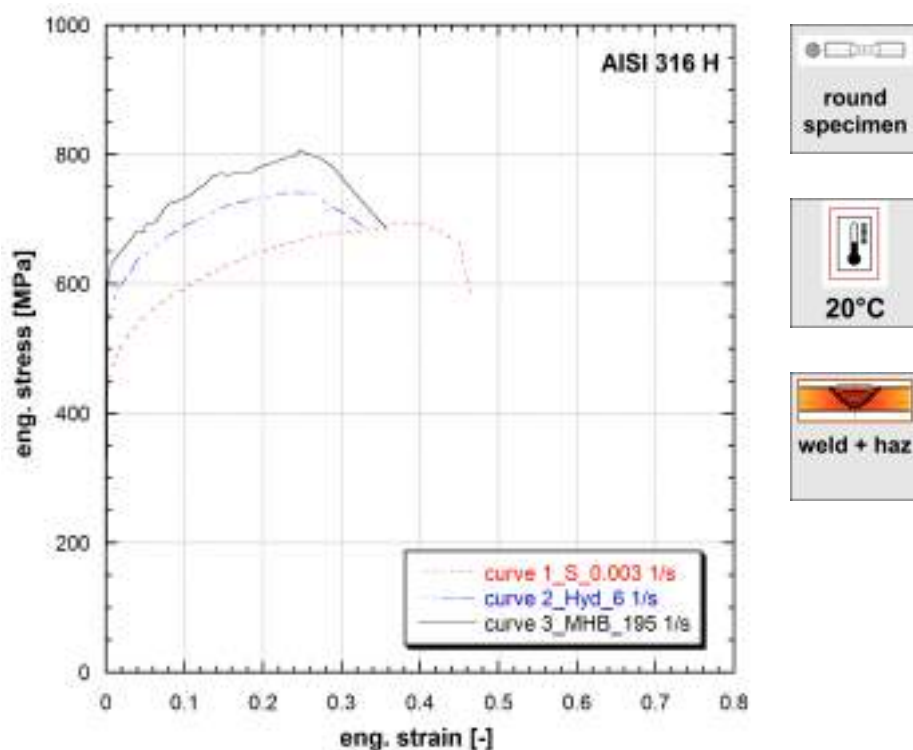


**Figure 9.134:** Stress vs strain curves of AISI 316 H (Ref.Mat.UKAEA)

**Note 9.134** Ref.Mat.UKAEA Argon arc welding.

Strain rate [1/s]	Yield stress [MPa]	Ultimate tensile strength [MPa]	Uniform strain [-]	Fracture stress [MPa]	Fracture strain [-]
0.003	453	695	0.389	580	0.465
6	547	741	0.259	687	0.331
195	617	805	0.247	685	0.357

**Table 134:** Mechanical properties of AISI 316 H (Ref.Mat.UKAEA)

Published in (Albertini and Montagnani, 1978).

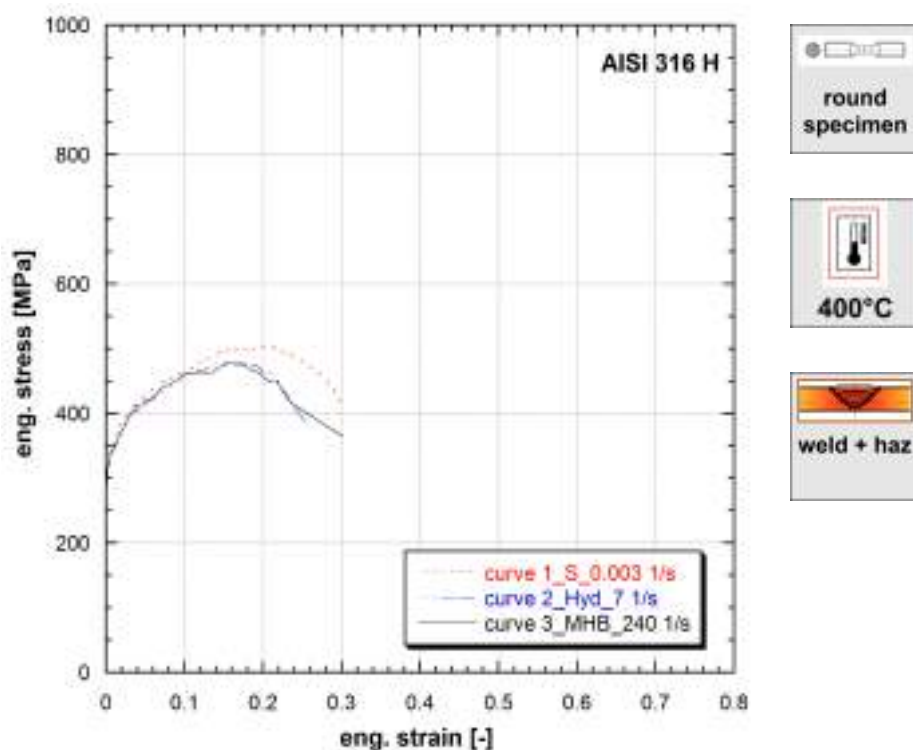


**Figure 9.135:** Stress vs strain curves of AISI 316 H (Ref.Mat.UKAEA)

**Note 9.135** Ref.Mat.UKAEA Argon arc welding.

Strain rate [1/s]	Yield stress [MPa]	Ultimate tensile strength [MPa]	Uniform strain [-]	Fracture stress [MPa]	Fracture strain [-]
0.003	327	504	0.209	415	0.301
7	320	480	0.151	387	0.255
240	322	480	0.165	364	0.302

**Table 135:** Mechanical properties of AISI 316 H (Ref.Mat.UKAEA)

Published in (Albertini and Montagnani, 1978).

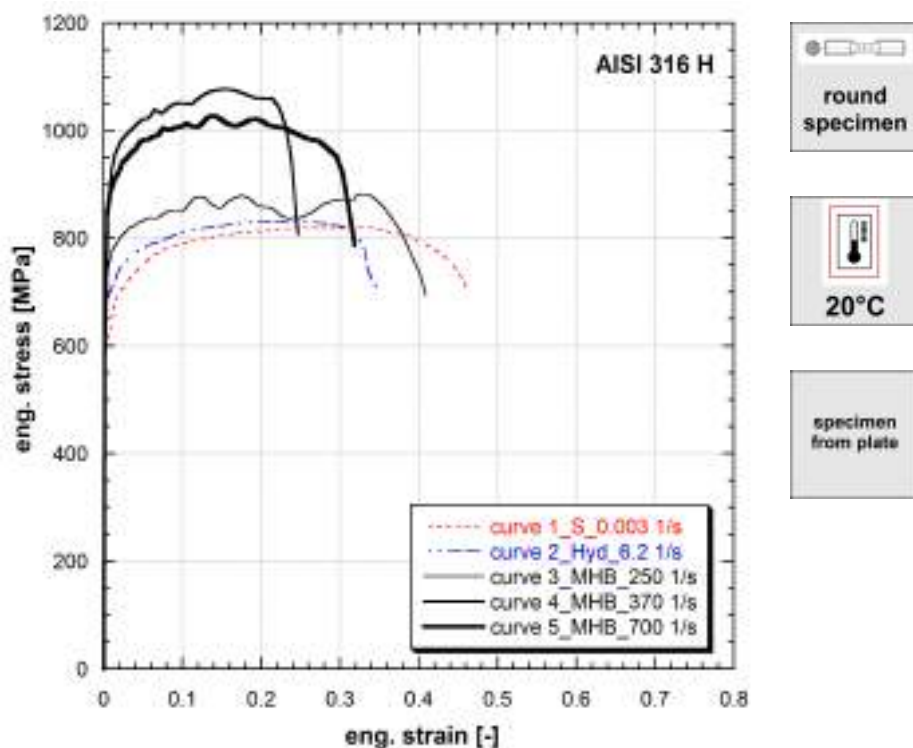


**Figure 9.136:** Stress vs strain curves of AISI 316 H (Ref.Mat.UKAEA)

**Note 9.136** Ref.Mat.UKAEA Argon arc welding.

Strain rate [1/s]	Yield stress [MPa]	Ultimate tensile strength [MPa]	Uniform strain [-]	Fracture stress [MPa]	Fracture strain [-]
0.003	597	820	0.335	706	0.461
6.2	680	830	0.211	702	0.348
250	710	882	0.326	693	0.409
370	797	1077	0.153	808	0.246
700	790	1028	0.137	787	0.319

**Table 136:** Mechanical properties of AISI 316 H (Ref.Mat.UKAEA)

Published in (Albertini and Montagnani, 1978).

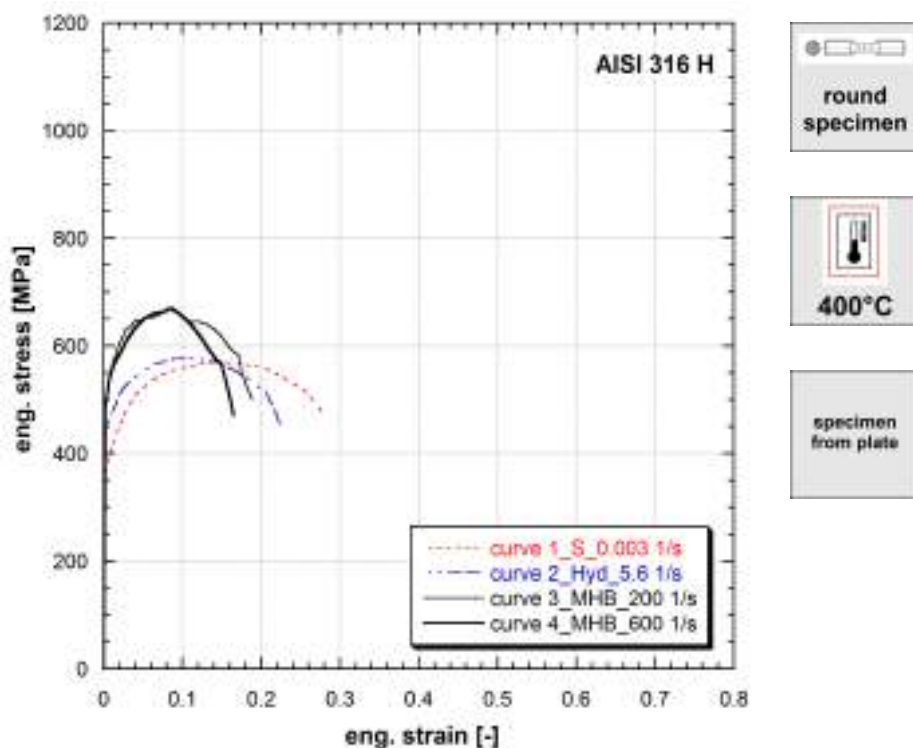


**Figure 9.137:** Stress vs strain curves of AISI 316 H (Ref.Mat.UKAEA)

**Note 9.137** Ref.Mat.UKAEA Argon arc welding.

Strain rate [1/s]	Yield stress [MPa]	Ultimate tensile strength [MPa]	Uniform strain [-]	Fracture stress [MPa]	Fracture strain [-]
0.003	369	570	0.152	472	0.279
5.6	444	578	0.111	444	0.228
200	507	671	0.088	500	0.189
600	509	669	0.083	471	0.165

**Table 137:** Mechanical properties of AISI 316 H (Ref.Mat.UKAEA)

Published in (Albertini and Montagnani, 1978), (Albertini and Montagnani, 1981a).

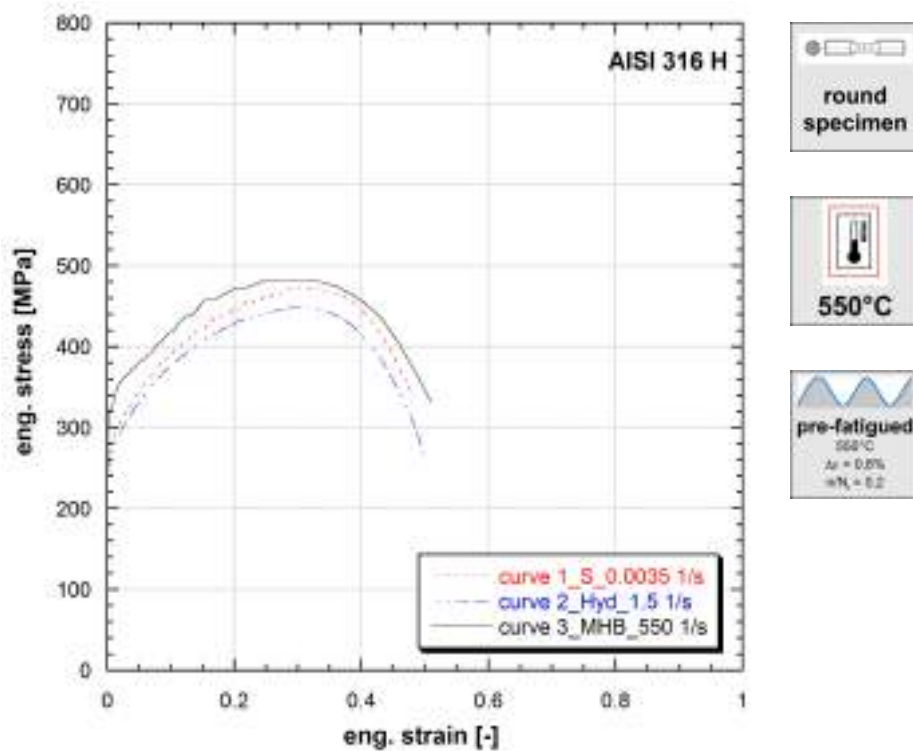


**Figure 9.138:** Stress vs strain curves of AISI 316 H (Ref.Mat.)

**Note 9.138** Ref.Mat.

Strain rate [1/s]	Yield stress [MPa]	Ultimate tensile strength [MPa]	Uniform strain [-]	Fracture stress [MPa]	Fracture strain [-]
0.0035	262	475	0.326	338	0.479
1.5	258	448	0.291	266	0.498
550	321	483	0.300	331	0.510

**Table 138:** Mechanical properties of AISI 316 H (Ref.Mat.)

Published in (Albertini et al., 1988), (Albertini and Montagnani, 1990).

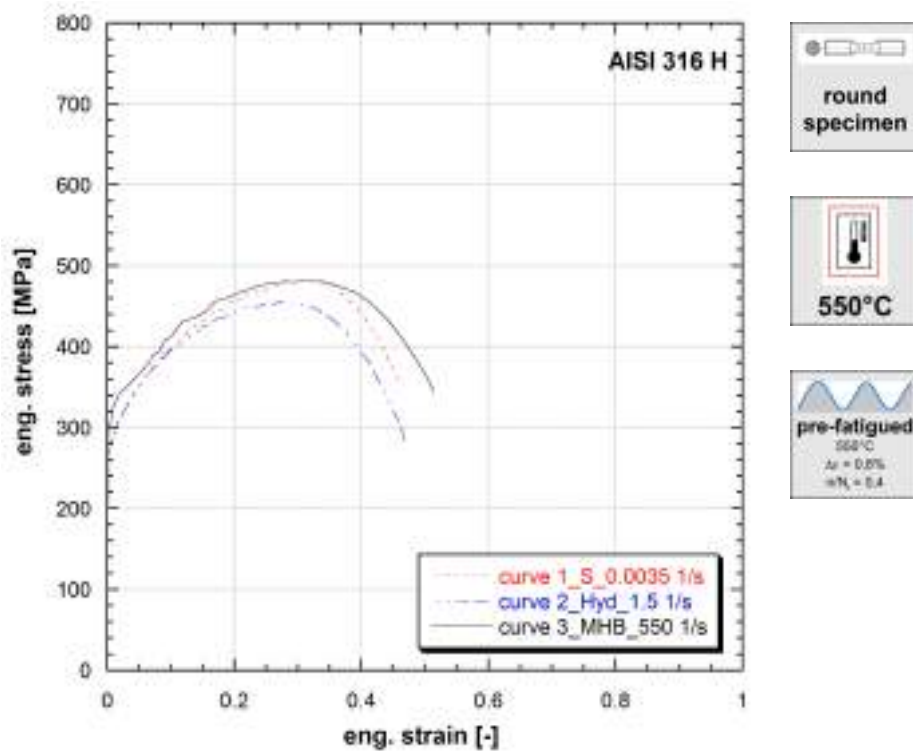


**Figure 9.139:** Stress vs strain curves of AISI 316 H (Ref.Mat.)

**Note 9.139** Ref.Mat.

Strain rate [1/s]	Yield stress [MPa]	Ultimate tensile strength [MPa]	Uniform strain [-]	Fracture stress [MPa]	Fracture strain [-]
0.0035	269	481	0.284	353	0.459
1.5	278	455	0.278	281	0.469
550	303	481	0.303	344	0.515

**Table 139:** Mechanical properties of AISI 316 H (Ref.Mat.)

Published in (Albertini et al., 1988), (Albertini and Montagnani, 1990).

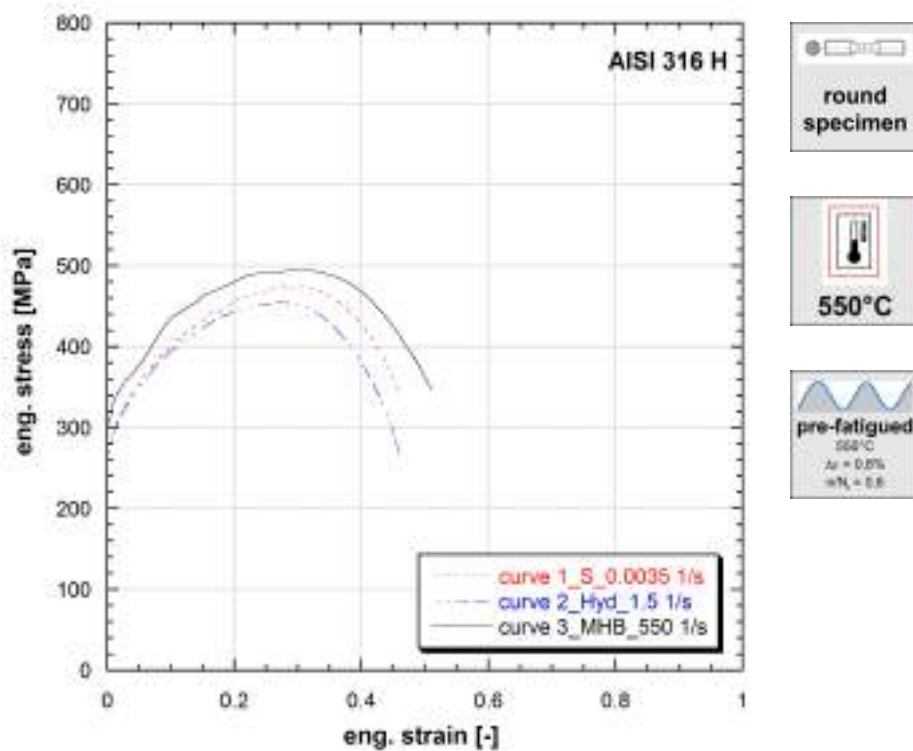


**Figure 9.140:** Stress vs strain curves of AISI 316 H (Ref.Mat.)

**Note 9.140** Ref.Mat.

Strain rate [1/s]	Yield stress [MPa]	Ultimate tensile strength [MPa]	Uniform strain [-]	Fracture stress [MPa]	Fracture strain [-]
0.0035	269	475	0.277	343	0.460
1.5	274	454	0.271	260	0.460
550	311	496	0.299	347	0.509

**Table 140:** Mechanical properties of AISI 316 H (Ref.Mat.)

Published in (Albertini et al., 1988), (Albertini and Montagnani, 1990).

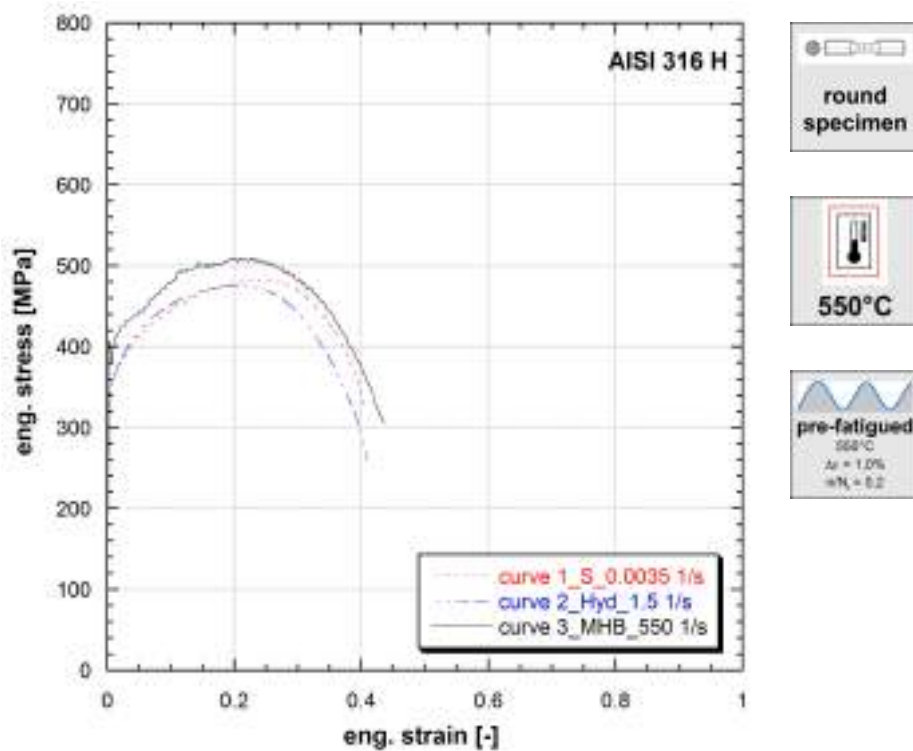


**Figure 9.141:** Stress vs strain curves of AISI 316 H (Ref.Mat.)

**Note 9.141** Ref.Mat.

Strain rate [1/s]	Yield stress [MPa]	Ultimate tensile strength [MPa]	Uniform strain [-]	Fracture stress [MPa]	Fracture strain [-]
0.0035	340	482	0.244	323	0.405
1.5	340	476	0.210	260	0.409
550	399	509	0.232	306	0.436

**Table 141:** Mechanical properties of AISI 316 H (Ref.Mat.)

Published in (Albertini et al., 1988), (Albertini and Montagnani, 1990).

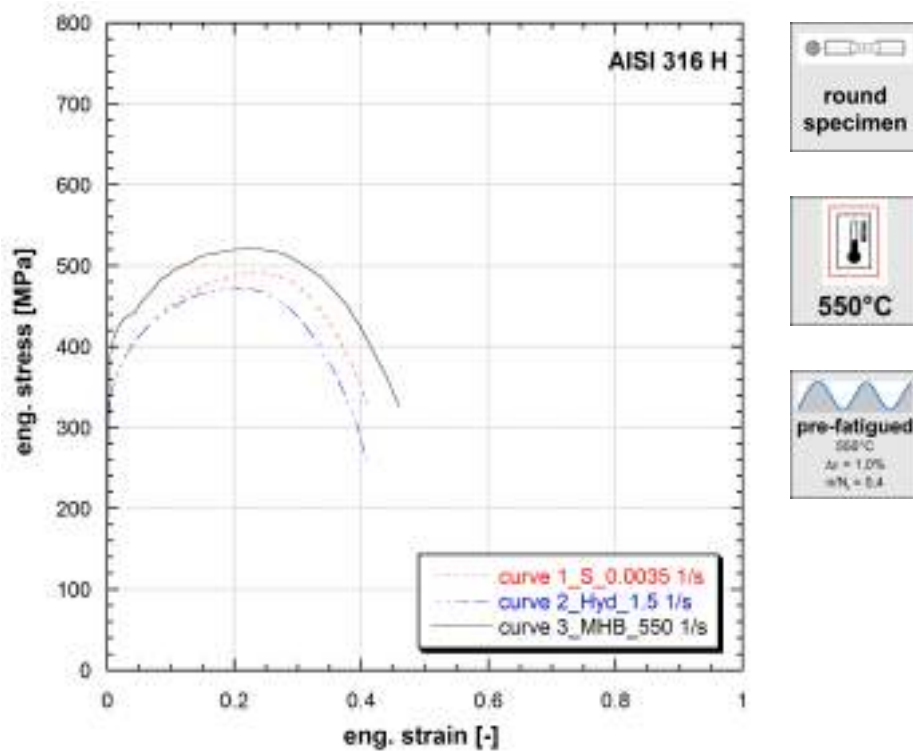


**Figure 9.142:** Stress vs strain curves of AISI 316 H (Ref.Mat.)

**Note 9.142** Ref.Mat.

Strain rate [1/s]	Yield stress [MPa]	Ultimate tensile strength [MPa]	Uniform strain [-]	Fracture stress [MPa]	Fracture strain [-]
0.0035	330	491	0.245	323	0.409
1.5	328	473	0.199	256	0.409
550	388	521	0.236	325	0.460

**Table 142:** Mechanical properties of AISI 316 H (Ref.Mat.)

Published in (Albertini et al., 1988), (Albertini and Montagnani, 1990).

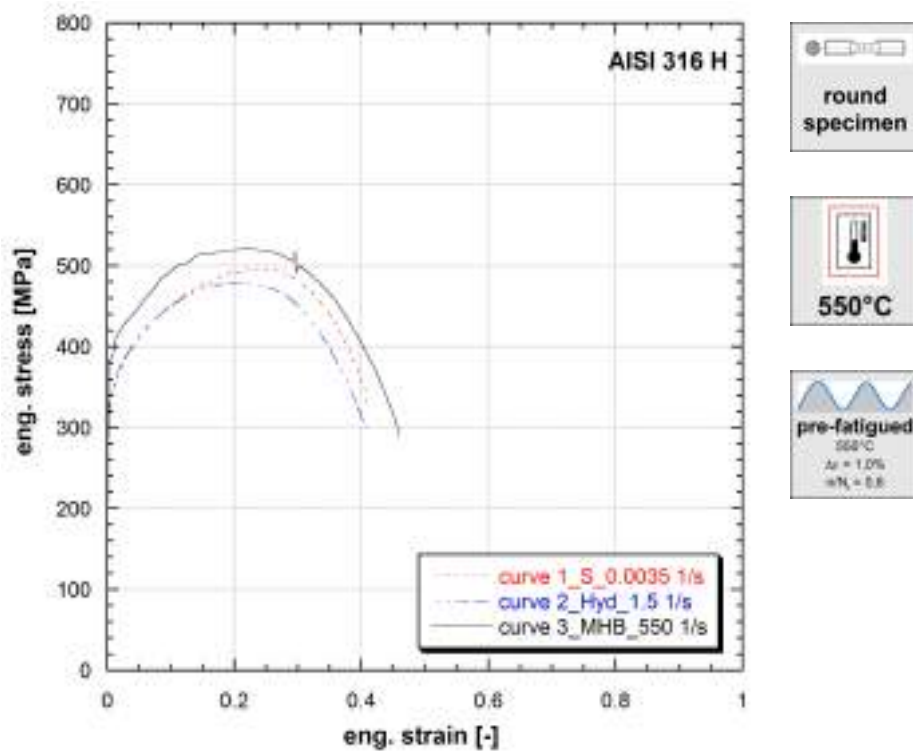


**Figure 9.143:** Stress vs strain curves of AISI 316 H (Ref.Mat.)

**Note 9.143** Ref.Mat.

Strain rate [1/s]	Yield stress [MPa]	Ultimate tensile strength [MPa]	Uniform strain [-]	Fracture stress [MPa]	Fracture strain [-]
0.0035	322	496	0.253	331	0.409
1.5	328	479	0.221	289	0.409
550	385	521	0.223	289	0.460

**Table 143:** Mechanical properties of AISI 316 H (Ref.Mat.)

Published in (Albertini et al., 1988), (Albertini and Montagnani, 1990).

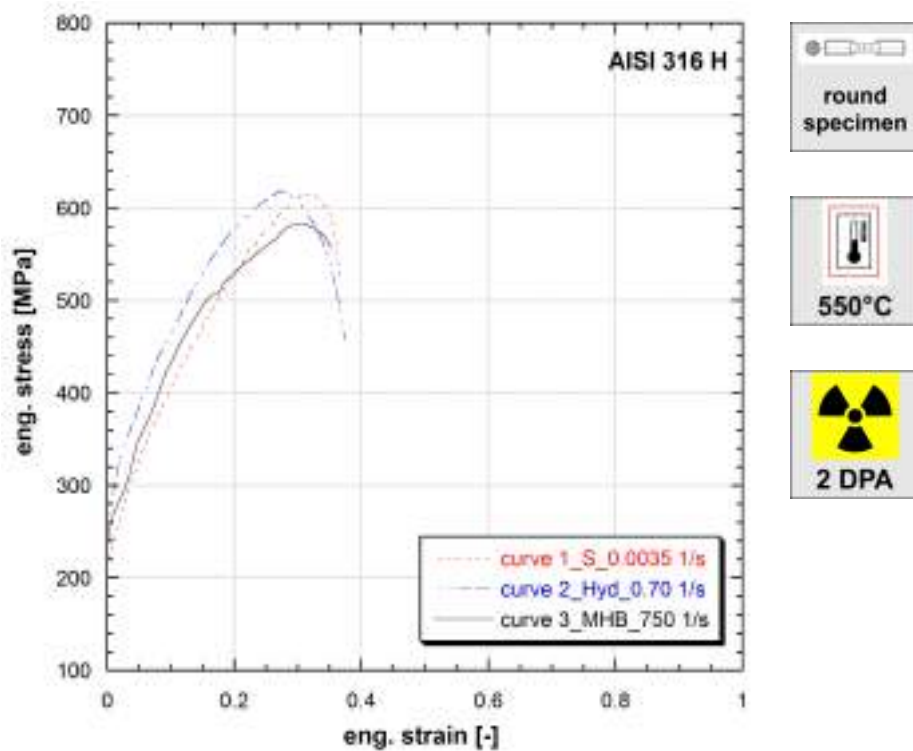


**Figure 9.144:** Stress vs strain curves of AISI 316 H (Ref.Mat.)

**Note 9.144** Ref.Mat.

*Irradiated in sodium at 550°C in HFR reactor, for 3000 hours.*

Strain rate [1/s]	Yield stress [MPa]	Ultimate tensile strength [MPa]	Uniform strain [-]	Fracture stress [MPa]	Fracture strain [-]
0.0035	215	615	0.322	526	0.366
0.7	272	619	0.273	457	0.374
750	240	583	0.311	556	0.353

**Table 144:** Mechanical properties of AISI 316 H (Ref.Mat.)

*Published in (Albertini et al., 1988), (Albertini and Montagnani, 1990).*

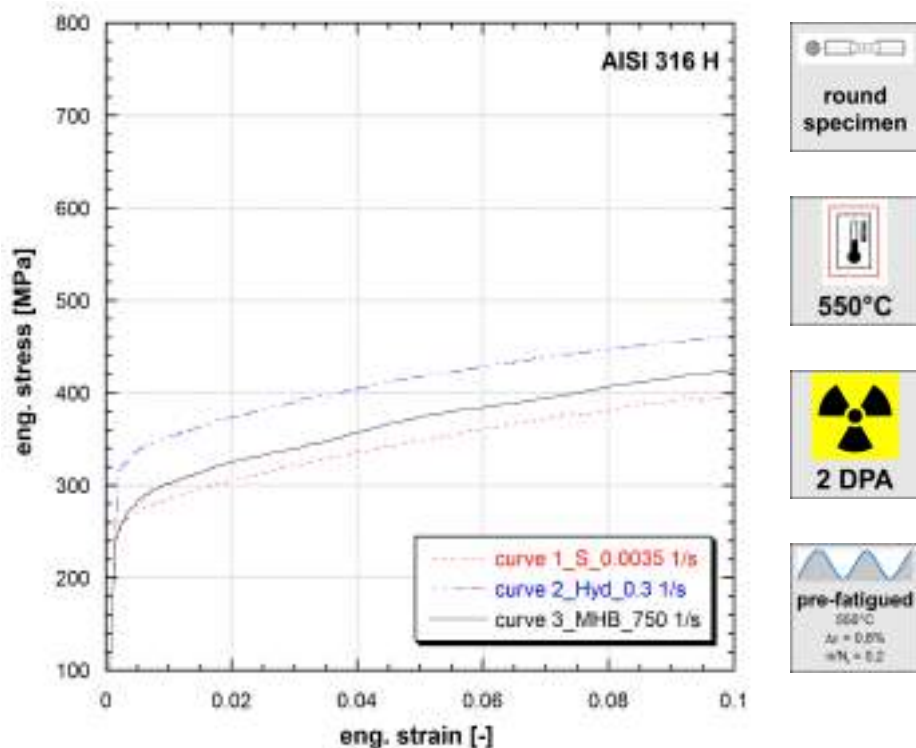


**Figure 9.145:** Stress vs strain curves of AISI 316 H (Ref.Mat.)

**Note 9.145** Ref.Mat.

Irradiated in sodium at 550°C in HFR reactor, for 3000 hours.

Strain rate [1/s]	Yield stress [MPa]	Ultimate tensile strength [MPa]	Uniform strain [-]	Fracture stress [MPa]	Fracture strain [-]
0.0035	265	-	-	-	-
0.3	330	-	-	-	-
750	273	-	-	-	-

**Table 145:** Mechanical properties of AISI 316 H (Ref.Mat.)

Published in (Albertini et al., 1988), (Albertini and Montagnani, 1990).

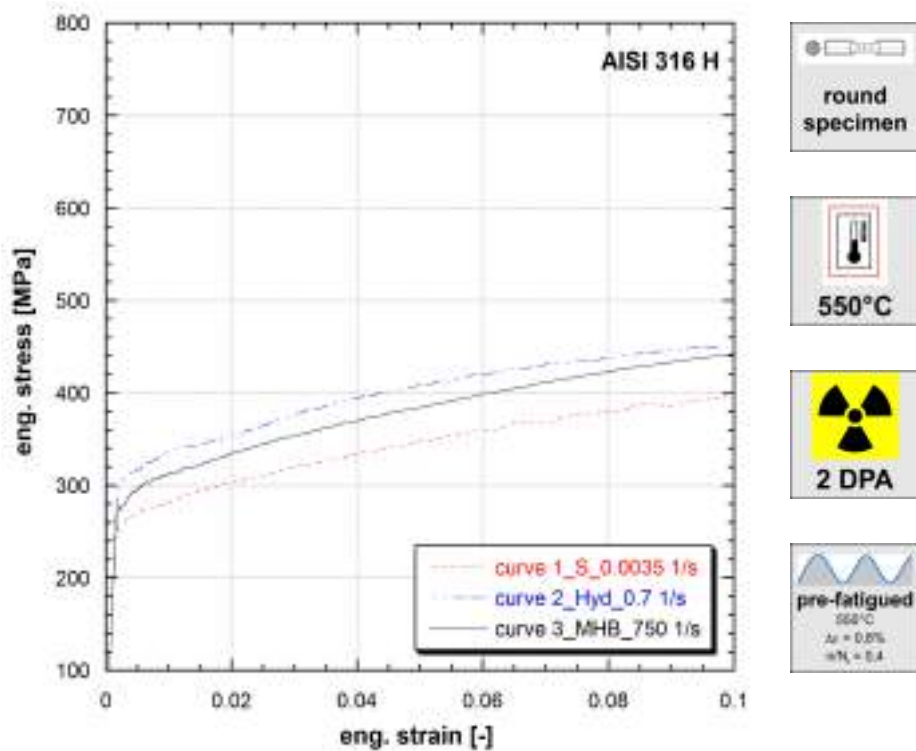


**Figure 9.146:** Stress vs strain curves of AISI 316 H (Ref.Mat.)

**Note 9.146** Ref.Mat.

Irradiated in sodium at 550°C in HFR reactor, for 3000 hours.

Strain rate [1/s]	Yield stress [MPa]	Ultimate tensile strength [MPa]	Uniform strain [-]	Fracture stress [MPa]	Fracture strain [-]
0.0035	264	-	-	-	-
0.7	316	-	-	-	-
750	288	-	-	-	-

**Table 146:** Mechanical properties of AISI 316 H (Ref.Mat.)

Published in (Albertini et al., 1988), (Albertini and Montagnani, 1990).

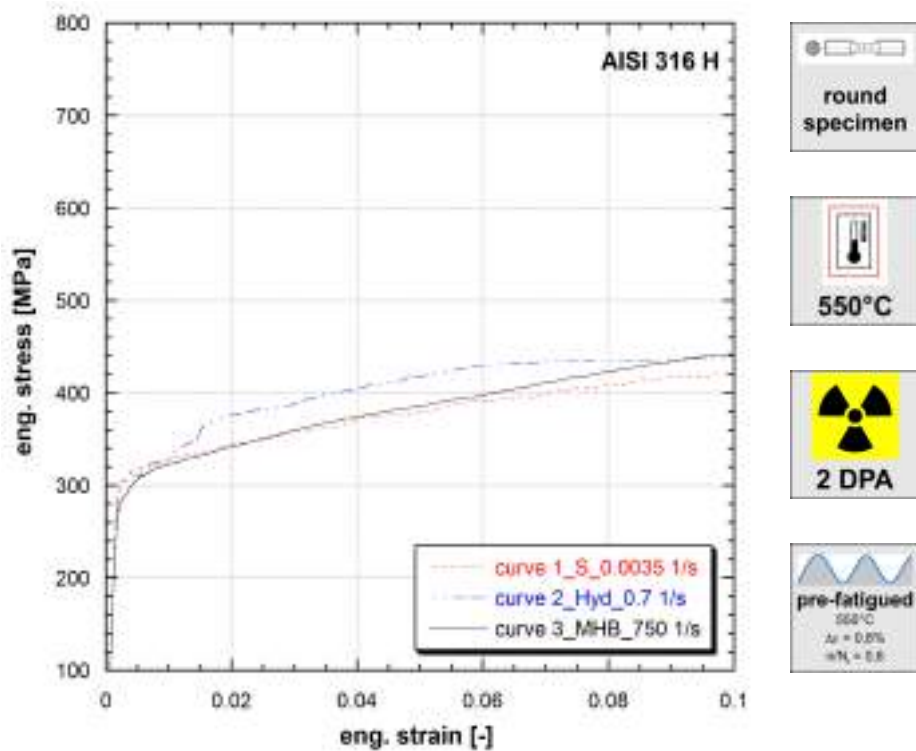


**Figure 9.147:** Stress vs strain curves of AISI 316 H (Ref.Mat.)

**Note 9.147** Ref.Mat.

Irradiated in sodium at 550°C in HFR reactor, for 3000 hours.

Strain rate [1/s]	Yield stress [MPa]	Ultimate tensile strength [MPa]	Uniform strain [-]	Fracture stress [MPa]	Fracture strain [-]
0.0035	314	-	-	-	-
0.7	307	-	-	-	-
750	297	-	-	-	-

**Table 147:** Mechanical properties of AISI 316 H (Ref.Mat.)

Published in (Albertini et al., 1988), (Albertini and Montagnani, 1990).

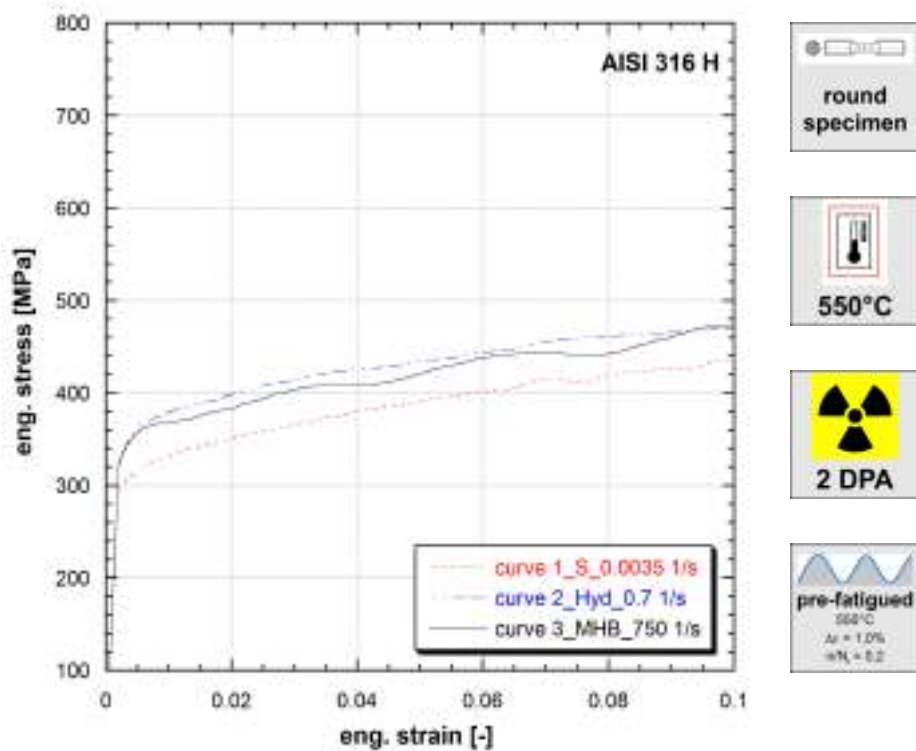


**Figure 9.148:** Stress vs strain curves of AISI 316 H (Ref.Mat.)

**Note 9.148** Ref.Mat.

Irradiated in sodium at 550°C in HFR reactor, for 3000 hours.

Strain rate [1/s]	Yield stress [MPa]	Ultimate tensile strength [MPa]	Uniform strain [-]	Fracture stress [MPa]	Fracture strain [-]
0.0035	312	-	-	-	-
0.7	357	-	-	-	-
750	352	-	-	-	-

**Table 148:** Mechanical properties of AISI 316 H (Ref.Mat.)

Published in (Albertini et al., 1988), (Albertini and Montagnani, 1990).

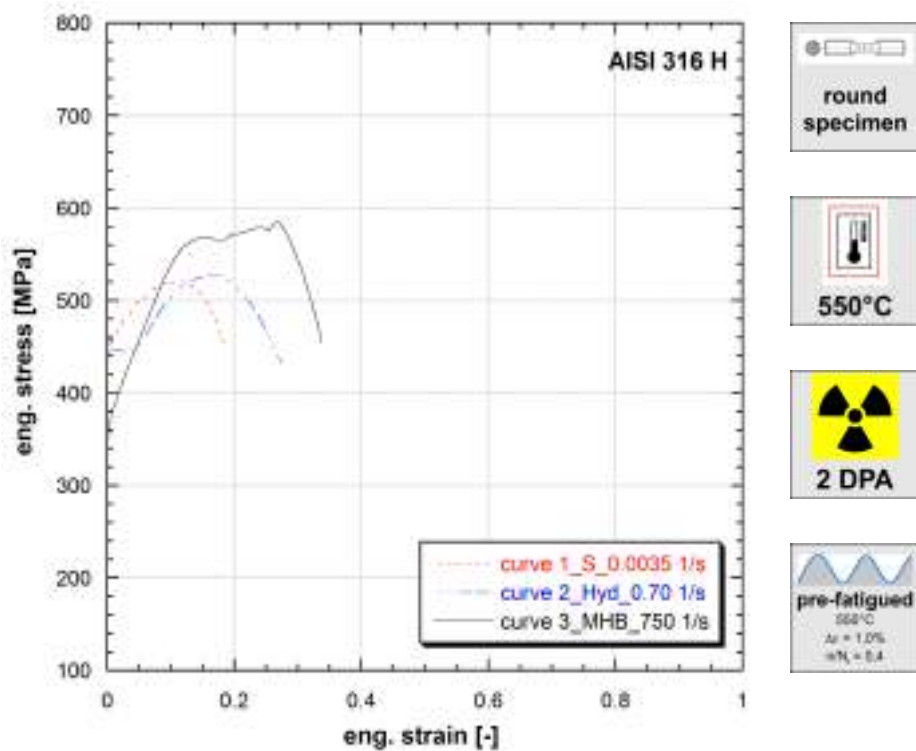


**Figure 9.149:** Stress vs strain curves of AISI 316 H (Ref.Mat.)

**Note 9.149** Ref.Mat.

Irradiated in sodium at 550°C in HFR reactor, for 3000 hours.

Strain rate [1/s]	Yield stress [MPa]	Ultimate tensile strength [MPa]	Uniform strain [-]	Fracture stress [MPa]	Fracture strain [-]
0.0035	452	520	0.124	454	0.184
0.7	348	526	0.156	433	0.274
750	355	585	0.270	452	0.338

**Table 149:** Mechanical properties of AISI 316 H (Ref.Mat.)

Published in (Albertini et al., 1988), (Albertini and Montagnani, 1990).

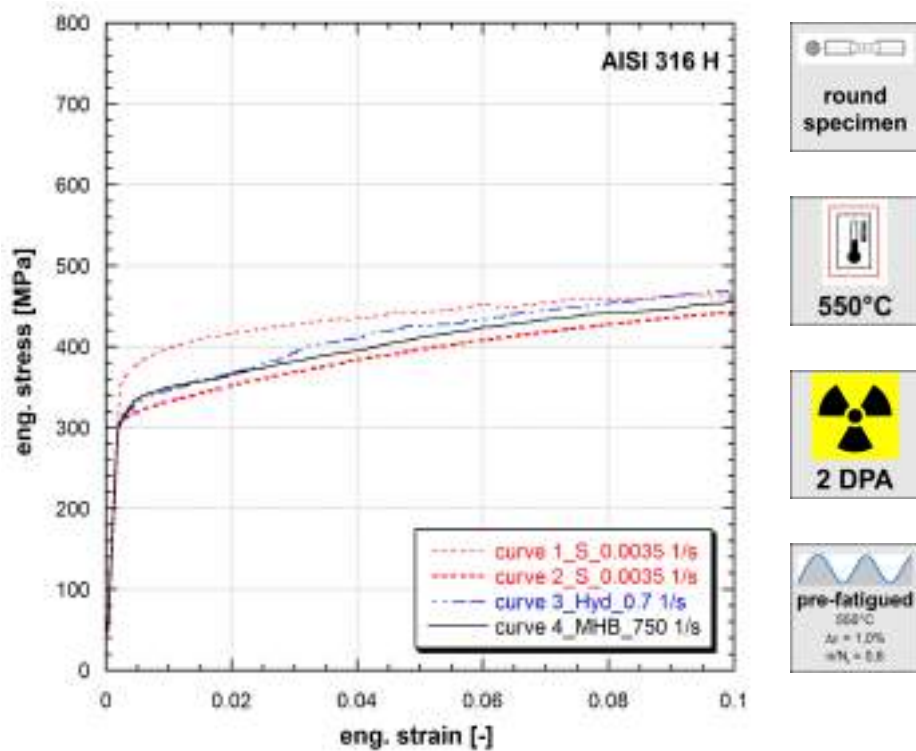


**Figure 9.150:** Stress vs strain curves of AISI 316 H (Ref.Mat.)

**Note 9.150** Ref.Mat.

Irradiated in sodium at 550°C in HFR reactor, for 3000 hours.

Strain rate [1/s]	Yield stress [MPa]	Ultimate tensile strength [MPa]	Uniform strain [-]	Fracture stress [MPa]	Fracture strain [-]
0.0035	374	-	-	-	-
0.0035	315	-	-	-	-
0.7	321	-	-	-	-
750	326	-	-	-	-

**Table 150:** Mechanical properties of AISI 316 H (Ref.Mat.)

Published in (Albertini et al., 1988), (Albertini and Montagnani, 1990).

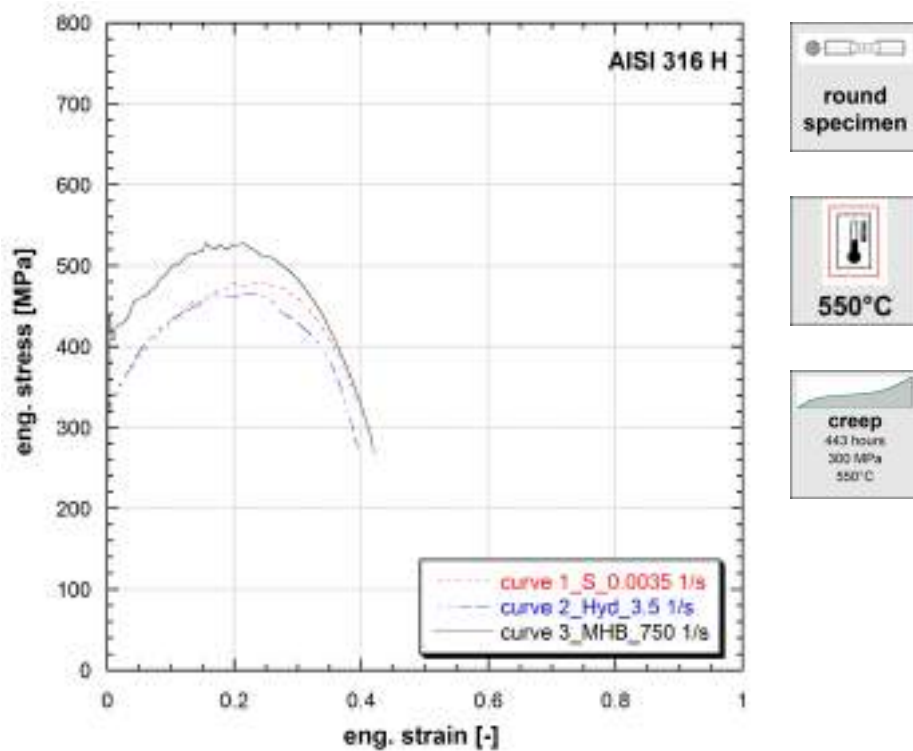


**Figure 9.151:** Stress vs strain curves of AISI 316 H (Ref.Mat.)

**Note 9.151** Ref.Mat.

Strain rate [1/s]	Yield stress [MPa]	Ultimate tensile strength [MPa]	Uniform strain [-]	Fracture stress [MPa]	Fracture strain [-]
0.0035	325	479	0.202	335	0.389
3.5	328	464	0.227	275	0.395
750	433	527	0.213	268	0.419

**Table 151:** Mechanical properties of AISI 316 H (Ref.Mat.)

Published in (Albertini et al., 1988), (Albertini et al., 1989c), (Albertini and Montagnani, 1990).

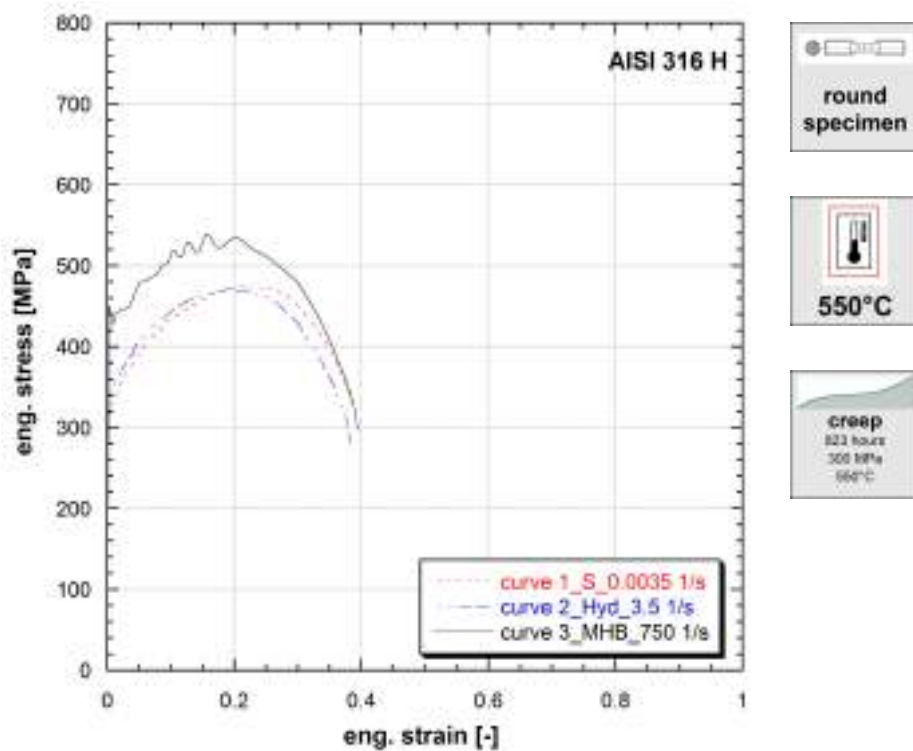


**Figure 9.152:** Stress vs strain curves of AISI 316 H (Ref.Mat.)

**Note 9.152** Ref.Mat.

Strain rate [1/s]	Yield stress [MPa]	Ultimate tensile strength [MPa]	Uniform strain [-]	Fracture stress [MPa]	Fracture strain [-]
0.0035	323	476	0.213	330	0.384
3.5	343	470	0.199	281	0.382
750	443	539	0.158	297	0.394

**Table 152:** Mechanical properties of AISI 316 H (Ref.Mat.)

Published in (Albertini et al., 1988), (Albertini et al., 1989c), (Albertini and Montagnani, 1990).

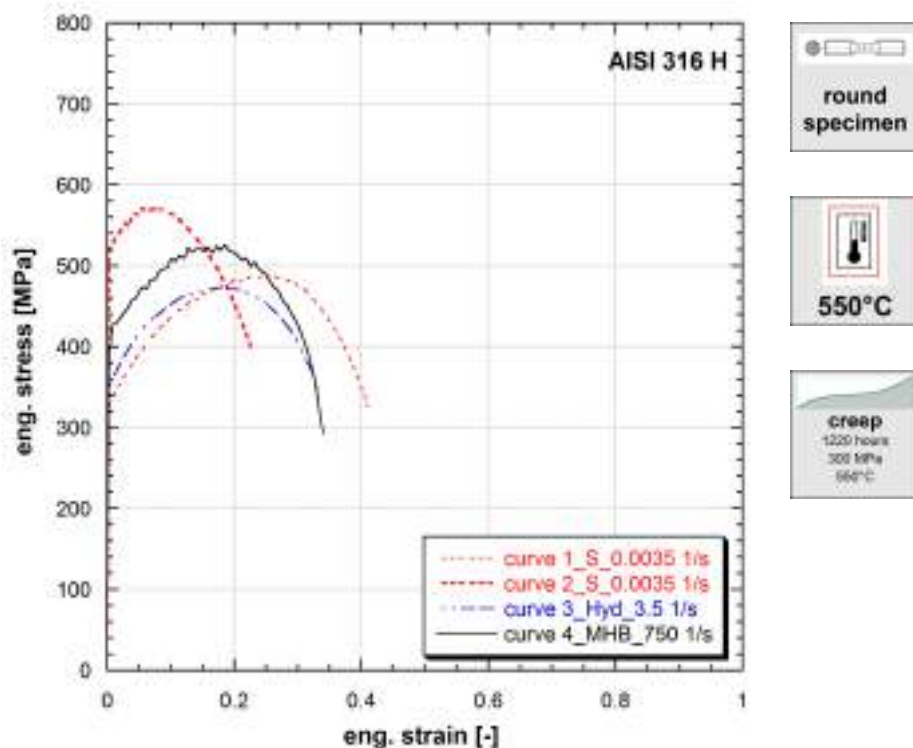


**Figure 9.153:** Stress vs strain curves of AISI 316 H (Ref.Mat.)

**Note 9.153** Ref.Mat.

Strain rate [1/s]	Yield stress [MPa]	Ultimate tensile strength [MPa]	Uniform strain [-]	Fracture stress [MPa]	Fracture strain [-]
0.0035	330	487	0.256	316	0.413
0.0035	527	571	0.052	393	0.228
3.5	352	472	0.179	332	0.334
750	397	525	0.185	292	0.339

**Table 153:** Mechanical properties of AISI 316 H (Ref.Mat.)

Published in (Albertini et al., 1988),(Albertini et al., 1989c), (Albertini and Montagnani, 1990).

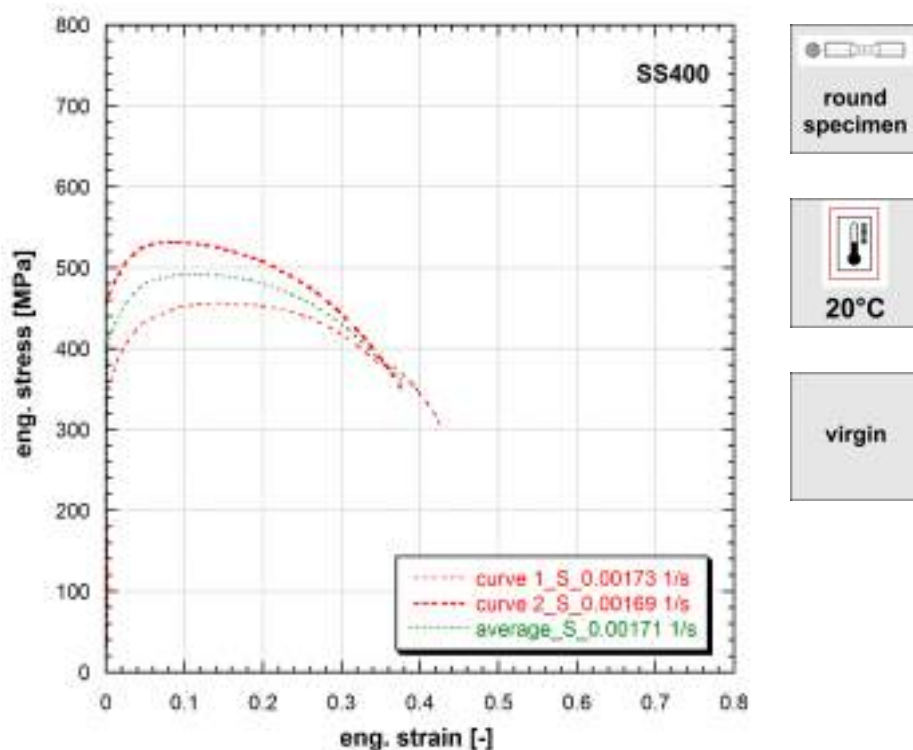


**Figure 9.154:** Stress vs strain curves of SS400

Strain rate [1/s]	Yield stress [MPa]	Ultimate tensile strength [MPa]	Uniform strain [-]	Fracture stress [MPa]	Fracture strain [-]
0.00173	348	456	0.157	304	0.426
0.00169	468	532	0.090	347	0.377
0.00171	409	492	0.111	343	0.402

**Table 154:** Mechanical properties of SS400

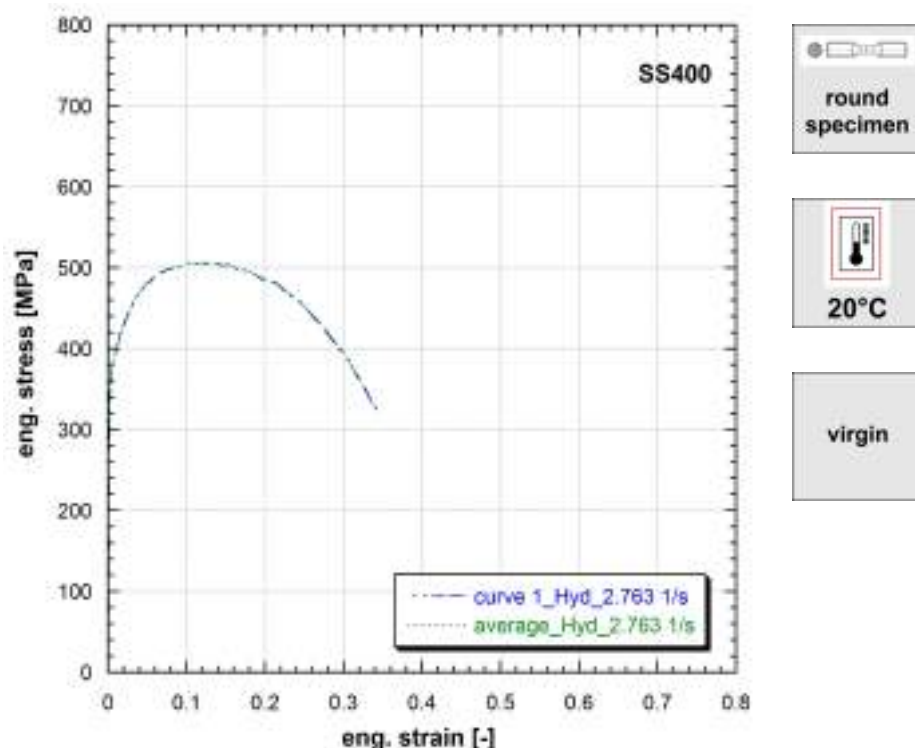


**Figure 9.155:** Stress vs strain curves of SS400

Strain rate [1/s]	Yield stress [MPa]	Ultimate tensile strength [MPa]	Uniform strain [-]	Fracture stress [MPa]	Fracture strain [-]
2.763	374	506	0.105	318	0.347
2.763	374	506	0.105	318	0.347

**Table 155:** Mechanical properties of SS400

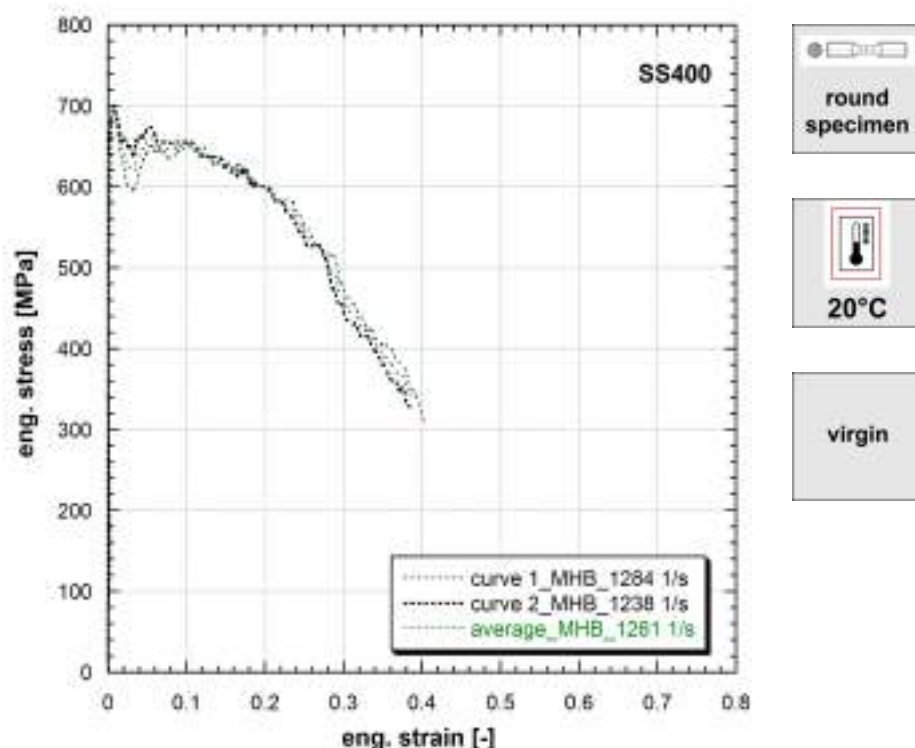


**Figure 9.156:** Stress vs strain curves of SS400

Strain rate [1/s]	Yield stress [MPa]	Ultimate tensile strength [MPa]	Uniform strain [-]	Fracture stress [MPa]	Fracture strain [-]
1284	-	651	0.104	304	0.403
1238	-	674	0.054	326	0.385
1261	-	662	0.056	338	0.394

**Table 156:** Mechanical properties of SS400

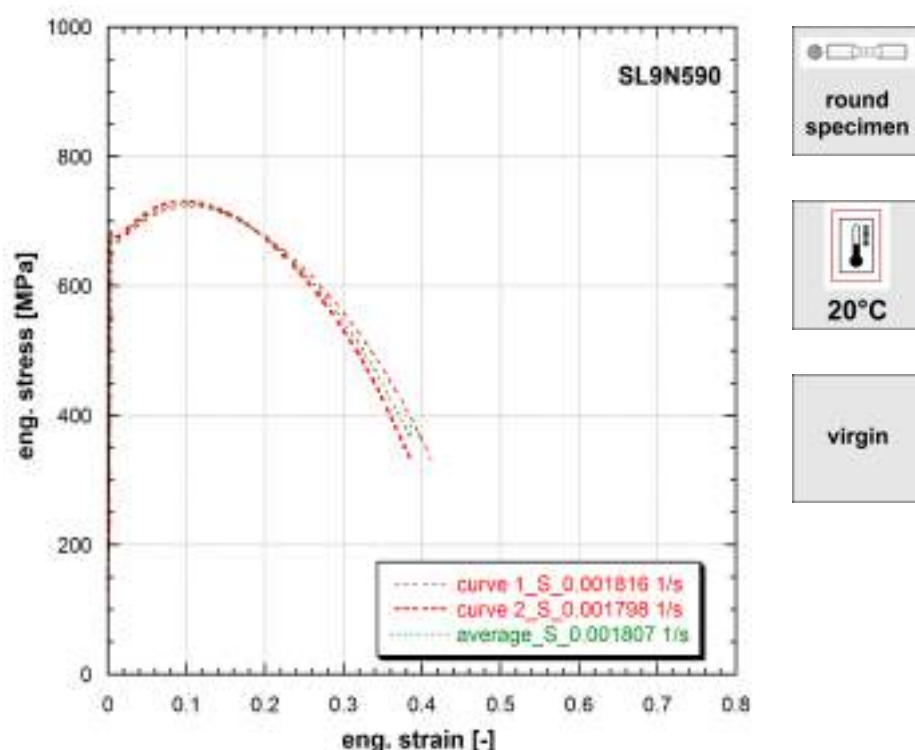


**Figure 9.157:** Stress vs strain curves of SL9N590

Strain rate [1/s]	Yield stress [MPa]	Ultimate tensile strength [MPa]	Uniform strain [-]	Fracture stress [MPa]	Fracture strain [-]
0.001816	664	722	0.111	332	0.412
0.001798	678	731	0.103	331	0.386
0.001807	677	727	0.102	365	0.399

**Table 157:** Mechanical properties of SL9N590

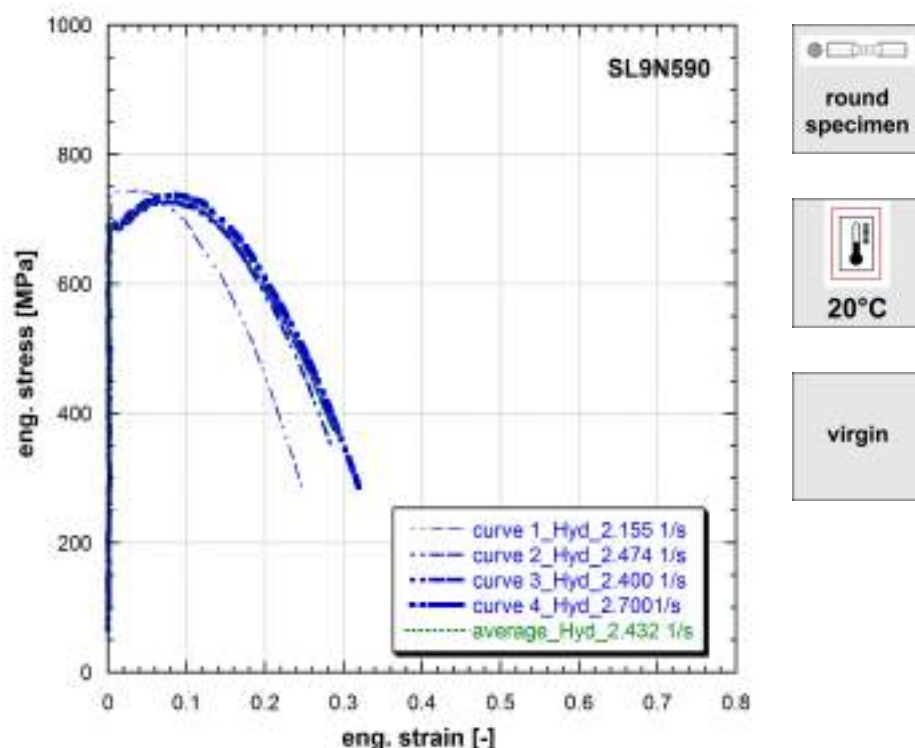


**Figure 9.158:** Stress vs strain curves of SL9N590

Strain rate [1/s]	Yield stress [MPa]	Ultimate tensile strength [MPa]	Uniform strain [-]	Fracture stress [MPa]	Fracture strain [-]
2.155	742	745	0.035	282	0.248
2.474	692	730	0.083	353	0.283
2.4	697	726	0.077	375	0.288
2.7	681	738	0.087	286	0.319
2.432	692	731	0.083	359	0.297

**Table 158:** Mechanical properties of SL9N590

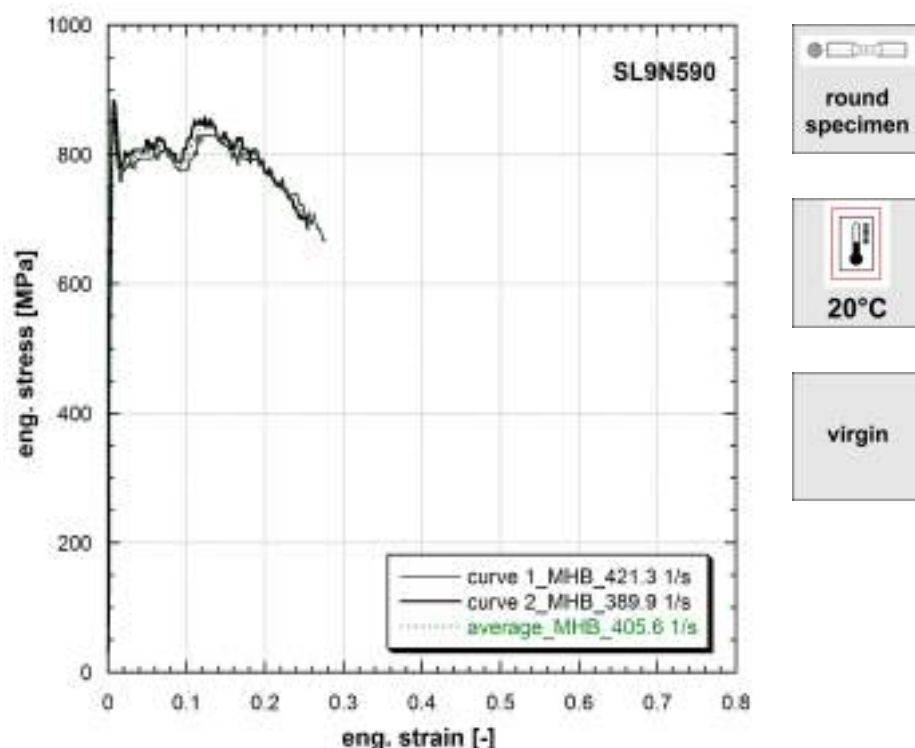


**Figure 9.159:** Stress vs strain curves of SL9N590

Strain rate [1/s]	Yield stress [MPa]	Ultimate tensile strength [MPa]	Uniform strain [-]	Fracture stress [MPa]	Fracture strain [-]
421.3	-	830	0.129	667	0.277
389.9	-	857	0.124	685	0.255
405.6	-	843	0.124	688	0.266

**Table 159:** Mechanical properties of SL9N590

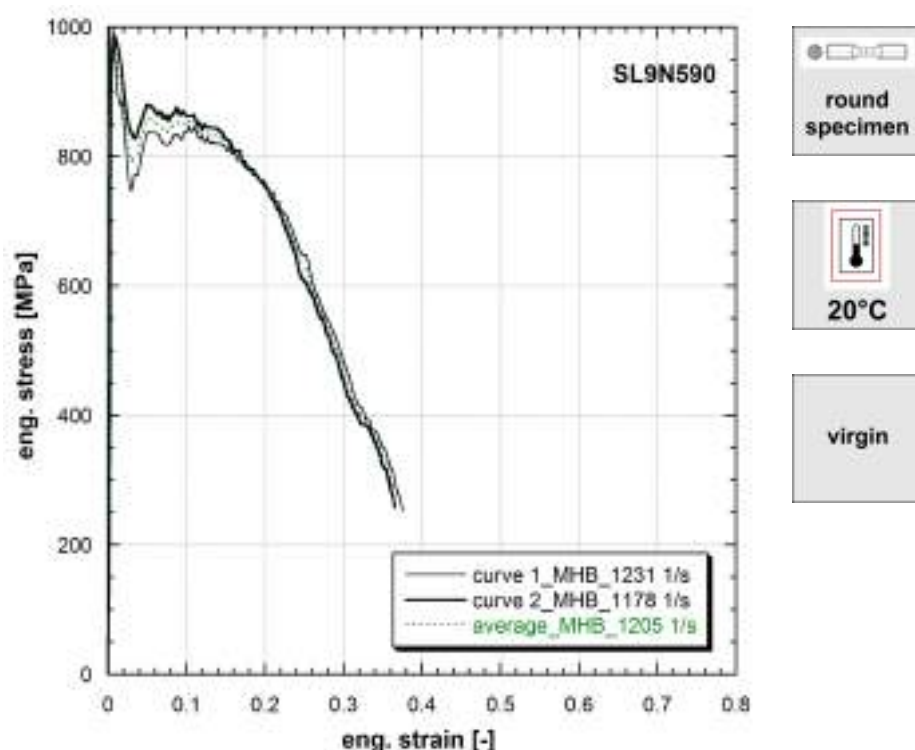


**Figure 9.160:** Stress vs strain curves of SL9N590

Strain rate [1/s]	Yield stress [MPa]	Ultimate tensile strength [MPa]	Uniform strain [-]	Fracture stress [MPa]	Fracture strain [-]
1231	-	846	0.103	252	0.375
1178	-	880	0.050	258	0.366
1205	-	858	0.053	277	0.371

**Table 160:** Mechanical properties of SL9N590

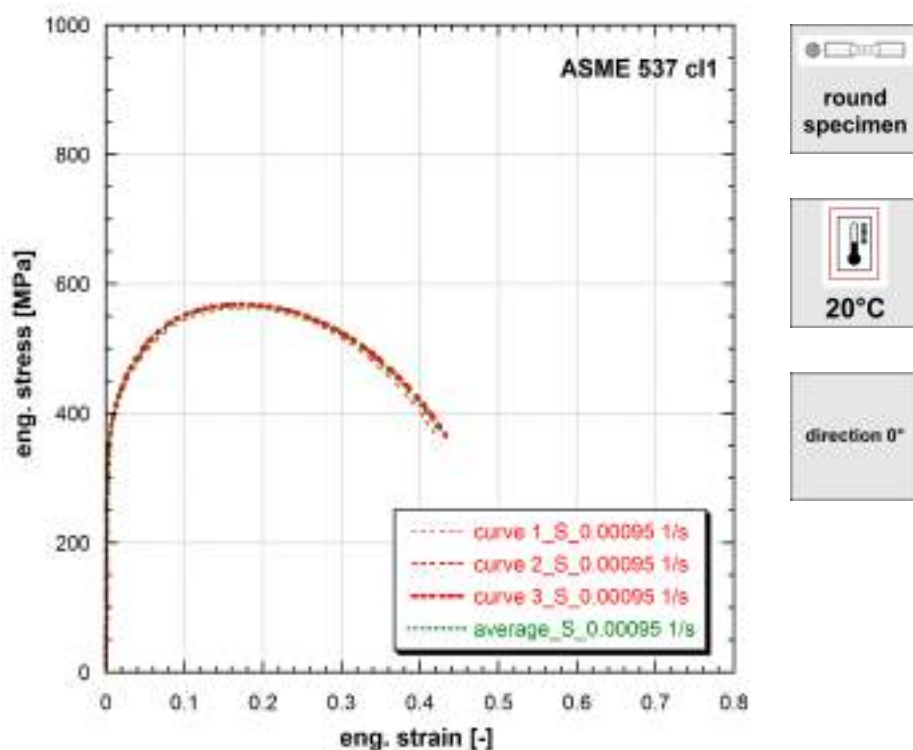


**Figure 9.161:** Stress vs strain curves of ASME 537cl1 (Ref.Mat.6)

**Note 9.161** Ref.Mat.6

Strain rate [1/s]	Yield stress [MPa]	Ultimate tensile strength [MPa]	Uniform strain [-]	Fracture stress [MPa]	Fracture strain [-]
0.00095	364	562	0.168	359	0.423
0.00095	374	569	0.181	371	0.431
0.00095	347	569	0.174	365	0.434
0.00095	363	566	0.181	373	0.429

**Table 161:** Mechanical properties of ASME 537cl1 (Ref.Mat.6)

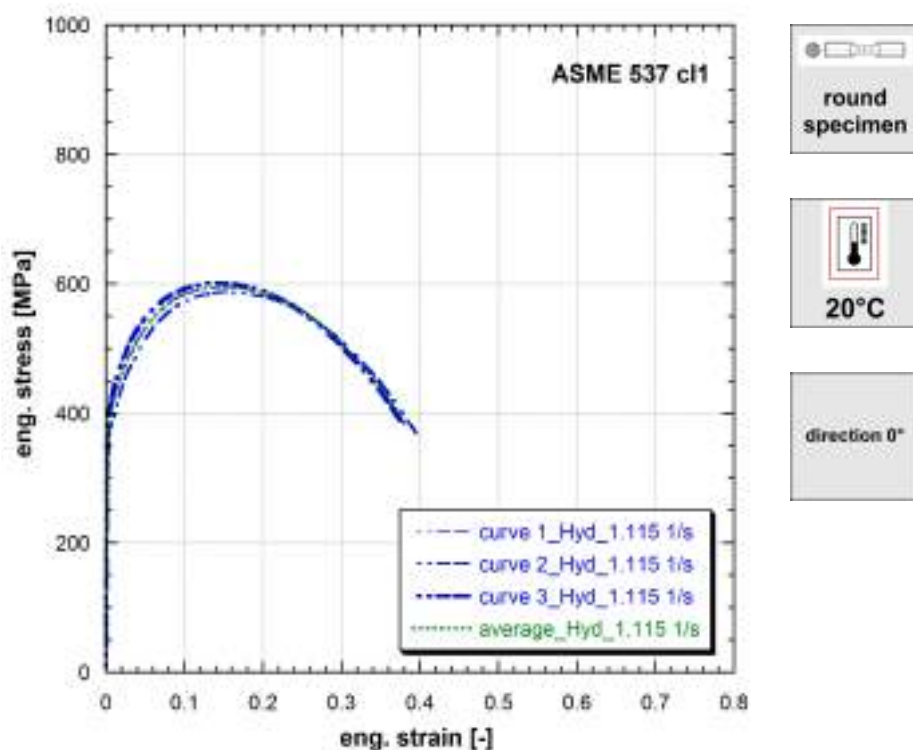


**Figure 9.162:** Stress vs strain curves of ASME 537cl1 (Ref.Mat.6)

**Note 9.162** Ref.Mat.6

Strain rate [1/s]	Yield stress [MPa]	Ultimate tensile strength [MPa]	Uniform strain [-]	Fracture stress [MPa]	Fracture strain [-]
1.115	387	596	0.150	382	0.382
1.115	353	588	0.156	361	0.399
1.115	408	602	0.141	389	0.375
1.115	385	595	0.151	387	0.385

**Table 162:** Mechanical properties of ASME 537cl1 (Ref.Mat.6)

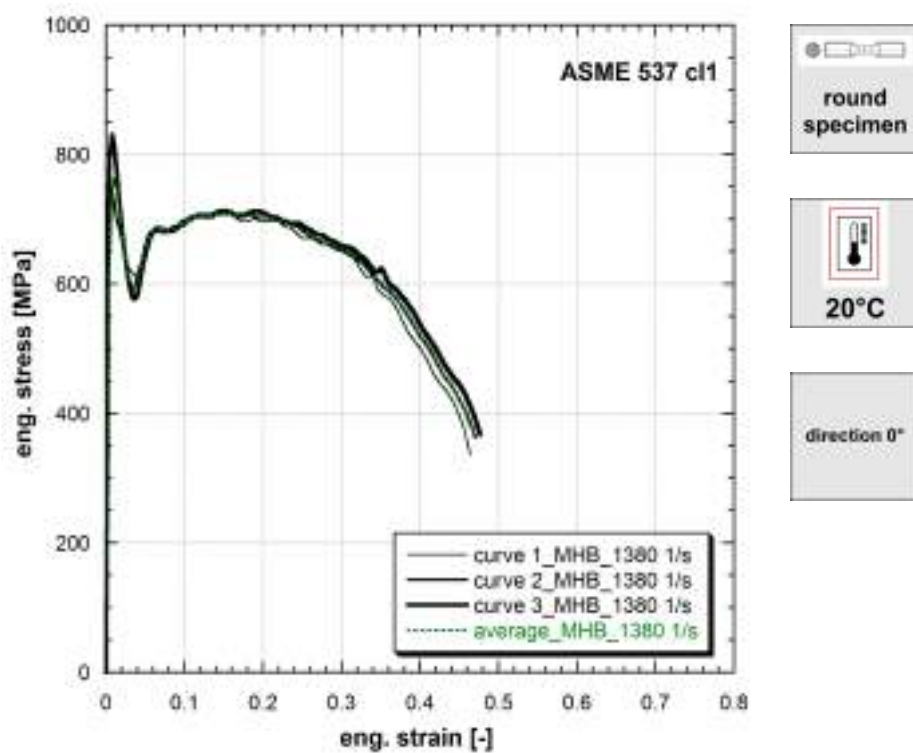


**Figure 9.163:** Stress vs strain curves of ASME 537cl1 (Ref.Mat.6)

**Note 9.163** Ref.Mat.6

Strain rate [1/s]	Yield stress [MPa]	Ultimate tensile strength [MPa]	Uniform strain [-]	Fracture stress [MPa]	Fracture strain [-]
1380	-	707	0.152	336	0.464
1380	-	708	0.181	362	0.471
1380	-	713	0.151	367	0.477
1380	-	709	0.151	366	0.470

**Table 163:** Mechanical properties of ASME 537cl1 (Ref.Mat.6)

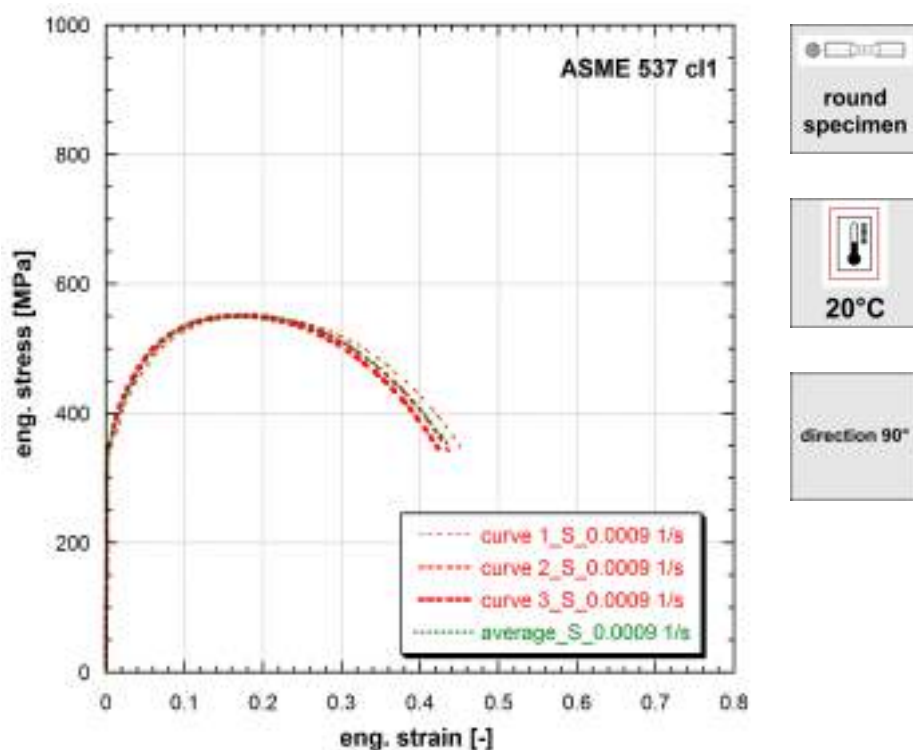


**Figure 9.164:** Stress vs strain curves of ASME 537cl1 (Ref.Mat.6)

**Note 9.164** Ref.Mat.6

Strain rate [1/s]	Yield stress [MPa]	Ultimate tensile strength [MPa]	Uniform strain [-]	Fracture stress [MPa]	Fracture strain [-]
0.0009	359	550	0.190	347	0.452
0.0009	353	554	0.176	337	0.438
0.0009	350	550	0.165	343	0.425
0.0009	354	551	0.176	346	0.438

**Table 164:** Mechanical properties of ASME 537cl1 (Ref.Mat.6)

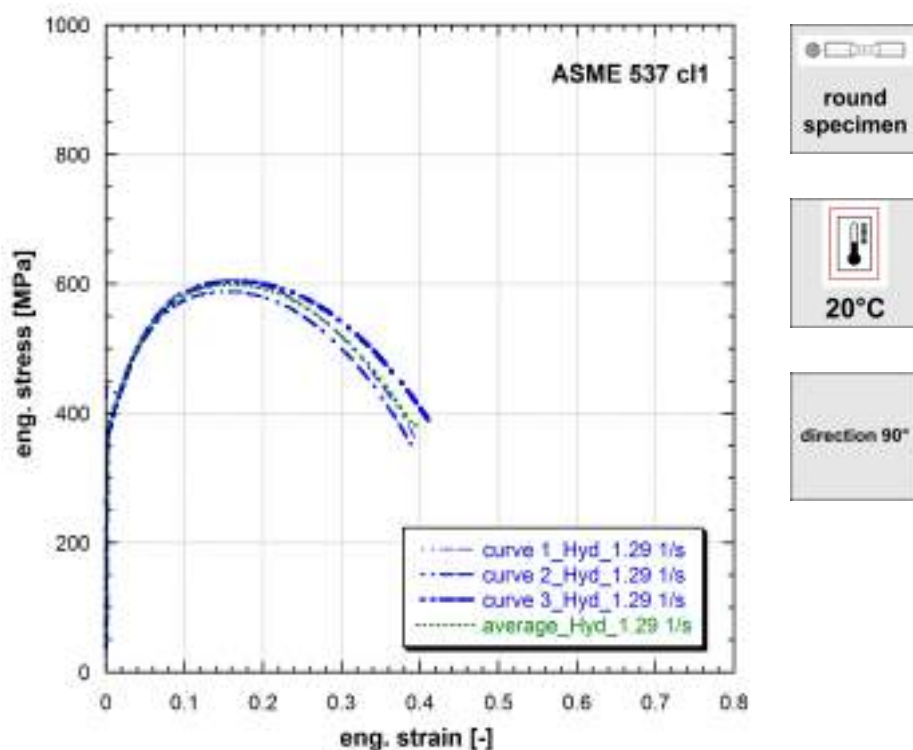


**Figure 9.165:** Stress vs strain curves of ASME 537cl1 (Ref.Mat.6)

**Note 9.165** Ref.Mat.6

Strain rate [1/s]	Yield stress [MPa]	Ultimate tensile strength [MPa]	Uniform strain [-]	Fracture stress [MPa]	Fracture strain [-]
1.29	437	605	0.152	363	0.393
1.29	373	588	0.150	352	0.389
1.29	375	605	0.174	390	0.411
1.29	395	599	0.157	376	0.397

**Table 165:** Mechanical properties of ASME 537cl1 (Ref.Mat.6)

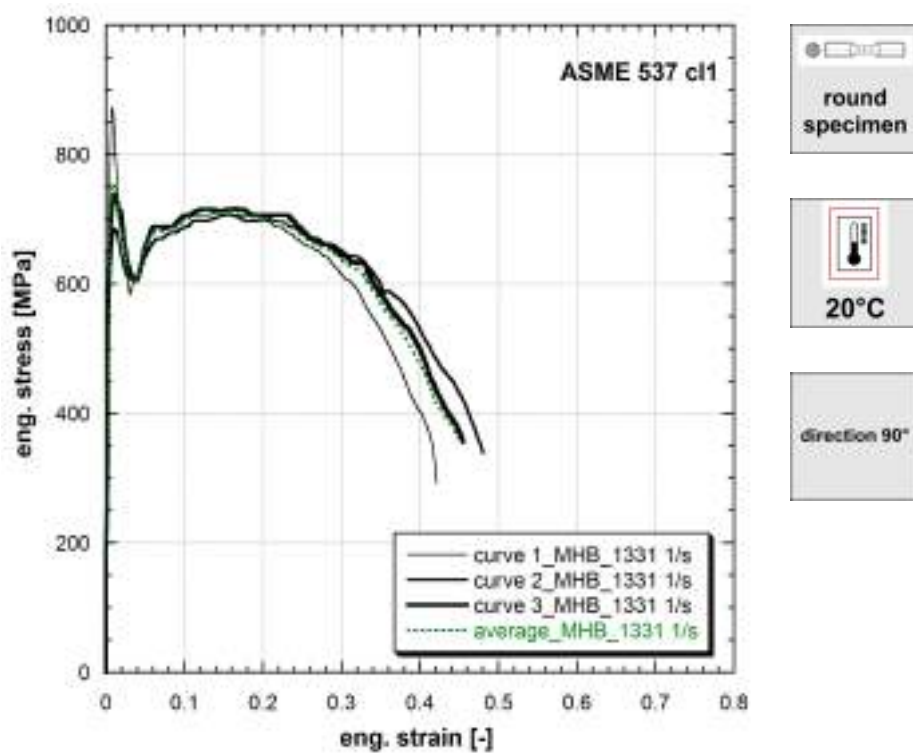


**Figure 9.166:** Stress vs strain curves of ASME 537cl1 (Ref.Mat.6)

**Note 9.166** Ref.Mat.6

Strain rate [1/s]	Yield stress [MPa]	Ultimate tensile strength [MPa]	Uniform strain [-]	Fracture stress [MPa]	Fracture strain [-]
1331	-	715	0.143	292	0.421
1331	-	706	0.161	339	0.481
1331	-	716	0.164	356	0.455
1331	-	711	0.146	355	0.452

**Table 166:** Mechanical properties of ASME 537cl1 (Ref.Mat.6)

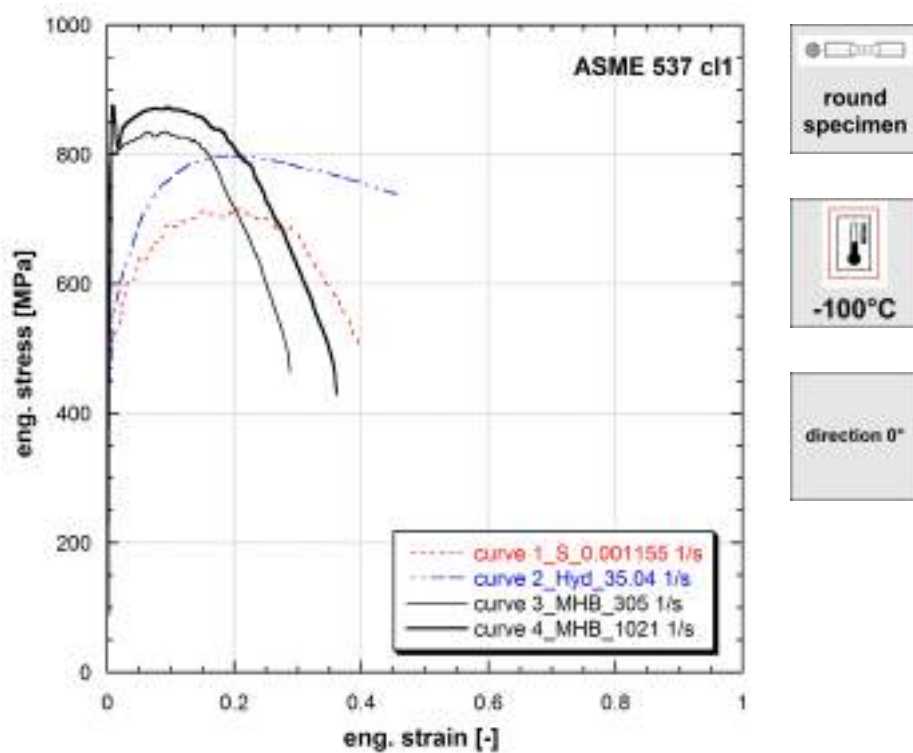


**Figure 9.167:** Stress vs strain curves of ASME 537cl1 (Ref.Mat.6)

**Note 9.167** Ref.Mat.6

Strain rate [1/s]	Yield stress [MPa]	Ultimate tensile strength [MPa]	Uniform strain [-]	Fracture stress [MPa]	Fracture strain [-]
0.001155	481	717	0.210	503	0.398
35.04	450	798	0.227	737	0.461
305	783	835	0.092	463	0.288
1021	858	873	0.095	431	0.361

**Table 167:** Mechanical properties of ASME 537cl1 (Ref.Mat.6)

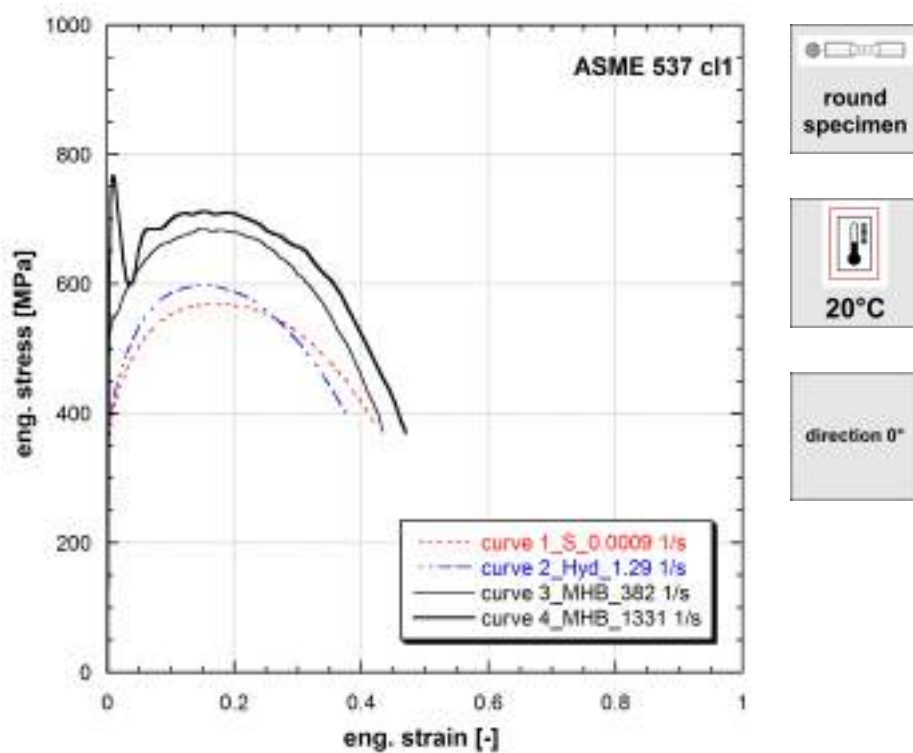


**Figure 9.168:** Stress vs strain curves of ASME 537cl1 (Ref.Mat.6)

**Note 9.168** Ref.Mat.6

Strain rate [1/s]	Yield stress [MPa]	Ultimate tensile strength [MPa]	Uniform strain [-]	Fracture stress [MPa]	Fracture strain [-]
0.0009	364	569	0.182	377	0.427
1.29	381	597	0.163	390	0.383
382	519	685	0.144	371	0.433
1331	-	712	0.151	369	0.470

**Table 168:** Mechanical properties of ASME 537cl1 (Ref.Mat.6)

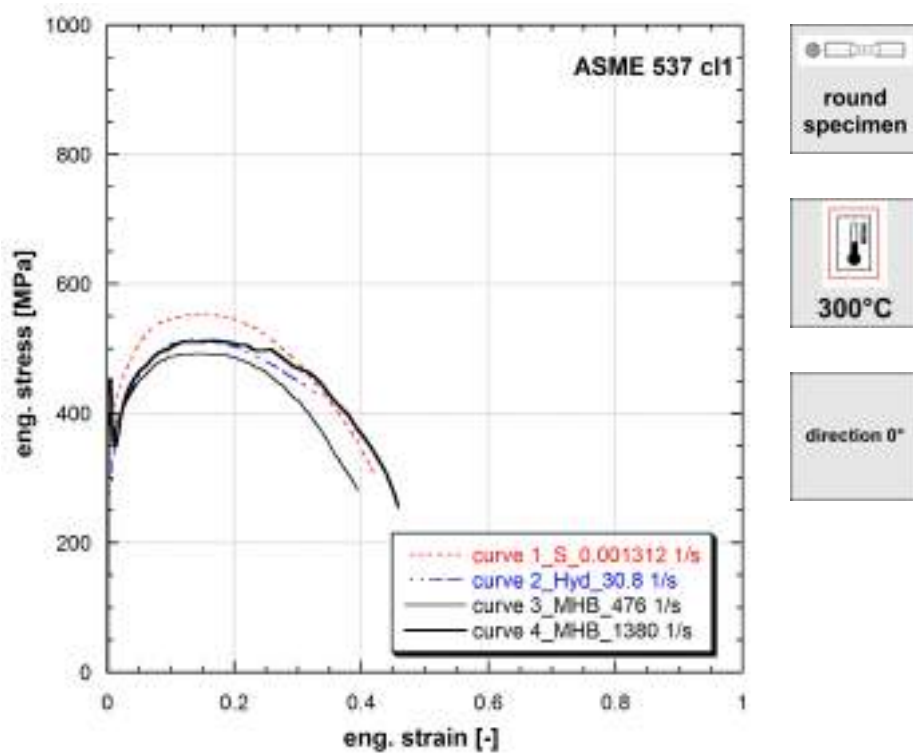


**Figure 9.169:** Stress vs strain curves of ASME 537cl1 (Ref.Mat.6)

**Note 9.169** Ref.Mat.6

Strain rate [1/s]	Yield stress [MPa]	Ultimate tensile strength [MPa]	Uniform strain [-]	Fracture stress [MPa]	Fracture strain [-]
0.001312	375	553	0.154	302	0.424
30.8	275	514	0.139	427	0.337
476	395	492	0.151	281	0.395
1380	452	513	0.168	256	0.458

**Table 169:** Mechanical properties of ASME 537cl1 (Ref.Mat.6)

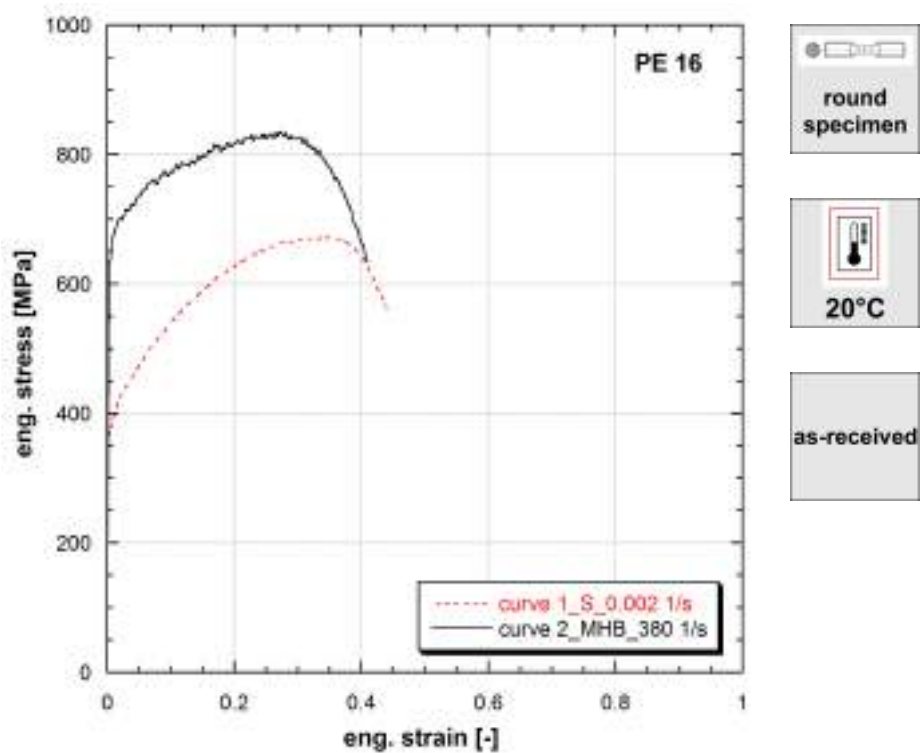


**Figure 9.170:** Stress vs strain curves of PE 16 (Ref.Mat.5)

**Note 9.170** Ref.Mat.5

Strain rate [1/s]	Yield stress [MPa]	Ultimate tensile strength [MPa]	Uniform strain [-]	Fracture stress [MPa]	Fracture strain [-]
0.002	372	671	0.344	554	0.445
380	636	835	0.273	634	0.410

**Table 170:** Mechanical properties of PE 16 (Ref.Mat.5)

Published in (Albertini et al., 1987a).

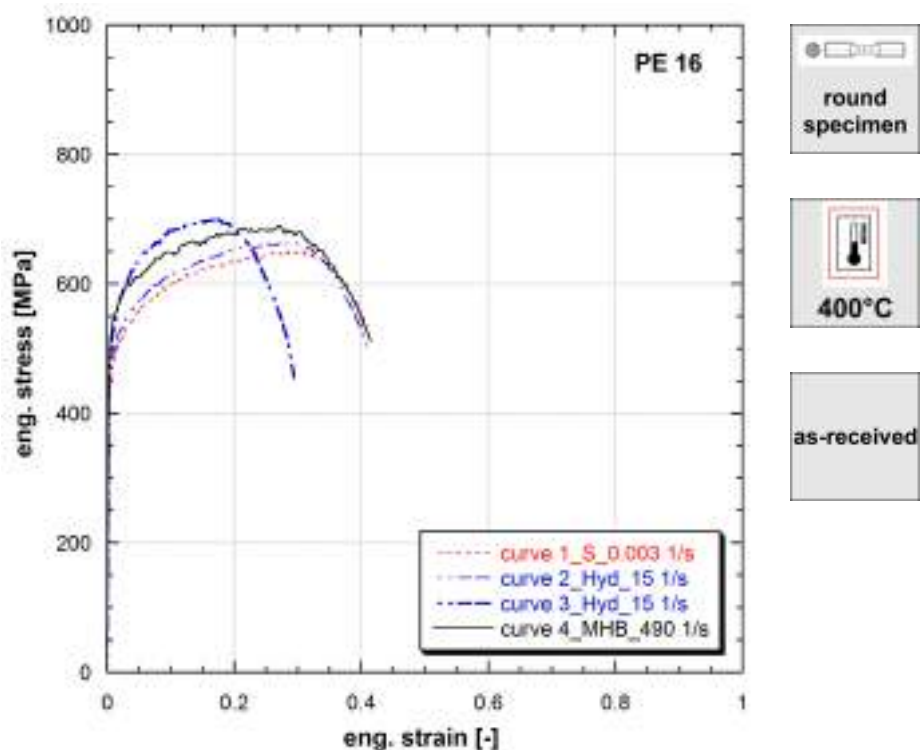


**Figure 9.171:** Stress vs strain curves of PE 16 (Ref.Mat.5)

**Note 9.171** Ref.Mat.5

Strain rate [1/s]	Yield stress [MPa]	Ultimate tensile strength [MPa]	Uniform strain [-]	Fracture stress [MPa]	Fracture strain [-]
0.003	442	650	0.283	536	0.410
15	460	663	0.298	504	0.408
15	496	700	0.170	453	0.295
490	517	690	0.270	511	0.415

**Table 171:** Mechanical properties of PE 16 (Ref.Mat.5)

Published in (Albertini et al., 1987a).

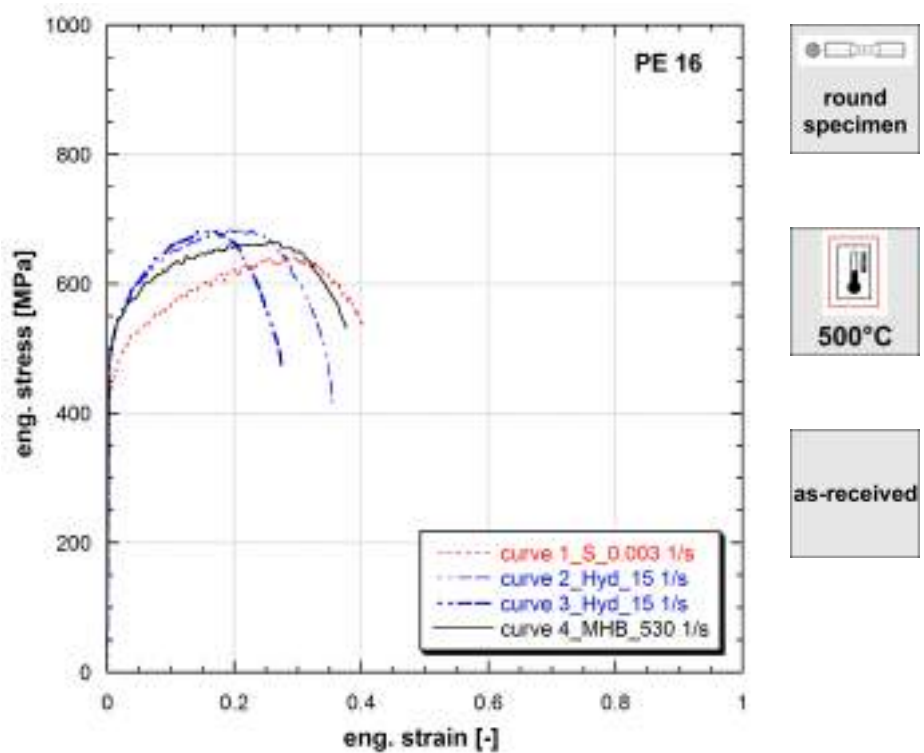


**Figure 9.172:** Stress vs strain curves of PE 16 (Ref.Mat.5)

**Note 9.172** Ref.Mat.5

Strain rate [1/s]	Yield stress [MPa]	Ultimate tensile strength [MPa]	Uniform strain [-]	Fracture stress [MPa]	Fracture strain [-]
0.003	434	641	0.279	536	0.406
15	482	683	0.195	414	0.355
15	492	681	0.170	473	0.274
530	486	668	0.257	532	0.376

**Table 172:** Mechanical properties of PE 16 (Ref.Mat.5)

Published in (Albertini et al., 1987a).

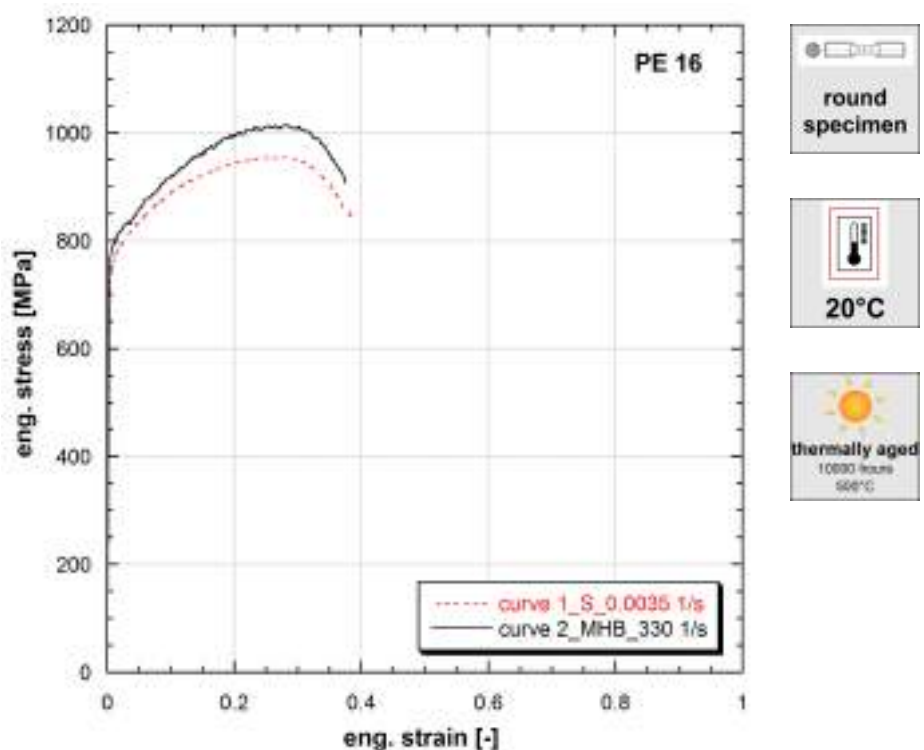


**Figure 9.173:** Stress vs strain curves of PE 16 (Ref.Mat.5)

**Note 9.173** Ref.Mat.5

Strain rate [1/s]	Yield stress [MPa]	Ultimate tensile strength [MPa]	Uniform strain [-]	Fracture stress [MPa]	Fracture strain [-]
0.0035	737	954	0.257	836	0.391
330	777	1014	0.282	907	0.376

**Table 173:** Mechanical properties of PE 16 (Ref.Mat.5)

Published in (Albertini et al., 1987a).

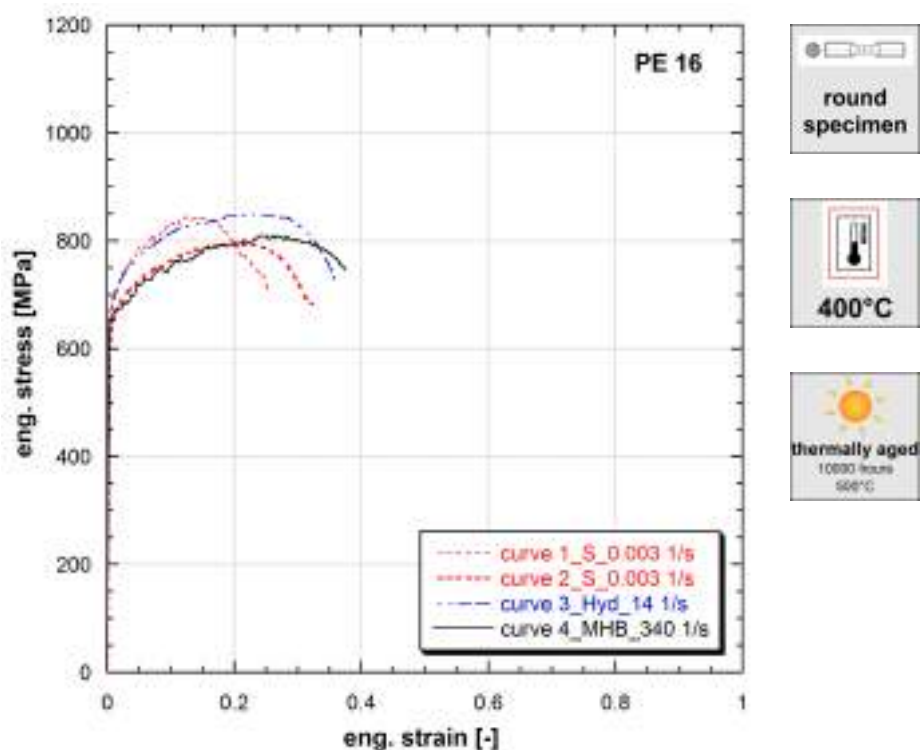


**Figure 9.174:** Stress vs strain curves of PE 16 (Ref.Mat.5)

**Note 9.174** Ref.Mat.5

Strain rate [1/s]	Yield stress [MPa]	Ultimate tensile strength [MPa]	Uniform strain [-]	Fracture stress [MPa]	Fracture strain [-]
0.003	680	844	0.125	702	0.255
0.003	621	799	0.197	683	0.324
14	668	849	0.239	717	0.361
340	647	809	0.262	746	0.375

**Table 174:** Mechanical properties of PE 16 (Ref.Mat.5)

Published in (Albertini et al., 1987a).

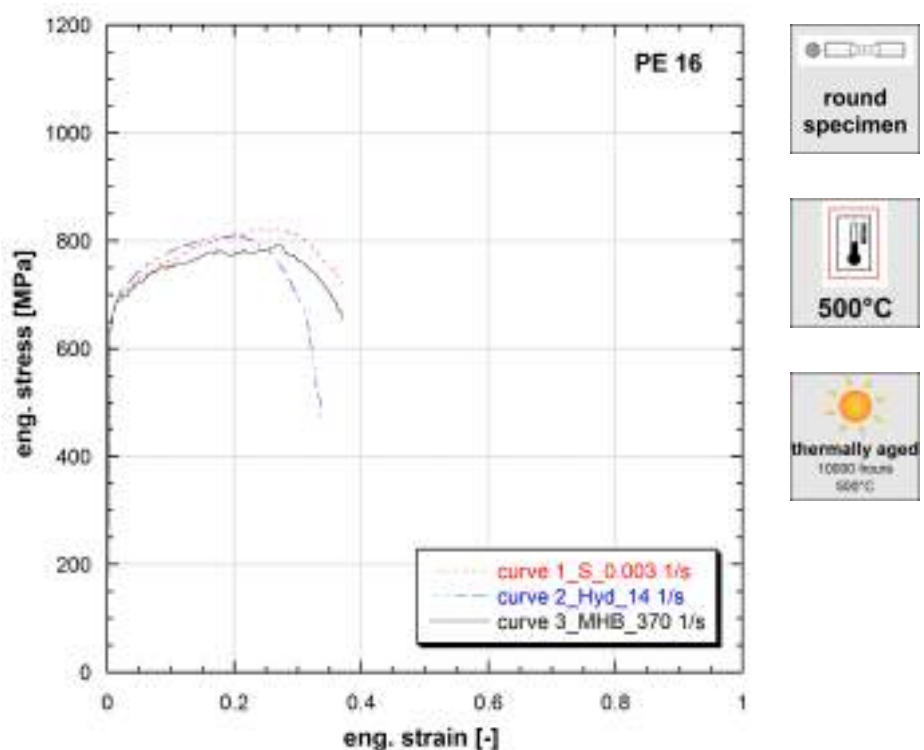


**Figure 9.175:** Stress vs strain curves of PE 16 (Ref.Mat.5)

**Note 9.175** Ref.Mat.5

Strain rate [1/s]	Yield stress [MPa]	Ultimate tensile strength [MPa]	Uniform strain [-]	Fracture stress [MPa]	Fracture strain [-]
0.003	642	822	0.247	719	0.370
14	650	809	0.191	467	0.338
370	642	791	0.270	654	0.370

**Table 175:** Mechanical properties of PE 16 (Ref.Mat.5)

Published in (Albertini et al., 1987a).

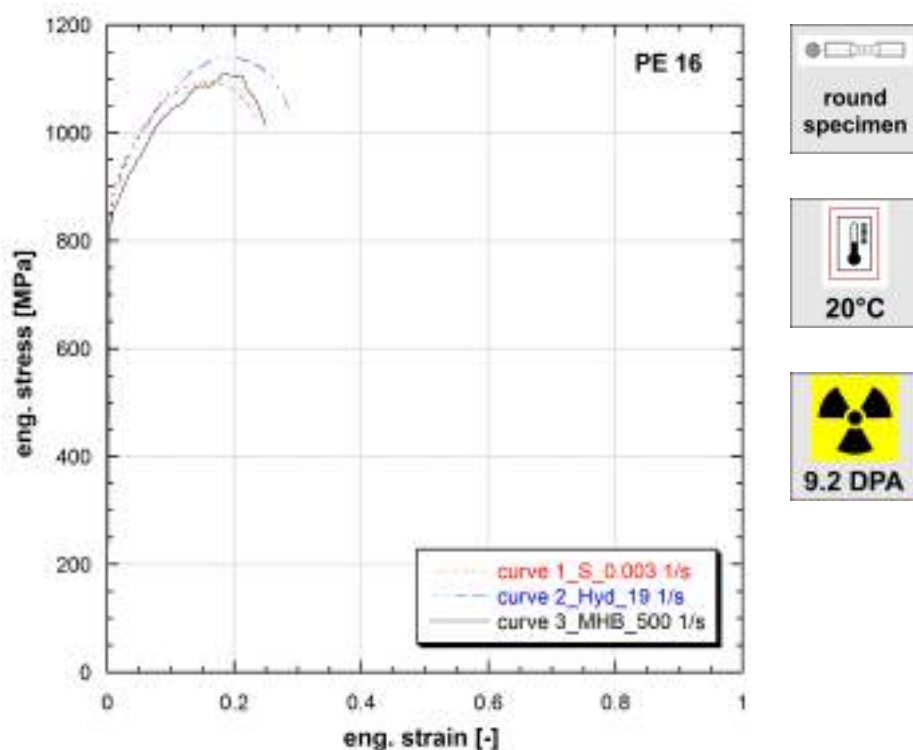


**Figure 9.176:** Stress vs strain curves of PE 16 (Ref.Mat.5)

**Note 9.176** Ref.Mat.5

*Irradiated in sodium at 500°C in HFR reactor, for 10000 hours.*

Strain rate [1/s]	Yield stress [MPa]	Ultimate tensile strength [MPa]	Uniform strain [-]	Fracture stress [MPa]	Fracture strain [-]
0.003	867	1094	0.161	1027	0.233
19	840	1141	0.190	1034	0.290
500	836	1110	0.197	1013	0.251

**Table 176:** Mechanical properties of PE 16 (Ref.Mat.5)

*Published in (Albertini et al., 1987a).*

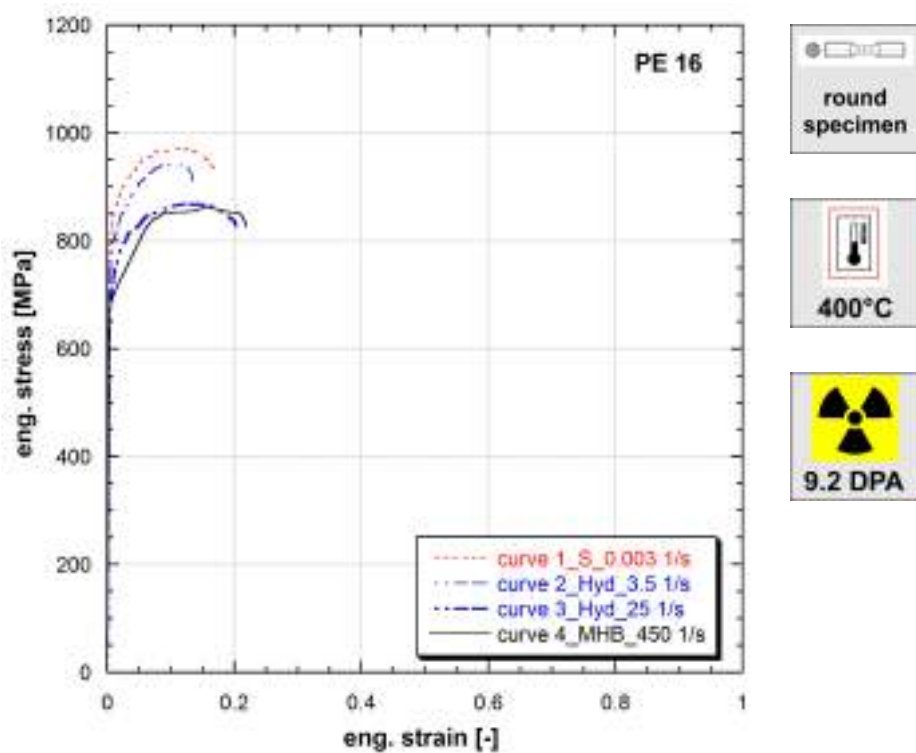


**Figure 9.177:** Stress vs strain curves of PE 16 (Ref.Mat.5)

**Note 9.177** Ref.Mat.5

*Irradiated in sodium at 500°C in HFR reactor, for 10000 hours.*

Strain rate [1/s]	Yield stress [MPa]	Ultimate tensile strength [MPa]	Uniform strain [-]	Fracture stress [MPa]	Fracture strain [-]
0.003	822	972	0.117	931	0.170
3.5	764	939	0.116	933	0.130
25	694	868	0.146	829	0.204
450	681	863	0.167	826	0.220

**Table 177:** Mechanical properties of PE 16 (Ref.Mat.5)

*Published in (Albertini et al., 1987a).*

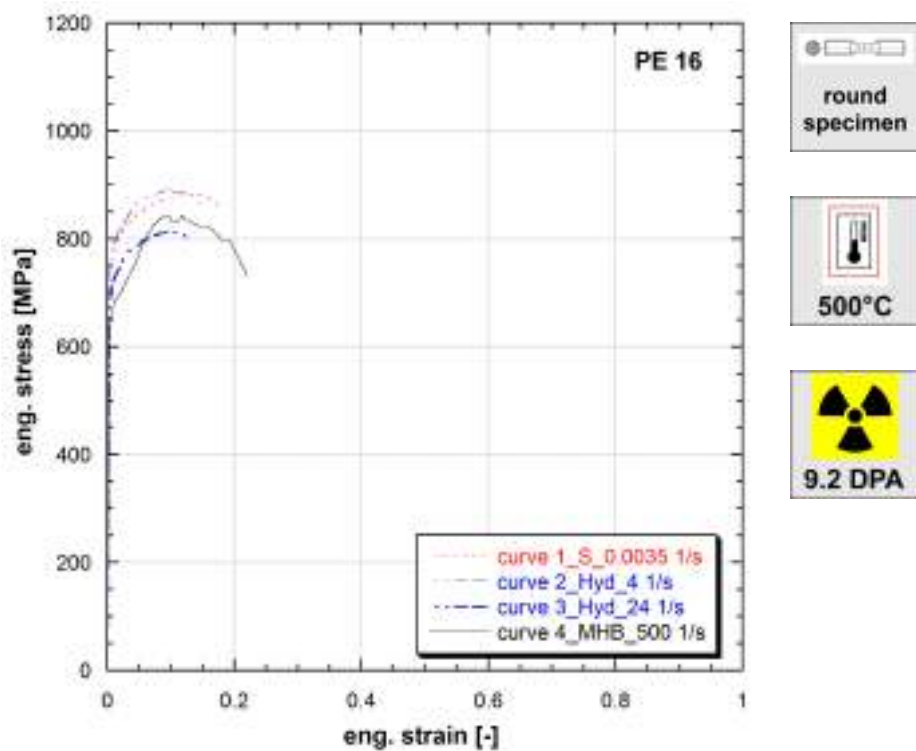


**Figure 9.178:** Stress vs strain curves of PE 16 (Ref.Mat.5)

**Note 9.178** Ref.Mat.5

*Irradiated in sodium at 500°C in HFR reactor, for 10000 hours.*

Strain rate [1/s]	Yield stress [MPa]	Ultimate tensile strength [MPa]	Uniform strain [-]	Fracture stress [MPa]	Fracture strain [-]
0.0035	761	882	0.132	859	0.175
4	753	889	0.102	858	0.149
24	700	814	0.099	794	0.132
500	650	844	0.117	733	0.220

**Table 178:** Mechanical properties of PE 16 (Ref.Mat.5)

*Published in (Albertini et al., 1987a).*

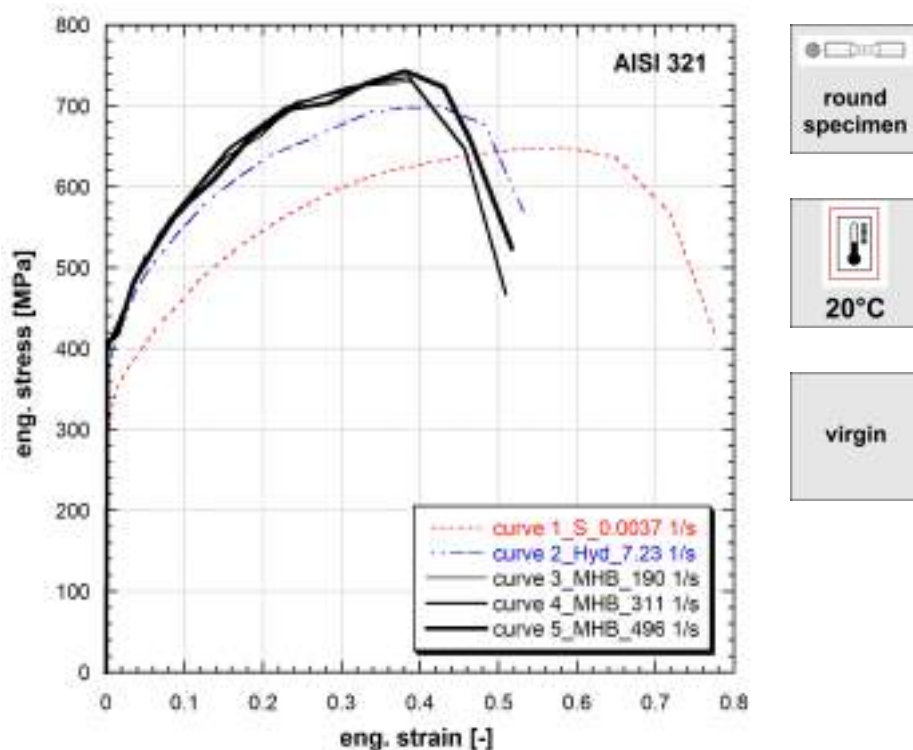


**Figure 9.179:** Stress vs strain curves of AISI 321 (Ref.Mat.2)

**Note 9.179** Ref.Mat.2

Strain rate [1/s]	Yield stress [MPa]	Ultimate tensile strength [MPa]	Uniform strain [-]	Fracture stress [MPa]	Fracture strain [-]
0.0037	291	648	0.586	417	0.776
7.23	371	699	0.426	569	0.532
190	402	730	0.390	-	-
311	407	736	0.385	467	0.509
496	409	743	0.381	523	0.517

**Table 179:** Mechanical properties of AISI 321 (Ref.Mat.2)

Published in (Albertini and Montagnani, 1983a), (Albertini and Montagnani, 1980).

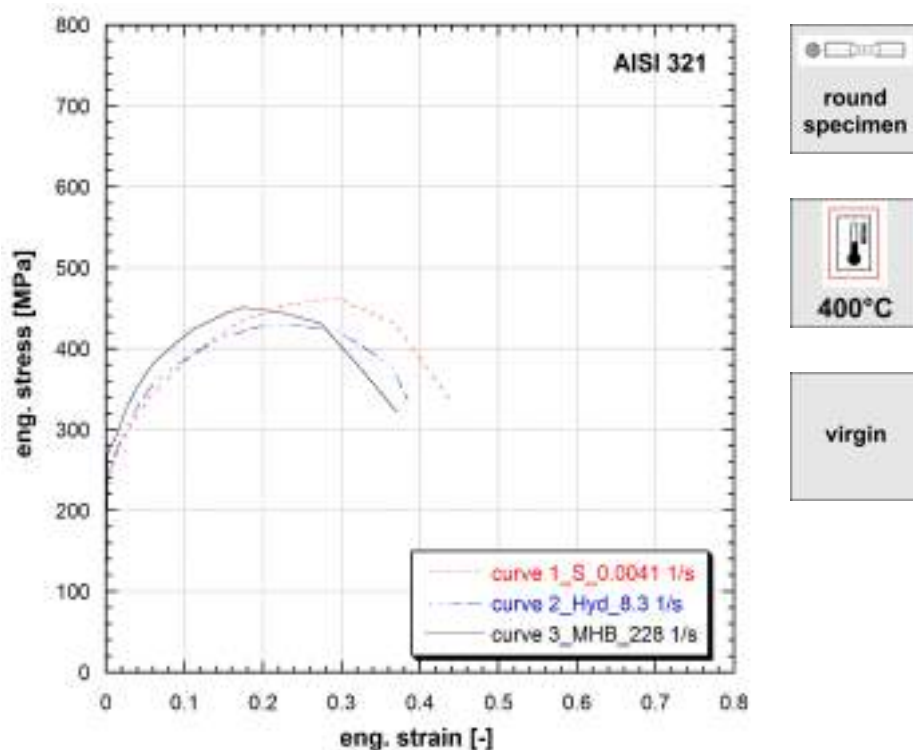


**Figure 9.180:** Stress vs strain curves of AISI 321 (Ref.Mat.2)

**Note 9.180** Ref.Mat.2

Strain rate [1/s]	Yield stress [MPa]	Ultimate tensile strength [MPa]	Uniform strain [-]	Fracture stress [MPa]	Fracture strain [-]
0.0041	218	462	0.295	329	0.444
8.3	238	429	0.243	336	0.385
228	274	451	0.176	321	0.371

**Table 180:** Mechanical properties of AISI 321 (Ref.Mat.2)

Published in (Albertini and Montagnani, 1980).

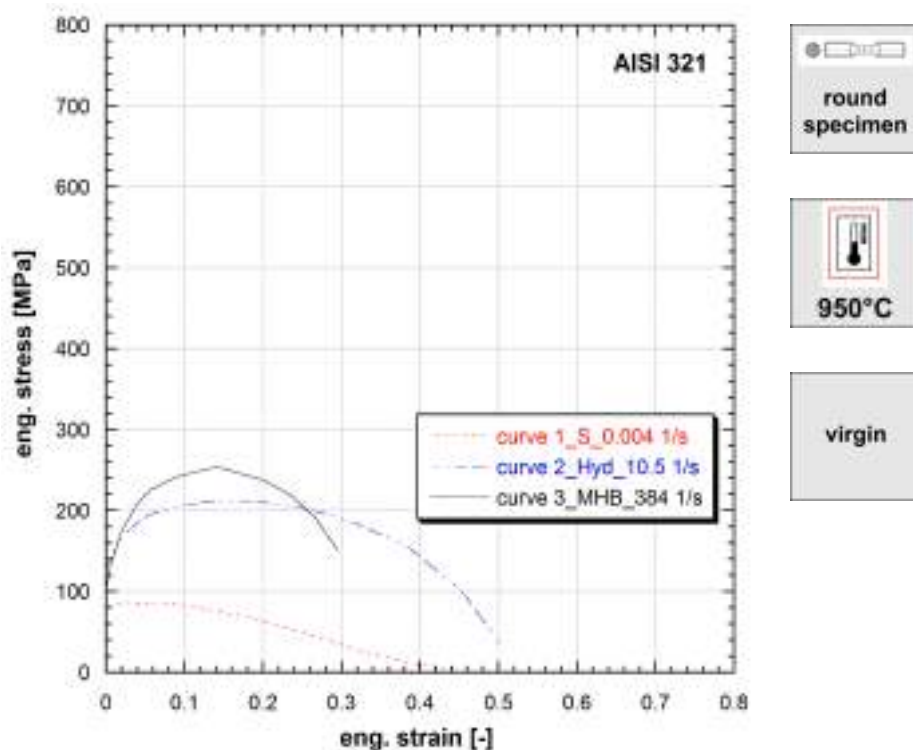


**Figure 9.181:** Stress vs strain curves of AISI 321 (Ref.Mat.2)

**Note 9.181** Ref.Mat.2

Strain rate [1/s]	Yield stress [MPa]	Ultimate tensile strength [MPa]	Uniform strain [-]	Fracture stress [MPa]	Fracture strain [-]
0.004	79	86	0.021	3	0.450
10.5	133	212	0.139	32	0.500
384	115	254	0.142	151	0.295

**Table 181:** Mechanical properties of AISI 321 (Ref.Mat.2)

Published in (Albertini and Montagnani, 1980).

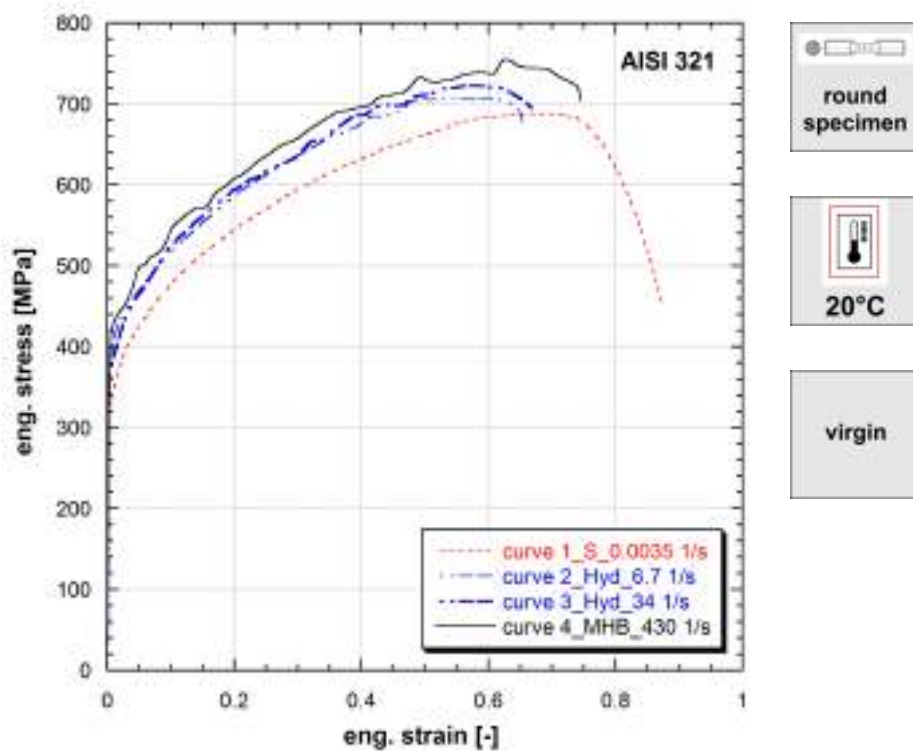


**Figure 9.182:** Stress vs strain curves of AISI 321 (Ref.Mat.2)

**Note 9.182** Specimens taken from a sheet of 1.6 mm thickness, JRC-COVA experiments.

Strain rate [1/s]	Yield stress [MPa]	Ultimate tensile strength [MPa]	Uniform strain [-]	Fracture stress [MPa]	Fracture strain [-]
0.0035	326	688	0.704	451	0.874
6.7	376	708	0.551	678	0.654
34	364	723	0.585	695	0.668
430	413	755	0.624	704	0.745

**Table 182:** Mechanical properties of AISI 321 (Ref.Mat.2)

Published in (Albertini and Montagnani, 1983a).

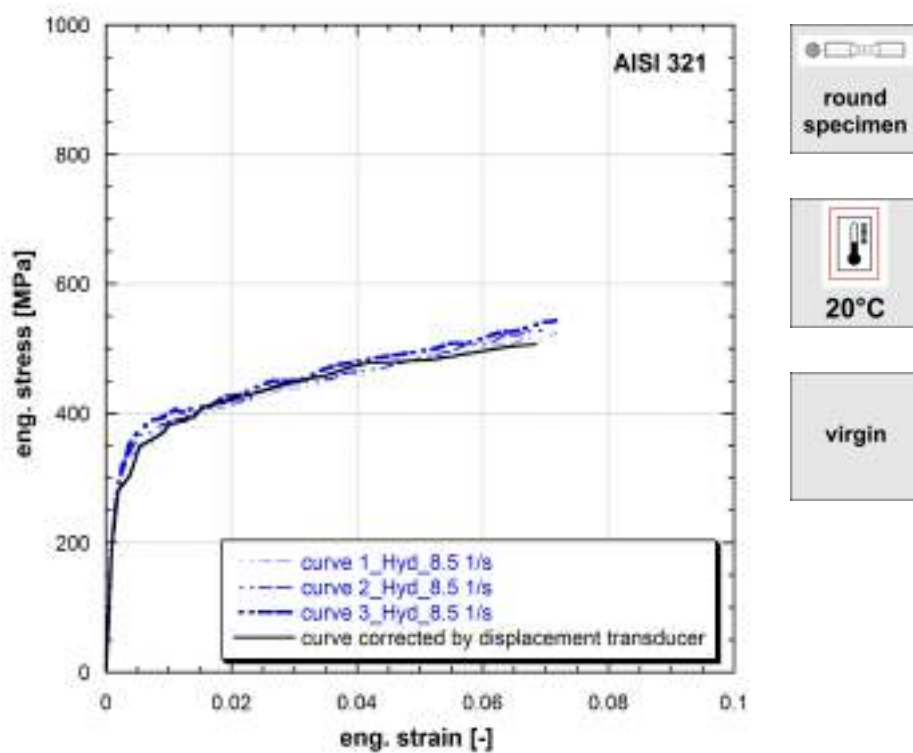


**Figure 9.183:** Stress vs strain curves of AISI 321 (Ref.Mat.2)

**Note 9.183** Comparison of flow curves with strains measured by strain gages directly on the specimen and strains from displacement transducer of the HPM, JRC-COVA experiments.

Strain rate [1/s]	Yield stress [MPa]	Ultimate tensile strength [MPa]	Uniform strain [-]	Fracture stress [MPa]	Fracture strain [-]
8.5	332	-	-	-	-
8.5	342	-	-	-	-
8.5	357	-	-	-	-

**Table 183:** Mechanical properties of AISI 321 (Ref.Mat.2)

Published in (Albertini and Montagnani, 1983a).

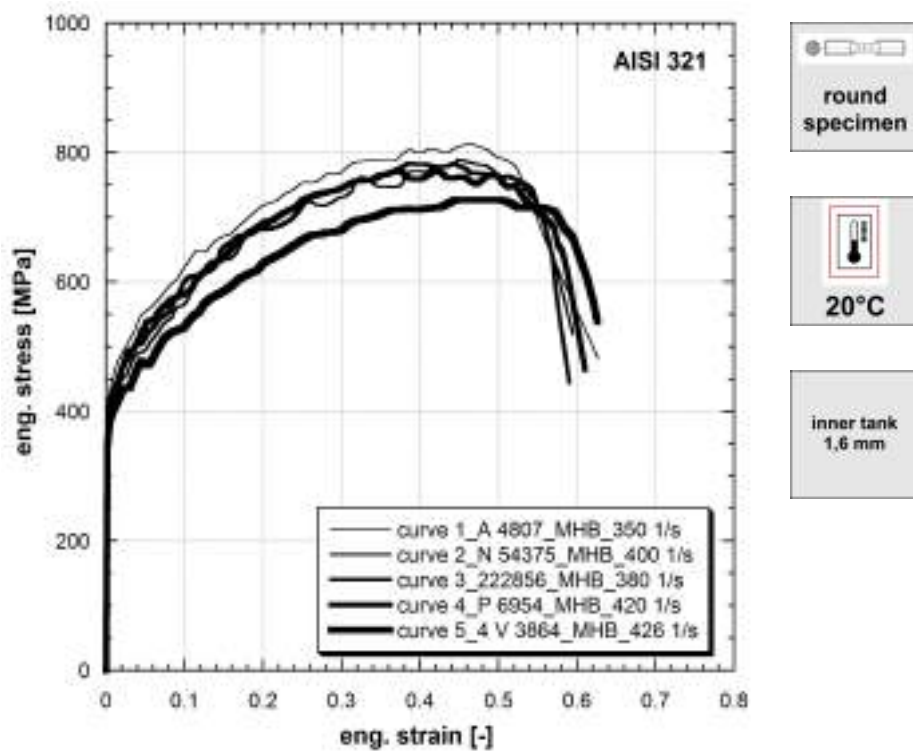


**Figure 9.184:** Stress vs strain curves of AISI 321 (Ref.Mat.2)

**Note 9.184** Comparison of flow curves at nearly the same strain-rate of specimens taken from different batches of sheets of 1.6 mm thickness, used in JRC-COVA experiments.

Strain rate [1/s]	Yield stress [MPa]	Ultimate tensile strength [MPa]	Uniform strain [-]	Fracture stress [MPa]	Fracture strain [-]
350	428	813	0.464	481	0.627
400	383	789	0.448	519	0.595
380	420	783	0.385	444	0.590
420	387	772	0.420	465	0.610
426	371	727	0.503	538	0.626

**Table 184:** Mechanical properties of AISI 321 (Ref.Mat.2)

Published in (Albertini and Montagnani, 1983a).

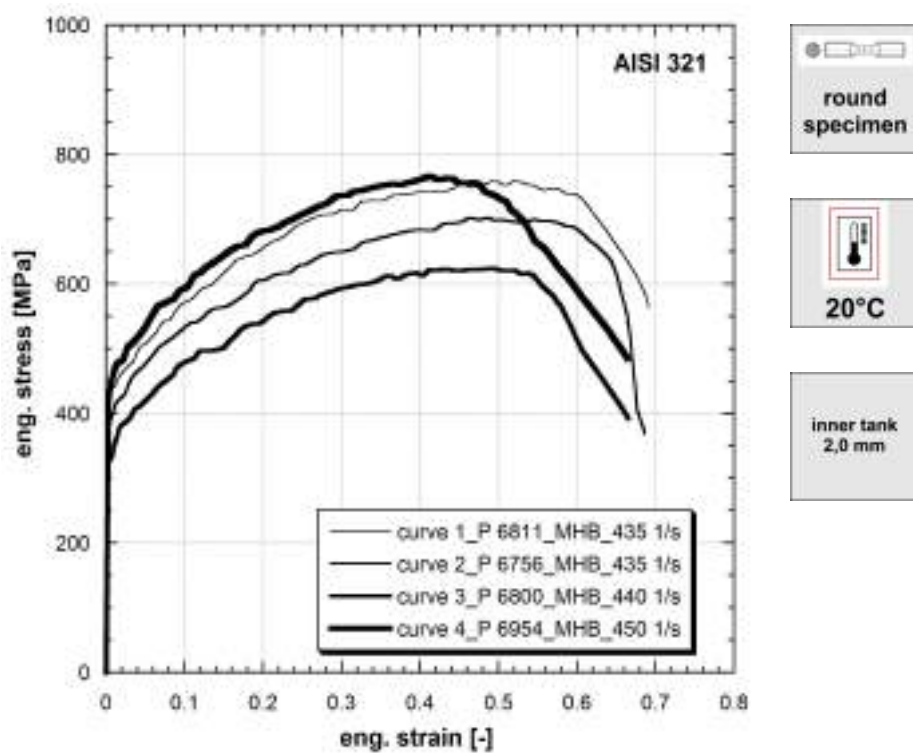


**Figure 9.185:** Stress vs strain curves of AISI 321 (Ref.Mat.2)

**Note 9.185** Comparison of flow curves at nearly the same strain-rate of specimens taken from different batches of sheets of 2 mm thickness, used in JRC-COVA experiments.

Strain rate [1/s]	Yield stress [MPa]	Ultimate tensile strength [MPa]	Uniform strain [-]	Fracture stress [MPa]	Fracture strain [-]
435	427	759	0.521	563	0.691
435	384	702	0.488	369	0.686
440	327	624	0.491	391	0.666
450	444	766	0.410	484	0.665

**Table 185:** Mechanical properties of AISI 321 (Ref.Mat.2)

Published in (Albertini and Montagnani, 1983a).

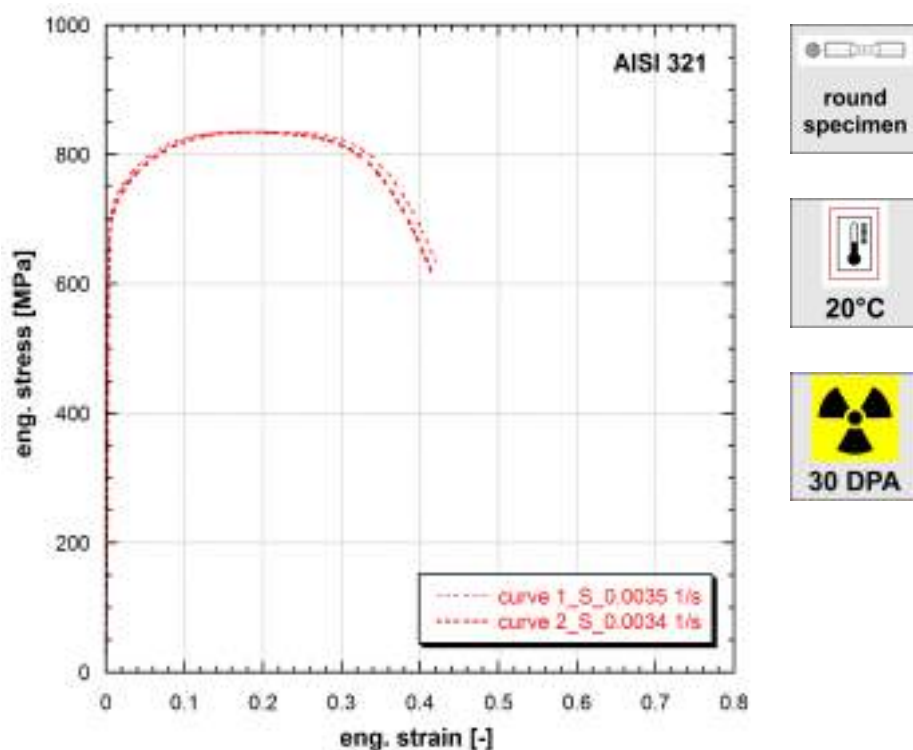


**Figure 9.186:** Stress vs strain curves of AISI 321 (Ref.Mat.2)

**Note 9.186** Ref.Mat.2

*Irradiated in sodium at 500°C in HFR reactor, for 30000 hours.*

Strain rate [1/s]	Yield stress [MPa]	Ultimate tensile strength [MPa]	Uniform strain [-]	Fracture stress [MPa]	Fracture strain [-]
0.0034	706	835	0.197	635	0.420
0.0035	686	835	0.185	618	0.415

**Table 186:** Mechanical properties of AISI 321 (Ref.Mat.2)

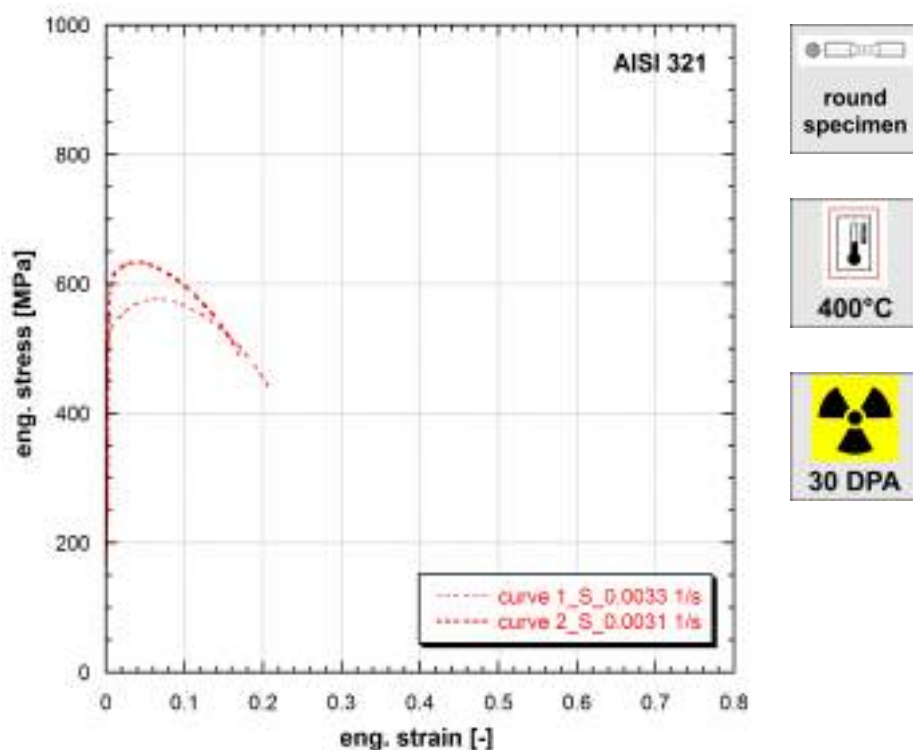


**Figure 9.187:** Stress vs strain curves of AISI 321 (Ref.Mat.2)

**Note 9.187** Ref.Mat.2

*Irradiated in sodium at 500°C in HFR reactor, for 30000 hours.*

Strain rate [1/s]	Yield stress [MPa]	Ultimate tensile strength [MPa]	Uniform strain [-]	Fracture stress [MPa]	Fracture strain [-]
0.0031	522	576	0.065	437	0.208
0.0033	589	634	0.041	492	0.169

**Table 187:** Mechanical properties of AISI 321 (Ref.Mat.2)

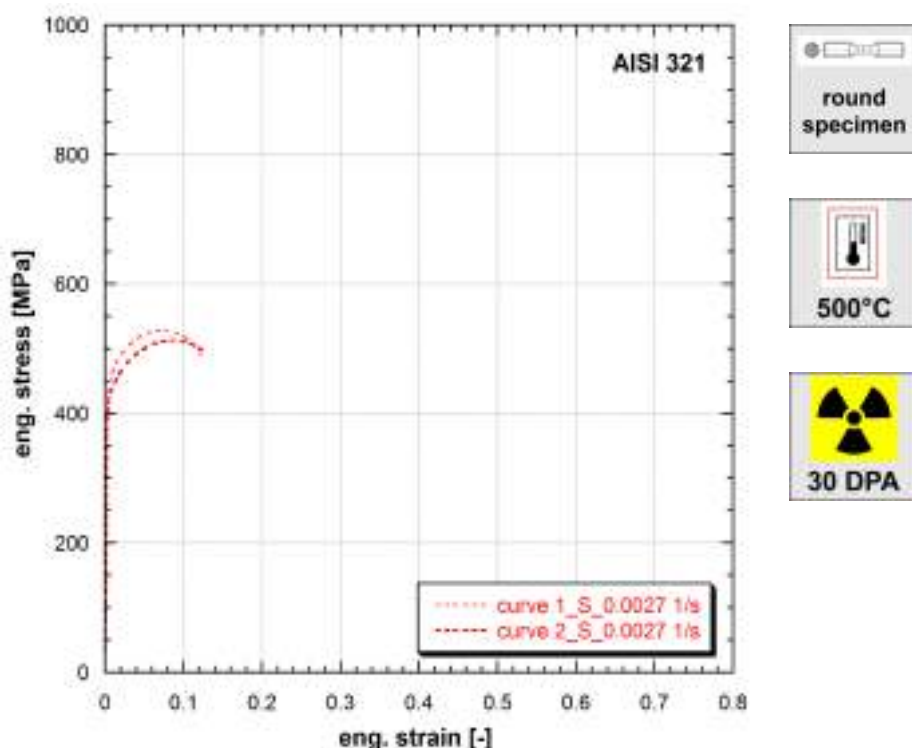


**Figure 9.188:** Stress vs strain curves of AISI 321 (Ref.Mat.2)

**Note 9.188** Ref.Mat.2

*Irradiated in sodium at 500°C in HFR reactor, for 30000 hours.*

Strain rate [1/s]	Yield stress [MPa]	Ultimate tensile strength [MPa]	Uniform strain [-]	Fracture stress [MPa]	Fracture strain [-]
0.0027	408	528	0.077	490	0.123
0.0027	403	513	0.090	488	0.131

**Table 188:** Mechanical properties of AISI 321 (Ref.Mat.2)

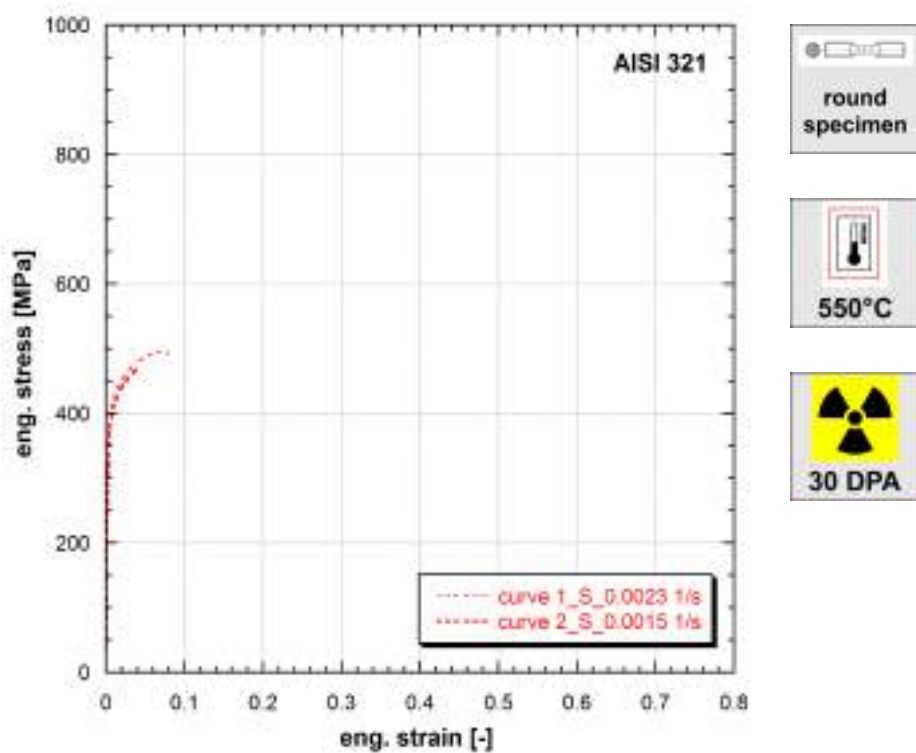


**Figure 9.189:** Stress vs strain curves of AISI 321 (Ref.Mat.2)

**Note 9.189** Ref.Mat.2

Irradiated in sodium at 500°C in HFR reactor, for 30000 hours.

Strain rate [1/s]	Yield stress [MPa]	Ultimate tensile strength [MPa]	Uniform strain [-]	Fracture stress [MPa]	Fracture strain [-]
0.0023	401	-	-	-	-
0.0015	371	-	-	-	-

**Table 189:** Mechanical properties of AISI 321 (Ref.Mat.2)

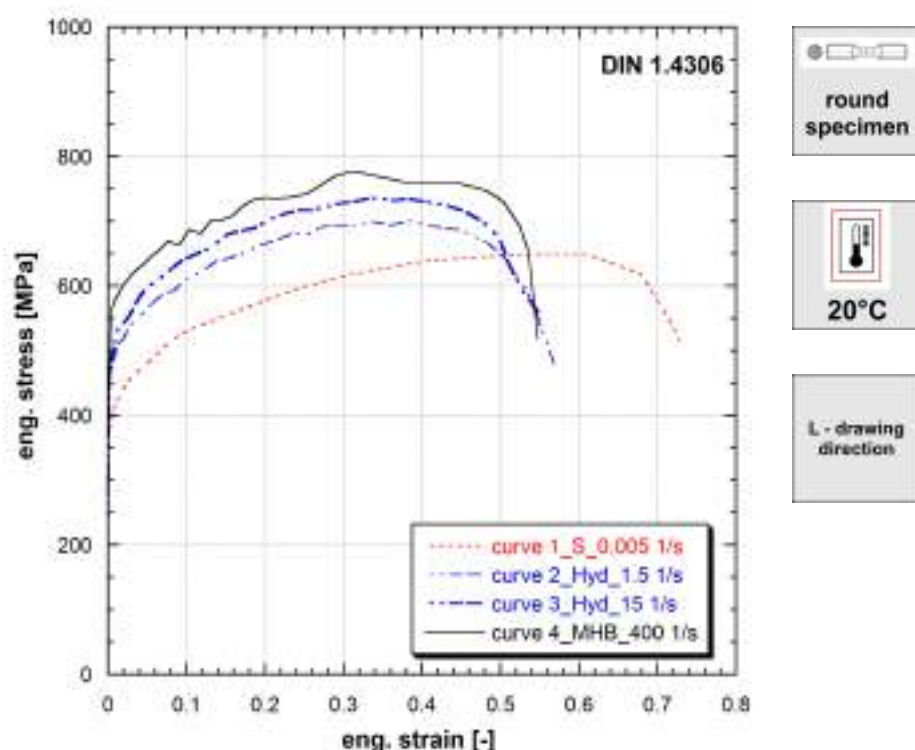


**Figure 9.190:** Stress vs strain curves of DIN 1.4306

Strain rate [1/s]	Yield stress [MPa]	Ultimate tensile strength [MPa]	Uniform strain [-]	Fracture stress [MPa]	Fracture strain [-]
0.005	383	649	0.610	515	0.730
1.5	461	700	0.380	471	0.570
15	483	736	0.330	557	0.549
400	503	775	0.320	517	0.550

**Table 190:** Mechanical properties of DIN 1.4306

Published in (Albertini and Montagnani, 1977).

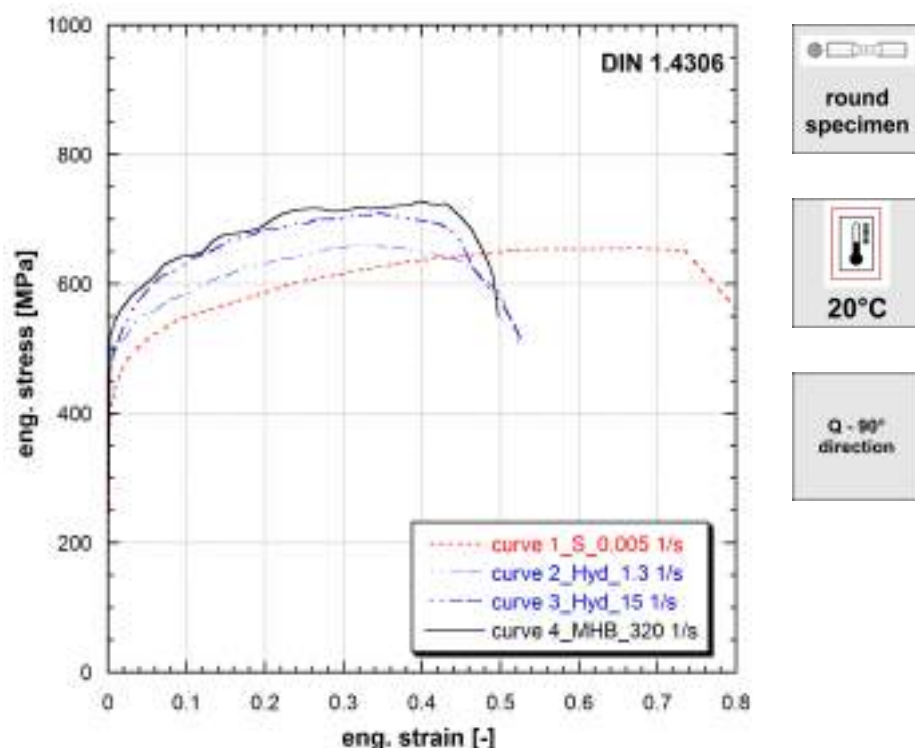


**Figure 9.191:** Stress vs strain curves of DIN 1.4306

Strain rate [1/s]	Yield stress [MPa]	Ultimate tensile strength [MPa]	Uniform strain [-]	Fracture stress [MPa]	Fracture strain [-]
0.005	406	655	0.676	557	0.800
1.3	481	659	0.331	508	0.520
15	474	709	0.346	514	0.530
320	524	728	0.399	549	0.497

**Table 191:** Mechanical properties of DIN 1.4306

Published in (Albertini and Montagnani, 1977).

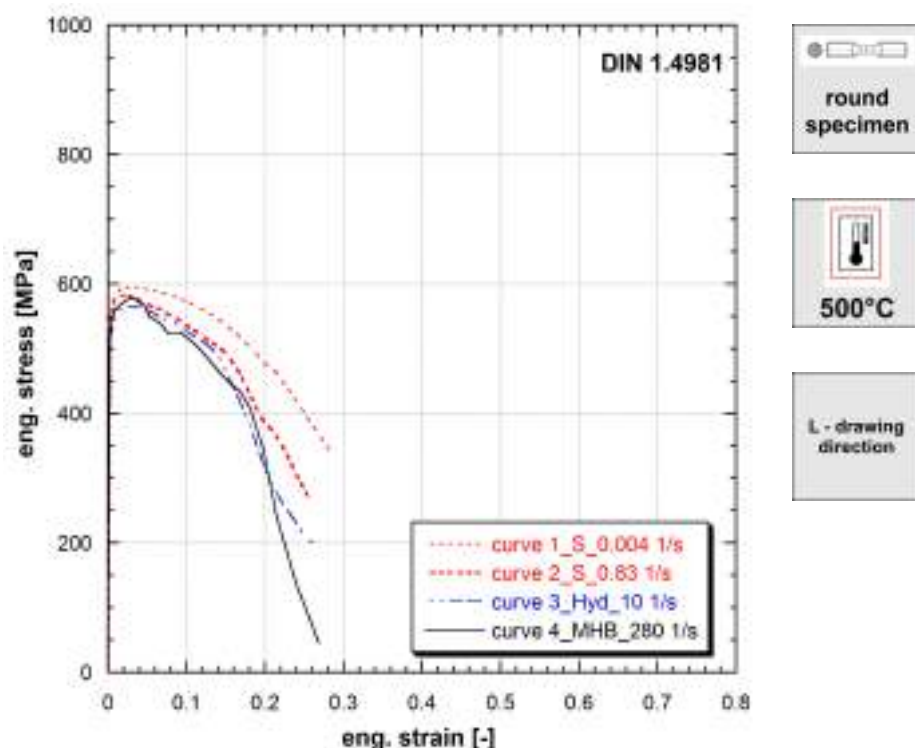


**Figure 9.192:** Stress vs strain curves of DIN 1.4981

Strain rate [1/s]	Yield stress [MPa]	Ultimate tensile strength [MPa]	Uniform strain [-]	Fracture stress [MPa]	Fracture strain [-]
0.004	564	595	0.020	343	0.280
0.83	551	582	0.020	273	0.250
10	527	566	0.044	188	0.270
280	538	579	0.029	45	0.270

**Table 192:** Mechanical properties of DIN 1.4981

Published in (Albertini and Montagnani, 1977), (Albertini and Montagnani, 1981b), (Albertini and Montagnani, 1981a).

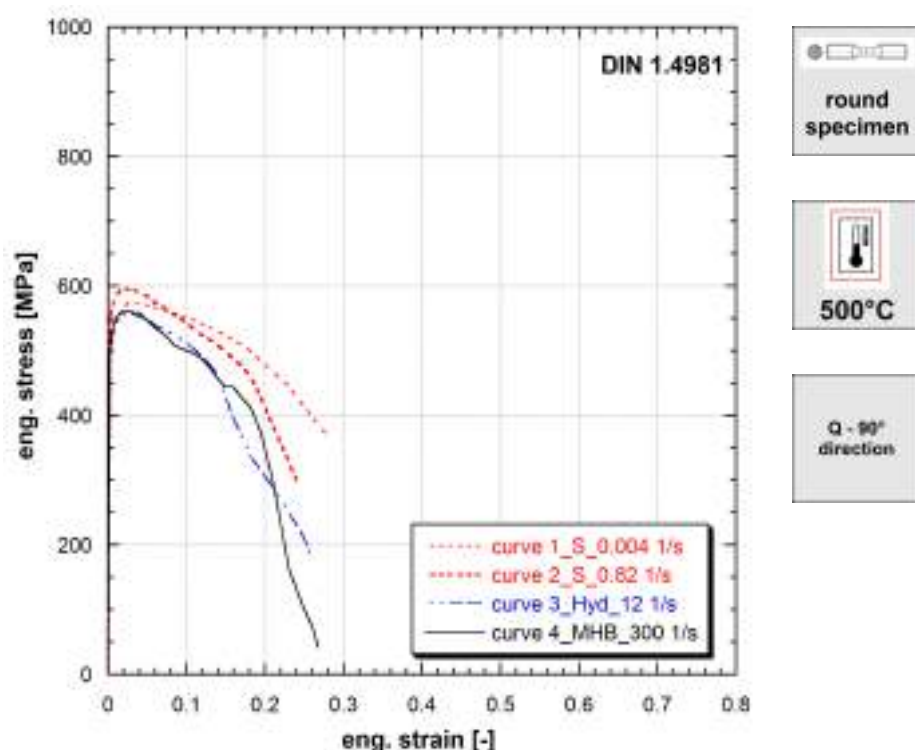


**Figure 9.193:** Stress vs strain curves of DIN 1.4981

Strain rate [1/s]	Yield stress [MPa]	Ultimate tensile strength [MPa]	Uniform strain [-]	Fracture stress [MPa]	Fracture strain [-]
0.004	506	574	0.026	367	0.280
0.82	566	596	0.020	300	0.240
12	516	556	0.024	174	0.260
300	521	562	0.029	41	0.268

**Table 193:** Mechanical properties of DIN 1.4981

Published in (Albertini and Montagnani, 1977).

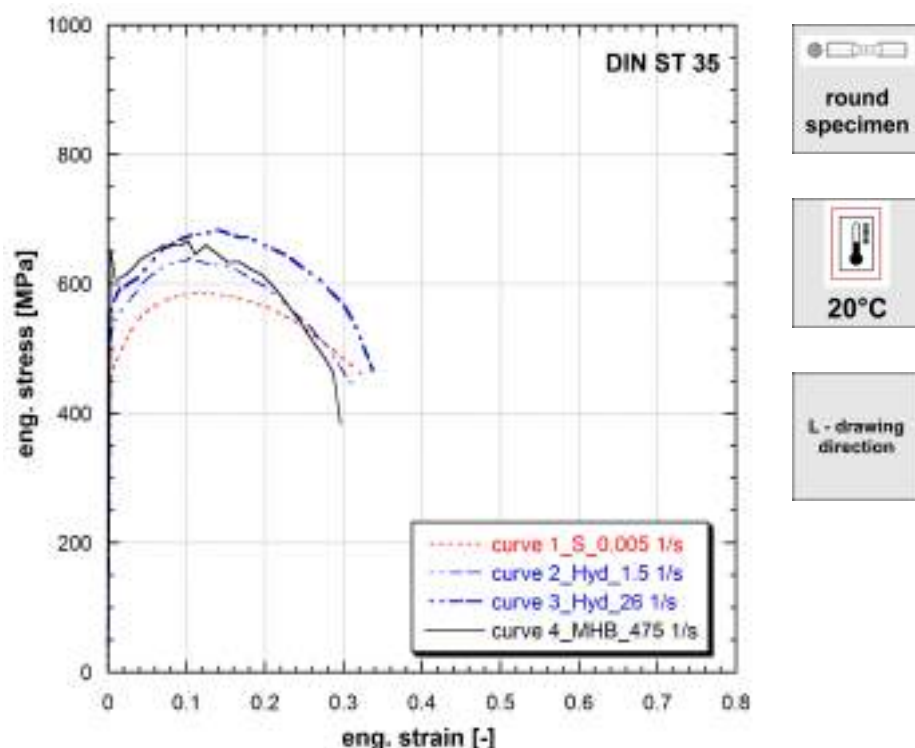


**Figure 9.194:** Stress vs strain curves of DIN ST 35

Strain rate [1/s]	Yield stress [MPa]	Ultimate tensile strength [MPa]	Uniform strain [-]	Fracture stress [MPa]	Fracture strain [-]
0.005	456	585	0.110	462	0.320
1.5	520	640	0.100	446	0.310
26	562	683	0.140	466	0.330
475	640	666	0.100	383	0.290

**Table 194:** Mechanical properties of DIN ST 35

Published in (Albertini and Montagnani, 1977).

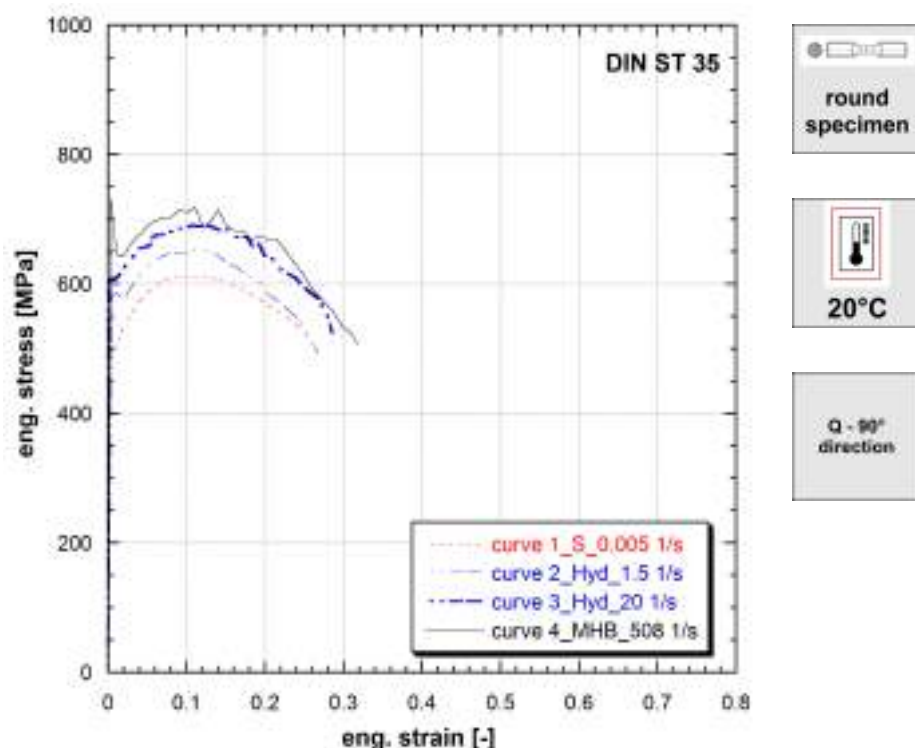


**Figure 9.195:** Stress vs strain curves of DIN ST 35

Strain rate [1/s]	Yield stress [MPa]	Ultimate tensile strength [MPa]	Uniform strain [-]	Fracture stress [MPa]	Fracture strain [-]
0.005	487	612	0.095	522	0.250
1.5	576	651	0.120	494	0.270
20	607	691	0.100	524	0.280
508	711	718	0.110	506	0.320

**Table 195:** Mechanical properties of DIN ST 35

Published in (Albertini and Montagnani, 1977).

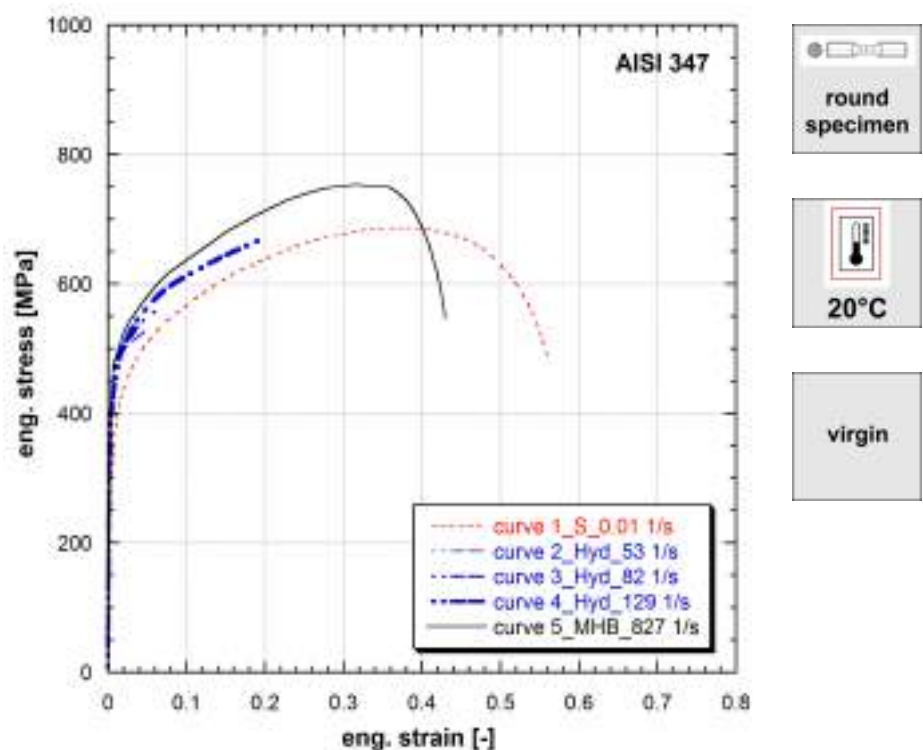


**Figure 9.196:** Stress vs strain curves of AISI 347

Strain rate [1/s]	Yield stress [MPa]	Ultimate tensile strength [MPa]	Uniform strain [-]	Fracture stress [MPa]	Fracture strain [-]
0.01	311	687	0.378	488	0.560
53	380	-	-	-	-
82	378	-	-	-	-
129	398	-	-	-	-
827	427	754	0.315	546	0.430

**Table 196:** Mechanical properties of AISI 347

Published in (Albertini and Montagnani, 1974).

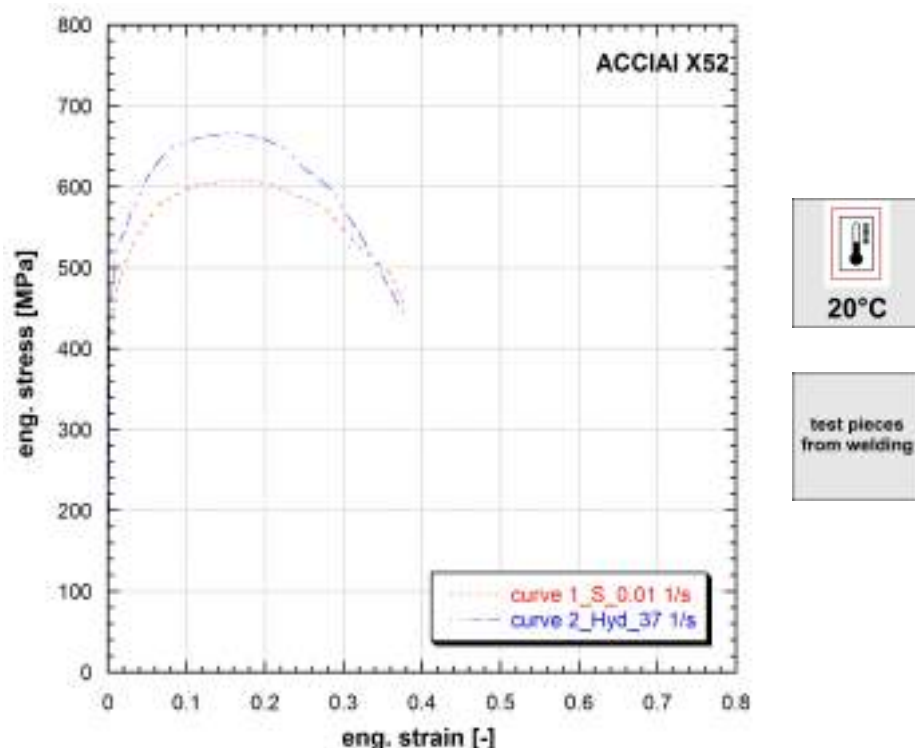


**Figure 9.197:** Stress vs strain curves of Steel X52

Strain rate [1/s]	Yield stress [MPa]	Ultimate tensile strength [MPa]	Uniform strain [-]	Fracture stress [MPa]	Fracture strain [-]
0.01	424	608	0.167	457	0.376
37	465	666	0.169	445	0.376

**Table 197:** Mechanical properties of Steel X52

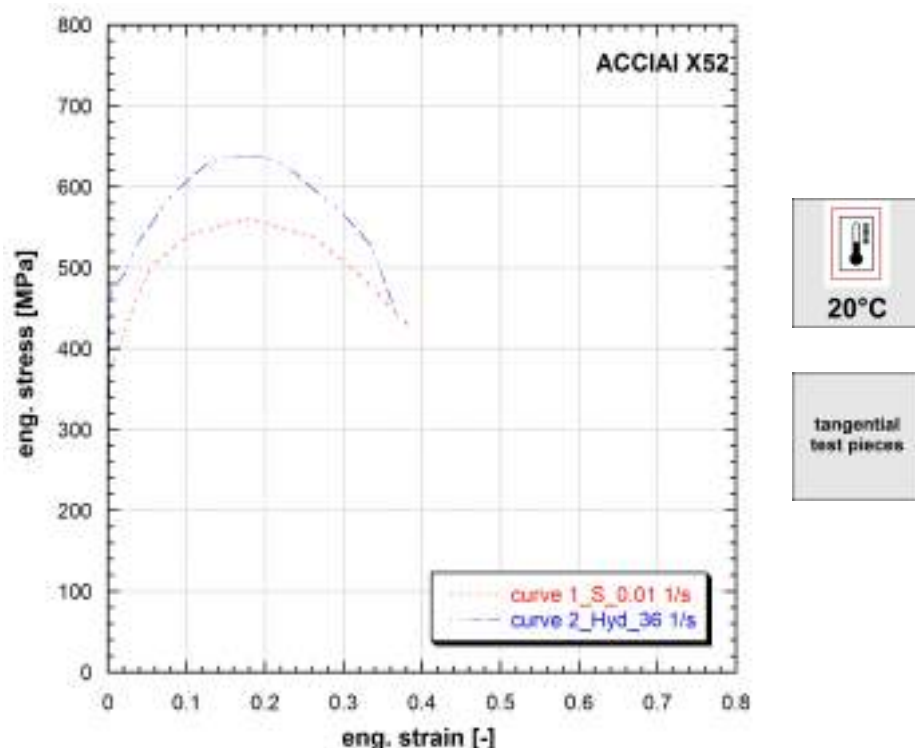


**Figure 9.198:** Stress vs strain curves of Steel X52

Strain rate [1/s]	Yield stress [MPa]	Ultimate tensile strength [MPa]	Uniform strain [-]	Fracture stress [MPa]	Fracture strain [-]
0.01	373	560	0.181	423	0.389
36	474	636	0.151	443	0.367

**Table 198:** Mechanical properties of Steel X52

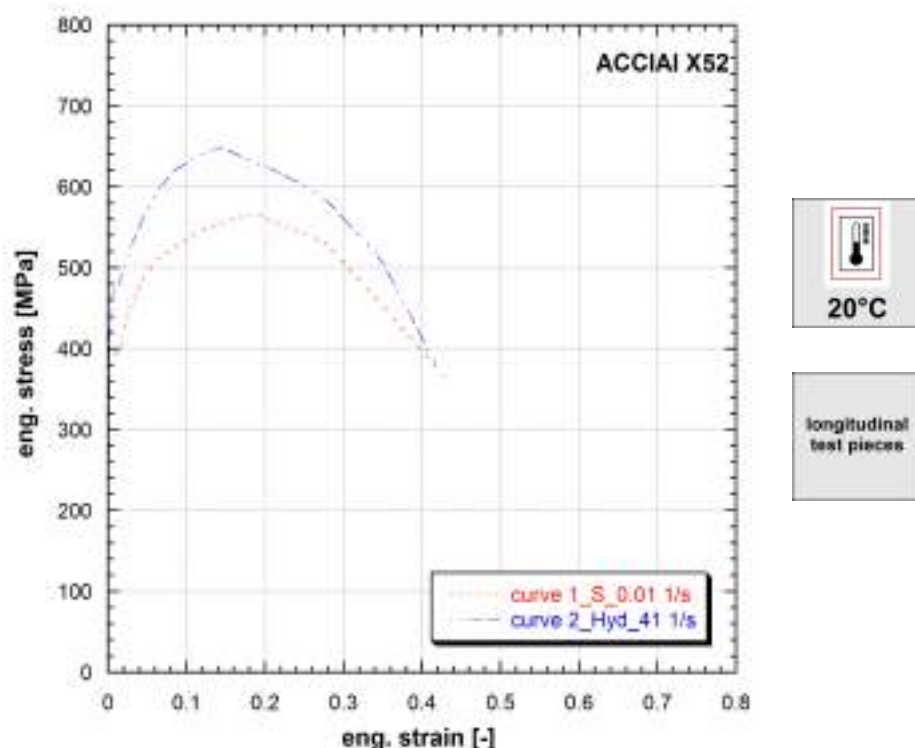


**Figure 9.199:** Stress vs strain curves of Steel X52

Strain rate [1/s]	Yield stress [MPa]	Ultimate tensile strength [MPa]	Uniform strain [-]	Fracture stress [MPa]	Fracture strain [-]
0.01	389	564	0.194	365	0.428
41	453	649	0.144	378	0.418

**Table 199:** Mechanical properties of Steel X52

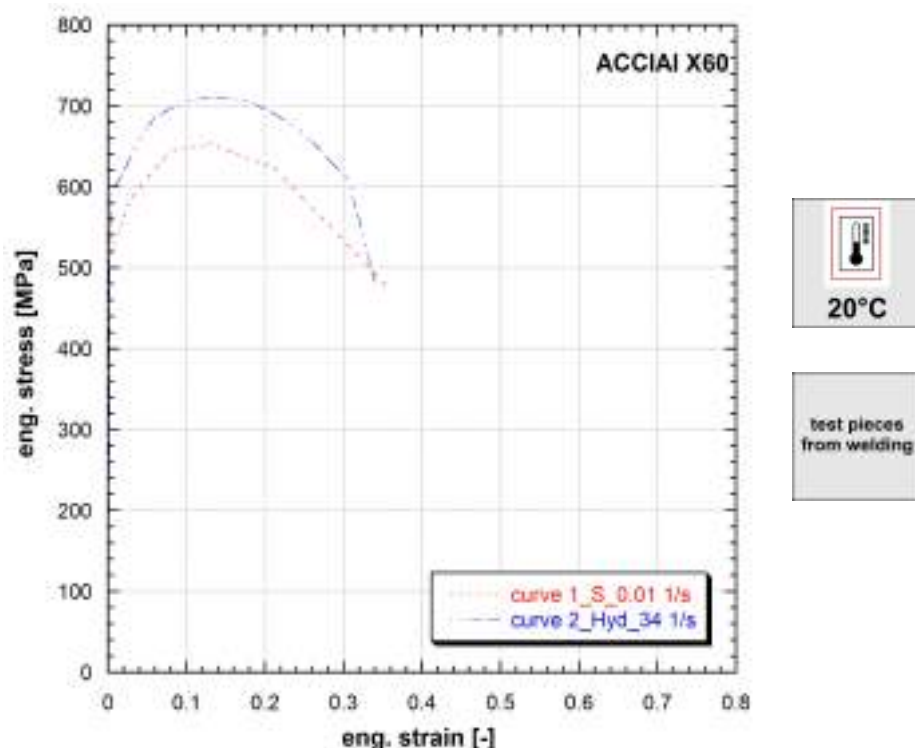


**Figure 9.200:** Stress vs strain curves of Steel X60

Strain rate [1/s]	Yield stress [MPa]	Ultimate tensile strength [MPa]	Uniform strain [-]	Fracture stress [MPa]	Fracture strain [-]
0.01	518	653	0.131	469	0.364
34	596	710	0.144	482	0.340

**Table 200:** Mechanical properties of Steel X60

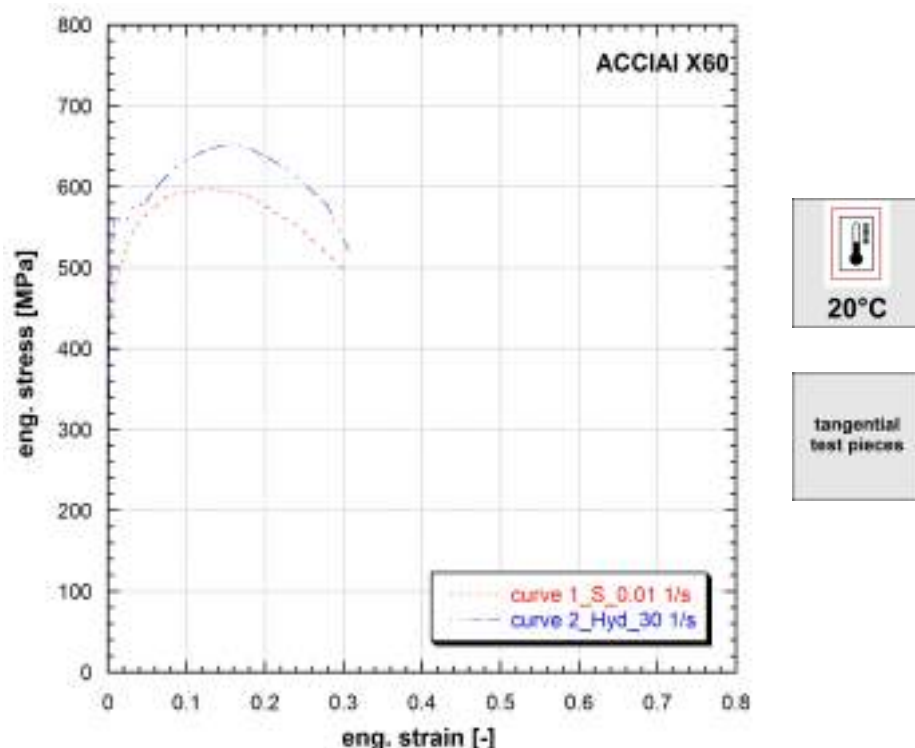


**Figure 9.201:** Stress vs strain curves of Steel X60

Strain rate [1/s]	Yield stress [MPa]	Ultimate tensile strength [MPa]	Uniform strain [-]	Fracture stress [MPa]	Fracture strain [-]
0.01	443	599	0.126	498	0.300
30	509	652	0.149	522	0.306

**Table 201:** Mechanical properties of Steel X60

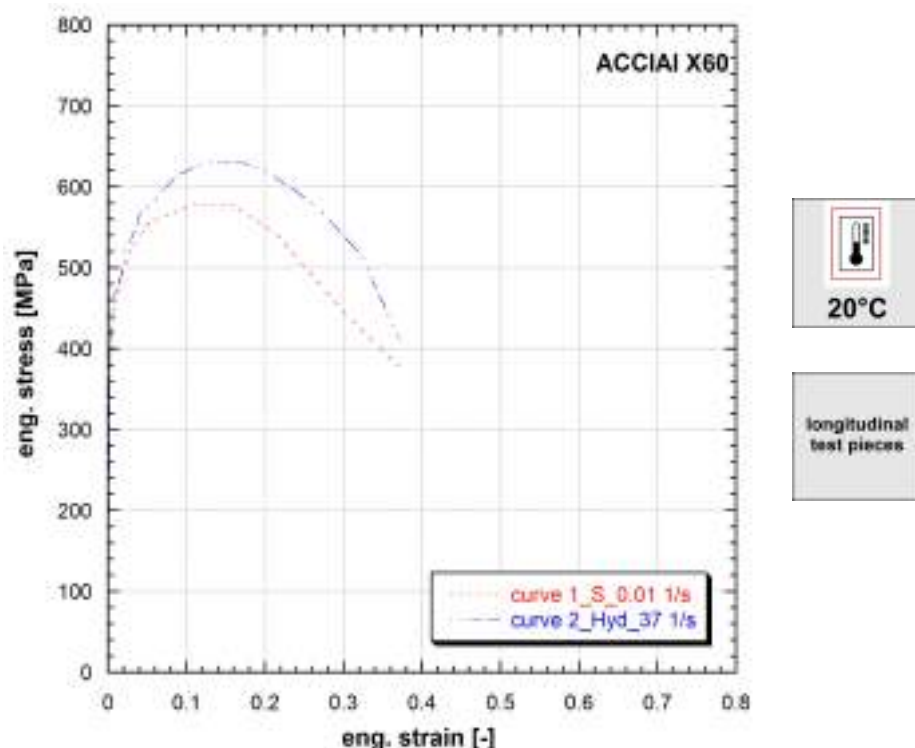


**Figure 9.202:** Stress vs strain curves of Steel X60

Strain rate [1/s]	Yield stress [MPa]	Ultimate tensile strength [MPa]	Uniform strain [-]	Fracture stress [MPa]	Fracture strain [-]
0.01	414	577	0.157	378	0.371
37	422	630	0.129	411	0.371

**Table 202:** Mechanical properties of Steel X60

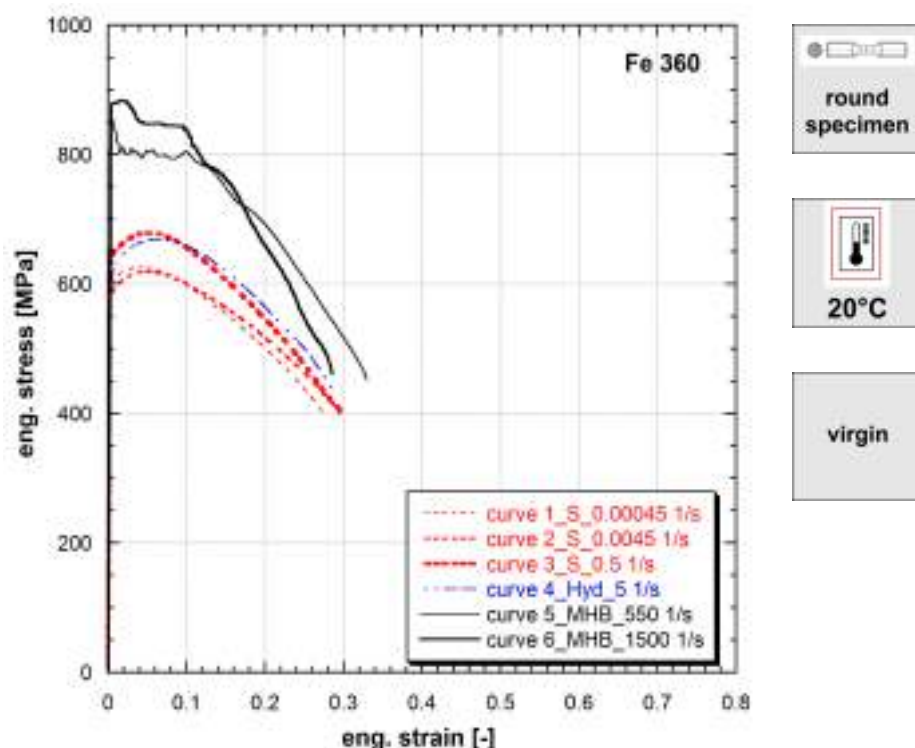


**Figure 9.203:** Stress vs strain curves of Fe360

Strain rate [1/s]	Yield stress [MPa]	Ultimate tensile strength [MPa]	Uniform strain [-]	Fracture stress [MPa]	Fracture strain [-]
0.00045	577	625	0.034	401	0.274
0.0045	582	619	0.047	400	0.295
0.5	639	679	0.047	401	0.299
5	609	668	0.056	433	0.287
550	851	854	0.005	451	0.330
1500	879	883	0.016	461	0.285

**Table 203:** Mechanical properties of Fe360

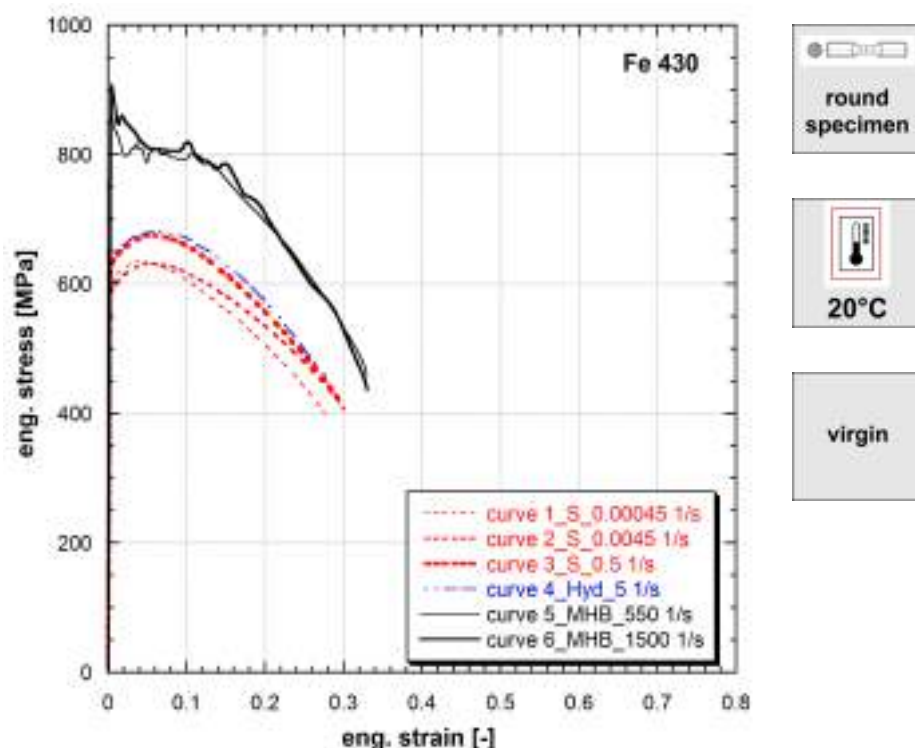


**Figure 9.204:** Stress vs strain curves of Fe430

Strain rate [1/s]	Yield stress [MPa]	Ultimate tensile strength [MPa]	Uniform strain [-]	Fracture stress [MPa]	Fracture strain [-]
0.00045	594	634	0.040	400	0.276
0.0045	585	631	0.049	407	0.300
0.5	624	675	0.050	414	0.299
1	638	681	0.061	453	0.280
550	857	862	0.005	457	0.330
1500	896	908	0.004	436	0.330

**Table 204:** Mechanical properties of Fe430

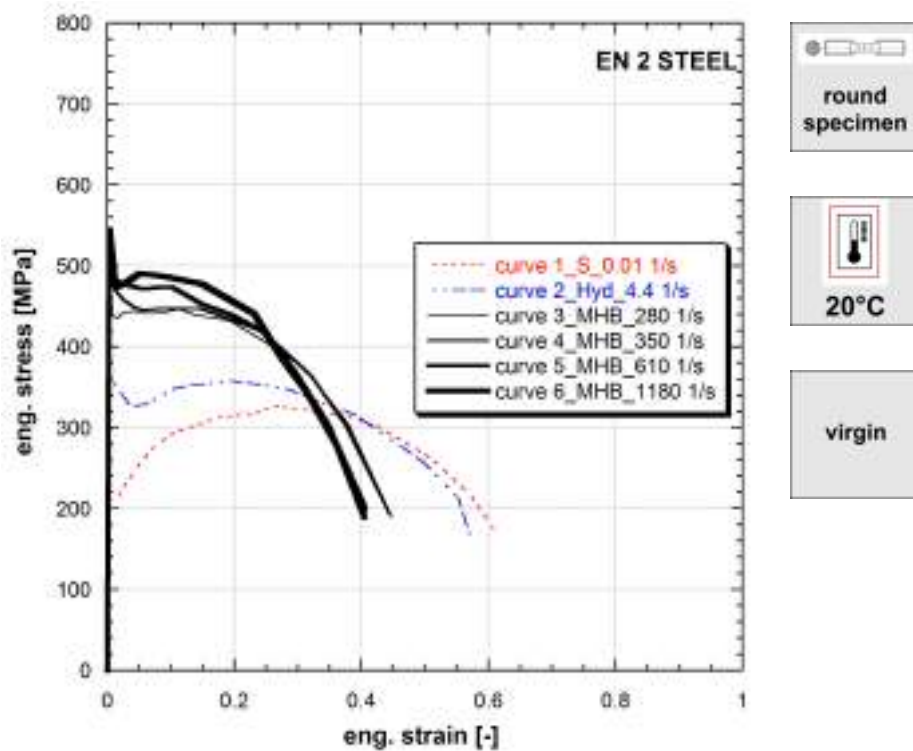


**Figure 9.205:** Stress vs strain curves of EN 2 STEEL

Strain rate [1/s]	Yield stress [MPa]	Ultimate tensile strength [MPa]	Uniform strain [-]	Fracture stress [MPa]	Fracture strain [-]
0.01	206	326	0.267	175	0.608
4.4	365	358	0.197	157	0.574
280	493	447	0.113	189	0.448
350	519	447	0.085	193	0.445
610	528	474	0.041	199	0.407
1180	538	490	0.050	189	0.405

**Table 205:** Mechanical properties of EN 2 STEEL

Published in (Albertini and Montagnani, 1976).

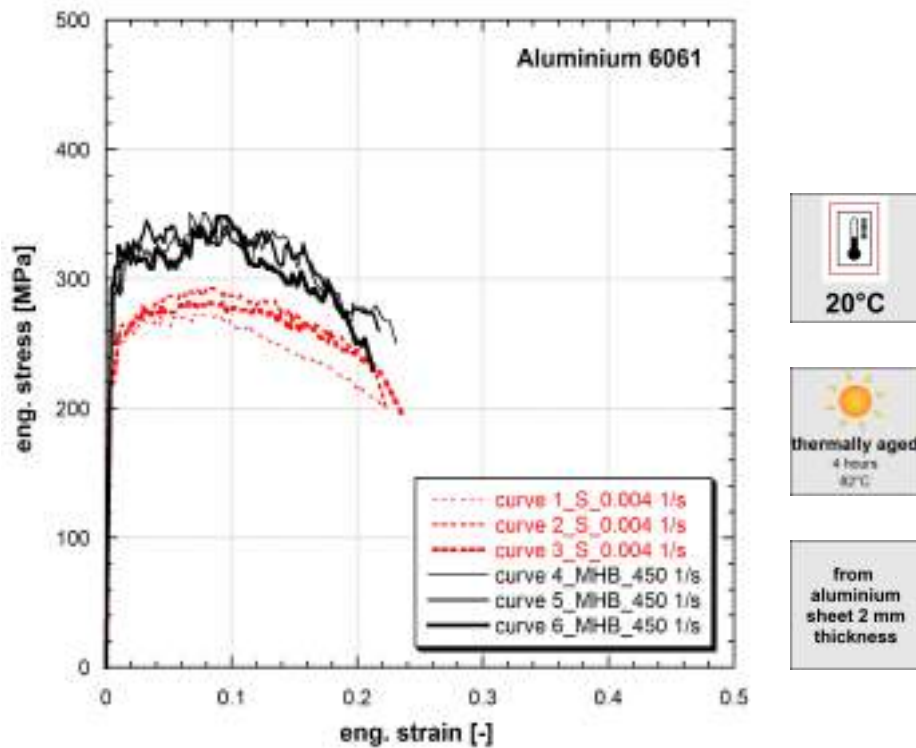


**Figure 9.206:** Stress vs strain curves of Aluminium 6061

Strain rate [1/s]	Yield stress [MPa]	Ultimate tensile strength [MPa]	Uniform strain [-]	Fracture stress [MPa]	Fracture strain [-]
0.004	243	272	0.064	203	0.219
0.004	218	293	0.081	197	0.224
0.004	225	284	0.066	196	0.235
450	251	351	0.066	250	0.231
450	299	345	0.032	260	0.217
450	296	348	0.090	229	0.212

**Table 206:** Mechanical properties of Aluminium 6061

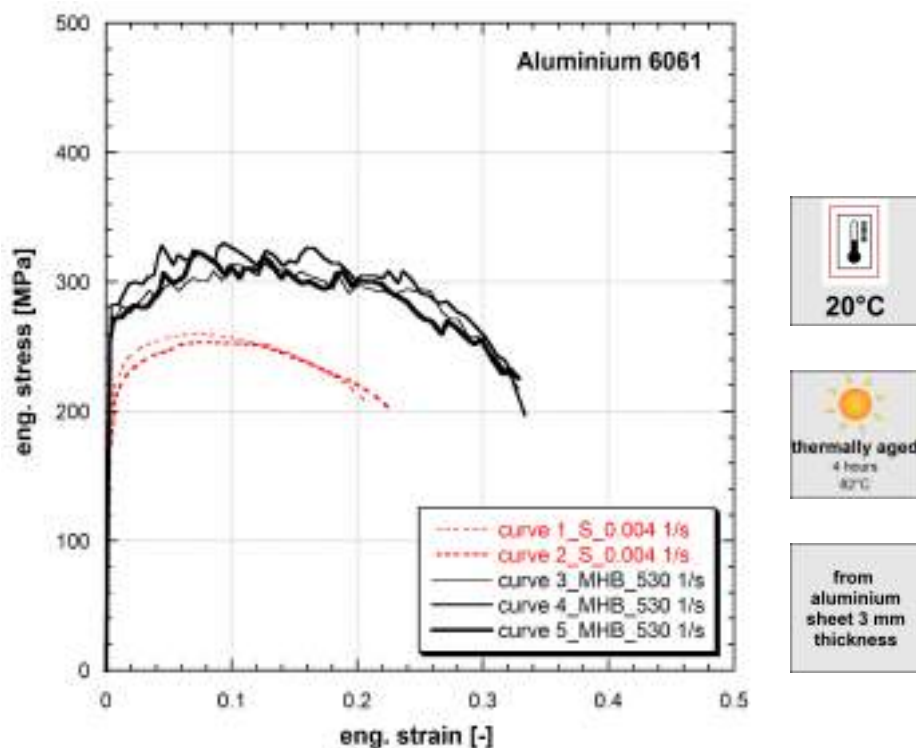


**Figure 9.207:** Stress vs strain curves of Aluminium 6061

Strain rate [1/s]	Yield stress [MPa]	Ultimate tensile strength [MPa]	Uniform strain [-]	Fracture stress [MPa]	Fracture strain [-]
0.004	206	260	0.076	208	0.207
0.004	176	253	0.070	203	0.224
530	265	314	0.126	217	0.328
530	282	330	0.090	197	0.330
530	268	324	0.070	225	0.330

**Table 207:** Mechanical properties of Aluminium 6061

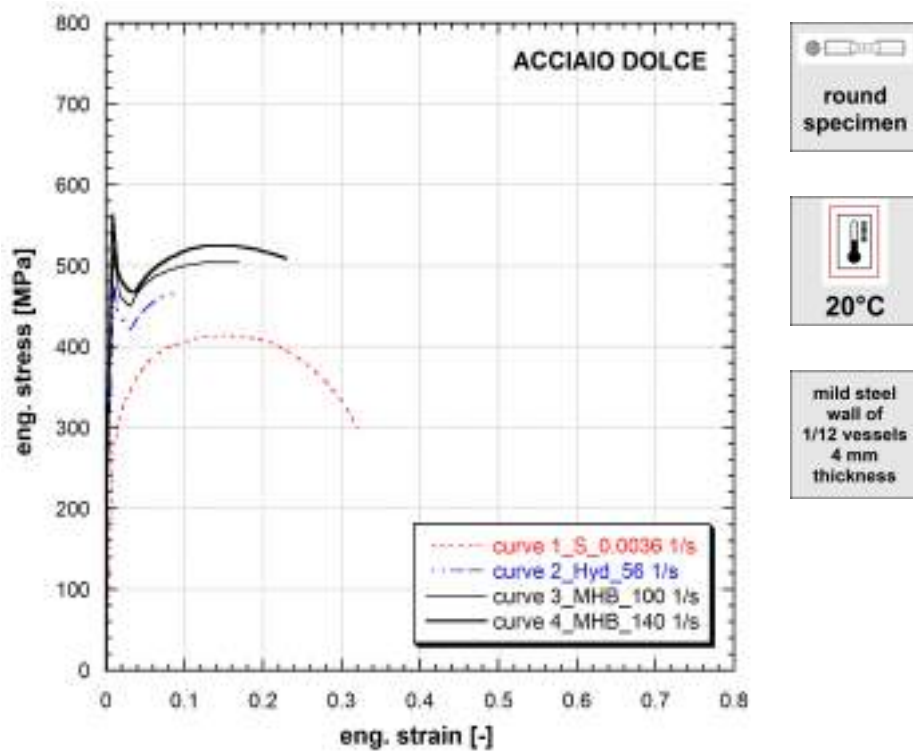


**Figure 9.208:** Stress vs strain curves of Mild Steel 4mm

Strain rate [1/s]	Yield stress [MPa]	Ultimate tensile strength [MPa]	Uniform strain [-]	Fracture stress [MPa]	Fracture strain [-]
0.0038	288	414	0.140	298	0.320
56	-	466	0.092	-	-
100	-	505	0.140	-	-
140	-	525	0.139	-	-

**Table 208:** Mechanical properties of Mild Steel 4mm

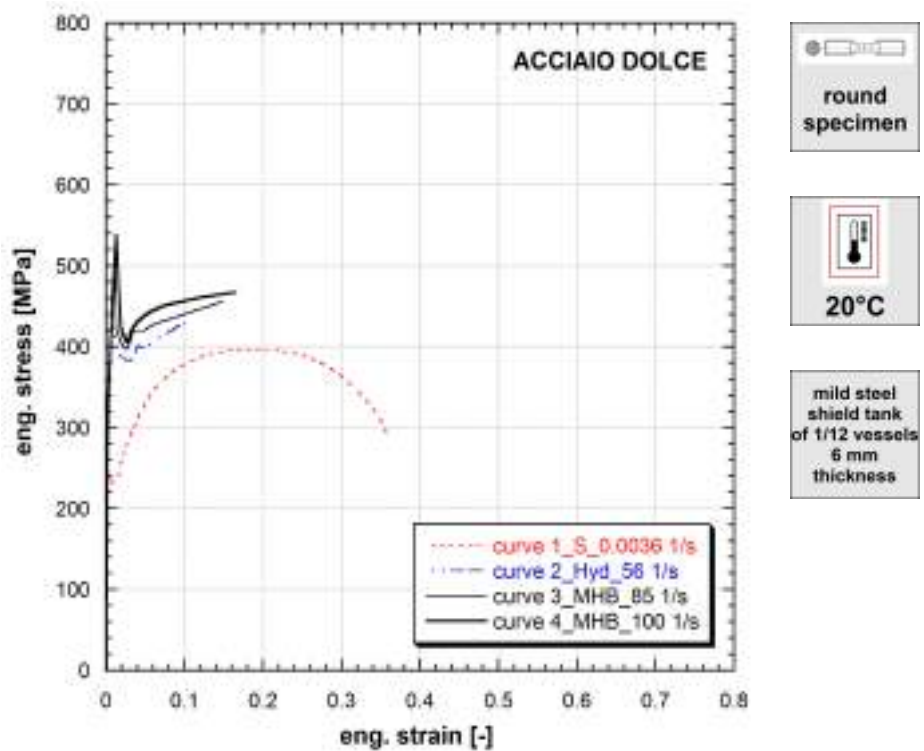


**Figure 9.209:** Stress vs strain curves of Mild Steel 6mm

Strain rate [1/s]	Yield stress [MPa]	Ultimate tensile strength [MPa]	Uniform strain [-]	Fracture stress [MPa]	Fracture strain [-]
0.0037	246	396	0.170	294	0.350
56	359	430	0.100	-	-
85	373	455	0.150	-	-
100	360	467	0.160	-	-

**Table 209:** Mechanical properties of Mild Steel 6mm

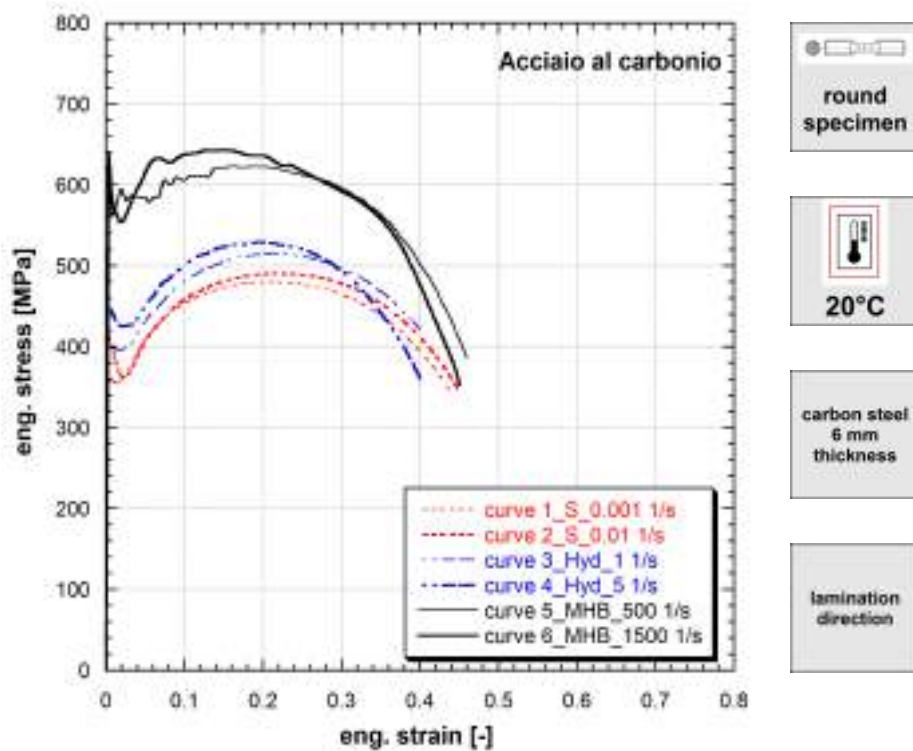


**Figure 9.210:** Stress vs strain curves of Carbon steel

Strain rate [1/s]	Yield stress [MPa]	Ultimate tensile strength [MPa]	Uniform strain [-]	Fracture stress [MPa]	Fracture strain [-]
0.001	361	480	0.200	342	0.440
0.01	408	491	0.220	345	0.450
1	405	515	0.210	422	0.400
5	454	530	0.190	361	0.400
500	596	623	0.160	386	0.460
1500	616	643	0.140	353	0.450

**Table 210:** Mechanical properties of Carbon steel

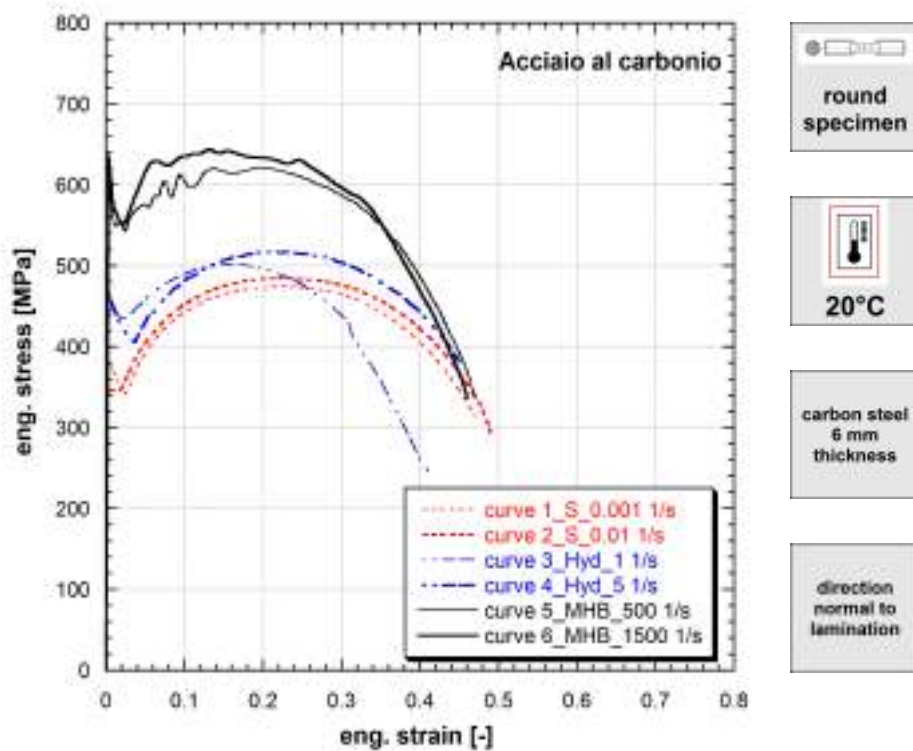


**Figure 9.211:** Stress vs strain curves of Carbon steel

Strain rate [1/s]	Yield stress [MPa]	Ultimate tensile strength [MPa]	Uniform strain [-]	Fracture stress [MPa]	Fracture strain [-]
0.001	382	474	0.237	313	0.470
0.01	345	485	0.233	294	0.490
1	443	502	0.157	247	0.410
5	463	517	0.233	382	0.450
500	598	620	0.214	336	0.470
1500	618	644	0.133	337	0.460

**Table 211:** Mechanical properties of Carbon steel

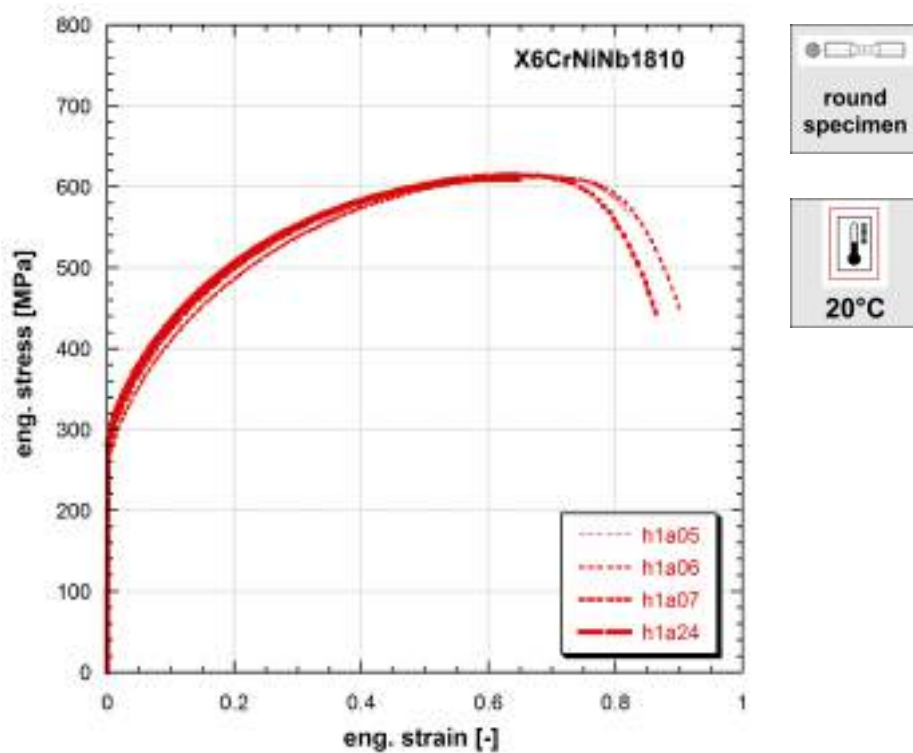


**Figure 9.212:** Stress vs strain curves of AUSTENITIC X6CrNiNb1810

Strain rate [1/s]	Yield stress [MPa]	Ultimate tensile strength [MPa]	Uniform strain [-]	Fracture stress [MPa]	Fracture strain [-]
0.002	257	615	0.649	566	0.821
0.002	267	614	0.677	450	0.900
0.002	283	616	0.627	436	0.867
0.002	296	611	0.623	609	0.648

**Table 212:** Mechanical properties of AUSTENITIC X6CrNiNb1810

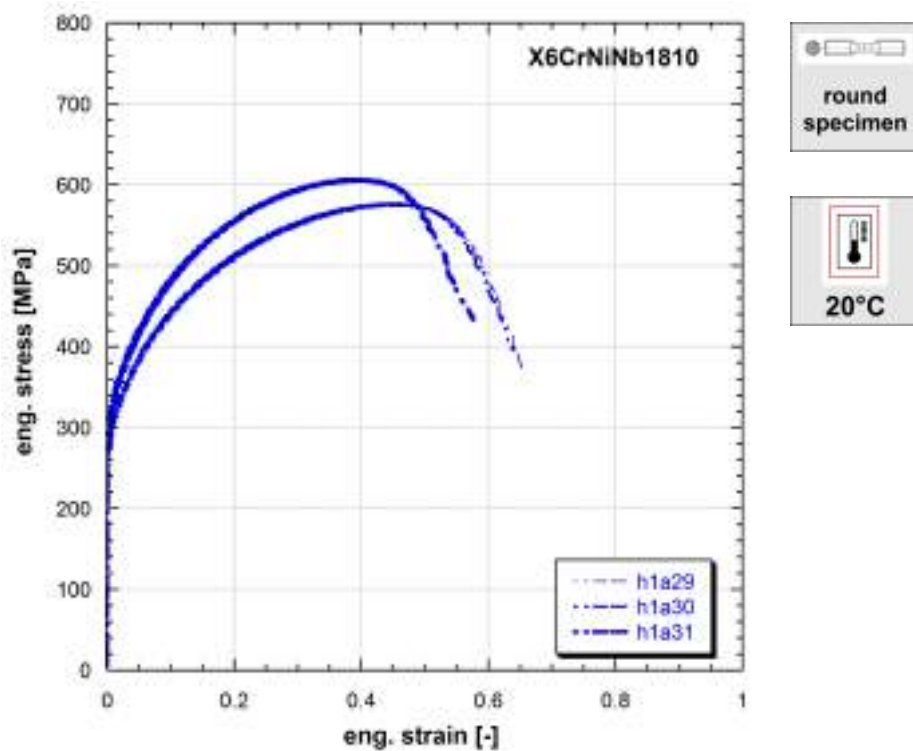


**Figure 9.213:** Stress vs strain curves of AUSTENITIC X6CrNiNb1810

Strain rate [1/s]	Yield stress [MPa]	Ultimate tensile strength [MPa]	Uniform strain [-]	Fracture stress [MPa]	Fracture strain [-]
0.1	270	576	0.458	374	0.653
0.1	285	577	0.463	395	0.640
0.1	300	607	0.382	433	0.577

**Table 213:** Mechanical properties of AUSTENITIC X6CrNiNb1810

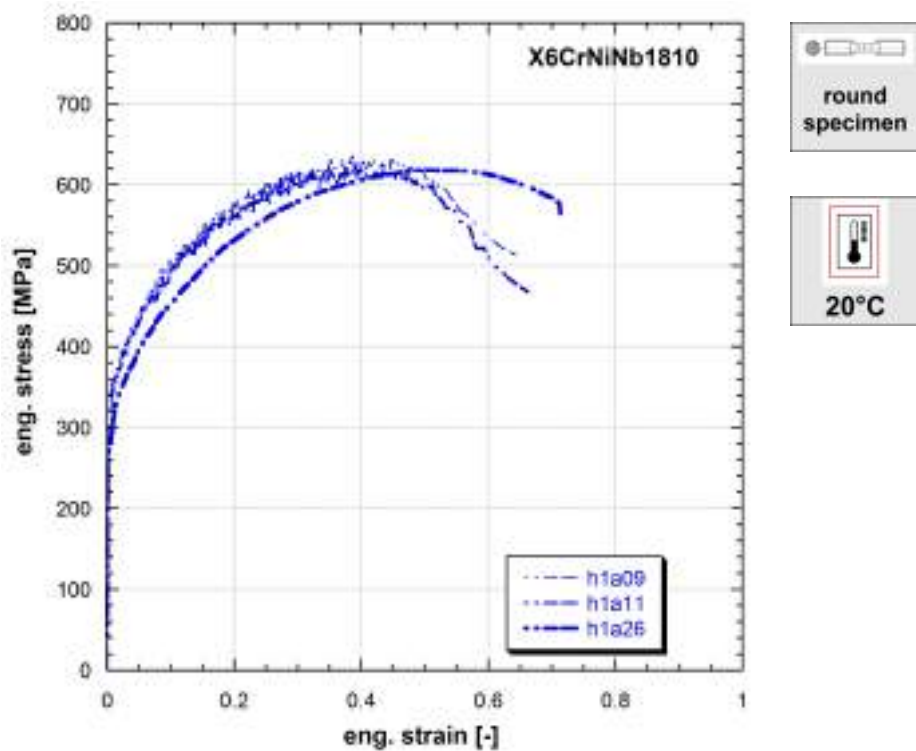


**Figure 9.214:** Stress vs strain curves of AUSTENITIC X6CrNiNb1810

Strain rate [1/s]	Yield stress [MPa]	Ultimate tensile strength [MPa]	Uniform strain [-]	Fracture stress [MPa]	Fracture strain [-]
10	322	636	0.386	513	0.643
10	297	624	0.388	468	0.662
10	274	618	0.494	564	0.713

**Table 214:** Mechanical properties of AUSTENITIC X6CrNiNb1810

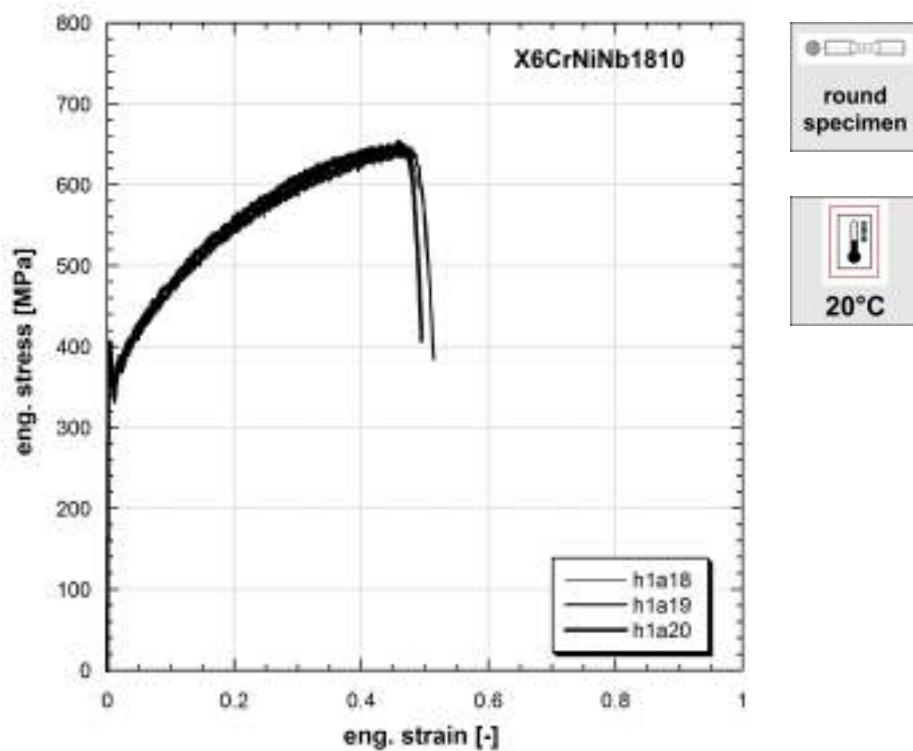


**Figure 9.215:** Stress vs strain curves of AUSTENITIC X6CrNiNb1810

Strain rate [1/s]	Yield stress [MPa]	Ultimate tensile strength [MPa]	Uniform strain [-]	Fracture stress [MPa]	Fracture strain [-]
200	383	641	0.457	430	0.511
200	381	648	0.468	384	0.514
200	405	653	0.458	407	0.495

**Table 215:** Mechanical properties of AUSTENITIC X6CrNiNb1810

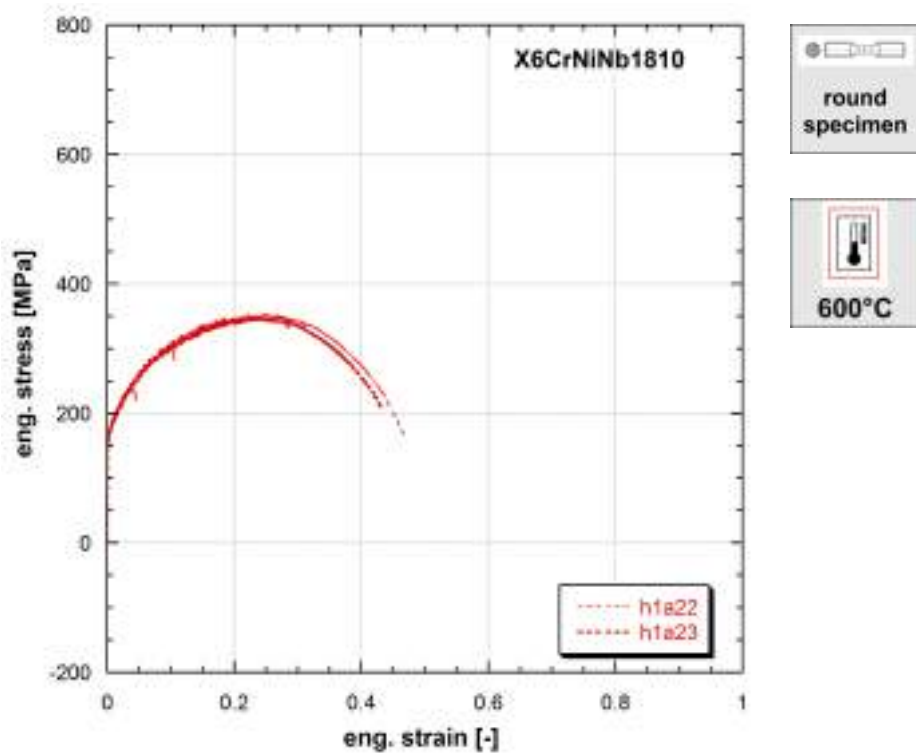


**Figure 9.216:** Stress vs strain curves of AUSTENITIC X6CrNiNb1810

Strain rate [1/s]	Yield stress [MPa]	Ultimate tensile strength [MPa]	Uniform strain [-]	Fracture stress [MPa]	Fracture strain [-]
0.002	168	353	0.248	168	0.466
0.002	167	346	0.230	204	0.433

**Table 216:** Mechanical properties of AUSTENITIC X6CrNiNb1810

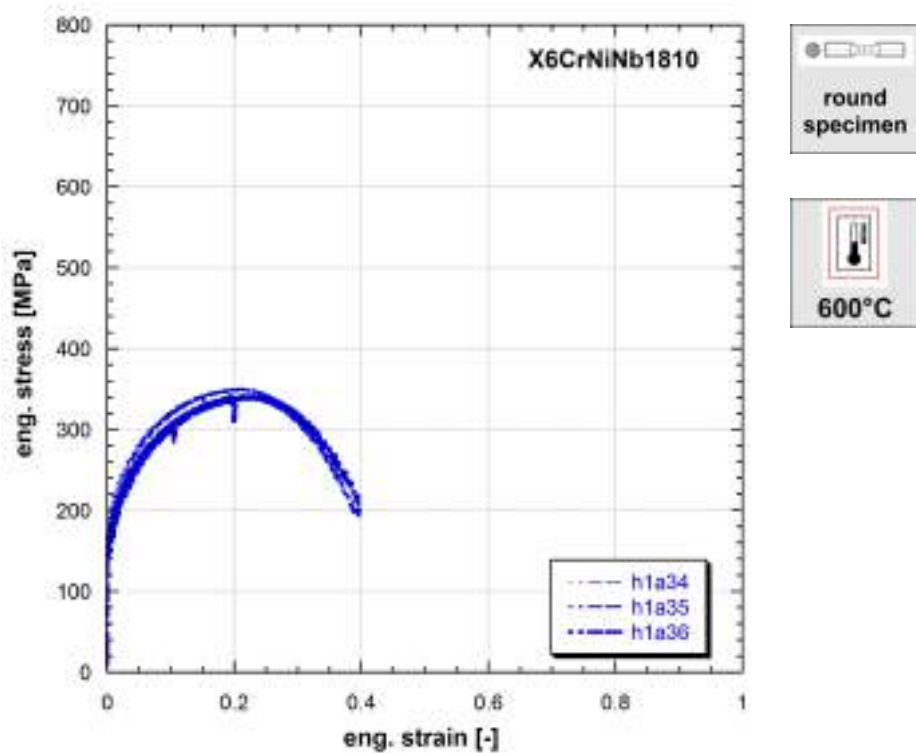


**Figure 9.217:** Stress vs strain curves of AUSTENITIC X6CrNiNb1810

Strain rate [1/s]	Yield stress [MPa]	Ultimate tensile strength [MPa]	Uniform strain [-]	Fracture stress [MPa]	Fracture strain [-]
0.1	185	351	0.210	196	0.389
0.1	168	341	0.213	193	0.397
0.1	163	342	0.230	199	0.397

**Table 217:** Mechanical properties of AUSTENITIC X6CrNiNb1810

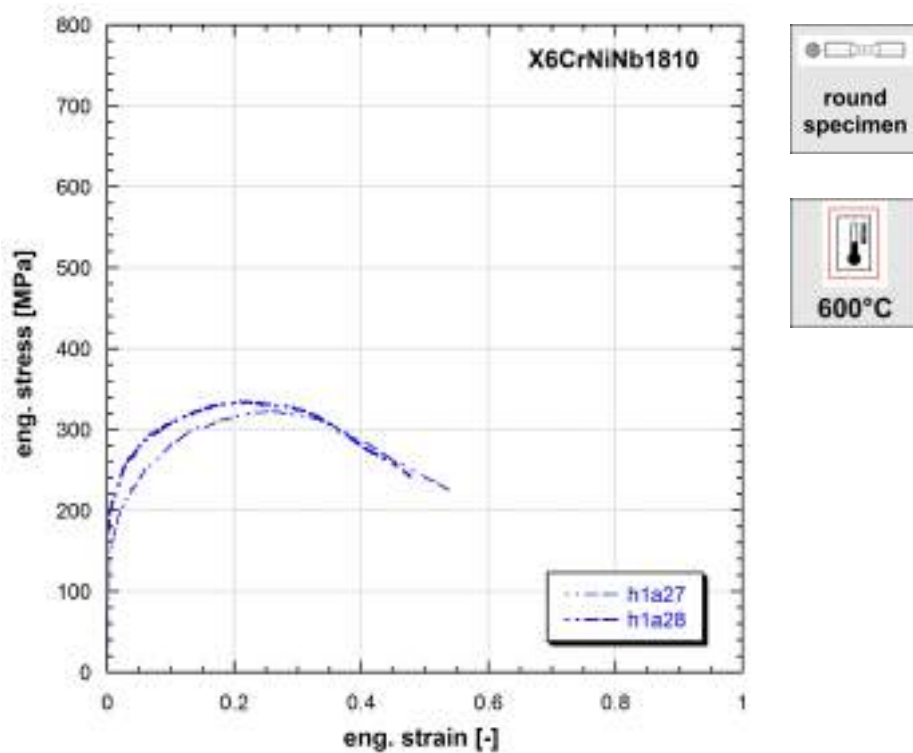


**Figure 9.218:** Stress vs strain curves of AUSTENITIC X6CrNiNb1810

Strain rate [1/s]	Yield stress [MPa]	Ultimate tensile strength [MPa]	Uniform strain [-]	Fracture stress [MPa]	Fracture strain [-]
10	147	323	0.254	225	0.538
10	190	335	0.211	242	0.477

**Table 218:** Mechanical properties of AUSTENITIC X6CrNiNb1810

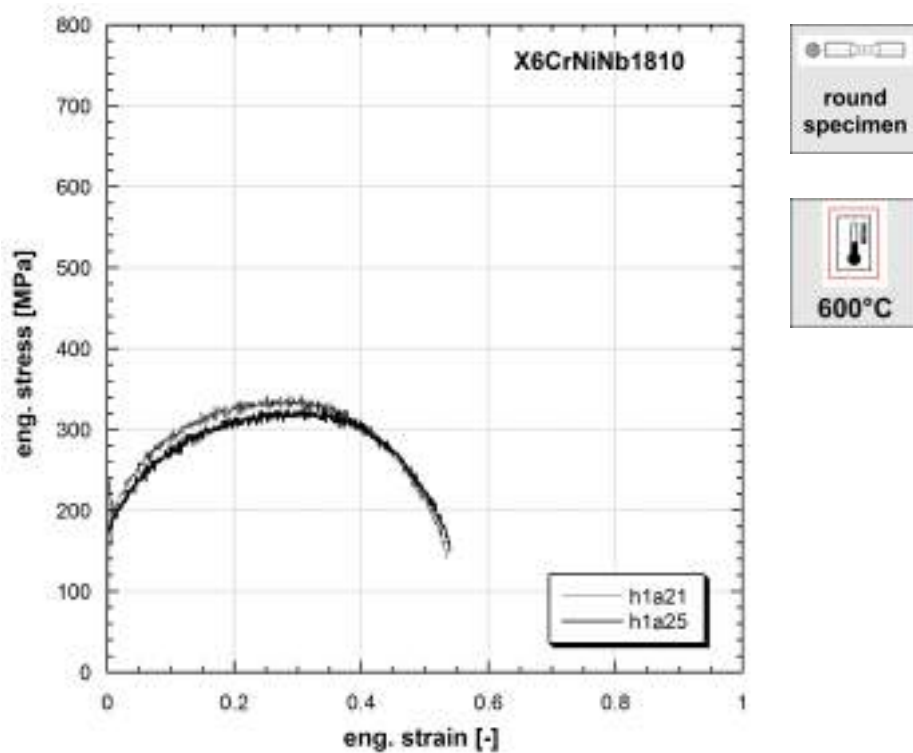


**Figure 9.219:** Stress vs strain curves of AUSTENITIC X6CrNiNb1810

Strain rate [1/s]	Yield stress [MPa]	Ultimate tensile strength [MPa]	Uniform strain [-]	Fracture stress [MPa]	Fracture strain [-]
250	237	342	0.307	140	0.534
250	176	326	0.310	150	0.539

**Table 219:** Mechanical properties of AUSTENITIC X6CrNiNb1810

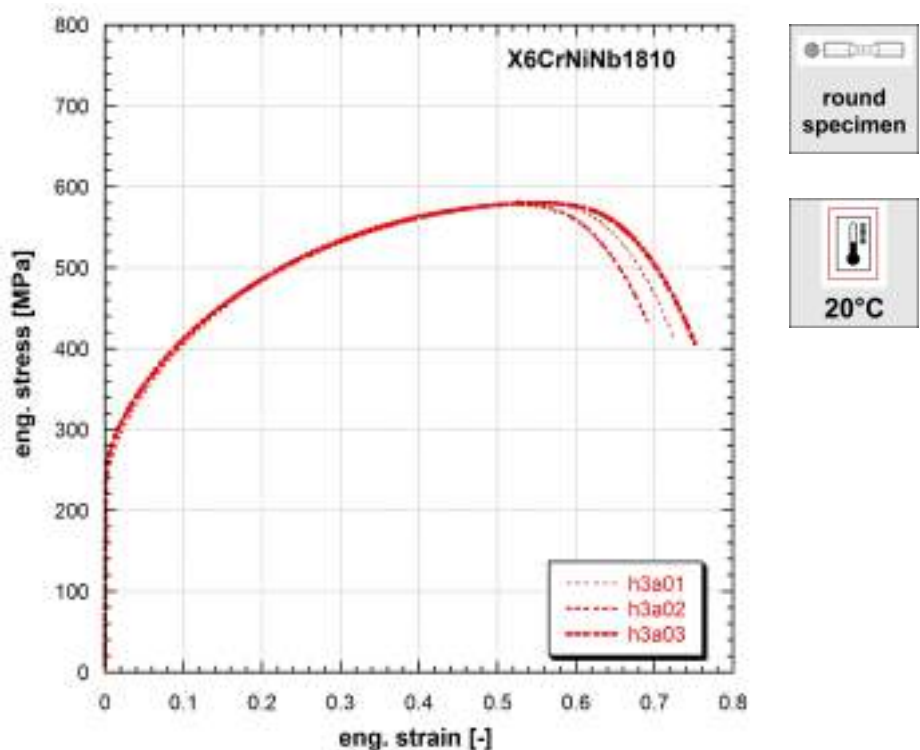


**Figure 9.220:** Stress vs strain curves of AUSTENITIC X6CrNiNb1810

**Note 9.220** Specimen diameter: 30 mm

Strain rate [1/s]	Yield stress [MPa]	Ultimate tensile strength [MPa]	Uniform strain [-]	Fracture stress [MPa]	Fracture strain [-]
0.001	238	581	0.541	409	0.725
0.001	250	578	0.512	434	0.691
0.001	260	582	0.557	406	0.751

**Table 220:** Mechanical properties of AUSTENITIC X6CrNiNb1810

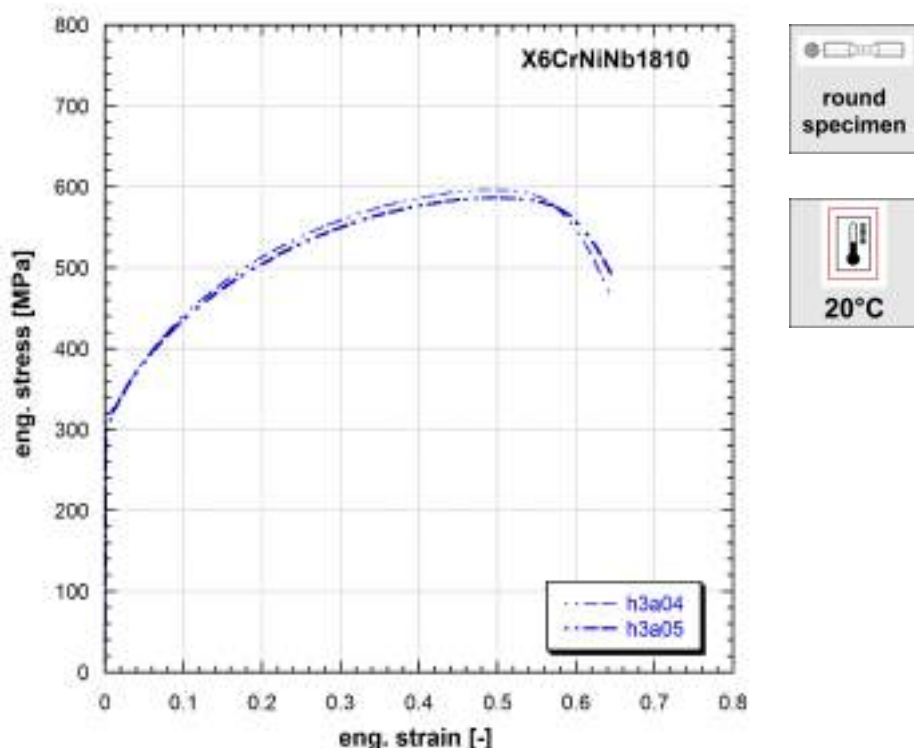


**Figure 9.221:** Stress vs strain curves of AUSTENITIC X6CrNiNb1810

**Note 9.221** Specimen diameter: 30 mm

Strain rate [1/s]	Yield stress [MPa]	Ultimate tensile strength [MPa]	Uniform strain [-]	Fracture stress [MPa]	Fracture strain [-]
0.1	318	596	0.498	463	0.645
0.1	303	587	0.501	489	0.646

**Table 221:** Mechanical properties of AUSTENITIC X6CrNiNb1810

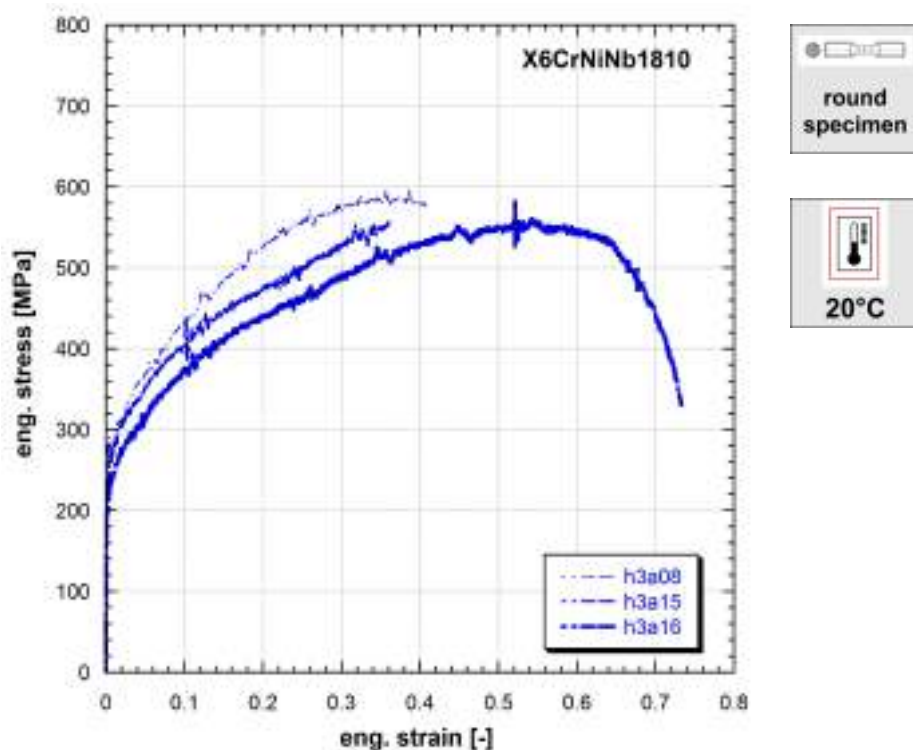


**Figure 9.222:** Stress vs strain curves of AUSTENITIC X6CrNiNb1810

**Note 9.222** Specimen diameter: 30 mm. Testing records were interrupted for h3a08 and h3a15.

Strain rate [1/s]	Yield stress [MPa]	Ultimate tensile strength [MPa]	Uniform strain [-]	Fracture stress [MPa]	Fracture strain [-]
25	280	596	0.356	-	-
25	227	557	0.472	-	-
25	204	581	0.521	330	0.730

**Table 222:** Mechanical properties of AUSTENITIC X6CrNiNb1810

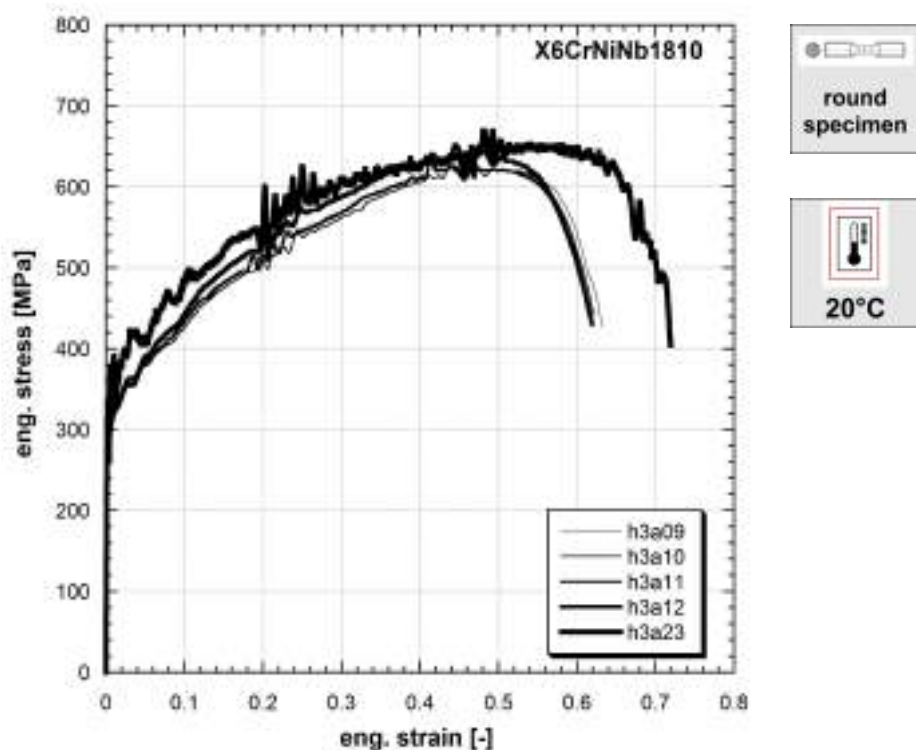


**Figure 9.223:** Stress vs strain curves of AUSTENITIC X6CrNiNb1810

**Note 9.223** Specimen diameter: 30 mm

Strain rate [1/s]	Yield stress [MPa]	Ultimate tensile strength [MPa]	Uniform strain [-]	Fracture stress [MPa]	Fracture strain [-]
150	282	636	0.415	426	0.632
150	270	629	0.438	442	0.621
150	279	632	0.414	569	0.576
150	280	652	0.445	430	0.619
150	280	670	0.482	404	0.719

**Table 223:** Mechanical properties of AUSTENITIC X6CrNiNb1810

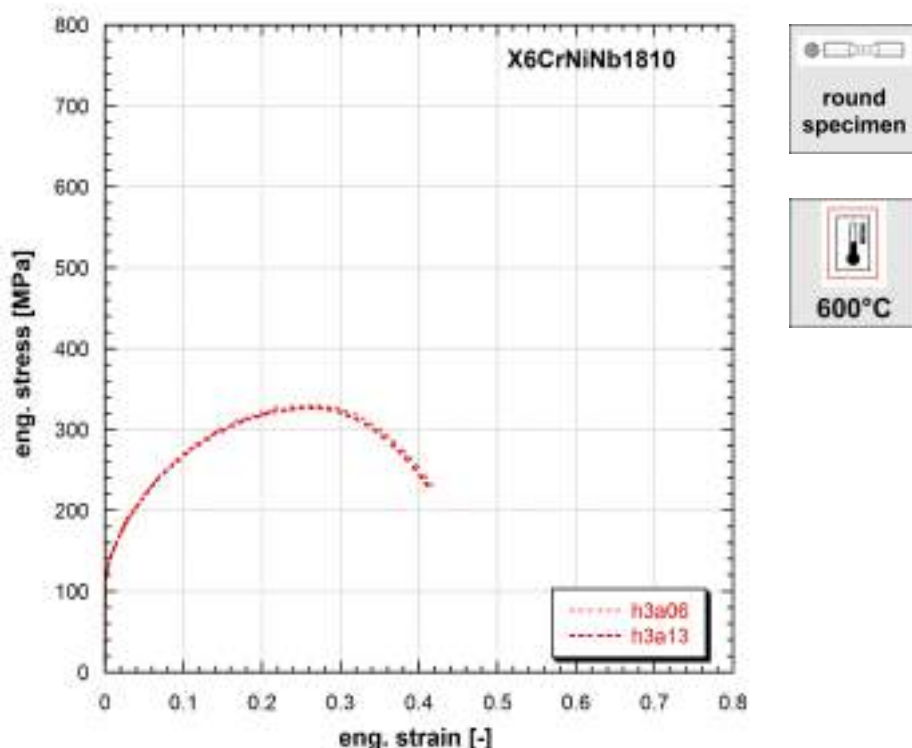


**Figure 9.224:** Stress vs strain curves of AUSTENITIC X6CrNiNb1810

**Note 9.224** Specimen diameter: 30 mm

Strain rate [1/s]	Yield stress [MPa]	Ultimate tensile strength [MPa]	Uniform strain [-]	Fracture stress [MPa]	Fracture strain [-]
0.001	122	329	0.270	230	0.417
0.001	124	326	0.261	230	0.411

**Table 224:** Mechanical properties of AUSTENITIC X6CrNiNb1810

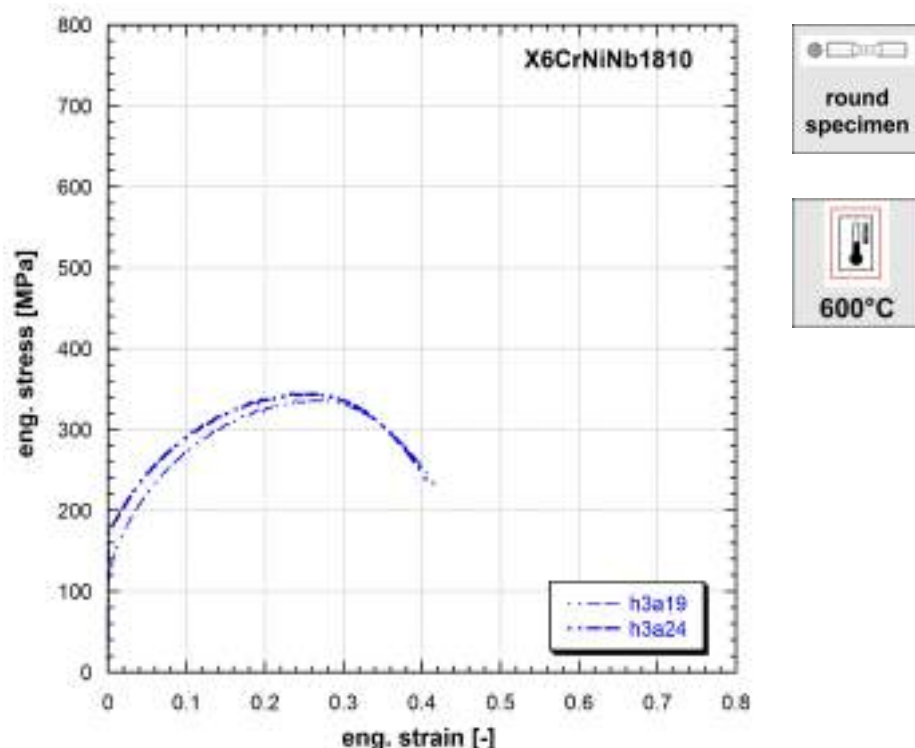


**Figure 9.225:** Stress vs strain curves of AUSTENITIC X6CrNiNb1810

**Note 9.225** Specimen diameter: 30 mm

Strain rate [1/s]	Yield stress [MPa]	Ultimate tensile strength [MPa]	Uniform strain [-]	Fracture stress [MPa]	Fracture strain [-]
0.1	125	336	0.266	231	0.416
0.1	177	344	0.237	336	0.407

**Table 225:** Mechanical properties of AUSTENITIC X6CrNiNb1810

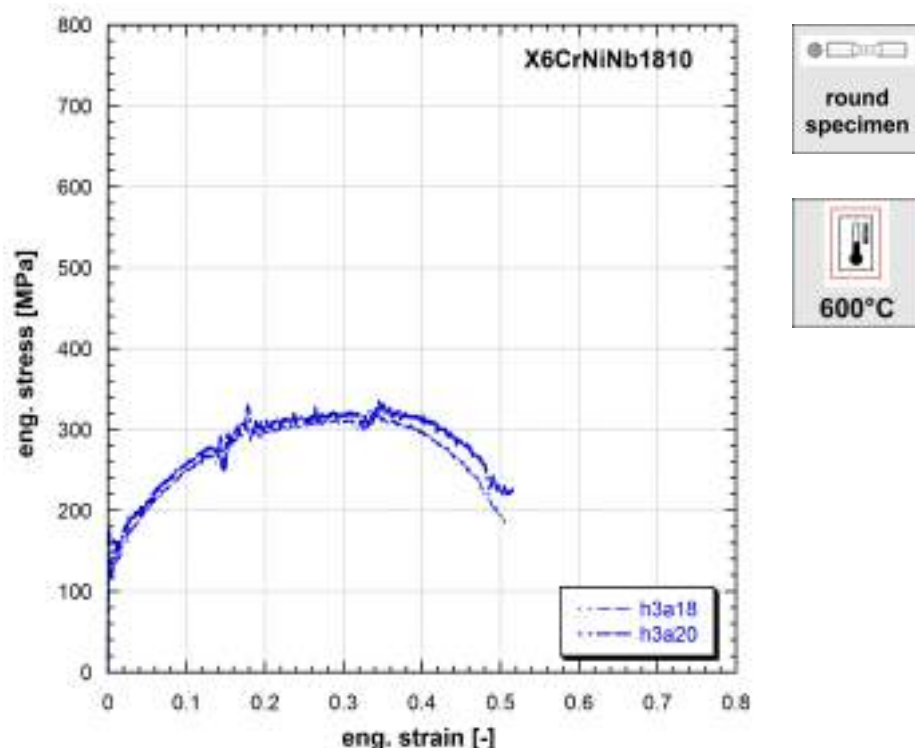


**Figure 9.226:** Stress vs strain curves of AUSTENITIC X6CrNiNb1810

**Note 9.226** Specimen diameter: 30 mm

Strain rate [1/s]	Yield stress [MPa]	Ultimate tensile strength [MPa]	Uniform strain [-]	Fracture stress [MPa]	Fracture strain [-]
50	132	322	0.345	185	0.505
50	152	335	0.345	226	0.516

**Table 226:** Mechanical properties of AUSTENITIC X6CrNiNb1810

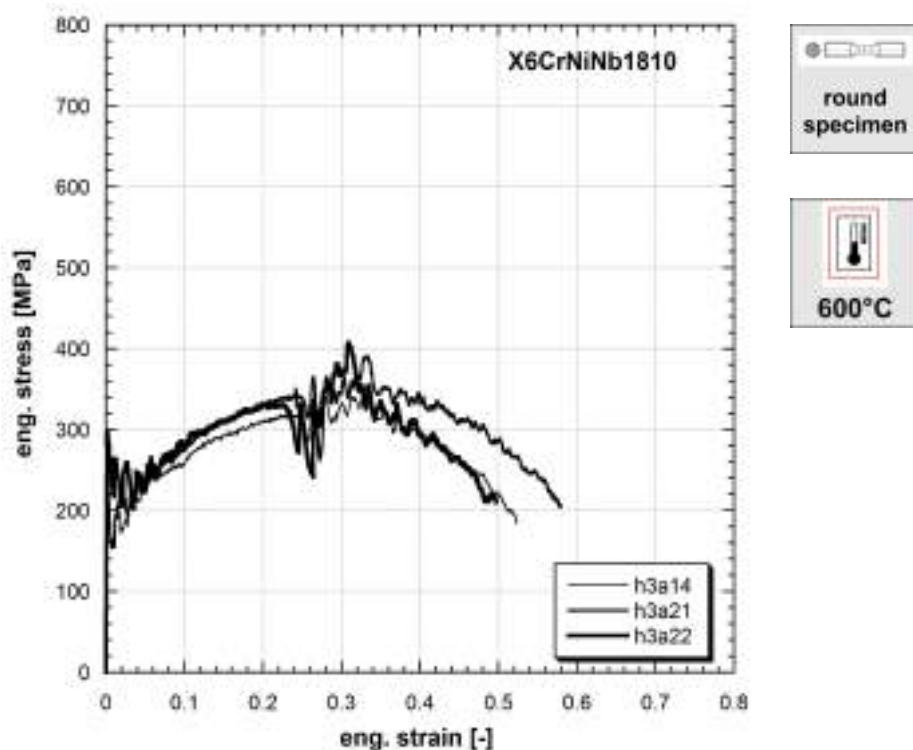


**Figure 9.227:** Stress vs strain curves of AUSTENITIC X6CrNiNb1810

**Note 9.227** Specimen diameter: 30 mm

Strain rate [1/s]	Yield stress [MPa]	Ultimate tensile strength [MPa]	Uniform strain [-]	Fracture stress [MPa]	Fracture strain [-]
150	222	331	0.319	184	0.523
150	223	350	0.329	206	0.580
150	281	341	0.316	210	0.497

**Table 227:** Mechanical properties of AUSTENITIC X6CrNiNb1810

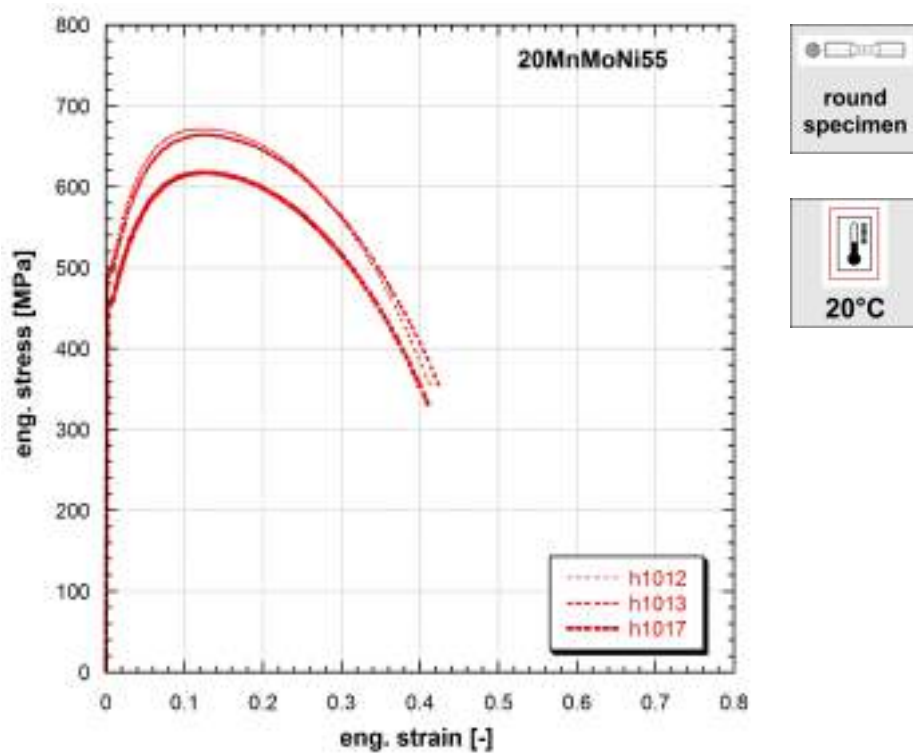


**Figure 9.228:** Stress vs strain curves of FERRITIC 20MnMoNi55

Strain rate [1/s]	Yield stress [MPa]	Ultimate tensile strength [MPa]	Uniform strain [-]	Fracture stress [MPa]	Fracture strain [-]
0.002	498	671	0.120	354	0.413
0.002	494	665	0.130	349	0.427
0.002	453	618	0.131	332	0.410

**Table 228:** Mechanical properties of FERRITIC 20MnMoNi55

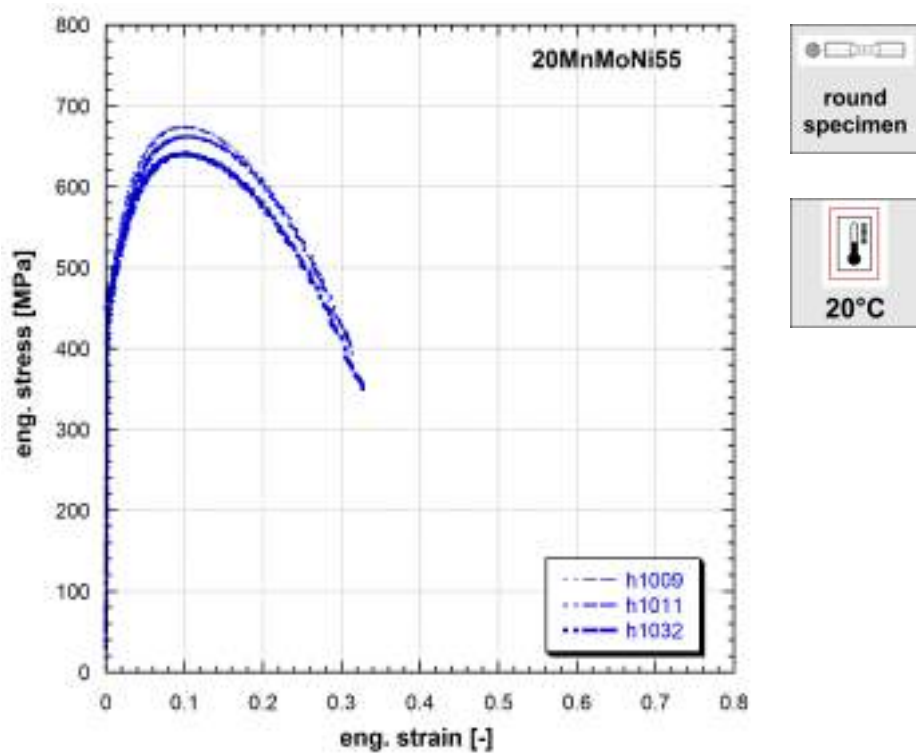


**Figure 9.229:** Stress vs strain curves of FERRITIC 20MnMoNi55

Strain rate [1/s]	Yield stress [MPa]	Ultimate tensile strength [MPa]	Uniform strain [-]	Fracture stress [MPa]	Fracture strain [-]
0.15	452	675	0.103	409	0.310
0.15	440	663	0.104	382	0.319
0.15	468	642	0.102	346	0.328

**Table 229:** Mechanical properties of FERRITIC 20MnMoNi55

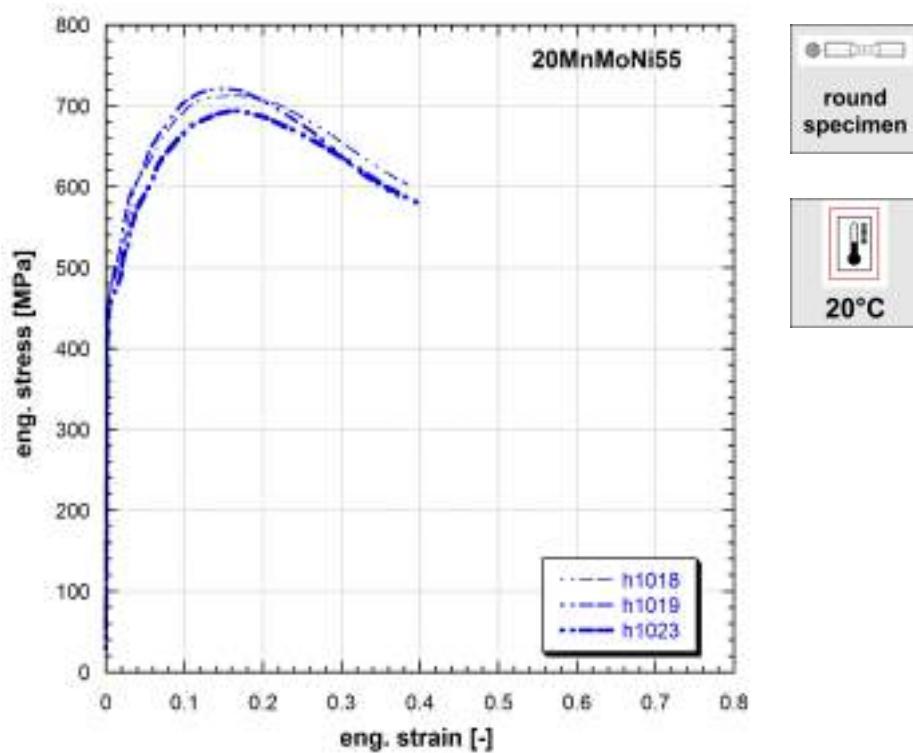


**Figure 9.230:** Stress vs strain curves of FERRITIC 20MnMoNi55

Strain rate [1/s]	Yield stress [MPa]	Ultimate tensile strength [MPa]	Uniform strain [-]	Fracture stress [MPa]	Fracture strain [-]
15	467	712	0.164	603	0.384
15	465	721	0.153	588	0.374
15	450	694	0.165	580	0.398

**Table 230:** Mechanical properties of FERRITIC 20MnMoNi55

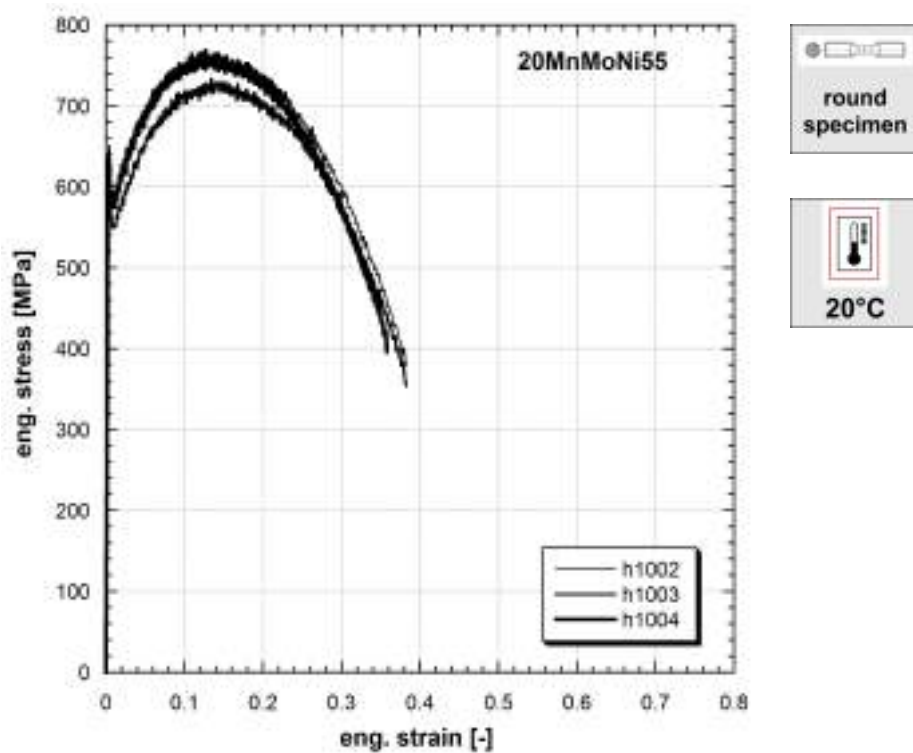


**Figure 9.231:** Stress vs strain curves of FERRITIC 20MnMoNi55

Strain rate [1/s]	Yield stress [MPa]	Ultimate tensile strength [MPa]	Uniform strain [-]	Fracture stress [MPa]	Fracture strain [-]
200	640	764	0.132	379	0.383
200	586	734	0.133	354	0.382
200	598	768	0.127	396	0.358

**Table 231:** Mechanical properties of FERRITIC 20MnMoNi55

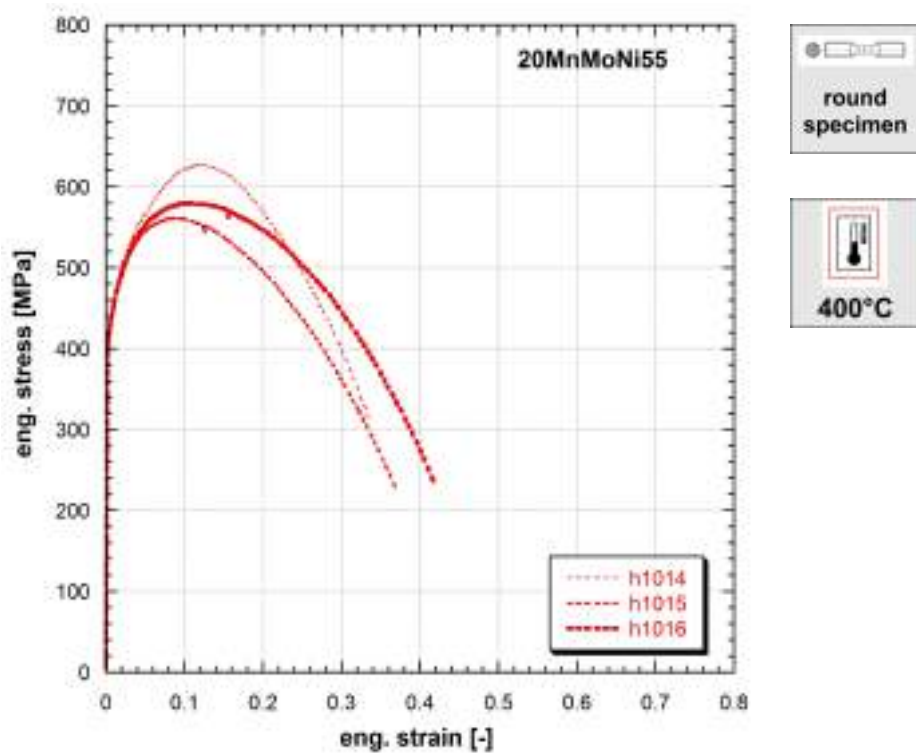


**Figure 9.232:** Stress vs strain curves of FERRITIC 20MnMoNi55

Strain rate [1/s]	Yield stress [MPa]	Ultimate tensile strength [MPa]	Uniform strain [-]	Fracture stress [MPa]	Fracture strain [-]
0.002	425	627	0.116	307	0.337
0.002	415	561	0.085	225	0.369
0.002	421	580	0.106	234	0.418

**Table 232:** Mechanical properties of FERRITIC 20MnMoNi55

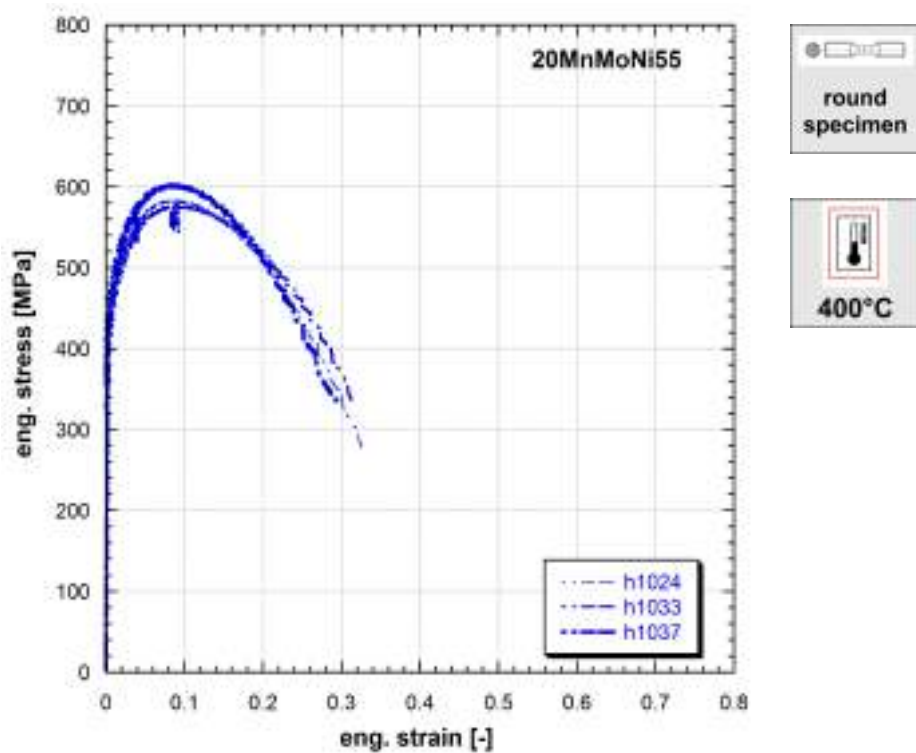


**Figure 9.233:** Stress vs strain curves of FERRITIC 20MnMoNi55

Strain rate [1/s]	Yield stress [MPa]	Ultimate tensile strength [MPa]	Uniform strain [-]	Fracture stress [MPa]	Fracture strain [-]
0.15	425	583	0.083	279	0.326
0.15	422	587	0.091	332	0.317
0.15	435	602	0.083	336	0.294

**Table 233:** Mechanical properties of FERRITIC 20MnMoNi55

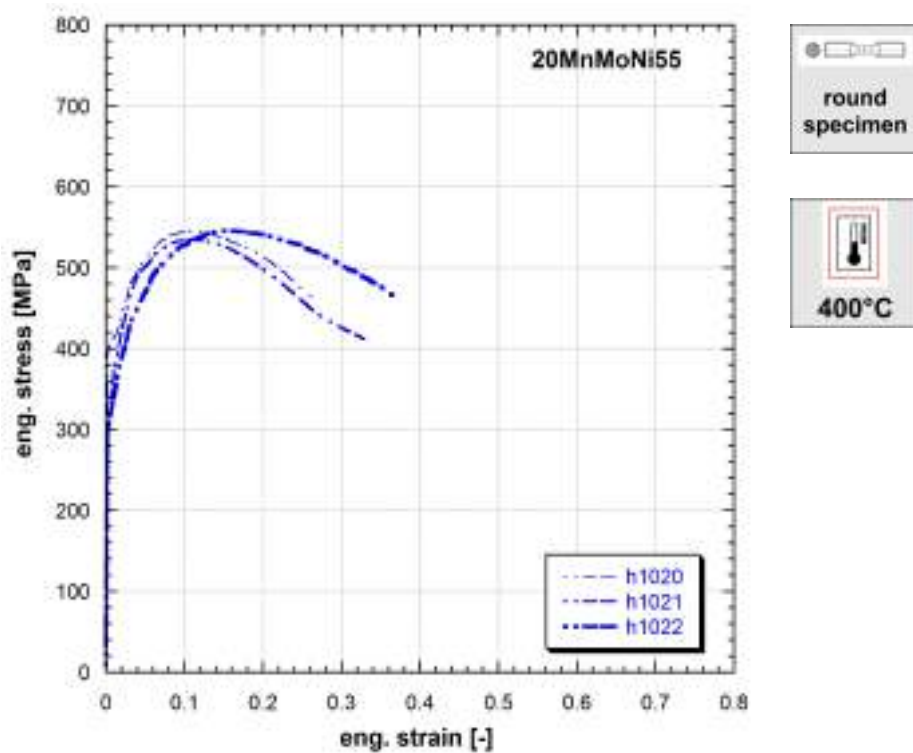


**Figure 9.234:** Stress vs strain curves of FERRITIC 20MnMoNi55

Strain rate [1/s]	Yield stress [MPa]	Ultimate tensile strength [MPa]	Uniform strain [-]	Fracture stress [MPa]	Fracture strain [-]
15	403	545	0.113	461	0.269
15	315	535	0.107	412	0.329
15	306	546	0.150	463	0.370

**Table 234:** Mechanical properties of FERRITIC 20MnMoNi55

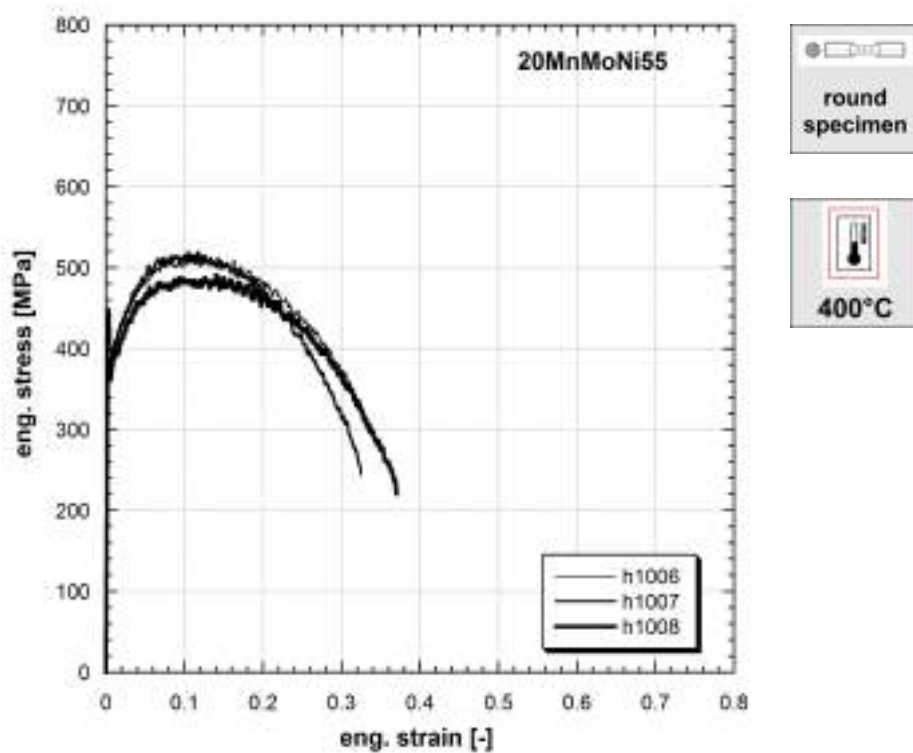


**Figure 9.235:** Stress vs strain curves of FERRITIC 20MnMoNi55

Strain rate [1/s]	Yield stress [MPa]	Ultimate tensile strength [MPa]	Uniform strain [-]	Fracture stress [MPa]	Fracture strain [-]
250	423	512	0.103	271	0.352
250	430	519	0.117	245	0.325
250	377	491	0.140	221	0.370

**Table 235:** Mechanical properties of FERRITIC 20MnMoNi55

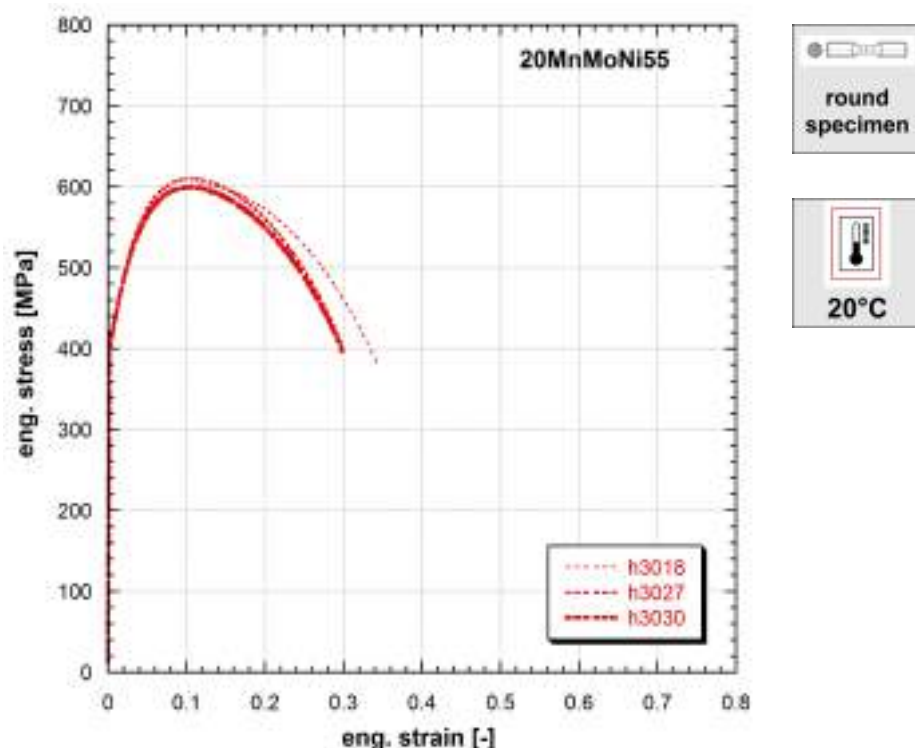


**Figure 9.236:** Stress vs strain curves of FERRITIC 20MnMoNi55

**Note 9.236** Specimen diameter: 30 mm

Strain rate [1/s]	Yield stress [MPa]	Ultimate tensile strength [MPa]	Uniform strain [-]	Fracture stress [MPa]	Fracture strain [-]
0.001	417	603	0.117	380	0.343
0.001	404	610	0.107	401	0.299
0.001	417	600	0.097	395	0.298

**Table 236:** Mechanical properties of FERRITIC 20MnMoNi55

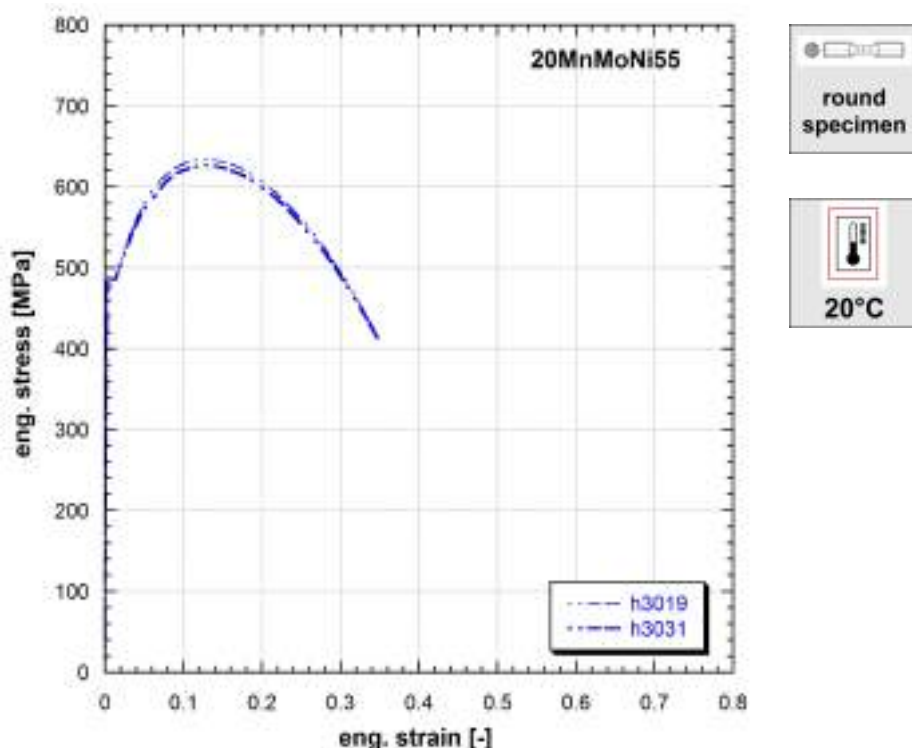


**Figure 9.237:** Stress vs strain curves of FERRITIC 20MnMoNi55

**Note 9.237** Specimen diameter: 30 mm

Strain rate [1/s]	Yield stress [MPa]	Ultimate tensile strength [MPa]	Uniform strain [-]	Fracture stress [MPa]	Fracture strain [-]
0.1	474	634	0.125	421	0.344
0.1	488	626	0.130	410	0.349

**Table 237:** Mechanical properties of FERRITIC 20MnMoNi55

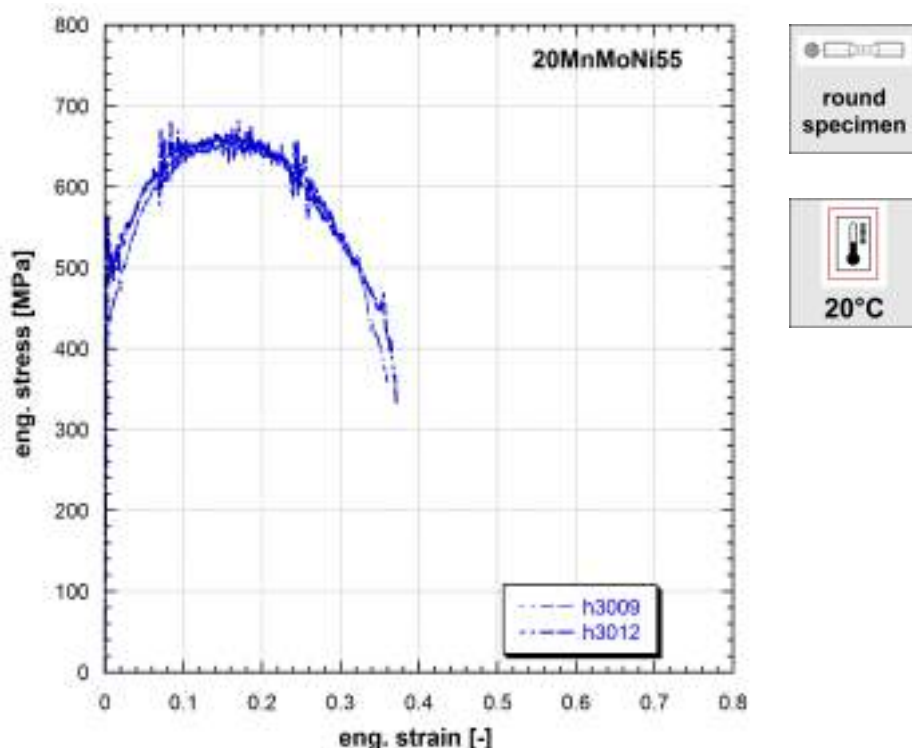


**Figure 9.238:** Stress vs strain curves of FERRITIC 20MnMoNi55

**Note 9.238** Specimen diameter: 30 mm

Strain rate [1/s]	Yield stress [MPa]	Ultimate tensile strength [MPa]	Uniform strain [-]	Fracture stress [MPa]	Fracture strain [-]
40	430	662	0.161	358	0.361
40	515	682	0.084	330	0.371

**Table 238:** Mechanical properties of FERRITIC 20MnMoNi55

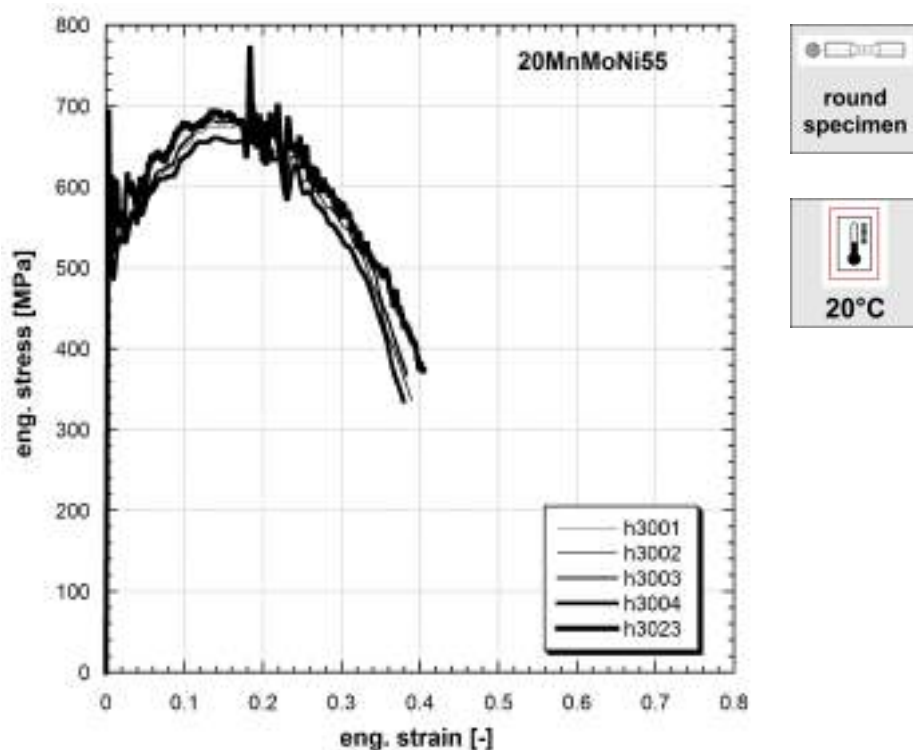


**Figure 9.239:** Stress vs strain curves of FERRITIC 20MnMoNi55

**Note 9.239** Specimen diameter: 30 mm

Strain rate [1/s]	Yield stress [MPa]	Ultimate tensile strength [MPa]	Uniform strain [-]	Fracture stress [MPa]	Fracture strain [-]
150	522	695	0.189	371	0.384
150	584	683	0.190	337	0.389
150	531	704	0.187	367	0.383
150	567	684	0.192	335	0.379
150	600	700	0.183	373	0.406

**Table 239:** Mechanical properties of FERRITIC 20MnMoNi55

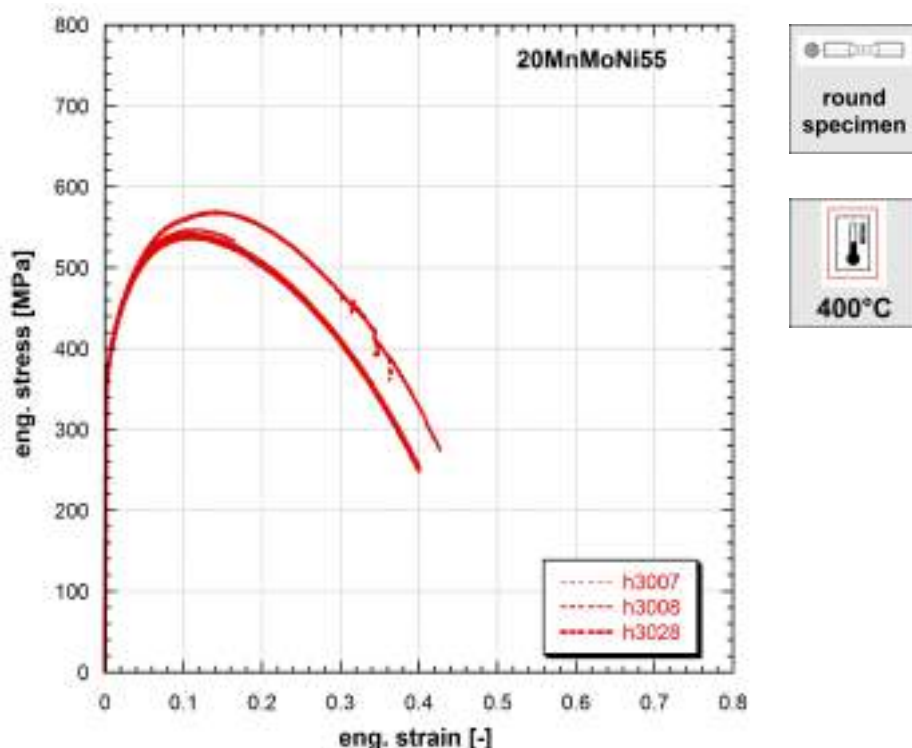


**Figure 9.240:** Stress vs strain curves of FERRITIC 20MnMoNi55

**Note 9.240** Specimen diameter: 30 mm

Strain rate [1/s]	Yield stress [MPa]	Ultimate tensile strength [MPa]	Uniform strain [-]	Fracture stress [MPa]	Fracture strain [-]
0.001	370	548	0.106	-	-
0.001	368	570	0.143	275	0.426
0.001	372	542	0.109	252	0.399

**Table 240:** Mechanical properties of FERRITIC 20MnMoNi55

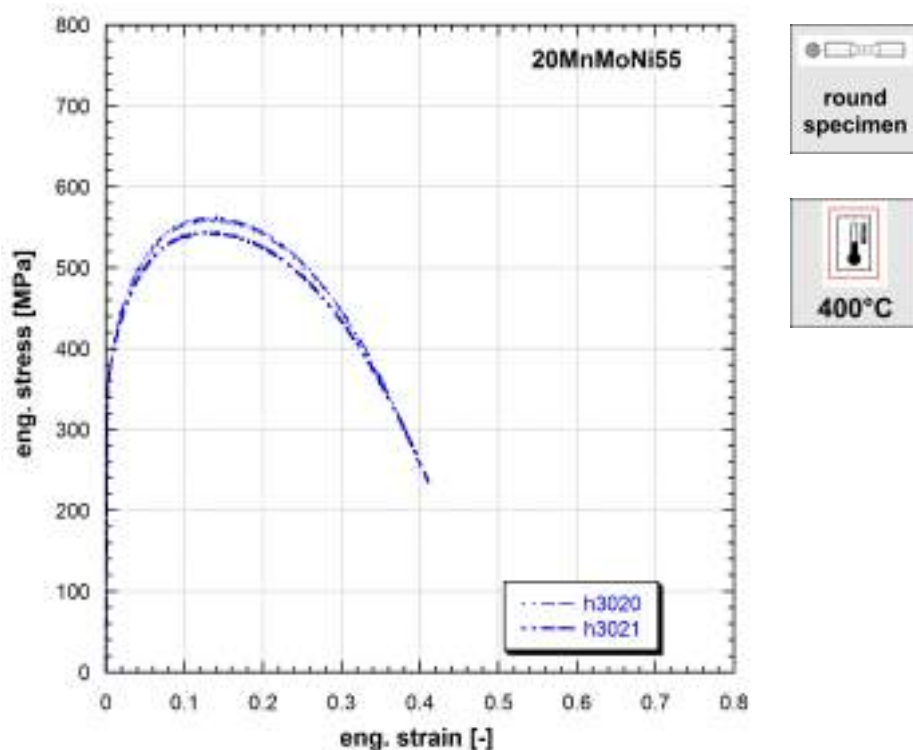


**Figure 9.241:** Stress vs strain curves of FERRITIC 20MnMoNi55

**Note 9.241** Specimen diameter: 30 mm

Strain rate [1/s]	Yield stress [MPa]	Ultimate tensile strength [MPa]	Uniform strain [-]	Fracture stress [MPa]	Fracture strain [-]
0.1	367	563	0.140	250	0.403
0.1	364	544	0.130	236	0.411

**Table 241:** Mechanical properties of FERRITIC 20MnMoNi55

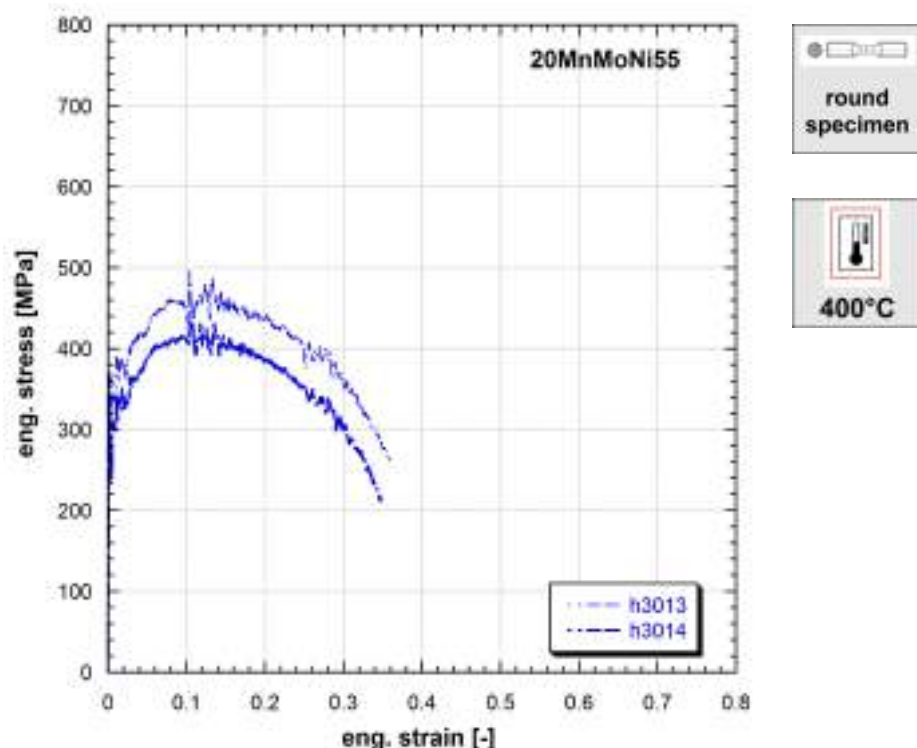


**Figure 9.242:** Stress vs strain curves of FERRITIC 20MnMoNi55

**Note 9.242** Specimen diameter: 30 mm

Strain rate [1/s]	Yield stress [MPa]	Ultimate tensile strength [MPa]	Uniform strain [-]	Fracture stress [MPa]	Fracture strain [-]
50	318	470	0.104	262	0.359
50	283	420	0.105	207	0.349

**Table 242:** Mechanical properties of FERRITIC 20MnMoNi55

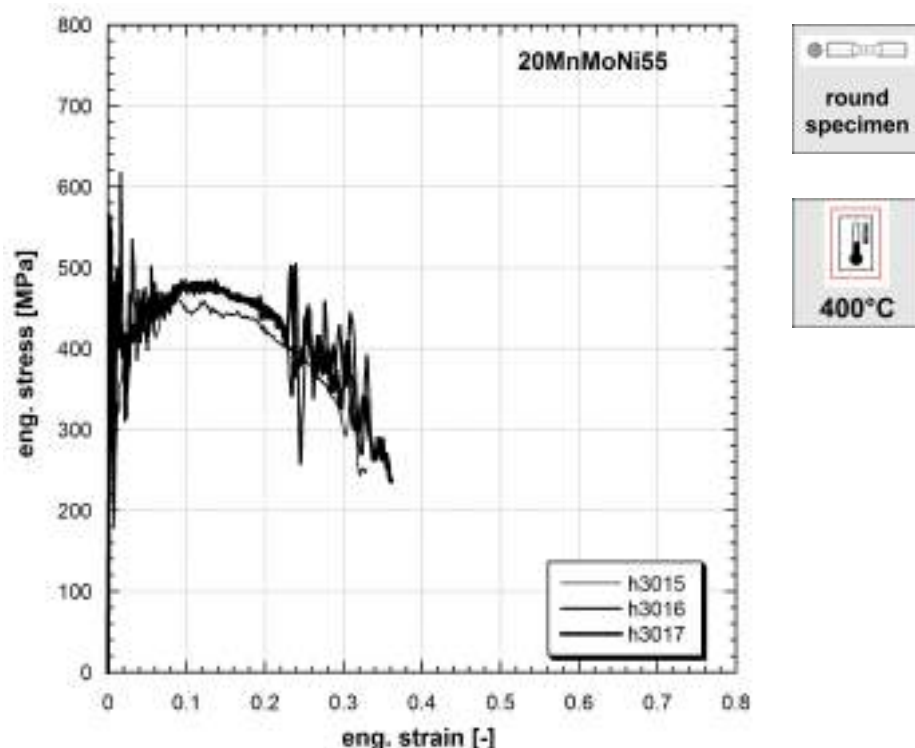


**Figure 9.243:** Stress vs strain curves of FERRITIC 20MnMoNi55

**Note 9.243** Specimen diameter: 30 mm

Strain rate [1/s]	Yield stress [MPa]	Ultimate tensile strength [MPa]	Uniform strain [-]	Fracture stress [MPa]	Fracture strain [-]
150	410	460	0.09	251	0.329
150	460	485	0.11	252	0.354
150	474	480	0.12	237	0.361

**Table 243:** Mechanical properties of FERRITIC 20MnMoNi55

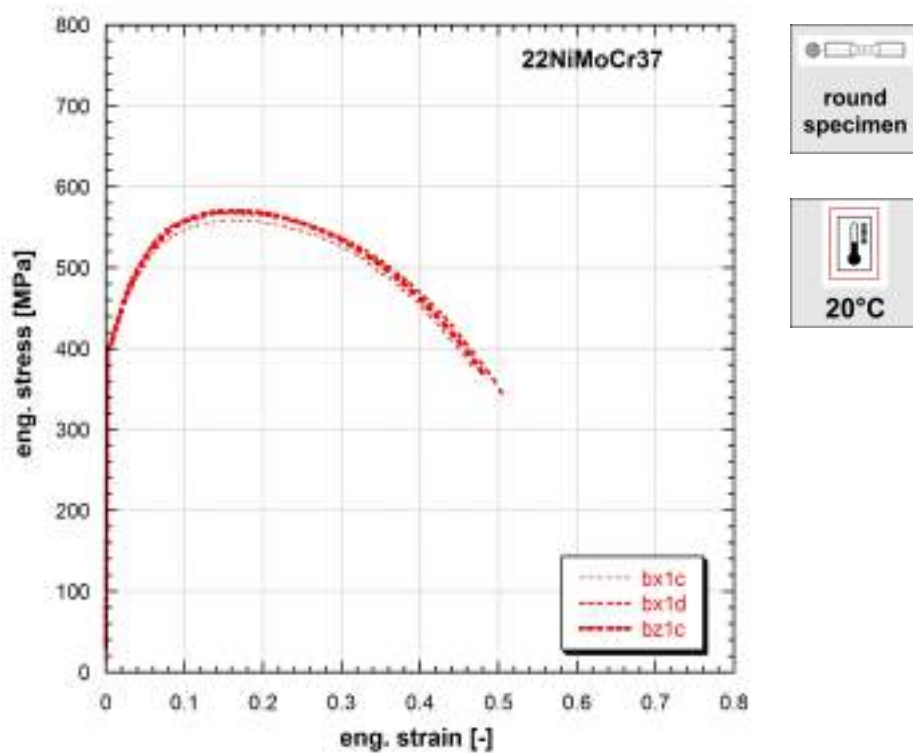


**Figure 9.244:** Stress vs strain curves of FERRITIC 20NiMoCr37

Strain rate [1/s]	Yield stress [MPa]	Ultimate tensile strength [MPa]	Uniform strain [-]	Fracture stress [MPa]	Fracture strain [-]
0.002	400	559	0.161	370	0.472
0.002	403	568	0.150	344	0.505
0.002	404	570	0.170	368	0.481

**Table 244:** Mechanical properties of FERRITIC 20NiMoCr37

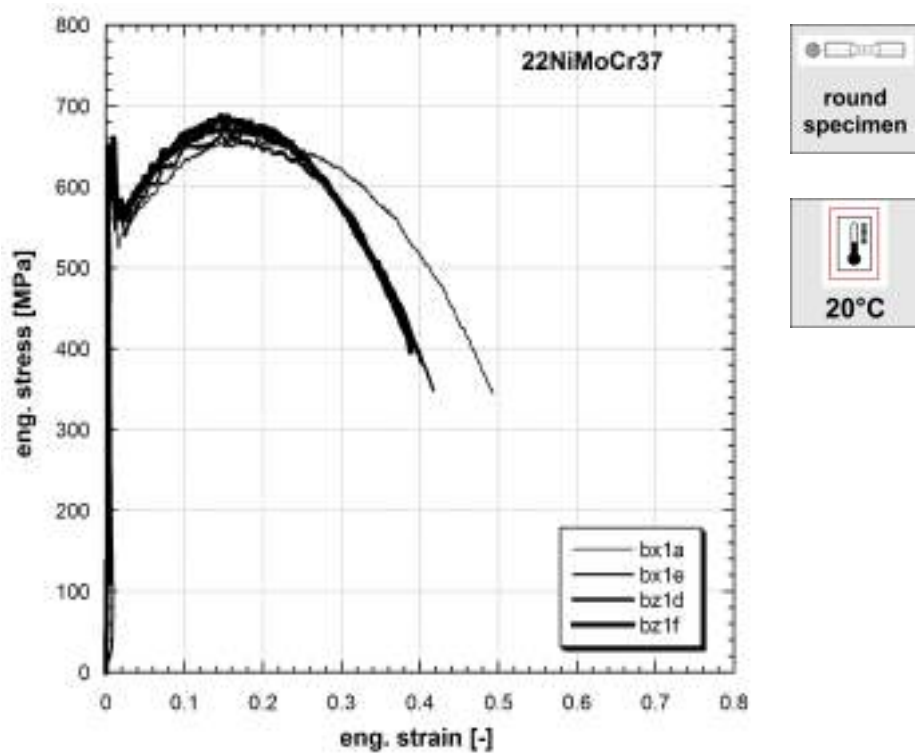


**Figure 9.245:** Stress vs strain curves of FERRITIC 20NiMoCr37

Strain rate [1/s]	Yield stress [MPa]	Ultimate tensile strength [MPa]	Uniform strain [-]	Fracture stress [MPa]	Fracture strain [-]
250	639	660	0.193	345	0.493
250	591	661	0.143	349	0.417
250	605	676	0.153	382	0.403
250	605	688	0.147	396	0.388

**Table 245:** Mechanical properties of FERRITIC 20NiMoCr37

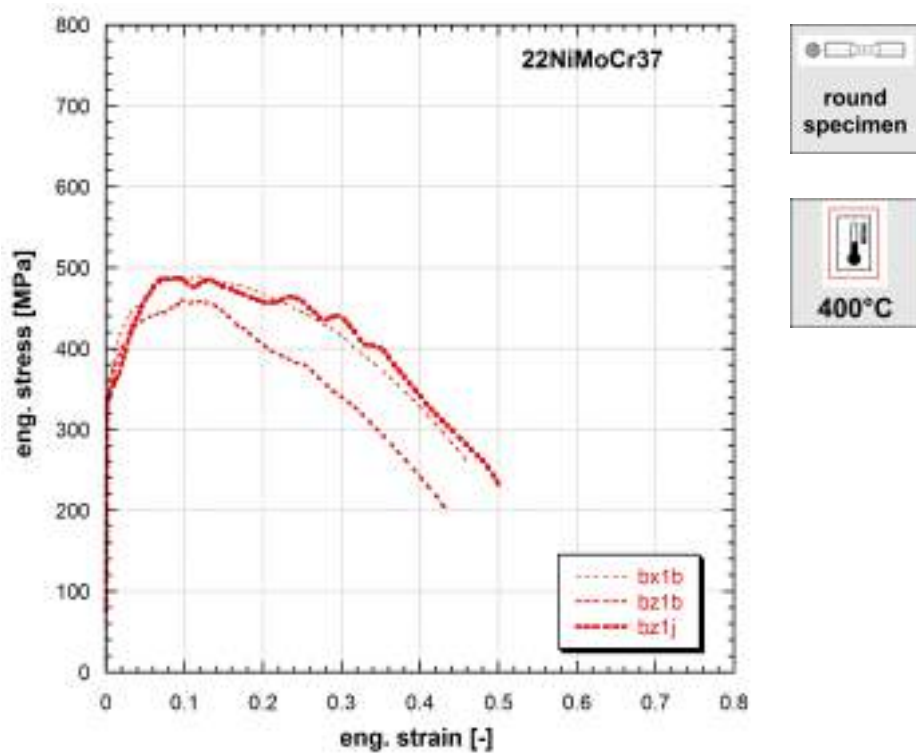


**Figure 9.246:** Stress vs strain curves of FERRITIC 20NiMoCr37

Strain rate [1/s]	Yield stress [MPa]	Ultimate tensile strength [MPa]	Uniform strain [-]	Fracture stress [MPa]	Fracture strain [-]
0.002	353	490	0.114	254	0.464
0.002	342	460	0.096	198	0.436
0.002	336	488	0.090	232	0.500

**Table 246:** Mechanical properties of FERRITIC 20NiMoCr37

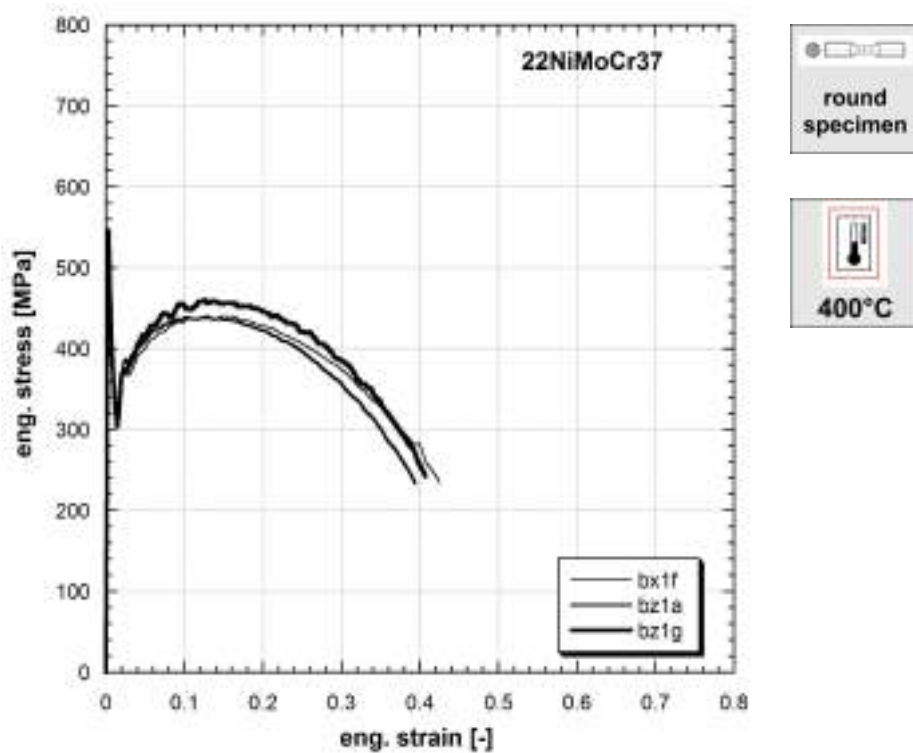


**Figure 9.247:** Stress vs strain curves of FERRITIC 20NiMoCr37

Strain rate [1/s]	Yield stress [MPa]	Ultimate tensile strength [MPa]	Uniform strain [-]	Fracture stress [MPa]	Fracture strain [-]
300	401	440	0.129	234	0.425
300	433	439	0.103	233	0.394
300	497	460	0.126	242	0.407

**Table 247:** Mechanical properties of FERRITIC 20NiMoCr37

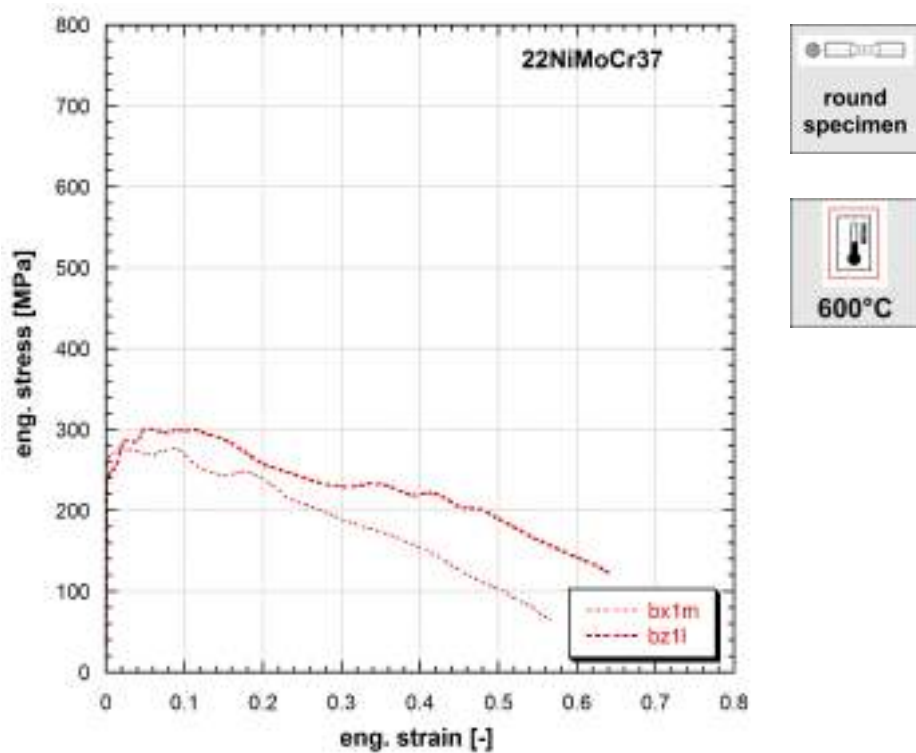


**Figure 9.248:** Stress vs strain curves of FERRITIC 20NiMoCr37

Strain rate [1/s]	Yield stress [MPa]	Ultimate tensile strength [MPa]	Uniform strain [-]	Fracture stress [MPa]	Fracture strain [-]
0.002	274	277	0.088	64	0.566
0.002	283	301	0.052	121	0.641

**Table 248:** Mechanical properties of FERRITIC 20NiMoCr37

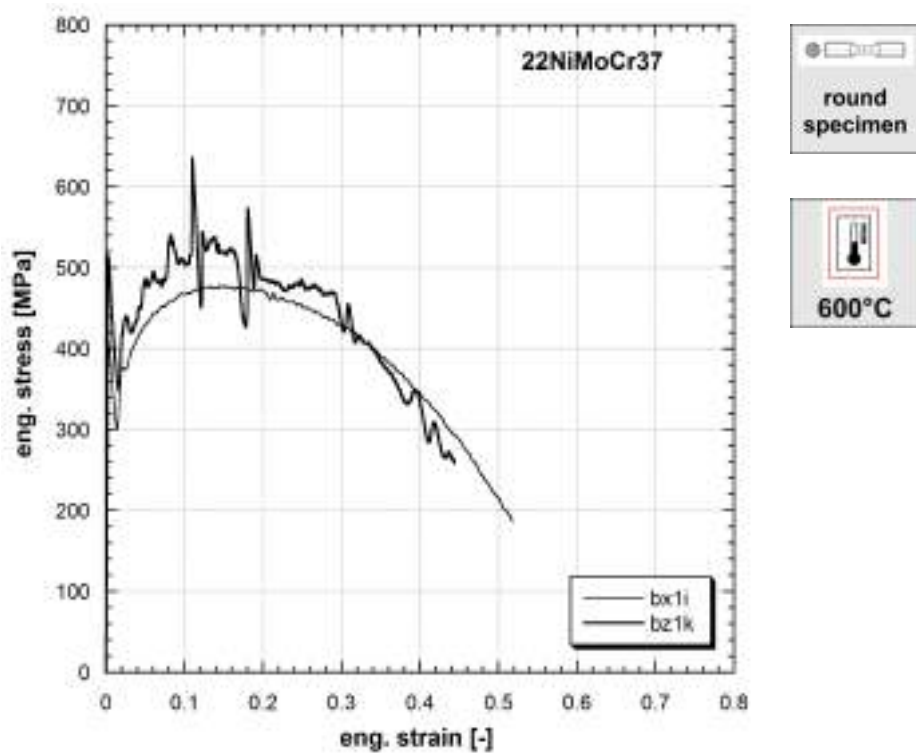


**Figure 9.249:** Stress vs strain curves of FERRITIC 20NiMoCr37

Strain rate [1/s]	Yield stress [MPa]	Ultimate tensile strength [MPa]	Uniform strain [-]	Fracture stress [MPa]	Fracture strain [-]
250	375	477	0.145	186	0.518
250	438	535	0.140	259	0.444

**Table 249:** Mechanical properties of FERRITIC 20NiMoCr37

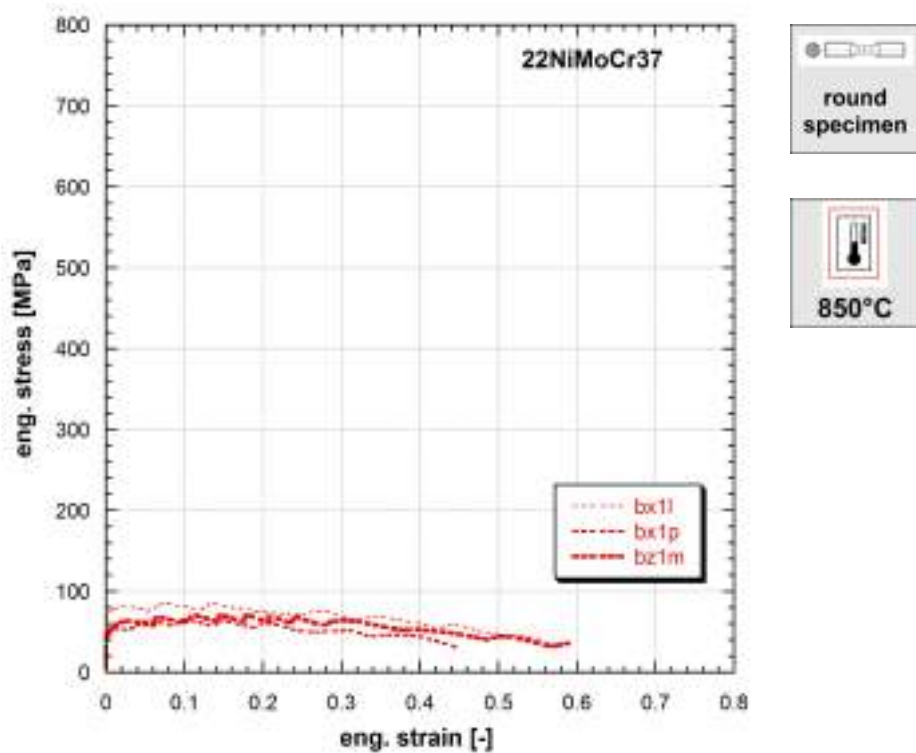


**Figure 9.250:** Stress vs strain curves of FERRITIC 20NiMoCr37

Strain rate [1/s]	Yield stress [MPa]	Ultimate tensile strength [MPa]	Uniform strain [-]	Fracture stress [MPa]	Fracture strain [-]
0.002	80	85	0.075	37	0.561
0.002	53	66	0.099	31	0.447
0.002	62	71	0.145	35	0.591

**Table 250:** Mechanical properties of FERRITIC 20NiMoCr37

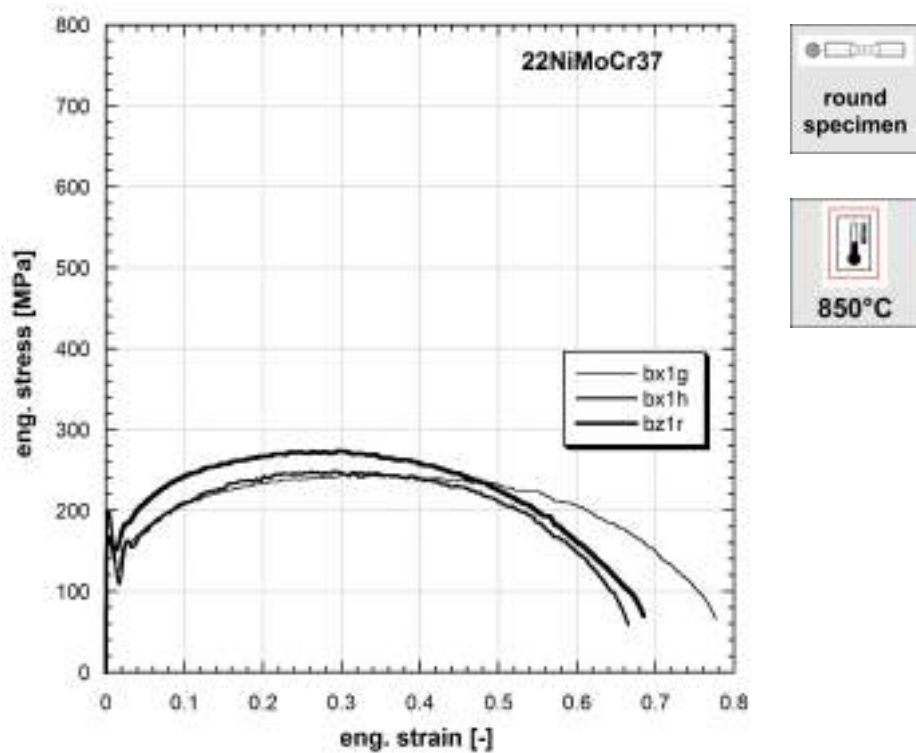


**Figure 9.251:** Stress vs strain curves of FERRITIC 20NiMoCr37

Strain rate [1/s]	Yield stress [MPa]	Ultimate tensile strength [MPa]	Uniform strain [-]	Fracture stress [MPa]	Fracture strain [-]
350	152	245	0.314	66	0.777
350	135	249	0.294	59	0.666
350	178	274	0.299	69	0.685

**Table 251:** Mechanical properties of FERRITIC 20NiMoCr37

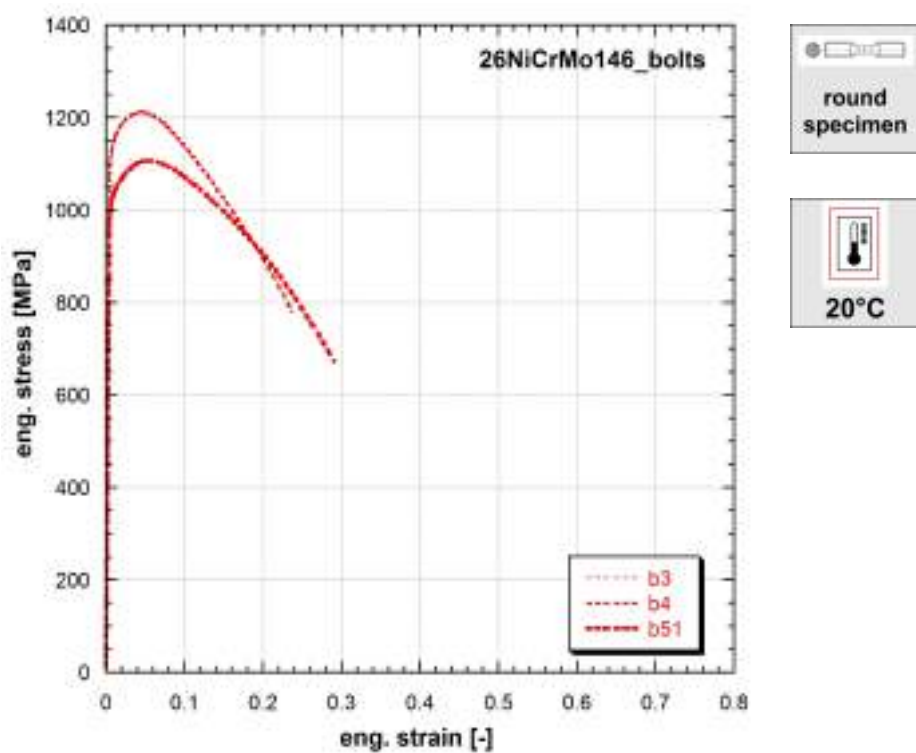


**Figure 9.252:** Stress vs strain curves of FERRITIC 26NiCrMo146

Strain rate [1/s]	Yield stress [MPa]	Ultimate tensile strength [MPa]	Uniform strain [-]	Fracture stress [MPa]	Fracture strain [-]
0.001	1147	1209	0.045	779	0.237
0.001	1151	1212	0.047	777	0.237
0.001	1035	1107	0.053	673	0.291

**Table 252:** Mechanical properties of FERRITIC 26NiCrMo146

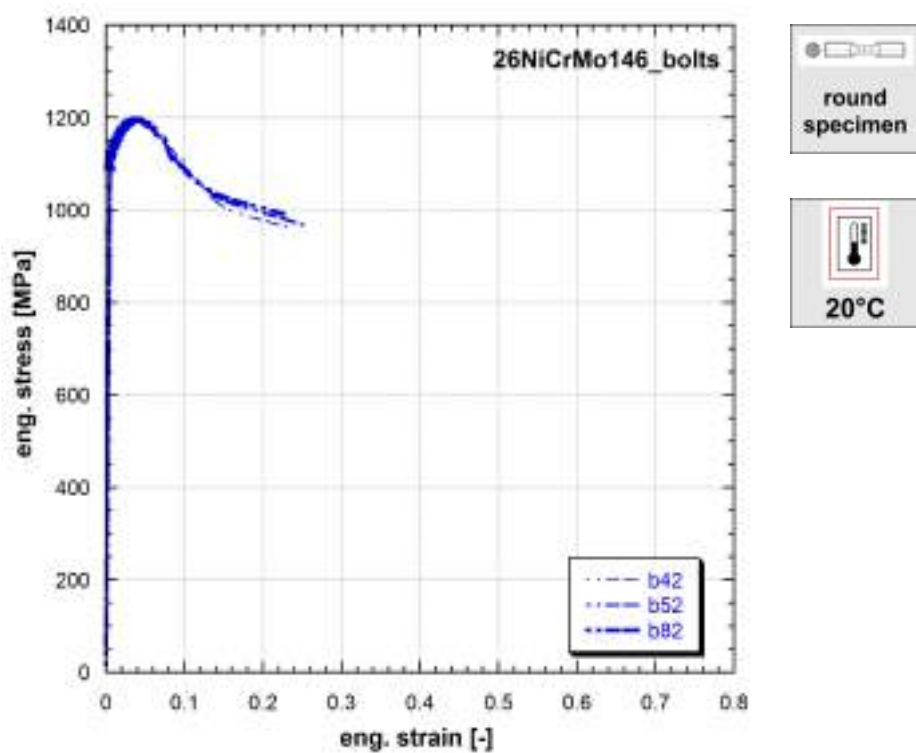


**Figure 9.253:** Stress vs strain curves of FERRITIC 26NiCrMo146

Strain rate [1/s]	Yield stress [MPa]	Ultimate tensile strength [MPa]	Uniform strain [-]	Fracture stress [MPa]	Fracture strain [-]
0.1	1098	1191	0.045	959	0.238
0.1	1104	1194	0.039	967	0.253
0.1	1111	1199	0.038	989	0.231

**Table 253:** Mechanical properties of FERRITIC 26NiCrMo146

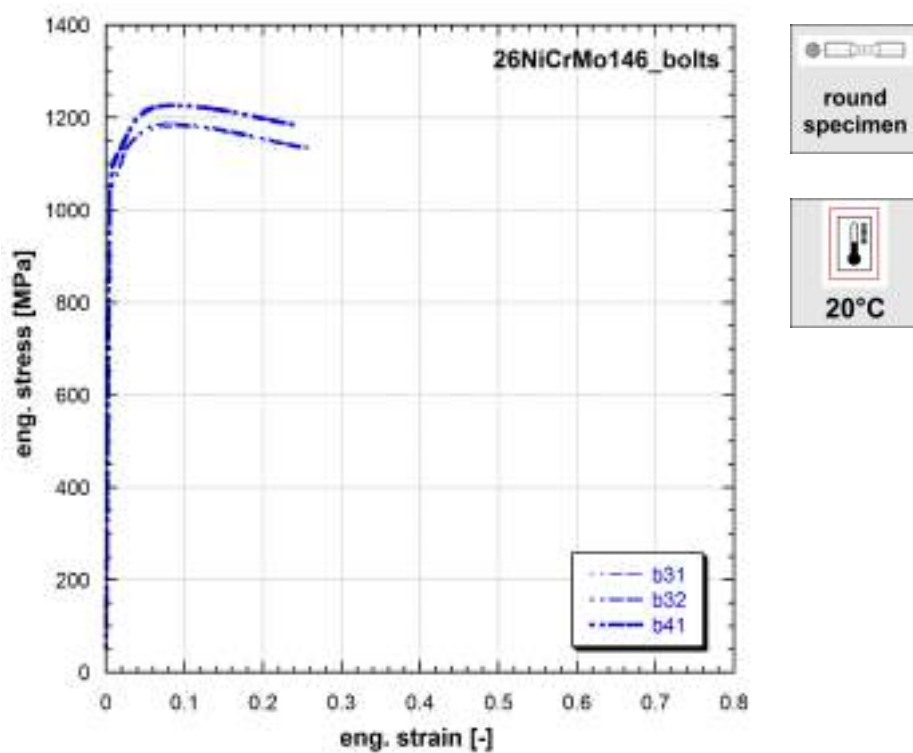


**Figure 9.254:** Stress vs strain curves of FERRITIC 26NiCrMo146

Strain rate [1/s]	Yield stress [MPa]	Ultimate tensile strength [MPa]	Uniform strain [-]	Fracture stress [MPa]	Fracture strain [-]
10	1065	1180	0.089	1134	0.248
10	1050	1186	0.077	1135	0.256
10	1085	1226	0.084	1183	0.200

**Table 254:** Mechanical properties of FERRITIC 26NiCrMo146

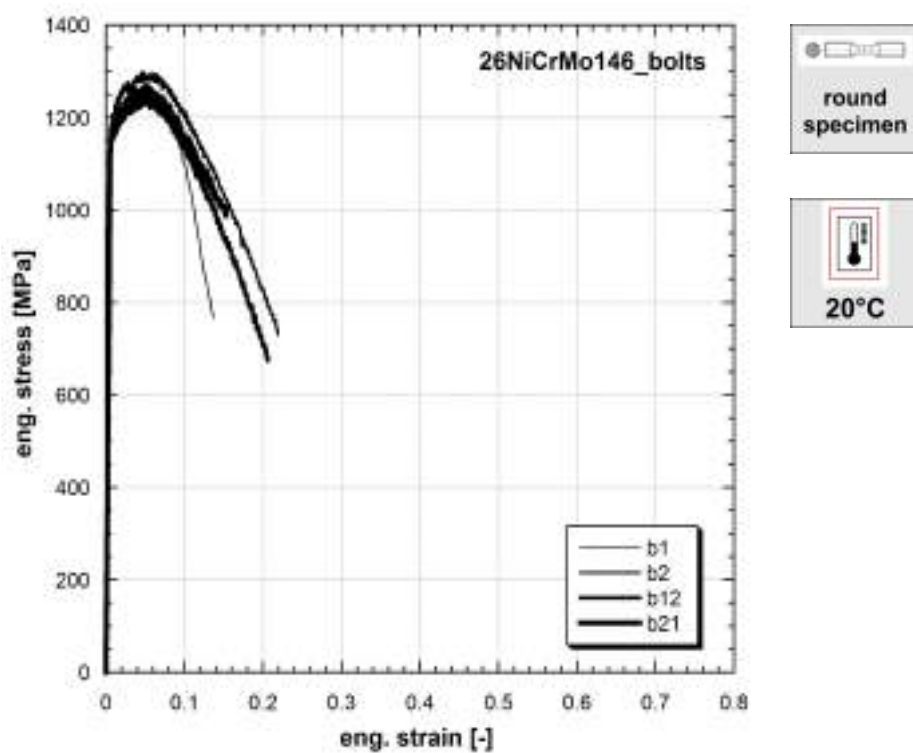


**Figure 9.255:** Stress vs strain curves of FERRITIC 26NiCrMo146

Strain rate [1/s]	Yield stress [MPa]	Ultimate tensile strength [MPa]	Uniform strain [-]	Fracture stress [MPa]	Fracture strain [-]
150	1145	1266	0.050	767	0.137
150	1169	1299	0.047	730	0.219
150	1147	1247	0.053	674	0.206
150	1173	1268	0.052	988	0.153

**Table 255:** Mechanical properties of FERRITIC 26NiCrMo146

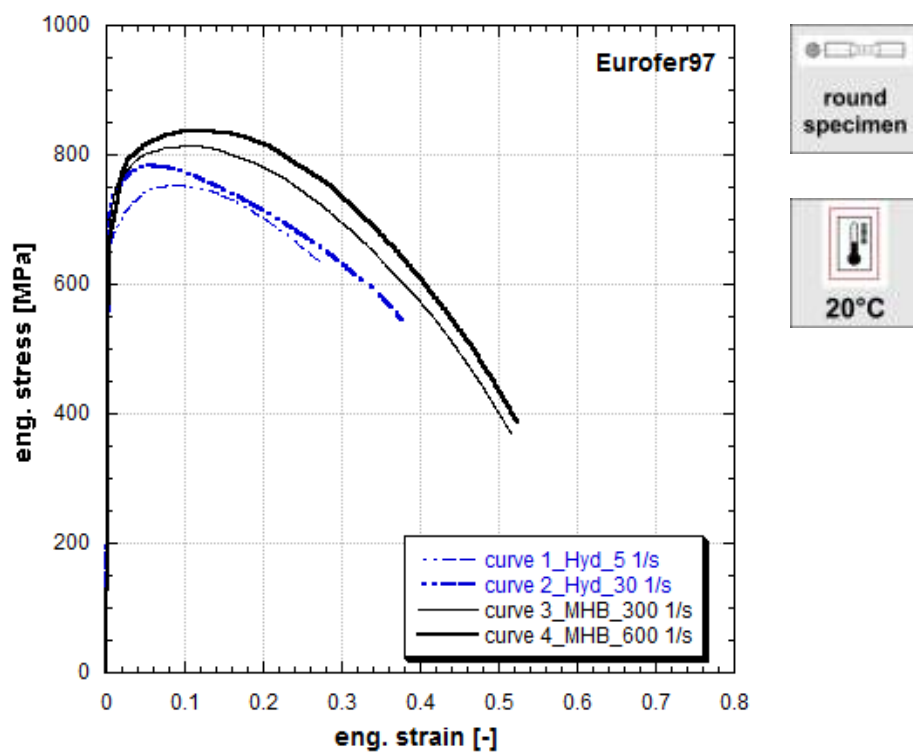


**Figure 9.256:** Stress vs strain curves of Eurofer97

Strain rate [1/s]	Yield stress [MPa]	Ultimate tensile strength [MPa]	Uniform strain [-]	Fracture stress [MPa]	Fracture strain [-]
5	665	753	0.086	636	0.333
30	690	770	0.082	546	0.399
300	716	814	0.010	370	0.519
600	720	837	0.011	387	0.531

**Table 256:** Mechanical properties of Eurofer97

Published in (Cadoni et al., 2011), (Cadoni et al., 2015).

## References

- Albertini, C., 'Material properties of reactor pressure vessels and containment shells under dynamic loading', *Nuclear Engineering and Design*, Vol. 174, No 2, October 1997, pp. 135–141.
- Albertini, C., Blery Blionas, E., Micunovic, M. and Montagnani, M. *Biaxial strain rate controlled viscoplastic experiments on cruciform specimens of AISI 316H up to 100 1/s*, Institute of Physics, Conference Series n°102, 1989a. pp. 173–180.
- Albertini, C., Boone, P. M. and Montagnani, M., 'Development of the Hopkinson Bar for testing large specimens in tension', *Journal de Physique Colloques*, Vol. 46, 1985a, pp. C5–499–C5–503.
- Albertini, C., Brusa, F., Grande, A. D., Mogilevsky, M., Pizzinato, E., Quik, M., Schnabel, W., Crutzen, Y., Inzaghi, A. and Caravati, D., 'Dynamic uniaxial and quasi-static biaxial tensile properties of aluminium alloy Al 7108', Tech. Rep. I.96.148, JRC Ispra, August 1996a.
- Albertini, C., Cadoni, E., Crutzen, Y., Francocci, P., Inzaghi, A., Labibes, K. and Petrangeli, A., 'Crash Worthiness Studies of Thin Sheet Metal Structures by Means of a Large Hopkinson bar; Benefits for Calibration of Impact Rigs and Validation of Numerical Crash Simulation', *Proceedings of the International Crashworthiness and design Symposium*, May 1995a, pp. 11–26.
- Albertini, C., Cadoni, E. and Labibes, K., 'Anisotropy and strain rates effects on dynamic testing of thin sheet boxes used as automotive crash energy absorbers', *Chinese Mechanics Journal - 2nd International Symposium on Impact Engineering*, September 1996b, pp. 106–110.
- Albertini, C., Cadoni, E. and Labibes, K., 'Precision Measurements of Vehicle Crashworthiness by Means of a Large Hopkinson Bar', *J. Phys. IV France*, Vol. 07, No C3, August 1997a, pp. C3–79–C3–84.
- Albertini, C., Cadoni, E. and Labibes, K., 'Study of the mechanical properties of plain concrete under dynamic loading', *Experimental Mechanics*, Vol. 39, No 2, June 1999, pp. 137–141.
- Albertini, C., Cadoni, E. and Solomos, G., 'Advances in the Hopkinson bar testing of irradiated/non-irradiated nuclear materials and large specimens', *Philosophical Transactions of the Royal Society A: Mathematical, Physical and Engineering Sciences*, Vol. 372, No 2015, 2014, p. 20130197. .
- Albertini, C., Cenerini, R., Curioni, S., Griffiths, L. J. and Montagnani, M., 'Constitutive equations of steels in dynamics as a function of temperature and strain rate. Techniques and results', *Proceedings of the II International Conference on Dynamic Mechanical Properties and Fracture Dynamics of Engineering Materials, Institute of Metallurgy, Czechoslovak Academy of Science*, June 1983a.
- Albertini, C., Cenerini, R., Curioni, S. and Montagnani, M., 'Radiation, welding, temperature and strain rate influence on material properties in fast breeder reactors', *Journal Archives of Mechanics*, Vol. 32, No 4, June 1980, pp. 549–577.
- Albertini, C., Cenerini, R., Curioni, S. and Montagnani, M., 'Constitutive equations of austenitic stainless steels in dynamics. Experiments and calibration procedure', *Proceedings of the 2nd Cairo University Conference on Mechanical Design and Production*, December 1982.
- Albertini, C., Cenerini, R., Curioni, S. and Montagnani, M., 'Dynamic mechanical properties of austenitic stainless steels. Fitting of experimental data on constitutive equations', *Transactions of the 7th International Conference On Structural Mechanics in Reactor Technology, SMIRT*, Vol. L, August 1983b.
- Albertini, C., Del Grande, A. and Montagnani, M. *Effects of irradiation on the constitutive equations of austenitic stainless steels under dynamic loading*, ASTM International, West Conshohocken, PA, January 1979. pp. 546–556.
- Albertini, C., Del Grande, A. and Montagnani, M. *Dynamic mechanical properties of AISI 304L irradiated to 2.2 dpa*, ASTM International, West Conshohocken, PA, January 1981. pp. 431–442.
- Albertini, C., Del Grande, A. and Montagnani, M. *Mechanical properties at high strain rate of AISI 316L stainless steel irradiated to 9.2 dpa*, ASTM International, West Conshohocken, PA, June 1984a. pp. 783–794.
- Albertini, C., Del Grande, A., Montagnani, M. and Pachera, A. *Mechanical Properties at Low and High Strain Rates of PE 16 Alloys Irradiated to 9.2 dpa*, ASTM International, West Conshohocken, PA, 01 1987a. pp. 151–161.
- Albertini, C., Eleiche, A. M. and Montagnani, M., 'Constitutive equation of AISI 316 at high rate of strain', *Proceedings of the Third International Conference on Mechanical Properties of Materials at High Rates of Strain. The Institute of Physics Conference series No 70, The University of Oxford*, April 1984b.

Albertini, C., Eleiche, A. M. and Montagnani, M., 'Strain rate history effect on dynamic mechanical properties of aisi 316 stainless steel', *Proceedings of the International Conference on Metallurgical Applications of Shock-Wave and High-Strain-Rate Phenomena, Explomet 85*, July 1985b, pp. 583 – 603.

Albertini, C., Eleiche, A. M. and Montagnani, M., 'The influence of strain rate history on the stress strain diagram of aisi 316 at high temperatures', *Journal Res Mechanica*, Vol. 27, 1989b, pp. 233–245.

Albertini, C., Eleiche, A. M. and Montagnani, M., 'Instabilities at high strain rate of AISI 316 damaged by creep, fatigue and irradiation. Discussion of adiabatic temperature oscillations', *Fourth International Conference on Mechanical Properties of Materials at High Rate of Strain. The Institute of Physics, conference Series No 102, The University of Oxford*, March 1989c.

Albertini, C. and Genet, F., 'Irradiations dans le reacteur H.F.R d'aciers austenitiques pour cuve de reacteur', *International Colloquium on Radiation Tests for Reactor Safety Programmes*, June 1979.

Albertini, C., Griffiths, L. J., Montagnani, M., Rodis, A., Mariotti, P., Paluffi, A. and Pazienza, G., 'Material characterization by an innovative biaxial shear experiment at very large strain rate', *J. Phys. IV France*, Vol. 01, No C3, 1991a, pp. C3–435–C3–440.

Albertini, C., Halleux, J. P. and Montagnani, M., 'Material behaviour and modelling in transient dynamic situations', *Lecture for Ispra Course on Advanced Structural Dynamics, JRC*, October 1978.

Albertini, C., Hanefi, E. and Wierzbicki, T., 'Calibration of impact rigs for dynamic crash testing', Tech. Rep. 16347EN, European Commission - Joint Research Centre, 1995b.

Albertini, C. and Labibes, K., 'Split Hopkinson bar compression testing apparatus. European patent EP 0849583, US Patent 6,109,093'. a.

Albertini, C. and Labibes, K., 'Stress wave bar transducer for measuring the local response of complex structures. European patent 0848241 and WO 9826268'. b.

Albertini, C., Labibes, K., Montagnani, M., Pizzinato, E. V., Solomos, G. and Viaccoz, B., 'Biaxial direct tensile tests in a large range of strain rate. Results on a ferritic nuclear steel', *J. Phys. IV France*, Vol. 10, No PR9, 2000, pp. Pr9–161–Pr9–166.

Albertini, C., Labibes, K. and Solomos, G., 'A liquid Hopkinson bar for impact compression test of soft tissues simulating human body parts and impact mitigation materials. European patent 01951834.9. British Patent 0015940.0. WO/PCT IBO 1/01141'.

Albertini, C., Labibes, K. and Solomos, G., 'Precision measurements of crash energy absorption: from material specimen to whole vehicle body', Tech. Rep. EUR 17293 EN, European Commission - Joint Research Centre, December 1997b.

Albertini, C., Micunovic, M. and Montagnani, M., 'Uniaxial viscoplastic experiments of predamaged AISI 316H', *4th IUTAM Symposium on Creep in Structures*, September 1990a.

Albertini, C., Micunovic, M. and Montagnani, M., 'Viscoplastic behaviour of AISI 316 H, multiaxial experimental results and numerical analysis', *Nuclear Engineering and Design*, Vol. 130, No 2, September 1991b, pp. 205–210.

Albertini, C. and Montagnani, M. *Testing techniques based on the split Hopkinson bar*, April 1974. pp. 22–32.

Albertini, C. and Montagnani, M., 'Wave propagation effects on dynamic loading', *Nuclear Engineering and Design*, Vol. 37, No 1, 4 1976, pp. 115–124.

Albertini, C. and Montagnani, M., 'Dynamic material properties of several steels for fast breeder reactor safety analysis', Final Report Collaboration Contract No 106-73 PIPGD EUR 5787E, collaboration EURATOM - G.F.K. KARLSRUHE, 1977. ISBN 92-825-0137-X Catalogue number CD-NE-77-066-EN-C.

Albertini, C. and Montagnani, M., 'Effect of welding on dynamic response of austenitic stainless steel for nuclear applications', *Third International Symposium on "Criteria for Preventing Service Failure in Welded Structures"*, September 1978, pp. 26–28.

Albertini, C. and Montagnani, M. *Testing techniques in dynamic biaxial loading*, Institute of Physics, Conference Series n°47, March 1979. pp. 25–34.

Albertini, C. and Montagnani, M., 'Dynamic uniaxial and biaxial stress-strain relationships for austenitic stainless steels', *Nuclear Engineering and Design*, Vol. 57, No 1, 1980, pp. 107–123.

Albertini, C. and Montagnani, M., 'Constitutive laws of materials in dynamics. Outlines of a programme of testing on small and large specimens for containment of extreme dynamic loading conditions', *Nuclear Engineering and Design*, Vol. 68, No 2, March 1981a, pp. 115–128.

Albertini, C. and Montagnani, M., 'Dynamic mechanical properties at high temperature of austenitic stainless steels for nuclear applications', *Proceedings of the International Conference on Mechanical Behavior and Nuclear Applications of Stainless Steels at Elevated Temperatures*, May 1981b.

Albertini, C. and Montagnani, M., 'Experimental determination of material's constitutive laws and of design criteria of reactor structures in extreme dynamic loading conditions', *Transactions of the 6th International Conference on Structural mechanics in Reactor Technology, SMiRT*, Vol. L, August 1981c.

Albertini, C. and Montagnani, M., 'Dynamic mechanical properties of the austenitic stainless steels used for the vessel models of COVA tests', Final report of the JRC COVA programme EUR 8705 EN CCGS(83) CONT-D 164, European Commission - Joint Research Centre, 1983a.

Albertini, C. and Montagnani, M., 'The behaviour of AISI 316 austenitic stainless steel at high rate of strain', *Journees d'Etudes, Deformations des Metaux aux Grandes Vitesses*, November 1983b.

Albertini, C. and Montagnani, M., 'Strain rate dependence of residual strength and ductility of aisi 316 stainless steel after creep, fatigue and irradiation', *Structural Mechanics in Reactor Technology: Transactions of the 9th International Conference on Structural Mechanics in Reactor Technology*, Vol. 30, August 1987, pp. 361–375.

Albertini, C. and Montagnani, M., 'Strain-rate dependence of residual strength and ductility of AISI 316H stainless steel after creep, fatigue and irradiation', *Journal Res Mechanica*, Vol. 30, 1990, pp. 361–375.

Albertini, C., Montagnani, M., Iida, K., Del Grande, A., Pachera, A. and Forlani, M. *Residual tensile properties at low and high strain-rate of AISI 316H pre-damaged by creep, low cycle fatigue and irradiation to 2 dpa*, ASTM International, West Conshohocken, PA, January 1988. pp. 387–403.

Albertini, C., Montagnani, M. and Pizzinato, V., 'Specimen size and shape effects at high strain rate on the mode of yielding and flow of AISI 316', *Proceedings of the International Conference on Impact Loading and Dynamic Behavior of Materials, Impact 87*, Vol. 1, May 1987b, pp. 461–468.

Albertini, C., Montagnani, M., Pizzinato, V., Rodis, A., Berlenghi, S., Berrini, G., Pazienza, G. and Paluffi, A., 'Mechanical properties in shear at very high strain rate of AISI 316 stainless steel and of a pure iron.', *Proceedings of the International Conference on Shock-Wave and High Strain Rate Phenomena in Materials. EXPLOMET 90*, August 1990b, pp. 681–691.

Albertini, C., Montagnani, M., Zyczkowski, M. and Laczek, S., 'Optimal design of a specimen for pure double shear tests', *International Journal of Mechanical Sciences*, Vol. 32, No 9, December 1990c, pp. 729–741.

Albertini, C., Pizzinato, V., Montagnani, M. and Rodis, A., 'Comparison of the equivalent flow curves in tension and shear at low and high strain rate for aisi 316 and armco iron', *Transactions of the 11th International Conference on Structural Mechanics in Reactor Technology, SMiRT 11*, Tokyo, Vol. L, August 1991c.

Albertini, C., Solomos, G. and Labibes, K., 'Calibration of impact rigs, crashworthiness testing of thin sheet metal boxes', *Proceedings of the 16th International Conference On the Enhanced Safety of Vehicles*, June 1998.

Bagchi, A., 'Conflicting nationalisms: the voice of the subaltern in Mahasweta Devi's *Bashai Tudu*', *Tulsa Studies in Women's Literature*, Vol. 15, No 1, 1996, pp. 41–50.

Baird, J. D., 'The effects of strain-ageing due to interstitial solutes on the mechanical properties of metals', *Metallurgical Reviews*, Vol. 16, No 1, July 1971, pp. 1–18.

Birch, R., Jones, N. and Jouri, W., 'Performance assessment of an impact rig', *Proceedings of the Institute of Mechanical Engineers*, Vol. 2, No C4, 1988, pp. 275–285.

Bragov, A. and Lomunov, A., 'Methodological aspects of studying dynamic material properties using the Kolsky method', *International Journal of Impact Engineering*, Vol. 16, No 2, 1995, pp. 321 – 330.

Bridgman, P. W., 'Studies in Large Plastic Flow and Fracture', McGraw Hill, 1952. Pp 9-37.

Cadoni, E., Albertini, C. and Solomos, G., 'Analysis of the concrete behaviour in tension at high strain-rate by a modified hopkinson bar in support of impact resistant structural design', *J. Phys. IV France*, Vol. 134, July 2006, pp. 647–652.

Cadoni, E., D'Aiuto, F. and Albertini, C., 'Dynamic behaviour of advanced high strength steels used in the automobile structures', *DYMAT 2009 - 9th International Conference on the Mechanical and Physical Behaviour of Materials under Dynamic Loading*, Vol. 1, September 2009a, pp. 135–141.

Cadoni, E., Dotta, M., Forni, D. and Spaetig, P., 'Strain-rate behavior in tension of the tempered martensitic reduced activation steel Eurofer97', *Journal of Nuclear Materials*, Vol. 414, No 3, 2011, pp. 360–366. ISSN 0022-3115.

Cadoni, E., Dotta, M., Forni, D. and Späti, P., 'Influence of the temperature on the tension behaviour of EUROFER97 alloy at high strain rate', Vol. 94, 2015, p. 01022.

Cadoni, E., Labibes, K. and Albertini, C., 'Dynamic behavior of plain concrete prisms in tension', Tech. Rep. I.96.175, European Commission - Joint Research Centre, 1996.

Cadoni, E., Labibes, K. and Albertini, C., 'Mechanical response in tension of plain concrete in a large range of strain-rates', Tech. Rep. I.97.194, European Commission - Joint Research Centre, 1997.

Cadoni, E., Labibes, K., Albertini, C., Berra, M. and Giangrasso, M., 'Strain-rate effect on the tensile behaviour of concrete at different relative humidity levels', *Materials and Structures*, Vol. 34, No 1, January 2001, pp. 21–26.

Cadoni, E., Solomos, G. and Albertini, C., 'Mechanical characterisation of concrete in tension and compression at high strain rate using a modified hopkinson bar', *Magazine of Concrete Research*, Vol. 61, No 3, April 2009b, pp. 221–230.

Campbell, J. D., 'Dynamic plasticity: Macroscopic and microscopic aspects', *Materials Science and Engineering*, Vol. 12, No 1, July 1973, pp. 3–21.

Chatani, A., Hojo, A. and Tachiya, H., 'The strength of hard steels at high strain rates', *Proceedings of the International conference Mechanical behaviour of materials*, Vol. 1, 1991, pp. 301–306.

Davis, R., 'A critical study of the Hopkinson pressure bar', *Philosophical Transactions of the Royal Society of London Series A, Mathematical and Physical Sciences*, Vol. 240, 1948, pp. 375–457.

Dieter, G. E., 'Mechanical Metallurgy', McGraw Hill, 1976.

Dodd, B., Stone, R. C. and Campbell, J. D., 'The Strain Rate Sensitivity of 304L Austenitic Stainless Steel in Uniaxial Tension', Tech. Rep. 1069/73, University Of Oxford, Engineering Laboratory, August 1973.

Duffey, T. *Structural Failure*, chap. Dynamic rupture of shells. John Wiley and Sons. ISBN 0-471-63733-5, 1988. pp. 161–192.

Eleiche, A. M., Albertini, C. and Montagnani, M., 'The influence of strain rate history on the ambient tensile strength of AISI type 316 stainless steel', *Nuclear Engineering and Design*, Vol. 88, No 2, 1985, pp. 131–141.

Hayhurst, D. R., 'A biaxial-tension creep rupture testing machine', *Journal Strain Analysis*, Vol. 8, No 2, April 1973, pp. 119–123.

Hecker, S., Stout, M. and Eash, D., 'Experiments on Plastic Deformation at Finite Strains', In 'Workshop on Plasticity of metals at Finite Strains', Stanford University, pp. 162–205.

Hopkinson, B., 'A method of measuring the pressure in the deformation of high explosive by impacts of bullets', *Philosophical Transactions of the Royal Society of London. Series A, Containing Papers of a Mathematical or Physical Character*, Vol. 213, 1914, pp. 437–456.

Hopkinson, J., 'On the rupture of an iron wire by a blow', *Proc. Manchester Literary Philosophical Society*, Vol. 11, 1872, pp. 40–45.

Jonas, J. J., Canova, G. R., Shrivastava, S. C. and Christodoulou, N., 'Sources of Discrepancies between the Flow Curves Determined in Torsion and Axisymmetric Tension and Compression testing', *Workshop on Plasticity of metals at Finite Strains*, January 1982, pp. 206–229.

Kaneko, F. and Malmberg, T., 'Theoretische Analyse eines Ersatzlaengenkonzepts fuer Zugproben nicht-konstanten Querschnitts', Tech. Rep. Ext.8/77-2, KfK Karlsruhe, December 1977.

Kolsky, H., 'An investigation of the mechanical properties of materials at very high rates of loading', *Proceedings of the Physical Society. Section B*, Vol. 62, No 11, November 1949, pp. 676–700.

Krieg, R., Devos, J., Caroli, C., Solomos, G., Ennis, P. J. and Kalkhof, D., 'On the prediction of the reactor vessel integrity under severe accident loadings (rpvs)', *Nuclear Engineering and Design*, Vol. 209, 2001, pp. 117–125.

Labibes, K., Albertini, C. and Solomos, G., 'Precision measurement technique of loads and displacements over an automotive body during crash testing', *SAE Technical Paper*, March 1999.

Lemaitre, J. and Chaboche, J. L., 'Materiaux solides', edited by D. E. Paris, 1985.

Lindholm, U., 'Techniques of metals research', edited by R. B. Editor, Vol. 5. J. Wiley, 1971.

Lindholm, U. and Yeakley, L., 'High strain rate testing: tension and compression', *Experimental Mechanics Journal*, January 1968.

Michel, D. J., Moteff, J. and Lovell, A. J., 'Substructure of type 316 stainless steel deformed in slow tension at temperatures between 21° and 816°C.', *Acta Metallurgica*, Vol. 21, No 9, 1973, pp. 1269 – 1277.

Micunovic, M., Albertini, C. and Montagnani, M., 'High strain rate thermo-inelasticity of damaged AISI 316H', *Int. J. Damage Mechanics*, Vol. 12, 2003, pp. 267–303.

Micunovic, M., Pino, G., Maresca, G. and Albertini, C., 'Some results concerning damage acquired by cruciform Hopkinson bar technique', *Proceedings of 10th European mechanics of materials conference, EMMC10*, 2007, pp. 185–194.

Mines, R. and Ruiz, C., 'The dynamic behaviour of the instrumented Charpy test', *Journal de Physique Colloques*, Vol. 46, No C5, January 1985, pp. C5–187–C5–196.

Mönch, E. and Galster, D., 'A method for producing a defined uniform biaxial tensile stress field', *British Journal of Applied Physics*, Vol. 14, No 11, November 1963, pp. 810–812.

Montagnani, M., Albertini, C., Buzzi, U. and Forlani, M., 'Dispositif de contrainte a accumulation mecanique pour essais dinamique de traction. Institut national de la propriete industrielle. A Paris Brevet No 74.17085. The Patent Office of London, Patent No 1.473.683, 1974. Italian Patent No 50008A'. 1973.

Nadai, A., 'Theory of flow and fracture of solids', McGraw Hill, 1950.

Perzyna, P., 'Modified Theory of Viscoplasticity. Application to Advanced Flow and Instability Phenomena', *Archives of Mechanics*, , No 32, 1980, pp. 403–420.

Pizzinato, E. V., Labibes, K., Schnabel, W., Solomos, G., Viaccoz, B., C.Albertini, Micunovic, M., Maresca, G. and Pino, G., 'Programma di prove per la valutazione di criteri di resistenza per i contenitori metallici di reattori nucleari sotto carichi da incidenti severi', Tech. Rep. I.00.74, JRC Ispra, 2000.

Polakowski, N. and Ripling, E., 'Strength and Structure of Engineering Materials', Prentice-Hall, Inc., Englewood Cliffs, 1966. Pp 382–383.

Pollan, M., 'The omnivore's dilemma', Penguin Group, New York, 2006.

Poston, T., 'A draft of history', edited by K. A. Hauke, University of Georgia Press, Athens, 2000.

Quik, M., Labibes, K., Albertini, C., Valentin, T. and Magain, P., 'Dynamic mechanical properties of some automotive thin sheet steels in tension, compression and shear', *J. Phys. IV France*, Vol. 07, No C3, September 1997, pp. C3–379 – C3–384.

Rodis, A., Del Grande, A., Pizzinato, E. V., Schnabel, W. and C.Albertini, 'Progetto di Barra di Hopkinson per lo studio delle proprietà meccaniche in tensione e taglio, ad alta velocità di deformazione, di acciai, materiali compositi e ceramiche', Tech. Rep. I.00.74, CCR Ispra, 1993.

Solomos, G., Albertini, C., Labibes, K., Pizzinato, E. V. and Viaccoz, B., 'Strain rate effects in nuclear steels at room and high temperature', *Nuclear Engineering and Design*, Vol. 229, No 2–3, April 2004, pp. 139–149.

Solomos, G., Albertini, C., Labibes, K., Pizzinato, V., Viaccoz, B., Delzano, C., Schnabel, W., Kiefer, R., Brogneri, E. and Rochez, E., 'Experimental investigation of strain rate, temperature and size effects in nuclear steels', Tech. Rep. I.00.76, EURATOM, 2000.

Solomos, G., Pizzinato, V., Kiefer, R. and Brogneri, E., 'Dynamic testing of pressure vessel steel 22nimocr37 at room and higher temperatures', Technical Note I.02.38, European Commission - Joint Research Centre, 2002.

Solomos, G., Pizzinato, V., Viaccoz, B., Dyngeland, T., Kiefer, R. and Brogneri, E., 'Results of dynamic tests of 22NiMoCr37 steel specimens.', Technical Note I.03.75, European Commission - Joint Research Centre, 2003.

Surname, F., 'JRC technical reports template', Tech. rep., Joint Research Centre, Via Enrico Fermi 2749, Ispra, VA, Italy, Nov. 2015.

Tarigopula, V., Albertini, C., Langseth, M., Hopperstad, O. S. and Clausen, A. H., 'A hydro-pneumatic machine for intermediate strain-rates: Set-up, tests and numerical simulations', *DYMAT - International Conference on the Mechanical and Physical Behaviour of Materials under Dynamic Loading*, Vol. 1, 2009, pp. 381–387.

Tong, J. W., Congfeng, G., Hongqi, L., Min, S., Albertini, C. and Pizzinato, E. V., 'Numerical analysis on the error in the split Hopkinson bar at temperature gradient', *Explosion and Shock Waves Journal*, Vol. 21, No 4, October 2001.

Verheyden, N., Montagnani, M., Albertini, C., Forlani, M. and Prosdocimi, G., 'Dispositif permettant de bloquer et de libérer brusquement une barre de test soumise à des efforts de traction et/ou de torsion. European Patent 0 364 919 B1'.

Yokoyama, T. and Kishida, K., 'A novel impact three-point bend test method for determining dynamic fracture-initiation toughness', *Experimental Mechanics*, Vol. 29, No 2, June 1989, pp. 188–194.

Zener, C. and Hollomon, J., 'Effect of Strain Rate Upon Plastic Flow of Steel', *Journal of Applied Physics*, Vol. 15, No 1, 1944, pp. 22–32.

Zerilli, F. J. and Armstrong, R. W., 'Dislocations Mechanics Based Constitutive Relations for Material Dynamics Calculations', *Journal of Applied Physics*, Vol. 61, No 5, 1987, pp. 1816–1825.

## List of figures

<b>Figure 2.1.</b> Stress vs. strain curves of AISI 316H stainless steel at different strain-rates and at room temperature. (S= Static, Hyd= Hydro-pneumatic machine, MHB= Modified Hopkinson Bar) . . . . .	7
<b>Figure 5.1.</b> Stress vs. strain curves of FEE355 at room temperature for a wide range of strain-rates. . . . .	12
<b>Figure 6.1.</b> Classical Split Hopkinson Pressure Bar (SHPB) . . . . .	13
<b>Figure 6.2.</b> Modified Hopkinson Bar with pre-stressed bar loading device for tensile testing . . . . .	14
<b>Figure 6.3.</b> Blocking system called $\theta$ theta clamp . . . . .	15
<b>Figure 6.4.</b> Record of a test with the MHB taken with a valve oscilloscope. . . . .	16
<b>Figure 6.5.</b> Record of a test with the MHB taken with modern transient recorder. . . . .	16
<b>Figure 6.6.</b> Specimen for a material tensile test with the MHB. . . . .	18
<b>Figure 6.7.</b> Engineering stress vs. strain curves of Ni201 steel in tension at room temperature. . . . .	19
<b>Figure 6.8.</b> Engineering stress vs. strain curves of AISI 316H steel in tension at different strain-rates and at 20°C. . . . .	19
<b>Figure 6.9.</b> Engineering stress vs. strain curves of AISI 316H steel in tension at different strain-rates and at 300°C. . . . .	20
<b>Figure 6.10.</b> Schematic of Hydro-Pneumatic Machine for dynamic tensile tests at constant strain-rate ( $10^{-1}$ - $100\text{ s}^{-1}$ ). . . . .	21
<b>Figure 6.11.</b> Record of a tension test with the Hydro-Pneumatic Machine, registered with a digital transient recorder. . . . .	22
<b>Figure 6.12.</b> Modified Hopkinson Bar with telemanipulators inside a large hot cell. . . . .	24
<b>Figure 6.13.</b> Modified Hopkinson Bar apparatus for dynamic tensile tests mounted in the hot cell. . . . .	24
<b>Figure 6.14.</b> Telemanipulators and instrumentation serving the MHB in the large hot cell. . . . .	25
<b>Figure 6.15.</b> Irradiated specimen connected to input and output bars of the MHB in the large hot cell. . . . .	25
<b>Figure 6.16.</b> Small hot cell with the input bar (right) and output passing through the shield walls. . . . .	26
<b>Figure 6.17.</b> Small hot cell with view of the input and pre-tensioned bar of the MHB and of the operating small telemanipulator. . . . .	26
<b>Figure 6.18.</b> Recording instrumentation serving the MHB installed in the small hot cell. . . . .	27
<b>Figure 6.19.</b> Interior of small hot cell: input, output bars and oven surrounding the specimen. . . . .	27
<b>Figure 6.20.</b> Hydro-Pneumatic machine for dynamic tensile test mounted in the large hot cell. . . . .	28
<b>Figure 6.21.</b> Specimen heating set-up for dynamic testing at high temperature with the MHB. . . . .	28
<b>Figure 6.22.</b> Large specimen for the study of the mechanical properties of real size welds at high strain-rate. 30	30
<b>Figure 6.23.</b> Specimens of 3, 9, 30mm diameter for the study of size effects at high strain-rate. . . . .	31
<b>Figure 6.24.</b> Schematic of Large MHB in the one-arm configuration for testing of large specimens. . . . .	31
<b>Figure 6.25.</b> Stress-strain curves of 3, 9, 30mm diameter specimens of austenitic steel X6CrNiNb1810. . . . .	31
<b>Figure 7.1.</b> Engineering stress vs. strain curves of AISI 304L steel as-received from quasi-static to high strain-rate, at ambient temperature (Albertini and Montagnani, 1980) (Ref.Mat.1). . . . .	33
<b>Figure 7.2.</b> Engineering stress vs. strain curves of AISI 321 stainless steel (Albertini and Montagnani, 1980), (Albertini and Montagnani, 1983a) from quasi-static to high strain-rate, at ambient temperature (Ref.Mat.2). . . . .	33
<b>Figure 7.3.</b> Engineering stress vs. strain curves of AISI 316L stainless steel from quasi-static to high strain-rate at ambient temperature (Albertini and Montagnani, 1978), (Albertini et al., 1978), (Albertini et al., 1979), (Albertini and Montagnani, 1980), (Albertini et al., 1980), (Albertini and Montagnani, 1981a), (Albertini et al., 1982), (Albertini and Montagnani, 1983b) (Ref.Mat.3). . . . .	34
<b>Figure 7.4.</b> Engineering stress vs. strain curves of AISI 316H as-received stainless steel from quasi-static to high strain-rate at ambient temperature (Albertini et al., 1983b), (Albertini et al., 1983a), (Albertini et al., 1984b). . . . .	34
<b>Figure 7.5.</b> Engineering stress vs. strain curves of X6CrNiNb1810 steel for several strain-rates and two temperatures (Solomos et al., 2004, Solomos et al., 2003). . . . .	35
<b>Figure 7.6.</b> Engineering stress vs. strain curves of ASME 537 cl1 steel from quasi-static to high strain-rate at ambient temperature (Albertini, 1997). . . . .	35
<b>Figure 7.7.</b> Engineering stress vs. strain curves of ASME 537 cl1 at 300°C at several strain-rates (Albertini, 1997). . . . .	36
<b>Figure 7.8.</b> Engineering stress vs. strain curves of 20MnMoNi55 at different strain-rates at R.T and 400°C (Solomos et al., 2004, Solomos et al., 2003). . . . .	36
<b>Figure 7.9.</b> Engineering stress vs. strain curves of AISI 316H (Ref.Mat) at different strain-rates and 100°C (Birch et al., 1988, Albertini et al., 1985b). . . . .	37
<b>Figure 7.10.</b> Engineering stress vs. strain curves of AISI 316H stainless steel at different strain-rates and 200°C (Birch et al., 1988, Albertini et al., 1985b). . . . .	37
<b>Figure 7.11.</b> Engineering stress vs. strain curves of AISI 316H stainless steel at different strain-rates and 300°C (Birch et al., 1988, Albertini et al., 1985b). . . . .	38

<b>Figure 7.12.</b> Engineering stress vs. strain curves of AISI 316H stainless steel at different strain-rates and 400°C (Birch et al., 1988, Albertini et al., 1985b) . . . . .	38
<b>Figure 7.13.</b> Engineering stress vs. strain curves of AISI 304L (Ref.Mat.1) stainless steel at 400°C (Albertini and Montagnani, 1980) at quasi-static and high strain-rate. . . . .	39
<b>Figure 7.14.</b> Engineering stress vs. strain curves of AISI 321(Ref.Mat.2) stainless steel at 400°C (Albertini and Montagnani, 1980) at quasi-static and high strain-rate. . . . .	39
<b>Figure 7.15.</b> Engineering stress vs. strain curves of AISI 316L (Ref.Mat.3) stainless steel at different strain-rates and 400°C (Albertini et al., 1983a, Eleiche et al., 1985). . . . .	40
<b>Figure 7.16.</b> Engineering stress vs. strain curves of AISI 316H stainless steel at different strain-rates and 550°C (Albertini et al., 1983a, Albertini and Montagnani, 1983b, Albertini and Labibes, a, Birch et al., 1988, Albertini et al., 1985b). . . . .	40
<b>Figure 7.17.</b> Engineering stress vs. strain curves of AISI 316L stainless steel at different strain-rates and 550°C (Albertini and Montagnani, 1978, Albertini and Montagnani, 1979, Albertini and Montagnani, 1980). . . . .	41
<b>Figure 7.18.</b> Engineering stress vs. strain curves of DIN 1.4981 stainless steel at different strain-rates and 550°C (Albertini et al., 1987b). . . . .	41
<b>Figure 7.19.</b> Engineering stress vs. strain curves of AISI 316H stainless steel at different strain-rates and 650°C (Birch et al., 1988, Albertini et al., 1985b). . . . .	42
<b>Figure 7.20.</b> Engineering stress vs. strain curves of AISI 304L as-received stainless steel at different strain-rates and 550°C (Albertini and Montagnani, 1976). . . . .	42
<b>Figure 7.21.</b> Engineering stress vs. strain curves of AISI 316L as-received stainless steel at different strain-rates and 950°C (Albertini et al., 1991b). . . . .	43
<b>Figure 7.22.</b> Engineering stress vs. strain curves of AISI 316L as-received stainless steel at different strain-rates and 750°C (Albertini and Montagnani, 1980). . . . .	43
<b>Figure 7.23.</b> Engineering stress vs. strain curves of AISI 321 as-received stainless steel at different strain-rates and 950°C (Albertini and Montagnani, 1980). . . . .	44
<b>Figure 7.24.</b> Effect of strain-rate on the engineering uniform elongation of AISI 316L at different temperatures. . . . .	44
<b>Figure 7.25.</b> Effect of strain-rate on the engineering uniform elongation of AISI 316H at different temperatures. . . . .	45
<b>Figure 7.26.</b> Effect of strain-rate on the ultimate tensile strength at room temperature and 650°C of AISI 316H as-received stainless steel. . . . .	45
<b>Figure 7.27.</b> Effect of strain-rate on the ultimate tensile strength at room temperature and 600°C of X6CrNiNb1810 as-received stainless steel. . . . .	46
<b>Figure 7.28.</b> Stress vs. strain curve of AISI 304L at different strain-rates and temperatures: a) As-received; b) Irradiated at 30 dpa. . . . .	47
<b>Figure 7.29.</b> Engineering stress vs. strain curves of AISI 316L as-received and irradiated to 9.2 dpa at 550°C and different strain-rates (Albertini et al., 1984a). . . . .	47
<b>Figure 7.30.</b> Effect of strain-rate on the 0.2% yield stress of AISI 316L stainless steel irradiated to 9.2 dpa in sodium at 550°C (Albertini et al., 1984a). . . . .	48
<b>Figure 7.31.</b> Effect of strain-rate on the uniform elongation of AISI 316L stainless steel irradiated to 9.2 dpa in sodium at 550°C (Albertini et al., 1984a). . . . .	48
<b>Figure 7.32.</b> Effect of dose on fracture strain and uniform deformation of AISI 316L stainless steel irradiated at 400°C (2.2 dpa) and at 500°C (9.2 dpa) (Albertini et al., 1984a). . . . .	49
<b>Figure 7.33.</b> Engineering stress vs. strain curves for PE16 nimonic alloy irradiated to 9.2 dpa tested at different strain-rates and 500°C (Albertini et al., 1987a). . . . .	49
<b>Figure 7.34.</b> Engineering stress vs. strain curves for PE16 nimonic alloy thermally aged for 9864 hours in sodium tested at different strain-rates and 500°C (Albertini et al., 1987a). . . . .	50
<b>Figure 7.35.</b> Engineering stress vs. strain curves for PE16 nimonic alloy as-received tested at different strain-rates and 500°C (Albertini et al., 1987a). . . . .	50
<b>Figure 7.36.</b> Engineering stress vs. strain curves for AISI 316H as-received and prefatigued tested at different strain-rates and 550°C . . . . .	51
<b>Figure 7.37.</b> Engineering stress vs. strain curves for AISI 316H as-received, prefatigued and irradiated to 2.2 dpa tested at different strain-rates and 550°C. . . . .	52
<b>Figure 7.38.</b> Engineering ultimate tensile strength vs. strain-rate, engineering 0.2% yield stress vs. strain-rate; AISI 316H stainless steel prefatigued with cycle strain range 1% and irradiated to 2.2 dpa (550°C). . . . .	52
<b>Figure 7.39.</b> Uniform strain vs. strain-rate, AISI 316H stainless steel prefatigued with cycle strain range 1% and irradiated to 2.2 dpa (550°C). . . . .	53
<b>Figure 7.40.</b> Fracture strain vs. strain-rate, AISI 316H stainless steel prefatigued with cycle strain range 1% and irradiated to 2.2 dpa (550°C). . . . .	53

<b>Figure 7.41.</b> Engineering stress vs. strain curves for AISI 316H as-received and after creep test (550°C) . . . . .	54
<b>Figure 7.42.</b> Engineering 0.2% yield stress and ultimate tensile strength of as-received and after creep test vs. strain-rate of AISI 316H stainless steel (550°C) . . . . .	54
<b>Figure 7.43.</b> Engineering uniform strain and fracture strain of as-received and after creep test vs. strain-rate of AISI 316H stainless steel (550°C) . . . . .	55
<b>Figure 7.44.</b> Engineering stress vs. strain curves for AISI 316H stainless steel base material (collaboration EURATOM-U.K.A.E.A.) tested at 400°C (Albertini and Montagnani, 1978) . . . . .	56
<b>Figure 7.45.</b> Engineering stress vs. strain curves for AISI 316H stainless steel weld+heat affected zone material tested at different strain-rates and 400°C (collaboration EURATOM-U.K.A.E.A.) (Albertini and Montagnani, 1978) . . . . .	56
<b>Figure 7.46.</b> Engineering stress vs. strain curves for AISI 316H stainless steel weld material tested at different strain-rates and 400°C (collaboration EURATOM-U.K.A.E.A.) (Albertini and Montagnani, 1978) . . . . .	57
<b>Figure 7.47.</b> Effect of strain-rate on 0.2% yield stress of AISI 316H stainless steel base, weld, weld+heat affected zone materials tested at room temperature and 400°C (collaboration EURATOM-U.K.A.E.A.) (Albertini and Montagnani, 1978) . . . . .	57
<b>Figure 7.48.</b> Effect of strain-rate on the ultimate tensile strength of AISI 316H stainless steel base, weld, weld+heat affected zone materials tested at room temperature and 400°C (collaboration EURATOM-U.K.A.E.A.) (Albertini and Montagnani, 1978) . . . . .	58
<b>Figure 7.49.</b> Effect of strain-rate on engineering fracture strain of AISI 316H stainless steel base, weld, weld+heat affected zone materials tested at room temperature and 400°C (collaboration EURATOM-U.K.A.E.A.) (Albertini and Montagnani, 1978) . . . . .	58
<b>Figure 7.50.</b> Wave transmission and reflection diagram along the Hopkinson bar, reconfigured with the addition of an extension bar and a ballistic pendulum. . . . .	60
<b>Figure 7.51.</b> Oscilloscope traces of the records of test performed with the Hopkinson bar, re-configured with the addition of a bar as a ballistic pendulum upstream (on the pre-tensioned bar) and of an extension bar downstream (on the transmitter bar) (Albertini et al., 1985b) . . . . .	60
<b>Figure 7.52.</b> True stress vs. true strain curves of AISI 316H for interrupted and monotonic quasi-static ( $0.004\text{ s}^{-1}$ ) and dynamic ( $500\text{s}^{-1}$ ) loading at 20°C (Albertini et al., 1985b) . . . . .	61
<b>Figure 7.53.</b> True stress vs. true strain curves of AISI 316H for interrupted and monotonic quasi-static ( $0.004\text{ s}^{-1}$ ) and dynamic ( $500\text{s}^{-1}$ ) loading at 550°C (Albertini et al., 1985b) . . . . .	61
<b>Figure 7.54.</b> Monotonic and interrupted quasi-static to dynamic jump true stress vs. true strain curves at 20°C (Albertini et al., 1985b) . . . . .	63
<b>Figure 7.55.</b> Monotonic and interrupted quasi-static to dynamic jump true stress vs. true strain curves at 300°C (Albertini et al., 1985b) . . . . .	64
<b>Figure 7.56.</b> Monotonic and interrupted quasi-static to dynamic jump true stress vs. true strain curves at 400°C (Albertini et al., 1985b) . . . . .	64
<b>Figure 7.57.</b> Monotonic and interrupted quasi-static to dynamic jump true stress vs. true strain curves at 550°C (Albertini et al., 1985b) . . . . .	65
<b>Figure 7.58.</b> Monotonic and interrupted quasi-static to dynamic jump true stress vs. true strain curves at 650°C (Albertini et al., 1985b) . . . . .	65
<b>Figure 7.59.</b> Monotonic and interrupted dynamic to quasi-static jump true stress vs. true strain curves at 20°C (Albertini et al., 1985b) . . . . .	66
<b>Figure 7.60.</b> Monotonic and interrupted dynamic to quasi-static jump true stress vs. true strain curves at 100°C (Albertini et al., 1985b) . . . . .	66
<b>Figure 7.61.</b> Monotonic and interrupted dynamic to quasi-static jump true stress vs. true strain curves at 200°C (Albertini et al., 1985b) . . . . .	67
<b>Figure 7.62.</b> Monotonic and interrupted dynamic to quasi-static jump true stress vs. true strain curves at 300°C (Albertini et al., 1985b) . . . . .	67
<b>Figure 7.63.</b> Monotonic and interrupted dynamic to quasi-static jump true stress vs. true strain curves at 400°C (Albertini et al., 1985b) . . . . .	68
<b>Figure 7.64.</b> Monotonic and interrupted dynamic to quasi-static jump true stress vs. true strain curves at 550°C (Albertini et al., 1985b) . . . . .	68
<b>Figure 7.65.</b> Monotonic and interrupted dynamic to quasi-static jump true stress vs. true strain curves at 650°C (Albertini et al., 1985b) . . . . .	69
<b>Figure 9.1.</b> Stress vs strain curves of AISI 304 (Ref.Mat.4) . . . . .	87
<b>Figure 9.2.</b> Stress vs strain curves of AISI 304 (Ref.Mat.4) . . . . .	88
<b>Figure 9.3.</b> Stress vs strain curves of AISI 304 (Ref.Mat.4) . . . . .	89
<b>Figure 9.4.</b> Stress vs strain curves of AISI 304 (Ref.Mat.4) . . . . .	90
<b>Figure 9.5.</b> Stress vs strain curves of AISI 304 (Ref.Mat.4) . . . . .	91
<b>Figure 9.6.</b> Stress vs strain curves of AISI 304 (Ref.Mat.4) . . . . .	92







<b>Figure 9.190.</b> Stress vs strain curves of DIN 1.4306 . . . . .	276
<b>Figure 9.191.</b> Stress vs strain curves of DIN 1.4306 . . . . .	277
<b>Figure 9.192.</b> Stress vs strain curves of DIN 1.4981 . . . . .	278
<b>Figure 9.193.</b> Stress vs strain curves of DIN 1.4981 . . . . .	279
<b>Figure 9.194.</b> Stress vs strain curves of DIN ST 35 . . . . .	280
<b>Figure 9.195.</b> Stress vs strain curves of DIN ST 35 . . . . .	281
<b>Figure 9.196.</b> Stress vs strain curves of AISI 347 . . . . .	282
<b>Figure 9.197.</b> Stress vs strain curves of Steel X52 . . . . .	283
<b>Figure 9.198.</b> Stress vs strain curves of Steel X52 . . . . .	284
<b>Figure 9.199.</b> Stress vs strain curves of Steel X52 . . . . .	285
<b>Figure 9.200.</b> Stress vs strain curves of Steel X60 . . . . .	286
<b>Figure 9.201.</b> Stress vs strain curves of Steel X60 . . . . .	287
<b>Figure 9.202.</b> Stress vs strain curves of Steel X60 . . . . .	288
<b>Figure 9.203.</b> Stress vs strain curves of Fe360 . . . . .	289
<b>Figure 9.204.</b> Stress vs strain curves of Fe430 . . . . .	290
<b>Figure 9.205.</b> Stress vs strain curves of EN 2 STEEL . . . . .	291
<b>Figure 9.206.</b> Stress vs strain curves of Aluminium 6061 . . . . .	292
<b>Figure 9.207.</b> Stress vs strain curves of Aluminium 6061 . . . . .	293
<b>Figure 9.208.</b> Stress vs strain curves of Mild Steel 4mm . . . . .	294
<b>Figure 9.209.</b> Stress vs strain curves of Mild Steel 6mm . . . . .	295
<b>Figure 9.210.</b> Stress vs strain curves of Carbon steel . . . . .	296
<b>Figure 9.211.</b> Stress vs strain curves of Carbon steel . . . . .	297
<b>Figure 9.212.</b> Stress vs strain curves of AUSTENITIC X6CrNiNb1810 . . . . .	298
<b>Figure 9.213.</b> Stress vs strain curves of AUSTENITIC X6CrNiNb1810 . . . . .	299
<b>Figure 9.214.</b> Stress vs strain curves of AUSTENITIC X6CrNiNb1810 . . . . .	300
<b>Figure 9.215.</b> Stress vs strain curves of AUSTENITIC X6CrNiNb1810 . . . . .	301
<b>Figure 9.216.</b> Stress vs strain curves of AUSTENITIC X6CrNiNb1810 . . . . .	302
<b>Figure 9.217.</b> Stress vs strain curves of AUSTENITIC X6CrNiNb1810 . . . . .	303
<b>Figure 9.218.</b> Stress vs strain curves of AUSTENITIC X6CrNiNb1810 . . . . .	304
<b>Figure 9.219.</b> Stress vs strain curves of AUSTENITIC X6CrNiNb1810 . . . . .	305
<b>Figure 9.220.</b> Stress vs strain curves of AUSTENITIC X6CrNiNb1810 . . . . .	306
<b>Figure 9.221.</b> Stress vs strain curves of AUSTENITIC X6CrNiNb1810 . . . . .	307
<b>Figure 9.222.</b> Stress vs strain curves of AUSTENITIC X6CrNiNb1810 . . . . .	308
<b>Figure 9.223.</b> Stress vs strain curves of AUSTENITIC X6CrNiNb1810 . . . . .	309
<b>Figure 9.224.</b> Stress vs strain curves of AUSTENITIC X6CrNiNb1810 . . . . .	310
<b>Figure 9.225.</b> Stress vs strain curves of AUSTENITIC X6CrNiNb1810 . . . . .	311
<b>Figure 9.226.</b> Stress vs strain curves of AUSTENITIC X6CrNiNb1810 . . . . .	312
<b>Figure 9.227.</b> Stress vs strain curves of AUSTENITIC X6CrNiNb1810 . . . . .	313
<b>Figure 9.228.</b> Stress vs strain curves of FERRITIC 20MnMoNi55 . . . . .	314
<b>Figure 9.229.</b> Stress vs strain curves of FERRITIC 20MnMoNi55 . . . . .	315
<b>Figure 9.230.</b> Stress vs strain curves of FERRITIC 20MnMoNi55 . . . . .	316
<b>Figure 9.231.</b> Stress vs strain curves of FERRITIC 20MnMoNi55 . . . . .	317
<b>Figure 9.232.</b> Stress vs strain curves of FERRITIC 20MnMoNi55 . . . . .	318
<b>Figure 9.233.</b> Stress vs strain curves of FERRITIC 20MnMoNi55 . . . . .	319
<b>Figure 9.234.</b> Stress vs strain curves of FERRITIC 20MnMoNi55 . . . . .	320
<b>Figure 9.235.</b> Stress vs strain curves of FERRITIC 20MnMoNi55 . . . . .	321
<b>Figure 9.236.</b> Stress vs strain curves of FERRITIC 20MnMoNi55 . . . . .	322
<b>Figure 9.237.</b> Stress vs strain curves of FERRITIC 20MnMoNi55 . . . . .	323
<b>Figure 9.238.</b> Stress vs strain curves of FERRITIC 20MnMoNi55 . . . . .	324
<b>Figure 9.239.</b> Stress vs strain curves of FERRITIC 20MnMoNi55 . . . . .	325
<b>Figure 9.240.</b> Stress vs strain curves of FERRITIC 20MnMoNi55 . . . . .	326
<b>Figure 9.241.</b> Stress vs strain curves of FERRITIC 20MnMoNi55 . . . . .	327
<b>Figure 9.242.</b> Stress vs strain curves of FERRITIC 20MnMoNi55 . . . . .	328
<b>Figure 9.243.</b> Stress vs strain curves of FERRITIC 20MnMoNi55 . . . . .	329
<b>Figure 9.244.</b> Stress vs strain curves of FERRITIC 20NiMoCr37 . . . . .	330
<b>Figure 9.245.</b> Stress vs strain curves of FERRITIC 20NiMoCr37 . . . . .	331
<b>Figure 9.246.</b> Stress vs strain curves of FERRITIC 20NiMoCr37 . . . . .	332
<b>Figure 9.247.</b> Stress vs strain curves of FERRITIC 20NiMoCr37 . . . . .	333
<b>Figure 9.248.</b> Stress vs strain curves of FERRITIC 20NiMoCr37 . . . . .	334
<b>Figure 9.249.</b> Stress vs strain curves of FERRITIC 20NiMoCr37 . . . . .	335
<b>Figure 9.250.</b> Stress vs strain curves of FERRITIC 20NiMoCr37 . . . . .	336

<b>Figure 9.251.</b> Stress vs strain curves of FERRITIC 20NiMoCr37 . . . . .	337
<b>Figure 9.252.</b> Stress vs strain curves of FERRITIC 26NiCrMo146 . . . . .	338
<b>Figure 9.253.</b> Stress vs strain curves of FERRITIC 26NiCrMo146 . . . . .	339
<b>Figure 9.254.</b> Stress vs strain curves of FERRITIC 26NiCrMo146 . . . . .	340
<b>Figure 9.255.</b> Stress vs strain curves of FERRITIC 26NiCrMo146 . . . . .	341
<b>Figure 9.256.</b> Stress vs strain curves of Eurofer97 . . . . .	342

## List of tables

<b>Table 1.</b> Mechanical properties of AISI 304 (Ref.Mat.4) . . . . .	87
<b>Table 2.</b> Mechanical properties of AISI 304 (Ref.Mat.4) . . . . .	88
<b>Table 3.</b> Mechanical properties of AISI 304 (Ref.Mat.4) . . . . .	89
<b>Table 4.</b> Mechanical properties of AISI 304 (Ref.Mat.4) . . . . .	90
<b>Table 5.</b> Mechanical properties of AISI 304 (Ref.Mat.4) . . . . .	91
<b>Table 6.</b> Mechanical properties of AISI 304 (Ref.Mat.4) . . . . .	92
<b>Table 7.</b> Mechanical properties of AISI 304 (Ref.Mat.4) . . . . .	93
<b>Table 8.</b> Mechanical properties of AISI 304 (Ref.Mat.4) . . . . .	94
<b>Table 9.</b> Mechanical properties of AISI 304 (Ref.Mat.4) . . . . .	95
<b>Table 10.</b> Mechanical properties of AISI 304 (Ref.Mat.4) . . . . .	96
<b>Table 11.</b> Mechanical properties of AISI 304 (Ref.Mat.4) . . . . .	97
<b>Table 12.</b> Mechanical properties of AISI 304 (Ref.Mat.4) . . . . .	98
<b>Table 13.</b> Mechanical properties of AISI 304 (Ref.Mat.4) . . . . .	99
<b>Table 14.</b> Mechanical properties of AISI 304 (Ref.Mat.4) . . . . .	100
<b>Table 15.</b> Mechanical properties of AISI 304 (Ref.Mat.4) . . . . .	101
<b>Table 16.</b> Mechanical properties of AISI 304 (Ref.Mat.4) . . . . .	102
<b>Table 17.</b> Mechanical properties of AISI 304 (Ref.Mat.4) . . . . .	103
<b>Table 18.</b> Mechanical properties of AISI 304 (Ref.Mat.4) . . . . .	104
<b>Table 19.</b> Mechanical properties of AISI 304 . . . . .	105
<b>Table 20.</b> Mechanical properties of AISI 304 . . . . .	106
<b>Table 21.</b> Mechanical properties of AISI 304 . . . . .	107
<b>Table 22.</b> Mechanical properties of AISI 304 . . . . .	108
<b>Table 23.</b> Mechanical properties of SUS 304 . . . . .	109
<b>Table 24.</b> Mechanical properties of SUS 304 . . . . .	110
<b>Table 25.</b> Mechanical properties of SUS 304 . . . . .	111
<b>Table 26.</b> Mechanical properties of SUS 304 . . . . .	112
<b>Table 27.</b> Mechanical properties of SUS 304 . . . . .	113
<b>Table 28.</b> Mechanical properties of SUS 304 . . . . .	114
<b>Table 29.</b> Mechanical properties of SUS 304 . . . . .	115
<b>Table 30.</b> Mechanical properties of SUS 304 . . . . .	116
<b>Table 31.</b> Mechanical properties of SUS 304 . . . . .	117
<b>Table 32.</b> Mechanical properties of SUS 304 . . . . .	118
<b>Table 33.</b> Mechanical properties of SUS 304 . . . . .	119
<b>Table 34.</b> Mechanical properties of SUS 304 . . . . .	120
<b>Table 35.</b> Mechanical properties of SUS 304 . . . . .	121
<b>Table 36.</b> Mechanical properties of Ni 201 . . . . .	122
<b>Table 37.</b> Mechanical properties of Ni 201 . . . . .	123
<b>Table 38.</b> Mechanical properties of Ni 201 . . . . .	124
<b>Table 39.</b> Mechanical properties of Ni 201 . . . . .	125
<b>Table 40.</b> Mechanical properties of AISI 304L . . . . .	126
<b>Table 41.</b> Mechanical properties of AISI 304L . . . . .	127
<b>Table 42.</b> Mechanical properties of AISI 304L . . . . .	128
<b>Table 43.</b> Mechanical properties of AISI 304L . . . . .	129
<b>Table 44.</b> Mechanical properties of AISI 304L (Ref.Mat.1) . . . . .	130
<b>Table 45.</b> Mechanical properties of AISI 304L (Ref.Mat.1) . . . . .	131
<b>Table 46.</b> Mechanical properties of AISI 304L (Ref.Mat.1) . . . . .	132
<b>Table 47.</b> Mechanical properties of AISI 304L (Ref.Mat.1) . . . . .	133
<b>Table 48.</b> Mechanical properties of AISI 304L (Ref.Mat.1) . . . . .	134
<b>Table 49.</b> Mechanical properties of AISI 304L (Ref.Mat.1) . . . . .	135
<b>Table 50.</b> Mechanical properties of AISI 304L (Ref.Mat.1) . . . . .	136
<b>Table 51.</b> Mechanical properties of AISI 304L (Ref.Mat.1) . . . . .	137
<b>Table 52.</b> Mechanical properties of AISI 304L (Ref.Mat.1) . . . . .	138
<b>Table 53.</b> Mechanical properties of AISI 304L (Ref.Mat.1) . . . . .	139
<b>Table 54.</b> Mechanical properties of AISI 304L (Ref.Mat.1) . . . . .	140
<b>Table 55.</b> Mechanical properties of AISI 304L (Ref.Mat.1) . . . . .	141
<b>Table 56.</b> Mechanical properties of AISI 304L (Ref.Mat.1) . . . . .	142
<b>Table 57.</b> Mechanical properties of AISI 304L (Ref.Mat.1) . . . . .	143
<b>Table 58.</b> Mechanical properties of AISI 304L (Ref.Mat.1) . . . . .	144
<b>Table 59.</b> Mechanical properties of AISI 304L (Ref.Mat.1) . . . . .	145





<b>Table 182.</b> Mechanical properties of AISI 321 (Ref.Mat.2) . . . . .	268
<b>Table 183.</b> Mechanical properties of AISI 321 (Ref.Mat.2) . . . . .	269
<b>Table 184.</b> Mechanical properties of AISI 321 (Ref.Mat.2) . . . . .	270
<b>Table 185.</b> Mechanical properties of AISI 321 (Ref.Mat.2) . . . . .	271
<b>Table 186.</b> Mechanical properties of AISI 321 (Ref.Mat.2) . . . . .	272
<b>Table 187.</b> Mechanical properties of AISI 321 (Ref.Mat.2) . . . . .	273
<b>Table 188.</b> Mechanical properties of AISI 321 (Ref.Mat.2) . . . . .	274
<b>Table 189.</b> Mechanical properties of AISI 321 (Ref.Mat.2) . . . . .	275
<b>Table 190.</b> Mechanical properties of DIN 1.4306 . . . . .	276
<b>Table 191.</b> Mechanical properties of DIN 1.4306 . . . . .	277
<b>Table 192.</b> Mechanical properties of DIN 1.4981 . . . . .	278
<b>Table 193.</b> Mechanical properties of DIN 1.4981 . . . . .	279
<b>Table 194.</b> Mechanical properties of DIN ST 35 . . . . .	280
<b>Table 195.</b> Mechanical properties of DIN ST 35 . . . . .	281
<b>Table 196.</b> Mechanical properties of AISI 347 . . . . .	282
<b>Table 197.</b> Mechanical properties of Steel X52 . . . . .	283
<b>Table 198.</b> Mechanical properties of Steel X52 . . . . .	284
<b>Table 199.</b> Mechanical properties of Steel X52 . . . . .	285
<b>Table 200.</b> Mechanical properties of Steel X60 . . . . .	286
<b>Table 201.</b> Mechanical properties of Steel X60 . . . . .	287
<b>Table 202.</b> Mechanical properties of Steel X60 . . . . .	288
<b>Table 203.</b> Mechanical properties of Fe360 . . . . .	289
<b>Table 204.</b> Mechanical properties of Fe430 . . . . .	290
<b>Table 205.</b> Mechanical properties of EN 2 STEEL . . . . .	291
<b>Table 206.</b> Mechanical properties of Aluminium 6061 . . . . .	292
<b>Table 207.</b> Mechanical properties of Aluminium 6061 . . . . .	293
<b>Table 208.</b> Mechanical properties of Mild Steel 4mm . . . . .	294
<b>Table 209.</b> Mechanical properties of Mild Steel 6mm . . . . .	295
<b>Table 210.</b> Mechanical properties of Carbon steel . . . . .	296
<b>Table 211.</b> Mechanical properties of Carbon steel . . . . .	297
<b>Table 212.</b> Mechanical properties of AUSTENITIC X6CrNiNb1810 . . . . .	298
<b>Table 213.</b> Mechanical properties of AUSTENITIC X6CrNiNb1810 . . . . .	299
<b>Table 214.</b> Mechanical properties of AUSTENITIC X6CrNiNb1810 . . . . .	300
<b>Table 215.</b> Mechanical properties of AUSTENITIC X6CrNiNb1810 . . . . .	301
<b>Table 216.</b> Mechanical properties of AUSTENITIC X6CrNiNb1810 . . . . .	302
<b>Table 217.</b> Mechanical properties of AUSTENITIC X6CrNiNb1810 . . . . .	303
<b>Table 218.</b> Mechanical properties of AUSTENITIC X6CrNiNb1810 . . . . .	304
<b>Table 219.</b> Mechanical properties of AUSTENITIC X6CrNiNb1810 . . . . .	305
<b>Table 220.</b> Mechanical properties of AUSTENITIC X6CrNiNb1810 . . . . .	306
<b>Table 221.</b> Mechanical properties of AUSTENITIC X6CrNiNb1810 . . . . .	307
<b>Table 222.</b> Mechanical properties of AUSTENITIC X6CrNiNb1810 . . . . .	308
<b>Table 223.</b> Mechanical properties of AUSTENITIC X6CrNiNb1810 . . . . .	309
<b>Table 224.</b> Mechanical properties of AUSTENITIC X6CrNiNb1810 . . . . .	310
<b>Table 225.</b> Mechanical properties of AUSTENITIC X6CrNiNb1810 . . . . .	311
<b>Table 226.</b> Mechanical properties of AUSTENITIC X6CrNiNb1810 . . . . .	312
<b>Table 227.</b> Mechanical properties of AUSTENITIC X6CrNiNb1810 . . . . .	313
<b>Table 228.</b> Mechanical properties of FERRITIC 20MnMoNi55 . . . . .	314
<b>Table 229.</b> Mechanical properties of FERRITIC 20MnMoNi55 . . . . .	315
<b>Table 230.</b> Mechanical properties of FERRITIC 20MnMoNi55 . . . . .	316
<b>Table 231.</b> Mechanical properties of FERRITIC 20MnMoNi55 . . . . .	317
<b>Table 232.</b> Mechanical properties of FERRITIC 20MnMoNi55 . . . . .	318
<b>Table 233.</b> Mechanical properties of FERRITIC 20MnMoNi55 . . . . .	319
<b>Table 234.</b> Mechanical properties of FERRITIC 20MnMoNi55 . . . . .	320
<b>Table 235.</b> Mechanical properties of FERRITIC 20MnMoNi55 . . . . .	321
<b>Table 236.</b> Mechanical properties of FERRITIC 20MnMoNi55 . . . . .	322
<b>Table 237.</b> Mechanical properties of FERRITIC 20MnMoNi55 . . . . .	323
<b>Table 238.</b> Mechanical properties of FERRITIC 20MnMoNi55 . . . . .	324
<b>Table 239.</b> Mechanical properties of FERRITIC 20MnMoNi55 . . . . .	325
<b>Table 240.</b> Mechanical properties of FERRITIC 20MnMoNi55 . . . . .	326
<b>Table 241.</b> Mechanical properties of FERRITIC 20MnMoNi55 . . . . .	327
<b>Table 242.</b> Mechanical properties of FERRITIC 20MnMoNi55 . . . . .	328

<b>Table 243.</b> Mechanical properties of FERRITIC 20MnMoNi55 . . . . .	329
<b>Table 244.</b> Mechanical properties of FERRITIC 20NiMoCr37 . . . . .	330
<b>Table 245.</b> Mechanical properties of FERRITIC 20NiMoCr37 . . . . .	331
<b>Table 246.</b> Mechanical properties of FERRITIC 20NiMoCr37 . . . . .	332
<b>Table 247.</b> Mechanical properties of FERRITIC 20NiMoCr37 . . . . .	333
<b>Table 248.</b> Mechanical properties of FERRITIC 20NiMoCr37 . . . . .	334
<b>Table 249.</b> Mechanical properties of FERRITIC 20NiMoCr37 . . . . .	335
<b>Table 250.</b> Mechanical properties of FERRITIC 20NiMoCr37 . . . . .	336
<b>Table 251.</b> Mechanical properties of FERRITIC 20NiMoCr37 . . . . .	337
<b>Table 252.</b> Mechanical properties of FERRITIC 26NiCrMo146 . . . . .	338
<b>Table 253.</b> Mechanical properties of FERRITIC 26NiCrMo146 . . . . .	339
<b>Table 254.</b> Mechanical properties of FERRITIC 26NiCrMo146 . . . . .	340
<b>Table 255.</b> Mechanical properties of FERRITIC 26NiCrMo146 . . . . .	341
<b>Table 256.</b> Mechanical properties of Eurofer97 . . . . .	342

## **GETTING IN TOUCH WITH THE EU**

### **In person**

All over the European Union there are hundreds of Europe Direct information centres. You can find the address of the centre nearest you at: [https://europa.eu/european-union/contact\\_en](https://europa.eu/european-union/contact_en)

### **On the phone or by email**

Europe Direct is a service that answers your questions about the European Union. You can contact this service:

- by freephone: 00 800 6 7 8 9 10 11 (certain operators may charge for these calls),
- at the following standard number: +32 22999696, or
- by electronic mail via: [https://europa.eu/european-union/contact\\_en](https://europa.eu/european-union/contact_en)

## **FINDING INFORMATION ABOUT THE EU**

### **Online**

Information about the European Union in all the official languages of the EU is available on the Europa website at: [https://europa.eu/european-union/index\\_en](https://europa.eu/european-union/index_en)

### **EU publications**

You can download or order free and priced EU publications from EU Bookshop at: <https://publications.europa.eu/en/publications>. Multiple copies of free publications may be obtained by contacting Europe Direct or your local information centre (see [https://europa.eu/european-union/contact\\_en](https://europa.eu/european-union/contact_en)).

## JRC Mission

As the Commission's in-house science service, the Joint Research Centre's mission is to provide EU policies with independent, evidence-based scientific and technical support throughout the whole policy cycle.

Working in close cooperation with policy Directorates-General, the JRC addresses key societal challenges while stimulating innovation through developing new methods, tools and standards, and sharing its know-how with the Member States, the scientific community and international partners.

*Serving society  
Stimulating innovation  
Supporting legislation*